EMERGING INFECTIOUS DISEASES®

U.S. CENTERS FOR DISEASE CONTROL AND PREVENTION

Foodborne Illnesses

November 2024

Abraham Mignon (1640–1679), *Still Life with Fruits, Oysters and a Porcelain Bowl* (1660–1679). Oil on panel, 21.7 in × 17.7 in/55 cm × 45 cm.
Digital image courtesy of Rijksmuseum, Amsterdam, the Netherlands.

EMERGING INFECTIOUS DISEASES®

Emerging Infectious Diseases is published monthly by the Centers for Disease Control and Prevention, 1600 Clifton Rd NE, Mailstop H16-2, Atlanta, GA 30329-4018, USA. Telephone 404-639-1960; email, eideditor@cdc.gov

EMERGING INFECTIOUS DISEASES®

Foodborne Illnesses **November 2024**

On the Cover

Abraham Mignon (1640–1679), *Still Life with Fruits, Oysters and a Porcelain Bowl* (1660–1679). Oil on panel, 21.7 in × 17.7 in/55 cm × 45 cm. Digital image courtesy of Rijksmuseum, Amsterdam, the Netherlands.

About the Cover p. 2454

Perspectives

Synopses

Research

EMERGING INFECTIOUS DISEASES®
November 2024

Dispatches

EMERGING INFECTIOUS DISEASES®
November 2024

Research Letters

Comment Letter

Books and Media

About the Cover

Online report

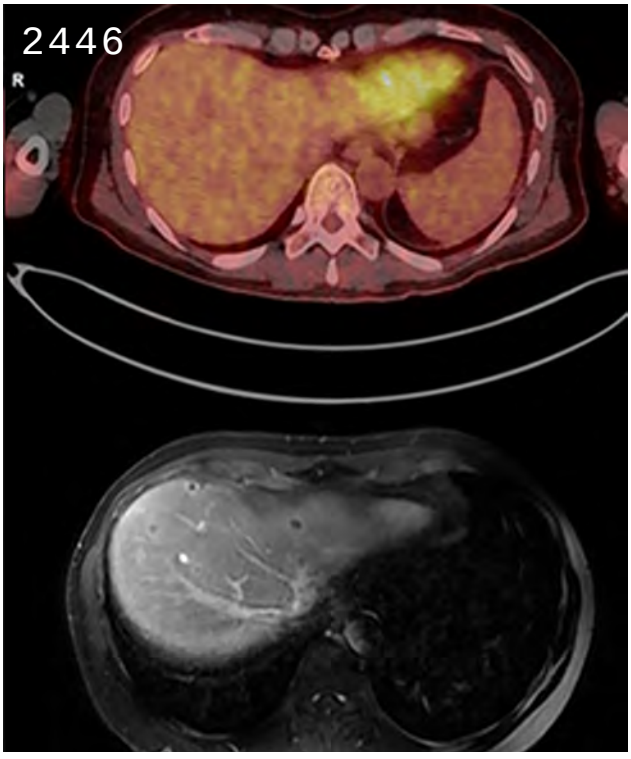

Emerging Infectious Diseases
Photo Quiz Articles

Volume 14, Number 9
September 2008

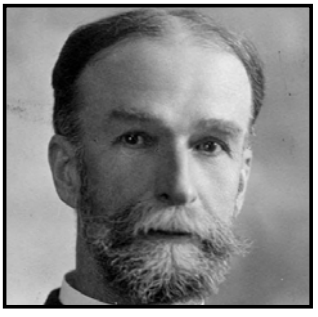

Volume 14, Number 12
December 2008

Volume 15, Number 9
September 2009

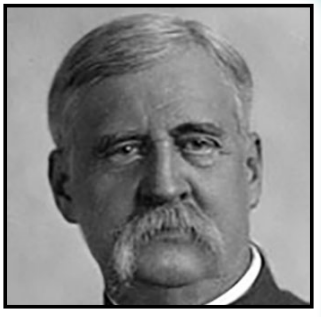

Volume 15, Number 10
October 2009

Volume 16, Number 6
June 2010

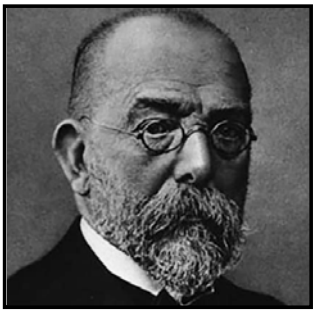

Volume 17, Number 3
March 2011

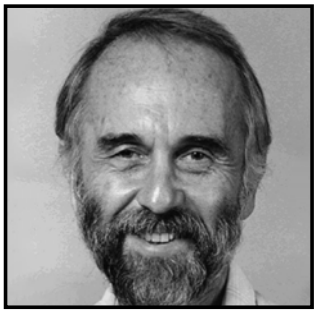

Volume 17, Number 12
December 2011

Volume 19, Number 4
April 2013

Volume 20, Number 5
May 2014

Volume 21, Number 9
September 2015

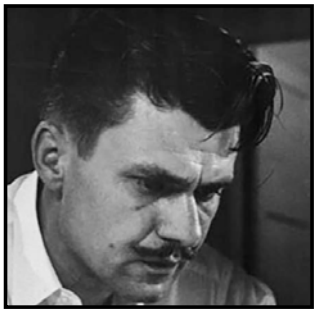

Volume 22, Number 8
August 2016

Volume 28, Number 3
March 2022

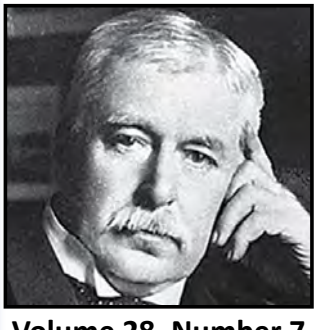

Volume 28, Number 7
July 2022

Click on the link below to read about the people behind the science.

https://bit.ly/3LN02tr

See requirements for submitting a photo quiz to EID.

https://bit.ly/3VUPqfj

EID Journal

Flexible Development Programs for Antibacterial Drugs to Address Unmet Medical Needs

Mayurika Ghosh, Dmitri Iarikov, Xiaojing (Karen) Qi, Daniel Rubin, Simone Shurland, Avery Goodwin, Xiaohui Wei, Dakshina Chilukuri, Owen McMaster, Terry Miller, Peter Kim, Adam Sherwat

The US Food and Drug Administration recognizes the unmet medical need for antibacterial drugs to treat serious bacterial diseases caused by resistant pathogens for which effective therapies are limited or lacking. The agency also recognizes that designing and conducting clinical trials to assess the safety and efficacy of drugs to treat resistant infections is challenging, especially for drugs only active against a single or a few bacterial species, and that a more flexible development program might be appropriate. In this article, we discuss several regulatory considerations for flexible development programs for antibacterial drugs intended to meet an unmet medical need. As an example, we use the recent approval of sulbactam for injection and durlobactam for injection (XACDURO) for the treatment of hospital-acquired bacterial pneumonia and ventilator-associated bacterial pneumonia caused by susceptible isolates of *Acinetobacter baumannii-calcoaceticus* complex.

As described in guidance from the US Food and Drug Administration (FDA), the evaluation of antibacterial drugs for serious bacterial diseases is associated with several challenges, such as the need to promptly initiate empiric antibacterial therapy that might obscure effects of the investigational drug(s) in noninferiority trials and difficulties with obtaining informed consent in acutely ill patients (*1*). Developing drugs that are active against a single resistant bacterial species presents additional challenges. The number of patients with infections with a targeted resistant phenotype can be relatively small, thereby slowing accrual of evaluable patients into the trial. Lack of rapid diagnostics can result in uncertainty regarding bacterial etiology at the time of enrollment, thereby necessitating continuation of empiric antibacterial therapy pending confirmation of the pathogen of interest. In potentially polymicrobial infections, such as nosocomial pneumonia, continuing broad-spectrum antibacterial therapy might be needed throughout the study to provide coverage for bacterial species against which the study drug is not active. Ideally, the spectrum of activity of the concomitant antibacterial therapy should not overlap with the activity of the antibacterial drug being studied, but that difference is not always feasible. When overlapping antibacterial therapy is necessary, it can confound assessments not only of efficacy but also of safety of the investigational drug.

For serious bacterial diseases for which effective treatment options exist, the efficacy of an investigational drug can be established in a noninferiority trial. The clinical trial population should include persons whose illness severity and comorbidities reflect the patient population with unmet medical need to ensure safety and efficacy findings are generalizable (*1*). Only patients who have pathogens against which the control drug has antibacterial activity should be included in the efficacy analyses in noninferiority trials. Thus, a higher than anticipated prevalence of resistance to the selected comparator might require increasing the initially planned sample size.

The Example of Sulbactam/Durlobactam

Infections caused by carbapenem-resistant (CR) *Acinetobacter baumannii-calcoaceticus* complex (ABC) constitute an area of high unmet medical need. They are associated with significant mortality rates, ranging from 38% to 76%; nosocomial pneumonia is the most common infection type (*2*–*5*). In 2020 in the United States, an estimated 7,500 cases of CR ABC infection occurred, resulting in 700 deaths (*6*). Therapies to treat CR ABC infections are limited because of multiple resistance mechanisms demonstrated by *A. baumannii*. In patients with hospital-acquired bacterial pneumonia (HABP) or ventilator-associated bacterial pneumonia

Author affiliation: Center for Drug Evaluation and Research, US Food and Drug Administration, Silver Spring, Maryland, USA

DOI: https://doi.org/10.3201/eid3011.231416

(VABP) caused by a CR pathogen that is sensitive only to polymyxins, treatment with intravenous polymyxins (colistin or polymyxin B) is an option (*7*). However, current treatment guidelines acknowledge that no clear standard-of-care regimen exists for the treatment of CR ABC infections (*8*).

XACDURO (Innoviva Specialty Therapeutics, Inc., https://www.xacduro.com) is a combination of sulbactam and durlobactam that is administered intravenously (*9*). Sulbactam is an Ambler class A β-lactamase inhibitor; however, against *A. baumannii*, sulbactam exerts its effect by binding to penicillin-binding proteins, thereby inhibiting cell-wall biosynthesis (*10*). An increasing number of isolates possess ≥1 β-lactamases that inactivate sulbactam (*11*). Durlobactam is a novel non–β-lactam β-lactamase inhibitor inactivating several serine β-lactamases expressed by *Acinetobacter* that degrade sulbactam including those of Ambler classes A, C, and D. Durlobactam does not have intrinsic antibacterial activity against *A. baumannii*.

Approval of sulbactam/durlobactam relied primarily on a single phase 3, randomized, independent assessor–blinded, active-controlled noninferiority study in adults with HABP or VABP caused by CR ABC in which sulbactam/durlobactam was compared with colistin (*12*). A noninferiority margin of 20% was used in the clinical trial (*13*). Both treatment arms also received imipenem/cilastatin as background therapy for potential HABP/VABP pathogens other than CR ABC. The primary efficacy endpoint for the study was 28-day all-cause mortality.

A total of 177 patients with documented ABC infections were randomized and received study drug (91 in the sulbactam/durlobactam group and 86 in the colistin group); 128 of 177 patients were found to have CR ABC infection susceptible to sulbactam/durlobactam and colistin. Among the 128 patients, 125 patients did not withdraw consent before assessment of survival status at day 28 and were included in the efficacy analyses. Sulbactam/durlobactam was found to be noninferior to colistin for the 28-day all-cause mortality primary endpoint (sulbactam/durlobactam 19% [12/63] vs. colistin 32.3% [20/62]; treatment difference: −13.2% [95% CI −30.0% to 3.5%]).

In many situations, FDA requires 2 adequate and well-controlled trials to establish effectiveness. Under certain circumstances, FDA can conclude that 1 adequate and well-controlled trial plus confirmatory evidence is sufficient to establish effectiveness. Factors considered when determining whether reliance on a single trial is appropriate include the persuasiveness of the single trial and the seriousness of the disease, particularly when an unmet medical need exists (*14*,*15*). Confirmatory evidence in the sulbactam/durlobactam development program was provided by in vitro studies, which were complemented by animal studies in murine neutropenic thigh abscess and lung infection models that established pharmacokinetic/pharmacodynamic targets for sulbactam/durlobactam combination and demonstrated that durlobactam restored sulbactam bactericidal activity against *A. baumannii* isolates producing serine β-lactamases (*15*,*16*).

Sulbactam and durlobactam pharmacokinetic data from phase 1, 2, and 3 studies were used for population pharmacokinetic modeling and probability of pharmacokinetic/pharmacodynamic target attainment analyses to inform the sulbactam/durlobactam dosage regimen and susceptibility breakpoints. Pharmacokinetic/pharmacodynamic target attainment results were also provided for drug exposures in epithelial lining fluid where animal and human data on the lung penetration for sulbactam and durlobactam were considered. Sulbactam and durlobactam pharmacokinetics were also evaluated in patients with altered renal function, which informed the dosage in such patients.

For a drug that is the subject of a more flexible development program, a safety database should generally include ≈300 persons at the dose and duration of therapy proposed for marketing. The safety database for the sulbactam/durlobactam new drug application included 158 participants who received sulbactam and durlobactam at the proposed dose and duration, including a phase 2 study in complicated urinary tract infections and the phase 3 study in HABP/VABP. The safety of durlobactam was also evaluated in 6 phase 1 studies in which 123 patients received durlobactam and 72 patients received sulbactam and durlobactam combinations.

No unexpected safety signals were identified in clinical studies during the development program, and the safety profile of sulbactam/durlobactam appeared consistent with other β-lactam/β-lactamase inhibitors. In the phase 3 trial, the incidence of acute kidney injury was lower in the sulbactam/durlobactam group (6%) than in the colistin group (36%) (*13*). No specific safety concerns were identified in nonclinical studies of sulbactam and durlobactam. In addition, clinical experience with sulbactam, which is approved in the United States in combination with ampicillin, was considered. Thus, although the safety database of the sulbactam/

durlobactam new drug application was relatively limited and some uncertainties remained, because this combination addresses an unmet medical need for a serious disease and demonstrated efficacy on the basis of an all-cause mortality endpoint, FDA determined that the database was adequate to inform the risk-benefit assessment. During an Antimicrobial Drugs Advisory Committee meeting on April 17, 2023, the Committee unanimously voted that the overall benefit–risk assessment was favorable for the use of sulbactam/durlobactam for the treatment of patients with HABP and VABP caused by susceptible strains of ABC organisms (*17*).

When the approval standard has been met but uncertainties remain about findings of a potentially serious risk, the FDA might determine that a postmarketing study is needed to further characterize the risk. In the case of sulbactam/durlobactam, a postmarketing requirement to conduct a single-arm, open-label, prospective, observational study to assess safety, including the risk for hypersensitivity reactions, in patients with ABC infection was issued at the time of approval to collect additional safety data.

In conclusion, FDA recognizes that challenges to developing antibacterial drugs to treat serious and life-threatening infections exist, especially for infections caused by highly drug-resistant pathogens for which treatment options are limited. The development program for sulbactam/durlobactam illustrates the successful use of a flexible development program for an antibacterial drug to address an unmet medical need.

The findings and conclusions in this report are those of the authors and do not necessarily represent the views of the US Food and Drug Administration.

M.G. wrote the original draft of the manuscript. D.I. revised the manuscript. M.G. and A.S. conceptualized the manuscript. D.I. and P.K. also contributed to the conceptualization of the manuscript. M.G., D.I., K.Q., O.M., S.S., and T.W. directly accessed and verified the underlying data. P.K., T.M., D.R., D.C., A.G., and A.S. reviewed and edited the manuscript.

About the Author

Dr. Ghosh is an infectious diseases specialist and medical officer in the Division of Anti-Infectives at the Food and Drug Administration. Her primary research interest is the development of antimicrobial drugs, including those to treat emerging pathogens and address unmet medical needs.

References

1. US Food and Drug Administration. Antibacterial therapies for patients with an unmet medical need for the treatment of serious bacterial diseases—questions and answers (revision 1) guidance for industry, May 2022 [cited 2023 Jul 10]. https://www.fda.gov/media/158589/download
2. Aydemir H, Akduman D, Piskin N, Comert F, Horuz E, Terzi A, et al. Colistin vs. the combination of colistin and rifampicin for the treatment of carbapenem-resistant *Acinetobacter baumannii* ventilator-associated pneumonia. Epidemiol Infect. 2013;141:1214–22. https://doi.org/10.1017/S095026881200194X
3. Lemos EV, de la Hoz FP, Einarson TR, McGhan WF, Quevedo E, Castañeda C, et al. Carbapenem resistance and mortality in patients with *Acinetobacter baumannii* infection: systematic review and meta-analysis. Clin Microbiol Infect. 2014;20:416–23. https://doi.org/10.1111/1469-0691.12363
4. Paul M, Daikos GL, Durante-Mangoni E, Yahav D, Carmeli Y, Benattar YD, et al. Colistin alone versus colistin plus meropenem for treatment of severe infections caused by carbapenem-resistant Gram-negative bacteria: an open-label, randomised controlled trial. Lancet Infect Dis. 2018;18:391–400. https://doi.org/10.1016/S1473-3099(18)30099-9
5. Weiner-Lastinger LM, Abner S, Edwards JR, Kallen AJ, Karlsson M, Magill SS, et al. Antimicrobial-resistant pathogens associated with adult healthcare-associated infections: summary of data reported to the National Healthcare Safety Network, 2015–2017. Infect Control Hosp Epidemiol. 2020;41:1–18. https://doi.org/10.1017/ice.2019.296
6. Castanheira M, Mendes RE, Gales AC. Global epidemiology and mechanisms of resistance of *Acinetobacter baumannii-calcoaceticus* complex. Clin Infect Dis. 2023;76(Suppl 2):S166–78. https://doi.org/10.1093/cid/ciad109
7. Kalil AC, Metersky ML, Klompas M, Muscedere J, Sweeney DA, Palmer LB, et al. Management of adults with hospital-acquired and ventilator-associated pneumonia: 2016 Clinical Practice Guidelines by the Infectious Diseases Society of America and the American Thoracic Society. Clin Infect Dis. 2016;63:e61–111. https://doi.org/10.1093/cid/ciw353
8. Tamma PD, Aitken SL, Bonomo RA, Mathers AJ, van Duin D, Clancy CJ. Infectious Diseases Society of America 2023 guidance on the treatment of antimicrobial resistant Gram-negative infections. Clin Infect Dis. 2023 Jul 18 [Epub ahead of print].
9. US Food and Drug Administration. XACDURO (sulbactam for injection; durlobactam for injection) prescribing information. May 2023 [cited 2023 Jul 10]. https://www.accessdata.fda.gov/drugsatfda_docs/label/2023/216974Orig1s000Correctedlbl.pdf
10. Penwell WF, Shapiro AB, Giacobbe RA, Gu RF, Gao N, Thresher J, et al. Molecular mechanisms of sulbactam antibacterial activity and resistance determinants in *Acinetobacter baumannii*. Antimicrob Agents Chemother. 2015;59:1680–9. https://doi.org/10.1128/AAC.04808-14
11. Shapiro AB, Moussa SH, McLeod SM, Durand-Réville T, Miller AA. Durlobactam, a new diazabicyclooctane β-lactamase inhibitor for the treatment of *Acinetobacter* infections in combination with sulbactam. Front Microbiol. 2021;12:709974. https://doi.org/10.3389/fmicb.2021.709974
12. Kaye KS, Shorr AF, Wunderink RG, Du B, Poirier GE, Rana K, et al. Efficacy and safety of sulbactam-durlobactam versus colistin for the treatment of patients with serious infections caused by *Acinetobacter baumannii-calcoaceticus* complex: a multicentre, randomised, active-controlled, phase 3,

non-inferiority clinical trial (ATTACK). Lancet Infect Dis. 2023; 23:1072–84. https://doi.org/10.1016/S1473-3099(23)00184-6
13. US Food and Drug Administration. Sulbactam-durlobactam new drug application. Integrated review, application number: 216974Orig1s000 [cited 2024 Apr 29]. https://www.accessdata.fda.gov/drugsatfda_docs/nda/2023/216974Orig1s000IntegratedR.pdf
14. US Food and Drug Administration. Demonstrating substantial evidence of effectiveness for human drug and biological products. Draft guidance for industry, December 2019 [cited 2023 Jul 10]. https://www.fda.gov/regulatory-information/search-fda-guidance-documents/demonstrating-substantial-evidence-effectiveness-human-drug-and-biological-products
15. US Food and Drug Administration. Demonstrating substantial evidence of effectiveness with one adequate and well-controlled clinical investigation and confirmatory evidence, September 2023 [cited 2024 Apr 29. https://www.fda.gov/regulatory-information/search-fda-guidance-documents/demonstrating-substantial-evidence-effectiveness-one-adequate-and-well-controlled-clinical
16. US Food and Drug Administration. Codevelopment of two or more new investigational drugs for use in combination, June 2013 [2024 Apr 29]. https://www.fda.gov/regulatory-information/search-fda-guidance-documents/codevelopment-two-or-more-new-investigational-drugs-use-combination
17. Antimicrobial Drugs Advisory Committee. Updated information: April 17, 2023: meeting of the Antimicrobial Drugs Advisory Committee meeting announcement [cited 2024 Aug 30]. https://www.fda.gov/advisory-committees/advisory-committee-calendar/updated-information-april-17-2023-meeting-antimicrobial-drugs-advisory-committee-meeting#event-materials

Address for correspondence: Mayurika Ghosh, Division of Anti-Infectives, Office of Infectious Diseases, Center for Drug Evaluation and Research, US Food and Drug Administration, 10903 New Hampshire Ave, Bldg 22, Silver Spring, MD 20993, USA; email: mayurika.ghosh@fda.hhs.gov

etymologia revisited

Picobirnavirus [pi-ko-burr′nə-vi″rəs]

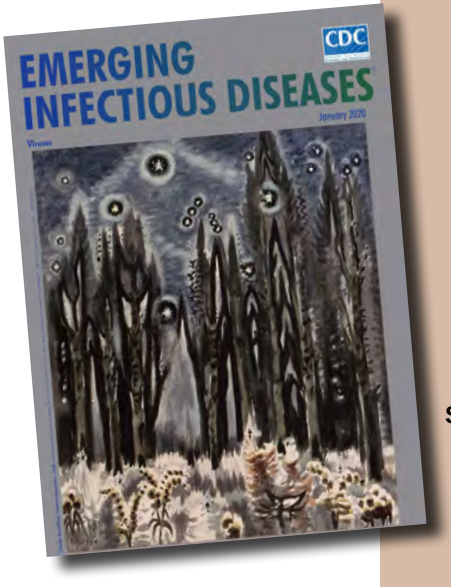

Originally published in January 2020

Picobirnavirus, the recently recognized sole genus in the family *Picobirnaviridae*, is a small (*Pico*, Spanish for small), bisegmented (*bi*, Latin for two), double-stranded RNA virus. Picobirnaviruses were initially considered to be birna-like viruses, and the name was derived from birnavirus (bisegmented RNA), but the virions are much smaller (diameter 35 nm vs. 65 nm).

Picobirnaviruses are reported in gastroenteric and respiratory infections. These infections were first described in humans and black-footed pigmy rice rats in 1988. Thereafter, these infections have been reported in feces and intestinal contents from a wide variety of mammals with or without diarrhea, and in birds and reptiles worldwide.

Sources

1. Delmas B, Attoui H, Ghosh S, Malik YS, Mundt E, Vakharia VN; ICTV Report Consortium. ICTV virus taxonomy profile: Picobirnaviridae. J Gen Virol. 2019;100:133–4. https://doi.org/10.1099/jgv.0.001186
2. Malik YS, Kumar N, Sharma K, Dhama K, Shabbir MZ, Ganesh B, et al. Epidemiology, phylogeny, and evolution of emerging enteric Picobirnaviruses of animal origin and their relationship to human strains. BioMed Res Int. 2014;2014:780752. https://doi.org/10.1155/2014/780752
3. Pereira HG, Flewett TH, Candeias JA, Barth OM. A virus with a bisegmented double-stranded RNA genome in rat (*Oryzomys nigripes*) intestines. J Gen Virol. 1988;69:2749–54. https://doi.org/10.1099/0022-1317-69-11-2749
4. Smits SL, van Leeuwen M, Schapendonk CM, Schürch AC, Bodewes R, Haagmans BL, et al. Picobirnaviruses in the human respiratory tract. Emerg Infect Dis. 2012;18:1539–40. https://doi.org/10.3201/eid1809.120507

https//wwwnc.cdc.gov/eid/article/26/1/et-2601_article

Conceptual Framework for Community-Based Prevention of Brown Dog Tick–Associated Rocky Mountain Spotted Fever

Maureen K. Brophy, Erica Weis, Naomi A. Drexler, Christopher D. Paddock, William L. Nicholson, Gilbert J. Kersh, Johanna S. Salzer

Rocky Mountain spotted fever (RMSF) is a severe tickborne disease that can reach epidemic proportions in communities with certain social and ecologic risk factors. In some areas, the case-fatality rate of brown dog tick-associated RMSF is up to 50%. Because of the spread of brown dog tick–associated RMSF in the southwestern United States and northern Mexico, the disease has the potential to emerge and become endemic in other communities that have large populations of free-roaming dogs, brown dog ticks, limited resources, and low provider awareness of the disease. By using a One Health approach, interdisciplinary teams can identify communities at risk and prevent severe or fatal RMSF in humans before cases occur. We have developed a conceptual framework for RMSF prevention to enable communities to identify their RMSF risk level and implement prevention and control strategies.

Rocky Mountain spotted fever (RMSF) is the deadliest tickborne disease in the Western Hemisphere. RMSF is caused by the bacterium *Rickettsia rickettsii*, which is primarily transmitted to humans by *Dermacentor* spp. ticks in the United States. RMSF exposures associated with the brown dog tick (*Rhipicephalus sanguineus* sensu lato) are different from those associated with *Dermacentor* spp. ticks. For brown dog tick–associated RMSF, the primary site of exposure is in the peridomestic environment, which is in and around homes. Circulation of the bacteria in the peridomestic environment may go unnoticed until there is a severe case or death. During July–November 2023, there were 5 confirmed cases of RMSF and 3 deaths in southern California, USA, all in people who had traveled to or resided in Tecate, Baja California, Mexico, where there is high incidence of RMSF associated with brown dog ticks (*1*,*2*). Those cases suggest the introduction of the pathogen to new locations is not only possible but likely. The travel-associated cases in California, along with recent emergence in Arizona, USA, and reemergence in Mexico, suggests that RMSF might occur in other global areas with similar community risk factors.

Author affiliations: Centers for Disease Prevention and Control, Atlanta, Georgia, USA (M.K. Brophy, N.A. Drexler, C.D. Paddock, W.L. Nicholson, G.J. Kersh, J.S. Salzer); Kapili Services, Honolulu, Hawaii, USA (E. Weis).

DOI: https://doi.org/10.3201/eid3011.240293

Brown Dog Tick–Associated RMSF in Mexico

Whereas cases of RMSF associated with brown dog tick transmission were not conclusively identified in the United States until 2005 (*3*), medical reports of a lethal illness described as a petechial rash and malignant scarlet fever in Mexico date back to 1903 (*4*). In 1943, epidemiologists identified this illness as the same RMSF that had been discovered in the United States around the turn of the 20th Century (*5*,*6*). They described the clinical manifestations and epidemiology of the disease and experimentally confirmed the association with brown dog ticks. Experimental studies in previous publications showed brown dog ticks were an efficient vector of *R. rickettsii* through 2 generations before this epidemiologic linkage (*7*). During 1918–1943, medical records indicate that ≥200 cases of RMSF occurred throughout Mexico, often clustered in neighborhoods or within households (*4*). The case clustering is a frequently observed characteristic of brown dog tick–associated RMSF transmission because the tick lives in and around human dwellings to be near its preferred host, domesticated dogs. A reduction in cases was reported after the 1940s, and whereas the reason for the decline is unknown, there is a possible

connection with high use of DDT to control malaria in endemic regions throughout Mexico and the United States (*8*). However, RMSF has resurged in northern Mexico; 1,394 cases and 247 deaths were reported during 2003–2016, and the case-fatality rate was 18%, higher than previously seen (*4*,*9*). The resurgence of RMSF in Mexico has been particularly evident in the states of Sonora and Baja California but includes many border states in the northern part of the country, such as Chihuahua, Coahuila, and Nuevo Leon (*10*–*14*).

Brown Dog Tick–Associated RMSF in Arizona

RMSF was historically rare in Arizona, consisting of only sporadic cases primarily associated with travel to endemic areas, until September 2003, when a fatal case occurred in an infant with no history of travel outside of their Indigenous Nation (*3*,*15*). During the investigation, 16 additional cases were identified in the original community and a neighboring Indigenous Nation; the earliest recognized case had occurred in 2002 (*3*). The typical vectors, *Dermacentor andersoni* or *D. variabilis* ticks, were absent, but many brown dog ticks on dogs secured on the property, free-roaming, and in the peridomestic environment were found. Of the brown dog ticks tested, 3% were positive for *R. rickettsii* (*3*). Implementation of intensive prevention measures reduced tick populations and temporarily halted cases. RMSF became endemic in the 2 communities, averaging 5–10 cases per year, with a case-fatality rate of ≈11% (*16*). During 2009–2011, cases of RMSF were confirmed on 4 other Indigenous Nations in Arizona. Those additional communities rapidly implemented prevention measures and have been able to reduce or eliminate additional human cases of RMSF to date.

Brown dog tick–associated RMSF emergence has historically been met with reactionary public health action, such as increased surveillance and intervention occurring after human cases are identified. However, evidence of *R. rickettsii* circulation in a zoonotic cycle before human cases were identified has been documented in countries including Brazil (*17*,*18*), Panama (*19*), and Costa Rica (*20*,*21*), suggesting early intervention could prevent the spread of RMSF to the human population. Within the United States, conditions for RMSF emergence are already present in some communities. A recent study found *R. rickettsii* in 1 of 10 adult and 1 of 20 larval brown dog ticks tested from Palm Beach, Florida, USA (*22*), where this tick species has not been reported to spread RMSF to date. In regions across the globe with similar suitable climates (i.e., 20°C–35°C and relative humidity 35%–95%) (*23*), if brown dog ticks carrying *R. rickettsii* were to infest free-roaming dogs or those with limited access to veterinary care, local circulation could follow and lead to outbreaks within the human population.

Local public health agencies should remain vigilant in monitoring for RMSF transmission, especially in regions with a suitable climate for brown dog ticks, large populations of free-roaming dogs, and limited access to medical and veterinary services. Identifying areas of high risk for brown dog tick–associated RMSF is necessary because mitigation efforts are expensive in terms of financial and human resource investment. Developing a conceptual framework for RMSF prevention can aid in identifying communities of high risk and implementing an early warning system that incorporates acarological surveillance. This early warning will increase preparedness and protect human lives while ensuring limited resources are appropriately allocated. This framework requires a One Health approach with expertise from medical, veterinary, and vector control professionals within each community (*9*,*24*,*25*).

Theoretical Framework

Preventing RMSF from emerging in a community at risk is necessary because it is difficult to eliminate the disease once it becomes endemic. We have provided a basic framework of risk factors (Figure 1) and outlined the indicators and action items established by an Arizona state interdisciplinary coalition, which is currently in use by Arizona communities, to assess the risk for brown dog tick–associated RMSF (Table). We believe that if a community has free-roaming dogs, high levels of brown dog ticks, and inadequate medical and veterinary care, there is a medium risk for emergence of RMSF. If *R. rickettsii* is established in the tick or dog population and there are gaps in community understanding and application of tickborne disease prevention, gaps in healthcare worker knowledge of RMSF diagnosis and treatment, or a combination of any of those factors, there is a high risk for emergence. Communities without free-roaming dogs and without high levels of brown dog ticks are considered low risk.

Once leaders of a community have assessed its risk level, they should identify key stakeholders within their network and develop an action plan to address those risk factors and implement RMSF prevention before human cases occur (Table 1; Figure 2). Implementing an early warning system for rickettsial diseases can prevent illness and death among the human and canine populations and prevent high medical and indirect costs associated with RMSF (*25*,*26*). Activities to include in the action plan range from lower cost and effort, such as implementing standard operating

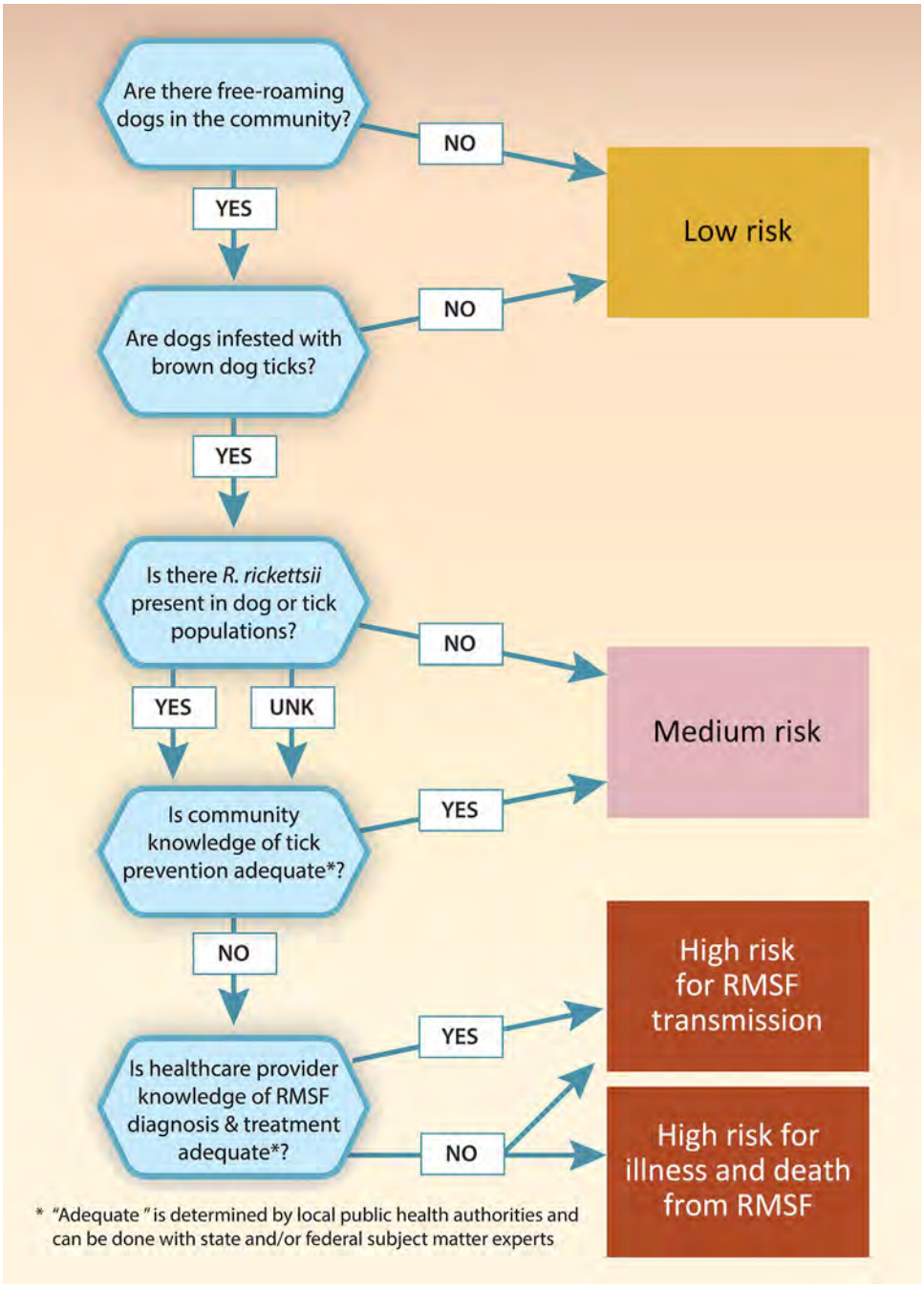

Figure 1. Community risk assessment for brown dog tick–associated RMSF. Communities with free-roaming dogs, high levels of brown dog ticks, and Rickettsia rickettsii in the dog or tick population are considered medium risk for RMSF transmission. Communities with those factors as well as inadequate community knowledge of tick prevention are considered high risk for RMSF transmission. If healthcare provider knowledge of RMSF diagnosis and treatment is also inadequate, the community is also considered high risk for severe illness or death from RMSF. RMSF, Rocky Mountain spotted fever.

procedures for identifying cases of RMSF in clinical settings, to high cost and effort, such as developing and maintaining a vector control program; feasibility and cost may depend on location and infrastructure. Communities should consider individual needs and resources to determine the level of RMSF risk response.

Core Functions of RMSF Control

During the emergence of RMSF in Arizona, 5 core functions were identified as critical to prevent and control RMSF: 1) health care system coordination and public health reporting; 2) community education and outreach; 3) animal control and veterinary programs; 4) environmental tick control and surveillance; and 5) finance and budget. Increasing awareness of RMSF symptoms and treatment in the healthcare system and community might be among the most cost-effective interventions available to reduce RMSF illness and death because the bulk of the cost would be personnel time. However, interventions at the animal and

environmental level are crucial to reducing tick populations and the potential for disease transmission.

Function 1: Healthcare System Coordination and Public Health Reporting

In the United States, RMSF is a nationally notifiable condition within the spotted fever rickettsiosis (SFR) standard case definition, which captures diseases caused by multiple rickettsial agents (*27*). Whereas RMSF is effectively treated with antimicrobial drugs if they are given within 5 days of symptom onset, the nonspecific clinical manifestations can lead to misdiagnosis. Clinical illness is characterized by acute fever and may include headache, malaise, myalgia, nausea, and vomiting. The pathognomonic spotted petechial rash that often involves the palms or soles

Table. Conceptual framework for community-based prevention of RMSF listing proposed indicators and action items for communities at medium and high risk for endemic transmission*

Core function	Recommended risk level indicators	Action	Relative cost
Healthcare system coordination and public health reporting	Presence or absence of provider education around ticks and tickborne diseases, provider understanding of diagnosing and treating tickborne diseases, diagnostic testing capacity, distance to healthcare, availability of medical transport	Implement standardized RMSF patient treatment protocol in all affected areas to include follow up contact to ensure treatment continues if the patient leaves endemic area health facilities	$
		Use RMSF patient treatment algorithm in patients experiencing with fever or a history of contact with ticks	$$
		Disseminate education on RMSF for support staff and healthcare providers	$
		Require continuing medical education for healthcare providers, including MDs in primary care, emergency care, internal care, family practice, and pediatrics, physician assistants, and nursing staff providing care; consider embedding RMSF training course into the onboarding process for new hires	$$
		Establish a clinical task force to address areas of varying needs and priorities	$
Community education and outreach	Percent of population below local poverty level, educational attainment in community; presence or absence of health education around ticks and tickborne diseases; knowledge, attitudes, and behaviors about personal and home tick prevention; percent of population with internet access	Disseminate education on RMSF for support staff and community health workers	$$
		Consider embedding RMSF training course into the onboarding process for new hires in public interfacing agencies	$
		Create an RMSF communication plan so all communities get consistent messaging	$
Animal control and veterinary programs	Wellness: presence or absence of veterinary services, availability of effective ectoparasite treatments for dogs in community, number of spayed or neutered animals, cost of effective ectoparasite treatments for dogs in community; free-roaming population status: density of free-roaming dogs, presence or absence of ordinance forbidding free roaming dogs, fencing and tethering behaviors across community; access to resources: presence or absence of animal control department, presence or absence of animal shelter space, number of low- or no-cost spay and neuter clinics	Establish animal control programs	$$$
		Establish veterinary services	$$$
Environmental tick surveillance and control	Harborage: presence or absence of municipal and community solid waste removal, landfill cost and availability; pesticide use: presence or absence of vector control program, presence or absence of certified pesticide applicators; community knowledge, Attitudes, and Practices about tickborne diseases: presence or absence of community education around ticks and tickborne diseases	Develop programs to provide regular tick control services for each home in affected areas	$$$
		Implement environmental tick surveillance to provide measurement and direction for prevention efforts	$$$
Finance and budget	Presence or absence of dedicated annual jurisdictional funding to all partners for RMSF prevention, presence or absence of personnel capable of writing and managing grants	Engage leadership to advocate for sustainable funding for all RMSF prevention partners	$
		Train personnel across all RMSF prevention partnering agencies in grant writing and management	$$

*Relative cost scale: $, lowest cost activities; $$, median cost activities; $$$, highest cost activities. RMSF, Rocky Mountain spotted fever.

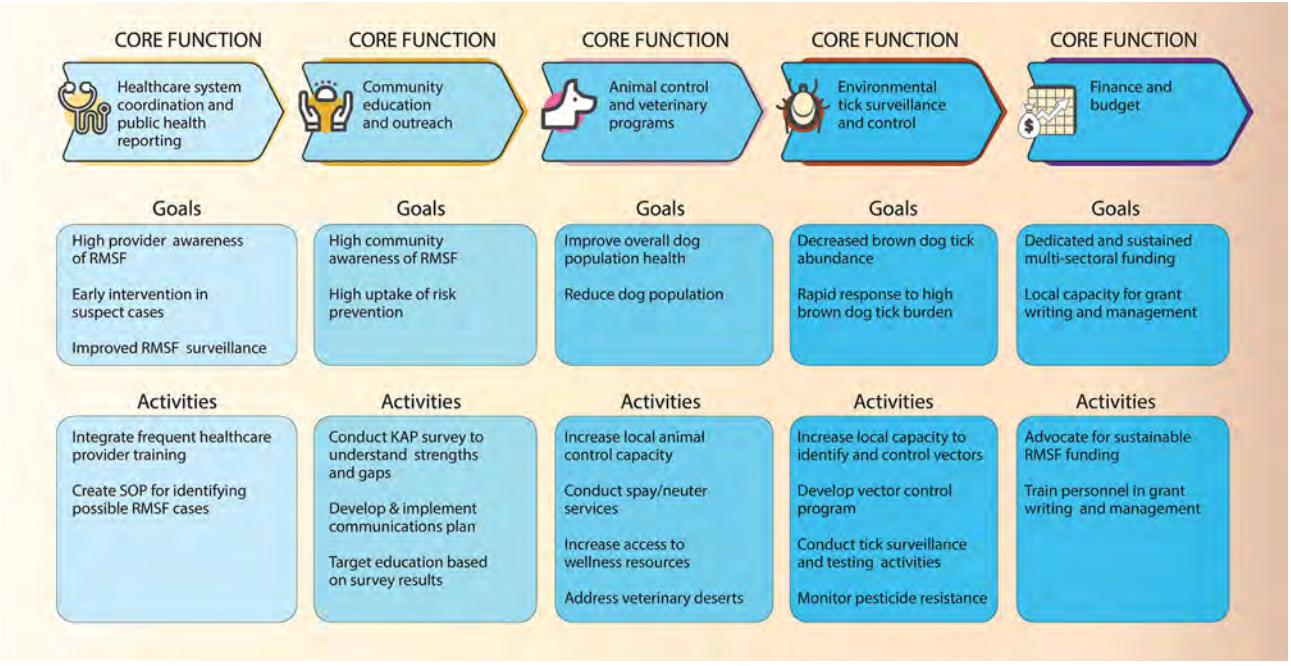

Figure 2. Recommended goals and activities for community-based prevention of brown dog tick–associated RMSF on the basis of the risk assessment road map for medium- or high-risk communities (Figure 1). KAP, knowledge, attitudes, and practices; RMSF, Rocky Mountain spotted fever; SOP, standard operating procedure.

does not typically appear until after day 5 or 6 of illness. It is imperative that clinicians in medium- and high-risk communities are capable of recognizing, treating, and diagnosing RMSF to prevent severe illness and death. Healthcare providers should be trained to prophylactically begin doxycycline treatment and to order appropriate laboratory tests for diagnosis, including whole blood and plasma specimens for molecular tests and acute and convalescent serum specimens for indirect fluorescence antibody tests (*28*). In addition to clinical manifestations, diagnostic confirmation can be made on the basis of a 4-fold change in *R. rickettsii*–specific or SFR IgG titers by indirect fluorescence antibody with paired serum specimens or PCR confirmation of SFR DNA in an acute clinical specimen. Patient history should include questions about tick bites or direct contact with a tick-infested dog, ticks identified in or around the household, or travel to or residence in an area where RMSF cases have recently been identified. However, patients may not recall tick bites; therefore, failure to self-report a tick bite should not exclude a RMSF diagnosis.

Our recommended indicators to assess risk level include the presence or absence of provider education around ticks and tickborne diseases, provider understanding of diagnosing and treating tickborne diseases, diagnostic testing capacity, distance to healthcare providers, and availability of medical transportation. We have identified many challenges in healthcare system coordination and public health reporting. Nonspecific symptoms may lead to misdiagnosis until the patient experiences critical clinical manifestations; laboratory testing is not always available, affordable, or expedient; PCR testing has low sensitivity in the acute stage of RMSF; serologic testing for detecting antibodies is frequently negative in the first week of illness, and the disease cannot be confirmed by using a single acute antibody result; patient loss to follow-up is high when a second visit to a healthcare provider is needed to collect a convalescent serum specimen, and the lack of convalescent titers has led to only 3% of SFR cases being reported as confirmed in the United States; surveillance may be limited when treatment is initiated on the basis of clinical manifestations and there is no laboratory confirmation of diagnosis; lack of case reporting reduces the ability of public health officials to conduct adequate surveillance and identify outbreaks; and misconceptions surrounding doxycycline administration to children persist, despite scientific studies showing its safety and efficacy.

Function 2: Community Education and Outreach

Community members and stakeholders that are well informed about RMSF may be able to recognize the risk for brown dog tick–associated RMSF without

knowing the infection rates in the brown dog tick or dog population. Some factors, such as fencing around property, conducting personal tick checks, and having community dogs spayed or neutered are protective against RMSF (*24*; M.K. Brophy, unpub. data). Other factors, such as solid waste or harborage near home and high dog density, especially free-roaming dogs, increase the risk for RMSF (*3*). Medium- and high-risk communities can prevent human illness and death from brown dog tick–associated RMSF by developing and implementing communications plans to inform the public about risk-mitigating factors. Public health outreach is more effective when tailored to the target population demographics (*29*–*32*). Communities should use locally minded verbiage and imagery and culturally relevant messaging and outreach through media with high uptake within the community.

Our recommended indicators to assess risk level include the percent of population below local poverty level, median years of educational attainment in community, presence or absence of health education around ticks and tickborne diseases, the community knowledge, attitudes, and behaviors surrounding personal and home tick prevention, and the percentage of the population with internet access. We have identified 3 challenges in community education and outreach. These challenges are the lack of culturally tailored educational materials, lack of staff to conduct outreach, and a low level of community resources to enable self-protective behaviors.

Function 3: Animal Control and Veterinary Programs

Across the world, ≈75% of the >700 million domestic dogs are classified as free-roaming, or without human restraint or control (*33*). High densities of free-roaming dogs are associated with many public health concerns, including transmission of zoonotic diseases (*34*). Canine serosurveys have revealed ≈50%–60% of dogs in outbreak communities were IgG-positive for SFRs, indicating RMSF was circulating in the canine population before human cases were detected (*15*,*35*–*37*). Over time, a correlation between canine seroprevalence and RMSF cases and deaths was established (*38*,*39*). A compartment model to understand the dynamics of brown dog tick–associated RMSF was developed and discovered an ≈2-year lag between introduction of the pathogen to a naive canine population and epidemic-level transmission, further solidifying the need for early intervention (*40*).

Communities without veterinary services or animal control agencies might be more likely to have large populations of free-roaming dogs who have not been spayed or neutered or treated with tick preventatives, fostering an ideal environment for brown dog ticks to flourish. Dogs that travel between homes can transport *R. rickettsii*–infected ticks throughout a community, leading to the establishment of the bacterium in the tick population (*37*). Treating dogs with acaricidal products and promoting responsible pet ownership, including safely securing owned dogs on property, are critical activities to reduce tick population (*25*,*41*). Access to programs that provide veterinary care, spay and neuter, and adoption services can have a protective effect against RMSF transmission and should be considered an integral measure to protect human life.

We recommend multiple indicators to assess risk level. The first indicator is the wellness of the animal population, which includes the presence or absence of veterinary services, availability of effective ectoparasite treatments for dogs in the community, the number of spayed or neutered animals, and the cost of effective ectoparasite treatments for dogs in community. The second indicator we recommend is evaluating the free-roaming dog population status, which includes the density of free-roaming dogs, presence or absence of ordinances forbidding free-roaming dogs, fencing or tethering behaviors across the community, and the rate of brown dog tick infestation in dog population. The final indicator is community access to resources, which includes the presence or absence of an animal control department, presence or absence of animal shelter space, and the number of low- or no-cost spay and neuter clinics.

Several challenges are present in animal control and veterinary programs in medium and high-risk communities. Those challenges include a lack of affordable and available veterinary services, low community prioritization of animal wellness, no animal control ordinances or programs, and a limited availability of animal wellness supplies and treatments.

Function 4: Environmental Tick Surveillance and Control

Whereas active surveillance of brown dog ticks and *R. rickettsii* is not feasible in most communities, if adequate vector control services are available, the burden of ticks on dogs and in the peridomestic environment can be loosely monitored. An increase in reports of ticks on dogs or around community homes could indicate increased risk for human infection.

Medium- and high-risk communities can use an integrative approach to prevent ticks by having solid waste removed and having homes treated with a properly applied acaricide in accordance with

product labels. Two high-risk communities in Arizona conduct regularly scheduled pesticide application campaigns, with teams going door-to-door to apply pesticide around the perimeter of homes and estimate tick burden on dogs. Additional measures include treating dogs with acaricidal products and promoting responsible pet ownership because the canine hosts play a large part in the ticks' ecology (*24*,*25*).

We recommend several indicators to assess risk level. The first is harborage, which includes the presence or absence of municipal or community solid waste removal and landfill cost and availability. The second indicator is pesticide use, which includes the presence or absence of vector control programs and the presence or absence of certified pesticide applicators. The final indicator is community knowledge, attitudes, and practices regarding tickborne diseases, which are influenced by the presence or absence of community education around ticks and tickborne diseases.

We have identified multiple challenges in environmental tick surveillance and control. Those challenges include the lack of vector control services specific to ticks, the lack of personnel trained in pesticide safety and application, the lack of solid waste removal, and the need for novel products and technologies for tick control.

Function 5: Finance and Budget

Addressing risk factors for preventing and controlling brown dog tick–associated RMSF requires coordinated, sustained efforts to reduce the free-roaming dog population, increase community awareness, and reduce the number of ticks in the environment. However, because the response requires a multisectoral approach, adequate funding must be distributed across partners, including those not traditionally considered in disease prevention. A key strategy to ensuring the sustainability of prevention activities in medium risk or high-risk communities is to work across sectors to identify short- and long-term funding opportunities, including grant funding.

We recommend 2 key indicators for use in evaluating the financial and budget risk level of communities. The first is the presence or absence of dedicated annual jurisdictional funding to all partners for RMSF prevention. Second is the presence or absence of personnel capable of writing and submitting grant applications.

We have identified 3 challenges to finance and budget security. First is the lack of sustainable funding, especially for tangential but necessary services. Second is the lack of infrastructure to house needed facilities. Last is the lack of financial commitment to ongoing prevention and control when the disease burden of RMSF is low.

Discussion

Emerging infectious diseases, which are pathogens that have newly appeared, reappeared, or are rapidly increasing in incidence or range, are a global threat of high public health importance. More than 60% of emerging human diseases are zoonotic (*42*), affecting humans and animals alike. The effect of vectorborne zoonotic diseases on human health outpaces many other infectious diseases, warranting consideration of new and creative prevention and mitigation strategies (*43*). Whereas we cannot predict the specifics of an individual disease emerging, vectorborne zoonotic diseases such as RMSF will continue to emerge and are likely to expand in range, especially in the light of land-use and climate changes. Understanding the key transmission drivers and mitigation strategies is imperative to identifying high-risk areas of emergence and rapidly responding to protect human and animal health.

Certain factors associated with climate change, including increases in vector range and abundance, increases in wildlife and human interaction because of land use changes, and pathogen host shifting, are especially relevant to emerging vectorborne zoonotic diseases. The effect of climate change related temperature increases on brown dog tick range and density is unclear because the peridomestic tick can be present in high abundance year-round in some parts of the world. However, previous studies suggest the risk for humans being bit and contracting a disease from brown dog ticks may increase with higher temperatures (*44*,*45*). The resistance of this tick species to low humidities, high temperatures, and other environmental conditions that are considered unsuitable for most tick species is remarkable and will likely exacerbate challenges to control brown dog ticks as changes to climates continue (*23*,*45*,*46*).

Brown dog tick–associated RMSF is an emerging public health concern that can be prevented through proper assessment and action. Often it is unclear a community is at risk for endemic RMSF transmission until the first fatal human case occurs; however, there are clear instances when canine cases precede human cases, which demonstrates that preparedness and early detection before human cases are identified may save lives (*39*). The complexities of the RMSF transmission cycle indicate that the pathogen and risk are not likely to disappear any time soon. Maintaining vigilance and implementing integrated pest management strategies,

including routine veterinary care and application of acaricides, in accordance with community risk level is crucial (*25*,*47*). The efforts to reduce tick populations and risk for RMSF transmission are cost- and labor-intensive endeavors that might prove unsustainable, especially in communities where access to resources are already restricted. Therefore, it is necessary to explore additional tools to add to the RMSF prevention toolbox, including novel prevention activities that are both scalable and sustainable, such as canine vaccine candidates against *R. rickettsii* or the brown dog tick itself (*48*). A vaccine might contribute greatly to reducing tick burdens on dogs or reduce the spread of *R. rickettsii* throughout the community.

Because of the interrelatedness of canine and human health regarding brown dog tick–associated RMSF, this complex One Health issue requires a communitywide multidisciplinary approach to reducing risk for disease in human and dog populations. Furthermore, the role of brown dog ticks in RMSF transmission is highly correlated with poverty and other social vulnerabilities, bringing health equity into focus (*4*,*14*,*49*–*51*). Most communities with endemic brown dog tick–associated RMSF are veterinary deserts with little or no access to care in the immediate area, which requires pet owners to travel long distances to seek veterinary care. In addition, many such communities in the United States are also in areas with limited access to medical care because of the rural nature of the environment. Increasing healthcare and veterinary services and accessibility in low-income settings are crucial goals to address health equity issues, including reducing RMSF risk. Until those goals can be realized, medium- and high-risk communities much establish realistic and scalable responses to help reduce RMSF risk on the basis of their resources and infrastructure abilities, such as ensuring human and animal healthcare providers are up to date in recognizing and treating this deadly disease.

Acknowledgments

We thank the Arizona Statewide RMSF Coalition for their efforts and contributions. We also thank the reviewers and editorial staff.

About the author

Dr. Brophy is an epidemiologist with the Centers for Disease Control and Prevention's Rickettsial Zoonoses Branch (National Center for Emerging and Zoonotic Infectious Diseases, Division of Vector-Borne Infectious Diseases). Her primary research interests are vectorborne and zoonotic diseases.

References

1. Centers for Disease Control and Prevention. Severe and fatal confirmed Rocky Mountain spotted fever among people with recent travel to Tecate, Mexico. 2023 [cited 2023 Dec 8]. https://stacks.cdc.gov/view/cdc/136450
2. Centers for Disease Control and Prevention. Rocky Mountain spotted fever in Mexico. [cited 2023 Dec 13]. https://wwwnc.cdc.gov/travel/notices/level1/rmsf-mexico
3. Demma LJ, Traeger MS, Nicholson WL, Paddock CD, Blau DM, Eremeeva ME, et al. Rocky Mountain spotted fever from an unexpected tick vector in Arizona. N Engl J Med. 2005;353:587–94. https://doi.org/10.1056/NEJMoa050043
4. Álvarez-Hernández G, Roldán JFG, Milan NSH, Lash RR, Behravesh CB, Paddock CD. Rocky Mountain spotted fever in Mexico: past, present, and future. Lancet Infect Dis. 2017;17:e189–96. https://doi.org/10.1016/S1473-3099(17)30173-1
5. Bustamante ME, Varela G. Una Nueva Rickettsiosis en Mexico. Rev Inst Salubr Enferm Trop. 1943;4.
6. Bustamante ME, Varela G. Caracteristicas de la Fiebre Manchada de las Montanas Rocosas en Sonora y Sinaloa, Mexico. Rev Inst Salubr Enferm Trop. 1944;5.
7. Parker RR, Philip CB, Jellison WL. Rocky Mountain spotted fever: potentialities of tick transmission in relation to geographic occurrence in the United States. Am J Trop Med. 1933;13:341–79. https://doi.org/10.4269/ajtmh.1933.s1-13.341
8. Newhouse VF, D'Angelo L, Holman RC. DDT use and the incidence of Rocky Mountain spotted fever: a hypothesis. Environ Entomol. 1979;8:777–81. https://doi.org/10.1093/ee/8.5.777
9. Straily A, Drexler N, Cruz-Loustaunau D, Paddock CD, Alvarez-Hernandez G. Notes from the field: community-based prevention of Rocky Mountain spotted fever—Sonora, Mexico, 2016. MMWR Morb Mortal Wkly Rep. 2016;65:1302–3. https://doi.org/10.15585/mmwr.mm6546a6
10. Alvarez-Hernandez G, Murillo-Benitez C, Candia-Plata MC, Moro M. Clinical profile and predictors of fatal Rocky Mountain spotted fever in children from Sonora, Mexico. Pediatr Infect Dis J. 2015;34:125–30. https://doi.org/10.1097/INF.0000000000000496
11. Beristain-Ruiz DM, Garza-Hernández JA, Figueroa-Millán JV, Lira-Amaya JJ, Quezada-Casasola A, Ordoñez-López S, et al. Possible association between selected tickborne pathogen prevalence and *Rhipicephalus sanguineus* sensu lato infestation in dogs from Juarez City (Chihuahua), northwest Mexico–US Border. Pathogens. 2022;11:552. https://doi.org/10.3390/pathogens11050552
12. Drexler NA, Yaglom H, Casal M, Fierro M, Kriner P, Murphy B, et al. Fatal Rocky Mountain spotted fever along the United States–Mexico Border, 2013–2016. Emerg Infect Dis. 2017;23:1621–6. https://doi.org/10.3201/eid2310.170309
13. López-Castillo DC, Vaquera-Aparicio D, González-Soto MA, Martínez-Ramírez R, Rodríguez-Muñoz L, Solórzano-Santos F. Rocky Mountain spotted fever: five years of active surveillance experience in a second-level pediatric hospital in northeastern Mexico [in Spanish]. Bol Med Hosp Infant Mex. 2018;75:303–8.
14. Zazueta OE, Armstrong PA, Márquez-Elguea A, Hernández Milán NS, Peterson AE, Ovalle-Marroquín DF, et al. Rocky Mountain spotted fever in a large metropolitan center, Mexico–United States border, 2009–2019. Emerg Infect Dis. 2021;27:1567–76. https://doi.org/10.3201/eid2706.191662
15. Nicholson WL, Gordon R, Demma LJ. Spotted fever group rickettsial infection in dogs from eastern Arizona: how long

has it been there? Ann N Y Acad Sci. 2006;1078:519–22. https://doi.org/10.1196/annals.1374.102
16. Arizona Department of Health Services. Arizona Rocky Mountain spotted fever handbook. 2020 [cited 2023 Dec 3]. https://www.azdhs.gov/documents/preparedness/epidemiology-disease-control/rocky-mountain-spotted-fever/rmsf-handbook.pdf
17. Moraes-Filho J, Pinter A, Pacheco RC, Gutmann TB, Barbosa SO, Gonzáles MARM, et al. New epidemiological data on Brazilian spotted fever in an endemic area of the state of São Paulo, Brazil. Vector Borne Zoonotic Dis. 2009;9:73–8. https://doi.org/10.1089/vbz.2007.0227
18. Pacheco RC, Moraes-Filho J, Guedes E, Silveira I, Richtzenhain LJ, Leite RC, et al. Rickettsial infections of dogs, horses and ticks in Juiz de Fora, southeastern Brazil, and isolation of *Rickettsia rickettsii* from *Rhipicephalus sanguineus* ticks. Med Vet Entomol. 2011;25:148–55. https://doi.org/10.1111/j.1365-2915.2010.00915.x
19. Martínez-Caballero A, Moreno B, González C, Martínez G, Adames M, Pachar JV, et al. Descriptions of two new cases of Rocky Mountain spotted fever in Panama, and coincident infection with *Rickettsia rickettsii* in *Rhipicephalus sanguineus* s.l. in an urban locality of Panama City, Panama. Epidemiol Infect. 2018;146:875–8. https://doi.org/10.1017/S0950268818000730
20. Argüello AP, Hun L, Rivera P, Taylor L. A fatal urban case of Rocky Mountain spotted fever presenting an eschar in San Jose, Costa Rica. Am J Trop Med Hyg. 2012;87:345–8. https://doi.org/10.4269/ajtmh.2012.12-0153
21. Pacheco-Solano K, Barrantes-González A, Dolz G, Troyo A, Jiménez-Rocha AE, Romero-Zuñiga JJ, et al. Exposure of dogs to *Rickettsia* spp. in Costa Rica: risk factors for PCR-positive ectoparasites and seropositivity. Parasite Epidemiol Control. 2019;7:e00118. https://doi.org/10.1016/j.parepi.2019.e00118
22. Tucker NSG, Weeks ENI, Beati L, Kaufman PE. Prevalence and distribution of pathogen infection and permethrin resistance in tropical and temperate populations of *Rhipicephalus sanguineus* s.l. collected worldwide. Med Vet Entomol. 2021;35:147–57. https://doi.org/10.1111/mve.12479
23. Dantas-Torres F. Biology and ecology of the brown dog tick, *Rhipicephalus sanguineus*. Parasit Vectors. 2010;3:26. https://doi.org/10.1186/1756-3305-3-26
24. Alvarez-Hernandez G, Drexler N, Paddock C, Licona J, Delgado de la Mora J, Straily A, et al. Community-based prevention of epidemic Rocky Mountain spotted fever among minority populations in Sonora, Mexico, using a one health approach. Trans R Soc Trop Med Hyg. 2020;114(4):293–300.
25. Drexler NA, Miller M, Gerding J, Todd S, Adams L, Dahlgren FS, et al. Community-based control of the brown dog tick in a region with high rates of Rocky Mountain spotted fever, 2012–2013. PLoS One. 2014;9:e112368. https://doi.org/10.1371/journal.pone.0112368
26. Drexler NA, Close R, Yaglom HD, Traeger M, Parker K, Venkat H, et al. Morbidity and functional outcomes following Rocky Mountain spotted fever hospitalization––Arizona, 2002–2017. Open Forum Infect Dis. 2022;9:ofac506. https://doi.org/10.1093/ofid/ofac506
27. United States Department of Health and Human Services. Spotted fever rickettsiosis (including Rocky Mountain spotted fever) (sfr, including rmsf) 2020 case definition. 2020 [cited 2023 Dec 4]. https://ndc.services.cdc.gov/case-definitions/spotted-fever-rickettsiosis-2020
28. Regan JJ, Traeger MS, Humpherys D, Mahoney DL, Martinez M, Emerson GL, et al. Risk factors for fatal outcome from Rocky Mountain spotted fever in a highly endemic area—Arizona, 2002–2011. Clin Infect Dis. 2015;60:1659–66. https://doi.org/10.1093/cid/civ116
29. Newell I, Wiskin C, Anthoney J, Meza G, de Wildt G. Preventing malaria in the Peruvian Amazon: a qualitative study in Iquitos, Peru. Malar J. 2018;17:31. https://doi.org/10.1186/s12936-018-2177-9
30. Bardosh KL, Jean L, Beau De Rochars VM, Lemoine JF, Okech B, Ryan SJ, et al. Polisye kont moustik: a culturally competent approach to larval source reduction in the context of lymphatic filariasis and malaria elimination in Haiti. Trop Med Infect Dis. 2017;2:39. https://doi.org/10.3390/tropicalmed2030039
31. Panter-Brick C, Clarke SE, Lomas H, Pinder M, Lindsay SW. Culturally compelling strategies for behaviour change: a social ecology model and case study in malaria prevention. Soc Sci Med. 2006;62:2810–25. https://doi.org/10.1016/j.socscimed.2005.10.009
32. Winch P, Kendall C, Gubler D. Effectiveness of community participation in vector-borne disease control. Health Policy Plan. 1992;7:342–51. https://doi.org/10.1093/heapol/7.4.342
33. Hughes J, Macdonald DW. A review of the interactions between free-roaming domestic dogs and wildlife. Biol Conserv. 2013;157:341–51. https://doi.org/10.1016/j.biocon.2012.07.005
34. Smith LM, Hartmann S, Munteanu AM, Dalla Villa P, Quinnell RJ, Collins LM. The effectiveness of dog population management: a systematic review. Animals (Basel). 2019;9:1020. https://doi.org/10.3390/ani9121020
35. Foley J, Álvarez-Hernández G, Backus LH, Kjemtrup A, Lopéz-Pérez AM, Paddock CD, et al. The emergence of Rocky Mountain spotted fever in the southwestern United States and northern Mexico requires a binational One Health approach. J Am Vet Med Assoc. 2024;262:698–704. https://doi.org/10.2460/javma.23.07.0377
36. Foley J, López-Pérez AM, Rubino F, Backus L, Ferradas C, Barrón-Rodriguez J, et al. Roaming dogs, intense brown dog tick infestation, and emerging rocky mountain spotted fever in Tijuana, México. Am J Trop Med Hyg. 2024;110:779–94. https://doi.org/10.4269/ajtmh.23-0410
37. López-Pérez AM, Orozco L, Zazueta OE, Fierro M, Gomez P, Foley J. An exploratory analysis of demography and movement patterns of dogs: new insights in the ecology of endemic rocky mountain-spotted fever in Mexicali, Mexico. PLoS One. 2020;15:e0233567. https://doi.org/10.1371/journal.pone.0233567
38. Demma LJ, Traeger M, Blau D, Gordon R, Johnson B, Dickson J, et al. Serologic evidence for exposure to *Rickettsia rickettsii* in eastern Arizona and recent emergence of Rocky Mountain spotted fever in this region. Vector Borne Zoonotic Dis. 2006;6:423–9. https://doi.org/10.1089/vbz.2006.6.423
39. McQuiston JH, Guerra MA, Watts MR, Lawaczeck E, Levy C, Nicholson WL, et al. Evidence of exposure to spotted fever group rickettsiae among Arizona dogs outside a previously documented outbreak area. Zoonoses Public Health. 2011;58:85–92. https://doi.org/10.1111/j.1863-2378.2009.01300.x
40. Backus L, Foley P, Foley J. A compartment and metapopulation model of Rocky Mountain spotted fever in southwestern United States and northern Mexico. Infect Dis Model. 2024;9:713–27. https://doi.org/10.1016/j.idm.2024.04.008
41. Dantas-Torres F, Otranto D. Best practices for preventing vector-borne diseases in dogs and humans. Trends Parasitol. 2016;32:43–55. https://doi.org/10.1016/j.pt.2015.09.004

42 Jones KE, Patel NG, Levy MA, Storeygard A, Balk D, Gittleman JL, et al. Global trends in emerging infectious diseases. Nature. 2008;451:990–3. https://doi.org/10.1038/nature06536
43. Swei A, Couper LI, Coffey LL, Kapan D, Bennett S. Patterns, drivers, and challenges of vector-borne disease emergence. Vector Borne Zoonotic Dis. 2020;20:159–70. https://doi.org/10.1089/vbz.2018.2432
44. Backus LH, López Pérez AM, Foley JE. Effect of temperature on host preference in two lineages of the brown dog tick, *Rhipicephalus sanguineus*. Am J Trop Med Hyg. 2021;104:2305–11. https://doi.org/10.4269/ajtmh.20-1376
45. Parola P, Socolovschi C, Jeanjean L, Bitam I, Fournier P-E, Sotto A, et al. Warmer weather linked to tick attack and emergence of severe rickettsioses. PLoS Negl Trop Dis. 2008;2:e338. https://doi.org/10.1371/journal.pntd.0000338
46. Dantas-Torres F. Climate change, biodiversity, ticks and tick-borne diseases: the butterfly effect. Int J Parasitol Parasites Wildl. 2015;4:452–61. https://doi.org/10.1016/j.ijppaw.2015.07.001
47. Alvarez-Hernandez G, Trejo AV, Ratti V, Teglas M, Wallace DI. Modeling of control efforts against *Rhipicephalus sanguineus*, the vector of Rocky Mountain spotted fever in Sonora Mexico. Insects. 2022;13:263. https://doi.org/10.3390/insects13030263
48. Walker DH, Blanton LS, Laroche M, Fang R, Narra HP. A vaccine for canine Rocky Mountain spotted fever: an unmet one health need. Vaccines (Basel). 2022;10:1626. https://doi.org/10.3390/vaccines10101626
49. Alvarez-Hernandez G, Rosales C, Sepulveda R. Rocky Mountain spotted fever, a reemerging disease in Arizona and Sonora—case study. J Case Rep Stud. 2014;2(3):301.
50. Foley J, Tinoco-Gracia L, Rodriguez-Lomelí M, Estrada-Guzmán J, Fierro M, Mattar-Lopez E, et al. Unbiased assessment of abundance of *Rhipicephalus sanguineus* sensu lato ticks, canine exposure to spotted fever group *Rickettsia*, and risk factors in Mexicali, México. Am J Trop Med Hyg. 2019;101:22–32. https://doi.org/10.4269/ajtmh.18-0878
51. Tinoco-Gracia L, Quiroz-Romero H, Quintero-Martínez MT, Rentería-Evangelista TB, González-Medina Y, Barreras-Serrano A, et al. Prevalence of *Rhipicephalus sanguineus* ticks on dogs in a region on the Mexico–USA border. Vet Rec. 2009;164:59–61. https://doi.org/10.1136/vr.164.2.59

Address for correspondence: Maureen Brophy, Centers for Disease Control and Prevention, 1600 Clifton Rd NE, Mailstop H24-12, Atlanta, GA 30329-4018, USA; email: qvw8@cdc.gov

etymologia revisited

Nipah Virus

[ne´-pə vī´-rəs]

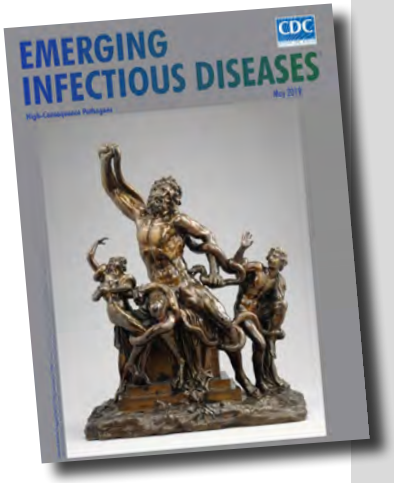

Originally published in May 2019

In 1994, a newly described virus, initially called equine morbillivirus, killed 13 horses and a trainer in Hendra, a suburb of Brisbane, Australia. The reservoir was subsequently identified as flying foxes, bats of the genus *Pteropus* (Greek pteron ["wing"] + *pous* ["foot"]). In 1999, scientists investigated reports of febrile encephalitis and respiratory illness among workers exposed to pigs in Malaysia and Singapore. (The pigs were believed to have consumed partially eaten fruit discarded by bats.)

The causative agent was determined to be closely related to Hendra virus and was later named for the Malaysian village of Kampung Sungai Nipah. The 2 viruses were combined into the genus *Henipavirus*, in the family *Paramyxoviridae*. Three additional species of *Henipavirus*—Cedar virus, Ghanaian bat virus, and Mojiang virus—have since been described, but none is known to cause human disease. Outbreaks of Nipah virus occur almost annually in India and Bangladesh, but *Pteropus* bats can be found throughout the tropics and subtropics, and henipaviruses have been isolated from them in Central and South America, Asia, Oceania, and East Africa.

References:

1. Centers for Disease Control and Prevention. Outbreak of Hendra-like virus—Malaysia and Singapore, 1998–1999. MMWR Morb Mortal Wkly Rep. 1999;48:265–9.
2. Selvey LA, Wells RM, McCormack JG, Ansford AJ, Murray K, Rogers RJ, et al. Infection of humans and horses by a newly described morbillivirus. Med J Aust. 1995;162:642–5.

https://wwwnc.cdc.gov/eid/article/25/5/et-2505_article

Reemergence of Oropouche Virus in the Americas and Risk for Spread in the United States and Its Territories, 2024

Sarah Anne J. Guagliardo, C. Roxanne Connelly, Shelby Lyons, Stacey W. Martin, Rebekah Sutter, Holly R. Hughes, Aaron C. Brault, Amy J. Lambert, Carolyn V. Gould, J. Erin Staples

Oropouche virus has recently caused outbreaks in South America and the Caribbean, expanding into areas to which the virus was previously not endemic. This geographic range expansion, in conjunction with the identification of vertical transmission and reports of deaths, has raised concerns about the broader threat this virus represents to the Americas. We review information on Oropouche virus, factors influencing its spread, transmission risk in the United States, and current status of public health response tools. On the basis of available data, the risk for sustained local transmission in the continental United States is considered low because of differences in vector ecology and in human–vector interactions when compared with Oropouche virus–endemic areas. However, more information is needed about the drivers for the current outbreak to clarify the risk for further expansion of this virus. Timely detection and control of this emerging pathogen should be prioritized to mitigate disease burden and stop its spread.

Oropouche virus (genus *Orthobunyavirus*, Simbu serogroup) has recently been identified as a reemerging cause of widespread disease throughout the Americas (*1*). First discovered in Trinidad and Tobago in 1955, the virus caused periodic outbreaks of acute febrile illness in a limited number of countries in South and Central America for decades (*2*). Starting in late 2023, outbreaks of Oropouche virus disease were reported in areas with known endemic disease, and the virus emerged in new areas where it had not been historically documented. During January 1–September 6, 2024, more than 9,000 confirmed Oropouche virus disease cases and 2 deaths were reported from 6 countries: Bolivia, Brazil, Colombia, Cuba, the Dominican Republic, and Peru (*1*). In addition, several travel-associated cases have been reported among persons in the United States, Canada, and Europe traveling back from Cuba and Brazil (*1*,*3*,*4*). The recent expansion of the virus into previously nonendemic areas, identification of vertical transmission, and first reports of death from Oropouche virus disease have raised concerns about the broader threat this virus represents to the Americas, including the United States (*1*).

Oropouche virus circulates in both a sylvatic and an urban cycle. Sylvatic transmission, although not well understood, suggests a wide range of possible mammalian and avian hosts; virus has been detected in sloths (*Bradypus tridactylus*) and in several species of nonhuman primates, and antibodies have been found in domestic and wild birds and a rodent (*5*–*7*). Vectors hypothesized to be involved in sylvatic transmission include *Aedes serratus* and *Coquillettidia venezuelensis* mosquitoes (*2*,*8*). Humans develop sufficient viremia to contribute to viral spread, serving as bridge hosts that introduce Oropouche virus from its sylvatic maintenance cycle to populated areas. Once in the urban cycle, the virus circulates between humans and biting midges, *Culicoides paraensis* (*9*,*10*). The ubiquitous southern house mosquito, *Culex quinquefasciatus*, has also been suggested to play a role in urban transmission, although vector competency evaluations have shown mixed results (*11*–*13*) (Table; Figure 1).

Epidemiology and Clinical Manifestations

Outbreaks of Oropouche virus have affected both urban and rural areas, and attack rates can be high; ≈30% of the population can be infected (*17*). Sex-specific

Author affiliation: Centers for Disease Control and Prevention, Fort Collins, Colorado, USA

DOI: https://doi.org/10.3201/eid3011.241220

Table. Possible vectors of Oropouche virus found in the United States and summary of laboratory and field data

Species	Laboratory evidence	Field data
Culicoides paraensis biting midge	Experimental infection from human to hamster through *Cu. paraensis* biting midge (*9*); efficient vector in laboratory studies (*9*)	Viral isolation from field collections during outbreaks in Para state, Brazil, 1978 (*14*); abundance correlated with higher seroprevalence in Para state, Brazil, 1975 (*10*)
Culex quinquefasciatus mosquito	Experimental infection from hamster to hamster via *Cx. quinquefasciatus* mosquito (*12*); found to be inefficient vector (possibly due to midgut barrier) in 1 study (*13*) but was found to have a low level of efficiency in other studies (*15*)	Viral Isolation from field collections in Para state, Brazil, 1961 and 1968 (*10*)
Culicoides sonorensis biting midge‡	Efficient vector in laboratory studies (*15*,*16*)	No viral isolations from field

attack rates have been inconsistent; some outbreaks disproportionately affect female persons and others affect more male persons (*17*,*18*). Some studies have shown that younger persons are more likely to be infected, possibly because of lack of previous exposure and immunity to the virus (*17*). A recent analysis of >5,000 confirmed cases identified in January 2015–March 2024 in Brazil showed approximately equal proportions of confirmed cases among male and female persons, and most reported infections occurred in persons 20–49 years of age (*19*). Those data suggest that persons with different demographic traits can be infected with Oropouche virus and that infection is driven by exposures, which might vary by sex, age, and daily activity (*18*).

The incubation period for Oropouche virus disease ranges from 3 to 10 days, and ≈60% of infected persons experience symptoms (*8*,*20*,*21*). Symptoms are similar to those of other vectorborne diseases, such as dengue, Zika, and chikungunya, and include acute onset of fever and severe headache, often with chills, myalgia, arthralgia, and fatigue. Other signs and symptoms can include photophobia, dizziness, retroorbital pain, nausea, vomiting, diarrhea, abdominal pain, conjunctival injection, and maculopapular rash (*17*,*22*,*23*). After the initial illness, up to 70% of persons can report relapse of symptoms, typically within a few days to weeks (*6*). Secondary episodes are clinically similar to the primary episode. No vaccines to prevent or medicines to treat Oropouche virus disease exist.

Although Oropouche virus disease is typically mild and reported deaths are rare, a small proportion of persons can develop more severe disease with hemorrhagic signs and symptoms (e.g., gingival bleeding, melena, and menorrhagia) or neurologic symptoms consistent with meningitis, meningoencephalitis, or Guillain-Barré syndrome (*1*,*21*,*23*,*24*). Of the 2 recent deaths associated with Oropouche virus among previously healthy young adult women, at least 1 patient had signs of hemorrhage (nasal, gingival, and vaginal bleeding and petechiae) starting 4 days after initial symptom onset (*1*). Neurologic symptoms have been reported in up to 4% of persons seeking clinical care (*25*). Signs and symptoms of neurologic disease can include occipital pain, dizziness, limb weakness, paresthesia, confusion, lethargy, photophobia, nausea, vomiting, nuchal rigidity, nystagmus, and paralysis (*17*,*24*,*25*).

In June 2024, vertical transmission of Oropouche virus was identified when RNA was detected in a stillborn infant born to a pregnant woman who had symptoms of Oropouche virus disease at 30 weeks' gestation (*1*). After this identification, a retrospective investigation identified 4 infants with microcephaly in whom Oropouche virus IgM was detected in serum samples or cerebrospinal fluid (CSF) samples collected shortly after birth (*26*). In August 2024, an additional infant with microcephaly associated with Oropouche virus infection was reported. The infant,

Figure 1. Possible biting midge and mosquito vectors of Oropouche virus found in United States in study of reemergence of Oropouche virus in the Americas, 2024. Possible vectors are presented in order of evidence for involvement in Oropouche virus transmission. A) *Culicoides paraensis* biting midge. Photo credit: "NACER355-12 Lateral"—BOLD:ABX5601 (compare *Culicoides paraensis*). Licensed under Creative Commons Attribution 4.0 International (https://creativecommons.org/licenses/by/4.0). B) *Culex quinquefasciatus* mosquito. Photo credit: Centers for Disease Control and Prevention Public Health Image Library. C) *Culicoides sonorensis* biting midge. Photo credit: Dominic Rose.

born in June 2024, tested positive for Oropouche virus IgM on the second day of life in serum and CSF. The infant later died at 47 days of life, and multiple tissues tested positive for Oropouche viral RNA (*26*). Further investigation is required to determine the frequency of vertical transmission and whether the timing of Oropouche virus disease during pregnancy increases the risk for an adverse outcome.

Testing

Testing for evidence of recent Oropouche virus infection can be performed on several different specimen types, though serum and CSF are used most often (*27*). During the first 7 days after infection, viral RNA can be detected through molecular testing such as reverse transcription PCR (RT-PCR). Most assays target the small (S) segment of the genome and cannot differentiate between Oropouche virus and other reassortant viruses (e.g., Iquitos virus) (*27*,*28*). After the first week of infection, antibody testing (e.g., IgM ELISA or plaque reduction neutralization test) is typically performed (*29*).

Viral RNA can be detected in the CSF of patients with neuroinvasive disease; however, it may not be present in the CSF at the time of clinical manifestation (because the virus is often cleared by that time), so serologic testing should be performed (*25*). Serologic testing is recommended for anyone experiencing a relapse of the disease because viral replication has not been detected during recurrence (*8*). Finally, in the event of fetal or infant death, postmortem tissues can be tested for evidence of antigen or viral RNA to assess causality (*1*).

Factors Affecting Risk for Spread

The current outbreak in Latin America could be the result of lack of population-level immunity and viral reemergence in endemic areas, but other factors are possibly contributing to the spread and higher case counts. For example, changes to the viral genome through reassortment or vector distribution and competence might have resulted in more efficient transmission. Increased contact between humans and vectors caused by land use changes also could be contributing, because transmission activity has previously been detected in areas affected by deforestation (*2*). Finally, poor case recognition in the context of a large dengue outbreak could have furthered unchecked spread (i.e., because of lack of public health action when authorities are unaware of ongoing transmission).

Oropouche virus, like other orthobunyaviruses, is susceptible to reassortment, owing to its tripartite RNA genome, which includes the S segment encoding the nucleocapsid, medium (M) segment encoding the glycoproteins, and large (L) segment encoding L protein, which has RNA-directed RNA polymerase functions (*30*,*31*). The strain causing the current outbreak has shown some evidence of successive reassortment with genetically similar viruses (e.g., Perdões virus, Iquitos virus). Although the manner in which this strain might have influenced vector competence, disease severity, virus transmissibility, and immune protective status is not clear, preliminary research suggests reduced cross-neutralization with prototype strains in vitro (*32*). Reassortment has been observed with other orthobunyaviruses in the Americas (e.g., Fort Sherman virus, Potosi virus) and experimentally between Oropouche virus and orthobunyaviruses in the Simbu serogroup from outside the Americas (*30*,*31*,*33*).

Limited data exist regarding the specific vectors associated with recent urban outbreaks, although viral RNA has historically been detected in biting midges, including *Cu. paraensis*, and in *Cx. quinquefasciatus* mosquitoes (*10*,*14*). *Cu. paraensis* midges are found throughout the tropics, subtropics, and temperate areas in the Americas in wetland, forest, agricultural, rural, and periurban areas. In addition, *Cx. quinquefasciatus* mosquitoes are relatively ubiquitous, having a broad distribution in the northern and southern hemispheres. Temporally, outbreaks in Latin America have mostly coincided with the rainy season, during which biting midge and mosquito populations are typically more abundant (*17*,*34*).

Currently, large dengue outbreaks are occurring throughout the world; the Americas have reported unprecedented numbers of cases totaling >11 million since late 2023 (*35*). Because Oropouche virus disease and dengue have similar symptomology, they are difficult to distinguish clinically, and dengue testing is usually conducted before Oropouche virus testing is considered (*29*). This factor, combined with limited Oropouche testing availability, could have led to an underrecognition of increasing disease burden, which in turn might have led to a further expansion of outbreak and spread of the virus through infected persons into new areas.

Risk for Sustained Local Transmission of Oropouche Virus in the United States

As of September 2024, local transmission of Oropouche virus had not been reported in the United States, although some cases have been reported in travelers (*4*; https://www.cdc.gov/oropouche/data-maps.) Various factors are likely to affect the risk for local spread of the virus, including the rate of introduction from travel-associated cases, the presence

and distribution of the vectors and potential host reservoirs, and potential virus adaptation.

Recent experiences with the introduction of chikungunya and Zika viruses to the United States could foretell what might occur with Oropouche virus, because all 3 arboviruses are maintained in an urban cycle between humans and arthropod vectors. During the chikungunya outbreak in 2014–2015, ≈3,700 travel-associated cases were reported in the continental United States. Despite thousands of possible introductions of viremic travelers, only 13 locally transmitted cases were identified in very limited areas of Florida and Texas (*36*). During the Zika virus outbreak in 2016–2017, US jurisdictions reported 5,389 travel-associated cases, resulting in 231 locally acquired cases, which also occurred in limited areas of Florida and Texas (*37*). Sustained local transmission of chikungunya and Zika was successfully thwarted by vector control and other public health interventions. Those experiences suggest that, even with frequent virus introductions through infected persons into the continental United States, large urban outbreaks of Oropouche are unlikely. For US territories, 4,900 locally acquired chikungunya cases were reported during 2014–2015 and 37,052 locally acquired cases of Zika virus were reported during 2016–2017 (*36*,*37*). Most of those cases were reported from Puerto Rico. On the basis of available data, the risk for sustained local transmission in the continental United States is likely low, whereas the risk for sustained transmission in Puerto Rico and the US Virgin Islands is unknown.

Most travel-associated Oropouche cases detected in Europe and the United States have been in travelers from Cuba (*3*,*4*). Cuba is in midst of its peak rainy season, which is associated with increased vector abundance (*17*,*34*), suggesting that more travel-associated cases might be expected from there. Previous research has not reported the primary vector of *Cu. paraensis* biting midges in Cuba, although *Cx. quinquefasciatus* mosquitoes and several biting midges of the *Ceratopogonidae* family have been detected there, including *Cu. furens* biting midges, which are also present in Florida (*38*). Vector competency evaluations have not been completed for many of those species, and a better understanding of transmission ecology in the Cuba outbreak and in the Dominican Republic will help to assess risk to the United States and, in particular, Puerto Rico.

Both chikungunya and Zika viruses in the United States are transmitted by *Aedes (Stegomyia)* mosquitoes, which oviposit and develop in containers in and around homes, making persons more susceptible to mosquito exposure and, ultimately, infection. In contrast, the primary Oropouche vector, the *Cu. paraensis* biting midge, has low abundance in North America and mostly resides in tree holes in the southeast and midwestern United States (*39*–*41*) (Figure 2). In addition, the *Cu. sonorensis* biting midge is an another possible Oropouche vector, according to laboratory competency evaluations (*15*,*16*). Located mainly west of the Mississippi, this biting midge would be unlikely to perpetuate local Oropouche virus transmission in humans, because it is found in rural areas around livestock operations (*15*,*42*). Overall, taken together, the spatial distribution of biting midges in rural areas and poor vector competence in laboratory studies of mosquitoes translate to reduced risk for urban transmission in the United States, if *Cu. paraensis* biting midges are indeed the primary vector in ongoing Oropouche outbreaks.

Figure 2. Distribution of biting midge and mosquito vectors in the United States and select territories based on field observations and modelling in study of reemergence of Oropouche virus in the Americas, 2024. Possible vectors are presented in order of evidence for involvement in Oropouche virus transmission. A) *Culicoides paraensis* biting midge; B) *Culex quinquefasciatus* mosquito; C) *Culicoides sonorensis* biting midge. Presence of vectors in a jurisdiction does not imply uniform distribution throughout an entire geographic area. A zone exists where *Cx. quinquefasciatus* mosquitoes hybridize with other *Culex* species; this zone is not accounted for in the map because no vector competence studies for Oropouche virus for those species have been conducted. USVI, US Virgin Islands.

Finally, despite its extreme abundance and enormous geographic range, the *Cx. quinquefasciatus* mosquito is not a very competent vector in laboratory studies and is the target of extensive West Nile virus vector control efforts (*15*,*43*,*44*). Existing control programs could therefore be adapted to the Oropouche context. On the other hand, *Cx. quinquefasciatus* mosquitoes have demonstrated widespread resistance to pyrethroids (particularly in parts of Florida), which could blunt the efficacy of vector control efforts. *Cx. quinquefasciatus* mosquitoes could represent a more serious threat to increase the risk for local transmission if it proves to be a competent vector. Of note, many mosquito (and *Culicoides* midge) species in the United States, which feed primarily on humans, have not been tested for vector competence of Oropouche virus.

Sylvatic transmission of Zika and chikungunya viruses has only been documented in Africa and relies on mosquitoes and nonhuman primates, whereas Oropouche virus maintenance in sylvatic settings can rely on wide array of species, on the basis of viral isolation and detection of antibodies in many different species (*6*). Oropouche virus has not been isolated or detected in birds, but Oropouche virus antibodies have been identified in ≥11 different families of wild and domestic birds in Brazil, raising questions about their role in transmission (5,*14*). Should the virus infect wild bird populations in North America, it is possible that Oropouche virus could become endemic, similar to the progression for West Nile virus. Oropouche virus's propensity for reassortment could affect its ability to infect new hosts, enhance vector competence, and evade host immune response (*45*). However, the probability of sustained local transmission at this time is thought to be low in the continental United States because Oropouche virus would be required to overcome a series of biologic and ecologic obstacles.

Preparedness for and Response to Oropouche Virus in the United States

In the past 25 years, the United States has experienced and responded to 4 different emergent mosquitoborne viral diseases, caused by West Nile, chikungunya, Zika, and dengue viruses. Given those experiences, preparation for potential Oropouche virus introductions into the United States could rely on several existing tools and interventions, including the current public health surveillance systems, case identification, vector control, personal protection, and public health communication.

ArboNET, the US national arboviral surveillance system, was established in 2000 in response to West Nile virus and can be adapted to capture data about new emerging and reemerging arboviruses (https://www.cdc.gov/oropouche/data-maps/current-year-data.html). ArboNET enables reporting of human disease cases, human infections (e.g., presumptive viremic donors), animal disease, sentinel animal infections, and vector infections. Human disease cases are reported from state and territorial health departments using standard case definitions. Case reports can include information on travel location, clinical manifestations, and transmission mechanisms (*46*).

Oropouche virus disease is not a nationally notifiable condition, but state and territorial health departments can voluntarily report identified cases to ArboNET. In addition, if Oropouche virus emerges in the United States, the Council of State and Territorial Epidemiologists can decide whether to make Oropouche virus disease nationally notifiable and determine whether a new case definition should be developed to capture potential fetal deaths or congenital infections, as was done for Zika virus previously (*47*).

Clinicians should report suspected Oropouche virus disease cases to state or local health departments to enable testing and to implement community prevention measures and messaging. Information about clinical features, diagnosis, and clinical management is available on the Centers for Disease Control and Prevention (CDC) website (https://www.cdc.gov/oropouche/hcp/clinical-overview). At this time, testing for Oropouche virus should be considered when a patient has traveled within 2 weeks of initial symptom onset (because patients can experience recurrent symptoms) to an area with documented or suspected Oropouche virus circulation and has an abrupt onset of fever, headache, and ≥1 of the following signs/symptoms: myalgia, arthralgia, photophobia, retroorbital/eye pain, or indications of neuroinvasive disease (e.g., stiff neck, altered mental status, seizures, limb weakness, or cerebrospinal fluid pleocytosis). If concern exists for local transmission in a nonendemic area, providers should consider whether the patient had contact with a person with confirmed Oropouche virus infection, lives in an area where travel-related cases have been identified, or has known vector exposure (e.g., mosquitoes or biting midges). In addition, testing should only be considered among patients who tested negative for other pathogens, in particular dengue. If strong suspicion of Oropouche virus disease exists on the basis of the patient's clinical features and history of travel to an area with virus circulation, providers should not wait on negative test results before sending specimens to CDC. This

guidance on clinical case identification will likely need to be modified as the epidemiologic situation evolves, including whether local transmission is identified, and as more is learned about clinical manifestations and transmission risk, including for vertical transmission and potential adverse birth outcomes.

Available vector control tools, such as insecticide spraying and source reduction (modification of larval habitats to prevent oviposition), are similar for biting midges and mosquitoes, but questions remain about the application of such tools in the context of Oropouche. Empirical evaluations of *Cu. paraensis* midge–specific control measures are lacking. Previous works have shown aerial spraying of the insecticide naled has resulted in substantial reduction (up to 99%) in pestiferous *Culicoides* species (*48*). Source reduction around dairy operations for *Cu. sonorensis* midges and removal of leaf waste for *Cu. paraensis* midges have also been used, with varying degrees of success (*49*). *Cx. quinquefasciatus* mosquitoes are abundant and widely distributed; therefore, control activities should be determined on the basis of mosquito surveillance data to more efficiently target when and where this species is active. A combination of larviciding and adulticiding will be most useful, given the asynchronous hatching of this mosquito's egg rafts. Challenges in implementing vector control include the limited scope of vector control agencies that primarily target mosquitoes and are not mandated to manage other arthropods, lack of acceptability of aerial spraying of insecticides, insecticide resistance, and limited utility of larval source reduction because of the cryptic nature of some larval habitats (i.e., tree holes for *Cu. paraensis* midges) (*39*).

Persons can protect themselves against both midge and mosquito bites by wearing long sleeves and pants and by using an insect repellant registered by the US Environmental Protection Agency. Those products are safe for pregnant and breastfeeding women when used as directed; for children <3 years of age, products containing oil of lemon eucalyptus or para-menthane-diol should not be used. Windows and door screens can also prevent mosquitoes from entering the home and protect against vectorborne diseases (*50*). However, *Culicoides* spp. midges are smaller than typical window screen holes and can pass through and enter the home. Mesh size 20 (or 20 × 20 mesh, which has 20 openings in 1 linear inch) is designed to exclude biting midges. Patients with suspected Oropouche virus disease should avoid being bitten by biting midges and mosquitoes for 1 week to prevent infection of naive vectors.

Strong engagement with the community is necessary to gain support for vector control activities, as well as to improve the uptake of personal protective measures, which are currently the only ways to prevent infection. Rapidly distributing information to public health professionals, providers, the public, and other stakeholders can lead to improved surveillance, diagnosis, and implementation of prevention strategies. The use of various platforms for distribution of communications (e.g., CDC website, Health Alert Network messages, social media posts, publications, and data dashboards) can improve the reach and distribution of messages about Oropouche virus and ways persons can prevent themselves from being infected and spreading the virus.

Summary

Overall, on the basis of current knowledge, the risk for localized outbreaks of Oropouche virus disease in most areas in the United States should be considered low because of differences in vectors and human-vector interactions (e.g., mitigation by widespread availability of closeable windows and air-conditioning) compared with endemic areas. Some states and territories are probably at elevated risk for local spread, including those where infected travelers are most likely to arrive and be readily exposed to vectors, such as southern Florida or Puerto Rico. Past experiences with several emerging and reemerging vectorborne diseases, as well as new information from Oropouche outbreaks (e.g., transmission ecology in Cuba), will help to inform and refine preparedness, detection, and response to Oropouche virus. Public health partners should prioritize timely detection and control of this emerging pathogen to prevent human disease cases and the spread of the virus.

Acknowledgments

We thank Roberto Barrera and Saul Lozano for their assistance with understanding geographic distribution of vectors.

About the Author

Dr. Guagliardo is an epidemiologist with the Division of Vector-Borne Diseases, National Center for Emerging and Zoonotic Infectious Diseases, Centers for Disease Control and Prevention in Fort Collins, Colorado. She has a longstanding interest in the epidemiology and ecology of vectorborne and zoonotic diseases.

References

1. Pan American Health Organization/World Health Organization. Epidemiological alerts and updates. [cited 2024 Sep 23]. https://www.paho.org/en/epidemiological-alerts-and-updates
2. Anderson CR, Spence L, Downs WG, Aitken TH. Oropouche virus: a new human disease agent from Trinidad, West Indies. Am J Trop Med Hyg. 1961;10:574–8. https://doi.org/10.4269/ajtmh.1961.10.574
3. European Centers for Disease Prevention and Control. Threat assessment brief: Oropouche virus disease cases imported into the European Union, 9 August 2024 [cited 2024 Sep 23]. https://www.ecdc.europa.eu/sites/default/files/documents/TAB-Oropouche-august-2024.pdf
4. Morrison A, White JL, Hughes HR, Guagliardo SAJ, Velez JO, Fitzpatrick KA, et al. Oropouche virus disease among U.S. travelers—United States, 2024. MMWR Morb Mortal Wkly Rep. 2024;73:769–73. PubMed https://doi.org/10.15585/mmwr.mm7335e1
5. Pinheiro FP, Travassos da Rosa AP, Travassos da Rosa JF, Bensabath G. An outbreak of Oropouche virus diease in the vicinity of santarem, para, barzil. Tropenmed Parasitol. 1976;27:213–23.
6. Azevedo RS, Nunes MR, Chiang JO, Bensabath G, Vasconcelos HB, Pinto AY, et al. Reemergence of Oropouche fever, northern Brazil. Emerg Infect Dis. 2007;13:912–5. https://doi.org/10.3201/eid1306.061114
7. Nunes MR, Martins LC, Rodrigues SG, Chiang JO, Azevedo RS, da Rosa AP, et al. Oropouche virus isolation, southeast Brazil. Emerg Infect Dis. 2005;11:1610–3. https://doi.org/10.3201/eid1110.050464
8. Pinheiro FP, Travassos da Rosa AP, Travassos da Rosa JF, Ishak R, Freitas RB, Gomes ML, et al. Oropouche virus. I. A review of clinical, epidemiological, and ecological findings. Am J Trop Med Hyg. 1981;30:149–60. PubMed https://doi.org/10.4269/ajtmh.1981.30.149
9. Pinheiro FP, Travassos da Rosa AP, Gomes ML, LeDuc JW, Hoch AL. Transmission of Oropouche virus from man to hamster by the midge *Culicoides paraensis*. Science. 1982;215:1251–3. https://doi.org/10.1126/science.6800036
10. Roberts DR, Hoch AL, Dixon KE, Llewellyn CH. Oropouche virus. III. Entomological observations from three epidemics in Pará, Brazil, 1975. Am J Trop Med Hyg. 1981;30:165–71. https://doi.org/10.4269/ajtmh.1981.30.165
11. Cardoso BF, Serra OP, Heinen LB, Zuchi N, Souza VC, Naveca FG, et al. Detection of Oropouche virus segment S in patients and in *Culex quinquefasciatus* in the state of Mato Grosso, Brazil. Mem Inst Oswaldo Cruz. 2015;110:745–54. https://doi.org/10.1590/0074-02760150123
12. Hoch AL, Pinheiro FP, Roberts DR, Gomes ML. Laboratory transmission of Oropouche virus by *Culex quinquefasciatus* Say. Bull Pan Am Health Organ. 1987;21:55–61.
13. de Mendonça SF, Rocha MN, Ferreira FV, Leite THJF, Amadou SCG, Sucupira PHF, et al. Evaluation of *Aedes aegypti*, *Aedes albopictus*, and *Culex quinquefasciatus* mosquitoes competence to Oropouche virus infection. Viruses. 2021;13:755. https://doi.org/10.3390/v13050755
14. LeDuc JW, Hoch AL, Pinheiro FP, da Rosa AP. Epidemic Oropouche virus disease in northern Brazil. Bull Pan Am Health Organ. 1981;15:97–103.
15. McGregor BL, Connelly CR, Kenney JL. Infection, dissemination, and transmission potential of North American *Culex quinquefasciatus*, *Culex tarsalis*, and *Culicoides sonorensis* for Oropouche virus. Viruses. 2021;13:226. https://doi.org/10.3390/v13020226
16. McGregor BL, Shults PT, McDermott EG. A review of the vector status of North American *Culicoides* (Diptera: Ceratopogonidae) for bluetongue virus, epizootic hemorrhagic disease virus, and other arboviruses of concern. Curr Trop Med Rep. 2022;9:130–9. https://doi.org/10.1007/s40475-022-00263-8
17. Pinheiro FP, Travassos da Rosa APA, Vasconcelos PF. Oropouche fever. In: Feigin RD, Demmler GJ, Cherry, JD, Kaplan SL, editors. Textbook of pediatric infectious diseases. Philadelphia: Elsevier; 2004. p. 2418–23.
18. Baisley KJ, Watts DM, Munstermann LE, Wilson ML. Epidemiology of endemic Oropouche virus transmission in upper Amazonian Peru. Am J Trop Med Hyg. 1998;59:710–6. https://doi.org/10.4269/ajtmh.1998.59.710
19. Martins-Filho PR, Carvalho TA, Dos Santos CA. Spatiotemporal epidemiology of Oropouche fever, Brazil, 2015–2024. Emerg Infect Dis. 2024;30:2196–8. https://doi.org/10.3201/eid3010.241088
20. Freitas RB, Pinheiro FP, Santos MAV, Travassos da Rodsa APA, Travassos da Rosa JFS, Nazareno de Freitas E. Oropouche virus epidemic in the eastern state of Para, 1979 [in Portuguese]. Rev Fundacao Servicos Saude Publica. 1980;25:59–72.
21. Vernal S, Martini CCR, da Fonseca BAL. Oropouche virus–associated aseptic meningoencephalitis, southeastern Brazil. Emerg Infect Dis. 2019;25:380–2. https://doi.org/10.3201/eid2502.181189
22. Vasconcelos PF, Travassos Da Rosa JF, Guerreiro SC, Dégallier N, Travassos Da Rosa ES, Travassos Da Rosa AP. 1st register of an epidemic caused by Oropouche virus in the states of Maranhão and Goiás, Brazil [in Portuguese]. Rev Inst Med Trop São Paulo. 1989;31:271–8. https://doi.org/10.1590/S0036-46651989000400011
23. Mourão MP, Bastos MS, Gimaqu JB, Mota BR, Souza GS, Grimmer GH, et al. Oropouche fever outbreak, Manaus, Brazil, 2007–2008. Emerg Infect Dis. 2009;15:2063–4. https://doi.org/10.3201/eid1512.090917
24. de Armas Fernández JR, Peña García CE, Acosta Herrera B, Betancourt Plaza I, Gutiérrez de la Cruz Y, Resik Aguirre S, et al. Report of an unusual

association of Oropouche Fever with Guillain-Barré syndrome in Cuba, 2024. Eur J Clin Microbiol Infect Dis. 2024 Sep 14 [Epub ahead of print]. https://doi.org/10.1007/s10096-024-04941-5
25. Pinheiro FP, Rocha AG, Freitas RB, Ohana BA, Travassos da Rosa AP, Rogério JS, et al. Meningitis associated with Oropouche virus infections [in Portuguese]. Rev Inst Med Trop Sao Paulo. 1982;24:246–51.
26. Ministry of Health Brazil, Secretariat of Health and Environment Surveillance. Joint technical note no. 135/2024-SVSA/SAPS/SAES/MS [in Portuguese] [cited 2024 Aug 14]. https://www.gov.br/saude/pt-br/centrais-de-conteudo/publicacoes/notas-tecnicas/2024/nota-tecnica-conjunta-no-135-2024-svsa-saps-saes-ms
27. Moreli ML, Aquino VH, Cruz AC, Figueiredo LT. Diagnosis of Oropouche virus infection by RT-nested-PCR. J Med Virol. 2002;66:139–42. https://doi.org/10.1002/jmv.2122
28. Naveca FG, Nascimento VAD, Souza VC, Nunes BTD, Rodrigues DSG, Vasconcelos PFDC. Multiplexed reverse transcription real-time polymerase chain reaction for simultaneous detection of Mayaro, Oropouche, and Oropouche-like viruses. Mem Inst Oswaldo Cruz. 2017;112:510–3. https://doi.org/10.1590/0074-02760160062
29. Pan American Health Organization/World Health Organization. Guidelines for the detection and surveillance of emerging arboviruses in the context of the circulation of other arboviruses [cited 2024 Sep 23]. https://www.paho.org/en/documents/guidelines-detection-and-surveillance-emerging-arboviruses-context-circulation-other
30. Briese T, Calisher CH, Higgs S. Viruses of the family Bunyaviridae: are all available isolates reassortants? Virology. 2013;446:207–16. https://doi.org/10.1016/j.virol.2013.07.030
31. Tilston-Lunel NL, Shi X, Elliott RM, Acrani GO. The potential for reassortment between Oropouche and Schmallenberg orthobunyaviruses. Viruses. 2017;9:220. https://doi.org/10.3390/v9080220
32. Naveca FG, de Almeida TAP, Souza V, Nascimento V, Silva D, Nascimento F, et al. Human outbreaks of a novel reassortant Oropouche virus in the Brazilian Amazon region. Nat Med. 2024; Epub ahead of print. https://doi.org/10.1038/s41591-024-03300-3
33. Briese T, Kapoor V, Lipkin WI. Natural M-segment reassortment in Potosi and Main Drain viruses: implications for the evolution of orthobunyaviruses. Arch Virol. 2007;152:2237–47. https://doi.org/10.1007/s00705-007-1069-z
34. Feitoza LHM, de Carvalho LPC, da Silva LR, Meireles ACA, Rios FGF, Silva GS, et al. Influence of meteorological and seasonal parameters on the activity of *Culicoides paraensis* (Diptera: Ceratopogonidae), an annoying anthropophilic biting midge and putative vector of Oropouche Virus in Rondônia, Brazilian Amazon. Acta Trop. 2023;243:106928. https://doi.org/10.1016/j.actatropica.2023.106928
35. Pan American Health Organization/World Health Organization. Dengue [cited 2024 Sep 23]. https://www3.paho.org/data/index.php/en/mnu-topics/indicadores-dengue-en.html
36. Centers for Disease Control and Prevention. Chikungunya in the United States [cited 2024 Sep 23]. https://www.cdc.gov/chikungunya/data-maps/chikungunya-us.html
37. Centers for Diseases Control and Prevention. Zika cases in the United States [cited 2024 Sep 23]. https://www.cdc.gov/zika/zika-cases-us/index.html
38. Borkent AD, Dominiak P. Catalog of the biting midges of the world (Diptera: Ceratopogonidae). Zootaxa. 2020;4787:001–377.
39. Pappas LG, Moyer S, Pappas CD. Tree hole Culicoides (Diptera: Ceratopogonidae) of the Central Plains in the United States. J Am Mosq Control Assoc. 1991;7:624–7.
40. Wirth WW, Dyce AL, Peterson BV. An atlas of wing photographs, with a summary of the numerical characters of the Nearctic species of Culicoides (Diptera: Ceratopogonidae). Contrib Am Entomol Inst. 1985;22:1–46.
41. Integrated Digitalized Biocollections (iDigBio). Specimen record: Culicoides paraensis [cited 2024 Sep 23]. https://www.idigbio.org/portal/records/b63faf1c-dd9f-4053-b600-001617263c5e
42. Schmidtmann ET, Herrero MV, Green AL, Dargatz DA, Rodriquez JM, Walton TE. Distribution of *Culicoides sonorensis* (Diptera: Ceratopogonidae) in Nebraska, South Dakota, and North Dakota: clarifying the epidemiology of bluetongue disease in the northern Great Plains region of the United States. J Med Entomol. 2011;48:634–43. https://doi.org/10.1603/ME10231
43. Gorris ME, Bartlow AW, Temple SD, Romero-Alvarez D, Shutt DP, Fair JM, et al. Updated distribution maps of predominant *Culex* mosquitoes across the Americas. Parasit Vectors. 2021;14:547. https://doi.org/10.1186/s13071-021-05051-3
44. Darcie RFJ, Ward RA. Identification and geographical distribution of the mosquitoes of North America, North of Mexico. Gainesville (FL): University Press of Florida; 2005.
45. Vijaykrishna D, Mukerji R, Smith GJ. RNA virus reassortment: an evolutionary mechanism for host jumps and immune evasion. PLoS Pathog. 2015;11:e1004902. https://doi.org/10.1371/journal.ppat.1004902
46. Centers for Disease Control and Prevention. Arboviral diseases, neuroinvasive and non-neuroinvasive: 2015 case definition [cited 2024 Sep 23]. https://ndc.services.cdc.gov/case-definitions/arboviral-diseases-neuroinvasive-and-non-neuroinvasive-2015
47. Council of State and Territorial Epidemiologists. Zika virus disease and Zika virus infection without disease,

including congenital infections case definitions and addition to the nationally notifiable diseases list [cited 2024 Sep 23]. https://cdn.ymaws.com/www.cste.org/resource/resmgr/2016PS/16_ID_01_edited7.29.pdf
48. Breidenbaugh MS, de Szalay FA. Effects of aerial applications of naled on nontarget insects at Parris Island, South Carolina. *Environ* Entomol. 2010;39:591–9. https://doi.org/10.1603/EN09087
49. Purse BV, Carpenter S, Venter GJ, Bellis G, Mullens BA. Bionomics of temperate and tropical *Culicoides* midges: knowledge gaps and consequences for transmission of *Culicoides*-borne viruses. Annu Rev Entomol. 2015;60:373–92. https://doi.org/10.1146/annurev-ento-010814-020614
50. Reiter P, Lathrop S, Bunning M, Biggerstaff B, Singer D, Tiwari T, et al. Texas lifestyle limits transmission of dengue virus. Emerg Infect Dis. 2003;9:86–9. https://doi.org/10.3201/eid0901.020220

Address for correspondence: Sarah Anne J. Guagliardo, Centers for Disease Control and Prevention, 3156 Rampart Rd, Fort Collins, CO 80521, USA; email: sguagliardo@cdc.gov

Clinical and Genomic Epidemiology of Coxsackievirus A21 and Enterovirus D68 in Homeless Shelters, King County, Washington, USA, 2019–2021

Sarah N. Cox, Amanda M. Casto, Nicholas M. Franko, Eric J. Chow, Peter D. Han, Luis Gamboa, Brian Pfau, Hong Xie, Kevin Kong, Jaydee Sereewit, Melissa A. Rolfes, Emily Mosites, Timothy M. Uyeki, Alexander L. Greninger, Marco Carone, M. Mia Shim, Trevor Bedford, Jay Shendure, Michael Boeckh, Janet A. Englund, Lea M. Starita, Pavitra Roychoudhury, Helen Y. Chu

In support of improving patient care, this activity has been planned and implemented by Medscape, LLC and Emerging Infectious Diseases. Medscape, LLC is jointly accredited with commendation by the Accreditation Council for Continuing Medical Education (ACCME), the Accreditation Council for Pharmacy Education (ACPE), and the American Nurses Credentialing Center (ANCC), to provide continuing education for the healthcare team.

Medscape, LLC designates this Journal-based CME activity for a maximum of 1.00 ***AMA PRA Category 1 Credit(s)™***. Physicians should claim only the credit commensurate with the extent of their participation in the activity.

Successful completion of this CME activity, which includes participation in the evaluation component, enables the participant to earn up to 1.0 MOC points in the American Board of Internal Medicine's (ABIM) Maintenance of Certification (MOC) program. Participants will earn MOC points equivalent to the amount of CME credits claimed for the activity. It is the CME activity provider's responsibility to submit participant completion information to ACCME for the purpose of granting ABIM MOC credit.

All other clinicians completing this activity will be issued a certificate of participation. To participate in this journal CME activity: (1) review the learning objectives and author disclosures; (2) study the education content; (3) take the post-test with a 75% minimum passing score and complete the evaluation at https://www.medscape.org/qna/processor/72826?showStandAlone=true&src=prt_jcme_eid_mscpedu; and (4) view/print certificate. For CME questions, see page 2458.

NOTE: It is Medscape's policy to avoid the use of Brand names in accredited activities. However, in an effort to be as clear as possible, trade names are used in this activity to distinguish between the mixtures and different tests. It is not meant to promote any particular product.

Release date: October 22, 2024; Expiration date: October 22, 2025

Learning Objectives

Upon completion of this activity, participants will be able to:

- Analyze the prevalence of enterovirus infection among persons experiencing homelessness
- Assess risk factors for enterovirus infection among persons experiencing homelessness
- Distinguish the clinical presentation of coxsackievirus A21 infection among persons experiencing homelessness
- Evaluate results of environmental testing for viruses in homeless shelters

CME Editor

Jude Rutledge, BA, Technical Writer/Editor, Emerging Infectious Diseases. *Disclosure: Jude Rutledge, BA, has no relevant financial relationships.*

CME Author

Charles P. Vega, MD, Health Sciences Clinical Professor of Family Medicine, University of California, Irvine School of Medicine, Irvine, California. *Disclosure: Charles P. Vega, MD, has the following relevant financial relationships: served as consultant or advisor for Boehringer Ingelheim; GlaxoSmithKline.*

Authors

Sarah N. Cox, MSPH; Amanda M. Casto, MD, PhD; Nicholas M. Franko, BS; Eric J. Chow, MD, MS, MPH; Peter D. Han, MS; Luis Gamboa, BSc; Brian Pfau, BS; Hong Xie, BSc (Medicine), MSc; Kevin Kong, BSc; Jaydee Sereewit, MSc; Melissa A. Rolfes, PhD, MPH; Emily Mosites, PhD, MPH; Timothy M. Uyeki, MD; Alexander L. Greninger, MD, PhD, MS, MPhil; Marco Carone, PhD; M. Mia Shim, MD, MPH; Trevor Bedford, PhD; Jay Shendure, MD, PhD; Michael Boeckh, MD, PhD; Janet A. Englund, MD; Lea M. Starita, PhD; Pavitra Roychoudhury, MSc, PhD; Helen Y. Chu, MD, MPH.

Congregate homeless shelters are disproportionately affected by infectious disease outbreaks. We describe enterovirus epidemiology across 23 adult and family shelters in King County, Washington, USA, during October 2019–May 2021, by using repeated cross-sectional respiratory illness and environmental surveillance and viral genome sequencing. Among 3,281 participants ≥3 months of age, we identified coxsackievirus A21 (CVA21) in 39 adult residents (3.0% [95% CI 1.9%–4.8%] detection) across 7 shelters during October 2019–February 2020. We identified enterovirus D68 (EV-D68) in 5 adult residents in 2 shelters during October–November 2019. Of 812 environmental samples, 1 was EV-D68–positive and 5 were CVA21–positive. Other enteroviruses detected among residents, but not in environmental samples, included coxsackievirus A6/A4 in 3 children. No enteroviruses were detected during April 2020–May 2021. Phylogenetically clustered CVA21 and EV-D68 cases occurred in some shelters. Some shelters also hosted multiple CVA21 lineages.

Enteroviruses are responsible for ≈10–15 million symptomatic illnesses in the United States annually; however, epidemiologic surveillance and genetic characterization of many enterovirus subspecies is limited (*1*–*3*). Coxsackievirus A21 (CVA21), discovered in 1947, and enterovirus D68 (EV-D68), discovered in 1962, can cause illnesses ranging from cold-like symptoms to difficulty breathing and wheezing (*2*,*4*,*5*–*9*). In recent years, interest and awareness of EV-D68 has grown because of temporal and geographic associations of outbreaks with clusters of acute flaccid myelitis in children (*4*,*5*). No specific treatments or vaccines are available for nonpolio enteroviruses (*4*), and the pathogenesis of the infections remain poorly understood (*10*). A need exists for phylogeographic epidemiology to define genomic variation and genetic changes over time and to determine transmission patterns in the community (*5*,*11*,*12*).

Persons experiencing homelessness are at increased risk for infectious diseases and complications, such as influenza, COVID-19, and hepatitis A (*13*,*14*). The risk for acquiring infections is considerably higher for those who live in congregate shelters because of challenges with overcrowding, maintaining physical distance, poor ventilation, and sharing of hygiene facilities (*15*–*18*). To our knowledge, minimal data are available to describe enterovirus transmission among persons experiencing homelessness.

Our study aimed to characterize the epidemiology of nonrhinovirus enteroviruses through nasal swab specimens and environmental samples collected from homeless shelters across King County, Washington, USA, during 2019–2021. We used genomic sequencing to describe the molecular diversity of enteroviruses within and across shelter sites.

Materials and Methods

Study Design and Population

We retrospectively analyzed cross-sectional respiratory virus surveillance data collected during October 1, 2019–May 31, 2021, across 23 homeless shelters in King County, which includes the city of Seattle. As previously described, the Seattle Flu Study instituted active routine surveillance through staffed shelter kiosks (*19*,*20*). Study enrollment was open to residents ≥3 months of age reporting new or worsening cough alone or onset of ≥2 other acute respiratory illness symptoms in the previous 7 days, including subjective fever, sore throat, rhinorrhea, shortness of breath, headache, and myalgias. Symptom criteria also included diarrhea, rash, and ear pain or discharge for children <18 years of age. Persons who did not meet the symptom requirements were allowed to enroll and submit a nasal swab specimen while asymptomatic up to once a month for shelter surveillance (i.e., inclusion criteria were broadened to allow a person to participate ≥1 time per month even if asymptomatic). Beginning April 1, 2020, eligibility expanded to all residents and staff regardless of symptoms as a result of the SARS-CoV-2 response (*19*). Nine shelters participated in the study, which included both participant and environmental testing, before the COVID-19 pandemic (October 2019–March 2020). An additional 14 shelters joined the study during April 2020–May 2021 but only for participant testing because of the need to shift resources toward identification and isolation of persons with SARS-CoV-2 infection.

We obtained written consent from participants ≥18 years of age or from a guardian for children <18

Author affiliations: University of Washington, Seattle, Washington, USA (S.N. Cox, A.M. Casto, N.M. Franko, E.J. Chow, H. Xie, K. Kong, J. Sereewit, A.L. Greninger, M.M. Shim, T. Bedford, J. Shendure, M. Boeckh, J.A. Englund, L.M. Starita, P. Roychoudhury, H.Y. Chu); Public Health Seattle and King County, Seattle (E.J. Chow, M.M. Shim); Brotman Baty Institute for Precision Medicine, Seattle (P.D. Han, L. Gamboa, B. Pfau, T. Bedford, J. Shendure, L.M. Starita); Centers for Disease Control and Prevention, Atlanta, Georgia, USA (M.A. Rolfes, E. Mosites, T.M. Uyeki); Fred Hutchinson Cancer Research Center, Seattle (A.L. Greninger, M. Carone, T. Bedford, M. Boeckh, P. Roychoudhury); Howard Hughes Medical Institute, Seattle (T. Bedford, J. Shendure); Seattle Children's Research Institute, Seattle (J.A. Englund)

DOI: https://doi.org/10.3201/eid3011.240687

years of age; we obtained assent from participants 13–17 years of age. We offered $5 gift cards to compensate participants for their time. This study was approved by the Human Subjects Division of the University of Washington Institutional Review Board (approval no. STUDY00007800).

Data Collection

Study staff recruited participants at each shelter site 3–6 days per week. All participants completed a questionnaire on an electronic tablet and submitted a nasal swab specimen at each enrollment. Questionnaires were stored in Research Electronic Data Capture (https://www.project-redcap.org) and included information on current symptoms, shelter site, and demographics.

We collected respiratory specimens by using midturbinate sterile nylon flocked nasal swabs (FLOQ Swab; Copan Diagnostics) during October 1, 2019–July 22, 2020, and then subsequently during November 1, 2020–May 31, 2021. During July 22–November 1, 2020, we briefly used anterior nares swabs (US Cotton; SteriPack) because of supply change resource limitations. Given the spread of SARS-CoV-2, we changed the specimen collection protocol to study staff–supervised self-collected swab specimen. We shared visual guides with participants before specimen collection to demonstrate self-swabbing.

We collected environmental samples weekly from 9 homeless shelters during November 20, 2019–April 10, 2020. We adapted collection methods described by Bailey et al. (*21*). With residents present, study staff swabbed a 10-cm^2 area of selected high-touch surfaces (e.g., kitchen counters, front desk, doors, and entrance and restroom doors) by using Berkshire Lab-Tip 125S swabs. We collected bioaerosol samples for 60 minutes in high-traffic areas by using an SKC QuickTake 30 air pump with ambient air pumped through Millipore filter papers. We stored all collected samples in Universal Transport Medium (Copan Diagnostics) and transported on ice.

Multiplex PCR Testing

We tested nasal swab specimens and environmental samples by using a multiplex reverse transcription PCR platform (Open Array; Thermo Fisher Scientific) for 28 viral respiratory pathogen targets, including pan-enterovirus, EV-D68, rhinovirus, influenza viruses (A, B, C), respiratory syncytial viruses (A and B), human parainfluenza viruses (1–4), human coronaviruses, human bocavirus, human parechovirus, human metapneumovirus, adenovirus, and SARS-CoV-2 (from specimens and samples collected beginning January 1, 2020). We generated a relative cycle threshold (Ct) value for each result.

We identified positive or inconclusive enterovirus swabs by using PCR on either pan-enterovirus (Thermo Fisher Scientific assay Vi06439631_s1) or EV-D68 (Thermo Fisher Scientific assay Vi06439669_s1) targets and using a relative Ct value of <28 as provided by the manufacturer. Because the enterovirus probe can produce a false-positive test result on a sample with high rhinovirus amplification, laboratory staff reviewed all specimens and samples initially positive on enterovirus-specific primers and evaluated them on the basis of the degree of enterovirus amplification, enterovirus relative Ct values, and degree of rhinovirus amplification. Finally, we attempted sequencing on all positive or inconclusive enterovirus swabs identified by PCR to confirm enterovirus positivity and subtype.

Genomic Sequencing and Analysis

To identify viral species and genotypes present in enterovirus-positive swabs, we performed sequencing with enrichment for respiratory viruses using a commercially available panel of capture probes that covered multiple enteroviruses. We attempted whole-genome sequencing on all specimens and environmental samples that were positive or inconclusive for either the pan-enterovirus or EV-D68 targets. In our process, we converted extracted RNA to double-stranded cDNA, purified by bead cleanup, enzymatically fragmented, end-repaired, amplified, indexed, and purified again by using the QIAseq FX DNA Library Kit (QIAGEN, https://www.qiagen.com). We performed hybridization capture by using the QIAseq xHYB Viral Respiratory Panel (QIAGEN) after pooling libraries by sample relative Ct values. After overnight hybridization with biotinylated probes and subsequent washing to remove unbound fragments, we amplified the enriched libraries and purified them by using bead clean-up. We sequenced the resulting libraries on Illumina NovaSeq 6000 or NextSeq 2000 instruments by using a 2 × 150 read format. We generated consensus genomes by using a custom bioinformatic pipeline described previously (Appendix, https://wwwnc.cdc.gov/EID/article/30/11/24-0687-App1.pdf) (*22*).

We categorized specimens and samples as enterovirus-positive when they were positive or inconclusive by PCR and were sequence-confirmed as coxsackievirus or enterovirus. We considered any other sequence-confirmed viruses as enterovirus-negative and grouped them with swabs identified as other respiratory virus (ORV)–positive through PCR testing. We defined enterovirus unknown as any swabs that

were initially identified as positive or inconclusive for pan-enterovirus or EV-D68 through PCR but were unable to be sequenced.

Computational Analysis

We analyzed demographic, symptom, respiratory virus, and environmental data descriptively by using R version 4.3.2 (The R Project for Statistical Computing). We linked multiple enrollments (i.e., encounters) from the same participant by name, date of birth, and sex, as previously described (*18*). We summarized enterovirus results by shelter type and highlighted shelter outbreaks with >5 enterovirus cases. We determined the frequency of enterovirus detection among shelter participants by dividing the number of sequence-confirmed positive specimens by the total number of participant encounters overall and during viral circulation. We used an intercept-only Poisson regression model fitted using generalized estimating equations to obtain robust SE estimates and 95% CIs, accounting for clustering by shelter site. We used NextStrain software to process consensus genomes and to generate and visualize phylogenetic trees (*23*). We calculated bootstrap values using IQ-TREE version 1.6.12 (*24*). In addition to the consensus genomes generated for this study (Appendix Table 1), we downloaded and included in our analyses full-length CVA21 and EV-D68 genomes available from GenBank.

Results

Participant Surveillance

During October 1, 2019–May 31, 2021, we collected 14,464 nasal swab specimens from 3,281 unique participants (22% staff, 78% residents) across 23 homeless shelters (Appendix Table 2, Figure 1). Swabs from children <18 years of age constituted 14% of all specimens collected.

PCR testing identified 83 participant specimens on either the pan-enterovirus (n = 73) or EV-D68 (n = 46) PCR targets. Upon sequencing, we found 55 confirmed enterovirus-positive specimens among 47 symptomatic shelter residents during October 3, 2019–March 6, 2020 (Figures 1, 2; Appendix Tables

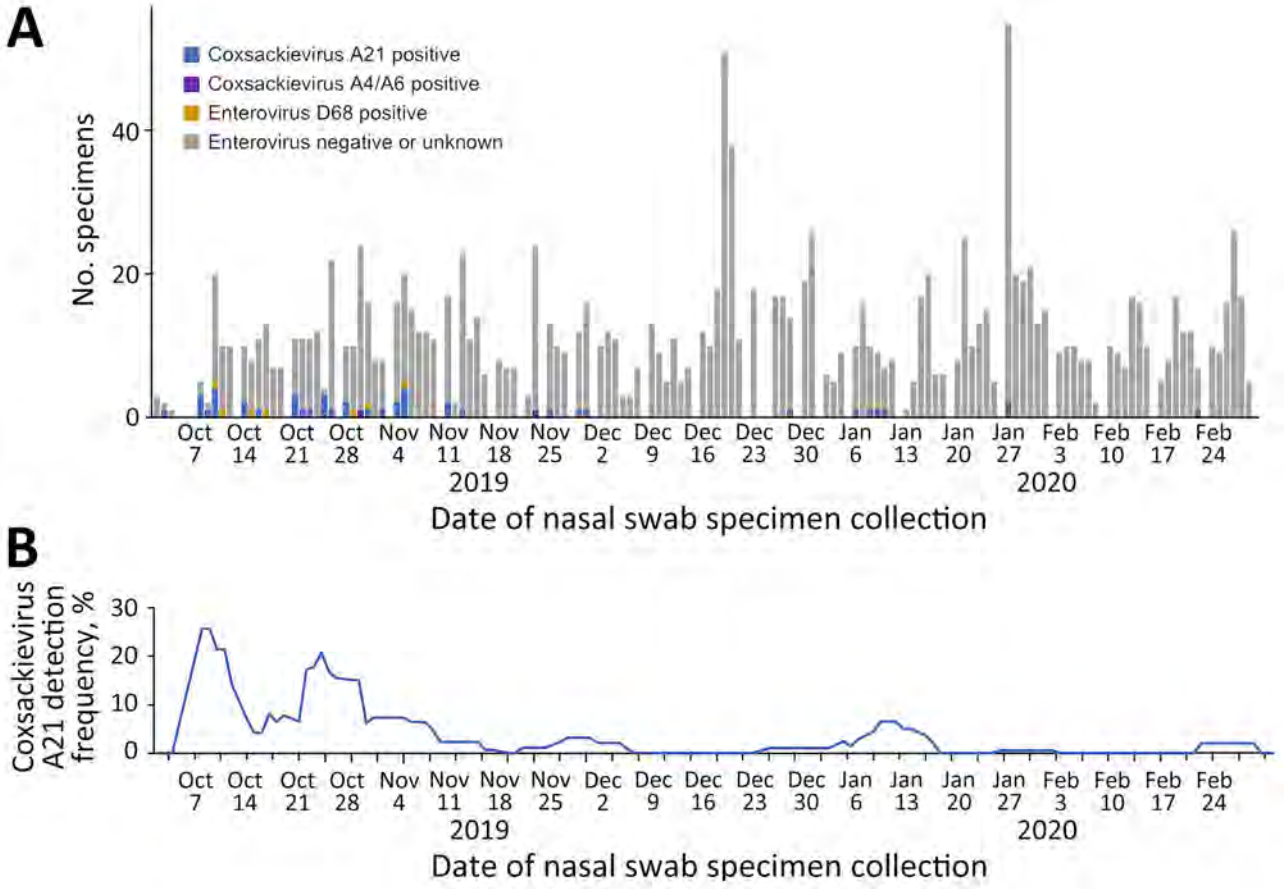

Figure 1. Nasal swab specimens (A) and enterovirus detection (B) in homeless shelters, King County, Washington, USA, October 2019–February 2020. Detection frequency represents a 7-day rolling average. No coxsackievirus A21-positive or enterovirus D68-positive specimens were detected during March 2020–May 2021.

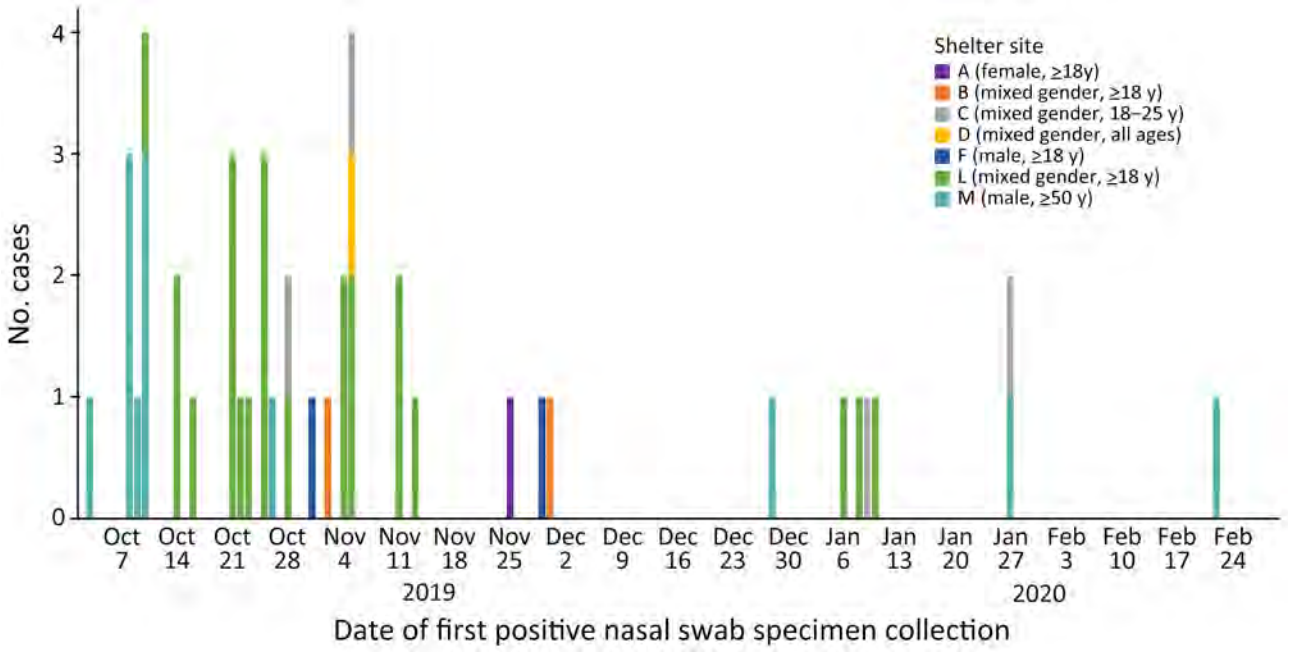

Figure 2. Unique participants with coxsackievirus A21 infection, by homeless shelter site, King County, Washington, USA, October 2019–February 2020.

2–4). We detected no enterovirus-positive specimens among shelter staff eligible to participate during April 2020–May 2021. Compared with episodes with enterovirus-negative specimens, episodes with enterovirus-positive specimens were associated with an older median age and being male, being a current tobacco smoker, experiencing chronic homelessness (≥1 year), and having underlying conditions (Appendix Table 2). Although the difference in age was attenuated when comparing specimens restricted to enrollment during October 2019–March 2020, other differences remained even after the expansion of eligibility during April 2020–May 2021 (Appendix Tables 3, 4).

We identified cases of CVA21 (n = 39) and EV-D68 (n = 5) among adults and CVA6 (n = 2) and CVA4 (n = 1) among children. Six residents tested CVA21-positive at 2 different timepoints, with a median of 9 days between positive tests (range 2–26 days). Two EV-D68–positive residents tested positive at 2 different timepoints (median 14 days, range 2–26 days). Four coxsackievirus-positive residents had rhinovirus co-detected.

The median age of CVA21-positive persons was 47 years (range 23–72 years). Most (90%) were male; 41% identified as White and 21% as Black/African-American (Appendix Table 2). The most commonly reported signs or symptoms of CVA21 infection included runny nose (85%) and cough (67%) (Figure 3; Appendix Tables 2, 5). Among the 39 unique persons with CVA21 infections, 51% (n = 20) reported a symptom or symptoms that prevented daily activity (Figure 3; Appendix Tables 5, 6). Half of the persons with CVA21 or EV-D68 indicated that their illness affected socialization, followed by those indicating that their illness affected their ability to take care of themselves or their family (36%), exercise (32%), and work (30%). Although 4 CVA21-positive persons sought care at a doctor's office or an urgent care setting, most (69% of persons with CVA21, 80% of persons with EV-D68) did not seek any medical care (Appendix Table 6).

Overall, CVA21 detection among all participant encounters was 0.3% (45/14,464 [95% CI 0.2%–0.5%]) during October 2019–May 2021 and 3.0% (45/1,485 [95% CI 1.9%–4.8%]) during viral circulation during October 2019–February 2020 (Figure 1; Appendix Table 7). Although we detected CVA21 across 7 shelter sites (Figure 1; Appendix Table 8), most cases occurred in outbreaks at 2 large adult shelters: 19 at mixed-gender shelter L with adults ≥18 years of age (October 10, 2019–January 10, 2020) (Figure 2; Video 1, https://wwwnc.cdc.gov/EID/article/30/11/24-0687-V1.htm) and 10 at all-male shelter M with older adults ≥50 years of age (October 3, 2019–January 27, 2019) (Figure 2; Video 2, https://wwwnc.cdc.gov/EID/article/30/11/24-0687-V2.htm).

Environmental Surveillance

Of 812 environmental swabs, we identified 18 on the pan-enterovirus (n = 8) or EV-D68 (n = 17) PCR targets, and we sequence-confirmed 6 as CVA21 (n = 5) or EV-D68 (n = 1) (Appendix Tables 8, 9, Figure 2). Detection

of enterovirus-positive environmental swabs occurred during November 20, 2019–March 12, 2020, across 3 shelters, all which also had resident cases detected. Most CVA21-positive environmental samples (n = 3) were detected at shelter L, which had the largest outbreak of cases among residents (Video 1). Despite having 10 unique CVA21-positive cases and 4 EV-D68-positive cases among its residents, the older adult male shelter (M) did not have any environmental samples that tested enterovirus-positive (Video 2). Surfaces where CVA21 was detected included bathroom doors and the front desk. We detected only 1 sequence-confirmed EV-D68–positive environmental sample from a bathroom door. We detected other viruses in environmental samples through PCR targets more frequently than enteroviruses; the highest rate of detection was for rhinovirus on children's playroom table (36%, n = 10), front desk (25%, n = 23), and restroom doors (23%, n = 31) (Appendix Table 9). Environmental surfaces tested consisted of plastic, Formica, or metal (Appendix Figure 3). None of the 99 bioaerosol samples tested were positive for enterovirus or another respiratory virus (Appendix Table 9).

Genomic Analysis

Because positive environmental samples may represent mixtures of viruses from multiple shelter residents or staff, we focused our genomic analysis on sequenced species from unique participants (Appendix Table 8). We collected all EV-D68 genomes from 5 unique participants during a 3-week period (October 10–31, 2019) from 2 shelters, L (n = 1) and M (n = 4). These formed a single cluster among 1,032 publicly available EV-D68 genomes downloaded from GenBank (Figure 4); specimens from shelter M did not cluster separately from the specimen from shelter L. All 5 genomes were of EV-D68 clade A2 and among the genomes from GenBank were most closely related to 2 genomes (GenBank accession nos. OR230417 and OR230423) collected in the United States in 2020. The environmental EV-D68 sample also was clade A2 but did not cluster with the participant specimens among the GenBank genomes (Appendix Figure 4).

All CVA21 genomes from 39 unique participants across 7 shelters formed a single phylogenetic cluster among 29 publicly available CVA21 genomes downloaded from GenBank (Figure 5, panel A). The study

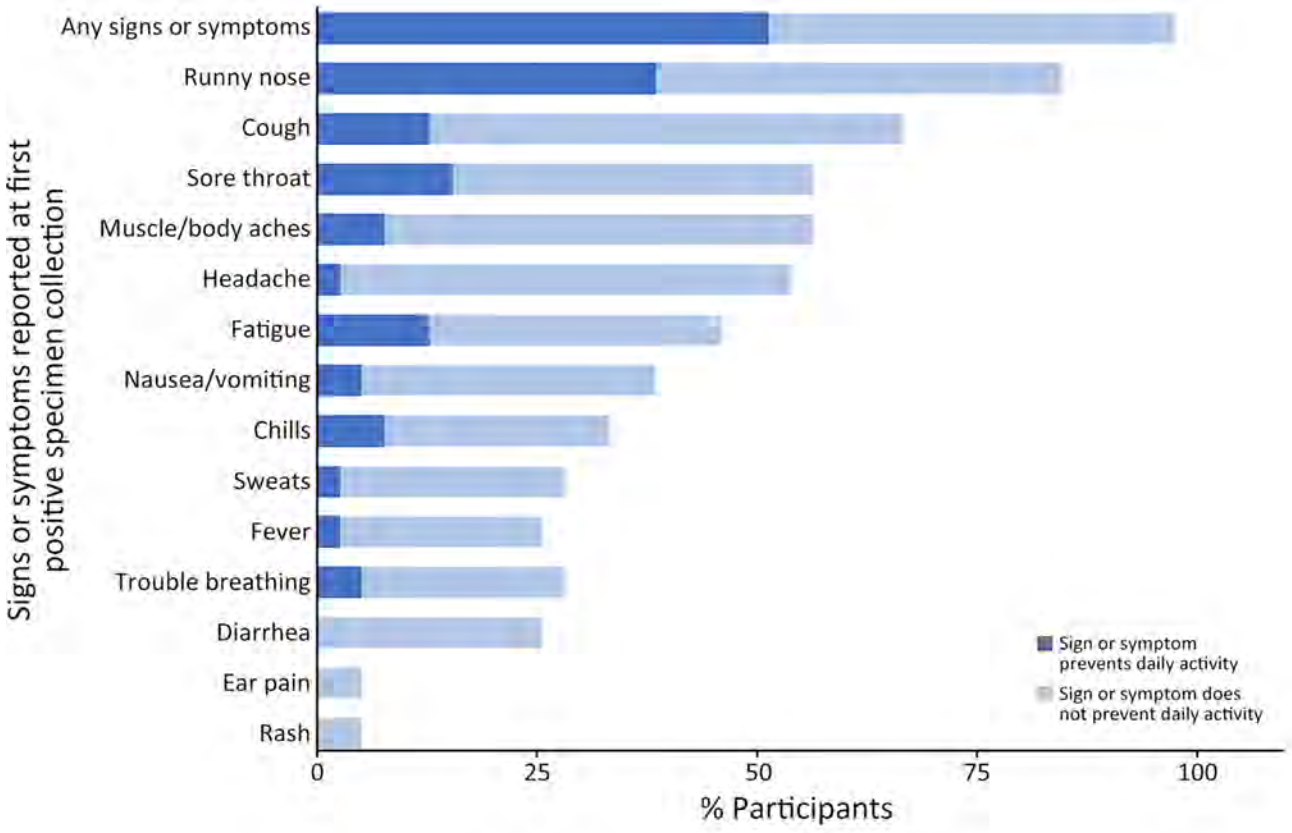

Figure 3. Signs or symptoms reported at specimen collection and effect on daily activity among adult homeless shelter residents with confirmed coxsackievirus A21 infection (n = 39), King County, Washington, USA, October 2019–January 2020. One person with coxsackievirus A21 infection was presymptomatic on initial encounter (first positive specimen collection) but symptomatic on subsequent encounter (second positive specimen collection).

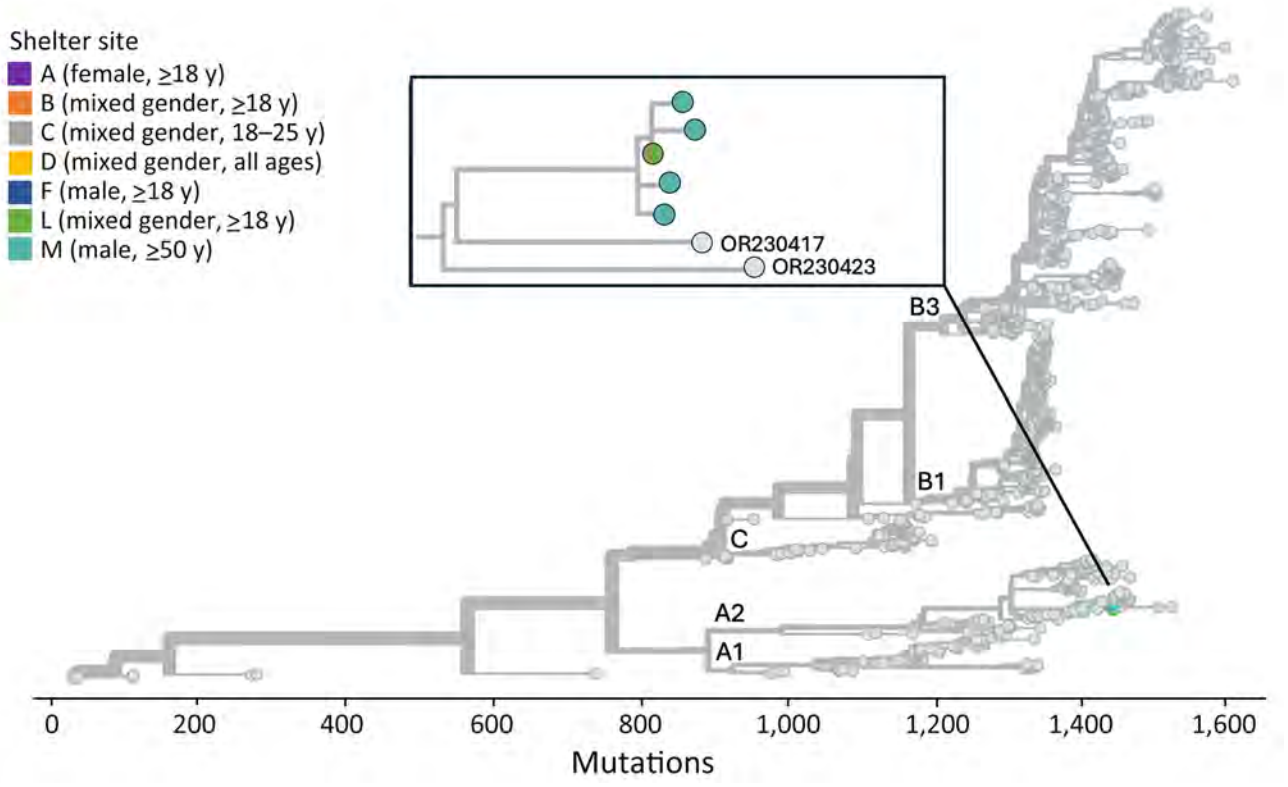

Figure 4. Phylogenetic tree of sequenced enterovirus D68 specimens of homeless shelter residents, King County, Washington, USA, October 2019–November 2019. Tips representing study specimens are colored according to shelter. Light gray tips represent enterovirus D68 genomes downloaded from GenBank. Inset shows a detailed view of the relationship among the study genomes. The x-axis represents the number of nucleotide changes in the genome relative to an enterovirus D68 reference genome (GenBank accession no. NC_038308.1).

genomes fall within CVA21 cluster I (*9*,*25*) and are mostly closely related to a genome collected in Nepal in 2017 (GenBank accession no. MZ396299). We observed some clustering by shelter (Figure 5, panels B, C) and instances of identical genomes at the same shelter. The mean pairwise genetic distances between specimens from the same shelter were lower than those from different shelters; however, this difference was not statistically significant (p = 0.0927 by analysis of variance) (Appendix Table 10). We observed no shelters with >2 sequenced participant specimens where all shelter genomes formed a single phylogenetic cluster and, among sequence clusters with >90% bootstrap support, we observed both single and multiple shelter groups. We also noted instances where >1 viral lineage of CVA21 appeared to be circulating at the same shelter at the same time (e.g., shelter M in October 2019). Finally, we observed an association between time of specimen collection and viral genotype given that all 6 specimens collected in 2020 formed a single cluster. Phylogenetic trees including the 5 sequenced environmental CVA21 samples (Appendix Figure 5) illustrate that 4 of 5 environmental samples were closely related to other specimens from the same shelter. The other sample from shelter L was not closely related to any other sequenced shelter specimens and, given its position in the tree, might represent a mixture of viral genotypes observed among the CVA21 shelter specimens.

We visualized the single sequenced CVA4 specimen in a phylogenetic tree among publicly available CVA4 genomes (Appendix Figure 6); the most closely related GenBank genome was collected in Tennessee in April 2015 (GenBank accession no. KY271949). The 2 sequenced CVA6 specimens cluster together among publicly available CVA6 genomes (Appendix Figure 7). The GenBank genome most closely related to these strains was collected in France in 2018 (GenBank accession no. MT814570).

Discussion

Our study characterizes the epidemiology of enteroviruses among persons experiencing homelessness by using respiratory specimen and environmental surveillance from a community-based shelter setting (*14*). Given the increased risk for infectious disease

transmission in congregate shelters and heightened potential for complications because of underlying conditions in many residents, understanding enterovirus epidemiology to prevent and support shelters during outbreaks is important. We detected CVA21 in 3% of all participant specimens tested among King County shelters during October 2019–February 2020, which falls within the range of findings in other global studies (<0.1%–57.0%) (*9*,*26*,*27*). Detection of EV-D68 in the shelters in 2019 is aligned with recent studies in Europe that found upsurges in the 2019 and 2021 seasons (*12*,*28*) compared with the previous biennial pattern observed in even years (e.g., 2014, 2016, 2018, and, to a lesser extent, 2020) (*7*,*29*). We detected no enteroviruses among shelter participants during April 2020–May 2021 despite ongoing surveillance during that period, possibly because stricter COVID-19 pandemic mitigation measures were in place.

All identified CVA21 and EV-D68 infections were in adult shelter residents in adult-only shelters, despite surveillance across children and adults, contributing to the scarce literature available on these viruses in adults (*30*). The manifestations of CVA21 and EV-D68 among symptomatic adult residents were similar and aligned with other adult case-patient reports (*30*,*31*). Half of persons with CVA21 reported a symptom that prevented daily activity; however, most enterovirus-positive persons did not seek any clinical care. Although previous studies have found that children are at higher risk for symptomatic EV-D68 infection than adults (*5*,*32*), we did not identify any positive cases among children in our study despite specimens from children constituting 14% of all specimens collected. In addition, we found no EV-D68–positive environmental surface samples in family shelters; we detected EV-D68–positive and CVA21-positive environmental samples in adult-only shelters.

Environmental monitoring is a minimally invasive method of surveillance for both endemic and emerging respiratory pathogens and could be

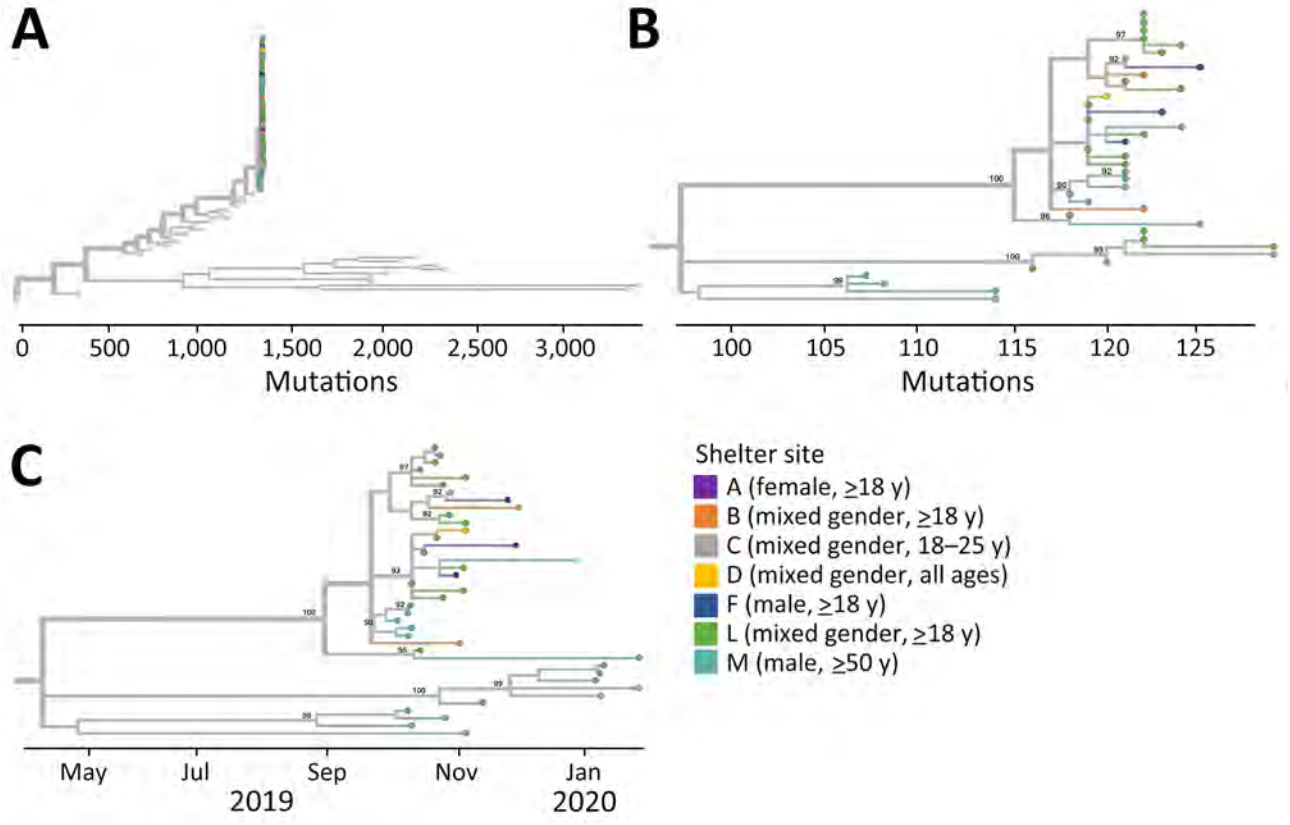

Figure 5. Phylogenetic trees of sequenced coxsackievirus A21 specimens of homeless shelter residents, King County, Washington, USA, October 2019–February 2020. A) Tree containing all shelter coxsackievirus A21 and all coxsackievirus A21 genomes deposited in GenBank. Tips representing study specimens are colored according to shelter. Light gray tips represent coxsackievirus A21 genomes downloaded from GenBank. The x-axis represents number of nucleotide changes in the genome relative to a coxsackievirus A21 reference genome (GenBank accession no. AF465515.1). B) Tree containing all shelter coxsackievirus A21 genomes. Internal nodes with >90% bootstrap support are labeled on tree. C) Tree containing all shelter coxsackievirus A21 genomes with x-axis corresponding to specimen collection date.

especially useful as an early indicator of viruses circulating in congregate settings. We found CVA21-positive environmental surface samples across 3 of the 7 shelters with CVA21 detection in nasal swabs. Although we did not find enteroviruses in the bioaerosol samples tested, previous studies have documented aerosol detection in the United States (*33*). We detected CVA21-positive environmental surface samples concurrently with the largest outbreak in adult shelter L, but we did not detect them in the older adult male shelter M outbreak, potentially because of enhanced cleaning procedures including ultraviolet disinfection (shelter M staff, pers. comm., 2020, staff meeting). Additional details on shelter disinfection practices were unavailable. Detection of CVA21 most commonly on bathroom doors may be suggestive of a fecal–oral route of transmission, as is observed with many enteroviruses (*2*,*34*). Although CVA21 was detected in nasal swab specimens before the positive environmental samples in 3 shelters, this finding probably is reflective of the earlier start of human specimen collection (October 2019) compared with environmental sampling (November 2020).

Our genomic analysis offers insight into the diversity of enteroviruses circulating in King County and the relationships among viruses of the same species within individual shelters and among different shelters. For EV-D68 and CVA21, the study specimens were closely related relative to the diversity represented by publicly available genomes of the same species. This finding may suggest that only 1 lineage of each of these viruses was circulating in King County during the study period, although other lineages not captured in our nasal swab specimens or environmental samples might have been present. Of note, very limited information about CVA21 genomic diversity is available, and the sequences generated by our study more than doubled the number of full genomes available for the virus.

The relationships among shelter CVA21 and EV-D68 genomes were complex. In some cases, viruses from the same shelter clustered together or were even identical, which is consistent with some intra-shelter viral spread. The phylogenetic analysis also identified instances in which viruses were more closely related to specimens from other shelters rather than the same shelter. This finding could be indicative of inter-shelter spread, although our limited knowledge of how quickly these viruses mutate prevents us from assessing whether this finding could represent direct transmission between shelters. For shelters B, C, L, and M, the phylogenetic tree was suggestive of >1 introduction of CVA21 into each shelter during the study period.

Because environmental samples can constitute mixtures of viruses from >1 person deposited at different times, interpretation of their placement in phylogenetic trees is difficult. We observed that CVA21 environmental samples grouped with other study specimens among the genomes from GenBank; in most cases, CVA21 environmental samples appeared most closely related to a participant specimen from the same shelter. This finding indicates that, despite the potentially complex origins of environmental samples, they can offer some insights into viral genotypes circulating at a location and as a result could be extremely valuable in cases where specimens from persons are unavailable.

This study describes the epidemiology of enteroviruses in congregate homeless shelters by using genetically sequenced surveillance data and associated symptom data. Although most previous studies on CVA21 and EV-D68 among adults are from hospitalization data and focus on case reports, our study provides both surveillance and environmental sampling data from a community setting.

Limitations of our study include the potential for a nonrepresentative sample because of voluntary participation, a lack of site-specific intervention data (e.g., disinfection practices), and a relatively small case count. In addition, limitations of testing include the sample type used (given that nasopharyngeal swab specimens historically are considered the standard), collection type used (given potential differences in quality between specimens that are self-collected versus staff-collected), and small sample size of enterovirus data (given the need to restrict to specimens confirmed through sequencing given the cross-reactivity of assays). Our conclusions also are limited by the study's cross-sectional nature because we could not follow up with participants about potential long-term complications and care-seeking (e.g., hospital admissions). Further research on longitudinal outcomes of enterovirus-positive participants is needed (*12*,*28*).

Our findings provide information on CVA21 and EV-D68 epidemiology, clinical characteristics, and transmission patterns to guide clinical diagnosis and public health interventions. Further understanding of enteroviruses can be used to develop effective preventative measures and treatment options. Surveillance of enteroviruses in shelters and other congregate settings may be warranted for early detection and implementation of control measures to reduce outbreaks.

Acknowledgments

We thank shelter program managers and staff for their active collaboration throughout the participant recruitment process. A special thanks to the research assistants who assisted with data collection and all residents who participated.

This study was funded by Gates Ventures and the Centers for Disease Control and Prevention (research contract no. 75D30120C09322 AM002 to H.Y.C.). The funders were not involved in the design of the study and do not have any ownership over the management and conduct of the study, the data, or the rights to publish. Computational analyses were supported by Fred Hutch Scientific Computing (National Institutes of Health Office of Research Infrastructure Programs grant no. S10OD028685) and University of Washington Laboratory Medicine Informatics. T.B. is a Howard Hughes Medical Institute Investigator.

S.N.C. reports honoraria from University of California–Berkeley and Fresno State for presentations on respiratory viruses. E.J.C. reports honoraria from Providence Health and Services, Seattle, Washington for presentations on COVID-19 and a travel grant received from the Infectious Diseases Society of America for travel to IDWeek 2022. A.L.G. reports contract testing from Abbott, Cepheid, Novavax, Pfizer, Janssen, and Hologic, research support from Gilead, outside of the work described in this article. J.A.E. reports consultation for Ark Biopharma, Astra Zeneca, Meissa Vaccines, Moderna, Sanofi Pasteur, and Pfizer, and has received research funding from AstraZeneca, GlaxoSmithKline, Merck, and Pfizer, outside the work described in this article. P.R. reports honoraria from the Bill and Melinda Gates Foundation for presentations on COVID-19. H.Y.C. reports consultation for Vir, Abbvie, and Merck outside the work described in this article. All other authors report no potential conflicts.

Author contributions: conception and design: S.N.C., A.M.C., E.J.C., P.R., and H.Y.C.; analysis and interpretation of the data: S.N.C., A.M.C., E.J.C., J.S., M.C., P.R., and H.Y.C.; drafting of the article: S.N.C., A.M.C., P.R., and H.Y.C; critical revision of the article for important intellectual content: S.N.C., A.M.C., N.M.F., E.J.C., P.D.H., L.G., B.P., H.X., K.K., J.S., M.A.R., E.M., T.M.U., A.L.G., M.C., M.M.S., T.B., J.S., M.B., J.A.E., L.M.S., P.R., and H.Y.C.; final approval of the article: S.N.C., A.M.C., N.M.F., E.J.C., P.D.H., L.G., B.P., H.X., K.K., J.S., M.A.R., E.M., T.M.U., A.L.G., M.C., M.M.S., T.B., J.S., M.B., J.A.E., L.M.S., P.R., and H.Y.C.; provision of study materials or patients: T.B., L.M.S., and H.Y.C; statistical expertise: M.C.; obtaining of funding: J.S., T.B., and H.Y.C.; administrative, technical, or logistic support: S.N.C., P.H., L.M.S., and H.Y.C.; collection and assembly of data: S.N.C., N.M.F., J.S., P.H., L.G., B.P., K.K., H.X., T.B., P.R., and H.Y.C.

About the Author

Dr. Cox is an epidemiologist at the University of Washington. Her primary research interests include infectious disease epidemiology and reducing health disparities.

References

1. Brouwer L, Moreni G, Wolthers KC, Pajkrt D. World-wide prevalence and genotype distribution of enteroviruses. Viruses. 2021;13:434. https://doi.org/10.3390/v13030434
2. Khetsuriani N, Lamonte-Fowlkes A, Oberst S, Pallansch MA; Centers for Disease Control and Prevention. Enterovirus surveillance—United States, 1970–2005. MMWR Surveill Summ. 2006;55:1–20.
3. Connell C, Tong HI, Wang Z, Allmann E, Lu Y. New approaches for enhanced detection of enteroviruses from Hawaiian environmental waters. PLoS One. 2012;7:e32442. https://doi.org/10.1371/journal.pone.0032442
4. Cassidy H, Poelman R, Knoester M, Van Leer-Buter CC, Niesters HGM. Enterovirus D68—the new polio? Front Microbiol. 2018;9:2677. https://doi.org/10.3389/fmicb.2018.02677
5. Dyda A, Stelzer-Braid S, Adam D, Chughtai AA, MacIntyre CR. The association between acute flaccid myelitis (AFM) and enterovirus D68 (EV-D68)—what is the evidence for causation? Euro Surveill. 2018;23:17–00310. https://doi.org/10.2807/1560-7917.ES.2018.23.3.17-00310
6. Dalldorf G, Sickles GM. An unidentified, filtrable agent isolated from the feces of children with paralysis. Science. 1948;108:61–2. https://doi.org/10.1126/science.108.2794.61
7. Centers for Disease Control and Prevention. Enterovirus D68 (EV-D68). 2022 [cited 2023 Feb 18]. https://www.cdc.gov/non-polio-enterovirus/about/ev-d68.html
8. Xiang Z, Gonzalez R, Wang Z, Ren L, Xiao Y, Li J, et al. Coxsackievirus A21, enterovirus 68, and acute respiratory tract infection, China. Emerg Infect Dis. 2012;18:821–4. https://doi.org/10.3201/eid1805.111376
9. Supian NI, Ng KT, Chook JB, Takebe Y, Chan KG, Tee KK. Genetic diversity of coxsackievirus A21 associated with sporadic cases of acute respiratory infections in Malaysia.. BMC Infect Dis. 2021;21:446. https://doi.org/10.1186/s12879-021-06148-x
10. Huang W, Wang G, Zhuge J, Nolan SM, Dimitrova N, Fallon JT. Whole-genome sequence analysis reveals the enterovirus d68 isolates during the United States 2014 outbreak mainly belong to a novel clade. Sci Rep. 2015;5:15223. https://doi.org/10.1038/srep15223
11. Hodcroft EB, Dyrdak R, Andrés C, Egli A, Reist J, García Martínez de Artola D, et al. Evolution, geographic spreading, and demographic distribution of Enterovirus D68. PLoS Pathog. 2022;18:e1010515. https://doi.org/10.1371/journal.ppat.1010515
12. Simoes MP, Hodcroft EB, Simmonds P, Albert J, Alidjinou EK, Ambert-Balay K, et al. Epidemiological and clinical insights into the enterovirus D68 upsurge in Europe 2021/22 and the emergence of novel B3-derived lineages, ENPEN multicentre study. J Infect Dis. 2024;jiae154. https://doi.org/10.1093/infdis/jiae154
13. Badiaga S, Raoult D, Brouqui P. Preventing and controlling emerging and reemerging transmissible diseases in the homeless. Emerg Infect Dis. 2008;14:1353–9. https://doi.org/10.3201/eid1409.080204
14. Chow EJ, Casto AM, Rogers JH, Roychoudhury P, Han PD, Xie H, et al. The clinical and genomic epidemiology

of seasonal human coronaviruses in congregate homeless shelter settings: a repeated cross-sectional study. Lancet Reg Health Am. 2022;15:100348. https://doi.org/10.1016/j.lana.2022.100348
15. Kuehn BM. Homeless shelters face high COVID-19 risks. JAMA. 2020;323:2240.
16. Leung CS, Ho MM, Kiss A, Gundlapalli AV, Hwang SW. Homelessness and the response to emerging infectious disease outbreaks: lessons from SARS. J Urban Health. 2008;85:402–10. https://doi.org/10.1007/s11524-008-9270-2
17. Imbert E, Kinley PM, Scarborough A, Cawley C, Sankaran M, Cox SN, et al. Coronavirus disease 2019 outbreak in a San Francisco homeless shelter. Clin Infect Dis. 2021;73:324–7. https://doi.org/10.1093/cid/ciaa1071
18. Rogers JH, Cox SN, Hughes JP, Link AC, Chow EJ, Fosse I, et al. Trends in COVID-19 vaccination intent and factors associated with deliberation and reluctance among adult homeless shelter residents and staff, 1 November 2020 to 28 February 2021—King County, Washington. Vaccine. 2022;40:122–32. https://doi.org/10.1016/j.vaccine.2021.11.026
19. Rogers JH, Link AC, McCulloch D, Brandstetter E, Newman KL, Jackson ML, et al.; Seattle Flu Study Investigators. Characteristics of COVID-19 in homeless shelters: a community-based surveillance study. Ann Intern Med. 2021;174:42–9. https://doi.org/10.7326/M20-3799
20. Newman KL, Rogers JH, McCulloch D, Wilcox N, Englund JA, Boeckh M, et al.; Seattle Flu Study Investigators. Point-of-care molecular testing and antiviral treatment of influenza in residents of homeless shelters in Seattle, WA: study protocol for a stepped-wedge cluster-randomized controlled trial. Trials. 2020;21:956. https://doi.org/10.1186/s13063-020-04871-5
21. Bailey ES, Choi JY, Zemke J, Yondon M, Gray GC. Molecular surveillance of respiratory viruses with bioaerosol sampling in an airport. Trop Dis Travel Med Vaccines. 2018;4:11. https://doi.org/10.1186/s40794-018-0071-7
22. Chow EJ, Casto AM, Sampoleo R, Mills MG, Han PD, Xie H, et al. Human parainfluenza virus in homeless shelters before and during the COVID-19 pandemic, Washington, USA. Emerg Infect Dis. 2022;28:2343–7. https://doi.org/10.3201/eid2811.221156
23. Hadfield J, Megill C, Bell SM, Huddleston J, Potter B, Callender C, et al. Nextstrain: real-time tracking of pathogen evolution. Bioinformatics. 2018;34:4121–3. https://doi.org/10.1093/bioinformatics/bty407
24. Nguyen LT, Schmidt HA, von Haeseler A, Minh BQ. IQ-TREE: a fast and effective stochastic algorithm for estimating maximum-likelihood phylogenies. Mol Biol Evol. 2015;32:268–74. https://doi.org/10.1093/molbev/msu300
25. Wang S, Xu M, Lin X, Liu Y, Xiong P, Wang L, et al. Molecular characterization of coxsackievirus A21 in Shandong, China. Arch Virol. 2016;161:437–44. https://doi.org/10.1007/s00705-015-2669-7
26. Zou L, Yi L, Song Y, Zhang X, Liang L, Ni H, et al. A cluster of coxsackievirus A21 associated acute respiratory illness: the evidence of efficient transmission of CVA21. Arch Virol. 2017;162:1057–9. https://doi.org/10.1007/s00705-016-3201-4
27. Hang J, Vento TJ, Norby EA, Jarman RG, Keiser PB, Kuschner RA, et al. Adenovirus type 4 respiratory infections with a concurrent outbreak of coxsackievirus A21 among United States Army Basic Trainees, a retrospective viral etiology study using next-generation sequencing. J Med Virol. 2017;89:1387–94. https://doi.org/10.1002/jmv.24792
28. Midgley SE, Benschop K, Dyrdak R, Mirand A, Bailly JL, Bierbaum S, et al. Co-circulation of multiple enterovirus D68 subclades, including a novel B3 cluster, across Europe in a season of expected low prevalence, 2019/20. Euro Surveill. 2020;25:1900749. https://doi.org/10.2807/1560-7917.ES.2020.25.2.1900749
29. Abedi GR, Watson JT, Nix WA, Oberste MS, Gerber SI. Enterovirus and parechovirus surveillance—United States, 2014–2016. MMWR Morb Mortal Wkly Rep. 2018;67:515–8. https://doi.org/10.15585/mmwr.mm6718a2
30. Waghmare A, Pergam SA, Jerome KR, Englund JA, Boeckh M, Kuypers J. Clinical disease due to enterovirus D68 in adult hematologic malignancy patients and hematopoietic cell transplant recipients. Blood. 2015;125:1724–9. https://doi.org/10.1182/blood-2014-12-616516
31. Giombini E, Rueca M, Barberi W, Iori AP, Castilletti C, Scognamiglio P, et al. Enterovirus D68-associated acute flaccid myelitis in immunocompromised woman, Italy. Emerg Infect Dis. 2017;23:1690–3. https://doi.org/10.3201/eid2310.170792
32. Centers for Disease Control and Prevention (CDC). Clusters of acute respiratory illness associated with human enterovirus 68—Asia, Europe, and United States, 2008–2010. MMWR Morb Mortal Wkly Rep. 2011;60:1301–4.
33. Lednicky JA, Bonny TS, Morris JG, Loeb JC. Complete genome sequence of enterovirus d68 detected in classroom air and on environmental surfaces. Genome Announc. 2016;4:e00579–16. https://doi.org/10.1128/genomeA.00579-16
34. Centers for Disease Control and Prevention. Non-polio enterovirus infection transmission. 2024 [cited 2024 Apr 11]. https://www.cdc.gov/non-polio-enterovirus/about/transmission.html

Address for correspondence: Sarah N. Cox, University of Washington Medicine, 750 Republican St, Seattle, WA 98109, USA; email: sarahcox@uw.edu

Mortality Rates after Tuberculosis Treatment, Georgia, USA, 2008–2019

Sarah Gorvetzian,[1] Antonio G. Pacheco, Erin Anderson, Susan M. Ray, Marcos C. Schechter

Limited data exist on mortality rates after tuberculosis (TB) treatment in the United States. We analyzed mortality rates for all adults in Georgia, USA, who had a TB diagnosis and finished treatment during January 1, 2008–December 31, 2019. We obtained posttreatment mortality rate data from the National Death Index and calculated standardized mortality ratios (SMRs) for TB treatment survivors and the general Georgia population. Among 3,182 TB treatment survivors, 233 (7.3%) had died as of December 31, 2019. The overall TB cohort age- and sex-adjusted SMR was 0.89 (95% CI 0.73–1.05). The SMR among US-born TB treatment survivors was 1.56 (95% CI 1.36–1.77). In the TB cohort, US-born status, HIV co-infection, excess alcohol use, diabetes mellitus, and end-stage renal disease were associated with increased risk for death after TB treatment. TB treatment survivors could benefit from improved linkage to primary and HIV comprehensive care to prevent posttreatment death.

Tuberculosis (TB) is a leading cause of death globally (*1*). However, TB-related mortality rate estimates usually do not account for posttreatment deaths (*1*). TB survivors are at increased risk for disability and death after treatment completion (*2*–*6*). The End TB Strategy focuses on TB prevention, diagnosis, and treatment but does not directly address posttreatment mortality rates (*7*), a critical omission because the number of TB survivors alive in a 2020 study was shown to be ≥10 times the global TB incidence (*8*).

A 2019 meta-analysis found a pooled standardized mortality ratio (SMR) of 2.91 among persons who completed TB treatment compared with control groups (*4*). Only 1 US-based study has reportedly measured posttreatment mortality rates among persons from Texas, Massachusetts, and Washington treated during 1993–2002 (*9*). That study found a higher all-cause death rate among persons who completed treatment for active TB (20.6%) than among those treated for latent TB (3.1%); however, that study did not compare rates with those from the general population, report causes of death, or investigate individual-level risk factors for posttreatment death, aside from demographics and HIV status (*9*).

Understanding long-term outcomes among TB survivors is needed to inform post-TB care policies in Georgia and in the rest of the United States. We performed survival analyses to determine risk factors for posttreatment deaths among persons who survived TB treatment. We also performed SMR analysis to investigate whether TB treatment survivors have a higher risk for death than the general state population in Georgia (i.e., persons who had no TB). We did not adjust for individual-level medical characteristics, such as other illnesses, because those data are not available for the entire Georgia population. Institutional Review Boards of Emory University and the Georgia Department of Public Health (GDPH) in Atlanta, Georgia, USA, approved this study.

Methods

We included in the study persons who had a TB diagnosis in Georgia, USA, during January 1, 2008 (earliest date TB data were available) to December 31, 2019 (last date long-term mortality data were available). We included patients who were ≥18 years of age at the time of TB diagnosis and those who ended treatment by December 31, 2019, and had bacteriologic or clinical TB diagnoses along with pulmonary or extrapulmonary disease. Because we were investigating posttreatment deaths, we excluded persons who

Author affiliations: Emory University School of Medicine, Atlanta, Georgia, USA (S. Gorvetzian, S.M. Ray, M.C. Schechter); Fundação Oswaldo Cruz, Rio de Janeiro, Brazil (A.G. Pacheco); Georgia Department of Public Health, Atlanta (E. Anderson, S.M. Ray, M.C. Schechter)

DOI: https://doi.org/10.3201/eid3011.240329

[1]Current affiliation: University of Colorado Anschutz Medical Campus, Aurora, Colorado, USA.

died before or during TB treatment and those who had missing treatment dates. However, we included persons who did not complete TB treatment but were alive when treatment ended. We also excluded persons with insufficient identifiers to query the Centers for Disease Control and Prevention (CDC) National Death Index (NDI) (*10*). TB is a notifiable disease in Georgia, and directly observed therapy is the standard of care (*11*). Incentives, such as housing and food vouchers, are generally available to persons with TB during but not after treatment. Similar to current US guidelines, no guidance exists for posttreatment care in Georgia (*12*,*13*).

Data Sources

We obtained all TB data by using the GDPH's electronic records (hereafter TB database) (*14*). Whenever applicable, we reported which data were missing and for how many subjects. We obtained posttreatment death data from the NDI (*10*). The NDI assigns a probabilistic score of 1–5 by using matching identifying data, and we considered scores of 1–3 as true matches according to NDI guidance (*10*). We reviewed all matches to ensure a plausible timeline existed between treatment completion and death.

We obtained mortality data for residents of Georgia who were ≥18 years of age and did not have TB during 2008–2019 (hereafter Georgia population) by using GDPH's Online Analytical Statistical Information System (*15*). We collected prevalence data for diabetes (*16*), alcohol use (*17*), HIV infection (*18*), homelessness (*19*), and non–US-born residents (*20*) in Georgia from public databases; we show data from our study midpoint (2014) or from the closest timepoint, if 2014 data were not available. Tobacco use data were unavailable in the TB database.

Study Definitions

We classified TB cases as culture confirmed if ≥1 culture from any site was positive for *Mycobacterium tuberculosis*, as clinical if no positive culture was obtained, or as other if a positive acid-fast bacilli smear or nucleic acid amplification test was obtained without a positive culture. We classified cavitary and miliary disease on the basis of chest radiograph and chest computerized tomography data, when available.

We identified persons with >1 TB episode during the study period by searching the TB database for duplicated dates of birth, names, or Social Security identification numbers. We manually reviewed all potential duplicates; when >1 TB episode was observed, we used characteristics that manifested during the first TB episode as baseline data.

We classified TB treatment outcomes as either complete or incomplete. Reasons for incomplete treatment were being lost to follow-up, having adverse treatment events, declining treatment, or moving out of Georgia during treatment. Treatment failure as defined by the World Health Organization TB treatment outcome classification (i.e., *M. tuberculosis*–positive sputum cultures after >4 months of treatment) is not recorded in the Georgia TB database. We defined the person-time follow-up for the TB cohort as the difference between the treatment stop date (irrespective of treatment completion) and either death or the study end date (December 31, 2019), whichever came first. We defined follow-up time for the Georgia population as the sum of the adult population in Georgia for each study year (2008–2019). We calculated mortality rates for the Georgia population from 2008–2019 by dividing the total number of deaths each year by that year's total population.

The NDI reports patient-level causes of death and the Online Analytical Statistical Information System reports the proportion of deaths in the Georgia population according to codes from the International Classification of Diseases, 10th Revision (ICD-10). We grouped causes of death according to ICD-10 codes as follows: cardiovascular disease (I09.X–I80.X), HIV (B20.X–B24.X), malignancy (C01.X–C34.X), respiratory disease (A16.X, A31.X, J18.X–J69.X), trauma/poisoning (V.X, W.X, X.X), and all others.

Data Analysis

We performed analyses in R version 4.1.2 (The R Project for Statistical Computing, https://www.r-project.org). We reported continuous data as medians and interquartile ranges (IQRs) or means and SDs, where appropriate. We restricted the following analyses to the TB cohort and only included persons who survived TB treatment. We calculated posttreatment death rates stratified by demographic, medical, and TB diagnosis and treatment characteristics. Because persons co-infected with TB and HIV and US-born persons had higher death rates, we calculated the rates of HIV co-infection and births in the United States stratified by demographic, medical, and TB diagnosis and treatment characteristics. We then used Kaplan-Meier curves to depict survival after stratifying TB treatment according to HIV status and place of birth; we calculated p values by using the log-rank test. We censored persons at death or on December 31, 2019 (the last date NDI data are available), whichever came first. Finally, we used Cox proportional

hazard models to estimate the relationship between individual-level characteristics and posttreatment deaths. We verified that all models met proportional hazards assumptions. We selected the multivariable Cox proportional hazard final model according to the best fit of the Akaike Information Criterion (AIC) (*21*). The AIC is a model selection method that penalizes the usual goodness of fit measurement by 2 times the number of estimated parameters to avoid overfitting; the lower the AIC, the better the model.

To compare the age of death between TB treatment survivors and the overall Georgia population, we calculated the standardized mortality rate per 1,000 person-years. We defined the age of persons with TB as their age at the time of death or as of December 31, 2019, whichever came first. We used the CDC 2000 projected US population as the standard population (*22*), and we calculated standard populations for sex and age by using US census projection reports (*23*). We calculated odds ratios and 95% CIs to compare causes of death between TB treatment survivors and the general population. We followed the Strengthening the Reporting of Observational Studies in Epidemiology guidelines for observational cohort studies (*24*).

Results

Baseline Characteristics of TB Cohort Patients and Georgia Population

A total of 3,755 TB episodes among 3,722 unique persons were diagnosed in Georgia during the study period (Figure 1). Among the 3,722 patients, reasons for exclusion from the study were as follows: treatment dates were not available (n = 27), treatment ended after December 31, 2019 (n = 233), death occurred before or during treatment (n = 279), and insufficient data was available to query the NDI (n = 1). We included 3,182 patients in the TB cohort. The median age at TB diagnosis was 44 years (IQR 32–57 years); a total of 2,093 (66%) patients were male, 1,089 (34%) female, 1,625 (51%) non–US-born persons, and 420 (13%) non-Hispanic White persons (Table 1). During the same period, the average age of the overall Georgia population was 45 years (IQR 31–58 years); 48% were male, 52% female, and 57% non-Hispanic White persons. In 2016, a total of 10% of Georgia residents were non–US-born persons. The prevalence of several co-existing illnesses or risk factors was higher in the TB cohort than in the overall Georgia population in 2014 (our study midpoint), including HIV (10% vs. 0.5%), homelessness (10% vs. 0.12%), excess alcohol use (15% vs. 5.3%), and diabetes mellitus (12% vs. 11%).

TB Manifestations and Treatment Characteristics

Most (n = 2,391 [75%]) TB cases were culture confirmed. Pulmonary disease occurred in 2,551 (80%) cases and extrapulmonary disease in 631 (20%) cases; both pulmonary and extrapulmonary disease occurred in 253 (8%) cases. Among patients who had available drug susceptibility results, 2,077 (88%) of those had rifampin- and isoniazid-susceptible TB. The median TB treatment duration was 224 days (IQR 189–289 days); 211 (7%) patients did not complete TB treatment. Reasons for treatment noncompletion

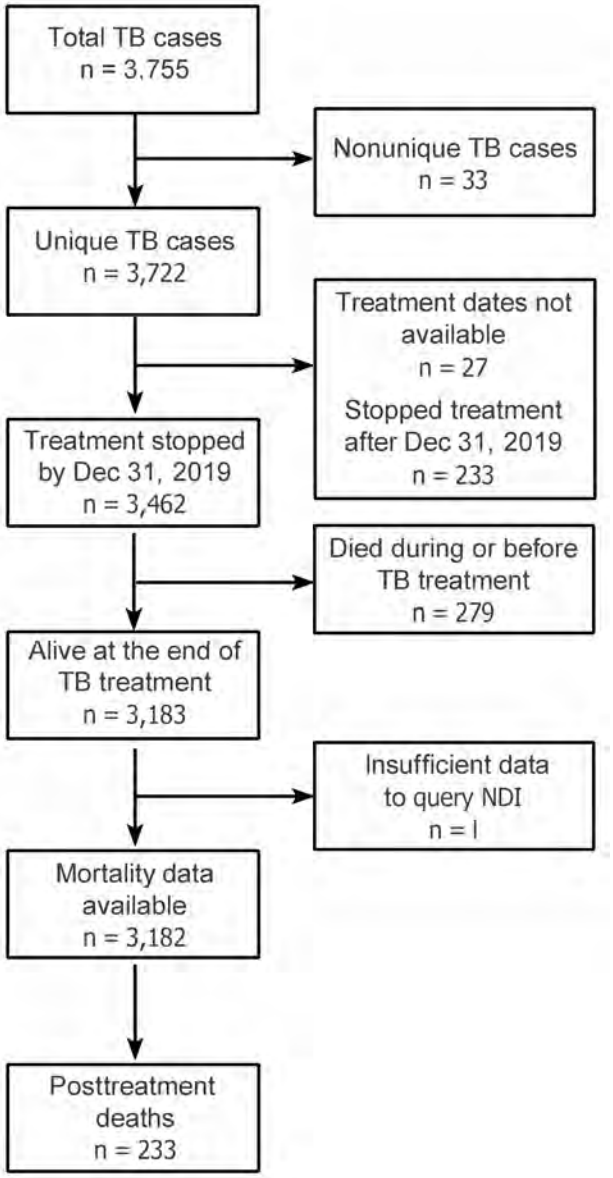

Figure 1. Flow chart of populations in study of mortality rates after TB treatment, Georgia, USA, 2008–2019. Persons who had a TB diagnosis in Georgia during January 1, 2008–December 31, 2019, were included in the study and compared with the general Georgia population. NDI, National Death Index; TB, tuberculosis.

Table 1. Characteristics of patients who finished TB treatment stratified according to posttreatment death, HIV infection, and place of birth in study of mortality rates after TB treatment, Georgia, USA, 2008–2019*

Characteristics	No. (%) patients			
	Overall cohort	Posttreatment deaths	HIV positive	US-born persons
Total no. patients	3,218	233	328	1,557
Age, y				
18–44	1,595 (50)	32 (2)	183 (11)	581 (36)
45–64	1,147 (36)	114 (10)	135 (12)	728 (63)
≥65	440 (14)	87 (20)	10 (2)	248 (56)
Sex				
F	1,089 (34)	70 (6)	93 (9)	477 (44)
M	2,093 (66)	163 (8)	235 (11)	1,080 (52)
Place of birth				
Non–US-born	1,625 (51)	32 (2)	113 (7)	NA
US-born	1,557 (49)	201 (13)	215 (14)	NA
Ethnicity				
Non-Hispanic White	420 (13)	59 (14)	14 (3)	368 (88)
Non-Hispanic Asian	669 (21)	21 (3)	18 (3)	19 (3)
Non-Hispanic Black	1,479 (46)	142 (10)	247 (17)	1,112 (75)
Hispanic, all races	559 (18)	11 (2)	40 (7)	29 (5)
Other	55 (2)	0 (0)	9 (16)	29 (53)
HIV status				
Negative	2,729 (86)	180 (7)	NA	1,292 (47)
Positive	328 (10)	38 (12)	NA	215 (66)
Missing data	125 (4)	15 (12)	NA	50 (40)
Injection drug use				
No	3,097 (97)	227 (7)	306 (10)	1,509 (49)
Yes	36 (1)	4 (11)	14 (39)	33 (92)
Missing data	49 (2)	2 (4)	8 (16)	15 (31)
Excess alcohol use				
No	2,659 (84)	162 (6)	257 (10)	1,169 (44)
Yes	467 (15)	69 (15)	65 (14)	370 (79)
Missing data	56 (2)	2 (4)	6 (11)	18 (32)
Homeless within year before TB diagnosis				
No	2,860 (90)	187 (7)	246 (9)	1,294 (45)
Yes	313 (10)	45 (14)	81 (26)	262 (84)
Missing data	9 (<1)	1 (11)	1 (11)	1 (11)
Diabetes mellitus				
No	2,791 (88)	178 (6)	319 (11)	1,368 (48)
Yes	391 (12)	55 (14)	9 (2)	189 (49)
End-stage renal disease				
No	3,139 (99)	224 (7)	324 (10)	1,527 (49)
Yes	43 (1)	9 (21)	4 (9)	30 (70)

*NA, not applicable; TB, tuberculosis.

included adverse events (n = 11), declined treatment (n = 12), loss to follow-up or moved during therapy (n = 93), and missing data/reason not recorded (n = 93).

TB Cohort Characteristics Stratified According to Posttreatment Death

Overall, 233 (7%) patients died after completing TB treatment (Table 1). Among 1,557 US-born persons, 201 (13%) died posttreatment compared with 32/1,625 (2%) of non–US-born persons. A total of 59/420 (14%) non-Hispanic White, 142/1,479 (10%) non-Hispanic Black, 21/669 (3%) non-Hispanic Asian, and 11/559 (2%) Hispanic patients died after completing TB treatment. Among 328 persons with TB co-infected with HIV, 38 (12%) died after TB treatment compared with 180/2,729 (7%) of persons who were not co-infected with HIV. Excess alcohol use, homelessness, diabetes mellitus, and end-stage renal disease were associated with a higher risk for posttreatment deaths (Table 1) Posttreatment death rates were the same among patients who completed treatment (218/2,973 [7%]) and those who did not complete treatment (15/211 [7%]) (Table 2).

TB Cohort Characteristics Stratified According to HIV Status and Birth Place

HIV infection occurred among 183/1,595 (11%) patients who were 18–44 years of age, 135/1,147 (12%) patients 45–65 years of age, and 10/440 (2%) patients ≥65 years of age at the time of TB diagnosis (Table 1). HIV co-infections occurred in 247/1,479 (17%) non-Hispanic Black, 14/420 (3%) non-Hispanic White, 18/669 (3%) non-Hispanic Asian, and 40/559 (7%) Hispanic persons with TB. Among persons who injected drugs, 14/36 (39%) were co-infected with HIV compared with 306/3,097 (10%) patients who did not inject drugs. Among patients who used excess alcohol, 65/467 (14%) had HIV

co-infections compared with 257/2,669 (10%) patients who did not use excess alcohol.

A total of 581/1,595 (36%) patients 18–44 years, 728/1,147 (63%) patients 45–64 years, and 248/440 (56%) patients ≥65 years of age at the time of TB diagnosis were US-born persons. We also found that 368/420 (88%) non-Hispanic White and 1,112/1,479 (75%) non-Hispanic Black patients were US-born persons with TB. Those rates were higher than for non-Hispanic Asian (19/669 [3%]) and Hispanic (29/559 [5%]) patients. US-born persons accounted for most persons who were HIV co-infected (215/328 [66%]), who injected drugs (33/36 [92%]), used excess alcohol (370/467 [79%]), had a history of homelessness (262/313 [84%]), or had end-stage renal disease (30/43 [70%]). Among 211/3,218 (7%) persons who did not complete TB treatment, 43 (21%) of those were US-born (Table 2).

TB Cohort Survival Analyses

The TB cohort median follow-up time was 5.8 years (IQR 2.8–8.7 years), for a total follow-up time of 18,426 person-years. We used Kaplan-Meier curves to depict posttreatment survival stratified by HIV status and place of birth (Figure 2). In univariate Cox proportional hazard models, older age at TB diagnosis was associated with increased risk for posttreatment death; the hazard ratio (HR) was 1.06 (95% CI 1.05–1.07) per year of age at the time of TB diagnosis (Table 3). Other risk factors for posttreatment death were being US-born (HR 6.68 [95% CI 4.60–9.70]), having HIV-positive (HR 1.70 [95% CI 1.22–2.45]) or missing HIV (HR 1.72 [95% CI 1.02–2.92]) status, using excess alcohol (HR 2.38 [95% CI 1.79–3.15]), having a history of homelessness (HR 2.19 [95% CI 1.58–3.04]), diabetes mellitus (HR 2.83 [95% CI 2.09–3.83]), and having end-stage renal disease (HR 3.36 [95% CI 1.73–6.54]). Extrapulmonary TB was associated with decreased risk for posttreatment death in univariate analysis (HR 0.62 [95% CI 0.43–0.91]). Compared with non-Hispanic White persons with TB, those of all other races/ethnicities had a lower posttreatment death HR. In multivariable Cox proportional hazard models (Table 3), factors associated with posttreatment death were older age at TB diagnosis (HR 1.06 [95% CI 1.05–1.07] per year), being US-born (HR 3.42 [95% CI 2.25–5.19]), HIV-positive status (HR 1.87 [95% CI 1.20–2.90]), excess alcohol use (HR 1.64 [95% CI 1.17–2.30]), missing homelessness history (HR 17.3 [95% CI 2.0–150.0]), diabetes mellitus (HR 2.05 [95% CI 1.44–2.91]), and end-stage renal disease (HR 2.24 [95% CI 1.05–4.80]).

TB Cohort and Georgia Population Mortality Rates

The median age at death for those who died after TB treatment was 64.0 years (IQR 55.7–75.3 years), whereas the average age at death in the Georgia population was 70.2 years. Among the deaths in the TB cohort, most were caused by cardiovascular disease

Table 2. TB diagnosis and treatment characteristics stratified according to posttreatment death, HIV infection, and place of birth in study of mortality rates after TB treatment, Georgia, USA, 2008–2019*

Characteristics	No. (%) patients			
	Overall cohort	Posttreatment deaths	HIV positive	US-born persons
Total no. patients	3,218	233	328	1,557
Case verification				
Culture confirmed	2,391 (75)	190 (8)	243 (10)	1,213 (51)
Clinical case	743 (23)	39 (5)	83 (11)	327 (44)
Other†	48 (2)	4 (8)	2 (4)	17 (35)
Site of TB disease				
Pulmonary	2,551 (80)	202 (8)	270 (11)	1,306 (51)
Extrapulmonary TB	631 (20)	31 (5)	58 (9)	251 (40)
Cavitary disease, n = 2,551 patients with pulmonary disease‡				
No	1,513 (59)	116(8)	214 (14)	729 (48)
Yes	1,038 (41)	86 (8)	56 (5)	577 (56)
Sputum smear, n = 2,551 patients with pulmonary disease‡				
Negative	1,254 (49)	95 (8)	137 (11)	650 (52)
Positive	1,192 (47)	98 (8)	124 (10)	600 (50)
Missing data	105 (4)	9 (9)	9 (9)	56 (53)
Drug susceptibility, n = 2,357 patients with available results‡				
RIF/INH susceptible	2,077 (88)	167 (8)	189 (9)	1,029 (50)
RIF susceptible/INH resistant	250 (11)	20 (8)	50 (20)	158 (63)
RIF resistant	30 (1)	1 (3)	3 (10)	10 (33)
Completed tuberculosis treatment				
Yes	2,973 (93)	218 (7)	303 (10)	1,514 (51)
No	211 (7)§	15 (7)	25 (12)	43 (21)

*INH, isoniazid; RIF, rifampin; TB, tuberculosis.
†Other comprised positive smear/tissue (n = 6) and positive nucleic acid amplification (n = 42).
‡Number of patients used in denominator to calculate percentage in overall cohort column.
§Incomplete treatment included adverse treatment events (n = 11), uncooperative or refused treatments (n = 12), lost to follow-up (n = 87), moved out of jurisdiction (n = 6), or reason was missing (n = 95).

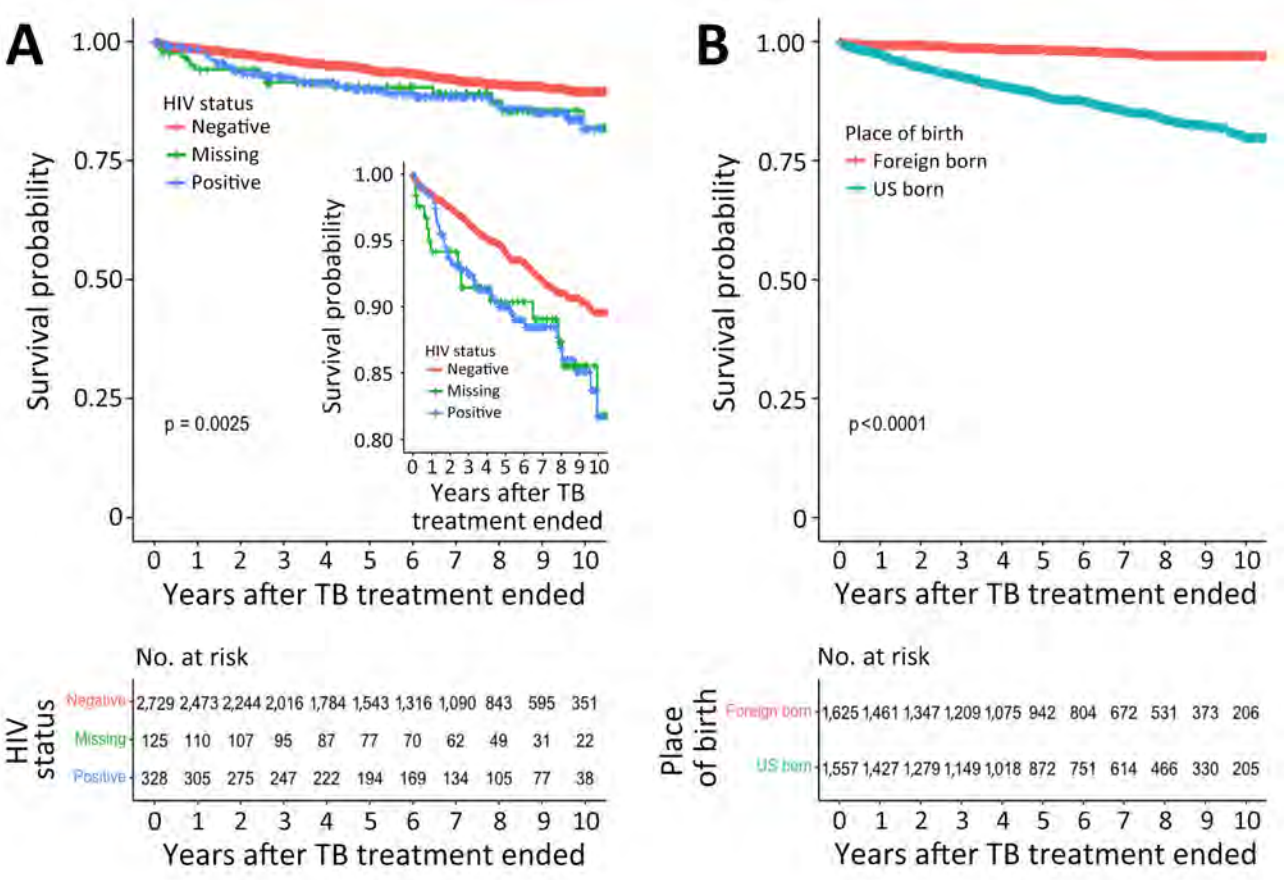

Figure 2. Survival probabilities in study of mortality rates after TB treatment, Georgia, USA, 2008–2019. Kaplan-Meier curves were used to plot survival probabilities of treated persons with TB over a 10-year period after treatment ended, stratified according to HIV status (A) and place of birth (B). Inset in panel A shows detailed curve with probabilities of 0.80–1.00. p values were calculated by log rank test. Number at risk tables below the curves indicate the total number of patients remaining in the study at each time point in each group, including any persons who experienced the event or were censored at that time point. Missing indicates missing data. TB, tuberculosis.

(56/233 [24.0%]) or malignancy (56/233 [24.0%]), followed by HIV infection (22/233 [9.9%]) (Table 4). Pulmonary malignancies (n = 21) accounted for 37.5% of total malignancies. Cardiovascular disease was a more frequent cause of death in the overall Georgia population (30.1%) compared with that in the TB cohort (24.0%). Conversely, HIV infection was a more frequent cause of death in the TB cohort (9.9%) compared with the overall Georgia population (0.05%). The mean age of death among those who died from HIV infection in the TB cohort was 49.6 years. No significant differences were observed for percentages of death from other causes between persons with TB and the general Georgia population.

Standardized Mortality Analyses Comparing Age of Death

The crude mortality rate for the overall TB cohort was 12.69/1,000 person-years (95% CI 11.12–14.3/1,000 person-years) (Table 5) compared with 9.92/1,000 person-years (95% CI 9.90–9.94/1,000 person-years); the Georgia population SMR was 0.89 (95% CI 0.73–1.05). We found similar results in a subgroup analysis restricted to culture-confirmed patients who completed treatment. In a subgroup analysis restricted to US-born persons in the TB cohort, the SMR was 1.58 (95% CI 1.41–1.76) (Table 5).

Discussion

We obtained data for persons who survived TB treatment in Georgia during 2008–2019 to report individual-level risk factors for posttreatment death and compared death rates and causes of death to those in the general Georgia population. This study fills a crucial knowledge gap because mortality rates after TB treatment in the United States were only reported >20 years ago (*9*). Among TB treatment survivors, 233/3,182 (7%) died, and the median time between treatment completion and death was 2.9 years. In a survival analysis restricted to the TB cohort, we

found that being a US-born patient, living with HIV, excess alcohol use, diabetes mellitus, and end-stage renal disease were significantly associated with post-TB treatment death. In contrast to studies in other countries (*4*,*6*,*25*–*27*), we found no difference between posttreatment mortality rates and mortality rates in the overall population (age- and sex-adjusted SMR of 0.91 [95% CI 0.75–1.07]). However, in a posthoc analysis, we found that US-born persons with TB had a higher mortality rate (age- and sex-adjusted SMR of 1.58 [95% CI 1.41–1.76]) than the Georgia population.

A landmark meta-analysis (*4*) of 10 studies investigating posttreatment deaths found an SMR of 2.91 (95% CI 2.21–3.84) among TB survivors, a finding that has been replicated by subsequent studies (*4*,*6*,*23*–*25*). Similar to this study, those studies have used the general population as a control (*4*). In this study, the follow-up time (18,426 person-years) was within the range (8,780–13.5 million person-years) of previous studies (*6*,*26*), and the HIV prevalence (10%) was also within the range (1.2%–16.0%) of previous studies (*9*,*29*,*30*). Thus, methodologic and study population differences are unlikely to explain why similar mortality rates existed among TB survivors in our cohort and the general Georgia population. However, increased life expectancy among immigrants in

Table 3. Hazard ratios for TB cohort groups defined by univariate and multivariable models in study of mortality rates after TB treatment, Georgia, USA, 2008–2019*

Characteristics	Univariate analysis, HR (95% CI)	Multivariate model, HR (95% CI)†
Age, per year	1.06 (1.05–1.07)	1.06 (1.05–1.07)
Sex		
F	Referent	NA
M	1.23 (0.92–1.63)	NA
US-born persons	6.68 (4.60–9.70)	3.42 (2.25–5.19)
Ethnicity‡		
Non-Hispanic White	Referent	NA
Non-Hispanic Asian	0.23 (0.14–0.37)	NA
Non-Hispanic Black	0.67 (0.49–0.91)	NA
Hispanic, all races	0.12 (0.06–0.23)	NA
HIV status		
Negative	Referent	Referent
Positive	1.70 (1.22–2.45)	1.87 (1.20–2.90)
Missing data	1.72 (1.02–2.92)	1.58 (0.90–2.78)
Injection drug use		
No	Referent	NA
Yes	1.44 (0.55–4.00)	NA
Missing data	1.46 (0.36–5.91)	NA
Excess alcohol use		
No	Referent	Referent
Yes	2.38 (1.79–3.15)	1.64 (1.17–2.30)
Missing data	1.30 (0.32–5.26)	1.51 (0.34–6.75)
Homeless within past year		
No	Referent	Referent
Yes	2.19 (1.58–3.04)	1.36 (0.89–2.08)
Missing data	1.81 (0.25–12.90)	17.3 (2.00–150.0)
Diabetes mellitus	2.83 (2.09–3.83)	2.05 (1.44–2.91)
End-stage renal disease	3.36 (1.73–6.54)	2.24 (1.05–4.80)
Case verification		
Culture confirmed	Referent	NA
Clinical case	0.66 (0.47–0.93)	NA
Other	1.12 (0.42–3.01)	NA
Extrapulmonary	0.62 (0.43–0.91)	NA
Cavitary disease, n = 2,511§	1.14 (0.86–1.50)	NA
Sputum smear, n = 2,511§		
Negative	Referent	NA
Positive	1.00 (0.76–1.33)	NA
Missing data	0.82 (0.41–1.63)	NA
Drug susceptibility, n = 2,318		
RIF/INH susceptible	Referent	Referent
RIF susceptible/INH resistant	0.99 (0.62–1.57)	0.89 (0.55–1.49)
RIF resistant	0.49 (0.07–3.47)	0.89 (0.12–6.39)
Incomplete TB treatment	0.83 (0.49–1.40)	NA

*HR, hazard ratio; INH, isoniazid; NA, not applicable; RIF, rifampin; TB, tuberculosis.
†Model selected according to best fit of Akaike Information Criterion (*21*).
‡Other category was excluded because no deaths occurred in this group (n = 55).
§Cavitary disease and sputum smear were not included in the multivariable models because the overall cohort included patients without pulmonary disease.

Table 4. Comparisons of causes of death between patients who finished TB treatment and the general population in study of mortality rates after TB treatment, Georgia, USA, 2008–2019*

Categories	No. (%) persons		Odds ratio (95% CI)†	Age at death, y, mean (SD)
	Posttreatment deaths	Georgia population deaths		
Total no. persons	233	900,874	NA	233
Cardiovascular disease	56 (24.0)	271,146 (30.1)	0.73 (0.54–0.99)	67.8 (14.8)
HIV	22 (9.9)	4,789 (0.5)	19.6 (12.6–30.4)	49.6 (11.3)
Malignancy	56 (24.0)‡	193,983 (21.5)	1.15 (0.85–1.55)	64.5 (12.0)
Pulmonary disease	26 (11.2)§	90,880 (10.1)	1.11 (0.74–1.68)	68.7 (14.9)
Trauma/poisoning	16 (6.9)	68,550 (7.6)	0.89 (0.53–1.48)	63.3 (14.3)
Other	57 (24.5)	271,526 (30.1)	0.75 (0.55–1.01)	68.0 (14.2)

*NA, not applicable; TB, tuberculosis.
†Odds of dying in posttreatment group compared with the general Georgia population.
‡Pulmonary malignancy, n = 21 (37.5% of total malignancies, 9% of total deaths).
§Pulmonary TB/mycobacterial infection, n = 7.

the United States compared with US-born persons (*31*) could explain our SMR findings; the SMR of 1.58 among US-born persons with TB in our cohort aligns with previously published studies.

Being a US-born TB patient was associated with higher rates of posttreatment death in the SMR and survival analyses. The increased death rate among US-born persons in the TB cohort could be, in part, because they were older, were more often HIV co-infected, and had higher rates of excess alcohol use, injection drug use, homelessness, and end-stage renal disease than did non–US-born persons. This finding is consistent with the higher life expectancy among non–US-born persons compared with US-born persons in the United States (*29*). However, it is possible that non–US-born TB treatment survivors emigrated from the United States more frequently than US-born TB treatment survivors, which might affect the mortality rate measurements because the NDI only captures deaths within the United States. We are unaware of US-based emigration data for TB treatment survivors, and challenges exist linking those data to minoritized populations within the NDI database because of higher rates of missing Social Security numbers (*32*) and differences in access to end-of-life care among immigrants (*33*). Those 2 limitations could lead to an undercount of posttreatment deaths among non–US-born persons. However, the other US-based study on mortality rates after TB treatment had a similar percentage of non–US-born persons compared with persons with TB identified in this study (58% vs. 51%) and also found a higher cumulative death rate among US-born persons (37%) compared with non–US-born persons (9%) (*9*). Other studies have also shown that co-existing illnesses are associated with increased posttreatment death rates (*6*,*26*,*34*). For example, a California-based study found that diabetes, HIV co-infection, and end-stage renal disease were associated with an increased death HR 1 year after TB diagnosis compared with age- and sex-matched control patients without TB (*34*). However, that study did not specifically measure TB mortality rates after treatment completion and did not stratify deaths by place of birth.

Table 5. Mortality rates and standardized mortality ratios for posttreatment groups compared with the general Georgia population in study of mortality rates after TB treatment, Georgia, USA, 2008–2019*

Groups	Mortality rate (95% CI)	Standardized mortality ratio (95% CI)
Overall TB cohort†		
Crude mortality rate	12.69 (11.12–14.43)	Referent
Mortality rate adjusted for age and sex	9.77 (8.29–11.43)	0.91 (0.75–1.07)
Mortality rate adjusted for age only	10.50 (9.09–12.07)	0.98 (0.84–1.12)
Culture confirmed and treatment completed‡		
Crude mortality rate	14.19 (12.20–16.41)	Referent
Mortality rate adjusted for age and sex	10.92 (9.08–13.03)	1.02 (0.84–1.20)
Non-Hispanic White and Black persons§		
Crude mortality rate	22.84 (19.79–26.23)	Referent
Mortality rate adjusted for age and race	19.73 (15.64–24.56)	1.82 (1.60–2.04)¶
US-born persons only#		
Crude mortality rate	22.51(19.50–25.84)	Referent
Mortality rate adjusted for age and sex	16.93 (14.10–20.15)	1.58 (1.41–1.76)

*All rates are per 1,000 person-years. Georgia population had 900,874 deaths; person-time = 90,796,252 person-years. SMR, standardized mortality ratio; TB, tuberculosis.
†Number of patients in TB cohort was 3,182. Overall TB cohort follow-up time was 18,426 person-years (no. deaths = 233).
‡Total number was 2,248. Culture-confirmed TB follow-up time was 12,820 person-years (no. deaths = 182).
§Total number was 1,899. Follow-up time was 10,797 person-years (no. deaths = 201).
¶Compared with non-Hispanic White and non-Hispanic Black persons in Georgia.
#Total number was 1,557. Follow-up time was 8,929 person-years (no. deaths = 201).

Persons with TB/HIV co-infection had a posttreatment death HR of 1.87 compared with non–co-infected persons (referent 1.0) in the TB cohort. Moreover, HIV-related deaths were ≈20-fold higher among those who died after TB treatment than those in the Georgia population (9.9% vs. 0.5%); TB/HIV co-infected persons also died at a younger mean age than those in the Georgia population (49.6 vs. 70.2 years). Persons with HIV/TB co-infection in the TB cohort were younger than non–co-infected persons but had higher rates of homelessness, excess alcohol use, and injection drug use. We have found that persons co-infected with HIV and TB in Atlanta, Georgia, had low rates of virus suppression after TB treatment (45% had virus suppression 1 year after TB treatment) (*35*), which might explain the poor post–TB treatment outcomes. Our findings suggest that strengthening the HIV care continuum might avert deaths among HIV co-infected TB survivors and should be a care priority after TB treatment.

The first limitation of our study is that we did not have individual-level data for the overall Georgia population. Second, the TB database has limitations, such as insufficient data needed to use the World Health Organization TB outcomes classification, lack of tobacco use data, and using nonstandardized definitions for alcohol use. Third, the NDI does not capture deaths that occurred outside of the United States. The strengths of our study are that TB disease notification is mandatory in Georgia and, thus, it is unlikely we missed TB cases, and we ascertained mortality rates through the NDI, which is the most complete database of deaths in the United States. Our findings might not be generalizable to the entire United States, and further studies that include nationwide data are needed.

In conclusion, we found that US-born TB survivors have higher mortality rates than persons in the general population in Georgia, and HIV, excess alcohol use, diabetes mellitus, and end-stage renal disease are risk factors for death after TB treatment. Currently, no guidance exists for post–TB treatment care in Georgia, and such care was not addressed in the latest American Thoracic Society/CDC/Infectious Diseases Society of America guidelines (*12*,*13*). The 2022 Canada TB standards recommend linkage of posttreatment care to primary care providers for TB survivors (*36*). Our findings support this recommendation because the conditions associated with increased posttreatment death in this study are usually treated by primary and HIV care providers in the United States. Most persons with TB in the United States receive ≥6 months of treatment, usually under directly observed therapy (*37*). Our findings indicate that, to prevent death after TB, comprehensive care during and after treatment should also consider social determinants of health and co-existing illnesses, which might be more prevalent among US-born persons.

The study was supported by the US National Institutes of Health, National Center for Advancing Translational Sciences (grant no. UL1TR002378) and National Institute of Allergy and Infectious Diseases (grant no. P30AI168386), and by the Conselho Nacional de Desenvolvimento Científico e Tecnológico of Brazil (grant no. 310566/2021-5 to A.G.P.).

About the Author

Dr. Gorvetzian is an internal medicine resident at the University of Colorado Anschutz Medical Campus. Her research interests focus on TB, HIV, and aging.

References

1. World Health Organization. Global tuberculosis report 2023 [cited 2024 Aug 1]. https://www.who.int/publications/i/item/9789240083851
2. Byrne AL, Marais BJ, Mitnick CD, Lecca L, Marks GB. Tuberculosis and chronic respiratory disease: a systematic review. Int J Infect Dis. 2015;32:138–46. https://doi.org/10.1016/j.ijid.2014.12.016
3. Huaman MA, Henson D, Ticona E, Sterling TR, Garvy BA. Tuberculosis and cardiovascular disease: linking the epidemics. Trop Dis Travel Med Vaccines. 2015;1:10. https://doi.org/10.1186/s40794-015-0014-5
4. Romanowski K, Baumann B, Basham CA, Ahmad Khan F, Fox GJ, Johnston JC. Long-term all-cause mortality in people treated for tuberculosis: a systematic review and meta-analysis. Lancet Infect Dis. 2019;19:1129–37. https://doi.org/10.1016/S1473-3099(19)30309-3
5. Menzies NA, Quaife M, Allwood BW, Byrne AL, Coussens AK, Harries AD, et al. Lifetime burden of disease due to incident tuberculosis: a global reappraisal including post-tuberculosis sequelae. Lancet Glob Health. 2021;9:e1679–87. https://doi.org/10.1016/S2214-109X(21)00367-3
6. Basham CA, Karim ME, Cook VJ, Patrick DM, Johnston JC. Post-tuberculosis mortality risk among immigrants to British Columbia, Canada, 1985–2015: a time-dependent Cox regression analysis of linked immigration, public health, and vital statistics data. Can J Public Health. 2021;112:132–41. https://doi.org/10.17269/s41997-020-00345-y
7. Uplekar M, Weil D, Lonnroth K, Jaramillo E, Lienhardt C, Dias HM, et al.; for WHO's Global TB Programme. WHO's new end TB strategy. Lancet. 2015;385:1799–801. https://doi.org/10.1016/S0140-6736(15)60570-0
8. Dodd PJ, Yuen CM, Jayasooriya SM, van der Zalm MM, Seddon JA. Quantifying the global number of tuberculosis survivors: a modelling study. Lancet Infect Dis. 2021;21:984–92. https://doi.org/10.1016/S1473-3099(20)30919-1
9. Miller TL, Wilson FA, Pang JW, Beavers S, Hoger S, Sharnprapai S, et al. Mortality hazard and survival after tuberculosis treatment. Am J Public Health. 2015;105:930–7. https://doi.org/10.2105/AJPH.2014.302431
10. Centers for Disease Control and Prevention, National Center for Health Statistics. National Death Index [cited 2024 Aug 1]. https://www.cdc.gov/nchs/ndi

11. Georgia Department of Public Health. 2020 Georgia TB reference guide [cited 2024 Aug 1]. https://dph.georgia.gov/document/document/2020georgiatbreferenceguidepdf/download
12. Nahid P, Mase SR, Migliori GB, Sotgiu G, Bothamley GH, Brozek JL, et al. Treatment of drug-resistant tuberculosis. An official ATS/CDC/ERS/IDSA clinical practice guideline. Am J Respir Crit Care Med. 2019;200:e93–142. https://doi.org/10.1164/rccm.201909-1874ST
13. Nahid P, Dorman SE, Alipanah N, Barry PM, Brozek JL, Cattamanchi A, et al. Official American Thoracic Society/Centers for Disease Control and Prevention/Infectious Diseases Society of America clinical practice guidelines: treatment of drug-susceptible tuberculosis. Clin Infect Dis. 2016;63:e147–95. https://doi.org/10.1093/cid/ciw376
14. Georgia Department of Public Health. State electronic notifiable disease surveillance system [cited 2024 Oct 4]. https://sendss.state.ga.us
15. Georgia Department of Public Health. Online analytical statistical information system [cited 2024 Oct 4]. https://oasis.state.ga.us
16. Georgia Department of Public Health. Diabetes [cited 2024 Jan 5]. https://dph.georgia.gov/chronic-disease-prevention/diabetes
17. Centers for Disease Control and Prevention. BRFSS prevalence and trends data, alcohol consumption, heavy drinking, 2014 [cited 2023 Jan 5]. https://nccd.cdc.gov/BRFSSPrevalence/rdPage.aspx
18. Georgia Department of Public Health. Georgia HIV surveillance data [cited 2024 Aug 2]. https://dph.georgia.gov/epidemiology/georgias-hivaids-epidemiology-section/georgia-hiv-surveillance-data
19. US Department of Housing and Urban Development, Office of Policy Development and Research. 2014 AHAR: Part 1—PIT estimates of homelessness in the US [cited 2024 Aug 2]. https://www.huduser.gov/portal/datasets/ahar/2014-ahar-part-1-pit-estimates-of-homelessness.html
20. World Population Review. Immigrants by state 2024 [cited 2024 Jan 5]. https://worldpopulationreview.com/state-rankings/immigrants-by-state
21. Akaike H. A new look at the statistical model identification. IEEE Trans Automat Contr. 1974;19:716–23. https://doi.org/10.1109/TAC.1974.1100705
22. Klein RJ, Schoenborn CA. Centers for Disease Control and Prevention. Age adjustment using the 2000 projected U.S. population. Statistical notes, January 2001 [cited 2024 Oct 4]. https://www.cdc.gov/nchs/data/statnt/statnt20.pdf
23. US Department of Commerce, Bureau of the Census. Population projections of the United States by age, sex, race, and Hispanic origin: 1995 to 2050 [cited 2024 Aug 1]. https://www.census.gov/content/dam/Census/library/publications/1996/demo/p25-1130.pdf
24. von Elm E, Altman DG, Egger M, Pocock SJ, Gøtzsche PC, Vandenbroucke JP; STROBE Initiative. The Strengthening the Reporting of Observational Studies in Epidemiology (STROBE) statement: guidelines for reporting observational studies. PLoS Med. 2007;4:e296. https://doi.org/10.1371/journal.pmed.0040296
25. Park SC, Kang MJ, Han CH, Lee SM, Kim CJ, Lee JM, et al. Long-term mortality of patients with tuberculosis in Korea. Int J Tuberc Lung Dis. 2020;24:492–8. https://doi.org/10.5588/ijtld.19.0324
26. Choi H, Han K, Jung J-H, Park SH, Kim SH, Kang HK, et al. Long-term mortality of tuberculosis survivors in Korea: a population-based longitudinal study. Clin Infect Dis. 2023;76:e973–81. https://doi.org/10.1093/cid/ciac411
27. Joseph Y, Yao Z, Dua A, Severe P, Collins SE, Bang H, et al. Long-term mortality after tuberculosis treatment among persons living with HIV in Haiti. J Int AIDS Soc. 2021;24:e25721. https://doi.org/10.1002/jia2.25721
28. Dangisso MH, Woldesemayat EM, Datiko DG, Lindtjørn B. Long-term outcome of smear-positive tuberculosis patients after initiation and completion of treatment: a ten-year retrospective cohort study. PLoS One. 2018;13:e0193396. https://doi.org/10.1371/journal.pone.0193396
29. Liu Y, Zheng Y, Chen J, Shi Y, Shan LY, Wang S, et al. Tuberculosis-associated mortality and its risk factors in a district of Shanghai, China: a retrospective cohort study. Int J Tuberc Lung Dis. 2018;22:655–60. https://doi.org/10.5588/ijtld.17.0726
30. Wang X-H, Ma A-G, Han X-X, Liang H, Wang D, Schouten E, et al. Survival and associated mortality risk factors among post-treatment pulmonary tubercolosis patients in the northwest of China. Eur Rev Med Pharmacol Sci. 2015;19:2016–25.
31. Hendi AS, Ho JY. Immigration and improvements in American life expectancy. SSM Popul Health. 2021;15:100914. https://doi.org/10.1016/j.ssmph.2021.100914
32. Miller EA, McCarty FA, Parker JD. Racial and ethnic differences in a linkage with the National Death Index. Ethn Dis. 2017;27:77–84.
33. Gray NA, Boucher NA, Cervantes L, Berlinger N, Smith SK, Johnson KS. Hospice access and scope of services for undocumented immigrants: a clinician survey. J Palliat Med. 2021;24:1167–73. https://doi.org/10.1089/jpm.2020.0547
34. Lee-Rodriguez C, Wada PY, Hung Y-Y, Skarbinski J. Association of mortality and years of potential life lost with active tuberculosis in the United States. JAMA Netw Open. 2020;3:e2014481. https://doi.org/10.1001/jamanetworkopen.2020.14481
35. Schechter MC, Bizune D, Kagei M, Holland DP, Del Rio C, Yamin A, et al. Challenges across the HIV care continuum for patients with HIV/TB co-infection in Atlanta, GA. Open Forum Infect Dis. 2018;5:ofy063. https://doi.org/10.1093/ofid/ofy063
36. Johnston JC, Cooper R, Menzies D. Chapter 5: treatment of tuberculosis disease. Can J Resp Crit Care Sleep Med. 2022;6:66–76. https://doi.org/10.1080/24745332.2022.2036504
37. Tsang CA, Patel NN, Stout JE, Fernando R, Pratt R, Goswami ND. Factors associated with receiving longer than recommended therapy among culture-negative pulmonary tuberculosis patients. Open Forum Infect Dis. 2022;9:ofac630. https://doi.org/10.1093/ofid/ofac630

Address for correspondence: Marcos C. Schechter, Department of Medicine, Division of Infectious Diseases, Emory University School of Medicine, 49 Jesse Hill Jr Drive SE, Atlanta, GA 30303, USA; email: mcoutin@emory.edu

Vibrio parahaemolyticus Foodborne Illness Associated with Oysters, Australia, 2021–2022

Emily Fearnley, Lex E.X. Leong, Alessia Centofanti, Paul Dowsett, Barry G. Combs, Anthony D.K. Draper, Helen Hocking, Ben Howden, Kristy Horan, Mathilda Wilmot, Avram Levy, Louise A. Cooley, Karina J. Kennedy, Qinning Wang, Alicia Arnott, Rikki M.A. Graham, Vitali Sinchenko, Amy V. Jennison, Stacey Kane, Rose Wright

The bacterium *Vibrio parahaemolyticus* is ubiquitous in tropical and temperate waters throughout the world and causes infections in humans resulting from water exposure and from ingestion of contaminated raw or undercooked seafood, such as oysters. We describe a nationwide outbreak of enteric infections caused by *Vibrio parahaemolyticus* in Australia during September 2021–January 2022. A total of 268 persons were linked with the outbreak, 97% of whom reported consuming Australia-grown oysters. Cases were reported from all states and territories of Australia. The outbreak comprised 2 distinct strains of *V. parahaemolyticus*, sequence types 417 and 50. We traced oysters with *V. parahaemolyticus* proliferation back to a common growing region within the state of South Australia. The outbreak prompted a national recall of oysters and subsequent improvements in postharvest processing of the shellfish.

Vibrio parahaemolyticus is a marine and estuarine bacterium that is ubiquitous in tropical and temperate waters worldwide (*1*). Infections, including wound infections, can occur in humans through exposure to water, and enteric infections are attributed most commonly to ingestion of raw or undercooked seafood. Invasive bloodstream infections and death rarely occur (*2*,*3*). Human infection is not associated with person-to-person spread or transmission through the fecal–oral route, and environmental presence of *V. parahaemolyticus* has not been linked to fecal contamination (*4*). The virulence of *V. parahaemolyticus* is associated with the presence of a thermostable direct hemolysin (coded by *tdh* gene) or thermostable related hemolysin (*trh* gene) (*5*).

Foodborne *V. parahaemolyticus* outbreaks have been reported across Asia, the United States, South America, Europe, and New Zealand, predominantly associated with consumption of filter-feeding bivalve shellfish, such as oysters and mussels (*6*–*12*). *V. parahaemolyticus* infections show seasonal patterns, with increases in warmer months, because *V. parahaemolyticus* will grow in seawater at temperatures >14°C–19°C (*6*). Climate change can increase the distribution and incidence of *V. parahaemolyticus* (*6*,*13*), and a rise in water temperature is the main environmental factor associated with growth of *V. parahaemolyticus* in oysters. Postharvest risk reduction strategies focus on rapid cooling and maintaining cold refrigeration of oysters throughout the supply chain to prevent bacterial growth, which occurs at air temperatures >10°C (*14*).

Until recently, foodborne outbreaks of *V. parahaemolyticus* were rare in Australia. Only 4 outbreaks

Author affiliations: South Australian Department for Health and Wellbeing, Adelaide, South Australia, Australia (E. Fearnley, A. Centofanti); University of South Australia, Adelaide (L.E.X. Leong); SA Pathology, Adelaide (L.E.X. Leong, H. Hocking); Department of Primary Industries and Regions, Adelaide (P. Dowsett); Department of Health Western Australia, Perth, Western Australia, Australia (B.G. Combs); Northern Territory Centre for Disease Control, Darwin, Northern Territory, Australia (A.D.K. Draper); The Peter Doherty Institute for Infection and Immunity, Melbourne, Victoria, Australia (B. Howden, K. Horan, M. Wilmont); PathWest Laboratory Medicine, Perth, (A. Levy); Royal Hobart Hospital, Hobart, Tasmania, Australia (L.A. Cooley); Canberra Hospital and Health Services, Canberra, Australian Capital Territory, Australia (K.J. Kennedy); Westmead Hospital, Westmead, New South Wales, Australia (Q. Wang); The University of Sydney, Sydney, New South Wales, Australia (A. Arnott, V. Sintchenko); Queensland Health Forensic and Scientific Services, Coopers Plains, Queensland, Australia (R.M.A. Graham, A.V. Jennison); Australian Government Department of Health and Aged Care, Canberra (S. Kane, R. Wright)

DOI: http://doi.org/10.3201/eid3011.240172

were reported during 2002–2019, affecting a total of 24 persons (*15*). Two previously reported outbreaks were linked to consumption of oysters; 1 from oysters produced in Tasmania and 1 from oysters grown in South Australia. Only 29 locally acquired, sporadic foodborne cases of *V. parahaemolyticus* were reported in Australia in 2016–2020; 22 of the infected persons reporting oyster consumption (76%) (*15*). *V. parahaemolyticus* infections might be underreported in Australia because pathology laboratories rarely include it in routine fecal testing procedures and the infection is a notifiable condition in only 4 of the 8 states and territories of Australia.

In September 2021, at the end of the winter season in the Southern Hemisphere, health officials identified an increase in locally acquired *V. parahaemolyticus* cases in South Australia, and a similar trend was later noted in other jurisdictions of Australia. In November 2021, through the OzFoodNet network, a multijurisdictional outbreak investigation commenced to coordinate the public health response. OzFoodNet is a network of epidemiologists across Australia who are responsible for undertaking surveillance and outbreak investigations of foodborne disease (*16*). Investigators worked closely with jurisdictional public health laboratories and with the Australia food regulatory authorities who implement control measures.

Methods

V. parahaemolyticus infection is a notifiable disease under legislation in the Australia jurisdictions of the Northern Territory, South Australia, Tasmania, and Western Australia, where laboratories are required to report cases to their respective health departments. Public health authorities contacted diagnostic laboratories in the remaining Australia jurisdictions to request reported detections of *V. parahaemolyticus* in fecal specimens (under the auspices of an OzFoodNet multijurisdictional outbreak investigation).

Epidemiologic Investigation

We defined an outbreak case as illness in any person with a fecal specimen testing positive for *V. parahaemolyticus* during September 7, 2021–February 18, 2022. We conducted a descriptive case series investigation, which entailed telephone interviews of case-patient using a standardized questionnaire to obtain demographic information (age, sex, jurisdiction of residence), onset of illness, symptoms, medications, risk factors, and consumption of seafood during the exposure period (defined as 7 days before onset).

We classified cases as confirmed outbreak cases if single-nucleotide polymorphism (SNP) cluster analysis was performed on sequence type (ST) 417 or ST50 *V. parahaemolyticus* isolates on AusTrakka (a national genomic surveillance platform) and determined to be highly related within each ST. We considered outbreak cases as probable if they were typed as ST417 or ST50 without further phylogenetic analysis on AusTrakka and as possible if isolates were unable to be further typed (no ST). Cases were excluded if case-patients had traveled overseas in the 7 days before onset, if another ST was identified, or if the sequences did not cluster by phylogenetic analysis on AusTrakka. We used a broad case definition to include both STs in the outbreak investigation to describe the overall increase in locally acquired *V. parahaemolyticus* cases.

We entered case data into REDCap v10.3.4 (Vanderbilt University, https://projectredcap.org). We calculated proportions, medians, and ranges by using Stata BE v17 (Stata, https://www.stata.com). Where data were missing, we calculated a proportion with known responses only.

Environmental Investigations

Jurisdictional food regulatory authorities conducted traceback investigations for oyster exposures. Traceback activity revealed harvest area and dates, and investigators then sought information relative to temperature control. Food regulatory personnel collected oyster samples from case households and retail premises. The South Australian Shellfish Quality Assurance Program collected oyster samples direct from growers. Technicians processed and tested oyster samples in approved laboratories across jurisdictions to determine the presence of *V. parahaemolyticus* according to the Australian standards for food microbiology examination for specific organisms. Methods involved grinding 25 g of oysters with alkaline peptone water before overnight incubation at 36°C ± 2°C. Laboratory technicians isolated *V. parahaemolyticus* from the ground samples on thiosulfate–citrate–bile salts–sucrose agar at 36°C ± 2°C. They collected positive green-colonies and sent the samples to public health laboratories for whole-genome sequencing (WGS).

Genomic Sequencing and Analysis of *V. parahaemolyticus*

Public health laboratories in each jurisdiction sequenced *V. parahaemolyticus* isolates from cases and food samples for species confirmation and ST determination through multilocus sequence typing (https://github.com/tseemann/mlst) (*17*). Technicians performed WGS by using Illumina platforms (MiSeq and NextSeq 500/550; Illumina, https://illumina.com) with paired-end reads. Public health

laboratories shared the raw sequencing reads of most isolates to AusTrakka (*18*). The national analysis team performed quality filtering, virulence gene detection, and phylogenetic analyses by using Snippy version 4.6.0 (https://github.com/tseemann/snippy) for cluster identification. Laboratory researchers determined genomic clusters for respective STs by using single-linkage clustering based on the SNP distance threshold of 5 SNPs, 10 SNPs, and 20 SNPs. The laboratories also performed pangenome analysis by using Roary version 3.13.0 (https://sanger-pathogens.github.io/Roary) (*19*) to include other publicly available *V. parahaemolyticus* genomes from PubMLST (https://pubmlst.org) and visualized a phylogenetic tree by using ggtree (https://guangchuangyu.github.io/software/ggtree). Genome sequences were uploaded to the National Center for Biotechnology Information's Sequence Read Archive under the BioProject Accession nos. PRJNA1129299, PRJNA783474, PRJNA856407, and PRJNA1131944.

Results

Epidemiologic Investigation

We investigated a total of 268 outbreak cases from all Australia jurisdictions:184 confirmed cases, 29 probable cases, and 55 possible cases (Figure 1). The outbreak occurred over a 5-month period, and the peak of cases occurred in mid-November 2021. Infections of ST50 were reported initially, followed by predominant reports of ST417 infections; subsequent reports then revealed a period of high overlap of the 2 STs. We noted the highest percentage of reported cases from residents of South Australia (28%, n = 76), followed by 2 jurisdictions where *V. parahaemolyticus* is not notifiable, Victoria (26%, n = 69) and Queensland (22%, n = 59) (Table 1). Some case-patients reported spending their entire incubation period in other jurisdictions, including a Tasmania resident exposed in South Australia and a South Australia resident exposed in Western Australia. More case-patients were male (57%) than female (43%). All jurisdictions with >5 outbreak cases included cases of both ST50 and ST417. The median age of case-patients was 52 years (range 1–90 years) (Table 2).

Of those with available information, 25% of case patients (51/206) sought treatment at hospital emergency departments and 13% (27/209) of case-patients were hospitalized; emergency department information was not reported for 3 case-patients. Of 24 cases with length of hospitalization recorded, the median stay was 2.5 days (range 1–7 days). There were no deaths. Of those who responded to symptom-specific questions, all 195 case-patients interviewed reported diarrhea, and 85% (165) reported abdominal pain. One case-patient had *V. parahaemolyticus* isolated from both a fecal specimen and blood culture. The median duration of illness for 131 cases with data available was 7 days (range 1–17 days); however, 40 cases were still unwell at the time of interview and were therefore not included in this calculation.

Of 206 case-patients interviewed, 199 (97%) reported consuming oysters, 189 (92%) reported consuming at least some of the oysters raw, and 25 (12%) reported consuming oysters for ≥1 meal in the week before onset. For case-patients who consumed oysters on only a single occasion (n = 131), the median incubation period was 1 day (range 4 hours to 7 days). The median number of oysters eaten per case-patient was 6 (range 1–31 oysters). Case-patients purchased oysters at a range of

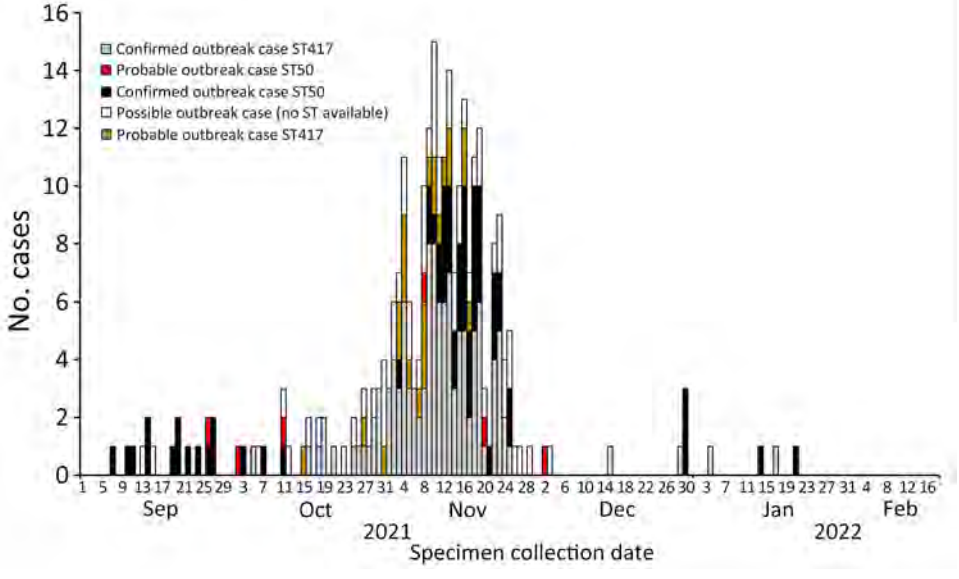

Figure 1. Epidemic curve of *Vibrio parahaemolyticus* outbreak cases by specimen collection date, outbreak case classification, and sequence typing, Australia, September 7, 2021–February 18, 2022. ST, sequence type.

Table 1. *Vibrio parahaemolyticus* outbreak cases (by jurisdiction of residence and ST, Australia, September 7,2021–February 18, 2022*

Jurisdiction of residence	ST50	ST417	No ST available	Total no. (%) cases
South Australia	31	44	1	76 (28)
Victoria	23	46	0	69 (26)
Queensland	4	11	44	59 (22)
Western Australia	7	23	3	33 (12)
New South Wales	5	15	6	26 (10)
Australian Capital Territory	0	3	0	3 (1)
Tasmania	0	1	0	1 (0.4)
Northern Territory	0	0	1	1 (0.4)
Total	70	143	55	268

*ST, sequence type.

venues, including restaurants (n = 71), supermarkets or seafood stores (n = 23), farms (n = 17), oyster tours (n = 9), and takeaway venues (n = 8). Exposure to other seafood was common, including 41% (n = 84) who reported consuming fish (varied types) and 37% (n = 76) who consumed prawns in the 7 days before onset. For those who consumed fish or prawns, most reported food to have been cooked. Less than 20% of case patients reported consuming seafood other than oysters, fish, or prawns (Table 3). From 166 case interviews, 25% (42) of case-patients reported they had taken medication that reduced stomach acid (e.g., reflux or ulcer medications) in the month before onset.

Environmental Investigation

Traceback of oysters was complex because the supply chain could include farmers, processors (harvesters), brokers, wholesalers, retailers, and food services. Brokers and processors could receive stock from multiple growers on the same day and often from different growing regions. Processors could manage multiple suppliers on the same day, and opportunities for traceability were sometimes lost because records lacked details of where batches had been distributed. Sometimes, processors recorded shuck dates but not harvest dates on packaging. There was no single method of easily identifying unlabeled oysters once original traceability was misplaced by the processor. Traceback indicated oysters had been sourced from different growing regions in South Australia, including Smoky Bay, Streaky Bay, and Coffin Bay, with the largest proportion traced back to Coffin Bay. Within Coffin Bay, there were 32 accredited growers, and it was impossible to definitively link oysters to any single grower. In total, 173 oyster exposures were able to be traced back to Coffin Bay.

Table 2. *Vibrio parahaemolyticus* outbreak cases by demographic and clinical characteristics, Australia, September 7, 2021–February 18, 2022

Characteristic	No. (%) cases, n = 268
Sex	
M	152 (57)
F	115 (43)
Not stated	1 (0.4)
Age group, y	
0–9	1 (0.4)
10–19	3 (1)
20–29	12 (5)
30–39	38 (14)
40–49	64 (24)
50–59	58 (22)
60–69	59 (22)
70–79	23 (9)
≥80	10 (4)
Symptoms*	
Diarrhea	206/206 (100)
Watery diarrhea	159/161 (99)
Abdominal pain	165/195 (85)
Lethargy	153/191 (80)
Nausea	138/200 (69)
Fever	98/203 (48)
Headache	96/198 (48)
Vomiting	71/204 (35)
Bloody diarrhea	8/181 (4)

*Values indicate number of case-patients who reported the symptom of those who answered the symptom question. Not all case-patients were asked about all symptoms.

Of 117 oyster samples tested for *V. parahaemolyticus,* 14 tested positive (7 from South Australia, 3 from Queensland, 3 from Victoria, 1 from Western Australia). All positive oysters were ST417. Those *V. parahaemolyticus*–positive oyster samples were from various sources, including case-patient households, retail vendors, distributors, and direct-purchase farms. We traced the original source of all 14 positive oyster samples to Coffin Bay.

The Department of Primary Industries and Regions of South Australia (PIRSA) closed the Coffin Bay growing area on November 16, 2021, for harvest of oysters. A national recall of Coffin Bay raw pacific oysters occurred on November 19, 2021, conducted via Emergency Orders under the South Australian Food Act 2001. PIRSA also served compliance orders on accredited growers in Coffin Bay on November 18, 2021, specifying legislative requirements for growers to resume harvesting. Growers were required to implement a *Vibrio* control program and provide evidence that they had infrastructure available to maintain cold chain, could address food safety requirements, could verify monitoring and traceability, and

could validate refrigeration capabilities. The *Vibrio* control program required growers to place oysters under active refrigeration within 7 hours of harvest, ensure oysters were at ≤10°C within 24 hours of harvest, ensure oysters were dispatched and transported at ≤10°C, and ensure enhanced traceability by including the harvest date, area, and aquaculture license number on invoices. *Vibrio* control programs were implemented in all oyster-growing areas across South Australia during this outbreak investigation. PIRSA also conducted microbiological sampling of oysters to clear growing zones in Coffin Bay before emergency orders were able to be lifted.

Genomic Epidemiology and Pathogenicity

Most outbreak cases (79%) could be classified as confirmed or probable cases, including 143 cases typed as ST417 and 70 cases typed as ST50. Cases of both STs occurred throughout the duration of the outbreak (Figure 1). All isolates from the 14 positive oyster samples were ST417 *V. parahaemolyticus*.

Phylogeny confirmed that ST417 and ST50 *V. parahaemolyticus* were not closely related (Figure 2, http://wwwnc.cdc.gov/EID/article/30/11/24-0172-F2.htm). Because of the distinct nature of those strains of *V. parahaemolyticus*, we performed phylogenetic SNP clustering analyses on each ST individually. We grouped all clinical cases of ST417 and oyster samples from Australia submitted for national analysis in AusTrakka (n = 135) into a single cluster at a 5-SNP threshold. Clustering analysis of *V. parahaemolyticus* ST50 grouped 65 clinical cases at the 10-SNP threshold. Further analysis at the narrower 5-SNP threshold revealed 2 distinct but related clusters (n = 35 and n = 28; 2 were unclustered at 5 SNPs). We excluded 4 cases from the outbreak based on genomic analysis: 1 ST50 case unclustered at the 10-SNP threshold on phylogenetic analysis in AusTrakka and 3 cases that were different STs (2 ST1140 and 1 ST36).

Both STs of *V. parahaemolyticus* isolated from cases in this outbreak investigation harbored virulence genes required for pathogenicity. Specifically, all *V. parahaemolyticus* ST417 isolates harbored the virulence gene *trh*, and all ST50 harbored 2 virulence genes, *tdh* and *trh*.

Discussion

This *V. parahaemolyticus* outbreak was caused by 2 STs and had a considerable effect on the population of Australia because of the nationwide distribution of oysters across mainland jurisdictions and cases occurring over a 5-month period. Recent investigations of other *V. parahaemolyticus* outbreaks have focused mostly on point source events, such as outbreaks on cruise ships (*8*,*20*,*21*). The communitywide outbreak in this report highlights the potential risks associated with consumption of raw oysters in Australia. Raw shellfish, particularly oysters, are known to be a common source of *Vibrio* foodborne illness, but recent trends observe increasing numbers of sporadic and outbreak cases, across an internationally wider span, somewhere cases had not been previously reported (*8*,*11*,*22*). *V. parahaemolyticus* has been isolated from other shellfish, including mussels, prawns, clams, and scallops during food surveillance studies, and has been identified as the cause of outbreaks in countries other than Australia (*3*,*23*–*25*).

The identification of 2 unrelated STs, ST417 and ST50, within this outbreak indicated the cause to be more relative to environmental factors influencing favorable growth conditions for *V. parahaemolyticus* across the oyster-growing region than to a single temperature-abuse error or single point source event. The appearance of those 2 strains could also be indicative of >1 outbreak occurring at the same time, with common contributing factors. However, multiple strains or types of a pathogen can cause discrete outbreaks and require a common public health investigation and response (*26*,*27*). The epidemiologic evidence in this investigation indicated raw oysters grown in South Australia as the cause of both ST417 and ST50 *V. parahaemolyticus* infections across Australia. Previous *V. parahaemolyticus* outbreaks have reported single-strain infections, predominantly by using traditional O and K serotyping methods (*8*,*25*). Longitudinal studies in Asia have identified a range of strains within a region (*28*), and other reports have highlighted highly virulent pandemic strains (e.g., ST36)

Table 3. *Vibrio parahaemolyticus* outbreak case-patients reporting exposure to seafood in the 7 days before onset of illness, Australia, September 7, 2021–February 18, 2022

Seafood	No. (%) cases exposed
Oysters	199 (97)
Oysters eaten raw	189 (95)
Fish*	84 (41)
Fish eaten raw	14 (17)
Prawns	76 (37)
Prawns eaten raw	4 (11)
Squid	37 (18)
Scallops	29 (14)
Mussels	19 (9)
Lobster/crayfish	17 (8)
Crab	13 (6)
Octopus	11 (5)
Clams/cockles	5 (2)
Roe	5 (2)
Abalone	3 (2)

*Fish includes multiple types of fresh fish and canned fish and different species of fish, including salmon, tuna, barramundi, kingfish, swordfish, whiting, snapper, and flathead.

detected across a widening international geographic range (*1*,*13*). Although minimal data are available in Australia regarding *V. parahaemolyticus* strains linked to locally acquired cases, recent increased use of genomic methods and practices will likely change that. The emergence of WGS characterization in Australia will also contribute to global knowledge regarding emerging and pathogenic strains. The presence of the *trh* virulence gene in both strains within this outbreak—and the additional *tdh* gene in the ST50 case isolates—correlates with prior literature noting that the presence of those virulence genes contributes to clinical symptoms but that both genes are not required to cause illness (*29*).

International risk assessments have been conducted for *V. parahaemolyticus* in seafood, noting the pathogenicity of the organism, the growth of *V. parahaemolyticus* increasing with increased water temperatures, and the need for strict postharvest controls to reduce the risk for foodborne disease (*6*,*12*). Outbreaks have occurred more frequently during warmer months (*3*) and at times when seawater temperatures have increased (*8*,*20*) or other environmental factors have had an influence (e.g., El Niño events or decreases in salinity) (*10*,*30*). In response to the outbreak we have described, oyster growers implemented postharvest controls through a *Vibrio* control program, where oysters were placed under active refrigeration. General trends of increased sea surface temperatures in Australia (*31*) and the seasonal occurrence of the Leeuwin current, which brings warm tropical waters to Western and South Australia (*31*), potentially created favorable conditions for growth of *V. parahaemolyticus* in South Australia oyster-growing bays. We believe that further research would improve understanding of risk factors for *V. parahaemolyticus* outbreaks in Australia's prone regions, including ongoing environmental surveillance at harvest sites to monitor seawater temperatures, salinity, and harvest conditions, as well as at points along the storage and transport chain to consumers.

We noted that many outbreak case-patients in this study consumed medication that reduces stomach acid, a finding noted in previous studies that investigated risk for *V. parahaemolyticus* and other bacterial gastroenteric infections (*32*,*33*). Gastric acidity also decreases with age (*34*); therefore, infection susceptibility could increase with age, which is consistent with our observed median case patient age of 52 years. The fact that a large portion of our case-patients were older adults might also be related to food consumption patterns in the general population of Australia, where mollusks are less commonly eaten by children compared with adults (*35*). The outbreak we studied showed higher severity of illness than some previous outbreaks; for example, we noted 13% of case patients hospitalized and a single case with septicemia, compared with a study that investigated an outbreak associated with Alaska oysters, where there were no hospitalizations (*8*). Conversely, we noted a lower hospitalization rate for case-patients (13%) compared with a longer-term study that reported a hospitalization rate of 44% (*9*). Individual factors and the pathogenicity of different strains could affect disease severity in outbreaks.

The first limitation of our investigation is that culture for *V. parahaemolyticus* is not always attempted on diarrheal samples in diagnostic laboratories in Australia, and *V. parahaemolyticus* targets are often omitted in routine fecal multiplex PCR kits employed for direct detection of enteropathogens. Also, there was likely underreporting of cases because *V. parahaemolyticus* is not a notifiable condition in all jurisdictions in Australia. However, public health laboratories were contacted by their respective health departments and asked to provide information on enteric *V. parahaemolyticus* cases. Further typing of strains by WGS is also not consistently conducted across Australia and sometimes must be specifically requested if an outbreak is suspected. During this outbreak, some requests for further typing were made several weeks after the initial isolation, at which point no specimens were available for shipment to the public health laboratories. Because of incomplete typing of all case isolates in this outbreak, some cases might have been of a different ST and might not have been specifically linked to the current outbreak. In addition, *V. parahaemolyticus* outbreak cases we studied coincided with a national surge in SARS-CoV-2 infections in Australia, putting strain on public health resources. Therefore, not all case-patients were able to be interviewed, and not all isolates were able to be further typed.

There were also limitations in the traceback of oysters within a complex supply chain, including distributors and retailers receiving stock from multiple growers and different growing regions, leading to potential mixing of stock, some incomplete records and invoicing, and case-patients having multiple exposures to oysters within their incubation period. Mixing of oyster stock could also have contributed to the identification of multiple strains of *V. parahaemolyticus* in cases included in this outbreak. Although traceback was unable to be completed for all cases, oysters consumed by most casepatients were traced to at least the harvest area.

In conclusion, evidence for the source of this outbreak was strong, considering the oyster consumption among case-patients, traceback of the source of oysters consumed by case-patients, and identification of the same strain of *V. parahaemolyticus* in both oysters and case patients. The reduction in cases of *V. parahaemolyticus* after the recall of oysters and wide implementation of *Vibrio* control programs supports this evidence. This outbreak of *V. parahaemolyticus* associated with consumption of Australia-grown oysters, largely consumed raw, has led to improvements in postproduction control and traceability in the oyster industry in South Australia. The outbreak also spotlighted the virulent potential of *V. parahaemolyticus* and the value in distinguishing it as a nationally notifiable disease in Australia. Improved surveillance data, including strain identification from a wider range of regions, and a clearer understanding of underreporting have been highlighted by the World Health Organization as priorities for improving risk assessment processes for *V. parahaemolyticus* (*22*). Increased surveillance across all jurisdictions in Australia would improve outbreak detection and ensure a prompt and coordinated public health response.

Acknowledgments

The authors thank the extended outbreak investigation team for contributions to this investigation, including the public health officers, food regulators, primary industry regulators, diagnostic laboratories, and public health laboratories in all jurisdictions. We thank specifically SA Pathology, PathWest Laboratory Medicine WA, Institute of Clinical Pathology and Medical Research-NSW Health Pathology, and Public Health Microbiology Forensic and Scientific Services (Queensland), Microbiological Diagnostic Unit. We also thank the AusTrakka National Analysis team as well as the OzFoodNet Network, which is funded by the Australian Government Department of Health and Aged Care. We extend thanks also to Food Standards Australia and New Zealand and the Department of Agriculture, Fisheries, and Forestry.

Ethics approval was not required for this study because the outbreak investigation was conducted under the relevant state, territory, and national public health legislation for investigation and response to acute public health events.

About the Author

Dr Fearnley is an infectious disease epidemiologist, working in the OzFoodNet network of epidemiologists in Australia. Her research interests include foodborne and zoonotic diseases and enteric disease modeling.

References

1. Baker-Austin C, Oliver JD, Alam M, Ali A, Waldor MK, Qadri F, et al. *Vibrio* spp. infections. Nat Rev Dis Primers. 2018;4:1. https://doi.org/10.1038/s41572-018-0005-8
2. Heymann DL. Control of communicable diseases manual, 20th edition. Washington: American Public Health Association; 2015.
3. Daniels NA, MacKinnon L, Bishop R, Altekruse S, Ray B, Hammond RM, et al. *Vibrio parahaemolyticus* infections in the United States, 1973–1998. J Infect Dis. 2000;181:1661–6. https://doi.org/10.1086/315459
4. Mannas H, Mimouni R, Chaouqy N, Hamadi F, Martinez-Urtaza J. Occurrence of *Vibrio* and *Salmonella* species in mussels (*Mytilus galloprovincialis*) collected along the Moroccan Atlantic coast. Springerplus. 2014;3:265. https://doi.org/10.1186/2193-1801-3-265
5. Lopez-Joven C, de Blas I, Furones MD, Roque A. Prevalences of pathogenic and non-pathogenic *Vibrio parahaemolyticus* in mollusks from the Spanish Mediterranean Coast. Front Microbiol. 2015;6:736. https://doi.org/10.3389/fmicb.2015.00736
6. Wang D, Flint SH, Palmer JS, Gagic D, Fletcher GC, On SLW. Global expansion of *Vibrio parahaemolyticus* threatens the seafood industry: perspective on controlling its biofilm formation. Lebensm Wiss Technol. 2022;158:113182. https://doi.org/10.1016/j.lwt.2022.113182
7. González-Escalona N, Cachicas V, Acevedo C, Rioseco ML, Vergara JA, Cabello F, et al. *Vibrio parahaemolyticus* diarrhea, Chile, 1998 and 2004. Emerg Infect Dis. 2005;11:129–31. https://doi.org/10.3201/eid1101.040762
8. McLaughlin JB, DePaola A, Bopp CA, Martinek KA, Napolilli NP, Allison CG, et al. Outbreak of *Vibrio parahaemolyticus* gastroenteritis associated with Alaskan oysters. N Engl J Med. 2005;353:1463–70. https://doi.org/10.1056/NEJMoa051594
9. Wu Y, Wen J, Ma Y, Ma X, Chen Y. Epidemiology of foodborne disease outbreaks caused by *Vibrio parahaemolyticus,* China, 2003–2008. Food Control. 2014;46:197–202. https://doi.org/10.1016/j.foodcont.2014.05.023
10. Daniels NA, Ray B, Easton A, Marano N, Kahn E, McShan AL II, et al. Emergence of a new *Vibrio parahaemolyticus* serotype in raw oysters: a prevention quandary. JAMA. 2000;284:1541–5. https://doi.org/10.1001/jama.284.12.1541
11. Newton A, Kendall M, Vugia DJ, Henao OL, Mahon BE. Increasing rates of vibriosis in the United States, 1996–2010: review of surveillance data from 2 systems. Clin Infect Dis. 2012;54(Suppl 5):S391–5. https://doi.org/10.1093/cid/cis243
12. Food and Agriculture Organization of the United Nations/World Health Organization. Risk assessment of *Vibrio parahaemolyticus* in seafood: Interpretative summary and technical report.. Microbiological Risk Assessment Series No. 16. Rome: The Organizations; 2011 [cited 2022 Jul 28]. https://www.who.int/publications/i/item/9789241548175
13. Martinez-Urtaza J, van Aerle R, Abanto M, Haendiges J, Myers RA, Trinanes J, et al. Genomic variation and evolution of *Vibrio parahaemolyticus* ST36 over the course of a transcontinental epidemic expansion. MBio. 2017;8:e01425–17. https://doi.org/10.1128/mBio.01425-17
14. Food and Drug Administration. U.S. Department of Health and Human Services, 2005. Quantitative risk assessment on the public health impact of pathogenic *Vibrio parahaemolyticus* in raw oysters. [cited 2022 Jun 7]. https://www.fda.gov/food/cfsan-risk-safety-assessments/

quantitative-risk-assessment-public-health-impact-pathogenic-vibrio-parahaemolyticus-raw-oysters
15. Harlock M, Quinn S, Turnbull AR. Emergence of non-choleragenic *Vibrio* infections in Australia. Commun Dis Intell. 2022;46. https://doi.org/10.33321/cdi.2022.46.8
16. Australian Government Department of Health and Aged Care. 2023. OzFoodNet network. [cited 2023 Oct 6]. https://www.health.gov.au/our-work/ozfoodnet-network
17. Jolley KA, Maiden MCJ. BIGSdb: Scalable analysis of bacterial genome variation at the population level. BMC Bioinformatics. 2010;11:595. https://doi.org/10.1186/1471-2105-11-595
18. Hoang T, da Silva AG, Jennison AV, Williamson DA, Howden BP, Seemann T. AusTrakka: Fast-tracking nationalized genomics surveillance in response to the COVID-19 pandemic. Nat Commun. 2022;13:865. https://doi.org/10.1038/s41467-022-28529-9
19. Page AJ, Cummins CA, Hunt M, Wong VK, Reuter S, Holden MTG, et al. Roary: rapid large-scale prokaryote pan genome analysis. Bioinformatics. 2015;31:3691–3. https://doi.org/10.1093/bioinformatics/btv421
20. Taylor M, Cheng J, Sharma D, Bitzikos O, Gustafson R, Fyfe M, et al. Outbreak of *Vibrio parahaemolyticus* associated with consumption of raw oysters in Canada, 2015. Foodborne Pathog Dis. 2018;15:554–9. https://doi.org/10.1089/fpd.2017.2415
21. Martinez-Urtaza J, Powell A, Jansa J, Rey JLC, Montero OP, Campello MG, et al. Epidemiological investigation of a foodborne outbreak in Spain associated with U.S. West Coast genotypes of *Vibrio parahaemolyticus*. Springerplus. 2016;5:87. https://doi.org/10.1186/s40064-016-1728-1
22. Food and Agriculture Organization of the United Nations/World Health Organization. Advances in science and risk assessment tools for *Vibrio parahaemolyticus* and *V. vulnificus* associated with seafood. Meeting report. Microbiological Risk Assessment Series No. 35. Rome: The Organizations; 2021 [cited 2022 Jun 7] https://doi.org/10.4060/cb5834en
23. Lopatek M, Wieczorek K, Osek J. Prevalence and antimicrobial resistance of *Vibrio parahaemolyticus* isolated from raw shellfish in Poland. J Food Prot. 2015;78:1029–33. https://doi.org/10.4315/0362-028X.JFP-14-437
24. Cruz CD, Hedderley D, Fletcher GC. Long-term study of *Vibrio parahaemolyticus* prevalence and distribution in New Zealand shellfish. Appl Environ Microbiol. 2015;81:2320–7. https://doi.org/10.1128/AEM.04020-14
25. Centers for Disease Control and Prevention. *Vibrio parahaemolyticus* infections associated with consumption of raw shellfish—three states, 2006. MMWR. 2006;55:854–6.
26. Garbuglia AR, Bruni R, Villano U, Vairo F, Lapa D, Madonna E, et al.; The Other Members Of The Hev Outbreak Working Group. Hepatitis E outbreak in the central part of Italy sustained by multiple HEV genotype 3 strains, June–December 2019. Viruses. 2021;13:1159. https://doi.org/10.3390/v13061159
27. European Centre for Disease Prevention and Control. Multi-country outbreak of multiple *Salmonella enterica* serotypes linked to imported sesame-based products—14 October 2021. European Food Safety Authority, 2021 [cited 2024 June 19] https://www.ecdc.europa.eu/sites/default/files/documents/ROA_S%20Mbandaka_S%20Havana_UI-716_14-October-2021.pdf
28. Li Y, Xie X, Shi X, Lin Y, Qiu Y, Mou J, et al. *Vibrio parahaemolyticus*, southern coastal region of China, 2007–2012. Emerg Infect Dis. 2014;20:685–8. https://doi.org/10.3201/eid2004.130744
29. Ragunath P. Roles of thermostable direct hemolysin (TDH) and TDH-related hemolysin (TRH) in *Vibrio parahaemolyticus*. Frontiers Microbiol. 2015;5:805.
30. Gonzalez-Escalona N, Gavilan RG, Toro M, Zamudio ML, Martinez-Urtaza J. Outbreak of *Vibrio parahaemolyticus* sequence type 120, Peru, 2009. Emerg Infect Dis. 2016;22:1235–7. https://doi.org/10.3201/eid2207.151896
31. Bureau of Meteorology. State of the climate report, 2022 [cited 2022 Jun 7] http://www.bom.gov.au/state-of-the-climate/oceans.shtml
32. Hassing RJ, Verbon A, de Visser H, Hofman A, Stricker BH. Proton pump inhibitors and gastroenteritis. Eur J Epidemiol. 2016;31:1057–63. https://doi.org/10.1007/s10654-016-0136-8
33. Cribb DM, Varrone L, Wallace RL, McLure AT, Smith JJ, Stafford RJ, et al. Risk factors for campylobacteriosis in Australia: outcomes of a 2018–2019 case-control study. BMC Infect Dis. 2022;22:586. https://doi.org/10.1186/s12879-022-07553-6
34. Koo J, Marshall DL, DePaola A. Antacid increases survival of *Vibrio vulnificus* and *Vibrio vulnificus* phage in a gastrointestinal model. Appl Environ Microbiol. 2001;67:2895–902. https://doi.org/10.1128/AEM.67.7.2895-2902.2001
35. Australian Bureau of Statistics. Australian Health Survey: Nutrition First results—foods and nutrients, 2011–2012 [cited 2024 Jan 18]. https://www.abs.gov.au/statistics/health/health-conditions-and-risks/australian-health-survey-nutrition-first-results-foods-and-nutrients/latest-release#data-downloads

Address for correspondence: Emily Fearnley, SA Health, SA Pathology, PO Box 14 Rundle Mall, Adelaide, South Australia 5000, Australia; email:emilyfearnley@sa.gov.au

Wastewater Surveillance for Poliovirus in Selected Jurisdictions, United States, 2022–2023

Erin R. Whitehouse, Nancy Gerloff, Randall English, Stacie K. Reckling, Mohammed A. Alazawi, Meghan Fuschino, Kirsten St George, Daniel Lang, Eli S. Rosenberg, Enoma Omoregie, Jennifer B. Rosen, Alyse Kitter, Colin Korban, Massimo Pacilli, Trisha Jeon, Joseph Coyle, Russell A. Faust, Irene Xagoraraki, Brijen Miyani, Charles Williams, James Wendt, Sarah M. Owens, Rosemarie Wilton, Rachel Poretsky, Lynn Sosa, Kathy Kudish, Manisha Juthani, Elizabeth F. Zaremski, Susan E. Kehler, Nagla S. Bayoumi, Sarah Kidd

Wastewater testing can inform public health action as a component of polio outbreak response. During 2022–2023, a total of 7 US jurisdictions (5 states and 2 cities) participated in prospective or retrospective testing of wastewater for poliovirus after a paralytic polio case was identified in New York state. Two distinct vaccine-derived poliovirus type 2 viruses were detected in wastewater from New York state and New York City during 2022, representing 2 separate importation events. Of those viruses, 1 resulted in persistent community transmission in multiple New York counties and 1 paralytic case. No poliovirus was detected in the other participating jurisdictions (Connecticut, New Jersey, Michigan, and Illinois and Chicago, IL). The value of routine wastewater surveillance for poliovirus apart from an outbreak is unclear. However, these results highlight the ongoing risk for poliovirus importations into the United States and the need to identify undervaccinated communities and increase vaccination coverage to prevent paralytic polio.

In June 2022, a case of paralytic polio caused by vaccine-derived poliovirus type 2 (VDPV2) was identified in an unvaccinated adult in Rockland County, New York, USA, historically a county with low vaccination coverage (*1*). In addition, poliovirus type 2 (PV2) genetically linked to the VDPV2 isolated from the patient was detected in wastewater samples from Rockland and several surrounding counties, indicating community transmission. This case was the first known case of paralytic polio in the United States since 2013 (*2*) and the first documented instance of community transmission of poliovirus in the United States since 2005 (*3*).

For decades, the Global Polio Eradication Initiative has used wastewater testing (or environmental surveillance) as a tool to describe the extent of poliovirus circulation when cases of paralytic polio were identified in a community or in at-risk communities with insufficient acute flaccid paralysis surveillance for paralytic polio (*4*,*5*). More recently, countries such as the United Kingdom, Israel, Netherlands, and France have implemented wastewater surveillance for poliovirus in the absence of reported cases of paralytic polio to identify when a community is at risk before a paralytic case occurs (*6*–*9*). Indeed, poliovirus can circulate for an extended period without causing

Author affiliations: Centers for Disease Control and Prevention, Atlanta, Georgia, USA (E.R. Whitehouse, N. Gerloff, R. English, S. Kidd); Agency for Toxic Substances and Disease Registry, Atlanta (S.K. Reckling); New York State Department of Health, Albany, New York, USA (M.A. Alazawi, D. Lang, E.S. Rosenberg); Wadsworth Center, New York State Department of Health, Albany (M. Fuschino, K. St George); New York City Department of Health and Mental Hygiene, Long Island City, New York, USA (E. Omoregie, J.B. Rosen); Chicago Department of Health, Chicago, Illinois, USA (A. Kitter, C. Korban, M. Pacilli); Rush University Medical Center, Chicago (T. Jeon); Michigan Department of Health and Human Services, Lansing, Michigan, USA (J. Coyle); Oakland County Health Division, Pontiac, Michigan, USA (R.A. Faust); Michigan State University, East Lansing, Michigan, USA (I. Xagoraraki, B. Miyani); Illinois Department of Public Health, Springfield, Illinois, USA (C. Williams, J. Wendt); Argonne National Laboratory, Lemont, Illinois, USA (S.M. Owens, R. Wilton); University of Illinois Chicago, Chicago (R. Poretsky); Connecticut Department of Public Health, Hartford, Connecticut, USA (L. Sosa, K. Kudish, M. Juthani); New Jersey Department of Health, Trenton, New Jersey, USA (E.F. Zaremski, S.E. Kehler, N.S. Bayoumi)

DOI: https://doi.org/10.3201/eid3011.240771

a paralytic case. Among unvaccinated persons, paralysis is estimated to occur in only 1 in 190 to 1 in 1,900 persons infected with poliovirus (depending on poliovirus type) (*10*). Further, inactivated polio vaccine, the only polio vaccine used in the United States since 2000, effectively prevents paralytic disease caused by poliovirus, but it does not prevent gastrointestinal infection or transmission (*11*). It is unknown how common the silent circulation of undetected poliovirus infections is in the United States.

After the paralytic polio case was identified in Rockland County, several surrounding jurisdictions (New York City [NYC], Connecticut, and New Jersey) participated in wastewater testing for poliovirus as part of the outbreak response to describe the geographic extent and duration of poliovirus transmission in the area. Subsequently, Michigan, Illinois, and the city of Chicago, Illinois, piloted poliovirus wastewater-testing projects in their jurisdictions. A previous report summarized results from New York state and NYC through November 2022 (*12*). This report describes the results from all 7 jurisdictions and includes results from samples collected through December 2023.

Methods

New York State and NYC

Initial wastewater testing for poliovirus was conducted by New York State Department of Health and NYC Department of Health and Mental Hygiene in collaboration with the Centers for Disease Control and Prevention (CDC) using the existing National Wastewater Surveillance System (NWSS) in NYC and 8 counties in New York state (Orange, Rockland, Nassau, Putnam, Sullivan, Ulster, Suffolk, and Westchester) that were proximal to Rockland County, where the case of paralytic polio was reported. We retrospectively tested stored wastewater samples for poliovirus; samples were originally collected for SARS-CoV-2 surveillance during March 9, 2022–July 25, 2022, in New York state and May 31, 2022–July 20, 2022, in NYC. After the sample from the paralytic case was confirmed positive at CDC on July 21, 2022, we collected and tested wastewater samples from NYC and the 8 New York counties in real time as part of the polio outbreak response through December 2023. Later, additional stored wastewater samples collected during June 2, 2022–December 14, 2022, from 47 other counties in New York were also retrospectively tested to more thoroughly assess the geographic scope of the outbreak.

In New York state, we collected 250 mL of 24-hour time-weighted or flow-weighted samples from the influent of wastewater treatment plants. In NYC, we collected 500 mL of 24-hour flow-weighted composite samples. Samples were collected approximately 1 or 2 times weekly from each site. We processed wastewater samples using either ultracentrifugation or polyethylene glycol precipitation for virus concentration followed by nucleic acid extraction (*13*). During June 2022–March 2023, we forwarded the extracts to the Wadsworth Center (state laboratory for the New York Department of Health) or the New York City Public Health Laboratory, where they were packaged and shipped to CDC. At CDC, we screened total nucleic acids (TNA) for the presence of poliovirus using the pan-poliovirus real-time reverse transcription PCR (rRT-PCR) assay and sequenced positive samples as previously described (*12*,*14*–*16*). We performed genetic linkage of the vaccine-derived poliovirus on the basis of World Health Organization (WHO) and Global Polio Eradication Initiative recommendations (*17*).

To increase sensitivity of the testing after receiving several indeterminate results in 2 sewersheds in NYC, we collected additional 500-mL wastewater specimens at the Newtown Creek–Brooklyn Queens sewershed (August 2022) and in Kings County, Owl's Head, sewershed (October 2022). Those specimens underwent enterovirus-specific concentration and WHO standard poliovirus isolation methods at CDC; we detected poliovirus presence by rRT-PCR and confirmed serotypes by genomic sequencing (*18*,*19*).

After March 2023, testing for NYC and New York state was performed locally, either at the NYC Public Health Laboratory or the Wadsworth Center. Sampling, processing, and extraction from select sewersheds continued unchanged. We screened extracts on an Applied Biosystems 7500 Fast Dx real-time PCR system (ThermoFisher Scientific, https://www.thermofisher.com) using identical pan-poliovirus rRT-PCR (*16*), after optimization of the primer and probe concentration at each respective laboratory (*15*). We sent extracts from positive samples, defined as a cycle threshold of <37, or indeterminate samples, defined as a cycle threshold of 37–40, to CDC for confirmation and genetic sequencing. Testing in NYC and New York state is ongoing; we present results through December 2023.

New Jersey and Connecticut

Given their states' proximity to the paralytic case, New Jersey Department of Health and Connecticut Department of Public Health released stored TNA samples that were collected weekly during May 11, 2022–August 8, 2022, in New Jersey and May 8, 2022–August

3, 2022, in Connecticut for SARS-CoV-2 surveillance as part of NWSS activities to the Polio Response at CDC (*20*). Wastewater samples submitted to NWSS were generally collected as 24-hour flow-weighted or time-weighted composites of ≈150 mL, although occasional post–grit removal or grab samples were collected. CDC tested the TNA for poliovirus using the same methods described previously (*12*,*15*,*16*).

Pilot Wastewater Surveillance in Additional Jurisdictions

As part of polio emergency response activities, we identified additional jurisdictions to pilot wastewater surveillance for poliovirus in nonoutbreak jurisdictions. Criteria for inclusion were existing participation in the NWSS to provide sufficient structure for reporting results, postal (ZIP) code–level data on vaccine coverage to identify areas with lower vaccine coverage, and identification of appropriately sized sewersheds for testing. Jurisdictions also used data on previous vaccine-preventable disease outbreaks (e.g., measles), a proxy for low vaccination coverage, to prioritize communities for testing (*21*). Illinois Department of Public Health opted for retrospective analysis using archived TNA extracted from wastewater samples in Kankakee, Rock Island, and St. Clair Counties collected during April 2022–April 2023. Chicago Department of Public Health and Michigan Department of Health and Human Services conducted prospective sampling and testing; Chicago officials tested in Cook County, Illinois, during March–July 2023 and Michigan officials conducted testing in Oakland County, Michigan, during June 2023–November 2023.

In Chicago and Illinois, the 24-hour time-weighted or volume-weighted influent composite 100 mL samples of wastewater were processed at the laboratory at the University of Illinois Chicago. After concentration using Ceres Nanotrap A Particles with Enhancement Reagent 1 (Ceres Nanosciences, https://www.ceresnano.com), we extracted RNA using the MagMax Viral Pathogen and Microbiome Ultra kits on the KingFisher Apex (both ThermoFisher Scientific, https://ww.thermofisher.com). We sequenced TNA of prospective Chicago samples at the Rush University Regional Innovative Public Health Laboratory, whereas archived TNA from Illinois samples were sequenced at the Argonne National Laboratory Environmental Sample Preparation and Sequencing Facility. Both laboratories used the methods developed by the Poliovirus Sequencing Consortium (https://polionanopore.org); data were analyzed using the PSC Piranha software package (https://github.com/polio-nanopore/piranha) (*22*,*23*).

Michigan prospectively collected 24-hour time-weighted composite 1-L samples of influent untreated wastewater weekly from 2 locations in Oakland County and processed wastewater samples using polyethylene glycol precipitation followed by nucleic acid extraction. After cDNA synthesis, we tested the samples with conventional PCR targeting the pan-polio viral protein 1 gene (*22*). PCR products from conventional PCR were visualized with gel electrophoresis and Sanger-sequenced. To confirm the sequencing results, all samples were also tested and analyzed with a GT molecular ddPCR Polio Typing Wastewater Surveillance Assay Kit (GT Molecular, https://www.gtmolecular.com) for the Bio-Rad QX200 Droplet Digital PCR System (Bio-Rad Laboratories, https://www.bio-rad.com) following the manufacturer's protocol.

Population estimates and percent coverage were reported by the jurisdiction or from CDC NWSS (for New Jersey and Connecticut) based on April 2020 US census data (*24*). This activity was reviewed by CDC, deemed not research, and conducted consistent with applicable federal law and CDC policy (e.g., 45 C.F.R. part 46.102(l)(2), 21 C.F.R. part 56; 42 U.S.C. §241(d); 5 U.S.C. §552a; 44 U.S.C. §3501 et seq).

Results

New York State and NYC

In New York state (excluding NYC), 86 samples collected from 7 sewersheds in 4 counties (Nassau, Orange, Rockland, and Sullivan) during May 23, 2022–February 22, 2023, tested positive by pan-poliovirus real-time PCR. Sequencing results confirmed PV2 that was genetically linked to VDPV2 isolated from the paralytic polio patient from Rockland County (Figure 1). In NYC, 6 samples collected during June 14, 2022–October 12, 2022, were PV2-positive and genetically linked to the outbreak. A second, genetically distinct VDPV2 was identified in a sample collected in NYC on July 10, 2022, representing a separate importation event into the United States. New York state also had 1 sample (April 21, 2022; Orange County) and NYC 4 samples (June 28, 2022–July 12, 2022) that tested positive for PV2, but genetic material was insufficient to determine linkage to the outbreak.

Overall, as a part of the outbreak response in New York state, a total of 3,985 samples across 46 sewersheds from 8 counties were collected during March 9, 2022–December 31, 2023; estimated coverage for each sewershed was 6%–96%, representing ≈2.9 million persons (Figure 2; Appendix Table, https://wwwnc.cdc.gov/EID/article/30/11/24-0771-App1.pdf). In NYC,

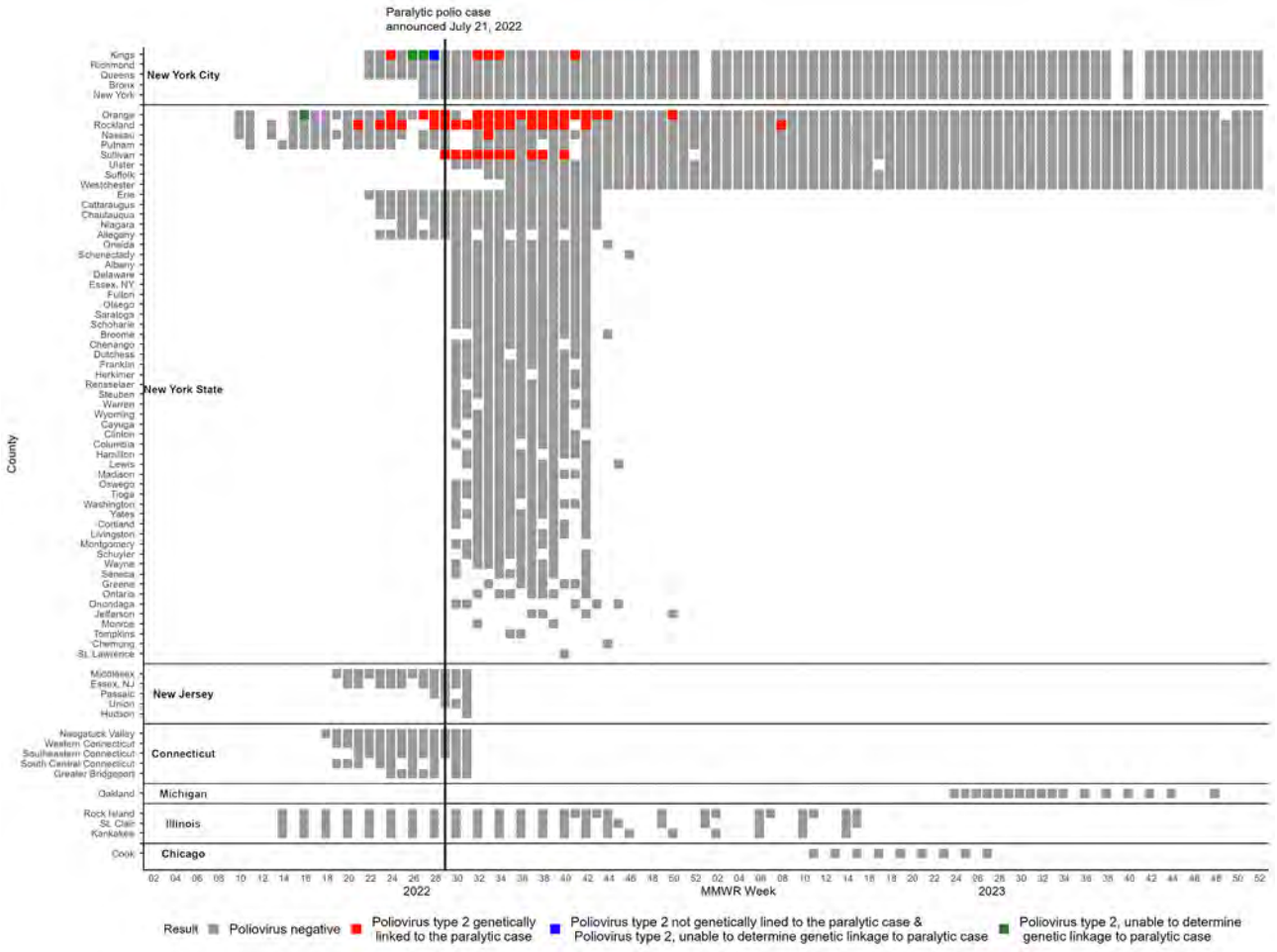

Figure 1. Positive and negative poliovirus results by MMWR week by county and jurisdiction in wastewater surveillance for poliovirus, United States, March 5, 2022–December 31, 2023. Colored squares represent poliovirus results for ≥1 wastewater samples collected during an MMWR week, including results from prospective testing (New York state, New York City, Chicago, Michigan) and retrospective testing of archived samples (New York state, New York City, Illinois, New Jersey, Connecticut). Any week with a positive poliovirus result is colored red, green, or blue, depending on genetic linkage to the case. Indeterminate results are not included in this figure. For context, the paralytic case was confirmed July 21, 2022 (MMWR week 29), with onset in June 2022. MMWR, Morbidity and Mortality Weekly Report.

a total of 1,888 samples across 16 sewersheds were collected during May 31, 2022–December 31, 2023, as a part of the outbreak response; the last positive test was October 2022. Some counties were represented by multiple unique sewersheds, so the coverage was additive (Appendix Table). The estimated combined percentage of population coverage of the sewersheds by county was 96%–99.5% in NYC. This coverage represents an estimated 8.5 million persons.

Subsequently, New York retrospectively tested samples from 47 additional counties that were not included in the original outbreak investigation. In those 47 counties, 1,032 samples collected during June 2, 2022–December 14, 2022, from 77 sewersheds were all negative for poliovirus (Figure 2; Appendix Table). The estimated coverage in this additional retrospective testing for each sewershed was 2%–85%, representing >2.7 million persons across the state.

New Jersey and Connecticut

We detected no poliovirus in the retrospective samples tested as a part of the outbreak response in New Jersey and Connecticut (Figure 1). In New Jersey, 32 samples collected during May 11, 2022–August 5, 2022, from 5 sewersheds in 7 counties were tested; 3 sewersheds covered multiple counties. The estimated combined percentage of population coverage of the sewersheds by county was 22%–88% and represented ≈3.2 million persons. In Connecticut, 87 samples collected during May 3, 2022–August 3, 2022, from 10 sewersheds in 5 planning regions (i.e., county equivalent in Connecticut) were tested. The estimated

percentage of planning region population covered by each sewershed was 22%–47% and represented ≈830,000 persons (Appendix Table).

Pilot Wastewater Surveillance in Additional Jurisdictions

We detected no poliovirus in wastewater surveillance in the 3 pilot jurisdictions (Figures 1, 2). In Chicago, we tested 36 prospectively collected samples from 4 sewersheds in Cook County during March 5, 2023–July 2, 2023, representing an estimated 4.6 million persons (88% coverage from the sewersheds). In Illinois, we tested 137 samples collected from 7 sewersheds in 3 counties during April 5, 2022–April 5, 2023. The estimated percentage of the county population covered by sewersheds was 48%–66%, a total of ≈300,000 persons. Finally, in Michigan, we tested 44 samples collected from 2 sewersheds in Oakland County during June 12, 2023–November 29, 2023. Those sewersheds represented ≈250,000–320,000 persons (20%–25% county coverage) (Appendix Table).

Discussion

Wastewater surveillance for poliovirus identified ongoing transmission of poliovirus in Rockland County and adjacent New York counties during an outbreak of poliovirus in the United States (*10*). It also retrospectively demonstrated the presence of poliovirus in the community for several months before the paralytic polio case was identified. Genetic characterization of the detected polioviruses confirmed that almost all wastewater detections were related to the virus isolated from the paralytic polio case. However, wastewater surveillance in NYC also identified a separate importation of VDPV2 that was not genetically related to the New York state case or other outbreaks globally. This second importation was an isolated detection and was not associated with a paralytic case. No related virus has been identified in subsequent testing in NYC or the surrounding counties, indicating that no sustained transmission occurred after that importation. An additional importation of poliovirus was identified in wastewater in Utah by researchers in 2022 and confirmed as poliovirus by CDC (*25*). Subsequent testing from the same site and from the surrounding areas failed to detect additional poliovirus-positive samples. Other researchers have likely tested wastewater for poliovirus in the United States, but CDC was not notified to confirm a positive result (*26*).

No poliovirus was detected in wastewater surveillance by the pilot jurisdictions (Michigan, Illinois, and Chicago) or the retrospective testing of samples from New Jersey, Connecticut, and 47 additional counties in New York. The last poliovirus-positive

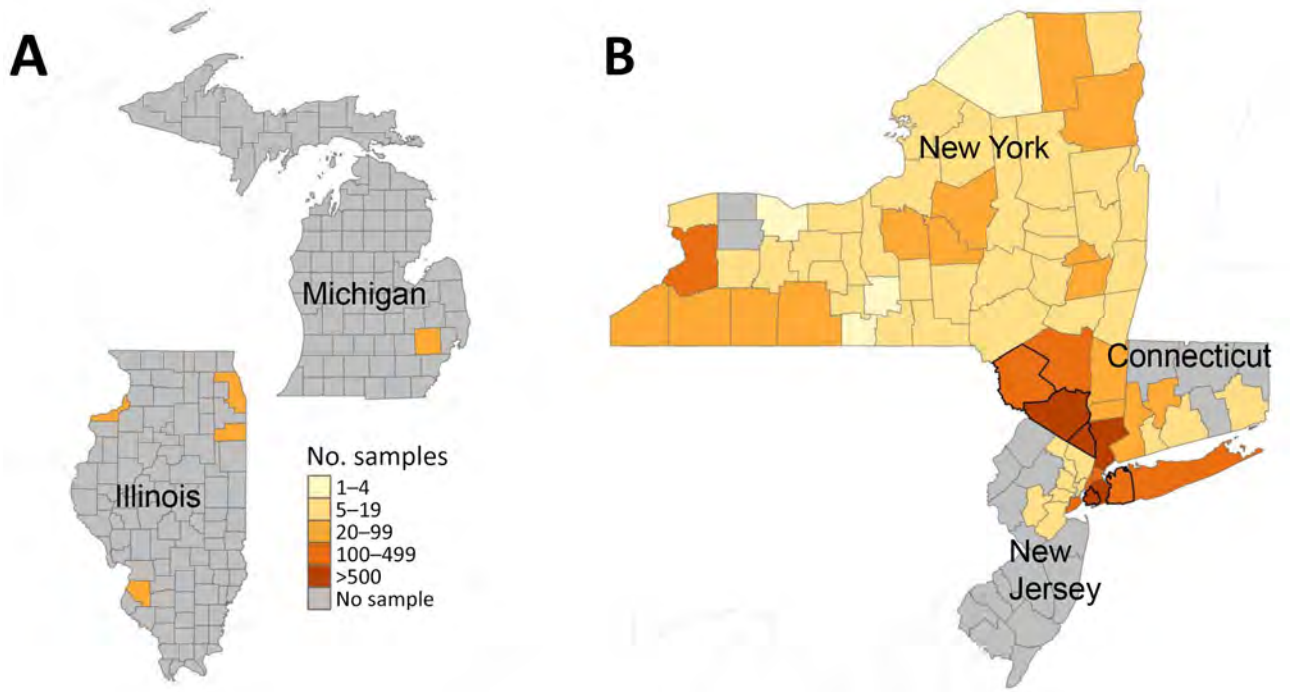

Figure 2. Total number of samples tested per county in participating jurisdictions in wastewater surveillance for poliovirus, United States, March 5, 2022–December 31, 2023. This figure represents the number of samples per county in participating jurisdictions on a logarithmic scale. A) Illinois, including the city of Chicago, and Michigan; B) New York, including New York City; Connecticut; and New Jersey. The thicker black borders in panel B show counties that had a positive sample for poliovirus.

samples detected in New York state and NYC, where wastewater testing has continued in the outbreak-affected areas, were collected on October 12, 2022, and February 22, 2023. As of October 2024, >2 years after the paralytic case and >1 year after the last positive wastewater detection, no further positive detections have been reported, suggesting the end of the outbreak (*27*,*28*).

The findings in this report indicate that the United States experiences periodic importations of poliovirus from other countries and is at risk for community transmission, especially in communities that are undervaccinated. However, even though this report was limited to 7 jurisdictions, the data suggest that sustained transmission after importation into the United States is likely a rare event, possibly because of high-quality water and sanitation services and generally high vaccination coverage in most of the country (*29*). Although the transition from oral poliovirus vaccination to inactivated polio vaccine in routine immunization in the United States might enable gastrointestinal poliovirus infection and extensive asymptomatic transmission, no evidence exists of widespread poliovirus transmission in the United States.

The first limitation of this study is that only 80% of US households are on a sewer system that can be sampled by sewershed wastewater surveillance, and this report includes data for just 7 jurisdictions (*30*). Further, outside of New York state, only a few counties in each jurisdiction participated, with limited sewersheds and for a limited period of time. Therefore, these data might not be representative of the United States as a whole, and poliovirus might have been present in wastewater in communities where testing did not occur. In addition, negative results should be interpreted with caution, because sensitivity and limits of detection of PCR testing for poliovirus in wastewater have not yet been defined. Every jurisdiction was responsible for their own test validation and testing methods were not validated by CDC. However, all jurisdictions reported identifying nonpolio enteroviruses. The selection of sewersheds, timing of poliovirus shedding, and the number of infected persons can all affect the ability to detect poliovirus if present. Some sewersheds included in this report had catchment areas that were larger than those recommended by the WHO (≈300,000 persons), potentially affecting the sensitivity of results (*31*,*32*). In addition, varying sewage treatment, concentration, and testing methods might affect the results. Any pretreatment of wastewater might affect the integrity of nucleic acids, giving false-negative results in downstream molecular testing.

As wastewater surveillance for other pathogens continues to expand, the appropriate role of wastewater surveillance for rare diseases like polio in nonendemic areas is still being refined. When used during an outbreak, as in New York, Connecticut, and New Jersey in 2022, wastewater surveillance is a useful tool for identifying the geographic and temporal scope of the outbreak and for identifying the communities at increased risk for poliovirus exposure. Outside of the outbreak setting, several key considerations exist for jurisdictions considering wastewater surveillance for poliovirus. Although instituting a new wastewater surveillance system is challenging, participating jurisdictions found that implementing poliovirus testing within an established wastewater surveillance infrastructure such as NWSS was generally feasible (*30*). However, implementing the additional precautions for poliovirus testing as described by the National Authority for Containment of Poliovirus can be burdensome, not only for health departments but also for laboratories and institutions located within the sewershed areas that are tested (*32*,*33*). Other considerations include ensuring that watershed companies and employees responsible for sample collection are not overburdened with collection processes, that the health and safety of workers are protected, and that any poliovirus detections are communicated clearly to workers and the general public (*32*).

When selecting sewersheds and communities for possible wastewater surveillance for poliovirus, health departments should consider the size of the sewershed catchment area and community perception of being selected for surveillance. A sewershed serving a population that is too small could lead to privacy concerns, whereas sewersheds with larger-than-recommended catchment area populations might compromise test sensitivity. Targeting specific communities for wastewater testing is controversial, and ethical considerations for testing should be taken into account, particularly when specific racial, ethnic, or religious communities might be identified by their sewershed (*32*,*34*,*35*). The same communities that are at risk for polio because of undervaccination might also be at increased risk for stigmatization and health inequities because of ethnic, religious, or racial makeup. Incidental identification of specific counties or communities because of wastewater surveillance could contribute to increased stigmatization (*36*). For those and other reasons, wastewater surveillance might not be acceptable to all communities. Health departments should consider the potential negative consequences of wastewater surveillance and collaborate with

at-risk communities when deciding if and where they conduct wastewater surveillance.

Health departments implementing wastewater surveillance for poliovirus should also develop clear communication plans for both negative and positive results to ensure affected populations understand the public health implications and the appropriate action to take, if any. Communication of any poliovirus detections should clarify that poliovirus in wastewater reflects the presence of poliovirus in the community (i.e., not just in sewage material) and should emphasize the importance of vaccination to prevent paralysis. All health departments conducting wastewater surveillance for poliovirus, especially those in communities with poliovirus detections, should anticipate an increase in inquiries about polio vaccination and whether the public needs additional doses. A substantial proportion of those inquiries might come from fully vaccinated persons and persons who are not at increased risk for infection; communication plans should also clarify who is at risk and provide reassurance for those who are not.

Ultimately, the primary purpose of wastewater surveillance for poliovirus is to prevent cases of paralytic polio by identifying communities at increased risk for poliovirus exposure and ensuring high vaccination coverage in those communities. However, how wastewater detections affect public perception of risk, or whether they lead to behavior change (i.e., vaccine uptake), is unclear. In New York state during the 2022 outbreak, publicity surrounding the presence of poliovirus in wastewater did not substantively increase vaccination rates in affected undervaccinated communities (*1*,*12*). Findings from focus groups have highlighted challenges involved in addressing barriers to vaccination (*12*,*34*). Similar challenges with barriers to vaccination and perceived low risk for poliovirus infection among communities with lower vaccine coverage were noted in the United Kingdom during a 2022 response to multiple detections of VDPV2 in sewage (*37*). Certainly, identifying undervaccinated communities and improving routine vaccination coverage are public health priorities. This work can and should be ongoing before, or even without, a wastewater detection.

Wastewater surveillance has the potential to be a vital public health tool for monitoring disease and promoting public health action in certain situations, as seen in the COVID-19 pandemic and during the outbreak response to the 2022 paralytic polio case in New York. However, outside of the outbreak setting, considering the public health resources required for ongoing surveillance and whether the data will lead to public health action are key (*38*). As long as poliovirus is circulating elsewhere in the world, periodic importations into the United States are to be expected (*7*). Regardless of wastewater surveillance availability in jurisdictions, vaccination, the most effective public health intervention to prevent paralytic polio, is readily available in the United States. State and local health departments should identify communities with low vaccination coverage and collaborate with those communities to improve vaccination rates to prevent paralytic polio and other vaccine preventable diseases.

Acknowledgments

We thank Kevin J. Kunstman and Stefan J. Green for support with laboratory testing, Janell Routh for leading this wastewater surveillance pilot project and providing input on this manuscript, Jeffrey Mercante for assistance with NWSS data, and Jane R. Zucker for assistance with this manuscript.

All authors have completed and submitted the International Committee of Medical Journal Editors form for disclosure of potential conflicts of interest. K.S.G. reports royalty-generating collaborative research agreement with Zeptometrix, with payments to institution; K.K. reports institutional support to the Connecticut Immunization Program from a grant from the CDC Vaccines for Children program; I.X. and B.M. report grant support from Michigan Department of Health and Human Services to their institution Michigan State University; A.K., C.K., T.J., and L.S. all report grant support from the CDC Epidemiology and Laboratory Capacity for Prevention and Control of Emerging Infectious Diseases cooperative agreement.

About the Author

Dr. Whitehouse is a nurse epidemiologist at the Centers for Disease Control and Prevention. She is currently working in the National Center for Immunizations and Respiratory Diseases in the Global Respiratory Viruses Branch.

References

1. Link-Gelles R, Lutterloh E, Schnabel Ruppert P, Backenson PB, St George K, Rosenberg ES, et al.; 2022 U.S. Poliovirus Response Team. Public health response to a case of paralytic poliomyelitis in an unvaccinated person and detection of poliovirus in wastewater—New York, June–August 2022. MMWR Morb Mortal Wkly Rep. 2022;71:1065–8. https://doi.org/10.15585/mmwr.mm7133e2
2. Trimble R, Atkins J, Quigg TC, Burns CC, Wallace GS, Thomas M, et al.; Centers for Disease Control and Prevention. Vaccine-associated paralytic poliomyelitis and

BCG-osis in an immigrant child with severe combined immunodeficiency syndrome—Texas, 2013. MMWR Morb Mortal Wkly Rep. 2014;63:721–4.
3. Alexander JP, Ehresmann K, Seward J, Wax G, Harriman K, Fuller S, et al.; Vaccine-Derived Poliovirus Investigations Group. Transmission of imported vaccine-derived poliovirus in an undervaccinated community in Minnesota. J Infect Dis. 2009;199:391–7. https://doi.org/10.1086/596052
4. Paul JR, Trask JD, Gard S. Poliomyelitic virus in urban sewage. J Exp Med. 1940;71:765–77. https://doi.org/10.1084/jem.71.6.765
5. World Health Organization. Guidelines for environmental surveillance of poliovirus circulation. 2003 [cited 2024 Apr 11]. https://iris.who.int/bitstream/handle/10665/67854/WHO_V-B_03.03_eng.pdf
6. Moran-Gilad J, Kaliner E, Gdalevich M, Grotto I. Public health response to the silent reintroduction of wild poliovirus to Israel, 2013–2014. Clin Microbiol Infect. 2016;22(Suppl 5):S140–5. https://doi.org/10.1016/j.cmi.2016.06.018
7. Klapsa D, Wilton T, Zealand A, Bujaki E, Saxentoff E, Troman C, et al. Sustained detection of type 2 poliovirus in London sewage between February and July, 2022, by enhanced environmental surveillance. Lancet. 2022;400:1531–8. https://doi.org/10.1016/S0140-6736(22)01804-9
8. Toro L, de Valk H, Zanetti L, Huot C, Tarantola A, Fournet N, et al. Pathogen prioritisation for wastewater surveillance ahead of the Paris 2024 Olympic and Paralympic Games, France. Euro Surveill. 2024;29:2400231. https://doi.org/10.2807/1560-7917.ES.2024.29.28.2400231
9. Duizer E, Ruijs WLM, Putri Hintaran AD, Hafkamp MC, van der Veer M, Te Wierik MJM. Wild poliovirus type 3 (WPV3)-shedding event following detection in environmental surveillance of poliovirus essential facilities, the Netherlands, November 2022 to January 2023. Euro Surveill. 2023; 28:2300049. https://doi.org/10.2807/1560-7917.ES.2023.28.5.2300049
10. Nathanson N, Kew OM. From emergence to eradication: the epidemiology of poliomyelitis deconstructed. Am J Epidemiol. 2010;172:1213–29. https://doi.org/10.1093/aje/kwq320
11. Kidd S, Clark T, Routh J, Cineas S, Bahta L, Brooks O. Use of inactivated polio vaccine among U.S. adults: updated recommendations of the Advisory Committee on Immunization Practices—United States, 2023. MMWR Morb Mortal Wkly Rep. 2023;72:1327–30. https://doi.org/10.15585/mmwr.mm7249a3
12. Ryerson AB, Lang D, Alazawi MA, Neyra M, Hill DT, St George K, et al.; 2022 U.S. Poliovirus Response Team. Wastewater testing and detection of poliovirus type 2 genetically linked to virus isolated from a paralytic polio case—New York, March 9–October 11, 2022. MMWR Morb Mortal Wkly Rep. 2022;71:1418–24. https://doi.org/10.15585/mmwr.mm7144e2
13. Hoar C, Chauvin F, Clare A, McGibbon H, Castro E, Patinella S, et al. Monitoring SARS-CoV-2 in wastewater during New York City's second wave of COVID-19: sewershed-level trends and relationships to publicly available clinical testing data. Environ Sci Water Res Technol. 2022;8:1021–35. https://doi.org/10.1039/D1EW00747E
14. Kilpatrick DR, Iber JC, Chen Q, Ching K, Yang SJ, De L, et al. Poliovirus serotype-specific VP1 sequencing primers. J Virol Methods. 2011;174:128–30. https://doi.org/10.1016/j.jviromet.2011.03.020
15. Gerloff N, Sun H, Mandelbaum M, Maher C, Nix WA, Zaidi S, et al. Diagnostic assay development for poliovirus eradication. J Clin Microbiol. 2018;56:e01624-17.
16. Sun H, Harrington C, Gerloff N, Mandelbaum M, Jeffries-Miles S, Apostol LNG, et al. Validation of a redesigned pan-poliovirus assay and real-time PCR platforms for the global poliovirus laboratory network. PLoS One. 2021;16:e0255795.
17. Global Polio Eradication Initiative. Classification and reporting of vaccine-derived polioviruses (VDPV). August 2016 [cited 2024 Aug 27]. https://polioeradication.org/wp-content/uploads/2016/09/Reporting-and-Classification-of-VDPVs_Aug2016_EN.pdf
18. Belgasmi H, Miles SJ, Sayyad L, Wong K, Harrington C, Gerloff N, et al. CaFÉ: A sensitive, low-cost filtration method for detecting polioviruses and other enteroviruses in residual waters. Front Environ Sci. 2022;10:10. https://doi.org/10.3389/fenvs.2022.914387
19. Global Polio Eradication Initiative. Guidelines on environmental surveillance for detection of polioviruses. 2015 [cited 2024 Apr 11]. https://polioeradication.org/wp-content/uploads/2016/07/WHO_V-B_03.03_eng.pdf
20. Adams C, Bias M, Welsh RM, Webb J, Reese H, Delgado S, et al. The National Wastewater Surveillance System (NWSS): from inception to widespread coverage, 2020–2022, United States. Sci Total Environ. 2024;924:171566. https://doi.org/10.1016/j.scitotenv.2024.171566
21. Cutts FT, Ferrari MJ, Krause LK, Tatem AJ, Mosser JF. Vaccination strategies for measles control and elimination: time to strengthen local initiatives. BMC Med. 2021;19:2. https://doi.org/10.1186/s12916-020-01843-z
22. Shaw AG, Majumdar M, Troman C, et al. Rapid and sensitive direct detection and identification of poliovirus from stool and environmental surveillance samples by use of nanopore sequencing. J Clin Microbiol. 2020;58:e00920–20.
23. Shaw A, Majumdar M, Troman C, Akello J, Martin J, Grassly N, et al. Nested VP1 PCR and nanopore sequencing from stool and ES samples v1.2 V.3. 2022 [cited 2024 Apr 11]. https://www.protocols.io/view/nested-vp1-pcr-and-nanopore-sequencing-from-stool-81wg-bpkmovpk/v3
24. United States Census Bureau. County population totals and components of change: 2020–2023. 2024 [cited 2024 Apr 11]. https://www.census.gov/data/datasets/time-series/demo/popest/2020s-counties-total.html#v2022
25. Roche L. A researcher found poliovirus in Utah wastewater last year. Here's why public health officials aren't concerned. Deseret News. 2023, March 20 [cited 2024 Apr 11]. https://www.deseret.com/utah/2023/3/20/23365690/polio-utah-wastewater-missouri-covid
26. Boss S, Baker H, Chang C-L. Poliovirus detection in Las Vegas wastewater. Undergraduate Research Symposium posters. 2022. Abstract 139 [cited 2024 Apr 11]. https://digitalscholarship.unlv.edu/durep_posters/139
27. World Health Organization. Standard operating procedures: responding to a poliovirus event or outbreak, version 4, 2022 [cited 2024 28 Aug]. https://polioeradication.org/wp-content/uploads/2022/09/Standard-Operating-Procedures-For-Responding-to-a-Poliovirus-Event-Or-Outbreak-20220905-V4-EN.pdf
28. Kalkowska DA, Badizadegan K, Routh JA, Burns CC, Rosenberg ES, Brenner IR, et al. Modeling undetected poliovirus circulation following the 2022 outbreak in the United States. Expert Rev Vaccines. 2024;23:186–95. https://doi.org/10.1080/14760584.2023.2299401
29. Centers for Disease Control and Prevention. Immunization: percentage of children vaccinated by age 24 months [cited 2024 Aug 27]. https://www.cdc.gov/nchs/fastats/immunize.htm

30. Centers for Disease Control and Prevention. National Wastewater Surveillance System (NWSS) [cited 2024 Apr 11]. https://www.cdc.gov/nwss/wastewater-surveillance.html
31. World Health Organization. Field guidance for the implementation of environmental surveillance for poliovirus [cited 2024 Apr 11]. https://polioeradication.org/wp-content/uploads/2023/06/Field-Guidance-for-the-Implementation-of-ES-20230007-ENG.pdf
32. Maal-Bared R, Brisolara K, Knight M, Mansfeldt C. To sample or not to sample: a governance-focused decision tree for wastewater service providers considering participation in wastewater-based epidemiology (WBE) in support of public health programs. Sci Total Environ. 2023;905:167128. https://doi.org/10.1016/j.scitotenv.2023.167128
33. Centers for Disease Control and Prevention. U.S. National Authority for Containment of Poliovirus [cited 2024 Apr 11]. https://www.cdc.gov/orr/polioviruscontainment
34. Kasstan B, Mounier-Jack S, Chantler T, Masters N, Flores SA, Stokley S, et al. Poliovirus outbreak in New York State, August 2022: qualitative assessment of immediate public health responses and priorities for improving vaccine coverage. Epidemiol Infect. 2022;2023:151.
35. European Union Drugs Agency. Ethical research guidelines for wastewater-based epidemiology and related fields [cited 2024 Apr 11]. https://www.emcdda.europa.eu/drugs-library/ethical-research-guidelines-wastewater-based-epidemiology-and-related-fields_en
36. Ram N, Shuster W, Gable L, Ram JL. Ethical and legal wastewater surveillance. Science. 2023;379:652–652. https://doi.org/10.1126/science.adg7147
37. Kasstan B, Mounier-Jack S, Zuriaga-Alvaro A, Weil LG, Chantler T. "We're potentially worsening health inequalities": evaluating how delivery of the 2022 London polio booster campaign was tailored to Orthodox Jewish families to reduce transmission vulnerability. SSM Qual Res Health. 2023;4:100365. https://doi.org/10.1016/j.ssmqr.2023.100365
38. Keshaviah A, Karmali RN, Vohra D, Huffman T, Hu XC, Diamond MB. The role of wastewater data in pandemic management [cited 2024 Apr 11]. https://www.rockefellerfoundation.org/wp-content/uploads/2022/04/The-Role-of-Wastewater-Data-in-Pandemic-Management-Survey-Research-Brief-Final.pdf

Address for correspondence: Sarah Kidd, Centers for Disease Control and Prevention, 1600 Clifton Rd NE, Mailstop 24-7, Atlanta, GA 30329-4018, USA; email: skidd@cdc.gov

etymologia revisited

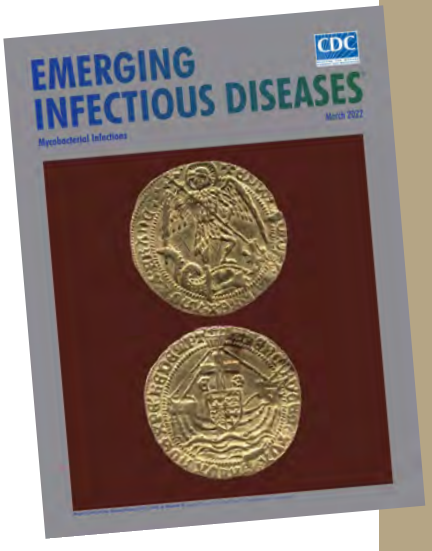

Originally published in March 2022

Schizophyllum commune

[skiz-of′-ĭ-ləm kom′-yoon]

Schizophyllum commune, or split-gill mushroom, is an environmental, wood-rotting basidiomycetous fungus. *Schizophyllum* is derived from "*Schíza*" meaning split because of the appearance of radial, centrally split, gill like folds; "*commune*" means common or shared ownership or ubiquitous. Swedish mycologist, Elias Magnus Fries (1794–1878), the Linnaeus of Mycology, assigned the scientific name in 1815. German mycologist Hans Kniep in 1930 discovered its sexual reproduction by consorting and recombining genomes with any one of numerous compatible mates (currently >2,800).

References

1. Chowdhary A, Kathuria S, Agarwal K, Meis JF. Recognizing filamentous basidiomycetes as agents of human disease: a review. Med Mycol. 2014;52: 782–97. https://doi.org/10.1093/mmy/myu047
2. Cooke WB. The genus *Schizophyllum*. Mycologia. 1961;53:575–99. https://doi.org/10.1080/00275514.1961.12017987
3. Greer DL. Basidiomycetes as agents of human infections: a review. Mycopathologia. 1978;65:133–9. https://doi.org/10.1007/BF00447184
4. O'Reilly P. *Schizophyllum commune*, split gill fungus, 2016 [cited 2021 Aug 23]. https://www.first-nature.com/fungi/schizophyllum-commune.php
5. Raper CA, Fowler TJ. Why study *Schizophyllum*? Fungal Genet Rep. 2004;51:30–6. https://doi.org/10.4148/1941-4765.1142

https//wwwnc.cdc.gov/eid/article/28/3/et-2803_article

Rocky Mountain Spotted Fever in Children along the US–Mexico Border, 2017–2023

Leslie Chiang,[1] Nanda Ramchandar, Jacquelyn Aramkul, Yaron Fireizen, Mark E. Beatty, Madeleine Monroe, Seema Shah, Jennifer Foley, Nicole G. Coufal

Rocky mountain spotted fever (RMSF) causes significant illness and death in children. Although historically rare in California, USA, RMSF is endemic in areas of northern Mexico that border California. We describe 7 children with RMSF who were hospitalized at a tertiary pediatric referral center in California during 2017–2023. Five children had recent travel to Mexico with presumptive exposure, but 2 children did not report any travel outside of California. In all 7 patients, *Rickettsia rickettsii* DNA was detected by plasma microbial cell-free next-generation sequencing, which may be a useful diagnostic modality for RMSF, especially early in the course of illness, when standard diagnostic tests for RMSF are of limited sensitivity. A high index of suspicion and awareness of local epidemiologic trends remain most critical to recognizing the clinical syndrome of RMSF and initiating appropriate antimicrobial therapy in a timely fashion.

Rocky Mountain spotted fever (RMSF) is a life-threatening infection caused by the tickborne pathogen *Rickettsia rickettsii*. The estimated overall case-fatality rate of RMSF is 7%–10% in the United States (*1*); however, case-fatality rates are considerably higher and approach ≥50% in several states along the US–Mexico border (*2*). Diagnosing RMSF requires a high degree of clinical suspicion; the organism is rarely isolated using standard culture methods, and ≈50% of case-patients do not report a history of tick bite (*3*). Moreover, diagnosis can be especially challenging in historically nonendemic regions because many of the signs and symptoms overlap with those of other infectious diseases. Serologic testing, PCR, immunostaining, or specialized culture methods may be used to diagnose RMSF on specimen types including whole blood or biopsy or autopsy tissue and are available through commercial, state health department, or Centers for Disease Control and Prevention (CDC) laboratories (*1*). Indirect immunofluorescence antibody (IFA) assays are a commonly used and widely commercially available diagnostic method; however, antibodies may not develop until the second week of illness (*1*). Prompt empiric administration of effective antimicrobial therapy is critical to averting illness and death.

Although historically rare in California, RMSF is endemic across areas of northern Mexico; since 2008, RMSF has reached epidemic proportions (*2*,*4*) with especially high case-fatality rates among children (*5*). Most cases of RMSF in southern California are associated with travel to Mexico; a recent update from the Centers for Disease Control and Prevention Health Alert Network reported 5 cases of severe RMSF during July–December 2023 with recent travel to Tecate, Mexico (*6*). Four of the 5 case-patients were children, and 4 case-patients died.

We describe 7 children with RMSF diagnoses in San Diego and in whom *R. rickettsii* was detected by plasma microbial cell-free next-generation sequencing (mcf-NGS). This study was approved by the Human Research Protections Program at the University of California, San Diego.

Methods

We conducted a retrospective chart review of case-patients who had a diagnosis of RMSF during January 1, 2017–August 30, 2023, and were admitted to Rady Children's Hospital (San Diego, CA, USA), a tertiary children's hospital with a broad referral base extending throughout the greater San Diego region. We obtained data from review of electronic medical records.

Author affiliations: University of California San Diego, San Diego, California, USA (L. Chiang, N. Ramchandar, Y. Fireizen, J. Foley, N.G. Coufal); Naval Medical Center San Diego, San Diego (N. Ramchandar); Rady Children's Hospital of San Diego, San Diego (N. Ramchandar, Y. Fireizen, J. Foley, N.G. Coufal); County of San Diego Health and Human Services Agency, San Diego (J. Aramkul, M.E. Beatty, M. Monroe, S. Shah)

DOI: http://doi.org/10.3201/eid3011.231760

[1]Current affiliation: University of California Davis, Davis, California, USA.

All mcf-NGS testing (Karius Inc., https://kariusdx.com) was sent at the clinical discretion of the treating infectious disease physicians. Cases were confirmed by either serology or PCR testing (Quest Diagnostics, https://www.questdiagnostics.com) and cross-referenced with cases reported to San Diego County Health and Human Services Agency to ensure that no additional pediatric cases occurred during the review period. There were no pediatric cases of RMSF in San Diego for which mcf-NGS was not sent or where mcf-NGS was negative but other testing was positive for RMSF.

Results

Seven cases of RMSF were diagnosed in the study period. There were no patients within the study period who had RMSF for whom plasma mcf-NGS was not obtained. The case-patients were 17 months to 14 years of age; mean age was 7.3 years and median 7 years (interquartile range [IQR] 4–10 years). Four case-patients (57%) were male and 3 (43%) were female. Case-patients had a median of 6 days of symptoms (range 5–7 days) before hospital admission. Care was sought for all case-patients during February–October (Table).

Six case-patients were critically ill and required admission to the pediatric intensive care unit (PICU). All case-patients had *R. rickettsii* detected by plasma mcf-NGS; 6 had the diagnosis of RMSF confirmed with serology and 1 by PCR, although 3 initially did not have detectable rickettsial antibodies (Appendix Table, https://wwwnc.cdc.gov/EID/article/30/11/23-1760-App1.pdf). The median time from specimen collection to result return was 3.3 days (IQR 3–3 days) for plasma mcf-NGS and 3.9 days (IQR 2.5–5 days) for serologic testing. Plasma PCR for *R. rickettsii* was sent in 1 case and the result received in 3 days. Antimicrobial therapy was altered because of the mcf-NGS result in 4/7 cases.

Case 1

A previously healthy 5-year-old boy residing in Tecate was brought to the emergency department of Rady Children's Hospital for 5 days of fever, abdominal pain, vomiting, rash, and altered mental status. The rash began on his face and extremities and subsequently generalized to the entire body. His family recalled a tick bite on his neck ≈2 weeks earlier. Physical examination disclosed a lethargic child with nystagmus, nuchal rigidity, and a diffuse petechial rash that was present on the palms and soles. The patient was admitted to the pediatric intensive care unit. Cerebrospinal fluid (CSF) analysis revealed elevated protein (175 mg/dL; reference range 15–40 mg/dL), glucose level within reference range, and CSF pleocytosis with 53 nucleated cells/μL (reference range 0–10 cells/μL), consisting of 47% neutrophils, 30% mononuclear cells, and 7% lymphocytes. Empiric ceftriaxone, vancomycin, and doxycycline were initiated. Magnetic resonance imaging (MRI) of the brain was notable for innumerable punctate foci of cytotoxic edema involving the supratentorial white matter (Figure 1). Rickettsial antibodies and plasma mcf-NGS were tested on hospital day (HD) 1. On HD3, mcf-NGS result returned with detection of *R. rickettsii*. Initial rickettsial antibodies results were negative, but plasma PCR tested on HD1 returned positive results on HD5. Vancomycin and ceftriaxone were discontinued on HD3, and doxycycline monotherapy was continued to complete a 19-day course. Follow-up serologic testing in the convalescent stage was not performed. The patient survived, with persistent deficits in gross motor function and speech with plans for ongoing rehabilitation.

Case 2

A previously healthy 10-year-old girl was brought for care for 7 days of fever, rash, and bilateral conjunctival injection. The rash began on the trunk and spread distally and involved the palms and soles (Figure 2). There was no history of insect bites or tick exposure. The patient lived in Calexico, California, but frequently traveled across the US–Mexico border, including recent travel to Ensenada in Baja California, Mexico. She was admitted to the pediatric intensive care unit for altered mental status and hypotension, and empiric vancomycin, meropenem, and doxycycline were initiated. Results of CSF analysis, other than an elevated protein of 72 mg/dL, were unremarkable. Results of

Table. Epidemiologic details for 7 cases of Rocky Mountain spotted fever at the US–Mexico border among children treated at Rady Children's Hospital, San Diego, California, USA

Case	Age/sex	Month of illness	Residence	Travel to/within Baja California, Mexico, in 14 d preceding admission	History of tick bite	History of other animal exposure
1	5 y/M	April	Tecate, Mexico	Primary residence in Tecate, Mexico	Yes	Dogs
2	10 y/F	June	Calexico, CA, USA	To Ensenada, Mexico	No	Goats, pigs
3	7 y/M	February	San Diego, CA, USA	None	No	Dogs
4	14 y/F	October	Mexicali, Mexico	Primary residence in Mexicali, Mexico	Yes	Dogs
5	10 y/F	July	El Centro, USA	To Mexicali, Mexico	No	Dogs
6	17 mo/M	August	El Cajon, USA	To Tecate, Mexico	No	Dogs
7	4 y/M	June	Alpine, CA, USA	None	No	Cats, chickens

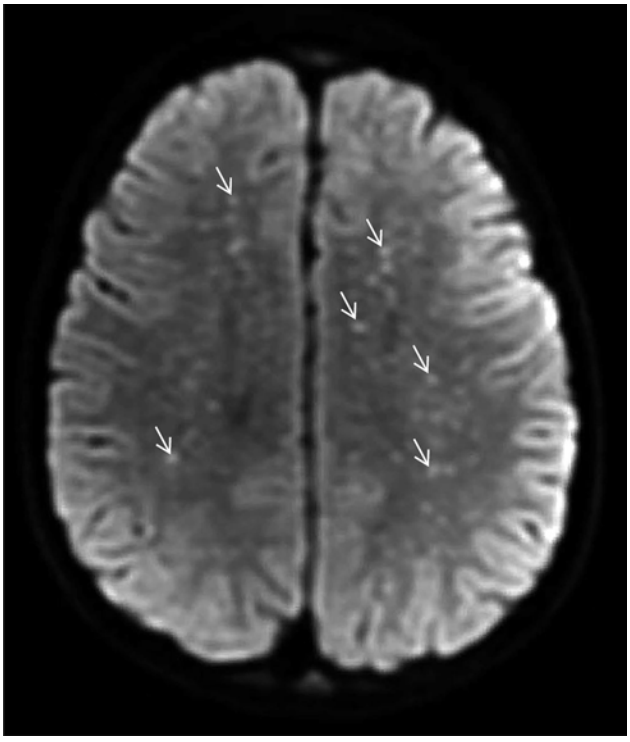

Figure 1. Diffusion-weight magnetic resonance imaging of the brain of a previously healthy 5-year-old boy from Tecate, Mexico, who had Rocky Mountain spotted fever and was treated at Rady Children's Hospital, San Diego, California, USA. The "starry sky" appearance shows numerous punctate foci of cytotoxic edema involving the supratentorial white matter (arrows), in keeping with acute to subacute injury from small vessel vasculitis.

MRI of the brain were unremarkable. Plasma mcf-NGS and rickettsial serology were tested on HD1; both tests had results on HD3. Mcf-NGS detected *R. rickettsii*; the finding was concordant with the *R. rickettsii* IgM. Vancomycin and meropenem were discontinued; the patient completed an 18-day course of doxycycline. The patient's altered mental status resolved completely before hospital discharge. At follow-up, she had returned to her baseline state of health.

Case 3

A previously healthy 7-year-old boy from San Diego was admitted to Rady Children's Hospital for evaluation of 6 days of fever, maculopapular rash, and joint pain in the ankles and feet. The rash first appeared on his face and spread to involve the trunk, palms, and soles. There was no history of tick exposure, and the family reported no recent travel outside of San Diego. Empiric antimicrobial therapy was not started. After 6 days of hospitalization, during which the fever persisted, mcf-NGS tested was performed, and results returned positive for *R. rickettsii* 2 days later. The rash, which was initially maculopapular in morphology, developed into petechiae during the hospital course. Lumbar puncture and central nervous system imaging was not performed. He was started on doxycycline, after which clinical symptoms resolved. The diagnosis of RMSF was confirmed with positive *R. rickettsii* IgG and IgM from testing sent on HD9 and results received 4 days later. He completed 7 days of doxycycline and returned to his baseline level of health.

Case 4

A previously healthy 14-year-old girl from a rural area of Mexico near Mexicali was admitted to the hospital with rash, fever, and altered mental status. Six days before care was sought, she had a presumed insect bite on her face, which developed a surrounding petechial rash. The rash subsequently generalized to her entire body, including the palms and soles. She was brought to Mexicali General Hospital, where she was stabilized, then transferred to Rady Children's Hospital for PICU level of care. Empiric vancomycin and ceftriaxone were initiated at Mexicali General Hospital, and doxycycline was initiated upon admission to Rady Children's Hospital. CSF analysis was notable for elevated protein 277 mg/dL, glucose level within reference range, and CSF pleocytosis with 83 nucleated cells/μL, 85% neutrophils, 12% lymphocytes, and 3% mononuclear cells. Brain MRI showed numerous punctate hemorrhages, thought to reflect small vessel ischemic changes from microvasculitis. Plasma mcf-NGS and rickettsial antibody testing were sent upon hospital admission. Test result for mcf-NGS were positive for *R. rickettsii* on HD4; initial rickettsial antibody testing was negative, but the patient demonstrated seroconversion with detectable *R. rickettsii* IgG antibody on HD7. Vancomycin and ceftriaxone were discontinued on HD4, and she continued doxycycline for a total 14-day course. Once her clinical condition stabilized, her family requested transfer back to the referring hospital to be closer to their home. She displayed significant gross motor, fine motor, and speech deficits at the time of hospital transfer.

Case 5

A previously healthy 10-year-old girl from El Centro, California, sought care for 5 days of fever, abdominal pain, emesis, dysuria, and rash on her torso, hands, and feet. The patient was initially seen at an outside hospital and noted to have elevated inflammatory markers, hypotension, and coagulopathy, prompting transfer to Rady Children's Hospital. There was a history of possible exposure to ticks found on the family dog, but the case-patient had not sustained any known tick bites. The family reported recent travel to

Mexicali, Mexico. At admission to the pediatric critical care unit, she was started on doxycycline and ceftriaxone. On HD2, she experienced altered mental status and lethargy. Computed tomography (CT) scan of the head showed no acute abnormality. A lumbar puncture showed elevated opening pressure of 26 mm Hg (reference range 7–15 mm Hg). CSF was notable for 48 nucleated cells/μL with 25% monocytes, 34% neutrophils, and 31% lymphocytes and for elevated protein 46 mg/dL; glucose level was within reference range. Testing obtained on HD1 included mcf-DNA, which detected *R. rickettsii*; the antibodies initially obtained from serum were negative. Serologic testing by IFA was repeated on HD7, revealing IgG and IgM reactive with *R. rickettsii*. The results became available 12 days after initial evaluation and 2 days after hospital discharge. She received 7 days of empiric ceftriaxone for a possible urinary tract infection and 14 days of doxycycline. Upon discharge, the patient was at baseline with no neurologic sequelae.

Case 6

A previously healthy 17-month-old boy from Tecate, Mexico, was brought for care with 1 week of fever and 3 days of lethargy, as well as 5 days of a diffuse maculopapular rash. At the emergency department, he was noted to have seizure activity with leftward eye and head deviation and a petechial rash on his palms, soles, and mucosal surfaces. He was admitted to the pediatric ICU. The family noted tick exposures around their rural home. Empiric meropenem and doxycycline were initiated. An MRI of the brain noted periventricular and subcortical white matter infarcts secondary to vasculitis. A lumbar puncture obtained at admission had 142 nucleated cells/μL with 61% neutrophils, 14% mononuclear cells, and 25% lymphocytes, elevated protein of 115 mg/dL, and glucose level within reference range. Both RMSF serology and mcf-DNA were sent on HD1, with mcf-DNA noting *Rickettsia* returning on HD3, 2 days before serology results returned. He was treated with 14 days of doxycycline and 5 days of ceftriaxone, followed by 5 days of meropenem, for ongoing fever and presumed culture negative sepsis. He was discharged to home with improved mental status and no focal deficits.

Case 7

A previously healthy 4-year-old boy from Alpine, California, a small town ≈18 miles north of the California–Mexico border, sought care for 6 days of fever accompanied by hypotension, abdominal pain, and periorbital and peripheral extremity edema. At the onset of fever, he was seen at an urgent care and prescribed amoxicillin for acute otitis media; 4 days before admission, a rash developed on his thighs and extremities that was initially attributed to drug reaction. The fever and rash persisted, and he came to the Rady Children's Hospital emergency department on day 6 of illness. He had a history of exposure to farm animals, including dogs and chickens, but no known tick exposure. Empiric ceftriaxone and vancomycin were started, and he was admitted to the pediatric ward. He was escalated to the intensive care unit on HD2 for bilateral pleural effusion and respiratory distress; empiric antimicrobial drugs were broadened to cefepime, doxycycline, and vancomycin upon admission to the PICU. Lumbar puncture and CNS imaging were not performed. Both RMSF serology and mcf-DNA were sent on HD3. Both mcf-DNA noting *Rickettsia* and serology results were returned after patient discharge, 6 days after being sent. He was treated with 10 days of doxycycline and a combined 7 days of cephalosporin therapy for presumed culture negative sepsis. He was discharged to home at his baseline level of health.

Figure 2. Characteristic petechial rash on the palms and soles of children with Rocky Mountain spotted fever treated at Rady Children's Hospital, San Diego, California, USA.

Discussion

We described 7 children with RMSF diagnosis at a tertiary academic center in San Diego, California, USA, in whom plasma mcf-NGS detected *R. rickettsii* over a 7-year period. Four of 7 patients had detectable rickettsial antibody titers on initial visit. All cases were independently verified with serology or PCR during their clinical course.

Although RMSF cases are not commonly diagnosed in southern California, RMSF has reached epidemic proportions in northern Mexico, where the brown dog tick, *Rhipicephalus sanguineus* sensu lato, serves as the principal vector (*7*,*8*). Exposures are occurring in domestic and peridomestic settings within urban centers because *Rh. sanguineus* ticks can complete their entire life cycle with dogs as its primary host (*4*,*9*). During 2020–2021, the overall RMSF case fatality rate was 32% across Baja California; Mexicali had the highest number of cases (*10*). Humans are infected in urban centers because of close contact with stray dogs. Domestic dogs may also become infested with brown dog ticks, and children may be especially at risk because they frequently interact with pet dogs and share peridomestic habitats with pet and stray dogs (*11*,*12*). Stray dogs are rare in southern California because of animal control regulations, and pets are often prophylactically treated to prevent tick infestation, likely decreasing *R. rickettsii* transmission by brown dog ticks in southern California. However, the potential for zoonotic disease spread remains as humans and their pets continue traveling to and from Mexico.

In this report, 5/7 patients reported travel to northern Mexico in the 2 weeks preceding hospital admission. San Diego County and neighboring Imperial County share an international border with Mexico; >100 million crossings were reported in 2022 through the public land ports (*13*). San Diego County exemplifies the fluid nature of RMSF transmission, with travelers frequently crossing and residing on both sides of the border. Of interest, 2 patients in this case series had no reported travel to Mexico. Families may travel with pets or bring dogs across the border, thereby importing *R. rickettsii* into southern California where foci of local infection can be established (*2*,*5*–*10*). Still, because the *Dermacentor occidentalis* tick is the sylvatic species that the California State Public Health Department attributed the source for certain non–travel associated RMSF cases (*8*,*14*) and because *R. rickettsii* has been detected in tick pools collected by the County of San Diego Vector Control Program as recently as 2023 (J. Aramkul, M.E. Beatty, M. Monroe, unpub. data), advising hikers and others engaged in outdoor activities in the habitat of *D. occidentalis* ticks on tick avoidance and removal is relevant.

The use of paired acute and convalescent specimens obtained 2–6 weeks apart for serologic testing is considered the reference standard for diagnosis of RMSF and achieves >90% sensitivity by day 14 of illness (*1*,*15*). However, patients may not develop detectable antibody titers until 7–10 days after illness onset, and they may die before detectable antibodies have developed (*16*). Given the high degree of virulence of RMSF, recognition of the risk factors and clinical syndrome of RMSF and prompt initiation of appropriate empiric antimicrobial therapy is critical; initial negative antibody testing results should not dissuade clinicians from the diagnosis. Although 5 patients in this case series had no known tick bites, all patients reported exposure to domestic animals, most commonly dogs. All patients in this series experienced fever and rash that involved the palms and soles and had common laboratory abnormalities, including hyponatremia, anemia, thrombocytopenia, transaminitis, and elevated C-reactive protein.

Physical examination, exposure and travel history, and a high index of suspicion are required for first-line healthcare providers to suspect RMSF. RMSF should be considered in the differential diagnosis for any seriously ill patient with recent travel to northern Mexico, even in the absence of classic risk factors or symptoms. Doxycycline is the treatment of choice in patients of all ages, is safe to administer to patients of any age, and should be initiated as soon as there is a clinical suspicion for RMSF without waiting for laboratory confirmation (*1*,*3*).

Plasma mcf-NGS is a noninvasive method of detecting microbial DNA in patient plasma (*17*). Turnaround times for plasma mcf-NGS approach 24–48 hours, short enough that the technology is an actionable method of achieving a diagnosis. In cases where infection is suspected but standard diagnostic tests fail to identify an infectious etiology, mcf-NGS may provide timely identification of a causative organism. In this single-center case series, the time for plasma mcf-NGS result was approximately half a day faster than serologic testing. Although mcf-NGS appears to be a promising diagnostic method for RMSF, doxycycline treatment should be initiated immediately without waiting for even a rapid diagnostic test result; therapeutic delay increases risk for death (*18*,*19*). Most children in our series were critically ill when they sought care and were started empirically on broad-spectrum antibiotics, including doxycycline. Once RMSF was diagnosed, antimicrobial therapy in 4/7 patients was eventually narrowed to doxycycline alone.

We described 7 children with RMSF who were admitted to our facility over 6.5 years. Our experience

aligns with recent epidemiologic trends indicating ongoing high levels of RMSF transmission in multiple border states in northern Mexico. Although our study is limited by its small sample size and retrospective nature, our findings suggest that plasma mcf-NGS may be a useful addition to the diagnostic armamentarium in situations where an infectious cause is suspected but the organism is difficult to isolate through standard methods, or where the clinical manifestation is atypical. This consideration is additionally salient in areas where the etiologic agent may not historically be considered endemic. We highlight the importance of closely monitoring epidemiologic trends in RMSF; early detection and treatment of this disease process are critical in averting serious illness.

About the Author

Dr. Chiang is an assistant professor in the division of Pediatric Infectious Diseases at University of California, Davis. Her primary interests are the clinical care of children with severe infections and the care of immunocompromised children.

References

1. Biggs HM, Behravesh CB, Bradley KK, Dahlgren FS, Drexler NA, Dumler JS, et al. Diagnosis and management of tickborne rickettsial diseases: Rocky Mountain spotted fever and other spotted fever group rickettsioses, ehrlichioses, and anaplasmosis—United States. MMWR Recomm Rep. 2016;65:1–44. https://doi.org/10.15585/mmwr.rr6502a1
2. Álvarez-Hernández G, Roldán JFG, Milan NSH, Lash RR, Behravesh CB, Paddock CD. Rocky Mountain spotted fever in Mexico: past, present, and future. Lancet Infect Dis. 2017;17:e189–96. https://doi.org/10.1016/S1473-3099(17)30173-1
3. Kimberlin DW, Barnett ED, Lynfield R, Sawyer MH; American Academy of Pediatrics Committee on Infectious Diseases. Red Book 2021–2024: report of the Committee on Infectious Diseases, 32nd edition. Itasca (NY): The Academy; 2021. https://doi.org/10.1542/9781610025225 https://doi.org/10.1542/9781610025225
4. Tinoco-Gracia L, Lomelí MR, Hori-Oshima S, Stephenson N, Foley J. Molecular confirmation of Rocky Mountain spotted fever epidemic agent in Mexicali, Mexico. Emerg Infect Dis. 2018;24:1723–5. https://doi.org/10.3201/eid2409.171523
5. Álvarez-Hernández G, Candia-Plata MC, Delgado-de la Mora J, Acuña-Meléndrez NH, Vargas-Ortega AP, Licona-Enríquez JD. Rocky Mountain spotted fever in Mexican children: Clinical and mortality factors [in Spanish]. Salud Publica Mex. 2016;58:385–92.
6. Centers for Disease Control and Prevention Health Alert Network. Severe and fatal confirmed Rocky Mountain spotted fever among people with recent travel to Tecate, Mexico. CDCHAN-00502. 2023 [cited 2023 Dec 24]. https://emergency.cdc.gov/han/2023/han00502.asp
7. Zazueta OE, Armstrong PA, Márquez-Elguea A, Hernández Milán NS, Peterson AE, Ovalle-Marroquín DF, et al. Rocky Mountain spotted fever in a large metropolitan center, Mexico–United States Border, 2009–2019. Emerg Infect Dis. 2021;27:1567–76. https://doi.org/10.3201/eid2706.191662
8. Drexler NA, Yaglom H, Casal M, Fierro M, Kriner P, Murphy B, et al. Fatal Rocky Mountain spotted fever along the United States–Mexico border, 2013–2016. Emerg Infect Dis. 2017;23:1621–6. https://doi.org/10.3201/eid2310.170309
9. Estrada-Mendizabal RJ, Tamez-Rivera O, Vela EH, Blanco-Murillo P, Alanis-Garza C, Flores-Gouyonnet J, et al. Rickettsial disease outbreak, Mexico, 2022. Emerg Infect Dis. 2023;29:1944–7. https://doi.org/10.3201/eid2909.230344
10. Waterman S, Gracia M. Rocky Mountain spotted fever in the California–Mexico border region: a growing vectorborne disease problem. San Diego Physician. 2023;12–5.
11. Demma LJ, Traeger MS, Nicholson WL, Paddock CD, Blau DM, Eremeeva ME, et al. Rocky Mountain spotted fever from an unexpected tick vector in Arizona. N Engl J Med. 2005;353:587–94. https://doi.org/10.1056/NEJMoa050043
12. Traeger MS, Regan JJ, Humpherys D, Mahoney DL, Martinez M, Emerson GL, et al. Rocky mountain spotted fever characterization and comparison to similar illnesses in a highly endemic area-Arizona, 2002-2011. Clin Infect Dis. 2015;60:1650–8. https://doi.org/10.1093/cid/civ115
13. US Department of Transportation. Border crossing entry data [cited 2023 Dec 7]. https://data.bts.gov/stories/s/Tables-Query-Tool/6rt4-smhh
14. Wikswo ME, Hu R, Dasch GA, Krueger L, Arugay A, Jones K, et al. Detection and identification of spotted fever group rickettsiae in *Dermacentor* species from southern California. J Med Entomol. 2008;45:509–16. https://doi.org/10.1093/jmedent/45.3.509
15. Kaplan JE, Schonberger LB. The sensitivity of various serologic tests in the diagnosis of Rocky Mountain spotted fever. Am J Trop Med Hyg. 1986;35:840–4. https://doi.org/10.4269/ajtmh.1986.35.840
16. Paddock CD, Greer PW, Ferebee TL, Singleton J Jr, McKechnie DB, Treadwell TA, et al. Hidden mortality attributable to Rocky Mountain spotted fever: immunohistochemical detection of fatal, serologically unconfirmed disease. J Infect Dis. 1999;179:1469–76. https://doi.org/10.1086/314776
17. Blauwkamp TA, Thair S, Rosen MJ, Blair L, Lindner MS, Vilfan ID, et al. Analytical and clinical validation of a microbial cell-free DNA sequencing test for infectious disease. Nat Microbiol. 2019;4:663–74. https://doi.org/10.1038/s41564-018-0349-6
18. Kirkland KB, Wilkinson WE, Sexton DJ. Therapeutic delay and mortality in cases of Rocky Mountain spotted fever. Clin Infect Dis. 1995;20:1118–21. https://doi.org/10.1093/clinids/20.5.1118
19. Minnich L, McJunkin JE, Bixler D, Slemp C, Haddy L, Busse F, et al.; Centers for Disease Control and Prevention (CDC). Consequences of delayed diagnosis of Rocky Mountain spotted fever in children—West Virginia, Michigan, Tennessee, and Oklahoma, May-July 2000. MMWR Morb Mortal Wkly Rep. 2000;49:885–8.

Address for correspondence: Leslie Chiang, University of California San Diego, 9500 Gilman Dr, Mail Code 0760, La Jolla CA 92093-0021, USA; email: lychiang@ucdavis.edu

Extrapulmonary *Mycobacterium abscessus* Infections, France, 2012–2020[1]

Benoît Heid-Picard, Faiza Mougari, Anne Pouvaret, Fanny Lanternier, Zeina Awad, Emmanuelle Bille, Olivier Lortholary,[2] Emmanuelle Cambau,[2] and the Mabsc Study Group[3]

Medscape CME Activity

In support of improving patient care, this activity has been planned and implemented by Medscape, LLC and Emerging Infectious Diseases. Medscape, LLC is jointly accredited with commendation by the Accreditation Council for Continuing Medical Education (ACCME), the Accreditation Council for Pharmacy Education (ACPE), and the American Nurses Credentialing Center (ANCC), to provide continuing education for the healthcare team.

Medscape, LLC designates this Journal-based CME activity for a maximum of 1.00 ***AMA PRA Category 1 Credit(s)™***. Physicians should claim only the credit commensurate with the extent of their participation in the activity.

Successful completion of this CME activity, which includes participation in the evaluation component, enables the participant to earn up to 1.0 MOC points in the American Board of Internal Medicine's (ABIM) Maintenance of Certification (MOC) program. Participants will earn MOC points equivalent to the amount of CME credits claimed for the activity. It is the CME activity provider's responsibility to submit participant completion information to ACCME for the purpose of granting ABIM MOC credit.

All other clinicians completing this activity will be issued a certificate of participation. To participate in this journal CME activity: (1) review the learning objectives and author disclosures; (2) study the education content; (3) take the post-test with a 75% minimum passing score and complete the evaluation at https://www.medscape.org/qna/processor/72828?showStandAlone=true&src=prt_jcme_eid_mscpedu; and (4) view/print certificate. For CME questions, see page 2459. NOTE: It is Medscape's policy to avoid the use of Brand names in accredited activities. However, in an effort to be as clear as possible, trade names are used in this activity to distinguish between the mixtures and different tests. It is not meant to promote any particular product.

Release date: October 21, 2024; Expiration date: October 21, 2025

Learning Objectives

Upon completion of this activity, participants will be able to:

- Assess anatomic infection sites of extrapulmonary infections due to *Mycobacterium abscessus* (EP-MAB)
- Analyze common clinical signs of EP-MAB
- Evaluate etiologies of infection with EP-MAB
- Assess clinical outcomes of EP-MAB infection

CME Editor

P. Lynne Stockton Taylor, VMD, MS, ELS(D), Technical Writer/Editor, Emerging Infectious Diseases. *Disclosure: P. Lynne Stockton Taylor, VMD, MS, ELS(D), has no relevant financial relationships.*

CME Author

Charles P. Vega, MD, Health Sciences Clinical Professor of Family Medicine, University of California, Irvine School of Medicine, Irvine, California. *Disclosure: Charles P. Vega, MD, has the following relevant financial relationships: served as a consultant or advisor for Boehringer Ingelheim; GlaxoSmithKline.*

Authors

Benoît Heid-Picard, MD, MSc; Faiza Mougari, MD, PhD; Anne Pouvaret, MD, MSc; Fanny Lanternier, MD, PhD; Zeina Awad, PharmD; Emmanuelle Bille, PharmD, PhD; Olivier Lortholary, MD, PhD; Emmanuelle Cambau, MD, PhD.

Author affiliation: Université Paris Cité, Paris, France

DOI: https://doi.org/10.3201/eid3011.240459

[1]Preliminary results from this study were displayed as oral communications at the 31st European Congress of Clinical Microbiology and Infectious Diseases (July 9–12, 2021, Vienna, Austria; abstract no. 04396) and at the 24èmes Journées Nationales d'Infectiologie (June 7–9, 2023, Grenoble, France; abstract no. PADS02-03).

[2]These authors contributed equally to this article.

[3]Mabsc Study Group members are listed at the end of this article.

Mycobacterium abscessus infection is challenging to treat. Extrapulmonary *M. abscessus* infections (EP-MAB) are less common than pulmonary *M. abscessus* infections. To evaluate treatment regimens, we retrospectively analyzed consecutive microbiologically confirmed EP-MAB cases diagnosed in France during 2012–2020. We studied 45 patients with EP-MAB, including 14 bone and joint infections, 10 skin and soft tissue infections, and 8 lymph node infections. Most (62%) patients had no reported immunodeficiency. In 27 patients, EP-MAB followed healthcare-associated (44%) or environmental (16%) injuries. Of the 45 isolates, 25 were subspecies *abscessus*, 10 *bolletii*, and 9 *massiliense*; 1 was unidentified. Cure was achieved for 36 (80%) patients who received a median antimicrobial regimen of 6 months; 22 (55%) also underwent surgery. Four patients died, and 5 were unavailable for follow-up. EP-MAB predominantly affects immunocompetent patients after an injury; outcomes are favorable. We propose a >6-month regimen of antimicrobial therapy with consideration for surgery and regular patient reassessment.

Nontuberculous mycobacteria (NTM) are found in the environment (*1*,*2*). They are increasingly recognized as causative agents of infections regardless of patient age or immune status, and in several countries they surpass tuberculosis in terms of prevalence (*3*–*5*).

Mycobacterium abscessus is a rapidly growing NTM (*6*,*7*), subcategorized as 3 subspecies: *abscessus*, *massiliense*, and *bolletii*. Subspecies affect pulmonary infection outcomes (*8*) because they correlate with the expression of the *erm*(41) gene (*9*), conferring inducible resistance to macrolides. Resistance has been noted for *M. abscessus* subsp. *bolletii* and *M. abscessus* subsp. *abscessus* sequevar T28 isolates, and susceptibility has been noted for *M. abscessus* subsp. *massiliense* and *M. abscessus* subsp. *abscessus* sequevar C28 isolates (*10*). Infection with those subspecies contributes to a poorer clinical outcome, restricting the effectiveness of macrolides, although they are recommended for pulmonary infections for all *M. abscessus* strains (*10*).

M. abscessus primarily causes pulmonary infections, particularly in patients with bronchiectasis (*10*). Despite multidrug antimicrobial therapy, cure rates remain <50%, and mortality rates are high (*11*). Extrapulmonary *M. abscessus* infections (EP-MAB) are rare, documented through localized outbreaks in single centers (*12*–*17*) or case series (*18*).

In France, *M. abscessus* accounts for 20%–25% of NTM clinical isolates received by the French National Reference Centre for Mycobacteria (CNR-MyRMA; https://cnrmyrma.fr) for identification and antimicrobial susceptibility testing in an infection context (E. Cambau, unpub. data). Although previous guidelines (*19*) provided advice about extrapulmonary NTM infections and proposed macrolide-based antimicrobial regimens and surgery and new guidelines have recently been updated for pulmonary *M. abscessus* infections (*10*), there are no specific recommendations for EP-MAB treatment duration. To investigate EP-MAB medical management (e.g., diagnostis, treatments, and outcomes), we retrospectively studied consecutive patients with microbiologically confirmed EP-MAB. In accordance with French law, our study protocol received approval by the "Comité d'éthique de la recherche AP-HP Centre" (IRB registration no. 00011928, Réf. 2020–12–04).

Material and Methods

Case Eligibility Criteria

We reviewed cases involving extrapulmonary infections associated with *M. abscessus* strains among all strains registered in the CNR-MyRMA database during January 2012–April 2020. Cases were eligible if they met the criteria of clinical signs/symptoms dependent on the site of the infection and ≥1 *M. abscessus* isolate was concurrently recovered from a sample from an extrapulmonary site (e.g., skin biopsy sample, articular fluid, blood). Multisite infections were defined as those involving 2 nonadjacent organs with concordant clinical, microbiological, or histologic criteria. Multisite infections that included pulmonary localization were eligible, and cases of pulmonary infection alone were not. The inclusion was assessed by authors B.H.P. and A.P.

Data Retrieval

We sent a questionnaire gathering epidemiologic, clinical, biological, radiologic, therapeutic, and follow-up data to physicians and microbiologists who reported a case. When needed, we also contacted them by phone or mail to request medical reports.

For injury-related infections, we set the geographic origin as the location where the injury occurred. For infections not associated with injury, the geographic origin was the location of the patient when initial symptoms were noted and, if that information was unavailable, the location where the diagnostic specimen was obtained. Healthcare-associated infections were defined as those following medical, surgical, or aesthetic procedures performed before the infection and at the same location. Antimicrobial regimens were recorded if administered for ≥7 days. We presented qualitative variables as medians (ranges). We considered patients cured if clinical reports indicated such; no microbiological evidence was required.

Identification and Antibiotic Susceptibility

We conducted mycobacterial identification and antimicrobial susceptibility testing (AST) in accordance with standard practice (*10*,*20*) and strain identification by using the GenoType *Mycobacterium* CM kit (Hain Lifescience, https://www.hain-lifescience.de), IVD MALDI Biotyper (Brucker Daltronics, https://www.bruker.com), and mass spectrometry Microflex LT MALDI-TOF MS (Brucker Daltronics), analyzed with the Mycobacteria Library MBT Compass3, (Bruker Daltonics) subspecies. We determined *erm*(41) sequevars by using the Genotype NTM-DR test (Hain Lifesciences, Bruker Daltronics) (*21*) complemented with *hsp65* or *rpoB* PCR Sanger sequencing when necessary. We performed AST in calcium-supplemented Mueller-Hinton medium and used Sensititre Myco AST Plate (Thermo Fisher Scientific, https://www.thermofisher.com) to determine MICs (*10*,*22*). To detect inducible clarithromycin resistance, we determined clarithromycin MICs after 3–5 days and after 14 days of incubation (*9*,*23*). We conducted molecular detection of mutations associated with antimicrobial resistance by targeting *rrl* for macrolides and *rrs* for aminoglycosides (*24*). We identified the *erm*(41) sequevar through PCR sequencing (*24*).

Results

During 2012–2020, CNR-MyRMA received 3,684 NTM strains for identification, including 736 (20%) *M. abscessus* strains, among which 56 (8%) were associated with EP-MAB (Figure 1). The average annual ratio of extrapulmonary to pulmonary strains was 0.07 (range 0.02–0.15) (Appendix Figure, https://wwwnc.cdc.gov/EID/article/30/11/24-0459-App1.pdf). Clinical data were collected for 47 (84%) strains isolated from the 45 patients (Table; Appendix Table 1).

Clinical and Biological Features

The 45 cases were distributed as 14 (31%) bone and joint infections (BJIs), 10 (22%) skin and soft tissue infections (SSTIs), 8 (18%) lymph node infections (LNIs), 4 (9%) bacteremia or catheter-related infections, 4 (9%) multisite infections, 3 (7%) breast

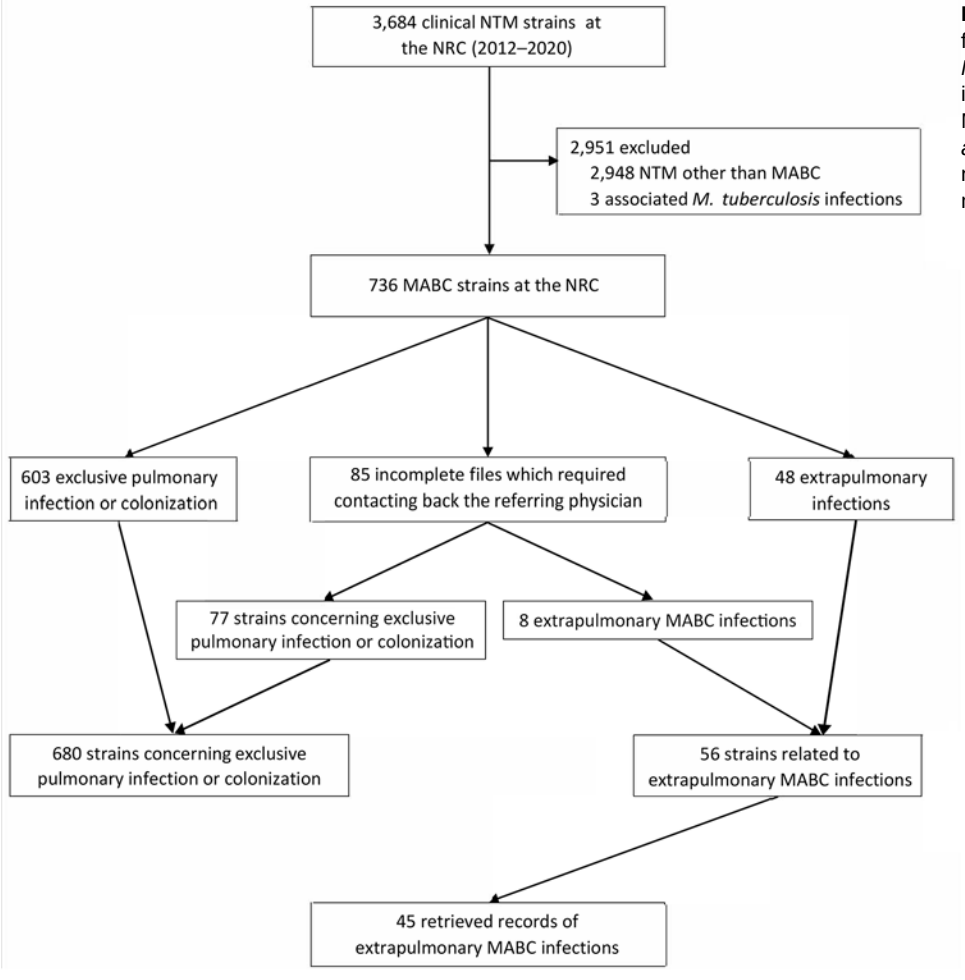

Figure 1. Flowchart of selection for study of extrapulmonary *Mycobacterium abscessus* infections, France, 2012–2020. MABC, *Mycobacterium abscessus* complex; NRC, national reference center; NTM, nontuberculous mycobacteria.

Table. Characteristics of 45 extrapulmonary *Mycobacterium abscessus* infections, France, 2012–2020*

Variable	Infections			Total
	Bone/joint	Skin/soft tissue	Lymph node	
Patients, no. (%)	14 (30)	10 (22)	8 (18)	45 (100)
Mean age, y, ± SD	50.2 ± 26.6	60.8 ± 21.2	43.7 ± 25.3	51.4 ± 24.5
M/F sex ratio	1.33	0.66	1	0.88
Geographic origin, no. (%)				
Metropolitan France	3	4	2	13 (29)
Overseas French territories	4	3	2	13 (29)
Foreign countries	7	3	4	19 (42)
Underlying immune disorder, no. (%)				
No known immunodeficiency	13	4	5	28 (62)
Immunosuppressive treatment	1	5	2	9 (20)
Solid tumor	0	0	1	4 (9)
Malignant hemopathy	0	1	0	2 (4)
Clinical features, no. (%)				
B symptoms†	7	4	2	17 (38)
Skin involvement	4	10	2	22 (49)
Initial injury	12	3	3	27 (60)
Median months to diagnosis [range]	4.5 [0.25–72]	1.5 [1–72]	1 [0.25–3]	3 [0.25–72]
Environmental	4	1	2	7 (16)
Healthcare associated	8	2	1	20 (44)
M. abscessus subspecies and *erm*(41) sequevars, no. (%)				
abscessus T28	7	5	1	19 (40)
abscessus C28	2	1	0	6 (13)
bolletii	2	2	4	12 (26)
massiliense	3	2	2	9 (19)
Medical management, no. (%)				
Surgery + antimicrobial regimen	11	3	3	22 (49)
Surgery alone	1	0	1	3 (7)
Antimicrobial regimen alone	2	6	3	13 (29)
Media months of antimicrobial regimen duration [range]	6 [2–12]	6 [3–15]	6 [1–6]	6 [1–long-term]
Outcome, no. (%)				
Cure	13	7	7	33 (73)
Relapse then cured	0	0	0	3 (7)
Not available for follow-up	1	2	1	5 (11)
Death	0	1	0	4 (9)

*Values are no. (%) except as indicated.
†Fever, night sweats, or weight loss.

infections, and 2 (4%) biliary tract infections. The median time between initial signs/symptoms and diagnosis was 2 months (range 1 week–2 years); 89% of cases were diagnosed in <6 months. The clinical signs were cutaneous lesions in 22 (46%) patients and palpable lymph nodes in 6 (13%) patients. Fever was noted for 9 (20%) patients, asthenia for 8 (17%), and night sweats for 2 (4%). BJIs were 7 monoarthritis, 4 lower limb osteitis, 2 spondylodiscitis, and 1 hip arthroplasty. Few details were available for SSTI descriptions; 7 cases were reported as cutaneous nodules. LNIs involved cervical lymph nodes in 4 patients, mediastinal lymph nodes in 3, and inguinal lymph nodes in 1. Median neutrophil count was 4.1×10^9 cells/L (range 0.93–11.64 $\times 10^9$ cells/L), median lymphocyte count was 1.2×10^9 cells/L (range 0.1–3.3 $\times 10^9$ cells/L), and median monocyte count was 0.6×10^9 cells/L (range 0.08–1.77 $\times 10^9$ cells/L). Median C-reactive protein concentration was 29 mg/L (range <5–230 mg/L). Thoracic computed tomography was available for 21 (47%) patients and revealed parenchymal infiltrates (including mostly condensations, nodules, or both) in 15 patients. After other diseases were excluded, pulmonary involvement was confirmed for only 2 of the 15 patients. For 2 of 4 patients with multisite *M. abscessus* infection, a thoracic computed tomography scan showed mediastinal lymph nodes in one and bilateral pulmonary nodules in the other. For the 2 patients with microbiologically proven spondylodiscitis, respiratory samples were also *M. abscessus* despite the absence of pulmonary signs or known underlying bronchopulmonary disease, suggesting probable colonization.

Epidemiology of Patients with Extrapulmonary Infections

The median patient age was 51.4 years (range 1–98 years); 6 (13%) were <18 years of age. The M:F sex ratio was 0.88. Underlying disease was documented for 19 (42%) patients, including 16 with immunodeficiency acquired by treatment or disease (Figure 2), 1 with inborn error of immunity (NEMO [nuclear factor κB essential modulator] mutation), and 2 with prior chronic pulmonary diseases. The remaining 26

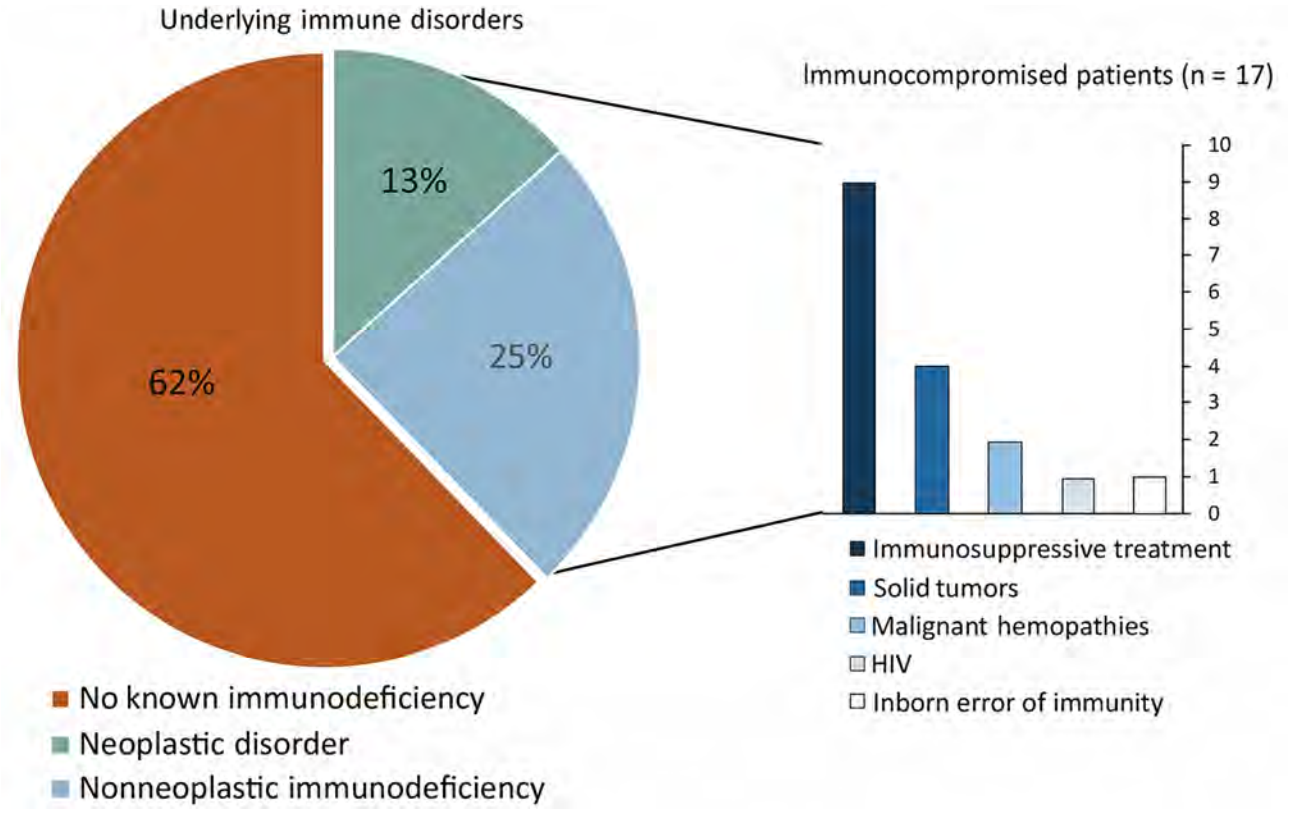

Figure 2. Medical conditions associated with extrapulmonary *M. abscessus* infections, France, 2012–2020.

patients were classified as immunocompetent, 2 of whom were negative for inborn immunodeficiency.

Penetrating injury was suspected as the portal of entry for 27 (60%) patients, including 20 (44%) with healthcare-related cases and 7 (16%) associated with an environmental source. The median time after injury was 3 months (range 1 week–5 years). Of the 14 BJIs, 11 (79%) followed an initial injury, which was either skin injury (all 4 osteitis) or articular infiltration (3 of 7 monoarthritis). The 3 breast infections were associated with healthcare injury, 2 after bilateral prosthetic implant procedures performed in Mauritius and 1 after breast biopsy. Of 4 patients who experienced bacteremia, 3 had an implantable venous access device. Of 10 SSTIs, 3 were associated with injury, 2 of them on tattoos.

Travel-related infection affected 32 (71%) patients, of which 13 (29%) of 45 cases were diagnosed in overseas France (6 in French West Indies, 4 in La Réunion Island, 1 in French Guyana, 1 in New Caledonia, and 1 in French Polynesia), 10 in Africa, 3 in the Americas, 3 in East Asia, 2 in Europe, and 1 in the Middle East. The remaining 13 (29%) patients were metropolitan France residents with no travel history that could be associated with *M. abscessus* infection.

Microbiological Results

The 47 strains collected for the 45 cases were distributed as 25 (53%) *M. abscessus* subsp. *abscessus* that included 19 (40%) *erm*(41) sequevar T28 and 6 (13%) sequevar C28, 12 (26%) *M. abscessus* subsp. *bolletii*, and 9 (19%) *M. abscessus* subsp. *massiliense* (Appendix Table 2). Subspecies identification was missing for 1 strain isolated in 2012. For the patient who experienced 2 relapses (patient 42), the same *M. abscessus* subsp. *bolletii* strain was isolated. All 9 strains of *M. abscessus* subsp. *massiliense* and 6 *M. abscessus* subsp. *abscessus erm*(41) sequevar C28 were susceptible to macrolides with a clarithromycin 90% MIC of 0.5 mg/L after 3–5 days and 1 mg/L after 14 days of incubation. For the 31 strains of *M. abscessus* subsp. *bolletii* and *M. abscessus* subsp. *abscessus erm*(41) sequevar T28, the clarithromycin 90% MIC was 8 mg/L after 3–5 days and >16 mg/L after 14 days of incubation. Sequences of *rrl* and *rrs* were available for all identified strains, and both were exhibited as a wild-type genotype.

Treatment

Before diagnosis, none of the patients had been treated with a drug that targeted *M. abscessus*. Antimycobacterial agents were administered to 35 (77%) patients, including 22 (49%) who also underwent

local surgery or local care; 3 (7%) patients underwent local surgery without antimicrobial drugs; 3 (7%) received local care alone; and 4 (9%) received no treatment (Appendix 2). Of the 35 initial antimicrobial drug regimens, 26 (74%) involved a combination of ≥3 drugs, 8 a combination of 2 drugs, and 1 was monotherapy. All regimens included macrolides for >3 weeks: clarithromycin (21 [62%]), azithromycin (11 [32%]), or sequential treatment with both (2 [6%]). For 30 (86%) patients, treatment started with an induction phase including ≥1 intravenous antimicrobial drug, and 4 (12%) patients received oral antimicrobial drugs only. For patients with BJIs, SSTIs, and LNIs, the median duration of the antimicrobial regimen was 6 months and the median duration of the induction phase was 6 weeks.

Outcomes

Cure rate with no relapse was 73% (33 patients), including 4 patients who received neither antimicrobial drugs nor surgery: 3 infections resolved with local care alone, and 1 patient with LNI experienced spontaneous resolution after 1 month. During the follow-up period, 4 (9%) patients experienced relapses (3 of whom eventually experienced cure and the other was not available for follow-up) and 4 (9%) patients died (3 died before receiving treatment for *M. abscessus* infection). Of the 4 who died, 2 had *M. abscessus* bacteremia and received supportive care for cancer, 1 had *M. abscessus* multisite infection diagnosed with a concomitant JC virus infection, and 1 had an SSTI and died of limb ischemia at 6 months of treatment. The 4 deaths were unrelated to *M. abscessus* infection. Five (11%) patients were unavailable for follow-up after 1 month of treatment. Overall cure was observed for 36 (80%) patients; median duration of patient follow-up was 32.5 months (1st quartile 26.25–3rd quartile 45.0 months). No explanatory factor was associated with the few infections that led to a negative outcome.

Immune reconstitution syndrome was noted for 1 patient (patient 25). The patient had an SSTI of the lower limb, and immune reconstitution syndrome affected the draining abdominal lymph nodes. The patient's condition improved after administration of steroids.

Discussion

M. abscessus is a challenging-to-treat pathogen (*10*), and EP-MAB is rarely described. In our series, EP-MAB often affected immunocompetent patients after injury, and for some patients, outcomes were favorable after antimicrobial therapy complemented with surgery.

In France, we benefit from the microbiological expertise of university hospital clinical microbiology national network reporting to CNR-MyRMA and from the monthly NTM treatment consilium organized by CNR-MyRMA. The collaborative network probably contributes to the widespread use of macrolides and the avoidance of antimicrobial monotherapy.

Although NTM are known as opportunistic pathogens with infections occurring in patients with underlying conditions or immunodeficiencies (*10*), in our series of EP-MAB, most (62%) patients had no reported immunodeficiency, although a few (15%) had undergone immunologic testing. Underlying inborn errors of immunity in children and adults have been revealed by NTM infections (*25*). We think that among patients with new EP-MAB infections, it is worthwhile to screen for immunodeficiencies (e.g., HIV serology testing or autoantibodies against interferon-γ [*26*]) as first-line tests in association with a clinical examination by a trained physician.

Unlike pulmonary infections, for which exposures are mainly unknown (*10*), in our study, the EP-MAB trigger was identified for 60% of the patients as a penetrating injury associated with healthcare or environmental inoculation. No outbreak was identified. Only the 3 patients with SSTIs remembered an injury, showing that small cutaneous injuries are almost unnoticed, as described previously (*27*–*29*). Considering the literature (*13*,*14*,*30*) and our data, *M. abscessus* infections might result from lack of antiseptic and aseptic procedures before joint infiltration, surgery, and aesthetic procedures including surgical tourism and thus might be avoidable.

Guidelines for treatment of NTM infections have recently been updated but only for pulmonary disease (*10*). Consequently, the recommendations for treatment of extrapulmonary NTM infections are those of the 2007 guidelines (*19*), which proposed a macrolide-based antimicrobial regimen and surgery but had no recommendations for treatment duration. With a cure rate of 80%, our study suggests that EP-MAB may have a much more favorable outcome than pulmonary *M. abscessus* diseases, which could result from the short time to diagnosis, because the median time to diagnosis observed in our study (2 months) aligns with findings from previous studies reporting outbreaks (*13*,*14*,*31*). Such a short time frame could be attributed to clinical similarities with tuberculosis, the ease of accessing sample sites, and the rapid growth ability of *M. abscessus*. It might contribute to the overall better prognosis for EP-MAB than for pulmonary *M. abscessus* infections. The clinical microbiology network reporting to

the CNR-MyRMA together with a monthly NTM treatment consilium probably contributes to the use of macrolides and the avoidance of antimicrobial monotherapy. The high proportion of surgeries could be attributed to specific infection sites, primarily involving BJIs and SSTIs. Some EP-MAB resolved spontaneously or with local care or surgery alone, a practice already described for LNIs in children (*32*). Overall, despite the relatively short duration of antimicrobial drug regimens, EP-MAB seems to have a favorable outcome with no sequelae and rare relapses, which contrasts with pulmonary infections, despite longer treatment durations (*10*). The discrepancy underscores the need for prospective studies specific for EP-MAB, specifically the optimal antimicrobial combinations, treatment duration, and criteria for associated or exclusive surgery.

The increase in cases reported to CNR-MyRMA during 2012–2020 was similar to reports from other northern countries (*33*–*36*), which could be attributed to awareness among physicians, along with improvements and standardization of the microbiological diagnosis of NTM (*37*). The increases may also indicate a growing prevalence of *M. abscessus* infections. Our findings underscore the value of increasing knowledge and monitoring of *M. abscessus*. In our cohort, the high number of infections originating from overseas territories of France or from countries in Africa suggests a higher risk for *M. abscessus* infection in tropical regions, consistent with previous reports (*13*,*14*,*31*,*38*). Factors such as climate change, globalization of trade, and medical tourism in tropical regions could contribute to the increased *M. abscessus* infections. Therefore, patients with EP-MAB should be asked about their detailed travel history (*13*). However, we did not identify any outbreaks, and isolates were not genotypically related (data not shown); 30% of the patients had infections diagnosed in metropolitan France, some of them having never traveled abroad. In temperate countries, *M. abscessus* has also been widely reported, primarily affecting patients with pulmonary infections, especially cystic fibrosis (*39*), but the *M. abscessus* environmental reservoir remains largely unknown.

Infection sites were diverse, localized primarily to 3 clinical manifestations: BJIs, SSTIs, and LNIs. Clinical manifestations varied, but classic tuberculosis symptoms (e.g., fever, night sweats, asthenia, or lymph node involvement), were reported for <40% of patients. Conversely, cutaneous signs were observed for 46% of patients, probably linked to a high proportion of SSTIs and BJIs. Enhanced clinical description of skin lesions could help clinicians determine severity and guide treatment decisions, particularly the need for surgery.

One of the main limitations of our study is its retrospective nature. Another limitation is that despite centralization at CNR-MyRMA, EP-MAB cases are not mandatorily reported, resulting in our data not being exhaustive. Less severe cases may not require specific medical management and microbiological diagnosis.

The results from our cohort of EP-MAB enables us to draw the following conclusions: there are no distinct underlying host characteristics but rather an association with penetrating injury and travel to tropical regions, and prognosis is generally favorable when multiple antimicrobial drugs are administered, with surgery if needed. We could not assess differences in outcomes based on clinical localization, causal subspecies, or underlying diseases. Such an assessment would require a collaborative study involving a larger number of cases, categorized by infection sites. While we wait for prospective data to become available, our data may support the benefits of treating EP-MAB with an antimicrobial regimen of >6 months including a macrolide, supplemented with surgery for BJIs and regular patient reassessment.

Acknowledgments

We thank all the patients who participated in this study. We also acknowledge the technical work done by the CNR-MyRMA team (Odile Vissouarn and all the technicians of the CNR-MyRMA during 2012–2020). We further acknowledge all the physicians of the Mabsc Study Group who contributed to these data by means of their involvement in the management of patients, expertise in diagnostic or characterization of mycobacterial isolates, listed alphabetically by location: M. Cihanek (Aix); C. Andrejak (Amiens); H. Cordel (Avicennes); R. Barruet (Beauvais); C. Chirouze (Besançon); A. Lesueur (Bligny); V. Castaigns, M.C. Receveur (Bordeaux); A.L. Roux (Boulogne); A. Desdoits, S. Deshayes, A. Laquievre (Caen); E. Beillard, L. Epelboin (Cayenne); M.E. Chanard (Centre Est); C. Bernard, C. Ragot (Clamart); V. Grobost, M. Vidal (Clermont-Ferrand); W. Vindrios (Créteil); J. Bador (Dijon); C. Etienne (Grasse); J. Claudeon, E. Curlier, U. Françoise, S. Guyomard, K. Pailla, E. Rossigneux (Guadeloupe); M. Gueye (Guyane); B. Hillion (Lagny); N. Allou, O. Belmonte, B. Kuli, R. Manaquin, L. Raffray, M. Verduyn (La Réunion); N. Crochette (Le Mans); V. Vieillefond (Levallois Perret); A.F. Georgel (Lille); P. Miailhes, C. Pariset, M.M. Ponsoda, E. Pricaz, A. Sénéchal, G. Singier (Lyon); L. Delapierre, H. Pegliasco (Marseille); O. Grossi (Nantes); G. Foulon (Neuilly); N. Ehret, J.M. Turmel (Martinique); K. Risso (Nice); I. Bourlaud, P. Lureau (Niort); J. Colot (Nouvelle-Calédonie); C. Bernigaud,

S. Bulifon, J. Bustamente, A. Canellas, E. Caumes, S. Chelabi, A. Contejean, F. Defournier, V. Delcey, L. Escaut, R. Gueneau, M. Humbert, V. Lalande, J. Lourtet, O. Paccoud, J. Pastre, G. Simonneau, C. Verdet, N. Veziris, V. Zeller (Paris); F. Chaix (Polynésie Française); D. Minette (Reims); V. Fabre (Rodez); I. Michelet (Rouen); M. Lagrange (Saint Denis); H. Tchero (Saint-Martin); P. Boyer (Strasbourg); E. Catherinot, I. Marroun (Suresnes); E. Oehler (Tahiti); K. Delavigne, M. Gauthier (Toulouse); G. Dewulf (Valenciennes); M. Amara, X. Brickley, A. Greder Belan, M. Groh, J. Vendroux (Versailles); E. Giroudon (Villefranche); E. Chachaty, E. Gallois, F. Griscelli (Villejuif).

The authors received no financial support for the research, authorship, or publication of this article. CNR-MyRMA is supported by Santé Publique France (Ministry of Health) by quinquennial grants for the periods 2009–2014 and 2015–2022. B.H.P., F.M., A.P., Z.A., E.B., E.C., and O.L. declare that they have no conflict of interest. F.L. received honoraria from Gilead, F2G, and Pfizer with no link to this work.

E.C., O.L., F.M., F.L., and E.B. designed the study. B.H.P. and A.P. were responsible for patients' recruitment and management. E.C., F.M., and Z.A. performed bacteriologic analysis. B.H.P., E.C., O.L., and A.P. drafted the manuscript. All authors contributed to revise the manuscript and all gave their approval for publication.

About the Author

Dr. Heid-Picard is a physician specialist in immunology and infectious diseases and a PhD student researching inborn errors of immunity and immune responses to viruses at the Imagine Institute, Paris.

References

1. Falkinham JO. Impact of human activities on the ecology of nontuberculous mycobacteria. Future Microbiol. 2010;5:951–60. https://doi.org/10.2217/fmb.10.53
2. Falkinham JO III. Nontuberculous mycobacteria from household plumbing of patients with nontuberculous mycobacteria disease. Emerg Infect Dis. 2011;17:419–24. https://doi.org/10.3201/eid1703.101510
3. Johnson MM, Odell JA. Nontuberculous mycobacterial pulmonary infections. J Thorac Dis. 2014;6:210–20.
4. von Reyn CF, Waddell RD, Eaton T, Arbeit RD, Maslow JN, Barber TW, et al. Isolation of *Mycobacterium avium* complex from water in the United States, Finland, Zaire, and Kenya. J Clin Microbiol. 1993;31:3227–30. https://doi.org/10.1128/jcm.31.12.3227-3230.1993
5. De Groote MA, Pace NR, Fulton K, Falkinham JO III. Relationships between *Mycobacterium* isolates from patients with pulmonary mycobacterial infection and potting soils. Appl Environ Microbiol. 2006;72:7602–6. https://doi.org/10.1128/AEM.00930-06
6. Runyon EH. Identification of mycobacterial pathogens utilizing colony characteristics. Am J Clin Pathol. 1970;54:578–86. https://doi.org/10.1093/ajcp/54.4.578
7. Lyle Cummins S, Williams EM. An "acid-fast" other than Koch's bacillus cultivated from sputum. Tubercle. 1933;15:49–53. https://doi.org/10.1016/S0041-3879(33)80019-5
8. Koh WJ, Jeon K, Lee NY, Kim BJ, Kook YH, Lee SH, et al. Clinical significance of differentiation of *Mycobacterium massiliense* from *Mycobacterium abscessus*. Am J Respir Crit Care Med. 2011;183:405–10. https://doi.org/10.1164/rccm.201003-0395OC
9. Nash KA, Brown-Elliott BA, Wallace RJ Jr. A novel gene, *erm*(41), confers inducible macrolide resistance to clinical isolates of *Mycobacterium abscessus* but is absent from *Mycobacterium chelonae*. Antimicrob Agents Chemother. 2009;53:1367–76. https://doi.org/10.1128/AAC.01275-08
10. Daley CL, Iaccarino JM, Lange C, Cambau E, Wallace RJ Jr, Andrejak C, et al. Treatment of nontuberculous mycobacterial pulmonary disease: an official ATS/ERS/ESCMID/IDSA clinical practice guideline. Eur Respir J. 2020;56:2000535. https://doi.org/10.1183/13993003.00535-2020
11. Mirsaeidi M, Machado RF, Garcia JGN, Schraufnagel DE. Nontuberculous mycobacterial disease mortality in the United States, 1999–2010: a population-based comparative study. PLoS One. 2014;9:e91879. https://doi.org/10.1371/journal.pone.0091879
12. Jeong SH, Kim SY, Huh HJ, Ki CS, Lee NY, Kang CI, et al. Mycobacteriological characteristics and treatment outcomes in extrapulmonary *Mycobacterium abscessus* complex infections. Int J Infect Dis. 2017;60:49–56. https://doi.org/10.1016/j.ijid.2017.05.007
13. Furuya EY, Paez A, Srinivasan A, Cooksey R, Augenbraun M, Baron M, et al. Outbreak of *Mycobacterium abscessus* wound infections among "lipotourists" from the United States who underwent abdominoplasty in the Dominican Republic. Clin Infect Dis. 2008;46:1181–8. https://doi.org/10.1086/529191
14. Cardoso AM, Martins de Sousa E, Viana-Niero C, Bonfim de Bortoli F, Pereira das Neves ZC, Leão SC, et al. Emergence of nosocomial *Mycobacterium massiliense* infection in Goiás, Brazil. Microbes Infect. 2008;10:1552–7. https://doi.org/10.1016/j.micinf.2008.09.008
15. Leao SC, Tortoli E, Viana-Niero C, Ueki SYM, Lima KVB, Lopes ML, et al. Characterization of mycobacteria from a major Brazilian outbreak suggests that revision of the taxonomic status of members of the *Mycobacterium chelonae–M. abscessus* group is needed. J Clin Microbiol. 2009;47:2691–8. https://doi.org/10.1128/JCM.00808-09
16. Chu HS, Chang SC, Shen EP, Hu FR. Nontuberculous mycobacterial ocular infections—comparing the clinical and microbiological characteristics between *Mycobacterium abscessus* and *Mycobacterium massiliense*. PLoS One. 2015;10:e0116236. https://doi.org/10.1371/journal.pone.0116236
17. Tiwari TSP, Ray B, Jost KC Jr, Rathod MK, Zhang Y, Brown-Elliott BA, et al. Forty years of disinfectant failure: outbreak of postinjection *Mycobacterium abscessus* infection caused by contamination of benzalkonium chloride. Clin Infect Dis. 2003;36:954–62. https://doi.org/10.1086/368192
18. Kim JH, Jung IY, Song JE, Kim EJ, Kim JH, Lee WJ, et al. Profiles of extrapulmonary nontuberculous mycobacteria infections and predictors for species: a multicenter retrospective study. Pathogens. 2020;9:949. https://doi.org/10.3390/pathogens9110949
19. Griffith DE, Aksamit T, Brown-Elliott BA, Catanzaro A, Daley C, Gordin F, et al.; ATS Mycobacterial Diseases Subcommittee; American Thoracic Society; Infectious Disease Society of America. An official ATS/IDSA statement: diagnosis, treatment, and prevention of

nontuberculous mycobacterial diseases. Am J Respir Crit Care Med. 2007;175:367–416. https://doi.org/10.1164/rccm.200604-571ST
20. Cornaglia G, Courcol R, Herrmann J-L, Kahlmeter G. European Manual of Clinical Microbiology [cited 2024 Oct 1]. https://www.decitre.fr/livres/european-manual-of-clinical-microbiology-9782878050264.html
21. Mougari F, Loiseau J, Veziris N, Bernard C, Bercot B, Sougakoff W, et al.; French National Reference Center for Mycobacteria. Evaluation of the new GenoType NTM-DR kit for the molecular detection of antimicrobial resistance in non-tuberculous mycobacteria. J Antimicrob Chemother. 2017;72:1669–77. https://doi.org/10.1093/jac/dkx021
22. Clinical and Laboratory Standards Institute. CLSI M24, susceptibility testing of mycobacteria, *Nocardia* spp., and other aerobic *Actinomycetes* [cited 2023 Apr 21]. https://clsi.org/standards/products/microbiology/documents/m24
23. Maurer FP, Castelberg C, Quiblier C, Böttger EC, Somoskövi A. Erm(41)-dependent inducible resistance to azithromycin and clarithromycin in clinical isolates of Mycobacterium abscessus. J Antimicrob Chemother. 2014;69:1559–63.
24. Bastian S, Veziris N, Roux AL, Brossier F, Gaillard JL, Jarlier V, et al. Assessment of clarithromycin susceptibility in strains belonging to the *Mycobacterium abscessus* group by *erm*(41) and *rrl* sequencing. Antimicrob Agents Chemother. 2011;55:775–81. https://doi.org/10.1128/AAC.00861-10
25. Bustamante J, Boisson-Dupuis S, Abel L, Casanova JL. Mendelian susceptibility to mycobacterial disease: genetic, immunological, and clinical features of inborn errors of IFN-γ immunity. Semin Immunol. 2014;26:454–70. https://doi.org/10.1016/j.smim.2014.09.008
26. Döffinger R, Helbert MR, Barcenas-Morales G, Yang K, Dupuis S, Ceron-Gutierrez L, et al. Autoantibodies to interferon-γ in a patient with selective susceptibility to mycobacterial infection and organ-specific autoimmunity. Clin Infect Dis. 2004;38:e10–4. https://doi.org/10.1086/380453
27. Grubbs J, Bowen C. *Mycobacterium abscessus* infection following home dermabrasion. Cutis. 2019;104:79–80.
28. Dickison P, Howard V, O'Kane G, Smith SD. *Mycobacterium abscessus* infection following penetrations through wetsuits. Australas J Dermatol. 2019;60:57–9. https://doi.org/10.1111/ajd.12915
29. Carter KK, Lundgren I, Correll S, Schmalz T, McCarter T, Stroud J, et al. First United States outbreak of *Mycobacterium abscessus* hand and foot disease among children associated with a wading pool. J Pediatric Infect Dis Soc. 2019;8:291–6. https://doi.org/10.1093/jpids/piy036
30. Pereira RT, Malone CM, Flaherty GT. Aesthetic journeys: a review of cosmetic surgery tourism. J Travel Med. 2018;25.
31. Baker AW, Maziarz EK, Lewis SS, Stout JE, Anderson DJ, Smith PK, et al. Invasive *Mycobacterium abscessus* complex infection after cardiac surgery: epidemiology, management, and clinical outcomes. Clin Infect Dis. 2021;72:1232–40. https://doi.org/10.1093/cid/ciaa215
32. Loizos A, Soteriades ES, Pieridou D, Koliou MG. Lymphadenitis by non-tuberculous mycobacteria in children. Pediatr Int. 2018;60:1062–7. https://doi.org/10.1111/ped.13708
33. Cristancho-Rojas C, Varley CD, Lara SC, Kherabi Y, Henkle E, Winthrop KL. Epidemiology of *Mycobacterium abscessus*. Clin Microbiol Infect. 2024;30:712–71.
34. Valadas E. Nontuberculous mycobacteria: clinical importance and relevance to bacille Calmette-Guérin vaccination. Clin Infect Dis. 2004;39:457–8. https://doi.org/10.1086/422326
35. Prevots DR, Shaw PA, Strickland D, Jackson LA, Raebel MA, Blosky MA, et al. Nontuberculous mycobacterial lung disease prevalence at four integrated health care delivery systems. Am J Respir Crit Care Med. 2010;182:970–6. https://doi.org/10.1164/rccm.201002-0310OC
36. Brode SK, Marchand-Austin A, Jamieson FB, Marras TK. Pulmonary versus nonpulmonary nontuberculous mycobacteria, Ontario, Canada. Emerg Infect Dis. 2017;23:1898–901. https://doi.org/10.3201/eid2311.170959
37. Tagliani E, Kohl TA, Ghodousi A, Groenheit R, Holicka Y, Niemann S, et al. Appeal from the European tuberculosis reference laboratory network (ERLTB-Net) for improving the diagnosis of infections due to nontuberculous mycobacteria. Clin Microbiol Infect. 2024;30:4–6. https://doi.org/10.1016/j.cmi.2023.06.005
38. Baker AW, Lewis SS, Alexander BD, Chen LF, Wallace RJ Jr, Brown-Elliott BA, et al. Two-phase hospital-associated outbreak of *Mycobacterium abscessus*: investigation and mitigation. Clin Infect Dis. 2017;64:902–11. https://doi.org/10.1093/cid/ciw877
39. Lipworth S, Hough N, Weston N, Muller-Pebody B, Phin N, Myers R, et al. Epidemiology of *Mycobacterium abscessus* in England: an observational study. Lancet Microbe. 2021;2:e498–507. https://doi.org/10.1016/S2666-5247(21)00128-2

Address for correspondence: Benoît Heid-Picard, Service de Maladies Infectieuses et Tropicales Adultes, Hôpital Necker, Enfants Malades, 149, Rue de Sèvres, 75015 Paris, France; email: benoit.heid@inserm.fr

Antiviral Susceptibility of Swine-Origin Influenza A Viruses Isolated from Humans, United States

Rongyuan Gao,[1] Philippe Noriel Q. Pascua,[1] Anton Chesnokov, Ha T. Nguyen, Timothy M. Uyeki, Vasiliy P. Mishin, Natosha Zanders, Dan Cui, Yunho Jang, Joyce Jones, Juan De La Cruz, Han Di, Charles Todd Davis, Larisa V. Gubareva

Since 2013, a total of 167 human infections with swine-origin (variant) influenza A viruses of A(H1N1)v, A(H1N2)v, and A(H3N2)v subtypes have been reported in the United States. Analysis of 147 genome sequences revealed that nearly all had S31N substitution, an M2 channel blocker-resistance marker, whereas neuraminidase inhibitor–resistance markers were not found. Two viruses had a polymerase acidic substitution (I38M or E199G) associated with decreased susceptibility to baloxavir, an inhibitor of viral cap-dependent endonuclease (CEN). Using phenotypic assays, we established subtype-specific susceptibility baselines for neuraminidase and CEN inhibitors. When compared with either baseline or CEN-sequence–matched controls, only the I38M substitution decreased baloxavir susceptibility, by 27-fold. Human monoclonal antibodies FI6v3 and CR9114 targeting the hemagglutinin's stem showed variable (0.03 to >10 μg/mL) neutralizing activity toward variant viruses, even within the same clade. Methodology and interpretation of laboratory data described in this study provide information for risk assessment and decision-making on therapeutic control measures.

Influenza A viruses are enzootic in swine populations worldwide. All swine influenza A viruses are 1 of 3 antigenic subtypes—H1N1, H1N2, and H3N2—and distinct differences in evolutionary patterns exist between North American and Eurasian viruses (*1*). Because pigs are susceptible to influenza viruses circulating in humans, birds, and other species, they are considered mixing vessels (*2*). Accordingly, co-infection with viruses from different species can generate reassortants with zoonotic and pandemic potential (*2*–*4*). Beginning in the late 1990s, swine influenza viruses containing gene segments from human, avian, and classical swine viruses became widespread in pigs in North America (*4*,*5*). Those viruses contained the triple-reassortment internal gene (TRIG) cassette consisting of human-lineage polymerase basic 1 (PB1); avian-lineage polymerase basic 2 (PB2) and polymerase acidic (PA); and classical swine-lineage nucleoprotein (NP), matrix (M), and nonstructural (NS) segments (*1*). This TRIG cassette pairs with various hemagglutinin (HA) and neuraminidase (NA) gene combinations derived from classical swine or human lineages (*1*,*4*,*5*).

Under World Health Organization (WHO) International Health Regulations (2005), human infections by swine-origin influenza A viruses are reportable (*6*). In 2007, the US Centers for Disease Control and Prevention (CDC) began a similar national notification mandate (*7*). Previously, such cases had been rare in the United States (*8*). However, a novel swine-origin influenza A(H1N1) virus emerged in 2009 in North America, causing the first influenza pandemic of the 21st Century. Genetically, that virus, designated A(H1N1)pdm09, closely resembled North American triple-reassortant swine A(H1N1) viruses but with NA and M segments from Eurasian swine lineage (*9*,*10*). By 2010, A(H1N1)pdm09 had replaced seasonal influenza A(H1N1) viruses previously circulating in humans. Furthermore, humans have repeatedly reintroduced A(H1N1)pdm09 into pigs (*11*,*12*). Those reverse zoonoses, followed by reassortment in pigs, increased the diversity of swine viruses, creating new genotypes of unknown epidemiologic implications. Swine-origin viruses that cause human infections are called variant viruses to distinguish them from seasonal viruses and are denoted as A(HxNx)v (*13*).

Author affiliation: Centers for Disease Control and Prevention, Atlanta, Georgia, USA

DOI: https://doi.org/10.3201/eid3011.240892

[1]These authors contributed equally to this article.

In 2012, influenza A(H3N2)v viruses containing A(H1N1)pdm09-derived M gene (M-pdm09) caused a large multistate outbreak of >300 human infections in the United States; M-pdm09 is now dominant in swine influenza A viruses of all subtypes (*14*,*15*). Moreover, the A(H1N1)pdm09-derived N1 segment (N1-pdm09) has become 1 of 4 cocirculating NA lineages, alongside classical swine-lineage N1 (N1-classical) and 2 human N2 lineages, N2-1998 and N2-2002 (*16*). N2-1998 and N2-2002 resulted from introductions of human influenza A(H3N2) viruses into pigs in 1998 and 2002 (*4*,*17*). Other gene segments from the A(H1N1)pdm09 lineage and some from live-attenuated influenza vaccine (LAIV) strains used in pigs during 2017–2020 have been detected sporadically (*16*,*18*,*19*). Variant virus infections in the United States are mostly associated with attendance at agricultural fairs or swine exhibitions (*20*). However, concerns remain that these viruses could cause broader spillover events or even trigger a new pandemic.

CDC and other laboratories of the WHO Global Influenza Surveillance and Research System regularly conduct virologic characterization of emerging zoonotic viruses. Laboratory data are used for risk assessment, pandemic preparedness, and antiviral treatment recommendations (*21*,*22*). Three classes of influenza antiviral drugs are approved by the Food and Drug Administration to manage influenza A virus infections: M2 channel blockers, NA inhibitors (NAIs), and a PA cap-dependent endonuclease (CEN) inhibitor (PA-CENI) (*23*). However, genetic changes caused by spontaneous mutations, gene reassortment, or selective pressure (caused by antiviral treatment) might compromise the usefulness of those drugs. For example, CDC recommends against the use of M2 blockers for seasonal influenza A viruses because of resistance, a characteristic independently acquired by A(H1N1)pdm09 and A(H3N2) subtypes. All variant viruses containing M-pdm09 are resistant to M2 blockers because of the presence of an S31N substitution in the M2 protein. In the United States, 3 NAIs (oseltamivir, zanamivir, and peramivir) are approved, and laninamivir is additionally approved in Japan only. The emergence and global spread of oseltamivir-resistant seasonal H1N1 virus in 2008–2010 and reports of community spread of oseltamivir-resistant A(H1N1)pdm09 viruses (*24*,*25*) demonstrate that broad circulation of antiviral resistant influenza virus is an ongoing public health concern.

The continuing pandemic threat posed by animal-origin influenza A viruses necessitates closely monitoring their antiviral susceptibilities, but phenotypic data for variant viruses are limited, and their interpretation is ill-defined. Here, we describe the testing algorithm and interpretation of phenotypic data for variant viruses collected in the United States since 2013.

Methods

Reagents

We dissolved NAIs (Biosynth, https://www.biosynth.com) oseltamivir carboxylate (oseltamivir), zanamivir, peramivir, and laninamivir in sterile distilled water. We dissolved baloxavir acid (MedChem Express, https://www.medchemexpress.com), an active metabolite of prodrug baloxavir marboxil, in dimethyl sulfoxide.

We purchased the broadly cross-reactive HA-stem targeting monoclonal antibodies (mAbs) FI6v3 and CR9114 from Creative Biolabs, Inc. (https://www.creativebiolabs.net). We collected antiserum from ferrets at 28 days postinfection and treated it with receptor-destroying enzyme (Denka Seiken, https://www.denka.co.jp) before use.

Viruses

Variant influenza viruses were submitted by US public health laboratories to the WHO Collaborating Center for Surveillance, Epidemiology and Control of Influenza at CDC and propagated in MDCK cells (ATCC, https://www.atcc.org) according to standard procedures (*26*). We used the CDC antiviral susceptibility reference virus panels (International Reagent Resource FR-1755 and FR-1678) as controls in phenotypic assays. Handling and testing of variant viruses were conducted in Biosafety Level 2 enhanced laboratories.

Next-Generation Sequencing and Analysis

We obtained whole-genome sequences by using the Illumina next-generation sequencing platform, analyzed by the iterative refinement meta-assembler (*27*), and deposited into GISAID (https://www.gisaid.org) (Appendix, https://wwwnc.cdc.gov/EID/article/30/11/24-0892-App1.pdf). We aligned sequences by using MAFFT version 7 (*28*).

Antiviral Susceptibility Assays

We examined NAI susceptibility using the fluorescent NA-Fluor kit (Applied Biosystems) (*29*). We assessed baloxavir susceptibility using the influenza replication inhibition neuraminidase-based assay (IRINA) in MDCK-SIAT1 cells (*30*). We determined the 50% inhibitory concentration (IC_{50}) and 50% effective concentration (EC_{50}) by curve-fitting analysis using nonlinear regression (*29*,*30*).

Virus Neutralization and HA Antigenic Analysis

To assess the neutralization activity of mAbs, we preincubated 2-fold serially diluted mAb (starting at 10 μg/ml) with virus for 1 hour. We performed IRINA as was done for baloxavir susceptibility testing. We assessed HA antigenicity by hemagglutination inhibition (HI) using 0.5% turkey red blood cells (Lampire Biological Laboratories, https://www.lampire.com) according to standard procedures (*26*) and subsequently by IRINA as previously described (*30*).

Results

Genome Sequence Analysis for Molecular Markers of Decreased Drug Susceptibility

During January 2013–April 2024, a total of 167 human infections caused by variant viruses were reported in 22 states across the United States; 17 cases were A(H1N1)v, 34 were (H1N2)v, and 116 were A(H3N2)v (*20*). In addition, 4 A(H1N1)pdm09 viruses from 2021 were recently reclassified as variant viruses based on their HA (*12*). We interrogated the deduced M2, NA, and PA protein sequences of 147 variant viruses to identify amino acid substitutions (molecular markers) associated with antiviral resistance or reduced antiviral susceptibility (Appendix Table 1).

Molecular markers of M2 blocker resistance are well defined; thus, sequence analysis is the primary method to determine susceptibility to this class of influenza antivirals (*31*). All but 1 variant virus had an M-pdm09 segment encoding a resistance-conferring S31N (Appendix Table 1). The exception—A/Hawaii/28/2020 (H3N2)v—had an M segment from the A(H3N2) component of a swine LAIV (*19*) and lacked M2 resistance markers.

Next, we examined sequence data for markers of NAI and PA-CENI resistance that are subtype-specific (*32*,*33*). None of the variant viruses had known markers of resistance to any NAI. However, A/Iowa/02/2021 (H1N1)v had S247N, a substitution that reduces oseltamivir inhibition for A(H5N1) (*34*) but not A(H1N1)pdm09 viruses (*35*) (Appendix Table 1). When analyzing the PA-CEN domain (Appendix Table 1), we identified 2 substitutions associated with decreased baloxavir susceptibility (*33*). I38M, together with the wild-type sequence, was present as a mixed virus population in A/Iowa/33/2017 (H1N1)v (Appendix Table 1) (*36*). The other substitution, E199G, was found in A/New Jersey/53/2015 (H3N2)v. In addition, all 3 subtypes had either serine (S) or proline (P) at position 28. In a seasonal A(H3N2) virus, L28P conferred 2.5-fold reduced baloxavir susceptibility (*37*). Finally, A/Iowa/04/2013 (H3N2)v had a rare I120V substitution, the effect of which was unknown; however, I120T reportedly decreased susceptibility to the PA-CENI, L-742,001 (*38*).

Assessment of Virus Susceptibility to NAIs

We assessed virus susceptibilities to NAIs using the surrogate phenotypic assay, NA inhibition. Conventionally, influenza A viruses are classified as displaying normal, reduced, or highly reduced inhibition if their IC_{50} is increased by <10-fold (normal), 10- to 100-fold (reduced), or >100-fold (highly reduced) over the subtype-specific median IC_{50} (baseline) (*32*). Therefore, our first task was to establish the variant viruses' baseline susceptibility. We assembled a panel of 53 viruses available for phenotypic testing that represented the 3 antigenic subtypes collected during 2007–2024 to test their susceptibility to each NAI (Appendix Table 2). We included the A/California/07/2009 (H1N1)pdm09 virus (CA/09) to represent the swine-origin virus that caused the 2009 pandemic.

The enzyme activity of all viruses was potently inhibited by oseltamivir, zanamivir, peramivir, and laninamivir; most IC_{50} fell in a sub-nanomolar range (Appendix Table 2). Among the 3 subtypes, A(H1N2)v exhibited 2- to 4-fold higher median IC_{50}, particularly for zanamivir and laninamivir, whereas A(H1N1)v produced 2- to 4-fold higher oseltamivir IC_{50} (Figure, panel A; Appendix Table 2). This analysis exemplifies the utility of subtype-specific baseline values for data interpretation, which we then subsequently used to conduct within-subtype analyses and determine whether individual viruses exhibited reduced antiviral inhibition. A/Iowa/02/2021 (H1N1)v (which had S247N) exhibited 2- to 3-fold increased IC_{50}, which is interpreted as normal inhibition (Table 1; Appendix Table 2). A similar outcome was attained when it was compared to its closest NA sequence–matched control or CA/09. Of note, an I427V substitution carried by a 2012 A(H1N1)v virus (A/Missouri/12/2012) conferred 17- to 21-fold reduced inhibition by oseltamivir when compared with the subtype-specific median and CA/09 IC_{50}s. To further demonstrate the value of subtype-specific baseline, we next analyzed results for an A(H3N2)v virus with S247P, A/Ohio/88/2012 (Table 1; Appendix Table 2) (*15*). That virus displayed reduced inhibition by oseltamivir and zanamivir using either baseline or a sequence-matched control as comparator.

To examine whether baseline IC_{50} values are NA-lineage specific, we grouped viruses according to their NA clade: N1-classical (n = 7), N1-pdm09 (n = 8), N2-1998 (n = 12), and N2-2002 (n = 23). Viruses possessing

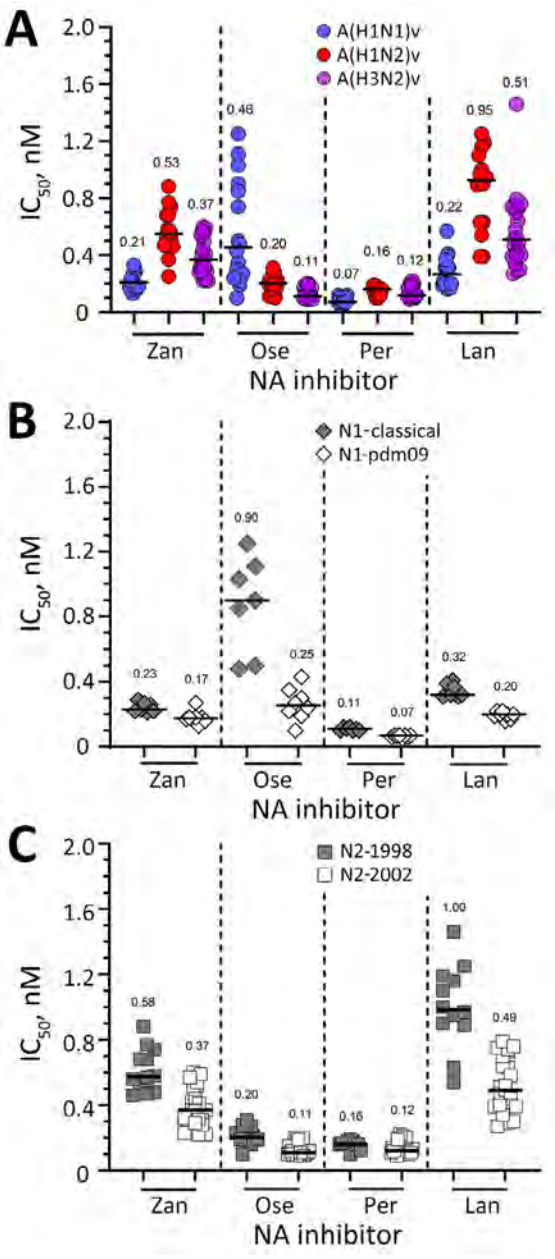

Figure. Susceptibility of variant viruses to NA inhibitors based on subtype and NA lineage in study of antiviral susceptibility of swine-origin influenza A viruses isolated from humans, United States. A) Susceptibility of A(H1N1)v (n = 15), A(H1N2)v (n = 14), and A(H3N2)v (n = 21) viruses to NA inhibitors determined in a fluorescence-based assay (*29*). The IC_{50}s of viruses lacking known or suspected molecular markers that reduce inhibition by NA inhibitors were used to calculate the subtype-specific median IC_{50}s (baseline susceptibility). B, C) Effect of NA lineage on inhibition by NA inhibitors. IC_{50}s obtained in NA inhibition assay were grouped according to their respective NA lineage: N1-classical (n = 7, closed diamond), N1-pdm09 (n = 8, open diamond), N2-1998 (n = 12, closed square), or N2-2002 (n = 23, open square). Horizontal bars and numbers indicate median IC_{50}s. IC_{50}, 50% inhibitory concentration; Lan, laninamivir; NA, neuraminidase; Ose, oseltamivir; Per, peramivir; Zan, zanamivir.

N1-classical had ≈4-fold higher median IC_{50} for oseltamivir compared with those containing N1-pdm09 (Figure, panel B; Appendix Table 2). Viruses possessing N2-1998 had ≈2-fold higher median IC_{50} for oseltamivir and laninamivir compared with those with N2-2002 (Figure, panel C). Overall, the observed interlineage differences were small but might affect interpretation of testing outcomes, particularly for N1 subtype against oseltamivir. For example, A/Missouri/12/2012 (H1N1)v would be reported either as displaying normal or reduced inhibition by oseltamivir, if the N1-classical baseline (8-fold) or the A(H1N1)v subtype-specific baseline (17-fold) was used for comparison (Table 1; Figure, panel B; Appendix Table 2).

Assessment of Susceptibility to Baloxavir

Susceptibility to baloxavir is assessed using cell culture-based assay. To report decreased susceptibility, the provisional cutoff was set at >3-fold above the subtype-specific baseline (*39*–*41*). Therefore, we first established baseline susceptibility using the same virus panel used previously except for 2 viruses with PA substitutions I38M and E199G. We tested viruses in the single-cycle replication assay IRINA (*30*) where the median EC_{50} values were 0.75 nM for A(H1N1)v, 0.98 nM for A(H1N2)v, and 1.27 nM for A(H3N2)v subtypes (Appendix Table 3). Of note, most A(H1N1)v viruses (11 of 16) had PA-pdm09, whereas PA-TRIG was dominant among A(H1N2)v and A(H3N2)v viruses. This finding raised the question of whether PA-pdm09 contributes to a somewhat lower A(H1N1)v baseline. However, we observed no apparent differences between A(H1N1)v viruses with PA-pdm09 or PA-TRIG (EC_{50} ranges 0.44–1.36 nM for PA-pdm09 and 0.50–1.58 nM for PA-TRIG) (Appendix Table 3). Therefore, the PA-lineage does not affect the susceptibility of US variant viruses to baloxavir. Of note, 2 viruses, A/Michigan/288/2019 (H1N1)v and A/Hawaii/28/2020 (H3N2)v, contained the LAIV virus–derived PA segment (*19*). Of those, 1 virus, A/Michigan/288/2019 (H1N1)v, exceeded the 3-fold provisional threshold compared to its subtype-specific baseline; however, substitutions in its PA-CEN domain associated with reduced baloxavir susceptibility were not present (Appendix Table 3).

A total of 11 viruses (e.g., A/Texas/14/2008) from all 3 subtypes shared the PA-CEN domain with identical amino acid sequence (Appendix Table 3). For those viruses, we again observed that A(H1N1)v viruses produced somewhat lower EC_{50} compared with A(H3N2)v (i.e., 0.54–0.93 nM vs. 1.0–1.85 nM). Therefore, A(H1N1)v viruses in this panel, except A/Michigan/288/2019, seemed slightly more susceptible

Table 1. NA inhibitor susceptibility of variant influenza viruses in a fluorescence-based neuraminidase inhibition assay in study of antiviral susceptibility of swine-origin influenza A viruses isolated from humans, United States*

Influenza A virus	Amino acid change in neuraminidase†	Mean IC_{50} ± SD, nM (fold change)			
		Zanamivir	Oseltamivir	Peramivir	Laninamivir
A(H1N1)v median IC_{50}, n = 15		0.21	0.43	0.07	0.22
A/Iowa/23/2020	–	0.18 ± 0.03 (1; 1)	0.27 ± 0.01 (1; 1)	0.07 ± 0.01 (1; 1)	0.22 ± 0.02 (1; 1)
A/Iowa/02/2021‡	S247N	0.33 ± 0.02 (2; 2)	1.05 ± 0.18 (2; 4)	0.20 ± 0.01 (3; 3)	0.57 ± 0.03 (3; 3)
A/Missouri/12/2012§	I427V	0.24 ± 0.06 (1; NA)	7.50 ± 0.73 (17; NA)¶	0.07 ± 0.01 (1; NA)	0.14 ± 0.02 (1; NA)
A(H1N2)v median IC_{50}, n = 14		0.55	0.20	0.16	0.92
A(H3N2) Median IC_{50}, n = 21		0.37	0.11	0.12	0.51
A/Ohio/83/2012	–	0.42 ± 0.12 (1; 1)	0.11 ± 0.02 (1; 1)	0.13 ± 0.02 (1; 1)	0.51 ± 0.05 (1; 1)
A/Ohio/88/2012#	S247P	34.78 ± 5.40 (94; 83)	5.09 ± 1.01 (46; 46)	0.20 ± 0.02 (2; 2)	4.45 ± 0.52 (9; 9)
Reference seasonal viruses**					
A/Illinois/45/2019 (H1N1)pdm09	–	0.15 ± 0.03	0.19 ± 0.03	0.05 ± 0.01	0.16 ± 0.03
A/Pennsylvania/46/2015 (H3N2)	–	0.24 ± 0.04	0.15 ± 0.03	0.09 ± 0.02	0.36 ± 0.06

*Each virus was tested in ≥3 independent experiments to determine IC_{50} value. Fold change values are given for the IC_{50} of variant virus containing amino acid substitution relative to subtype-specific median IC_{50} and wild-type NA sequence-matched virus IC_{50}, respectively. Viruses lacking known neuraminidase markers were used to determine the median IC_{50} (Appendix Table 2, https://wwwnc.cdc.gov/EID/article/30/11/24-0892-App1.pdf). Dashes indicate the absence of known or suspected molecular markers that reduce susceptibility to neuraminidase inhibitors. IC_{50}, 50% inhibitory concentration; NA, not applicable.
†The head domain of the neuraminidase that encompasses amino acid residues 82 to 470. Straight numbering is used to show amino acid substitutions. Residue 247 in N1 corresponds to residue 246 in N2.
‡A/Iowa/02/2021 (H1N1)v also contains N188S and V398I neuraminidase substitutions not present in the wild-type control virus, A/Iowa/23/2020 (H1N1)v.
§Wild-type control virus for A/Missouri/12/2012 (H1N1)v was not available for comparison.
¶The I427V neuraminidase substitution confers reduced inhibition by oseltamivir (17-fold increase) when compared with the A(H1N1)v median IC_{50} but normal inhibition (8-fold increase) when compared with the N1-classical IC_{50}.
#This virus was tested previously (*15*).
**Source: Centers for Disease Control and Prevention Neuraminidase Inhibitor Susceptibility Reference Virus Panel (IRR: FR-1755 ver3) (https://www.isirv.org/site/index.php/reference-panel).

to baloxavir. This difference is potentially because of differences in early-stage replication kinetics. Within each subtype, we noted no apparent difference in baloxavir susceptibility between viruses having S or P at residue 28 (Appendix Table 3).

A/Iowa/33/2017 (H1N1)v with I38M showed 27-fold decreased baloxavir susceptibility compared with the subtype-specific baseline and 15-fold decreased baloxavir susceptibility compared with the sequence-matched control (Table 2; Appendix Table 3). The observed effect is similar to that of I38M in a seasonal influenza A(H3N2) virus. Conversely, E199G found in A/New Jersey/53/2015 had no effect on baloxavir susceptibility when compared with either the subtype-specific baseline or a sequence-matched control (Table 2). I120V also did not alter baloxavir susceptibility of A/Iowa/04/2013 (Appendix Table 3).

Table 2. Baloxavir susceptibility of variant influenza viruses in cell culture-based IRINA in study of antiviral susceptibility of swine-origin influenza A viruses isolated from humans, United States*

Influenza viruses	Amino acid change in PA-CEN†	Mean EC_{50} ± SD, nM (fold change)
A(H1N1v) median EC_{50}, n = 15		0.75
A/Iowa/33/2017 clone 1‡	–	1.33 ± 0.07 (2; 1)
A/Iowa/33/2017 clone 2‡	I38M	19.98 ± 2.17 (27; 15)
A(H1N2v) median EC_{50}, n = 14	–	0.98
A(H3N2v) median EC_{50}, n = 21		1.27
A/Michigan/84/2016	–	1.53 ± 0.31 (1; 1)
A/New Jersey/53/2015	E199G	1.50 ± 0.17 (1; 1)
Reference seasonal viruses¶		
A/Louisiana/50/2017(H3N2)	–	1.08 ± 0.17 (NA; 1)
A/Louisiana/49/2017(H3N2)	I38M	14.06 ± 2.96 (13)

*Each virus was tested in ≥3 independent experiments to determine EC_{50} value. Fold-change: EC_{50} of variant virus containing PA amino acid substitution relative to subtype-specific median or the wild-type PA sequence-matched virus, respectively. Variant viruses lacking PA markers were used to determine the median EC_{50}s (Appendix Table 3, https://wwwnc.cdc.gov/EID/article/30/11/24-0892-App1.pdf). Dashes indicate the absence of known or suspected molecular markers for reduced baloxavir susceptibility. EC_{50}, 50% effective concentration; IRINA, influenza replication inhibition neuraminidase-based assay; NA, not applicable; PA, polymerase acidic; PA-CEN, PA cap-dependent endonuclease;.
†PA-CEN domain encompasses the N-terminal amino acid residues 1 to 209 in PA protein.
‡These viruses were previously tested (*40*).
¶Source: Centers for Disease Control and Prevention Baloxavir Susceptibility Reference Virus Panel (IRR: FR-1678 ver1.1) (https://www.isirv.org/site/index.php/reference-panel).

Overall, sequence analysis results supplemented with those from NA inhibition assay and IRINA suggest that the variant viruses isolated during January 2013–April 2024 maintain susceptibility to NAIs and PA-CENIs. Only 1 of 147 viruses (A/Iowa/33/2017 with PA-I38M) exhibited decreased susceptibility to baloxavir.

Neutralization by Antibodies Targeting HA

HA is considered an attractive target for development of mAbs as a non–small molecule treatment option (*23*). We next examined the neutralization activity of 2 human mAbs—FI6v3 and CR9114—targeting the HA-stem regions of group 1 and 2 influenza A viruses (*42*,*43*). Using IRINA, we observed a wide range of EC_{50}s (0.03 to >10 μg/mL) for both mAbs when tested against a subset of viruses (n = 22) from the 3 subtypes (Table 3). Specifically, we observed broad variation in EC_{50}s for A(H1N2)v viruses from clade 1B.2.1 (0.03 to >10 μg/mL for FI6v3 and 0.03–4.02 μg/mL for CR9114) (Table 3). In addition, within each subtype, ≥1 mAb failed to neutralize viruses even at the highest concentration tested (Table 3). We inspected HA sequences to identify variations in mAb epitopes (*42*,*43*), but none had an apparent effect (Appendix Table 4). Those observations suggest a role of amino acid differences outside the known epitopes. Overall, CR9114 was slightly more effective against the A(H1)v subtype compared with FI6V3.

Finally, to determine the antigenic relatedness between the variant viruses and select candidate vaccine viruses (CVVs), we used polyclonal postinfection ferret antiserum in an HI assay and IRINA. We specifically assessed the antigenic relatedness of clade 1B.2.1 (delta 2) A(H1N2)v viruses and A/Ohio/35/2017 (OH/17), a clade-specific CVV (Table 4). Results from both assays indicated that OH/17 antiserum had reduced reactivity to variant viruses (HI 4- to 64-fold; IRINA 9- to 144-fold). We observed the greatest reduction in neutralization activity for 2 viruses, both from 2023 (Table 4), that lack a potential glycosylation motif at residue 89 (H1 numbering) and contain substitutions at antigenic sites Ca (K168T, G237K), Sb (H193N) and 5 additional residues (Appendix Table 5). The OH/17 antiserum reacted somewhat better against the seasonal CVV A/Victoria/2570/2019 (H1N1)pdm09 than to variant viruses from 2023, indicating notable antigenic

Table 3. Neutralization of variant viruses by broadly reactive human mAbs in IRINA in study of antiviral susceptibility of swine-origin influenza A viruses isolated from humans, United States*

Influenza viruses	HA clade	Mean EC_{50} ± SD, μg/mL		HA Acc. ID†
		FI6v3	CR9114	
A(H1N1)v, n = 7				
A/California/07/2009	1A.3.3.2	>10	3.39 ± 0.74	EPI1161425
A/North Carolina/01/2021	1A.3.3.2	1.83 ± 0.35	0.48 ± 0.14	EPI1869574
A/North Dakota/12226/2021	1A.3.3.c-c1	7.91 ± 1.33	1.81 ± 0.25	EPI1918841
A/Missouri/12/2012	1A.3.3.3-c3	2.15 ± 0.15	0.62 ± 0.06	EPI395313
A/Arkansas/14/2013	1A.3.3.3-c3	7.79 ± 0.35	2.89 ± 0.18	EPI471102
A/Arkansas/15/2013	1A.3.3.3-c3	4.52 ± 0.94	1.38 ± 0.18	EPI482785
A/Wisconsin/03/2021	1A.3.3.3-c3	1.18 ± 0.20	0.55 ± 0.02	EPI1868840
A(H1N2)v, n = 7				
A/Ohio/24/2017	1A.1.1.3	>10	5.31 ± 0.66	EPI1056725
A/Pennsylvania/27/2024	1A.1.1.3	1.46 ± 0.06	1.01 ± 0.04	EPI3171496
A/Michigan/382/2018	1B.2.1	>10	4.02 ± 1.73	EPI1271034
A/Ohio/35/2017	1B.2.1	0.15 ± 0.01	0.16 ±0.03	EPI1056733
A/Iowa/04/2021	1B.2.1	0.03 ± 0.01	0.03 ± 0.01	EPI3215541
A/Ohio/28/2022	1B.2.1	3.72 ± 0.36	1.33 ± 0.06	EPI2193021
A/Michigan/48/2023	1B.2.1	5.75 ± 2.24	1.33 ± 0.24	EPI2687008
A(H3N2)v, n = 8				
A/Hawaii/28/2020	1990.1	>10	>10	EPI1804523
A/Iowa/04/2013	1990.4.a	5.94 ± 1.25	2.26 ±1.23	EPI516844
A/Wisconsin/24/2014	1990.4.a	>10	>10	EPI557542
A/Michigan/39/2015	1990.4.a	>10	>10	EPI642513
A/Ohio/02/2014	1990.4.b1	>10	6.59 ± 1.37	EPI539159
A/Ohio/27/2016	2010.1	5.82 ± 2.38	>10	EPI881739
A/Ohio/13/2017	2010.1	2.30 ± 0.54	>10	EPI1056653
A/Wisconsin/01/2021	2010.1	0.64 ± 0.11	4.48 ± 0.40	EPI1843130
Reference seasonal viruses‡				
A/Illinois/08/2018 (H1N1)pdm09	N/A	8.29 ± 1.11	1.69 ± 0.07	EPI1259741
A/Louisiana/50/2017 (H3N2)	N/A	6.41 ± 1.29	>10	EPI1259757

*Each virus was tested in ≥3 independent experiments to determine EC_{50}. EC_{50}, 50% effective concentration; HA, hemagglutinin; IRINA, influenza replication inhibition neuraminidase-based assay; N/A, not applicable.
†Accession number of HA sequences deposited to the GISAID database (https://gisaid.org) (accessed on April, 2024).
‡Source: Centers for Disease Control and Prevention antiviral susceptibility reference virus panels (FR-1678 ver1.1) (https://www.isirv.org/site/index.php/reference-panel).

Table 4. Antigenic analysis of A(H1N2)v viruses with ferret antiserum using HI and IRINA in study of antiviral susceptibility of swine-origin influenza A viruses isolated from humans, United States*

	Ferret antiserum, titer (fold change)					
	A/Ohio/35/2017		A/Michigan/48/2023		A/Victoria/2570/2019	
Influenza viruses	HI	IRINA	HI	IRINA	HI	IRINA
A(H1N2)v, clade 1B.2.1						
A/Ohio/35/2017, CVV	2,560 (1)	29,041 (1)	20 (64)	228 (79)	<10	<80
Test viruses						
A/Michigan/383/2018	320 (8)	1,131 (26)	80 (16)	469 (38)	<10	<80
A/Iowa/04/2021	640 (4)	3,290 (9)	160 (8)	620 (29)	<10	<80
A/Ohio/28/2022	160 (16)	1,542 (19)	640 (2)	11,677 (2)	<10	<80
A/Montana/28/2023	80 (32)	252 (115)	2,560 (1)	21,399 (1)	<10	<80
A/Michigan/48/2023	40 (64)	201 (144)	1,280 (1)	17,987 (1)	<10	<80
Reference seasonal A(H1N1)pdm09						
A/Victoria/2570/2019, CVV	160 (16)	1,269 (23)	<10	134 (134)	5,120 (1)	81,920 (1)

*HI titer determined using conventional method. IRINA titer determined using curve-fitting, 50% neutralization. Titers are reciprocal of antiserum dilution factor. Underlined values are reactivity titers of antiserum to homologous virus antigens. CVV, candidate vaccine virus; HI, hemagglutination inhibition; IRINA, influenza replication inhibition neuraminidase-based assay.

evolution among swine-origin viruses. Antiserum raised against A/Michigan/48/2023 reacted poorly (HI 8- to 64-fold; IRINA 29-79-fold) against A(H1N2)v viruses collected during 2017–2021 and very poorly (IRINA 134-fold) against A/Victoria/2570/2019 (H1N1)pdm09. As we expected, antiserum raised against A/Victoria/2570/2019 (H1N1)pdm09 produced poor cross-reactivity with A(H1N2)v viruses in both assays (Table 4).

Discussion

In this study, we assessed the susceptibility of US influenza variant viruses to influenza antiviral drugs approved by the Food and Drug Administration using a combination of sequence-based analysis and phenotypic testing. In recent years, low proportions (<1%) of seasonal viruses contained mutations that might reduce their susceptibility to antiviral drugs recommended by CDC (*39*,*41*). Our results indicated that the frequency of variant viruses resistant to those antiviral drugs was also low (<1%). As for seasonal viruses, variant viruses collected after the A(H3N2)v virus outbreaks in 2011–2012 were resistant to M2 blockers because of S31N in M2 protein. Whole-genome sequence data supports the conclusion that this resistance was acquired through reverse zoonosis and reassortment (*11*). Conversely, all 2013–2024 variant viruses were deemed susceptible to NAIs because no markers of resistance were identified, and we observed normal inhibition in an NA inhibition assay. Of the known PA substitutions of interest (*33*), only I38M was detected in a single A(H1N1)v virus, which displayed decreased baloxavir susceptibility, as expected.

With the goal of improving interpretation and harmonizing reporting of testing outcomes, we generated subtype-specific baseline antiviral susceptibilities of variant viruses. In the NA inhibition assay, 1 flagged virus with S247N displayed up to 4-fold increase in IC_{50} for NAIs regardless of the comparator. This finding is similar to other reports and was interpreted as normal inhibition (*35*,*44*,*45*). However, S247N in a clade 2.3.4 A(H5N1) virus was associated with reduced inhibition by oseltamivir (*34*). Another A(H1N1)v virus, A/Missouri/12/2012, had I427V substitution. Its effect on oseltamivir susceptibility remains unknown because a sequence-matched control was unavailable for testing. However, I427V would be reported as conferring reduced inhibition (17-fold) by oseltamivir when comparison is done using the A(H1N1)v subtype-specific baseline but not for the N1-classical virus baseline (8-fold). Those results underscore the uncertainties in the current interpretation of NA inhibition data and a need to refine the WHO Global Influenza Surveillance and Research System reporting criteria for zoonotic viruses.

In addition to assessing NAI susceptibility, we performed phenotypic testing with baloxavir using IRINA, a new assay developed to improve antiviral phenotyping throughput and turnaround time (*30*). In this assay, I38M in A(H1N1)v virus conferred decreased susceptibility to baloxavir compared with either sequence-matched control or the subtype-specific baseline. In seasonal viruses, E199G confers a variable effect (1- to 7-fold) on EC_{50} (*33*,*46*). In this study, E199G did not alter baloxavir susceptibility of an A(H3N2)v virus when compared in a similar manner, indicating the role of a virus's genetic background.

While establishing the baloxavir susceptibility baseline, we noticed that A(H1N1)v viruses appeared to be slightly more susceptible, even when they shared an identical PA-CEN domain sequence with viruses from the 2 other subtypes. Baloxavir exerts its antiviral effect by inhibiting synthesis of viral mRNA, thus preventing synthesis of viral

proteins. In IRINA, baloxavir and virus are added to cells simultaneously, and viral replication is limited to a single cycle because of the absence of TPCK-trypsin in media. Under such conditions, viruses displaying slower binding and internalization might appear to be slightly more susceptible to baloxavir. Therefore, when interpreting baloxavir EC_{50} of variant viruses, using a subtype-specific baseline might be prudent, especially considering the rather low provisional cutoff (3-fold) for reporting reduced drug susceptibility. Alternatively, the cutoff could be adjusted to a greater value (e.g., >5-fold over baseline) to prevent overreporting decreased susceptibility, such as for A/Michigan/288/2019 (H1N1)v, which exceeded the 3-fold threshold for the A(H1N1)v subtype, despite lacking PA-CEN substitutions.

IRINA was developed to test viruses against antiviral drugs with different mechanisms of action (*30*). In this study, mAbs targeting the HA stem region, FI6V3 and CR9114, demonstrated broad activity. However, 1 or both mAbs failed to neutralize one third of variant viruses. Variations in the mapped antigenic epitopes were observed, but they could not explain the observed neutralization patterns, indicating an involvement of residues outside of the identified epitopes. Of note, IRINA measures direct neutralization, and HA-targeting antibodies could possibly produce antiviral effects through alternative mechanisms when used in vivo (e.g., antibody effector functions) (*30*).

We used IRINA alongside HI assay to antigenically characterize A(H1N2)v viruses from clade 1B.2.1. As expected, IRINA titers were greater than those determined in HI assay because only a portion of neutralizing antibodies can prevent agglutination of erythrocytes. Moreover, IRINA titers are determined using curve-fitting and IC_{50}-based calculations. Despite differences in absolute titers between IRINA and HI, the fold changes in both assays indicated similar reactivity patterns. Moreover, antiserum raised against OH/17 (CVV for clade 1B.2.1), poorly neutralized viruses from the same clade collected in 2023, which indicated antigenic divergence. Taken together, the IRINA and HI data underscore the need to closely monitor antigenic properties of variant viruses and to promptly update CVVs as part of pandemic preparedness.

Although sequencing information is indispensable for risk assessment, sequence-only analysis might fail to predict the effect of mutations and their combinations on antiviral susceptibility as it could be specific to virus type, subtype, clade, or strain (*31*–*33*). Nonetheless, sequence-only data can be used to generate recombinant NA proteins (*15*) or reverse genetics-derived viruses to conduct antiviral testing (*35*).

The first limitation of our study is that not all variant viruses collected since 2013 were subjected to phenotypic testing. Therefore, we cannot rule out that few untested viruses with rare mutations would exhibit decreased drug susceptibility. In addition, interpreting laboratory phenotypic data is challenging because of the lack of laboratory correlates for clinically relevant antiviral resistance, even for the commonly used oseltamivir. Last, antiviral susceptibility testing is done using in-house–developed assays, which are known to produce different IC_{50}/EC_{50} results. Criteria used to report viruses that are potentially resistant are arbitrarily based on fold change in IC_{50}/EC_{50} values, which are assay dependent (*31*).

Variant viruses have been detected and characterized in many countries, including recently from Brazil, Spain, and the United Kingdom (*47*,*48*). The genetic makeup differs in swine viruses from different parts of the world, which might manifest in different susceptibilities to antiviral drugs. Laboratories that are unable to establish baseline susceptibility for variant viruses using their phenotypic assays may benefit from including well-characterized reference seasonal influenza A viruses when testing newly emerged viruses. This practice would help harmonize testing methodologies and interpretation of laboratory data to improve our knowledge of the viruses that continuously pose a pandemic threat.

Acknowledgements

We thank our colleagues from the Virology, Surveillance and Diagnosis Branch, Influenza Division, National Center for Immunization and Respiratory Diseases, Centers for Disease Control and Prevention (CDC), for their valuable support and contributions to this project. We also thank the US Public Health Laboratories for the submission of variant influenza viruses, other members of the Influenza Division at CDC for their valuable contributions to this study, and Trent Bullock for editorial assistance.

This study was supported by the Influenza Division of CDC.

About the Author

Dr. Gao is an associate service fellow in the Influenza Division, National Center for Immunization and Respiratory Diseases, Centers for Disease Control and Prevention, Atlanta, GA. His current research focuses on antigenic characterization and antiviral susceptibility of seasonal and emerging novel influenza viruses.

References

1. Vincent A, Awada L, Brown I, Chen H, Claes F, Dauphin G, et al. Review of influenza A virus in swine worldwide: a call for increased surveillance and research. Zoonoses Public Health. 2014;61:4–17. https://doi.org/10.1111/zph.12049
2. Scholtissek C, Bürger H, Kistner O, Shortridge KF. The nucleoprotein as a possible major factor in determining host specificity of influenza H3N2 viruses. Virology. 1985; 147:287–94. https://doi.org/10.1016/0042-6822(85)90131-X
3. Ito T, Couceiro JN, Kelm S, Baum LG, Krauss S, Castrucci MR, et al. Molecular basis for the generation in pigs of influenza A viruses with pandemic potential. J Virol. 1998;72:7367–73. https://doi.org/10.1128/JVI.72.9.7367-7373.1998
4. Zhou NN, Senne DA, Landgraf JS, Swenson SL, Erickson G, Rossow K, et al. Genetic reassortment of avian, swine, and human influenza A viruses in American pigs. J Virol. 1999;73:8851–6. https://doi.org/10.1128/JVI.73.10.8851-8856.1999
5. Olsen CW. The emergence of novel swine influenza viruses in North America. Virus Res. 2002;85:199–210. https://doi.org/10.1016/S0168-1702(02)00027-8
6. World Health Organization. International health regulations, 2nd edition. Geneva: The Organization; 2005.
7. Council of State and Territorial Epidemiologists. Council of State and Territorial Epidemiologists Position statement: national reporting for initial detections of novel influenza A viruses [cited 2024 Jun 17]. https://cdn.ymaws.com/www.cste.org/resource/resmgr/PS/07-ID-01.pdf
8. Shu B, Garten R, Emery S, Balish A, Cooper L, Sessions W, "et al. Genetic analysis and antigenic characterization of swine origin influenza viruses isolated from humans in the United States, 1990–2010. Virology. 2012;422:151–60. https://doi.org/10.1016/j.virol.2011.10.016
9. Dawood FS, Jain S, Finelli L, Shaw MW, Lindstrom S, Garten RJ, et al.; Novel Swine-Origin Influenza A (H1N1) Virus Investigation Team. Emergence of a novel swine-origin influenza A (H1N1) virus in humans. N Engl J Med. 2009;360:2605–15. https://doi.org/10.1056/NEJMoa0903810
10. Garten RJ, Davis CT, Russell CA, Shu B, Lindstrom S, Balish A, et al. Antigenic and genetic characteristics of swine-origin 2009 A(H1N1) influenza viruses circulating in humans. Science. 2009;325:197–201. https://doi.org/10.1126/science.1176225
11. Anderson TK, Chang J, Arendsee ZW, Venkatesh D, Souza CK, Kimble JB, et al. Swine influenza A viruses and the tangled relationship with humans. Cold Spring Harb Perspect Med. 2021;11:a038737. https://doi.org/10.1101/cshperspect.a038737
12. Markin A, Ciacci Zanella G, Arendsee ZW, Zhang J, Krueger KM, Gauger PC, et al. Reverse-zoonoses of 2009 H1N1 pandemic influenza A viruses and evolution in United States swine results in viruses with zoonotic potential. PLoS Pathog. 2023;19:e1011476. https://doi.org/10.1371/journal.ppat.1011476
13. World Health Organization. Standardization of terminology for the influenza virus variants infecting humans: update [cited 2024 Jun 17]. https://www.who.int/publications/m/item/standardization-of-terminology-for-the-influenza-virus-variants-infecting-humans-update
14. Jhung MA, Epperson S, Biggerstaff M, Allen D, Balish A, Barnes N, et al. Outbreak of variant influenza A(H3N2) virus in the United States. Clin Infect Dis. 2013;57:1703–12. https://doi.org/10.1093/cid/cit649
15. Sleeman K, Mishin VP, Guo Z, Garten RJ, Balish A, Fry AM, et al. Antiviral susceptibility of variant influenza A(H3N2) v viruses isolated in the United States from 2011 to 2013. Antimicrob Agents Chemother. 2014;58:2045–51. https://doi.org/10.1128/AAC.02556-13
16. Nelson MI, Stratton J, Killian ML, Janas-Martindale A, Vincent AL. Continual reintroduction of human pandemic H1N1 influenza A viruses into swine in the United States, 2009 to 2014. J Virol. 2015;89:6218–26. https://doi.org/10.1128/JVI.00459-15
17. Webby RJ, Swenson SL, Krauss SL, Gerrish PJ, Goyal SM, Webster RG. Evolution of swine H3N2 influenza viruses in the United States. J Virol. 2000;74:8243–51. https://doi.org/10.1128/JVI.74.18.8243-8251.2000
18. Rajão DS, Walia RR, Campbell B, Gauger PC, Janas-Martindale A, Killian ML, et al. Reassortment between swine H3N2 and 2009 pandemic H1N1 in the United States resulted in influenza A viruses with diverse genetic constellations with variable virulence in pigs. J Virol. 2017;91:e01763-16. https://doi.org/10.1128/JVI.01763-16
19. Sharma A, Zeller MA, Li G, Harmon KM, Zhang J, Hoang H, et al. Detection of live attenuated influenza vaccine virus and evidence of reassortment in the U.S. swine population. J Vet Diagn Invest. 2020;32:301–11. https://doi.org/10.1177/1040638720907918
20. Centers for Disease Control and Prevention. Novel influenza A virus infections [cited 2024 Apr 24]. https://gis.cdc.gov/grasp/fluview/Novel_Influenza.html
21. Cox NJ, Trock SC, Burke SA. Pandemic preparedness and the Influenza Risk Assessment Tool (IRAT). Curr Top Microbiol Immunol. 2014;385:119–36. https://doi.org/10.1007/82_2014_419
22. World Health Organization. Tool for influenza pandemic risk assessment (TIPRA), version 2 release. January 2020 [cited 2024 Jun 17]. https://www.who.int/publications/i/item/tool-for-influenza-pandemic-risk-assessment-(tipra)-2nd-edition
23. Jones JC, Yen HL, Adams P, Armstrong K, Govorkova EA. Influenza antivirals and their role in pandemic preparedness. Antiviral Res. 2023;210:105499. https://doi.org/10.1016/j.antiviral.2022.105499
24. Hurt AC. The epidemiology and spread of drug resistant human influenza viruses. Curr Opin Virol. 2014;8:22–9. https://doi.org/10.1016/j.coviro.2014.04.009
25. Takashita E, Ejima M, Itoh R, Miura M, Ohnishi A, Nishimura H, et al. A community cluster of influenza A(H1N1)pdm09 virus exhibiting cross-resistance to oseltamivir and peramivir in Japan, November to December 2013. Euro Surveill. 2014;19:20666. https://doi.org/10.2807/1560-7917.ES2014.19.1.20666
26. World Health Organization. Global Influenza Surveillance Network: manual for the laboratory diagnosis and virological surveillance of influenza. Geneva: The Organization; 2011.
27. Shepard SS, Meno S, Bahl J, Wilson MM, Barnes J, Neuhaus E. Viral deep sequencing needs an adaptive approach: IRMA, the iterative refinement meta-assembler. BMC Genomics. 2016;17:708. https://doi.org/10.1186/s12864-016-3030-6
28. Katoh K, Standley DM. MAFFT multiple sequence alignment software version 7: improvements in performance and usability. Mol Biol Evol. 2013;30:772–80. https://doi.org/10.1093/molbev/mst010
29. Okomo-Adhiambo M, Sleeman K, Ballenger K, Nguyen HT, Mishin VP, Sheu TG, et al. Neuraminidase inhibitor susceptibility testing in human influenza viruses: a laboratory surveillance perspective. Viruses. 2010;2:2269–89. https://doi.org/10.3390/v2102269
30. Patel MC, Flanigan D, Feng C, Chesnokov A, Nguyen HT, Elal AA, et al. An optimized cell-based assay to assess

influenza virus replication by measuring neuraminidase activity and its applications for virological surveillance. Antiviral Res. 2022;208:105457. https://doi.org/10.1016/j.antiviral.2022.105457
31. World Health Organization. Meetings of the WHO working group on surveillance of influenza antiviral susceptibility—Geneva, November 2011 and June 2012. Wkly Epidemiol Rec. 2012;87:369–74.
32. World Health Organization. Laboratory methodologies for testing the antiviral susceptibility of influenza viruses: neuraminidase inhibitor (NAI) [cited 2024 Jun 17]. https://www.who.int/teams/global-influenza-programme/laboratory-network/quality-assurance/antiviral-susceptibility-influenza/neuraminidase-inhibitor
33. World Health Organization. Laboratory methodologies for testing the antiviral susceptibility of influenza viruses: polymerase acidic (PA) inhibitor, baloxavir [cited 2024 Jun 17]. https://www.who.int/teams/global-influenza-programme/laboratory-network/quality-assurance/antiviral-susceptibility-influenza/polymerase-acidic-protein-inhibitor
34. Boltz DA, Douangngeun B, Phommachanh P, Sinthasak S, Mondry R, Obert C, et al. Emergence of H5N1 avian influenza viruses with reduced sensitivity to neuraminidase inhibitors and novel reassortants in Lao People's Democratic Republic. J Gen Virol. 2010;91:949–59. https://doi.org/10.1099/vir.0.017459-0
35. Hurt AC, Lee RT, Leang SK, Cui L, Deng YM, Phuah SP, et al. Increased detection in Australia and Singapore of a novel influenza A(H1N1)2009 variant with reduced oseltamivir and zanamivir sensitivity due to a S247N neuraminidase mutation. Euro Surveill. 2011;16:19884. https://doi.org/10.2807/ese.16.23.19884-en
36. Mishin VP, Patel MC, Chesnokov A, De La Cruz J, Nguyen HT, Lollis L, et al. Susceptibility of influenza A, B, C, and D viruses to baloxavir. Emerg Infect Dis. 2019;25:1969–72. https://doi.org/10.3201/eid2510.190607
37. Omoto S, Speranzini V, Hashimoto T, Noshi T, Yamaguchi H, Kawai M, et al. Characterization of influenza virus variants induced by treatment with the endonuclease inhibitor baloxavir marboxil. Sci Rep. 2018;8:9633. https://doi.org/10.1038/s41598-018-27890-4
38. Stevaert A, Dallocchio R, Dessì A, Pala N, Rogolino D, Sechi M, et al. Mutational analysis of the binding pockets of the diketo acid inhibitor L-742,001 in the influenza virus PA endonuclease. J Virol. 2013;87:10524–38. https://doi.org/10.1128/JVI.00832-13
39. Govorkova EA, Takashita E, Daniels RS, Fujisaki S, Presser LD, Patel MC, et al. Global update on the susceptibilities of human influenza viruses to neuraminidase inhibitors and the cap-dependent endonuclease inhibitor baloxavir, 2018–2020. Antiviral Res. 2022;200:105281. https://doi.org/10.1016/j.antiviral.2022.105281
40. Gubareva LV, Mishin VP, Patel MC, Chesnokov A, Nguyen HT, De La Cruz J, et al. Assessing baloxavir susceptibility of influenza viruses circulating in the United States during the 2016/17 and 2017/18 seasons. Euro Surveill. 2019;24:1800666. https://doi.org/10.2807/1560-7917.ES.2019.24.3.1800666
41. Takashita E, Daniels RS, Fujisaki S, Gregory V, Gubareva LV, Huang W, et al. Global update on the susceptibilities of human influenza viruses to neuraminidase inhibitors and the cap-dependent endonuclease inhibitor baloxavir, 2017–2018. Antiviral Res. 2020;175:104718. https://doi.org/10.1016/j.antiviral.2020.104718
42. Corti D, Voss J, Gamblin SJ, Codoni G, Macagno A, Jarrossay D, et al. A neutralizing antibody selected from plasma cells that binds to group 1 and group 2 influenza A hemagglutinins. Science. 2011;333:850–6. https://doi.org/10.1126/science.1205669
43. Dreyfus C, Laursen NS, Kwaks T, Zuijdgeest D, Khayat R, Ekiert DC, et al. Highly conserved protective epitopes on influenza B viruses. Science. 2012;337:1343–8. https://doi.org/10.1126/science.1222908
44. Leung RC, Ip JD, Chen LL, Chan WM, To KK. Global emergence of neuraminidase inhibitor-resistant influenza A(H1N1)pdm09 viruses with I223V and S247N mutations: implications for antiviral resistance monitoring. Lancet Microbe. 2024;5:627–8. https://doi.org/10.1016/S2666-5247(24)00037-5
45. Patel, M, Nguyen HT, Pascua, PNQ, Gao, R, Steel J, Kondor RJ, Gubareva LV. 2024. Multicountry spread of influenza A(H1N1)pdm09 viruses with reduced inhibition by oseltamivir, May 2023–February 2024. Emerg Infect Dis. 2024;30:1410–5.
46. Takashita E, Fujisaki S, Morita H, Nagata S, Miura H, Matsuura Y, et al. A community cluster of influenza A(H3N2) virus infection with reduced susceptibility to baloxavir due to a PA E199G substitution in Japan, February to March 2023. Euro Surveill. 2023;28:2300501. https://doi.org/10.2807/1560-7917.ES.2023.28.39.2300501
47. World Health Organization. 2024. Influenza at the human-animal interface summary and risk assessment, 26 February 2024 [cited 2024 Jun 17]. https://www.who.int/publications/m/item/influenza-at-the-human-animal-interface-summary-and-assessment-26--february-2024
48. Cogdale J, Kele B, Myers R, Harvey R, Lofts A, Mikaiel T, et al.; Influenza A(H1N2)v Incident Management Team. A case of swine influenza A(H1N2)v in England, November 2023. Euro Surveill. 2024;29:2400002. https://doi.org/10.2807/1560-7917.ES.2024.29.3.2400002

Address for correspondence: Larisa V. Gubareva, Centers for Disease Control and Prevention, 1600 Clifton Rd NE, Mailstop H17-5, Atlanta, GA 30329-4018, USA; email: lgubareva@cdc.gov

Risk for Facial Palsy after COVID-19 Vaccination, South Korea, 2021–2022

Dongwon Yoon,[1] Kyungyeon Jung,[1] Ju Hwan Kim, Hwa Yeon Ko, Byeol-A Yoon,[2] Ju-Young Shin,[2] CoVaSC Investigators

We conducted a self-controlled case series study to investigate the association between COVID-19 vaccination and facial palsy (FP) in South Korea. We used a large immunization registry linked with the national health information database. We included 44,564,345 patients ≥18 years of age who received ≥1 dose of COVID-19 vaccine (BNT162b2, mRNA-1273, ChAdOx1 nCoV-19, or Ad.26.COV2.S) and had an FP diagnosis and corticosteroid prescription within 240 days postvaccination. We compared FP incidence in a risk window (days 1–28) with a control window (the remainder of the 240-day observation period, excluding any risk windows). We found 5,211 patients experienced FP within the risk window and 10,531 experienced FP within the control window. FP risk increased within 28 days postvaccination, primarily after first and second doses and was observed for both mRNA and viral vaccines. Clinicians should carefully assess the FP risk-benefit profile associated with the COVID-19 vaccines and monitor neurologic signs after vaccination.

Amid the COVID-19 pandemic, vaccines were widely distributed under emergency use authorizations worldwide (*1*,*2*). During the development phase of COVID-19 vaccines, although no severe safety concerns were evident in any of the pivotal clinical trials, an imbalance in facial palsy (FP) incidence after vaccination was observed in vaccinated persons compared with the general population (*3*–*6*). Although the exact etiology of FP remains elusive, infection, autoimmune mechanisms, or vaccination are considered potential contributors to its development (*7*,*8*). Because of its sudden and acute symptom onset, characterized by facial muscle paralysis, FP has been included in the priority list of adverse events of special interest generated by the Safety Platform for Emergency vACcines (SPEAC) (*9*).

Multiple studies on the association of FP after COVID-19 vaccination have been reported (*10*–*14*), but the results from those studies have been inconsistent and lack a clear consensus. The variability in study results may be attributed to several factors, including limited statistical power because of small study populations and heterogeneity among studies in terms of population, ethnicity, vaccine types, doses, observation periods, and statistical methods. Even though a systematic review and meta-analysis were conducted to address those concerns (*15*,*16*), reaching definitive conclusions was challenging because the limited definition of eligibility criteria in that analysis, such as types of studies or study participants, did not fully encompass all available evidence on FP.

Because of the controversial and inconclusive results of existing studies, previous evidence necessitates an in-depth body of evidence and a clear consensus on the safety of COVID-19 vaccines concerning FP. Using 2 large, linked databases in South Korea, we conducted a self-controlled case series analysis to address the inconsistent findings of previous studies and provide an updated overall assessment of the potential association between FP and COVID-19 vaccines.

Methods

Data Sources

This research was conducted as part of COVID-19 Vaccine Safety Research Committee (CoVaSC) in South Korea with the aim of providing evidence on

Author affiliations: Sungkyunkwan University Department of Biohealth Regulatory Science, Suwon, South Korea (D. Yoon, K. Jung, J.H. Kim, J.-Y. Shin); Sungkyunkwan University School of Pharmacy, Suwon (D. Yoon, J.H. Kim, H.Y. Ko, J.-Y. Shin); Dong-A University College of Medicine Department of Neurology, Busan, South Korea (B.-A. Yoon); Sungkyunkwan University Samsung Advanced Institute for Health Sciences & Technology (SAIHST), Seoul, South Korea (J.-Y. Shin)

DOI: https://doi.org/10.3201/eid3011.240610

[1]These first authors contributed equally to this article.

[2]These last authors contributed equally to this article.

the safety of COVID-19 vaccines for immunization. In South Korea, several types of COVID-19 vaccine were available during the study period: BNT162b2 (Pfizer-BioNTech, https://www.pfizer.com), mRNA-1273 (Moderna, https://www.modernatx.com), ChAdOx1 nCoV-19 (AstraZeneca, https://www.astrazeneca.com), Ad.26.COV2.S (Janssen, https://www.janssen.com), and NVX-CoV2373 (Novavax, https://www.novavax.com) (*17*).

To obtain vaccine and adverse event data, we linked data from 2 large databases: the COVID-19 immunization registry (February 26, 2021–October 31, 2022) managed by the Korea Disease Control and Prevention Agency (KDCA) and healthcare claims data (January 1, 2002–October 31, 2022) provided by National Health Insurance Service (NHIS). During the COVID-19 pandemic in South Korea, KDCA and the government oversaw the distribution of vaccines and established the immunization registry covering the entire population. The registry included crucial information, such as age at vaccination, date of vaccination, type of vaccine administered, and dosing schedule of specific vaccines.

In accordance with the single-payer insurance provider system in South Korea, the NHIS covers the entire population of >50 million. The claims database of NHIS contains comprehensive healthcare utilization information on reimbursed patient visits, such as medical diagnoses, drug prescriptions, and medical screening data, which can be provided in an anonymized format. Diagnosis records are coded according to the International Classification of Disease 10th Revision (ICD-10), and drug prescriptions can be identified by national drug codes based on the Anatomic Therapeutic Chemical (ATC) classification of the World Health Organization.

This study followed the Strengthening the Reporting of Observational Studies in Epidemiology (STROBE) reporting guideline and was approved by the Public Institutional Review Board Designated by Ministry of Health and Welfare (approval no. P01-202203-01-005) and performed in accordance with the principles of the Declaration of Helsinki (World Medical Association, https://www.wma.net). The requirement of informed consent was waived because this study used anonymized administrative claims data.

Study Population

We identified persons ≥18 years of age who received an initial COVID-19 vaccine dose during February 26, 2021–March 1, 2022. Among that population, we identified and included patients with a primary FP diagnosis accompanied by a prescription for corticosteroids during February 26, 2021–October 31, 2022. Because we adopted a self-controlled case series analysis (SCCS), we further included patients who received a COVID-19 vaccination and had incident FP diagnosed within a prespecified observation period. Exclusion criteria comprised foreign born residents, participants in clinical trials, persons vaccinated abroad, and persons deviating from vaccination guidelines (i.e., incomplete immunization information) to account for potential exposure misclassification. In addition, we excluded persons with a history of FP in the year preceding the observation period and those whose FP cases occurred after the end of observation period (Figure 1).

SCCS Design

To investigate the risk for FP after COVID-19 vaccination, we used an SCCS design (*18*). SCCS uses within-person comparisons, which offers the advantage of minimizing the potential effects of time-invariant confounders that could be major limitations of the conventional cohort designs. We adopted the SCCS design because we recognized that selecting appropriate comparison groups would be challenging because of the high COVID-19 immunization rates in South Korea. We specified an observation period of 240 days after the first dose of any COVID-19 vaccine. We defined the risk window as days 1–28 after each dose of COVID-19 vaccination, with day 0 indicating the time of vaccination. We chose that timeframe as the risk window because persons are at a higher risk for FP occurrence during that period (Appendix Figure, https://wwwnc.cdc.gov/EID/article/30/11/24-0610-App1.pdf). We selected a 28-day risk window on the basis of previous studies (*10*,*19*) and observations from clinical trials of COVID-19 vaccines that indicated that neutralizing antibodies against SARS-CoV-2 peaked 28 days after vaccination (*20*,*21*). We defined the control windows as the periods outside the risk windows during the observation period.

COVID-19 Vaccination

Since the implementation of a massive immunization campaign against COVID-19 in South Korea, KDCA has collected detailed information on immunization for each available vaccine. For the Ad26.COV2.S vaccine, a single dose was regarded as a complete primary series, whereas other vaccines required 2 doses for completion. We obtained immunization information on those COVID-19 vaccines and defined their receipt as exposures. To consider the potential effect of administering different types of vaccines, we

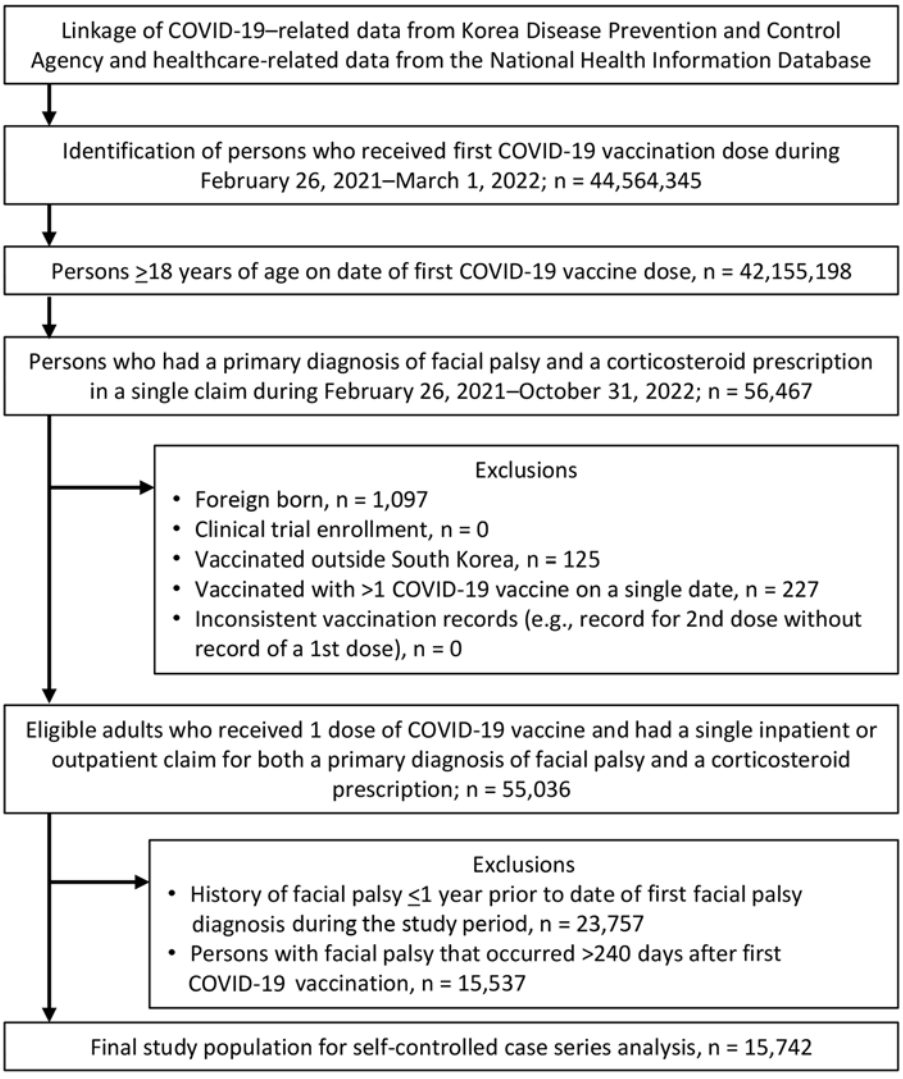

Figure 1. Flowchart of participant selection in study of risk for facial palsy after COVID-19 vaccination in South Korea, 2021–2022. The Korea Disease Control and Prevention Agency database has operated since 2020 and collects information on age, sex, type of vaccine and lot number, vaccinating healthcare provider, and date of vaccination for all COVID-19 vaccines. The National Health Information Database includes data collected by the National Health Insurance Service, which is the single-payer health insurance in South Korea, covering 97% of total population (≈50 million persons). The overall positive predictive value of the diagnoses recorded in the National Health Information Database is 82%.

categorized vaccinees as homologously vaccinated if they received the same type of COVID-19 vaccine throughout their dosing series and heterologously vaccinated otherwise. To assess the differential risk for FP occurrence on the basis of the biologic mechanism of action, we categorized specific vaccine types: BNT162b2 and mRNA-1273 as mRNA vaccines, ChAdOx1 nCoV-19 and Ad26.COV2.S as viral vector vaccines, and NVX-CoV2373 as a recombinant protein vaccine.

Outcomes

The outcome of interest was FP, which we defined as a primary diagnosis of FP accompanied by a prescription for oral or parenteral corticosteroid on the same day. We included oral or parenteral corticosteroid prescription to enhance the outcome validity of FP because of the clinical context of administration to patients experiencing acute FP in South Korea. The CoVaSC clinical research committee reviewed and approved our case definition. Incident FP cases were identified by ICD-10 codes G51.0, G51.8, or G51.9, and corticosteroid prescription was identified by ATC code H02AB (Appendix Table 1). We observed all FP cases that occurred within the observation period in the eligible population and calculated the incidence rate ratio (IRR) by comparing the incidence rate of FP between the risk and control windows.

Statistical Analysis

We summarized demographic characteristics according to the risk or control window, including age, sex, region of residence, health insurance type, and history of underlying conditions assessed ≤1 year before the first vaccine dose, including myocardial infarction, congestive heart failure, peripheral vascular

disease, stroke, dementia, chronic pulmonary disease, rheumatic disease, peptic ulcer disease, mild liver disease, diabetes mellitus, diabetic complications, hemiplegia or paraplegia, renal disease, cancer, serious liver disease, solid or metastatic tumor, and HIV infection. Statistical analyses involved *t*-tests for continuous variables and χ^2 tests for categorial variables. We considered $p<0.05$ statistically significant.

We measured the number of events and person-years to estimate the incidence rate of FP in the risk and control windows. We used a conditional Poisson regression model to estimate IRRs and 95% CIs, comparing the FP incidence rates in the risk window with FP incidence in the control window. In secondary analyses, we explored vaccine-specific risks, considering doses (first, second, third, fourth, or first/second [a first dose of BNT162b2, mRNA-1273, ChAdOx1 nCoV-19, or Ad26.COV2.S and a second dose of BNT162b2, mRNA-1273, or ChAdOx1 nCoV-19]) and homologous or heterologous vaccination within the dose series.

We conducted subgroup analyses stratified by age groups (18–29, 30–39, 40–49, 50–59, 60–69, 70–79, ≥80 years of age), sex, type of insurance (health insurance or medical aid), region of residence (metropolitan or rural), Charlson Comorbidity Index score (<5 or ≥5), and history of underlying conditions. We applied a Benjamini-Hochberg adjustment to address the inflation of type I error resulting from multiple comparisons (22).

To assess the robustness of our findings under various assumptions, we further conducted several sensitivity analyses. First, we repeated the main analysis by varying risk windows to 1–14 days or 1–42 days to assess the potential effects of different risk windows on the FP occurrence. Second, we

Table 1. Baseline characteristics stratified by exposure windows in a study of risk for facial palsy after COVID-19 vaccination, South Korea, 2021–2022*

Baseline characteristics	Risk window, n = 5,211	Control window, n = 10,531	p value
Mean age, y (SD)	53.1 (15.9)	52.8 (16.0)	0.3147
Age group, y			0.1587
18–29	506 (9.7)	1,005 (9.5)	
30–39	597 (11.5)	1,310 (12.4)	
40–49	990 (19.0)	1,955 (18.6)	
50–59	1,204 (23.1)	2,472 (23.5)	
60–69	1,099 (21.1)	2,176 (20.7)	
70–79	599 (11.5)	1,113 (10.6)	
≥80	216 (4.1)	500 (4.7)	
Sex			0.0417
M	2,849 (54.7)	5,938 (56.4)	
F	2,362 (45.3)	4,593 (43.6)	
Health insurance type			0.4262
National health insurance	5,045 (96.8)	10,170 (96.6)	
Medical aid	166 (3.2)	361 (3.4)	
Region of residence			0.7853
Metropolitan	3,485 (66.9)	7,020 (66.7)	
Rural	1,726 (33.1)	3,511 (33.3)	
Mean CCI (SD)	1.3 (1.8)	1.3 (1.7)	0.0540
CCI group			0.1488
CCI <5	4,866 (93.4)	9,896 (94.0)	
CCI ≥5	345 (6.6)	635 (6.0)	
Underlying conditions			
Myocardial infarction	41 (0.8)	115 (1.1)	0.0689
CHF	164 (3.1)	383 (3.6)	0.1144
Peripheral vascular disease	620 (11.9)	1,139 (10.8)	0.0424
Cerebrovascular disease	315 (6.0)	696 (6.6)	0.1742
Dementia	198 (3.8)	366 (3.5)	0.3031
CPD	676 (13.0)	1,408 (13.4)	0.4886
Rheumatic disease	137 (2.6)	301 (2.9)	0.4107
Peptic ulcer	848 (16.3)	1,634 (15.5)	0.2199
Mild liver disease	1,105 (21.2)	2,179 (20.7)	0.4553
Diabetes mellitus	1,190 (22.8)	2,236 (21.2)	0.0217
Diabetic complications	337 (6.5)	665 (6.3)	0.0289
Hemiplegia or paraplegia	20 (0.4)	56 (0.5)	0.2076
Renal disease	110 (2.1)	222 (2.1)	0.9906
Cancer	258 (5.0)	455 (4.3)	0.0734
Serious liver disease	15 (0.3)	21 (0.2)	0.2743
Solid metastatic tumor	22 (0.4)	32 (0.3)	0.2322
HIV infection	1 (0.0)	6 (0.1)	0.2900

*Values are no. (%) except as indicated. CCI, Charlson Comorbidity Index score; CHF, congestive heart failure; CPD, chronic pulmonary disease.

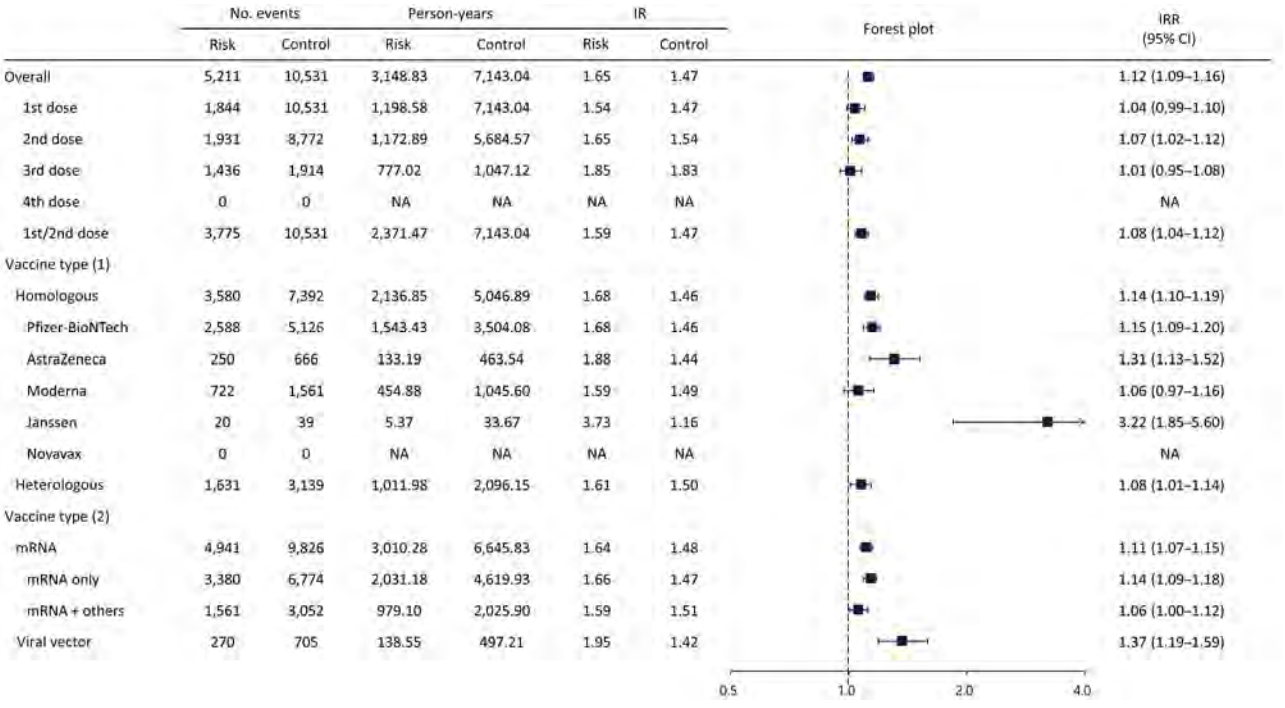

Figure 2. Forest plot of risk for facial palsy after COVID-19 vaccination in South Korea, 2021–2022. Plot assess facial palsy risk within 28 days of COVID-19 vaccination. Overall risk is shown, as is risk stratified by dose and vaccine type. Squares indicate IRRs; bars indicate 95% CIs. Vaccine types were BNT162b2 (Pfizer-BioNTech, https://www.pfizer.com), mRNA-1273 (Moderna, https://www.modernatx.com), ChAdOx1 nCoV-19 (AstraZeneca, https://www.astrazeneca.com), Ad.26.COV2.S (Janssen, https://www.janssen.com), and NVX-CoV2373 (Novavax, https://www.novavax.com). 1st/2nd dose indicates a first dose of BNT162b2, mRNA-1273, ChAdOx1 nCoV-19, or Ad26.COV2.S and a second dose of BNT162b2, mRNA-1273, or ChAdOx1 nCoV-19. IR, incidence rate; IRR, incidence rate ratio; NA, not applicable.

excluded persons who died within 7 days after FP diagnosis to exclude susceptible persons. Third, because COVID-19 infection poses a potential risk factor for FP, as reported in previous studies (*23*–*25*), we excluded persons who had COVID-19 infection within 90 days before vaccination or who had COVID-19 infection before their FP diagnosis. Fourth, we restricted cases to inpatient or emergency department visits to minimize outcome misclassification due to the definition of outcome identification. Fifth, we further restricted cases to persons simultaneously prescribed corticosteroids and antiviral medications to consider various clinical aspect of managing FP in South Korea. Last, we restricted cases to Bell's palsy diagnosis only (ICD-10 code G51.0) to account for the possibility of lower outcome validity of other FP diagnosis codes (ICD-10 codes G51.8 and G51.9). We used SAS Enterprise Guide version 8.3 (SAS Institute Inc., https://www.sas.com) for all statistical analyses.

Results

A total of 44,564,345 persons in South Korea were administered 129,956,027 COVID-19 vaccine doses during February 26, 2021–March 1, 2022 (Figure 1). We identified 15,742 FP cases with corticosteroid prescriptions during the study period. Among those cases, 5,211 occurred within 1–28 days postvaccination, corresponding to 4.0 FP cases/1 million doses. Among the FP study population, the mean age at first COVID-19 vaccination was 53.1 (SD 15.9) years; 54.7% (n = 2,849) were male and 45.3% (n = 2,362) were female (Table 1).

Our study showed FP risk increased within 1–28 days after any COVID-19 vaccine dose (IRR 1.12 [95% CI 1.09–1.16]). We observed increased FP risks (IRR 1.07 [95% CI 1.02–1.12]) with the second dose and combined first and second doses (IRR 1.08 [95% CI 1.04–1.12]) but identified no association for the third dose (IRR 1.01 [95% CI 0.95–1.08]). Regardless of whether persons received homologous or heterologous vaccination, we observed FP increased after vaccination; for homologous doses IRR was 1.14 (95% CI 1.10–1.19) and for heterologous doses IRR was 1.08 (95% CI 1.01–1.14). Furthermore, we found increased FP risks across vaccine types, in patients vaccinated with at least one mRNA vaccine IRR was 1.11 (95% CI 1.07–1.15) and in those vaccinated with viral vector vaccines only IRR was 1.37 (95% CI 1.19–1.59) (Figure 2; Appendix Table 2).

Table 2. Incidence risk and incidence risk ratios in a study of risk for facial palsy after COVID-19 vaccination, South Korea, 2021–2022*

Subgroup analyses	No. events		Person-years		IR		IRR (95% CI)
	Risk window	Control window	Risk window	Control window	Risk window	Control window	
Age group, y							
18–29	506	1,005	296.63	693.22	1.71	1.45	1.18 (1.06–1.31)†
30–39	597	1,310	345.53	907.82	1.73	1.44	1.20 (1.09–1.32)†
40–49	990	1,955	579.31	1,347.76	1.71	1.45	1.18 (1.09–1.27)†
50–59	1,204	2,472	760.05	1,647.95	1.58	1.50	1.06 (0.99–1.13)
60–69	1,099	2,176	683.97	1,453.30	1.61	1.50	1.07 (1.00–1.15)
70–79	599	1,113	351.39	760.24	1.70	1.46	1.16 (1.05–1.29)†
≥80	216	500	131.96	332.74	1.64	1.50	1.09 (0.93–1.28)
Sex							
M	2,849	5,938	1,766.69	3,981.28	1.61	1.49	1.08 (1.03–1.13)†
F	2,362	4,593	1,382.14	3,161.77	1.71	1.45	1.18 (1.12–1.24)†
Health insurance type							
National health insurance	5,045	10,170	3,043.69	6,908.08	1.66	1.47	1.13 (1.09–1.16)†
Medical aid	166	361	105.15	234.96	1.58	1.54	1.03 (0.86–1.23)
Region of residence							
Metropolitan	3,485	7,020	2,099.87	4,770.18	1.66	1.47	1.13 (1.08–1.17)†
Rural	1,726	3,511	1,048.96	2,372.86	1.65	1.48	1.11 (1.05–1.18)†
Charlson Comorbidity Index score							
<5	4,866	9,896	2,948.41	6,705.30	1.65	1.48	1.12 (1.08–1.16)†
≥5	345	635	200.43	437.75	1.72	1.45	1.19 (1.04–1.35)†

*Date of vaccination considered day 0, risk window considered days 1–28 postvaccination, and control window considered days 29–240 postvaccination. IR, incidence rate; IRR, incidence rate ratio.
†These results remained significant (p<0.05) after applying the Benjamini-Hochberg adjustment to account for multiple comparisons (*22*).

IRRs were generally consistent across age groups (Table 2; Appendix Table 3), and we identified elevated risks irrespective of sex. Among male persons, IRR was 1.08 (95% CI 1.03–1.13) and for female persons IRR was 1.18 (95% CI 1.12–1.24). After applying the Benjamini-Hochberg adjustment, those results generally remained consistent.

Sensitivity analyses demonstrated the robustness of the main results. The results remained consistent across both shorter and longer risk windows. IRR was 1.15 (95% CI 1.11–1.20) for the 1–14-day window and 1.12 (95% CI 1.09–1.16) for the 1–42-day window. Excluding persons who died within 7 days after FP diagnosis showed the FP risk was comparable to the main findings (IRR 1.12 [95% CI 1.09–1.16]). Moreover, we noted increased risks for FP regardless of COVID-19 infection, and those risks increased when we excluded cases of COVID-19 infection within 90 days before vaccination (IRR 1.12 [95% CI 1.09–1.16]) and COVID-19 cases before FP diagnosis (IRR 1.13 [95% CI 1.10–1.17]). Elevated risks of FP were shown when we restricted cases to inpatient or emergency department visits (IRR 1.21 [95% CI 1.14–1.28), to persons simultaneously prescribed corticosteroids and antiviral medication (IRR 1.24 [95% CI 1.17–1.32]), and to Bell's palsy diagnosis (IRR 1.13 [95% CI 1.09–1.17]) (Figure 3).

Discussion

Using 2 large, linked databases from the national COVID-19 immunization registry and NHIS claims data, we identified a positive association between COVID-19 vaccination and FP in the population of South Korea. The overall transient risk for postvaccination FP was primarily determined by the events that occurred within 28 days after the first and second doses of COVID-19 vaccines. We observed increased FP risks across all vaccine types, among homologous and heterologous vaccinees, and for mRNA and viral vaccines.

Our findings contribute to the evidence of a positive association between FP and COVID-19 vaccination, aligning with other studies. In a study of 2.6 million patients in Israel vaccinated with BNT162b2 during December 20, 2020–April 30, 2021, the standardized FP IRR at 21 days after the first dose was 1.36 (95% CI 1.14–1.61) compared with the period before the COVID-19 pandemic (*11*). Another SCCS analysis in the United Kingdom showed a positive association with FP for ChAdOx1 nCoV-19 vaccine during the 15–21 days after vaccination (IRR 1.29 [95% CI 1.08–1.56]) (*14*). Furthermore, our study aligns with a population-based study conducted in Hong Kong, China, which reported an overall increased risk for Bell's palsy after the first and second BNT162b2 vaccinations (adjusted odds ratio 1.54 [95% CI 1.12–2.12]) (*10*). Specifically, that study reported a substantially increased risk for Bell's palsy within the first 14 days after the second dose in both nested case–control (adjusted odds ratio 2.33 [95% CI 1.41–3.82]) and SCCS (IRR 2.44 [95% CI 1.32–4.50]) analyses (*10*). Those

findings are consistent with our findings, which also showed an increased risk for FP after the second COVID-19 vaccine dose.

Although the exact biological mechanism for development of FP after vaccination is unknown, plausible links between FP and both mRNA and viral vector COVID-19 vaccines have been proposed. First, mRNA vaccines use lipid nanoparticles to encapsulate SARS-CoV-2 spike antigen (*26*). When the mRNA lipid nanoparticles are recognized as foreign materials, the innate immune system is induced, stimulating production of type I interferons (*27*–*29*). As the immune response acts against myelin basic proteins, proinflammatory cytokines are profoundly released, damaging the myelin sheath and thereby attenuating peripheral tolerance (*30*–*32*). That proposed mechanism is supported by prior studies where Bell's palsy occurred in patients undergoing interferon therapy (*33*,*34*).

Similar to results for previous studies (*10*,*35*), our study revealed increased FP risks in persons

Sensitivity analyses	No. events		Person-years		IR		Forest plot	IRR (95% CI)
	Risk	Control	Risk	Control	Risk	Control		
Varying the risk window length, 1–14 days								
Overall	2,779	12,963	1,622.44	8,719.20	1.71	1.49		1.15 (1.11–1.20)
1st dose	1,045	12,963	629.74	8,719.20	1.66	1.49		1.12 (1.05–1.19)
2nd dose	999	10,379	589.53	6,662.31	1.69	1.56		1.09 (1.02–1.16)
3rd dose	735	2,615	402.91	1,432.68	1.82	1.83		1.00 (0.92–1.08)
4th dose	0	0	NA	NA	NA	NA		NA
1st/2nd dose	2,097	12,963	1,306.39	8,719.20	1.61	1.49		1.08 (1.03–1.13)
Varying the risk window length, 1–42 days								
Overall	7,314	8,428	4,508.47	5,833.17	1.62	1.44		1.12 (1.09–1.16)
1st dose	2,454	8,428	1,622.11	5,833.17	1.51	1.44		1.05 (1.00–1.09)
2nd dose	2,817	7,307	1,766.45	4,802.68	1.59	1.52		1.05 (1.00–1.09)
3rd dose	2,043	1,307	1,119.56	715.94	1.82	1.83		1.00 (0.93–1.07)
4th dose	0	0	NA	NA	NA	NA		NA
1st/2nd dose	5,271	8,428	3,388.57	5,833.17	1.56	1.44		1.08 (1.04–1.11)
Excluded deaths that occurred within 7 days of facial palsy analysis								
Overall	5,211	10,530	3,148.70	7,142.88	1.65	1.47		1.12 (1.09–1.16)
1st dose	1,844	10,530	1,198.53	7,142.88	1.54	1.47		1.04 (0.99–1.10)
2nd dose	1,931	8,771	1,172.81	5,684.41	1.65	1.54		1.07 (1.02–1.12)
3rd dose	1,436	1,914	777.02	1,047.12	1.85	1.83		1.01 (0.95–1.08)
4th dose	0	0	NA	NA	NA	NA		NA
1st/2nd dose	3,775	10,530	2,371.34	7,142.88	1.59	1.47		1.08 (1.04–1.12)
Excluded persons infected with COVID-19 within 90 days before vaccination								
Overall	5,211	10,531	3,148.83	7,143.04	1.65	1.47		1.12 (1.09–1.16)
1st dose	1,844	10,531	1,198.58	7,143.04	1.54	1.47		1.04 (0.99–1.10)
2nd dose	1,931	8,772	1,172.89	5,684.57	1.65	1.54		1.07 (1.02–1.12)
3rd dose	1,436	1,914	777.02	1,047.12	1.85	1.83		1.01 (0.95–1.08)
4th dose	0	0	NA	NA	NA	NA		NA
1st/2nd dose	3,775	10,531	2,371.47	7,143.04	1.59	1.47		1.08 (1.04–1.12)
Excluded persons with COVID-19 prior to facial palsy diagnosis								
Overall	5,211	10,528	3,045.38	6,976.13	1.71	1.51		1.13 (1.10–1.17)
1st dose	1,844	10,528	1,154.23	6,976.13	1.6	1.51		1.06 (1.01–1.11)
2nd dose	1,931	8,770	1,128.33	5,532.14	1.71	1.59		1.08 (1.03–1.13)
3rd dose	1,436	1,912	762.48	1,031.94	1.88	1.85		1.02 (0.95–1.09)
4th dose	0	0	NA	NA	NA	NA		NA
1st/2nd dose	3,775	10,528	2,282.56	6,976.13	1.65	1.51		1.10 (1.06–1.14)
Inpatients or emergency department settings of outcome								
Overall	1,723	3,019	1,003.90	2,127.97	1.72	1.42		1.21 (1.14–1.28)
1st dose	641	3,019	383.74	2,127.97	1.67	1.42		1.18 (1.08–1.28)
2nd dose	651	2,489	373.06	1,642.27	1.75	1.52		1.15 (1.06–1.26)
3rd dose	431	494	246.94	279.84	1.75	1.77		0.99 (0.87–1.12)
4th dose	0	0	NA	NA	NA	NA		NA
1st/2nd dose	1,292	3,019	756.80	2,127.97	1.71	1.42		1.20 (1.13–1.29)
Persons simultaneously prescribed corticosteroid and antiviral medication								
Overall	1,658	3,064	934.49	2,149.71	1.77	1.43		1.24 (1.17–1.32)
1st dose	616	3,064	358.07	2,149.71	1.72	1.43		1.21 (1.11–1.32)
2nd dose	634	2,516	346.90	1,656.02	1.83	1.52		1.20 (1.10–1.31)
3rd dose	408	511	229.38	285.73	1.78	1.79		0.99 (0.87–1.13)
4th dose	0	0	NA	NA	NA	NA		NA
1st/2nd dose	1,250	3,064	704.97	2,149.71	1.77	1.43		1.24 (1.16–1.33)
Persons with only a Bell's palsy diagnosis								
Overall	4,909	9,897	2,956.02	6,721.93	1.66	1.47		1.13 (1.09–1.17)
1st dose	1,726	9,897	1,127.05	6,721.93	1.53	1.47		1.04 (0.99–1.09)
2nd dose	1,831	8,259	1,102.05	5,343.34	1.66	1.55		1.08 (1.02–1.13)
3rd dose	1,352	1,788	726.58	980.16	1.86	1.82		1.02 (0.95–1.09)
4th dose	0	0	NA	NA	NA	NA		NA
1st/2nd dose	3,557	9,897	2,229.10	6,721.93	1.60	1.47		1.08 (1.04–1.13)

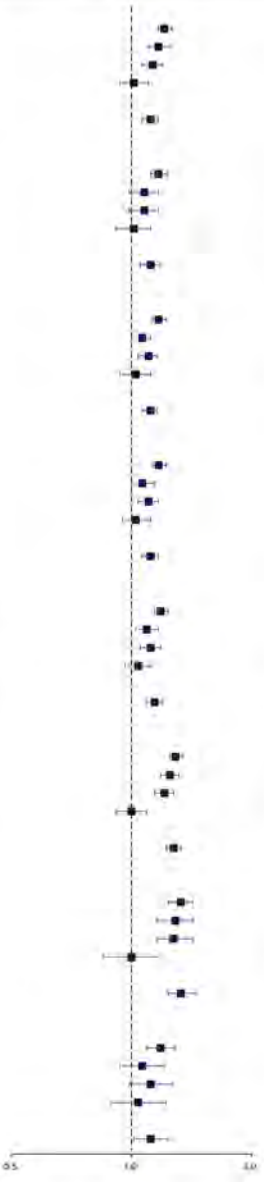

Figure 3. Forest plot of sensitivity analyses of risk for facial palsy after COVID-19 vaccination in South Korea, 2021–2022. Overall risk is shown, as is risk stratified by adverse events of interest. Squares indicate IRRs; bars indicate 95% CIs. 1st/2nd dose indicates a first dose of BNT162b2, mRNA-1273, ChAdOx1 nCoV-19, or Ad26.COV2.S and a second dose of BNT162b2, mRNA-1273, or ChAdOx1 nCoV-19. IR, incidence rate; IRR, incidence rate ratio; NA, not applicable.

homologously vaccinated with mRNA vaccines, especially for BNT162b2 (IRR 1.15 [95% CI 1.09–1.12]) and in those with at least a single dose of mRNA vaccine (IRR 1.11 [95% CI 1.07–1.15]). In addition, viral vector vaccines may trigger production of antibodies against virus proteins. Because of molecular mimicry between viral and peripheral nerve antigens, those antibodies can react with myelin antigens, causing demyelination. In addition, bystander activation of autoreactive T cells by viral vector vaccines can also provoke autoimmune phenomena (*36*,*37*). In line with a previous study that showed high T-cell responses after ChAdOx1 nCoV-19 vaccination (*38*), our study revealed elevated risks FP among patients who received homologous dosing of viral vector vaccines: IRR 1.31 (95% CI 1.13–5.52) for ChAdOx1 nCoV-19 and IRR 3.22 (95% CI 1.85–5.60) for Ad26.COV2.S vaccines. Moreover, recipients of viral vector vaccines had a much higher risk for FP (IRR 1.37 [95% CI 1.19–1.59]). However, that interpretation should be approached with caution because of the small number of FP cases, particularly with Ad26.COV2.S vaccines.

Recent studies have suggested that COVID-19 infection itself could also be a risk factor for FP onset (*23*) because it may lead to nerve compressions resulting from inflammation in response to viral infections (*39*). In South Korea, the annual incidence of Bell's palsy increased from 23.0 to 30.8 cases/100,000 persons from 2008 to 2018 (*40*) and reached 32.5 cases/100,000 persons during 2021–2022 (*24*), suggesting an increasing trend during the COVID-19 pandemic. In addition, a retrospective cohort study in South Korea indicated that COVID-19 infection is associated with a higher risk for Bell's palsy for both COVID-19 vaccine recipients (IRR 1.20 [95% CI 1.15–1.25]) and nonrecipients (IRR 1.84 [95% CI1.59–2.12]) (p<0.001) (*24*). In our SCCS study, a design widely used for vaccine safety evaluation, postvaccination FP risk was identified despite the previously recognized risk for FP after COVID-19 infection. The postvaccination risk is further supported by the consistent increase in FP risk observed in our sensitivity analysis, in which we excluded persons infected with COVID-19 from the study cohort.

By using a large, linked database in South Korea that covered >44 million persons vaccinated with >130 million vaccine doses, our study revealed an increased risk for FP after COVID-19 vaccination, providing supportive real-world evidence on postvaccination FP. We could address the inconsistencies observed in previous studies resulting from various limitations, including limited statistical power resulting from a small number of FP cases (*13*), and heterogeneity in vaccine types and doses studied for each analysis.

The first limitation of our study is the possible misclassification of FP cases because we relied on ICD-10 codes and could not apply the Brighton Collaboration's definition for FP because of the lack of laboratory data in our database (*41*). Nevertheless, we defined our case definition to include only FP patients with prescriptions for corticosteroids, and we applied several other definitions of FP in sensitivity analyses to assess the robustness of our main results. The second limitation is that the actual timing of FP occurrence and diagnosis recorded might differ, potentially leading cases to be included in control window. Nevertheless, our sensitivity analyses by varying the length of risk windows showed comparable findings. Furthermore, even though we conducted sensitivity analyses to adjust for the effects of COVID-19 infection, residual confounding may remain among patients who did not undergo a COVID-19 testing and were later received an FP diagnosis or COVID-19 vaccination.

In conclusion, our study revealed a transient risk for FP after any dose of COVID-19 vaccine, irrespective of homologous and heterologous dosing or vaccine type. However, of note, although the risk for FP appears elevated, the absolute number of FP cases was small, and risk for FP should not discourage patients from receiving COVID-19 vaccinations. Because FP is generally mild and manageable, physicians should monitor neurologic signs after COVID-19 vaccination and provide patients with a comprehensive evaluation of the risk–benefit profile associated with COVID-19 vaccines.

Acknowledgments

The authors thank the Korea Disease Control and Prevention Agency, National Academy of Medicine of Korea, and the National Health Insurance Service for their collaborative effort in making the nationwide data readily available for analysis and providing necessary assistance to conduct this study.

This study was supported by the Korea Disease Control and Prevention Agency (grant no. 2021-05-008). The funders of the study had no role in design and conduct of the study; collection, management, analysis, and interpretation of the data; preparation, review, or approval of the manuscript; and decision to submit the manuscript for publication.

J.-Y.S. received grants from the Ministry of Food and Drug Safety, the Ministry of Health and Welfare, the National Research Foundation of Korea, and the Government-wide

R&D Fund for Infectious Disease Research and Pharmaceutical Companies, including Pfizer, UCB, and LG Chem. No other relationships or activities have influenced the submitted work.

About the Authors

Dr. Yoon is a postdoctoral research fellow at the School of Pharmacy, Sungkyunkwan University, Suwon, South Korea. His research interests are pharmacoepidemiology, particularly in generating real-world evidence, and vaccine safety. Ms. Jung is a researcher at the College of Biohealth Regulatory Science, Sungkyunkwan University, Suwon, South Korea. Her research interests are pharmacoepidemiology using real-world data.

References

1. Wollersheim S; US Food and Drug Administration. Vaccines and Related Biological Products Advisory Committee meeting: FDA review of efficacy and safety of Pfizer-BioNTech COVID-19 vaccine emergency use authorization request [cited 2023 Sep 1]. https://www.fda.gov/media/144337/download
2. US Food and Drug Administration. Vaccines and Related Biological Products Advisory Committee meeting presentation: FDA review of efficacy and safety of Moderna COVID-19 vaccine emergency use authorization request [cited 2023 Sep 1]. https://www.fda.gov/media/144585/download
3. Polack FP, Thomas SJ, Kitchin N, Absalon J, Gurtman A, Lockhart S, et al.; C4591001 Clinical Trial Group. Safety and efficacy of the BNT162b2 mRNA Covid-19 vaccine. N Engl J Med. 2020;383:2603–15. https://doi.org/10.1056/NEJMoa2034577
4. El Sahly HM, Baden LR, Essink B, Doblecki-Lewis S, Martin JM, Anderson EJ, et al.; COVE Study Group. Efficacy of the mRNA-1273 SARS-CoV-2 vaccine at completion of blinded phase. N Engl J Med. 2021;385:1774–85. https://doi.org/10.1056/NEJMoa2113017
5. Falsey AR, Sobieszczyk ME, Hirsch I, Sproule S, Robb ML, Corey L, et al.; AstraZeneca AZD1222 Clinical Study Group. Phase 3 safety and efficacy of AZD1222 (ChAdOx1 nCoV-19) Covid-19 vaccine. N Engl J Med. 2021;385:2348–60. https://doi.org/10.1056/NEJMoa2105290
6. Sadoff J, Gray G, Vandebosch A, Cárdenas V, Shukarev G, Grinsztejn B, et al.; ENSEMBLE Study Group. Final Analysis of Efficacy and Safety of Single-Dose Ad26.COV2.S. N Engl J Med. 2022;386:847–60. https://doi.org/10.1056/NEJMoa2117608
7. Eviston TJ, Croxson GR, Kennedy PG, Hadlock T, Krishnan AV. Bell's palsy: aetiology, clinical features and multidisciplinary care. J Neurol Neurosurg Psychiatry. 2015;86:1356–61. https://doi.org/10.1136/jnnp-2014-309563
8. Mutsch M, Zhou W, Rhodes P, Bopp M, Chen RT, Linder T, et al. Use of the inactivated intranasal influenza vaccine and the risk of Bell's palsy in Switzerland. N Engl J Med. 2004;350:896–903. https://doi.org/10.1056/NEJMoa030595
9. Law B. Safety Platform for Emergency vACcines (SPEAC) Project: SO2-D2.1.2 priority list of COVID-19 adverse events of special interest: quarterly update December 2020. Oslo, Norway: Coalition for Epidemic Preparedness Innovations; 2020.
10. Wan EYF, Chui CSL, Ng VWS, Wang Y, Yan VKC, Lam ICH, et al. Messenger RNA coronavirus disease 2019 (COVID-19) vaccination with BNT162b2 increased risk of Bell's palsy: a nested case-control and self-controlled case series study. Clin Infect Dis. 2023;76:e291–8. https://doi.org/10.1093/cid/ciac460
11. Shibli R, Barnett O, Abu-Full Z, Gronich N, Najjar-Debbiny R, Doweck I, et al. Association between vaccination with the BNT162b2 mRNA COVID-19 vaccine and Bell's palsy: a population-based study. Lancet Reg Health Eur. 2021;11:100236. https://doi.org/10.1016/j.lanepe.2021.100236
12. Kim S, Kang M, Park JS, Seok HY. Risk and characteristics of Bell's palsy in adults as an adverse event following COVID-19 vaccination: a retrospective study. Acta Neurol Belg. 2023;123:2185–93. https://doi.org/10.1007/s13760-023-02204-2
13. Li X, Raventós B, Roel E, Pistillo A, Martinez-Hernandez E, Delmestri A, et al. Association between COVID-19 vaccination, SARS-CoV-2 infection, and risk of immune mediated neurological events: population based cohort and self-controlled case series analysis. BMJ. 2022;376:e068373. https://doi.org/10.1136/bmj-2021-068373
14. Patone M, Handunnetthi L, Saatci D, Pan J, Katikireddi SV, Razvi S, et al. Neurological complications after first dose of COVID-19 vaccines and SARS-CoV-2 infection. Nat Med. 2021;27:2144–53. https://doi.org/10.1038/s41591-021-01556-7
15. Rafati A, Pasebani Y, Jameie M, Yang Y, Jameie M, Ilkhani S, et al. Association of SARS-CoV-2 vaccination or infection with Bell palsy: a systematic review and meta-analysis. JAMA Otolaryngol Head Neck Surg. 2023;149:493–504. https://doi.org/10.1001/jamaoto.2023.0160
16. Shahsavarinia K, Mahmoodpoor A, Sadeghi-Ghyassi F, Nedayi A, Razzaghi A, Zehi Saadat M, et al. Bell's palsy and COVID-19 vaccination: a systematic review. Med J Islam Repub Iran. 2022;36:85. https://doi.org/10.47176/mjiri.36.85
17. Nham E, Song JY, Noh JY, Cheong HJ, Kim WJ. COVID-19 vaccination in Korea: past, present, and the way forward. J Korean Med Sci. 2022;37:e351. https://doi.org/10.3346/jkms.2022.37.e351
18. Petersen I, Douglas I, Whitaker H. Self controlled case series methods: an alternative to standard epidemiological study designs. BMJ. 2016;354:i4515. https://doi.org/10.1136/bmj.i4515
19. Walker JL, Schultze A, Tazare J, Tamborska A, Singh B, Donegan K, et al. Safety of COVID-19 vaccination and acute neurological events: a self-controlled case series in England using the OpenSAFELY platform. Vaccine. 2022;40:4479–87. https://doi.org/10.1016/j.vaccine.2022.06.010
20. Zhu FC, Li YH, Guan XH, Hou LH, Wang WJ, Li JX, et al. Safety, tolerability, and immunogenicity of a recombinant adenovirus type-5 vectored COVID-19 vaccine: a dose-escalation, open-label, non-randomised, first-in-human trial. Lancet. 2020;395:1845–54. https://doi.org/10.1016/S0140-6736(20)31208-3
21 García-Pérez J, González-Pérez M, Castillo de la Osa M, Borobia AM, Castaño L, Bertrán MJ, et al.; CombiVacS Study Group. Immunogenic dynamics and SARS-CoV-2 variant neutralisation of the heterologous ChAdOx1-S/BNT162b2 vaccination: secondary analysis of the randomised CombiVacS study. EClinicalMedicine. 2022;50:101529. https://doi.org/10.1016/j.eclinm.2022.101529
22. Benjamini Y, Hochberg Y. Controlling the false discovery rate: a practical and powerful approach to multiple testing. J R Stat Soc Series B Stat Methodol. 1995;57:289–300. https://doi.org/10.1111/j.2517-6161.1995.tb02031.x
23. Tamaki A, Cabrera CI, Li S, Rabbani C, Thuener JE, Rezaee RP, et al. Incidence of Bell palsy in patients with COVID-19.

JAMA Otolaryngol Head Neck Surg. 2021;147:767–8. https://doi.org/10.1001/jamaoto.2021.1266
24. Kim HJ, Jeong S, Song J, Park SJ, Oh YH, Jung J, et al. Risk of Bell's palsy following SARS-CoV-2 infection: a nationwide cohort study. Clin Microbiol Infect. 2023;29:1581–6. https://doi.org/10.1016/j.cmi.2023.08.014
25. Khurshid A, Khurshid M, Sohail A, Raza IM, Ahsan MK, Alam Shah MUF, et al. Facial palsy as a manifestation of COVID-19: a systematic review of cases. Health Sci Rep. 2022;5:e887. https://doi.org/10.1002/hsr2.887
26. Lamprinou M, Sachinidis A, Stamoula E, Vavilis T, Papazisis G. COVID-19 vaccines adverse events: potential molecular mechanisms. Immunol Res. 2023;71:356–72. https://doi.org/10.1007/s12026-023-09357-5
27. Ozonoff A, Nanishi E, Levy O. Bell's palsy and SARS-CoV-2 vaccines. Lancet Infect Dis. 2021;21:450–2. https://doi.org/10.1016/S1473-3099(21)00076-1
28. Lee Y, Jeong M, Park J, Jung H, Lee H. Immunogenicity of lipid nanoparticles and its impact on the efficacy of mRNA vaccines and therapeutics. Exp Mol Med. 2023;55:2085–96. https://doi.org/10.1038/s12276-023-01086-x
29. Soeiro T, Salvo F, Pariente A, Grandvuillemin A, Jonville-Béra AP, Micallef J. Type I interferons as the potential mechanism linking mRNA COVID-19 vaccines to Bell's palsy. Therapie. 2021;76:365–7. https://doi.org/10.1016/j.therap.2021.03.005
30. Principi N, Esposito S. Do vaccines have a role as a cause of autoimmune neurological syndromes? Front Public Health. 2020;8:361. https://doi.org/10.3389/fpubh.2020.00361
31. Gorodezky C, Carranza JM, Bustamante A, Yescas P, Martinez A, Alonso Vilatela ME. The HLA system and T-cell subsets in Bell's palsy. Acta Otolaryngol. 1991;111:1070–4. https://doi.org/10.3109/00016489109100758
32. Mañós-Pujol M, Buendia E, Mestre M, Jimenéz R, Gil E, Menén JP, et al. Cellular immunity abnormalities in patients with recurrent Bell's palsy. Clin Otolaryngol Allied Sci. 1987;12:283–7. https://doi.org/10.1111/j.1365-2273.1987.tb00203.x
33. Hwang I, Calvit TB, Cash BD, Holtzmuller KC. Bell's palsy: a rare complication of interferon therapy for hepatitis C. Dig Dis Sci. 2004;49:619–20. https://doi.org/10.1023/B:DDAS.0000026389.56819.0c
34. Yalçindağ FN, Alay C. Bell's palsy during interferon alpha 2a treatment in a case with Behçet uveitis. F1000 Res. 2013;2:245. https://doi.org/10.12688/f1000research.2-245.v1
35. Shoaibi A, Lloyd PC, Wong HL, Clarke TC, Chillarige Y, Do R, et al. Evaluation of potential adverse events following COVID-19 mRNA vaccination among adults aged 65 years and older: two self-controlled studies in the U.S. Vaccine. 2023;41:4666–78. https://doi.org/10.1016/j.vaccine.2023.06.014
36. Fujinami RS, von Herrath MG, Christen U, Whitton JL. Molecular mimicry, bystander activation, or viral persistence: infections and autoimmune disease. Clin Microbiol Rev. 2006;19:80–94. https://doi.org/10.1128/CMR.19.1.80-94.2006
37. Kim TS, Shin EC. The activation of bystander $CD8^+$ T cells and their roles in viral infection. Exp Mol Med. 2019;51:1–9. https://doi.org/10.1038/s12276-019-0316-1
38. Aguinam ET, Nadesalingam A, Chan A, Smith P, Paloniemi M, Cantoni D, et al. Differential T-cell and antibody responses induced by mRNA versus adenoviral vectored COVID-19 vaccines in patients with immunodeficiencies. J Allergy Clin Immunol Glob. 2023;2:100091. https://doi.org/10.1016/j.jacig.2023.100091
39. Baugh RF, Basura GJ, Ishii LE, Schwartz SR, Drumheller CM, Burkholder R, et al. Clinical practice guideline: Bell's palsy. Otolaryngol Head Neck Surg. 2013;149(Suppl):S1–27.
40. Lee JS, Kim YH. Epidemiological trends of Bell's palsy treated with steroids in Korea between 2008 and 2018. Muscle Nerve. 2021;63:845–51. https://doi.org/10.1002/mus.27213
41. Rath B, Gidudu JF, Anyoti H, Bollweg B, Caubel P, Chen YH, et al.; Brighton Collaboration Bell's Palsy Working Group. Facial nerve palsy including Bell's palsy: Case definitions and guidelines for collection, analysis, and presentation of immunisation safety data. Vaccine. 2017;35:1972–83. https://doi.org/10.1016/j.vaccine.2016.05.023

Address for correspondence: Ju-Young Shin, School of Pharmacy, Sungkyunkwan University, 2066, Seobu-ro, Jangan-gu, Suwon, Gyeonggi-do 16419, South Korea; email: shin.jy@skku.edu

Detection in Orchards of Predominant Azole-Resistant *Candida tropicalis* Genotype Causing Human Candidemia, Taiwan

Kuo-Yun Tseng,[1] Yin-Zhi Chen,[1] Zi-Li Zhou, Jyh-Nong Tsai, Min-Nan Tseng, Hsing-Lung Liu, Chi-Jung Wu, Yu-Chieh Liao, Chih-Chao Lin, De-Jiun Tsai, Feng-Jui Chen, Li-Yun Hsieh, Kuan-Chung Huang, Chun-Hua Huang, Kai-Ting Chen, Wen-Li Chu, Chiao-Mei Lin, Shu-Man Shih, Chao Agnes Hsiung, Yee-Chun Chen, Huey-Kang Sytwu, Yun-Liang Yang, Hsiu-Jung Lo

Fluconazole-resistant clade 4 *Candida tropicalis* causing candidemia in humans has been detected in tropical/subtropical areas, including those in China, Singapore, and Australia. We analyzed 704 individual yeasts isolated from fruits, soil, water, and farmers at 80 orchards in Taiwan. The most common pathogenic yeast species among 251 isolates recovered from farmers were *Candida albicans* (14.7%) and *C. parapsilosis* (11.6%). In contrast, *C. tropicalis* (13.0%), *C. palmioleophila* (6.6%), and *Pichia kudriavzevii* (6.0%) were prevalent among 453 environmental isolates. Approximately 18.6% (11/59) of *C. tropicalis* from the environment were resistant to fluconazole, and 81.8% (9/11) of those belonged to the clade 4 genotype. *C. tropicalis* susceptibility to fluconazole correlated with susceptibilities to the agricultural azole fungicides, difenoconazole, tebuconazole, and triadimenol. Tandem gene duplications of mutated *ERG11* contributed to azole resistance. Agriculture environments are a reservoir for azole-resistant *C. tropicalis*; discontinuing agricultural use of azoles might reduce emergence of azole-resistant *Candida* spp. strains in humans.

Candida spp. account for ≈8%–15% of invasive infections leading to hospitalization; the emergence of drug-resistant non–*C. albicans Candida* spp. is particularly troublesome for optimal health recovery of immunocompromised patients, especially those in hospital intensive care units (*1,2*). *C. tropicalis* is one of the leading non–*C. albicans* species causing candidemia in humans residing in tropical Asia and Latin America (*3*–*5*) and is also the leading cause of invasive candidiasis in patients with hematologic malignancies (*4,6*). Because of major differences in geographic distribution of human-invasive *Candida* spp., each country or region must conduct its own surveillance program to assess the dominant species and emergence of drug-resistant strains (*1,2,7*). The recent sporadic outbreaks of multidrug-resistant *C. auris* infections in >14 countries located in 5 continents demonstrate the still unmet need for this surveillance (*8,9*).

The National Health Research Institutes (NHRI) of Taiwan established the Taiwan Surveillance of Antimicrobial Resistance of Yeasts (TSARY) program in 1999 to periodically monitor national trends in species distribution and antifungal drug susceptibility of pathogenic yeasts isolated from patients (*10*). Subsequent surveillance was conducted in 2002, 2006, 2010, 2014, and 2018 (*11*–*15*). Resistance to fluconazole was found in 25 of 294 *C. tropicalis* isolates from TSARY 2014 and in 31 of 314 *C. tropicalis* isolates from TSARY

Author affiliations: National Tsing Hua University, Hsinchu, Taiwan (K.-Y. Tseng); National Health Research Institutes, Miaoli, Taiwan (K.-Y. Tseng, Y.-Z. Chen, Z.-L. Zhou, C.-J. Wu, Y.-C. Liao, C.-C. Lin, D.-J. Tsai, F.-J. Chen, L.-Y. Hsieh, K.-C. Huang, C.-H. Huang, K.-T. Chen, W.-L. Chu, C.-M. Lin, S.-M. Shih, C.A. Hsiung, Y.-C. Chen, H.-K. Sytwu, H.-J. Lo); National Yang Ming Chiao Tung University, Hsinchu (Z.-L. Zhou, Y.-L. Yang, H.-J. Lo); Taiwan Agricultural Research Institute, Taichung, Taiwan (J.-N. Tsai); Kaohsiung District Agricultural Research and Extension Station, Pingtung, Taiwan (M.-N. Tseng); Taichung District Agricultural Research and Extension Station, CHangHua, Taiwan (H.-L. Liu); National Cheng Kung University Hospital and Medical College, Tainan, Taiwan (C.-J. Wu); National Taiwan University Hospital College of Medicine, Taipei, Taiwan (Y.-C. Chen); China Medical University, Taichung (H.-J. Lo)

DOI: https://doi.org/10.3201/eid3011.240545

[1]These authors contributed equally to this article.

2018; moreover, 91.1% (51/56) of fluconazole-resistant *C. tropicalis* belonged to the clade 4 genotype (*15*). Since 2014, other studies have also reported the isolation of azole-resistant *C. tropicalis*, particularly in the Asia-Pacific region (*16*–*18*). Tandem gene duplications of the *ERG11* gene encoding a Y132F amino acid mutation have reportedly contributed to azole-resistant phenotypes in clade 4 *C. tropicalis* isolates from China, Singapore, and Australia (*19*). However, little data have been generated regarding the genetics of *Candida* spp. collected from environmental sources.

C. tropicalis has been recovered from soil and aquatic environments (*20,21*). Furthermore, the azole-resistant *C. tropicalis* clade 4 genotype has been isolated from fruits purchased at a supermarket in northern Taiwan (*22*). Thus, identifying potential sources of the fluconazole-resistant *C. tropicalis* clade 4 genotype became critical. *Aspergillus fumigatus* fungi recovered from soil and compost have been reported to be genetically related to clinically resistant isolates, raising the possibility that an environmental source of azole-resistant *C. tropicalis* might account for resistant strains in humans (*23*). Through collaborations with healthcare and agriculture sectors, we determined whether the azole-resistant *C. tropicalis* clade 4 genotype existed in orchard environments by investigating the distribution of yeasts in 3 different types of orchards. We also analyzed potential mechanisms contributing to azole resistance in *C. tropicalis*.

Materials and Methods

Study Design

We designed this study to evaluate yeast species distribution by using an orchard survey and to investigate the genetic relatedness among fluconazole-resistant *C. tropicalis* isolates. NHRI designed an orchard survey that was used by agricultural research institutes and stations located in representative regions of Taiwan. NHRI's Human Experiment and Ethics Committee approved the orchard survey (study no. EC1070117).

Most orchards in Taiwan are located in central and southern areas; therefore, we surveyed a total of 80 orchards—31 papaya, 28 wax apple, and 21 grape orchards—located in those 2 areas during July 2012–January 2013. We designated this survey as orchard survey 2012. We collected 1 fruit and 1 soil sample from east, west, south, north, and center collection points within each orchard. Thus, we collected 5 fruit and 5 soil samples from each orchard. From the orchard farmers, we collected swab samples from armpits and hands, as well as oral mouth rinse samples. We analyzed a total of 400 fruit and 400 soil samples, 80 samples of water, and 80 samples each of armpit swab, hand swab, and mouth rinse samples.

Microbiologic Processing

We isolated yeasts from samples as previously described (*21,24*). In brief, we maintained all swab samples at room temperature and transported them to the laboratory within 24 hours after collection. We streaked the samples onto BBL CHROMagar *Candida* plates (BD Biosciences, https://www.bdbiosciences.com). We identified the isolates by rDNA sequencing of the internal transcribed spacer or the D1/D2 domain regions (*25*) and submitted all novel rDNA sequences to GenBank (Appendix Table 1, 2, https://wwwnc.cdc.gov/EID/article/30/11/24-0545-App1.pdf). We further analyzed 1 isolate per species per type of sample. We labeled the strains from orchard survey 2012 with YFA12 and strains from TSARY 2014 with YM14 followed by 4 numbers.

Drug Susceptibility Testing

Because *Pichia kudriavzevii* (formerly *C. krusei*) is intrinsically resistant to fluconazole, we determined susceptibilities of *C. albicans*, *C. parapsilosis*, *C. tropicalis*, and *Nakaseomyces glabratus* (formerly *C. glabrata*), all common yeasts causing human infections, to 2–64 mg/L fluconazole. We analyzed susceptibilities of all 66 *C. tropicalis* isolates to difenoconazole (1–32 mg/L), tebuconazole (1–32 mg/L), and triadimenol (2–64 mg/L), 3 commonly used fungicides in agriculture in Taiwan. We incubated cultures at 35°C for 24 hours in RPMI medium 1640 (Thermo Fisher Scientific, https://www.thermofisher.com) and measured the growth of each isolate by using a Multiskan FC microplate photometer (Thermo Fisher Scientific). We defined MICs as the concentration of drug capable of reducing the turbidity of cells by >50%. We used procedures and clinical breakpoints for yeast strains as previously described (*26*). For fluconazole, the clinical breakpoints for *C. albicans*, *C. parapsilosis*, and *C. tropicalis* were MICs of ≤2 mg/L for susceptible, ≥8 mg/L for resistant, and 4 mg/L for susceptible-dose dependent. For *N. glabratus*, we considered a fluconazole MIC of ≤32 mg/L to be susceptible-dose dependent and ≥64 mg/L resistant. The breakpoints for fungicides in agriculture have not been defined. We used Spearman correlation coefficient analysis to evaluate the correlations between susceptibilities to fluconazole and to agricultural fungicides. We used the following guide to evaluate the strength of the correlation: very weak, 0.00–0.19; weak, 0.20–0.39; moderate, 0.40–0.59; strong, 0.60–0.79; and very strong, 0.80–1.0.

Multilocus Sequence Typing

We conducted multilocus sequence typing (MLST) as described previously (*27*,*28*). In brief, we sequenced DNA fragments of 6 *C. tropicalis* genes, *ICL1*, *MDR1*, *SAPT2*, *SAPT4*, *XYR1*, and *ZWF1a*, by using specific primers (Appendix Table 2) and included those sequences in the analyses. We aligned the sequences by using BioNumerics 3.0 (Applied Maths, https://www.applied-maths.com) and compared them with *C. tropicalis* sequences in the public MLST database (http://pubmlst.org) to determine the level of sequence identities and diploid sequence type (DST). We performed phylogenetic analysis by using the unweighted pair group method with arithmetic means algorithm and MEGA 11 software (https://www.megasoftware.net) as previously described (*29*). We determined the genome types of 66 *C. tropicalis* isolates recovered from the orchards and chose a cutoff p-distance value of 0.01 because it separated clades that contained known isolates. We generated a global phylogenetic tree of *C. tropicalis* composed of 1,368 DSTs listed in the *C. tropicalis* MLST database, as previously described (*22*).

Qualitative Analysis of *CDR1*, *ERG11*, and *MDR1* Transcripts by Real-Time PCR

We determined the expression levels of genes involved in azole resistance in 17 *C. tropicalis* isolates collected from orchards and patients, including 14 fluconazole-resistant (11 clade 4 and 1 each of clades 2, 3, and 8) and 3 fluconazole-susceptible isolates. We harvested the cells after growing them to an optical density of 0.7–0.9 in YPD liquid medium (BD Biosciences) at 30°C for 6 hours. After sequencing *CDR1*, *ERG11*, and *MDR1* gene fragments (Appendix Table 2), we normalized expression levels against *ACT1* in each isolate. Then, we used the mRNA levels in a fluconazole-susceptible isolate, YFA120877 (control strain), recovered from orchard survey 2012, as the denominator for normalization.

Whole-Genome Sequencing and *ERG11* Copy Number Variant Detection

We conducted whole-genome sequencing (WGS) of 14 orchard-derived *C. tropicalis* isolates that had different genotypes, including 8 isolates resistant and 6 susceptible to fluconazole. We also sequenced 16 isolates from patients in TSARY 2014, including 7 resistant and 9 susceptible to fluconazole, and the *C. tropicalis* strain ATCC750 (American Type Culture Collecton, https://www.atcc.org). We constructed a multiplexing nanopore sequencing library with high molecular weight DNAs by using the Ligation Sequencing Kit and Native Barcoding Expansion Kit (both Oxford Nanopore Technologies, https://www.nanoporetech.com) according to the manufacturer's instructions. We analyzed a standard 72-hour sequencing script by using MinKNOW software (Oxford Nanopore Technologies), collected raw reads, and then basecalled and demultiplexed by using the standalone application guppy (*30*). After inputting an estimated genome size of 15 Mbp, we obtained long-length and high-quality (coverage ×80; i.e., 1.2 Gbp) sequencing reads by using a customized script, GetFastq.py (*31*). We then filtered and aligned the reads against the *ERG11* gene (GenBank accession no. XM_002550939) by using minimap2 (https://github.com/lh3/minimap2) and a customized script to test for copy number variants. This script separated reads containing *ERG11* sequences into 3 groups: single copy *ERG11* reads, multiple-copy *ERG11* reads, and unsure *ERG11* reads that included partial *ERG11* sequences. For the single and multiple copy groups, we selected a reference read and polished with Medaka version 1.4.3 (https://github.com/nanoporetech/medaka).

Use of Azole Compounds in Taiwan

Fluconazole (1992), itraconazole (1992), ketoconazole (1981), and voriconazole (2004) have been available in Taiwan for ≥2 decades. Posaconazole was introduced in 2010. We retrospectively analyzed systemic antifungal drugs administered in healthcare settings in Taiwan by using data obtained from the Taiwan National Health Insurance Research database; the details of the database and methods have been described previously (*32*). We determined the defined daily dose (DDD) of total azole, fluconazole, itraconazole, ketoconazole, and voriconazole in 2005 (1 year after voriconazole was introduced) and 2013 (1 year before TSARY 2014). We did not include the DDD for posaconazole because it was introduced after 2005. We estimated the amounts of azole-type compounds used in agriculture in Taiwan according to Domestic Manufacturers Production & Sale of Pesticides, an annual publication by the Taiwan Crop Protection Industry Association (*33*).

Results

Distribution of Yeasts Isolated from Orchard Environment and Farmers

We isolated 704 individual yeasts from 310 samples, including 74 from fruit, 63 from soil, 59 from hand, 58 from oral rinse, 31 from water, and 25 from armpit samples. The isolated yeasts comprised 34 genera

and 83 species; 41 of those species have been reported to cause disease in humans. Of the 704 yeasts, 453 (64.3%) were isolated from the environment and 251 (35.7%) from farmers (Table 1; Appendix Table 3). Most (251/453 [55.4%]) environmental isolates were from fruits, and most (126/251 [50.2%]) isolates from farmers were from hand swab samples.

The most common human pathogenic yeasts recovered from the environment were *C. tropicalis* (59/453 [13.0%]), *Candida palmioleophila* (30/453 [6.6%]), and *P. kudriavzevii* (27/453 [6.0%]), whereas the leading 2 human pathogenic yeasts recovered from the farmers were *C. albicans* (37/251 [14.7%]) and *C. parapsilosis* (29/251 [11.6%]) (Figure 1). Furthermore, yeast species had different prevalences according to the collection site (Table 1). *C. tropicalis* (32/153 [20.9%]) and *C. palmioleophila* (26/153 [17%]) were 2 major species found in soil, and *P. kudriavzevii* was prevalent in water (7/49 [14.3%]). Most (35/37) *C. albicans* and all 3 *N. glabratus* isolated from farmers were found in oral rinse samples. Of the 35 armpit swab samples, 12 (34.3%) contained *C. parapsilosis* and 5 (14.3%) *Rhodotorula mucilaginosa*.

Susceptibility of 4 Major *Candida* spp. to Fluconazole

All 39 *C. albicans*, 29 *C. parapsilosis*, and 3 *N. glabratus* isolates were susceptible to fluconazole (≤2 mg/L), whereas 11 (16.7%) *C. tropicalis* isolates were resistant (≥8 mg/L), 14 susceptible-dose dependent (4 mg/L), and 41 susceptible (≤2 mg/L) to fluconazole (Table 2). In addition, we found that yeast susceptibilities to fluconazole were positively correlated with susceptibilities to 3 azole fungicides used in agriculture (Table 2). All 11 fluconazole-resistant *C. tropicalis* isolates were collected from the environment in 3 different orchards: grape (n = 4 isolates), papaya (n = 4), and wax apple (n = 3) (Appendix Table 4).

Table 1. Distribution of yeasts according to source in study of detection in orchards of predominant azole-resistant *Candida tropicalis* genotype causing human candidemia, Taiwan*

	Environment				Farmers†				
Yeast species (former species name)	Fruit	Soil	Water	Subtotal	Armpit	Hand	Oral	Subtotal	Total
Pathogenic yeasts									
Candida tropicalis	18	32	9	59	0	4	3	7	66
C. albicans	0	0	2	2	0	2	35	37	39
C. palmioleophila	3	26	1	30	1	1	0	2	32
Pichia kudriavzevii (*C. krusei*)	11	9	7	27	0	2	2	4	31
C. parapsilosis	0	0	0	0	12	12	5	29	29
Nakaseomyces glabratus (*C. glabrata*)	0	0	0	0	0	0	3	3	3
Hanseniaspora opuntiae	11	3	5	19	1	0	3	4	23
Moesziomyces aphidis (*Pseudozyma aphidis*)	11	1	0	12	1	7	2	10	22
Pichia terricola (*Issatchenkia terricola*)	9	8	1	18	0	2	1	3	21
Rhodotorula mucilaginosa	6	1	0	7	5	9	0	14	21
Moesziomyces antarcticus (*Pseudozyma antarctica*)	13	1	0	14	0	5	1	6	20
Meyerozyma caribbica (*C. fermentati*)	7	3	4	14	1	1	2	4	18
Hanseniaspora uvarum	6	3	0	9	0	3	3	6	15
Kodamaea ohmeri	5	1	2	8	0	3	2	5	13
Meyerozyma guilliermondii (*C. guilliermondii*)	1	2	0	3	0	1	2	3	6
Other 27 species	13	10	4	27	5	15	7	27	54
Subtotal	114	100	35	249	26	67	71	164	413
Nonpathogenic yeasts									
Rhodotorula taiwanensis	26	7	2	35	4	14	3	21	56
Rhodotorula paludigena (*Rhodosporidium paludigenum*)	30	8	4	42	0	4	1	5	47
Sporobolomyces pararoseus (*Sporidiobolus pararoseus*)	16	3	2	21	0	15	1	16	37
Rhodosporidiobolus ruineniae (*Sporidiobolus ruineniae*)	15	5	0	20	0	1	2	3	23
Hanseniaspora thailandica	6	5	1	12	0	1	2	3	15
Papiliotrema aurea (*Cryptococcus aureus*)	7	0	1	8	0	3	0	3	11
Pichia occidentalis	2	7	1	10	0	0	1	1	11
Starmerella bacillaris (*C. zemplinina*)	4	0	0	4	0	5	0	5	9
Rhodotorula toruloides (*Rhodosporidium toruloides*)	4	0	0	4	0	4	0	4	8
Debaryomyces nepalensis	2	3	0	5	1	0	1	2	7
Pichia manshurica	3	0	0	3	0	2	2	4	7
Papiliotrema ruineniae (*Cryptococcus ruineniae*)	5	0	0	5	0	1	0	1	6
Other 30 species	17	15	3	35	4	9	6	19	54
Subtotal	137	53	14	204	9	59	19	87	291
Total	251	153	49	453	35	126	90	251	704

*Values are numbers of each yeast species isolated from different sources.
†Swab samples were collected from hands and armpits of orchard farmers; oral rinse samples were also collected from orchard farmers.

Genetic Relatedness of *C. tropicalis* Isolates

We analyzed the DSTs of all 66 *C. tropicalis* isolates (Appendix Table 4). The genotype distribution among the 42 fluconazole-susceptible isolates was more diverse, and they were classified into 12 different genotypes: clade 8 (n = 12 isolates); clades 3 and 6 (n = 6 each); clade 4 (n = 5); clade 1 (n = 4); clade 5 (n = 3); clades 2, 10, and 17 (n = 1 each); and DST1394, DST1402, and DST564 (n = 1 each). The 13 fluconazole–susceptible-dose dependent isolates were classified into 5 genotypes: clade 4 (n = 9), clades 8 and 10 (n = 1 each), and DST1394 and DST598 (n = 1 each). Most (≈69%) fluconazole–susceptible-dose dependent isolates belonged to clade 4, of which 88.9% (8/9) belonged to DST225. Furthermore, 9 (81.8%) of 11 fluconazole-resistant isolates belonged to clade 4, consistent with the finding among fluconazole-resistant *C. tropicalis* causing infections in patients.

Molecular Characteristics of *C. tropicalis* Isolates

We analyzed the expression of genes involved in fluconazole resistance in *C. tropicalis* isolated from orchards and patients (Table 3). *ERG11* mRNA levels increased 3.8–13-fold in all 11 clade 4 isolates compared with that of the azole-susceptible control strain, YFA120877. In contrast, the levels of *ERG11* mRNA in 3 non–clade 4 fluconazole-resistant isolates, including clades 2, 3, and 8, were not increased. In addition to *ERG11*, the expression of *MDR1* in 3 clade 4 fluconazole-resistant and 1 clade 5 fluconazole-susceptible isolates was increased compared with the control. *CDR1* expression in the clade 8 fluconazole-resistant isolate was also increased.

To further investigate mutations of the azole drug target, *ERG11*, that contributes to fluconazole resistance, we completed WGS of 31 isolates (Table 3). Sequence comparisons indicated that all but 1 clade 4 isolates clustered together (Figure 2), confirming genetic relatedness among fluconazole-resistant isolates from orchards and patients. All 12 clade 4, but not the 3 non–clade 4 (clades 2, 3, and 8), fluconazole-resistant isolates contained Y132F or S154F mutations in the Erg11 protein. In contrast, all but 1 fluconazole-susceptible isolates had wild-type Erg11 protein. The difference between the clade 4 fluconazole-resistant

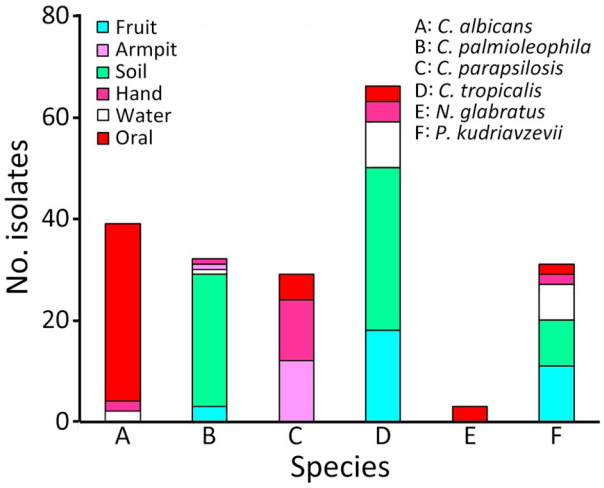

Figure 1. Detection in orchards of predominant azole-resistant *Candida tropicalis* genotype causing human candidemia, Taiwan. Samples from fruit, soil, and water at different orchards were collected. Swab samples from the hands and armpits and oral rinse samples were collected from orchard farmers. Colors indicate source of different yeast species. Numbers of *Candida* spp., *Nakaseomyces glabratus* (formerly *C. glabrata*), and *Pichia kudriavzevii* (formerly *C. krusei*) yeast isolates were determined for each sample type.

Table 2. Correlations between susceptibilities to fluconazole and 3 fungicides in study of detection in orchards of predominant azole-resistant *Candida tropicalis* genotype causing human candidemia, Taiwan*

	Fluconazole MICs, mg/L								
Fungicide MICs, mg/L	≤2	4	8	16	32	≥64	Total no.	Spearman ρ	p value
Difenoconazole								0.636	<0.001
≤1	41	14	1	0	2	0	58		
2	0	0	0	1	2	1	4		
4	0	0	0	0	1	0	1		
≥8	0	0	0	0	1	2	3		
Tebuconazole								0.758	<0.001
≤1	41	13	0	0	0	0	54		
2	0	1	1	1	5	1	9		
4	0	0	0	0	1	1	2		
≥8	0	0	0	0	0	1	1		
Triadimenol								0.875	<0.001
≤2	36	1	0	0	0	0	37		
4	1	0	0	0	0	0	1		
8	2	3	1	1	0	0	7		
16	2	9	0	0	0	0	11		
32	0	1	0	0	0	0	1		
≥64	0	0	0	0	6	3	9		

*Values are numbers of *C. tropicalis* isolates except as indicated. Spearman correlation coefficients were used to determine correlations between fluconazole susceptibility and susceptibility to 3 different fungicides used in agriculture in Taiwan.

Table 3. Characteristics of *Candida tropicalis* isolates from agricultural and clinical settings in study of detection in orchards of predominant azole-resistant *C. tropicalis* genotype causing human candidemia, Taiwan*

Strain	Source	Clade	DST	Fluconazole S/R	Fluconazole MIC, mg/L	Erg11† Y132F/S154F	Upc2† L168P/A251T/ Q287S	mRNA level‡ *ERG11*	mRNA level‡ *CDR1*	mRNA level‡ *MDR1*	MLST ID§
ATCC750	Patient	N914¶	914	S	2	YS/YS	LTS/LTS	ND	ND	ND	1829
YM140066	Ascites	4	506	R	64	YS/FF (9)	LAQ/PTS	5.44	0.64	0.36	831
YM140132	Urine	4	506	R	32	YS/FF (4)	LAQ/LTS	3.08	0.56	0.31	1765
YM140298	Urine	3	585	R	8	YS/YS	LAQ/LAQ	0.67	0	0.26	825
YM140372	Sputum	4	225	R	32	YS/FF (6)	LAQ/LAQ	4.59	0.41	0.24	1762
YM140441	Urine	4	506	R	32	YS/FF (5)	LAQ/PTS	4.88	0.48	0.22	1766
YM140586	Blood	4	225	R	64	YS/FF (9)	LAQ/LTS	4.56	0.57	0.07	833
YM141055	Sputum	2	153	R	>64	YS/YS	LAQ/LAQ	1.24	0.71	1.3	1753
YFA120301	Soil	4	225	R	32	YS/FF (6)	LAQ/PTS	9.59	0.61	2.43	1756
YFA120472	Fruit	8	169	R	16	YS/YS	LAQ/LAQ	1.08	4.24	0.62	1754
YFA120760	Fruit	4	225	R	64	YS/FF (9)	LAQ/PTS	12.98	0.78	2.96	1757
YFA121702	Soil	4	506	R	32	YS/FF (6)	LAQ/PTS	5.81	0.83	2.38	1763
YFA121900-2	Fruit	4	225	R	64	YS/FF (4)	LAQ/PTS	ND	ND	ND	1759
YFA122361	Soil	4	506	R	32	YS/FF (5)	LAQ/LTS	3.81	0.61	0.54	1764
YFA123343-1	Fruit	4	225	R	32	YS/FF (8)	LAQ/PTS	10.85	0.92	0.53	1760
YFA123757	Soil	4	225	R	64	YS/FF (8)	LAQ/PTS	11.28	0.77	1.11	1761
YM140156	Blood	7	139	S	0.25	YS/YS	LAQ/LAQ	ND	ND	ND	1748
YM140225	Blood	5	140	S	0.25	YS/YS	LTS/LTS	ND	ND	ND	1750
YM140458	Sputum	11	923	S	0.25	YS/YS	LAQ/LAS	ND	ND	ND	1767
YM140470	Urine	6	149	S	0.5	YS/YS	LAQ/LAQ	ND	ND	ND	1752
YM140518	Urine	2	134	S	0.25	YS/YS	LAQ/LAQ	ND	ND	ND	1747
YM140896	Blood	5	911	S	0.25	YS/YS	LTS/LTS	1.06	0.57	2.53	843
YM140912	Blood	5	910	S	0.5	YS/YS	LAQ/LAQ	ND	ND	ND	845
YM140977	Blood	5	140	S	0.25	YS/YS	LTS/LTS	ND	ND	ND	1751
YM141031	Urine	4	667	S	0.25	YS/YS	LAQ/LTS	ND	ND	ND	847
YFA120622	Soil	5	928	S	≤2	YS/YS	LAQ/LAQ	ND	ND	ND	818
YFA120679	Hand	5	140	S	≤2	YS/YS	LTS/LTS	ND	ND	ND	1749
YFA120727	Fruit	8	169	S	≤2	YS/YS	LAQ/LAQ	ND	ND	ND	1755
YFA120766	Fruit	1	587	S	≤2	YS/YS	LAQ/LAQ	ND	ND	ND	827
YFA121078	Soil	4	225	S	≤2	YS/FF	LAQ/PTS	1.12	0.8	1.41	1758
YFA121513	Fruit	6	577	S	≤2	YS/YS	LAQ/LAQ	ND	ND	ND	817

*DST, diploid sequence type; ID, identification; MLST, multilocus sequence typing; ND, not determined; R, resistant; S, susceptible.
†Locations of amino acid mutations in Erg11 and Upc2 proteins are indicated by numbers. Letter combinations indicate amino acid changes in both alleles of each isolate. Copy numbers of *ERG11* gene are indicated in parentheses, when >1 copy per allele was present.
‡Numbers are fold change in mRNA levels for each gene compared with the control strain (YFA120877).
§ID numbers are from the pubMLST database (https://pubmlst.org).
¶Clades were labeled with N followed by DST number if the isolates were not classified into a specific clade.

and fluconazole-susceptible isolates was the 4–9 tandem gene duplications of *ERG11* found in resistant isolates, whereas the susceptible isolate, YFA121078, had only 1 copy of the *ERG11* gene.

Discussion

We found that fluconazole-resistant *C. tropicalis* isolated from fruits, soils, and water in orchards in Taiwan were genetically similar to those causing prolonged colonization and tissues damage in humans. This finding might be associated with both increasingly frequent clinical use of azoles in humans and intense use of azole fungicides in agriculture in Taiwan. We provide epidemiologic evidence indicating that orchards are a reservoir for clade 4 fluconazole-resistant *C. tropicalis*. First, infections in humans were sporadic and unrelated to each other (*15*,*34*), and no identifiable hospital outbreaks occurred. Second, most patients had major underlying conditions and had not been treated with azole drugs within 6 months before hospital admission (*15*). Last, we identified a specific causative clade 4 that shared the same DST genotypes common to both orchards and patients.

Sequential accumulation of adaptive chromosomal mutations has been reported to be associated with drug resistance in fungi (*35*,*36*). Selection of azole-resistant *A. fumigatus* has been associated with agricultural use of azoles (*37*); isolates carrying tandem repeat 34/L98H mutations in the Cyp51A (Erg11) protein were recovered from 2 azole-naive patients with pulmonary aspergillosis (*38*). *C. albicans* and other yeast species isolated from patients with HIV infections and from vine grapes in Bavaria, Germany, were also cross-resistant to medical and agricultural azole drugs (*39*); however, the genetic relatedness among those resistant isolates was not determined.

The YFA121078 isolate was susceptible to fluconazole even though it had both Y132F and S154F mutations in the Erg11 protein, suggesting that ≥1 mutation in Erg11 might not be sufficient to contribute

to treatment failure, but might allow *C. tropicalis* to survive when low levels of azole are present in the environment. The expression of *MDR1* mRNA in YM140896, a fluconazole-susceptible isolate, was 2.5-fold higher than that of the control strain. Furthermore, the expression of *MDR1* mRNA in 3 clade 4 fluconazole-resistant isolates was also higher than that of the control strain. Those findings suggest that overexpression of *MDR1* alone might not cause treatment failure. Our findings are consistent with a concept that fluconazole resistance might be caused by accumulation of molecular changes in different genes, including mutations and overexpression.

An outbreak of *C. auris* in a neuroscience intensive care unit in the United Kingdom was linked to reusable axillary temperature probes (*40*). Among 21 fluconazole-susceptible *C. tropicalis* isolates collected from patients in Italy who had neurologic disorders, 9 belonged to DST747 and 6 to DST333. Isolates from door handles, bedside tables, bed handles, and the hands of healthcare workers also belonged to 1 of those DSTs (*41*). Hence, a specific *Candida* spp. clone can persist in the environment and be horizontally transmitted within a healthcare setting.

The detection of the same clade 4 genotype of fluconazole-resistant *C. tropicalis* from agricultural sites and infected humans suggests that fluconazole-resistant *C. tropicalis* in environments can be a threat to healthcare. A 7-year (2011–2017) observational study of adult patients with *C. tropicalis* bloodstream infections at National Taiwan University Hospital showed that 9 of 58 fluconazole-resistant *C. tropicalis* isolates were DST225 and 6 were DST506, all belonging to clade 4 (*34*). Furthermore, 23 of 30 fluconazole-resistant *C. tropicalis* isolates from Shanghai, China, belonged to clade 4 DST505–7 (*42*). Therefore, active surveillance to detect emergence and dissemination of azole-resistant *C. tropicalis* in clinical settings should be considered and should not be limited to tropical Asia and Latin America.

Because 29 of 31 fluconazole-resistant *C. tropicalis* isolated during TSARY 2018 belonged to the clade 4 genotype, we conducted a follow-up survey of orchards in 2018. Preliminary data showed that >90% of fluconazole-resistant *C. tropicalis* isolates from orchard environments in that survey belonged to clade 4 (H.J. Lo, unpub. data). Our findings demonstrate that the clade 4 fluconazole-resistant *C. tropicalis* genotype is persistent in Taiwan in both clinical settings and the environment.

MLST is a convenient and cost-effective tool to study genetic relatedness and diversity of mi-

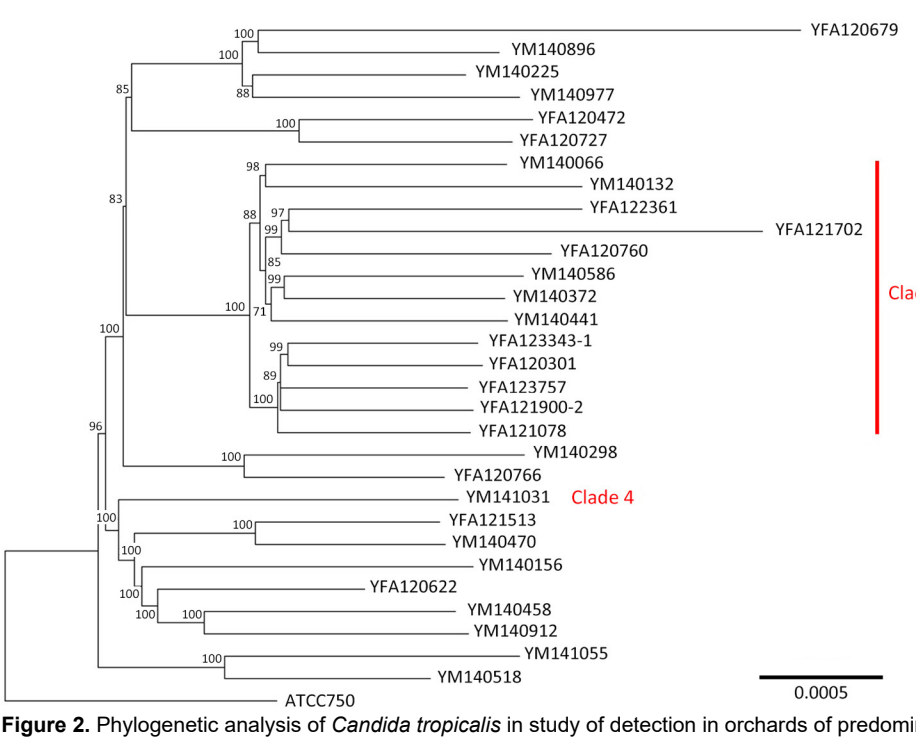

	Source	Clade	DST	MIC
YFA120679	Hand	5	140	≤2
YM140896	Blood	5	911	0.25
YM140225	Blood	5	140	0.25
YM140977	Blood	5	140	0.25
YFA120472	Fruit	8	169	16
YFA120727	Fruit	8	169	≤2
YM140066	Ascites	4	506	64
YM140132	Urine	4	506	32
YFA122361	Soil	4	506	32
YFA121702	Soil	4	506	32
YFA120760	Fruit	4	225	64
YM140586	Blood	4	225	64
YM140372	Sputum	4	225	32
YM140441	Urine	4	506	32
YFA123343-1	Fruit	4	225	32
YFA120301	Soil	4	225	32
YFA123757	Soil	4	225	64
YFA121900-2	Fruit	4	225	64
YFA121078	Soil	4	225	≤2
YM140298	Urine	3	585	8
YFA120766	Fruit	1	587	≤2
YM141031	Urine	4	667	0.25
YFA121513	Fruit	6	557	≤2
YM140470	Urine	6	149	0.5
YM140156	Blood	7	139	0.25
YFA120622	Soil	5	928	≤2
YM140458	Sputum	11	923	0.25
YM140912	Blood	5	910	0.5
YM141055	Sputum	2	153	>64
YM140518	Urine	2	134	0.25
ATCC750	ATCC	ND	914	2

Figure 2. Phylogenetic analysis of *Candida tropicalis* in study of detection in orchards of predominant azole-resistant genotype causing human candidemia, Taiwan. Red numbers indicate fluconazole resistance at MICs of ≥8 mg/L. We conducted whole-genome sequencing of 31 isolates. Sequence comparisons indicated that all but 1 clade 4 isolate was fluconazole resistant and that isolates from orchards and patients were genetically related. Scale bar indicates nucleotide substitutions per site. ATCC, American Type Tissue Collection; DST, diploid sequence type, ND, not determined.

crobes. We showed that clade assignment from MLST aligned well with the tree topology according to WGS results, which is consistent with our previous report of genetic relatedness among 2 clades detected by MLST and confirmed by mitochondrial genome sequencing (*43*). Nevertheless, when we compared the WGS results among clade 4 strains, we ruled out the possibility that YM141031, which fell outside of the clade 4 cluster (Figure 2), had large insertions or deletions within its genome. Therefore, it is possible that the clade 4 *C. tropicalis* ancestor was divided into 2 different progenies because of drug selection pressure. The fluconazole-susceptible ancestor of YM141031 has wild-type *ERG11* and survives in an azole drug-free environment, whereas the ancestor of YFA121078, found in the clade 4 cluster, has mutations in *ERG11* and survives in the presence of low levels of azole drugs. YFA121078 developed into a fully fluconazole-resistant strain by *ERG11* copy number variation or other potential mechanisms contributing to drug resistance. Thus, the combination of clade 4 genotype and *ERG11* mutations might help to rapidly identify drug-resistant clade 4 *C. tropicalis*.

Twenty-nine different types of azole fungicides have been used in Taiwan. The annual azole fungicide use in agriculture in Taiwan increased from 82.1 tons in 2005 to 145.7 tons in 2013 (*33*). Difenoconazole use increased from 9.2 tons in 2005 to 32 tons in 2013 and tebuconazole increased from 2.1 tons in 2005 to 12.7 tons in 2013; ≈0.5 tons of triadimenol were used during both periods. Correlations between increased agricultural azole use and the appearance of azole resistance in human fungal pathogens have been found. We found that *C. tropicalis* could be traced to a few farmers. However, no farmers harbored clade 4 azole-resistant isolates. Nevertheless, we have established a foundation for more in-depth and systematic studies to evaluate the horizontal transmission of the *C. tropicalis* genotype in the agricultural setting and its implications in the clinical setting.

In conclusion, our findings reemphasize the importance of the One Health concept. In Taiwan, total clinical azole use increased from 14,691 DDD in 2005 to 21,991 DDD in 2013; fluconazole increased from 12,707 DDD in 2005 to 19,053 DDD in 2013, itraconazole increased from 362 DDD in 2005 to 760 DDD in 2013, and voriconazole increased from 332 DDD in 2005 to 1,396 DDD in 2013, whereas ketoconazole decreased from 1,291 DDD in 2005 to 677 DDD in 2013, according to data derived from the Taiwan National Health Insurance Research database (*32*). Antimicrobial drug stewardship efforts in hospitals can reduce the selection of drug-resistant organisms. However, if no efforts are made in agriculture to discontinue use of antimicrobial drug classes used in human medicine, vulnerable patients will continue to become infected with highly resistant organisms and have fewer treatment options. Our findings indicate that agriculture environments are one reservoir for azole-resistant *C. tropicalis*; discontinuing agricultural use of azoles might reduce emergence of azole-resistant *Candida* spp. strains in humans.

Acknowledgments

We thank Calvin Kunin, Shau-Ku Huang, Clifford McDonald, Geneviève Milon, and Mark Swofford for their assistance with the manuscript; Pfizer for supplying fluconazole; and Mission Biotech for assistance with techniques for sequencing and real-time PCR.

This work was supported in part by grants from the Ministry of Science and Technology, Taiwan (grant nos. 112-2314-B-400-007 and 112-0324-01-30-06), National Health Research Institutes (grant nos. IV-112-PP-02, IV-112-PP-11, IV-113-PP-01, and IV-113-PP-05), Taiwan Centers for Disease Control (grant no. MOHW111-CDCC-114-124301).

About the Author

Mr. Tseng is an epidemiologist at the Taiwan National Health Research Institutes. His research interests focus on molecular epidemiology, mechanisms of antimicrobial drugs, and bioinformatics.

References

1. Warnock DW. Trends in the epidemiology of invasive fungal infections. Nihon Ishinkin Gakkai Zasshi. 2007;48:1–12. https://doi.org/10.3314/jjmm.48.1
2. Yang YL, Cheng MF, Wang CW, Wang AH, Cheng WT, Lo HJ, et al. The distribution of species and susceptibility of amphotericin B and fluconazole of yeast pathogens isolated from sterile sites in Taiwan. Med Mycol. 2010;48:328–34. https://doi.org/10.3109/13693780903154070
3. Colombo AL, Júnior JNA, Guinea J. Emerging multidrug-resistant *Candida* species. Curr Opin Infect Dis. 2017;30:528–38. https://doi.org/10.1097/QCO.0000000000000411
4. Tan BH, Chakrabarti A, Li RY, Patel AK, Watcharananan SP, Liu Z, et al.; Asia Fungal Working Group (AFWG). Incidence and species distribution of candidaemia in Asia: a laboratory-based surveillance study. Clin Microbiol Infect. 2015;21:946–53. https://doi.org/10.1016/j.cmi.2015.06.010
5. Wu PF, Liu WL, Hsieh MH, Hii IM, Lee YL, Lin YT, et al. Epidemiology and antifungal susceptibility of candidemia isolates of non-albicans *Candida* species from cancer patients. Emerg Microbes Infect. 2017;6:e87. https://doi.org/10.1038/emi.2017.74
6. Lortholary O, Renaudat C, Sitbon K, Desnos-Ollivier M, Bretagne S, Dromer F; French Mycoses Study Group. The risk and clinical outcome of candidemia depending on

underlying malignancy. Intensive Care Med. 2017;43:652–62. https://doi.org/10.1007/s00134-017-4743-y
7. Pfaller M, Neofytos D, Diekema D, Azie N, Meier-Kriesche HU, Quan SP, et al. Epidemiology and outcomes of candidemia in 3648 patients: data from the Prospective Antifungal Therapy (PATH Alliance®) registry, 2004–2008. Diagn Microbiol Infect Dis. 2012;74:323–31. https://doi.org/10.1016/j.diagmicrobio.2012.10.003
8. Akinbobola AB, Kean R, Hanifi SMA, Quilliam RS. Environmental reservoirs of the drug-resistant pathogenic yeast *Candida auris*. PLoS Pathog. 2023;19:e1011268. https://doi.org/10.1371/journal.ppat.1011268
9. Jeffery-Smith A, Taori SK, Schelenz S, Jeffery K, Johnson EM, Borman A, et al.; Candida auris Incident Management Team. *Candida auris*: a review of the literature. Clin Microbiol Rev. 2017;31:e00029-17. https://doi.org/10.1128/CMR.00029-17
10. Yang YL, Cheng HH, Ho YA, Hsiao CF, Lo HJ. Fluconazole resistance rate of *Candida* species from different regions and hospital types in Taiwan. J Microbiol Immunol Infect. 2003;36:187–91.
11. Yang YL, Chen HT, Lin CC, Chu WL, Lo HJ; TSARY Hospitals. Species distribution and drug susceptibilities of *Candida* isolates in TSARY 2010. Diagn Microbiol Infect Dis. 2013;76:182–6. https://doi.org/10.1016/j.diagmicrobio.2013.03.003
12. Yang YL, Li SY, Cheng HH, Lo HJ; TSARY Hospitals. Susceptibilities to amphotericin B and fluconazole of *Candida* species in TSARY 2002. Diagn Microbiol Infect Dis. 2005;51:179–83. https://doi.org/10.1016/j.diagmicrobio.2004.11.004
13. Yang YL, Wang AH, Wang CW, Cheng WT, Li SY, Lo HJ; TSARY Hospitals. Susceptibilities to amphotericin B and fluconazole of *Candida* species in Taiwan surveillance of antimicrobial resistance of yeasts 2006. Diagn Microbiol Infect Dis. 2008;61:175–80. https://doi.org/10.1016/j.diagmicrobio.2008.01.011
14. Zhou ZL, Lin CC, Chu WL, Yang YL, Lo HJ; TSARY Hospitals. The distribution and drug susceptibilities of clinical *Candida* species in TSARY 2014. Diagn Microbiol Infect Dis. 2016;86:399–404. https://doi.org/10.1016/j.diagmicrobio.2016.09.009
15. Zhou ZL, Tseng KY, Chen YZ, Tsai DJ, Wu CJ, Chen YC, et al. Genetic relatedness among azole-resistant *Candida tropicalis* clinical strains in Taiwan from 2014 to 2018. Int J Antimicrob Agents. 2022;59:106592. https://doi.org/10.1016/j.ijantimicag.2022.106592
16. Fernández-Ruiz M, Puig-Asensio M, Guinea J, Almirante B, Padilla B, Almela M, et al.; CANDIPOP Project; GEIH-GEMICOMED (SEIMC); REIPI. *Candida tropicalis* bloodstream infection: incidence, risk factors and outcome in a population-based surveillance. J Infect. 2015;71:385–94. https://doi.org/10.1016/j.jinf.2015.05.009
17. Tan TY, Hsu LY, Alejandria MM, Chaiwarith R, Chinniah T, Chayakulkeeree M, et al. Antifungal susceptibility of invasive *Candida* bloodstream isolates from the Asia-Pacific region. Med Mycol. 2016;54:471–7. https://doi.org/10.1093/mmy/myv114
18. Teo JQ, Candra SR, Lee SJ, Chia SY, Leck H, Tan AL, et al. Candidemia in a major regional tertiary referral hospital—epidemiology, practice patterns and outcomes. Antimicrob Resist Infect Control. 2017;6:27. https://doi.org/10.1186/s13756-017-0184-1
19. Fan X, Dai RC, Zhang S, Geng YY, Kang M, Guo DW, et al. Tandem gene duplications contributed to high-level azole resistance in a rapidly expanding *Candida tropicalis* population. Nat Commun. 2023;14:8369. https://doi.org/10.1038/s41467-023-43380-2
20. Berger CN, Sodha SV, Shaw RK, Griffin PM, Pink D, Hand P, et al. Fresh fruit and vegetables as vehicles for the transmission of human pathogens. Environ Microbiol. 2010;12:2385–97. https://doi.org/10.1111/j.1462-2920.2010.02297.x
21. Lo HJ, Tsai SH, Chu WL, Chen YZ, Zhou ZL, Chen HF, et al. Fruits as the vehicle of drug resistant pathogenic yeasts. J Infect. 2017;75:254–62. https://doi.org/10.1016/j.jinf.2017.06.005
22. Chen YZ, Tseng KY, Wang SC, Huang CL, Lin CC, Zhou ZL, et al. Fruits are vehicles of drug-resistant pathogenic *Candida tropicalis*. Microbiol Spectr. 2023;11:e0147123. https://doi.org/10.1128/spectrum.01471-23
23. Snelders E, Huis In 't Veld RA, Rijs AJ, Kema GH, Melchers WJ, Verweij PE. Possible environmental origin of resistance of *Aspergillus fumigatus* to medical triazoles. Appl Environ Microbiol. 2009;75:4053–7. https://doi.org/10.1128/AEM.00231-09
24. Hung CC, Yang YL, Lauderdale TL, McDonald LC, Hsiao CF, Cheng HH, et al. Colonization of human immunodeficiency virus-infected outpatients in Taiwan with *Candida* species. J Clin Microbiol. 2005;43:1600–3. https://doi.org/10.1128/JCM.43.4.1600-1603.2005
25. Leaw SN, Chang HC, Barton R, Bouchara JP, Chang TC. Identification of medically important *Candida* and non-*Candida* yeast species by an oligonucleotide array. J Clin Microbiol. 2007;45:2220–9. https://doi.org/10.1128/JCM.00543-07
26. Clinical and Laboratory Standards Institute. Performance standards for antifungal susceptibility testing of yeasts. 1st edition, informational supplement (M60). Wayne (PA): The Institute; 2017.
27. Chou HH, Lo HJ, Chen KW, Liao MH, Li SY. Multilocus sequence typing of *Candida tropicalis* shows clonal cluster enriched in isolates with resistance or trailing growth of fluconazole. Diagn Microbiol Infect Dis. 2007;58:427–33. https://doi.org/10.1016/j.diagmicrobio.2007.03.014
28. Tavanti A, Davidson AD, Johnson EM, Maiden MCJ, Shaw DJ, Gow NAR, et al. Multilocus sequence typing for differentiation of strains of *Candida tropicalis*. J Clin Microbiol. 2005;43:5593–600. https://doi.org/10.1128/JCM.43.11.5593-5600.2005
29. Wang SH, Shen M, Lin HC, Sun PL, Lo HJ, Lu JJ. Molecular epidemiology of invasive *Candida albicans* at a tertiary hospital in northern Taiwan from 2003 to 2011. Med Mycol. 2015;53:828–36. https://doi.org/10.1093/mmy/myv065
30. Chien YS, Chen FJ, Wu HC, Lin CH, Chang WC, Perera D, et al. Cost-effective complete genome sequencing using the MinION platform for identification of recombinant enteroviruses. Microbiol Spectr. 2023;11:e0250723. https://doi.org/10.1128/spectrum.02507-23
31. Liao YC, Cheng HW, Wu HC, Kuo SC, Lauderdale TY, Chen FJ. Completing circular bacterial genomes with assembly complexity by using a sampling strategy from a single MinION run with barcoding. Front Microbiol. 2019;10:2068. https://doi.org/10.3389/fmicb.2019.02068
32. Kuo SC, Shih SM, Hsieh LY, Lauderdale TY, Chen YC, Hsiung CA, et al. Antibiotic restriction policy paradoxically increased private drug consumptions outside Taiwan's National Health Insurance. J Antimicrob Chemother. 2017;72:1544–5. https://doi.org/10.1093/jac/dkw595
33. Wang HC, Huang JC, Lin YH, Chen YH, Hsieh MI, Choi PC, et al. Prevalence, mechanisms and genetic relatedness of the human pathogenic fungus *Aspergillus fumigatus* exhibiting resistance to medical azoles in the environment of Taiwan. Environ Microbiol. 2018;20:270–80. https://doi.org/10.1111/1462-2920.13988

34. Chen PY, Chuang YC, Wu UI, Sun HY, Wang JT, Sheng WH, et al. Clonality of fluconazole-nonsusceptible *Candida tropicalis* in bloodstream infections, Taiwan, 2011–2017. Emerg Infect Dis. 2019;25:1660–7. https://doi.org/10.3201/eid2509.190520
35. Cowen LE. Predicting the emergence of resistance to antifungal drugs. FEMS Microbiol Lett. 2001;204:1–7. https://doi.org/10.1111/j.1574-6968.2001.tb10853.x
36. Cowen LE, Sanglard D, Calabrese D, Sirjusingh C, Anderson JB, Kohn LM. Evolution of drug resistance in experimental populations of *Candida albicans*. J Bacteriol. 2000;182:1515–22. https://doi.org/10.1128/JB.182.6.1515-1522.2000
37. Chowdhary A, Kathuria S, Xu J, Meis JF. Emergence of azole-resistant *Aspergillus fumigatus* strains due to agricultural azole use creates an increasing threat to human health. PLoS Pathog. 2013;9:e1003633. https://doi.org/10.1371/journal.ppat.1003633
38. Wu CJ, Wang HC, Lee JC, Lo HJ, Dai CT, Chou PH, et al. Azole-resistant *Aspergillus fumigatus* isolates carrying TR_{34}/L98H mutations in Taiwan. Mycoses. 2015;58:544–9. https://doi.org/10.1111/myc.12354
39. Müller FMC, Staudigel A, Salvenmoser S, Tredup A, Miltenberger R, Herrmann JV. Cross-resistance to medical and agricultural azole drugs in yeasts from the oropharynx of human immunodeficiency virus patients and from environmental Bavarian vine grapes. Antimicrob Agents Chemother. 2007;51:3014–6. PubMed https://doi.org/10.1128/AAC.00459-07
40. Eyre DW, Sheppard AE, Madder H, Moir I, Moroney R, Quan TP, et al. A *Candida auris* outbreak and its control in an intensive care setting. N Engl J Med. 2018;379:1322–31. https://doi.org/10.1056/NEJMoa1714373
41. Scordino F, Giuffrè L, Barberi G, Marino Merlo F, Orlando MG, Giosa D, et al. Multilocus sequence typing reveals a new cluster of closely related *Candida tropicalis* genotypes in Italian patients with neurological disorders. Front Microbiol. 2018;9:679. https://doi.org/10.3389/fmicb.2018.00679
42. Wang Y, Shi C, Liu JY, Li WJ, Zhao Y, Xiang MJ. Multilocus sequence typing of *Candida tropicalis* shows clonal cluster enrichment in azole-resistant isolates from patients in Shanghai, China. Infect Genet Evol. 2016;44:418–24. https://doi.org/10.1016/j.meegid.2016.07.026
43. Tseng KY, Liao YC, Chen FC, Chen FJ, Lo HJ. A predominant genotype of azole-resistant *Candida tropicalis* clinical strains. Lancet Microbe. 2022;3:e646. https://doi.org/10.1016/S2666-5247(22)00179-3

Address for correspondence: Hsiu-Jung Lo, Taiwan Mycology Reference Center, National Institute of Infectious Diseases and Vaccinology, National Health Research Institutes, 35 Keyan Rd, Zhunan, Miaoli County 350, Taiwan; email: hjlo@nhri.edu.tw

etymologia revisited

Enterocytozoon bieneusi

[ˈentərəˌsaitəˈʒu:ən bɪəˈnəʊsɪ]

From the Greek *en'tĕr-ō-sī'tōn* (intestine), *kútos* (vessel, cell), and *zō'on* (animal), and the surname Bieneus, in memory of the first infected patient whose case was reported in Haiti during 1985. *Enterocytozoon bieneusi*, a member of the wide-ranging phylum Microsporidia, is the only species of this genus known to infect humans. Microsporidia are unicellular intracellular parasites closely related to fungi, although the nature of the relationship is not clear.

E. bieneusi, a spore-forming, obligate intracellular eukaryote, was discovered during the HIV/AIDS pandemic and is the main species responsible for intestinal microsporidiosis, a lethal disease before widespread use of antiretroviral therapies. More than 500 genotypes are described, which are divided into different host-specific or zoonotic groups. This pathogen is an emerging issue in solid organ transplantation, especially in renal transplant recipients.

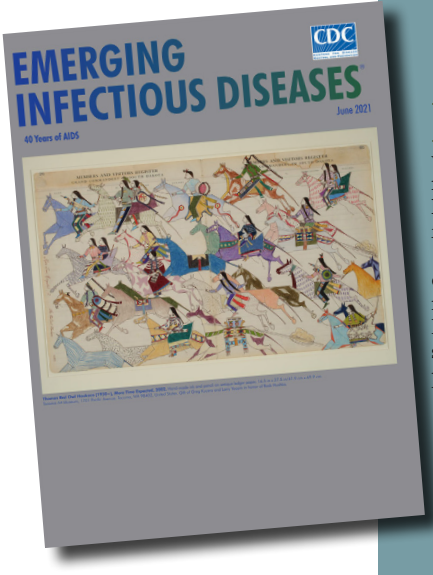

Originally published in June 2021

Sources

1. Desportes I, Le Charpentier Y, Galian A, Bernard F, Cochand-Priollet B, Lavergne A, et al. Occurrence of a new microsporidan: *Enterocytozoon bieneusi* n.g., n. sp., in the enterocytes of a human patient with AIDS. J Protozool. 1985;32:250–4. https://doi.org/10.1111/j.1550-7408.1985.tb03046.x
2. Didier ES, Weiss LM. Microsporidiosis: not just in AIDS patients. Curr Opin Infect Dis. 2011;24:490–5. https://doi.org/10.1097/QCO.0b013e32834aa152
3. Han B, Weiss LM. Microsporidia: obligate intracellular pathogens within the fungal kingdom. Microbiol Spectr. 2017;5:97–113. https://doi.org/10.1128/microbiolspec.FUNK-0018-2016
4. Moniot M, Nourrisson C, Faure C, Delbac F, Favennec L, Dalle F, et al. Assessment of a multiplex PCR for the simultaneous diagnosis of intestinal cryptosporidiosis and microsporidiosis: epidemiologic report from a French prospective study. J Mol Diagn. 2021;23:417–23. https://doi.org/10.1016/j.jmoldx.2020.12.005

https//wwwnc.cdc.gov/eid/article/27/6/et2706_article

Spatiotemporal Ecologic Analysis of COVID-19 Vaccination Coverage and Outcomes, Oklahoma, USA, February 2020–December 2021

Kai Ding, Ozair H. Naqvi, R. Jackson Seeberger, Dale W. Bratzler, Aaron M. Wendelboe

Data on COVID-19 cases, deaths, hospitalizations, and vaccinations in Oklahoma, USA, have not been systematically described. The relationship between vaccination and COVID-19–related outcomes over time has not been investigated. We graphically described data c ollected during February 2020–December 2021 and conducted spatiotemporal modeling of monthly increases in COVID-19 cumulative death and hospitalization rates, adjusting for cumulative case rate, to explore the relationship. A 1 percentage point increase (absolute change) in the cumulative vaccination rate was associated with a 6.3% (95% CI 1.4%–10.9%) relative decrease in death outcome during April–June 2021, and a 1.9% (95% CI 1.1%–2.6%) relative decrease in death outcome and 1.1% (95% CI 0.5%–1.7%) relative decrease in hospitalization outcome during July–December 2021; the effect on hospitalizations was driven largely by data from urban counties. Our findings from Oklahoma suggest that increasing cumulative vaccination rates might reduce the increase in cumulative death and hospitalization rates from COVID-19.

COVID-19 dramatically increased severe outcomes in the United States, based on >5 million hospitalizations and >1 million deaths being reported as of late 2022 (*1*). In Oklahoma (Figure 1), a state in the south-central United States, the pandemic resulted in >101,000 hospitalizations and >14,000 deaths during that period (*1*). On the basis of provisional mortality data from the Centers for Disease Control and Prevention (CDC), COVID-19 was the third leading cause of death in the United States in both 2020 and 2021 (*2*,*3*). Furthermore, COVID-19 led to decreases in US life expectancy from 77.3 years in 2020 to 76.1 years in 2021 (*4*,*5*). In late 2020, the US Food and Drug Administration provided emergency use authorization for 2 separate COVID-19 vaccines, developed by Pfizer-BioNTech (https://www.pfizer.com) and Moderna (https://www.modernatx.com) pharmaceutical companies, followed promptly by recommendations from the Advisory Committee on Immunization Practices for prioritization and use of the vaccines (*6*,*7*). By April 2021, COVID-19 vaccines were available in Oklahoma for all persons >16 years of age (*8*). At that point, ≈5,000 deaths involving COVID-19 had occurred in the state, making the need for further medical interventions critical to preventing further loss of life (*1*). The resulting vaccination campaign led to declines in rates of COVID-19 incidence, emergency department visits, hospitalizations, and deaths across the nation (*9*).

However, implementation of preventive measures and severe COVID-19 outcomes were uneven depending on where persons lived (*10*–*12*). Despite the disease's severity, many persons living in the United States have been skeptical about their risk of experiencing a COVID-19–related hospitalization or death and even more skeptical about receiving a COVID-19 vaccine to reduce such risks (*13*–*15*). Those views have been disproportionately shared by persons living in rural areas, based on the unsupported belief that COVID-19 poses a greater risk in urban settings (*15*–*17*). Current evidence indicates that rural residents are less likely to vaccinate against COVID-19 than are urban residents (*18*–*20*). For persons less skeptical of vaccination, the risk factors associated with adverse COVID-19 outcomes, such as older persons living in multigenerational households or lower socioeconomic status among residents of sparsely populated regions, should encourage COVID-19 vaccine uptake (*19*,*21*,*22*). Moreover, analyses of cumulative death

Author affiliation: University of Oklahoma Health Sciences, Oklahoma City, Oklahoma, USA

DOI: https://doi.org/10.3201/eid3011.231852

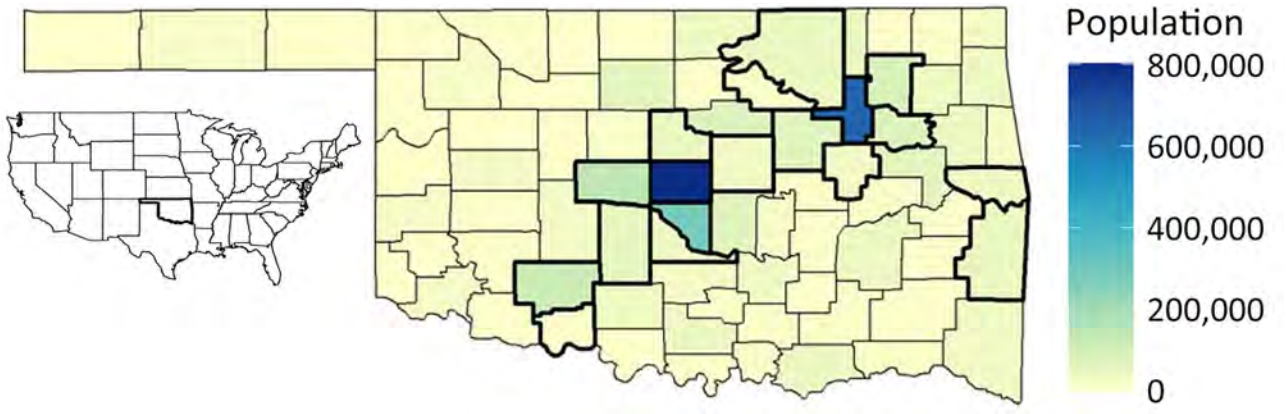

Figure 1. Geography of Oklahoma, USA, and population by county (range 2,137–797,434 residents). Counties with thick boundary lines are metropolitan. The 2 most populous are Oklahoma County (population 797,434) and Tulsa County (population 651,552). Inset map shows location of Oklahoma in the mainland United States.

rates from COVID-19 have pointed to disproportionate burdens borne by residents of rural compared with urban counties (*23*,*24*).

Similar disparities have been reported in terms of COVID-19 vaccination coverage, which is lower in rural than urban counties in Oklahoma (*25*), including in its 2 large metropolitan counties. Vaccination coverage even varied among counties by a wide margin, from 43% of persons receiving ≥1 dose in rural Cimarron County (county seat Boise City) to 88.3% in mostly urban Oklahoma County (county seat Oklahoma City) as of December 2021 (*26*). Other studies have also described disparities between urban and rural counties in COVID-19 vaccination coverage; that coverage gap more than doubled from April 2021 through January 2022 (*25*,*27*). Although national studies have linked counties on the fringes of large metropolitan areas and nonmetropolitan counties to greater COVID-19 disparities (*28*), further research is needed to characterize that relationship between county metropolitan status and vaccination coverage on the state level to evaluate how local public health interventions to increase vaccination coverage can be improved.

Spatiotemporal epidemiology can be used to integrate the investigation of health outcomes across geography and time (*29*,*30*). Prior studies have taken county of residence and underlying medical conditions into consideration when evaluating the spread of COVID-19 across communities over time (*31*–*33*); however, the time-varying effect of vaccination on both death and hospitalization related to COVID-19 has not been thoroughly explored.

We used county-level COVID-19 data from Oklahoma to conduct a spatiotemporal ecologic study with 2 objectives: to describe the distribution of COVID-19–related cases, deaths, hospitalizations, and vaccinations over time and to investigate the correlation between COVID-19 cumulative death and hospitalization rates and vaccination coverage. Furthermore, we assessed whether the correlation varied between urban and rural counties. The University of Oklahoma Health Sciences institutional review board determined this study (review no. 17463) did not meet criteria for human subjects research.

Methods

Data Sources

We obtained county-level cumulative vaccination rates and individual-level data on COVID-19 cases and outcomes (death and hospitalization) from the CDC National Notifiable Disease Surveillance System (NNDSS) COVID-19 Case Surveillance Restricted Access Dataset (*34*). The dataset included deidentified individual-level data on confirmed and probable COVID-19 cases, hospitalizations, and deaths reported from local and state public health jurisdictions (*35*). We accessed data for the excess death plot from the CDC National Center for Health Statistics, modified it to reflect the February 2020–December 2021 study period, and accessed county-level vaccination data from the CDC COVID Data Tracker, which included county-level population data (*1*,*36*).

Measures

The primary exposure was the cumulative vaccination rate, which we defined as the percentage of the county population that had completed the 2-dose series by a given date. We included both probable and laboratory-confirmed COVID-19 cases in our analyses. Because of an issue involving incomplete reporting of death events, we restricted analyses to data collected through December 4, 2021. We defined an absolute cumulative event (COVID-19 case, death, or

hospitalization) rate as the county's cumulative event count on a specific date normalized to 100,000 residents. For spatiotemporal modeling, we calculated the increases in the cumulative rate of COVID-19 death and hospitalization outcomes over a time interval by subtracting the county's absolute cumulative rate on the day before the start of the time interval from that rate at the end of the time interval. We defined counties as urban if designated metropolitan according to the CDC National Center for Health Statistics urban/rural classification scheme for counties (*37*).

Statistical Analysis

We determined county-level cumulative vaccination, death, and hospitalization rates at selected time points in spatial plots. We computed Pearson correlation coefficients and 95% CIs between cumulative vaccination rates and cumulative rates of outcomes weighted by county population size at selected time points. We also used scatter plots with weighted least-squares lines to visualize the relationship between vaccination coverage and the absolute cumulative outcome rates. On the basis of epidemic curve of COVID-19–related deaths (Figure 2, panel A), we studied the relationship between cumulative vaccination rates and COVID-19–related outcomes during 3 intervals: January 1–March 31, 2021; April 1–June 30, 2021; and July 1–December 4, 2021. Within each time interval, we created a scatter plot of the averaged cumulative vaccination rate, calculated as the average of the cumulative vaccination rates at the start and the end dates

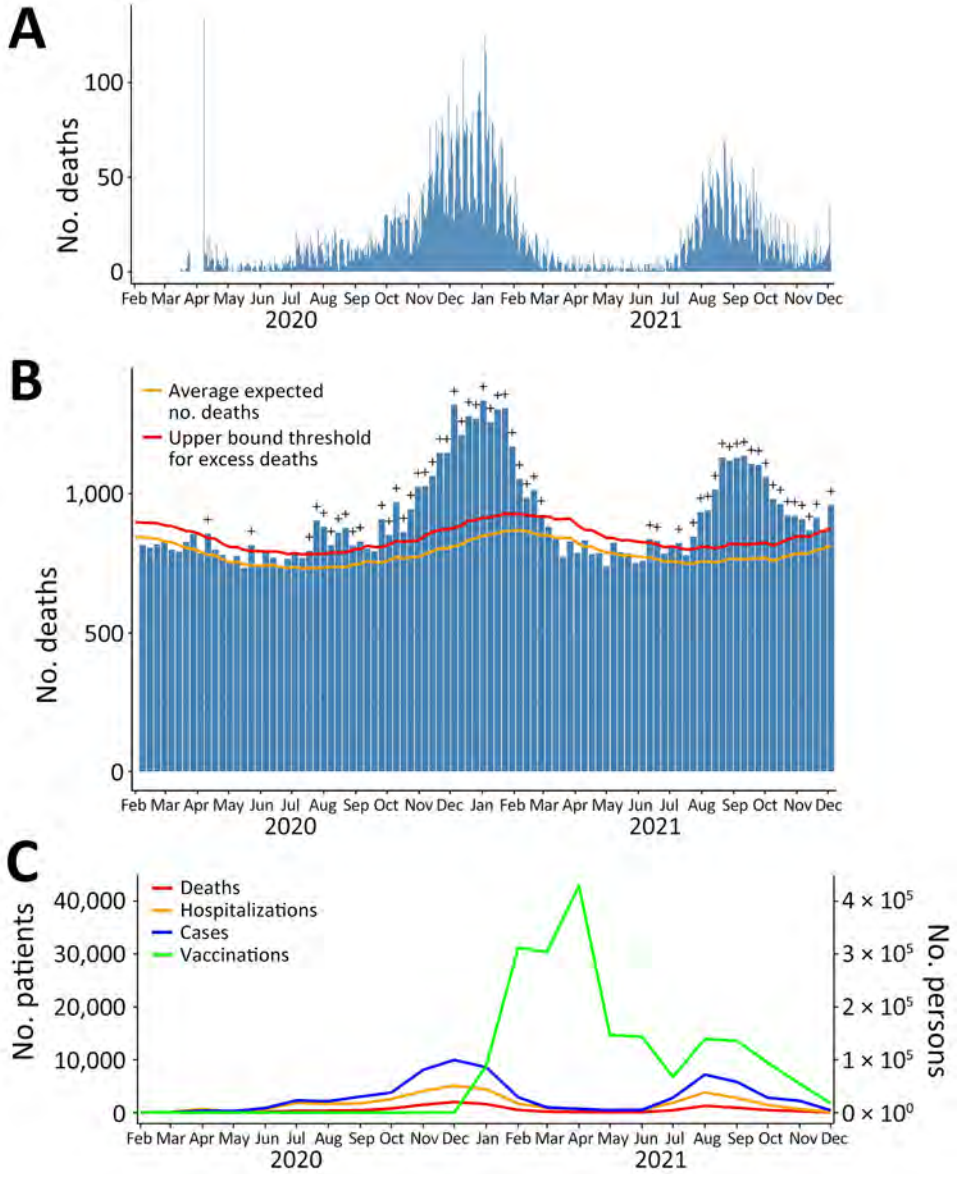

Figure 2. Distribution of COVID-19 deaths (A), all-cause and excess mortality (B), and COVID-19 cases, hospitalization, deaths, and rates of vaccination against COVID-19 (C) in analysis of COVID-19 vaccination coverage and outcomes, Oklahoma, USA, February 2020–December 2021. The spike in the number of deaths on April 8, 2020, was caused by the delay in death reporting early in the pandemic. The excess mortality plot was accessed from the Centers for Disease Control and Prevention National Center for Health Statistics and modified to reflect the study period February 2020–December 2021. Plus (+) symbol indicates observed count above threshold (defined as the upper bound of the 95% prediction interval of the expected number of deaths). In panel C, scales for the y-axes differ substantially to underscore patterns but do not permit direct comparisons. Data sources: https://covid.cdc.gov/covid-data-tracker; https://data.cdc.gov/Case-Surveillance/COVID-19-Case-Surveillance-Restricted-Access-Detai/mbd7-r32t

of the interval, compared with the increase in the cumulative death or hospitalization rate during the same interval.

We based spatiotemporal analysis (Appendix, https://wwwnc.cdc.gov/EID/article/30/11/23-1582-App1.pdf) on the generalized additive model, including a linear term in averaged cumulative vaccination rate and a nonparametric function of the spatial location and time. Specifically, for each interval, we modeled county-level monthly data on averaged cumulative vaccination rates and the increase in cumulative death or hospitalization rates by mixed-effects quasi-Poisson regression using the function GAM in the R package MGCV (The R Project for Statistical Computing, https://www.r-project.com), where the spatiotemporal data structure was captured through a tensor-product of spline-based spatial and temporal basis functions and the tuning parameters in the number of knots were selected based on the generalized cross-validation score (*30*). All models adjusted for the monthly cumulative COVID-19 case rate (averaged between the first and last days of each month) as a potential confounder. In those models, we treated the averaged cumulative vaccination and cumulative COVID-19 case rates as fixed effects and used the tensor-product terms with random coefficients (random effects) to model the spatial and temporal correlation in the data. We chose the quasi-Poisson model, in which we used the log link function and logarithm of the county population as the offset, to account for overdispersion in the data; all dispersion parameter estimates were >1. We also investigated the interaction between averaged cumulative vaccination rate and county metropolitan status and presented stratified results where warranted. We reported both point estimates and 95% CIs. Statistical significance was reached if the 2-sided p value was <0.05. We performed all analyses using R software version 4.2.1 (The R Project for Statistical Computing, https://cran.r-project.org/bin/windows/base/old/4.2.1).

Results

COVID-19–Related Cases, Deaths, Hospitalizations, and Vaccinations over Time

As of December 4, 2021, the data cutoff date for our study, 663,350 reported cases, 11,962 reported provisional deaths, and 38,232 hospitalizations had been attributed to COVID-19 across all 77 counties in Oklahoma. Of those totals, 308,694 (46.5%) cases, 5,914 (49.4%) deaths, and 18,760 (49.1%) hospitalizations were reported by December 31, 2020, before COVID-19 vaccines were sufficiently available to have a meaningful effect on reported cases. We plotted the epidemic curve for COVID-19–related deaths in Oklahoma (Figure 2, panel A). Excess mortality from all causes followed the same trend over time as COVID-19 deaths (Figure 2, panels A, B). We also plotted epidemic curves by month for COVID-19 cases, deaths, patients ever hospitalized, and prime doses of COVID-19 vaccines (Figure 2, panel C). COVID-19–related hospitalizations and deaths followed similar time trends as cases, and peaks were associated with multiple SARS-CoV-2 variants in January 2021 and the Delta variant in August 2021. There was an initial demand for COVID-19 vaccines when they were first made available; peak distribution occurred in March 2021. Demand has largely decreased over time, except for a temporary increase in demand during the August 2021 surge in cases caused by the Delta variant.

County-Level COVID-19–Related Death and Vaccination

We used spatial plots to visualize county-level cumulative vaccination and cumulative death rates at selected time points (Figure 3). Among the 77 counties in Oklahoma, by December 4, 2021, cumulative vaccination rates were 24.1%–59.1% (weighted average 48.8%); cumulative death rates were 155.5–551.2 (weighted average 302.3) deaths/100,000 residents. We also calculated weighted Pearson correlation coefficients between cumulative vaccination and cumulative death rates at selected time points (Table 1). Except for the first time point, at which we observed a positive correlation, cumulative vaccination and cumulative death rates were negatively correlated, and the magnitudes of association were moderate (Appendix Figure 1). We also illustrated county-level averaged cumulative vaccination rates versus increases in cumulative death rates per 100,000 residents for selected time intervals (Figure 4, panel A). Again, except during the January 1–March 31, 2021 time period, averaged cumulative vaccination rates and increases in cumulative death rates were negatively associated (i.e., for April 1–June 30, 2021 and July 1–December 4, 2021).

Through modeling monthly data on averaged cumulative vaccination rates and increases in cumulative death rates (death outcome), a 1 percentage point increase (absolute change) in cumulative vaccination rate was associated with a decrease of 6.3% (95% CI 1.4%–10.9%; p = 0.014) (relative change) in the death outcome for the April–June 2021 time interval and a decrease of 1.9% (95% CI 1.1%–2.6%; p<0.0001) for the July–December 2021 time interval (Table 2); however, we found no association for the January–March 2021 time interval. The interaction between cumulative

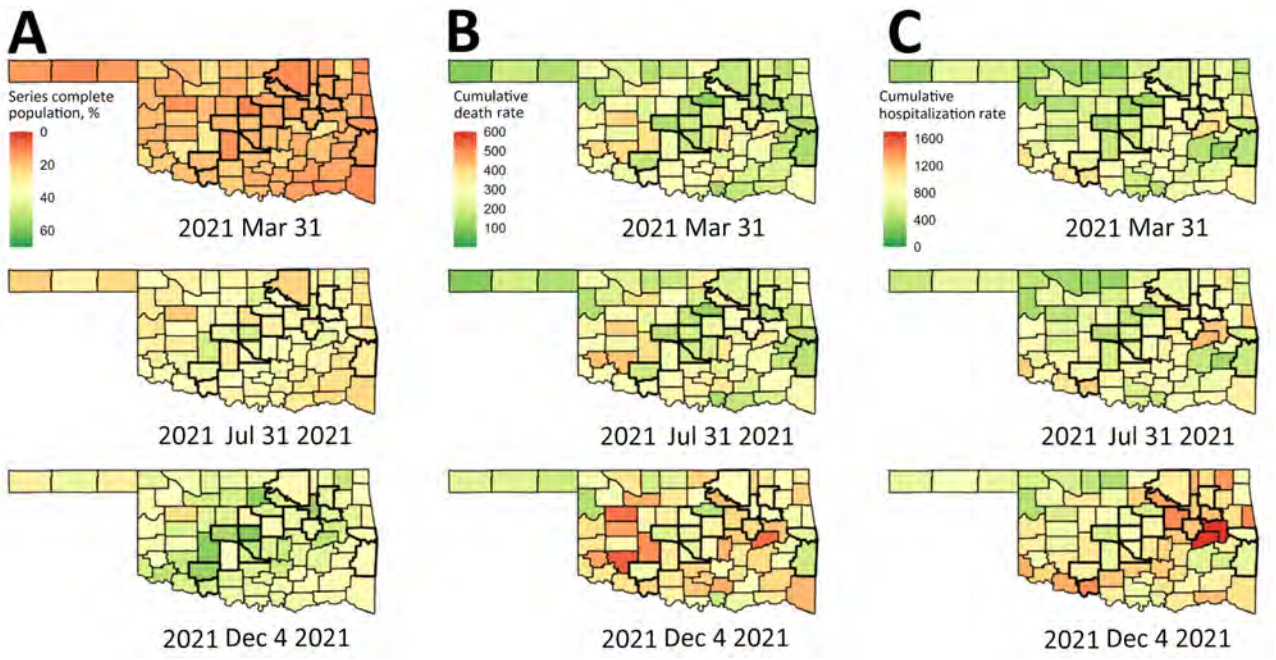

Figure 3. Spatial plots of county-level cumulative vaccination rates and cumulative death and hospitalization rates per 100,000 residents at selected time points in analysis of COVID-19 vaccination coverage and outcomes, Oklahoma, USA, February 2020–December 2021. A) Vaccination rates; B) death rates; C) hospitalization rates. Counties with thick boundary lines are metropolitan.

vaccination rates and metropolitan status of the county was not significant (p = 0.282 for January–March 2021, 0.144 for April–June 2021 and 0.125 for July–December 2021), suggesting that the association between cumulative vaccination rates and the death outcome also did not change according to county metropolitan status. We obtained similar results from sensitivity analyses using the cumulative vaccination rate on the first day of each month, and by including or excluding December 2021 (results not shown).

County-Level COVID-19–Related Hospitalization and Vaccination

We used spatial plots to visualize county-level cumulative vaccination rates and cumulative hospitalization rates at selected time points (Figure 3). Among the 77 counties in Oklahoma, by December 4, 2021, cumulative hospitalization rates were 415.4–1,678.9 (weighted average 966.2)/100,000 residents. We found a positive association between cumulative vaccination and cumulative hospitalization rates for the first time point, but the correlation coefficient was negative for the second and the third time points; however, the magnitude of the negative associations was relatively small (Table 1). We generated scatter plots to illustrate those associations (Appendix Figure 2). We also generated scatter plots of county-level averaged cumulative vaccination rates versus increases in cumulative hospitalization rates per 100,000 residents for selected time intervals (Figure 4, panel B). Again, descriptively, we found a positive association for the January 1–March 31, 2021 time period but observed little association for the April 1–June 30, 2021 and July 1–December 4, 2021 time periods.

Through modeling monthly data on averaged cumulative vaccination rates and increases in cumulative hospitalization rates (hospitalization outcome), we found a significant positive association for the time interval January–March 2021, but found no significant association for the time interval April–June 2021 (Table 2). For the time interval July–December 2021, there was a negative association, but the magnitude of association was relatively small; a 1 percentage point increase (absolute change) in cumulative vaccination rate was associated with a decrease of 1.1% (95% CI 0.5%–1.7%; p = 0.001) (relative change)

Table 1. Pearson correlations and 95% CIs between cumulative vaccination rate and COVID-related outcomes at selected time points in analysis of COVID-19 vaccination coverage and outcomes, Oklahoma, USA, February 2020–December 2021*

Date	Cumulative death rate (crude 95% CIs)	Cumulative hospitalization rate (crude 95% CIs)
2021 Mar 31	0.182 (0.135–0.223)	0.250 (0.204–0.290)
2021 Jul 31	–0.319 (–0.362 to –0.281)	–0.037 (–0.082 to 0.009)
2021 Dec 4	–0.391 (–0.432 to –0.355)	–0.013 (–0.059 to 0.033)

*95% Cis weighted by county population size; crude 95% CIs were reported.

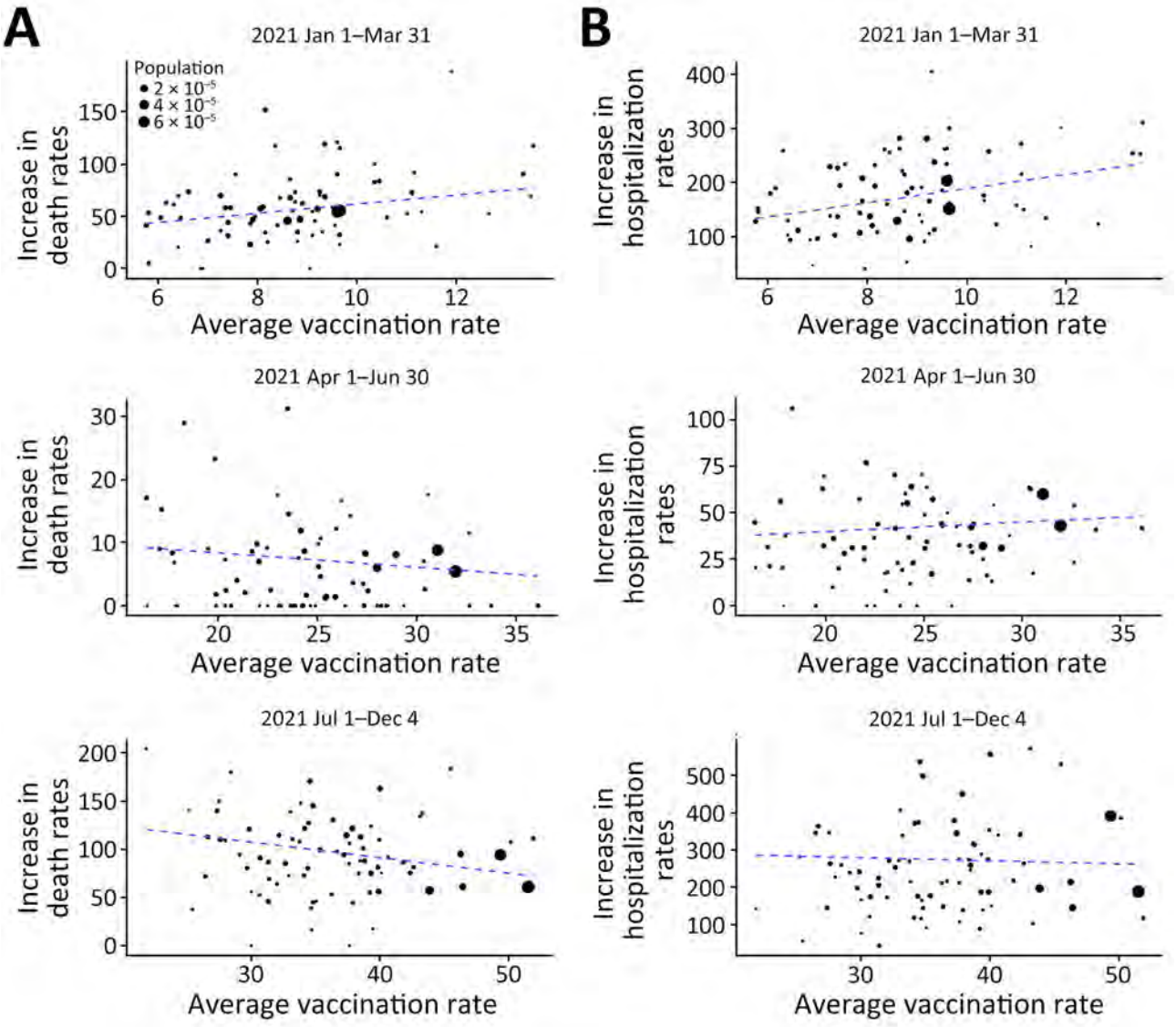

Figure 4. Scatter plot of county-level population percentage of complete vaccination series (averaged between the start and the end dates) versus increase in cumulative death rates (A) and cumulative hospitalization rates (B) per 100,000 residents for selected time intervals in analysis of COVID-19 vaccination coverage and outcomes, Oklahoma, USA, February 2020–December 2021. The dashed line is the weighted (by county population size) least-squares line. The 2 largest solid dots in the plot correspond to the 2 largest counties (i.e., Oklahoma and Tulsa) in Oklahoma.

in the hospitalization outcome. The p values for the interaction between cumulative vaccination rates and county metropolitan status were 0.023 for January–March 2021, 0.173 for April–June 2021, and 0.031 for July–December 2021. Those values suggest that the association between cumulative vaccination rates and the hospitalization outcome differed according to county metropolitan status for the first and the third time periods but not for the second. The overall negative association for the time interval July–December 2021 was largely driven by data from metropolitan counties (Table 3). We obtained similar results from sensitivity analyses using the cumulative vaccination rate on the first day of each month and by including or excluding December 2021 (results not shown).

Discussion

Using county-level data, we conducted a spatiotemporal ecologic analysis to investigate the relationship between both COVID-19–related deaths and hospitalizations and COVID-19 vaccination coverage in the state of Oklahoma, USA. Overall, the findings from this study describe how severe COVID-19–related outcomes changed in Oklahoma over time and based on county urban/rural status. Debate about the accuracy of attributing the correct cause of death to patients diagnosed

Table 2. Association between population percentage of complete vaccination series and increases in cumulative death rates and cumulative hospitalization rates, respectively, for selected time intervals in analysis of COVID-19 vaccination coverage and outcomes, Oklahoma, USA, February 2020–December 2021*

	Death		Hospitalization	
Time interval	Relative decrease for 1 percentage point increase in vaccination (95% CI)	p value	Relative decrease for 1 percentage point increase in vaccination (95% CI)	p value
Jan–Mar 2021	–4.4% (–10.5% to 1.4%)	0.130	–7.4% (–11.0% to –3.8%)	<0.0001
Apr–Jun 2021	6.3% (1.4%–10.9%)	0.014	1.1% (–0.7%–2.8%)	0.231
Jul–Dec 2021	1.9% (1.1%–2.6%)	<0.0001	1.1% (0.5%–1.7%)	0.001

*Monthly data were modeled with (log-link) quasi-Poisson regression using the GAM function in R package "MGCV." All models adjusted for averaged cumulative case rate as potential confounder.
†Sensitivity analysis showed similar results when December 2021 data were excluded or using cumulative vaccination rate on the first day of each month

with COVID-19 has occurred; some persons have been concerned that COVID-19–related deaths were being overreported (*36*) and others concerned those deaths were being underreported (*38*). The time trend of excess deaths from all causes was similar to the epidemic curve of COVID-19–related deaths in Oklahoma, which supports COVID-19 as a cause of excess mortality.

We found a negative correlation between vaccination coverage and COVID-19–related mortality during April–June 2021 and July–December 2021, meaning that higher vaccination coverage was associated with lower increases in cumulative mortality rates during those time periods. The significant association between cumulative vaccination and cumulative death rates was largely driven by data from Oklahoma and Tulsa Counties, the 2 largest counties in Oklahoma (Figure 4, panel A; Appendix Figure 1). The strength of the association was stronger during April–June 2021 than July–December 2021, indicating a possible waning effect for vaccines in protection from death. For COVID-19–related hospitalizations, we did not find a negative correlation with vaccination coverage until July–December 2021; in addition, the magnitude of association was weaker than for COVID-19–related deaths. We also found a positive association between cumulative vaccination rates and outcomes during the early time periods of our study (through March 31, 2021). However, vaccination coverage was low across all counties during the first few months after vaccines first became available. Although Oklahoma implemented rapid initial rollout of COVID-19 vaccines, a time lag would be expected between when vaccinations first became available and reached sufficient population immunity to observe a protective effect.

Our findings were consistent with documented national spatial and temporal progression of COVID-19 up through September 2021 (*39*). In addition, another analysis (*40*) underscored the association of spatial vaccination heterogeneity with intensified COVID-19 surges, particularly in rural counties, which constitute most areas with low vaccination rates. Those studies emphasize the pivotal role of COVID-19 vaccination coverage in mitigating effects of the pandemic in urban and rural settings (*39*,*40*). Our study offers granular, state-level insight into that relationship in Oklahoma, elucidating the nuanced relationship between vaccination coverage and severe COVID-19 outcomes in urban versus rural contexts.

The protective benefit of COVID-19 vaccines has been reported at both the population and individual levels on the basis of data from clinical trials and observational studies (*41*–*48*). Despite that evidence, resistance to uptake of COVID-19 vaccine persists. Through experience as healthcare providers participating in the public health response to the pandemic, we have heard anecdotal accounts of persons from rural counties expressing a belief that risk for COVID-19 infection is lower among persons who live in rural than in urban settings. The data do not support this belief and instead show similar cumulative case rates between urban and rural counties during March 2020–March 2021. Furthermore, studies have linked rural counties with higher CDC Social Vulnerability Index (SVI) scores, which are linked to locations with higher poverty, crowded housing, and

Table 3. Association between population percentage of complete vaccination series and the increases in cumulative hospitalization rate stratified by county metropolitan status, for selected time intervals in analysis of COVID-19 vaccination coverage and outcomes, Oklahoma, USA, February 2020–December 2021*

	Metropolitan counties		Nonmetropolitan counties	
Time interval	Relative decrease for 1 percentage point increase in vaccination (95% CI)	p value	Relative decrease for 1 percentage point increase in vaccination (95% CI)	p value
Jan–Mar 2021	–11.7% (–17.9% to –5.9%)	0.0003	–5.7% (–10.5% to –1.1%)	0.017
Apr–Jun 2021	–0.2% (–2.2% to 1.7%)	0.816	–0.9% (–4.1% to 2.2%)	0.575
Jul–Dec 2021	1.1% (0.2%–1.9%)	0.016	–2.3% (–3.8% to –0.9%)	0.001

*Monthly data were modeled with (log-link) quasi-Poisson regression using the GAM function in R package "MGCV." All models adjusted for averaged cumulative case rate as potential confounder

other community attributes associated with adverse health outcomes (*49*,*50*). Many counties in Oklahoma score high in the SVI, and many of those same counties report lower rates of vaccination coverage, similar to associations observed on the national level between high SVI scores and low vaccination rates (*28*).

Among strengths of this study, we provided a systematic description of COVID-19 cases, deaths, hospitalizations, and vaccination data in the state of Oklahoma during different time periods that roughly correspond with surges in case numbers during the timeframes of the original and Delta variant of SARS-COV-2 virus and the time period between those surges. We also used a mixed-effects model to account for the correlations and spatiotemporal structure in our data when evaluating associations between COVID-19 vaccination coverage and outcomes.

Among limitations of this study, the data we used for analyses were ecologic and aggregate in nature so that we could not determine if persons infected with COVID-19 or who died from COVID-19 had been vaccinated. Second, the exact dates associated with outcomes were not available. Instead, we defined those dates as the earlier of the clinical date (date of illness onset or specimen collection) or the date the case report was received by CDC. Third, we used cumulative vaccination rate over time in our modeling and therefore could not account for the waning effect of vaccines in our analyses. Fourth, although it was not a primary outcome, the cumulative number of COVID-19 cases was potentially undercounted, and discrepancies between urban and rural counties in COVID-19 testing practices might have existed, which might have affected our findings. Last, although we adjusted for cumulative case rates in our models and conclusions were similar after further adjusting for county-level median age and income (data not shown), potential uncontrolled confounding effects cannot be ruled out.

In conclusion, we found a moderate correlation between higher COVID-19 vaccination coverage and lower increase in cumulative COVID-19 death rates but a weaker association with COVID-19–related hospitalization. Future studies using individual-level data are needed to gain further insight into vaccine efficacy. This study provides evidence of the demonstrable benefit to both urban and rural populations in Oklahoma getting vaccinated against COVID-19. That evidence could aid public health officials, healthcare providers, and others to communicate through written and visual media the likely benefits population-level immunity vaccination can provide.

About the Author

Dr. Ding is professor of biostatistics, Department of Biostatistics and Epidemiology, University of Oklahoma Health Sciences in Oklahoma City, Oklahoma, USA. His research interests include survival analysis, high dimensional data, gastrointestinal and gynecological cancers, and ophthalmology.

References

1. Centers for Disease Control and Prevention. COVID data tracker [cited 2022 Nov 7]. https://covid.cdc.gov/covid-data-tracker
2. Ahmad FB, Cisewski JA, Miniño A, Anderson RN. P rovisional mortality data—United States, 2020. MMWR Morb Mortal Wkly Rep. 2021;70:519–22. Erratum in: MMWR Morb Mortal Wkly Rep. 2021;70:900. https://doi.org/10.15585/mmwr.mm7014e1
3. Ahmad FB, Cisewski JA, Anderson RN. Provisional mortality data—United States, 2021. MMWR Morb Mortal Wkly Rep. 2022;71:597–600. https://doi.org/10.15585/mmwr.mm7117e1
4. Arias E, Tejada-Vera B, Kochanek KD, Ahmad F. Centers for Disease Control and Prevention. Provisional life expectancy estimates for 2021 [cited 2023 Nov 1]. https://www.cdc.gov/nchs/data/vsrr/vsrr023.pdf
5. Arias E, Tejada-Vera B, Ahmad F, Kochanek KD. Centers for Disease Control and Prevention. Provisional life expectancy estimates for 2020 [cited 2023 Nov 1]. https://www.cdc.gov/nchs/data/vsrr/vsrr015-508.pdf
6. Oliver SE, Gargano JW, Marin M, Wallace M, Curran KG, Chamberland M, et al. The Advisory Committee on Immunization Practices' Interim Recommendation for Use of Moderna COVID-19 Vaccine—United States, December 2020. MMWR Morb Mortal Wkly Rep. 2021; 69:1653–6. https://doi.org/10.15585/mmwr.mm695152e1
7. Oliver SE, Gargano JW, Marin M, Wallace M, Curran KG, Chamberland M, et al. The Advisory Committee on Immunization Practices' Interim Recommendation for Use of Pfizer-BioNTech COVID-19 Vaccine—United States, December 2020. MMWR Morb Mortal Wkly Rep. 2020;69:1922–4. https://doi.org/10.15585/mmwr.mm6950e2
8. Oklahoma State Department of Health. COVID-19 vaccination [cited 2023 Nov 1]. https://vaccinate.oklahoma.gov/en-US
9. Christie A, Henley SJ, Mattocks L, Fernando R, Lansky A, Ahmad FB, et al. Decreases in COVID-19 cases, emergency department visits, hospital admissions, and deaths among older adults following the introduction of COVID-19 vaccine—United States, September 6, 2020–May 1, 2021. MMWR Morb Mortal Wkly Rep. 2021;70:858–64. https://doi.org/10.15585/mmwr.mm7023e2
10. Hernandez I, Dickson S, Tang S, Gabriel N, Berenbrok LA, Guo J. Disparities in distribution of COVID-19 vaccines across US counties: a geographic information system-based cross-sectional study. PLoS Med. 2022;19:e1004069. https://doi.org/10.1371/journal.pmed.1004069
11. Sun Y, Monnat SM. Rural-urban and within-rural differences in COVID-19 vaccination rates. J Rural Health. 2022;38:916–22. https://doi.org/10.1111/jrh.12625
12. Cuadros DF, Branscum AJ, Mukandavire Z, Miller FD, MacKinnon N. Dynamics of the COVID-19 epidemic in urban and rural areas in the United States. Ann Epidemiol. 2021; 59:16–20. https://doi.org/10.1016/j.annepidem.2021.04.007
13. Levin J, Bradshaw M. Determinants of COVID-19 skepticism and SARS-CoV-2 vaccine hesitancy: findings from a national

population survey of U.S. adults. BMC Public Health. 2022;22:1047. https://doi.org/10.1186/s12889-022-13477-2
14. Kaiser Family Foundation. KFF COVID-19 vaccine monitor: September 2022 [cited 2023 Nov 1]. https://www.kff.org/coronavirus-covid-19/poll-finding/kff-covid-19-vaccine-monitor-september-2022
15. Callaghan T, Lueck JA, Trujillo KL, Ferdinand AO. Rural and urban differences in COVID-19 prevention behaviors. J Rural Health. 2021;37:287–95. https://doi.org/10.1111/jrh.12556
16. Probst JC, Crouch EL, Eberth JM. COVID-19 risk mitigation behaviors among rural and urban community-dwelling older adults in summer, 2020. J Rural Health. 2021;37:473–8. https://doi.org/10.1111/jrh.12600
17. McElfish PA, Willis DE, Shah SK, Bryant-Moore K, Rojo MO, Selig JP. Sociodemographic determinants of COVID-19 vaccine hesitancy, fear of infection, and protection self-efficacy. J Prim Care Community Health. 2021; 12:21501327211040746. https://doi.org/10.1177/21501327211040746
18. Bennett NG, Bloom DE, Ferranna M. Factors underlying COVID-19 vaccine and booster hesitancy and refusal, and incentivizing vaccine adoption. PLoS One. 2022;17:e0274529. https://doi.org/10.1371/journal.pone.0274529
19. Wong R, Grullon JR, Lovier MA. COVID-19 risk factors and predictors for handwashing, masking, and social distancing among a national prospective cohort of US older adults. Public Health. 2022;211:164–70. https://doi.org/10.1016/j.puhe.2022.08.002
20. Sparks G, Hamel L, Kirzinger A, Stokes M, Brodie M. KFF COVID-19 vaccine monitor: differences in vaccine attitudes between rural, suburban, and urban areas [cited 2023 Nov 1]. https://www.kff.org/coronavirus-covid-19/poll-finding/kff-covid-19-vaccine-monitor-vaccine-attitudes-rural-suburban-urban
21. Zang E, West J, Kim N, Pao C. U.S. regional differences in physical distancing: evaluating racial and socioeconomic divides during the COVID-19 pandemic. PLoS One. 2021;16:e0259665. https://doi.org/10.1371/journal.pone.0259665
22. Ghosh AK, Venkatraman S, Soroka O, Reshetnyak E, Rajan M, An A, et al. Association between overcrowded households, multigenerational households, and COVID-19: a cohort study. Public Health. 2021;198:273–9. https://doi.org/10.1016/j.puhe.2021.07.039
23. Ullrich F, Mueller K; RUPRI Center for Rural Health Policy Analysis. COVID-19 cases and deaths, metropolitan and nonmetropolitan counties over time (update) [cited 2023 Nov 1]. https://rupri.public-health.uiowa.edu/publications/policybriefs/2020/COVID%20Longitudinal%20Data.pdf
24. Curtin SC, Heron M. COVID-19 death rates in urban and rural areas: United States, 2020. NCHS Data Brief. 2022;447:1–8. https://doi.org/10.15620/cdc:121523
25. Saelee R, Zell E, Murthy BP, Castro-Roman P, Fast H, Meng L, et al. Disparities in COVID-19 vaccination coverage between urban and rural counties—United States, December 14, 2020–January 31, 2022. MMWR Morb Mortal Wkly Rep. 2022;71:335–40. https://doi.org/10.15585/mmwr.mm7109a2
26. Oklahoma State Department of Health. COVID-19 weekly epidemiology report: December 5–11, 2021 [cited 2023 Nov 1]. https://oklahoma.gov/content/dam/ok/en/covid19/documents/weekly-epi-report/2021/2021.12.15%20Weekly%20Epi%20Report.pdf
27. Murthy BP, Sterrett N, Weller D, Zell E, Reynolds L, Toblin RL, et al. Disparities in COVID-19 vaccination coverage between urban and rural counties—United States, December 14, 2020–April 10, 2021. MMWR Morb Mortal Wkly Rep. 2021;70:759–64. https://doi.org/10.15585/mmwr.mm7020e3
28. Barry V, Dasgupta S, Weller DL, Kriss JL, Cadwell BL, Rose C, et al. Patterns in COVID-19 vaccination coverage, by social vulnerability and urbanicity—United States, December 14, 2020–May 1, 2021. MMWR Morb Mortal Wkly Rep. 2021;70:818–24. https://doi.org/10.15585/mmwr.mm7022e1
29. Meliker JR, Sloan CD. Spatio-temporal epidemiology: principles and opportunities. Spat Spatiotemporal Epidemiol. 2011;2:1–9. https://doi.org/10.1016/j.sste.2010.10.001
30. Wikle CK, Zammit-Mangion A, Cressie N. Spatio-temporal statistics with R. Boca Raton (FL): Chapman and Hall/CRC Press; 2019.
31. Correa-Agudelo E, Mersha TB, Branscum AJ, MacKinnon NJ, Cuadros DF. Identification of vulnerable populations and areas at higher risk of COVID-19–related mortality during the early stage of the epidemic in the United States. Int J Environ Res Public Health. 2021;18:4021. https://doi.org/10.3390/ijerph18084021
32. Paul R, Arif AA, Adeyemi O, Ghosh S, Han D. Progression of COVID-19 from urban to rural areas in the United States: a spatiotemporal analysis of prevalence rates. J Rural Health. 2020;36:591–601. https://doi.org/10.1111/jrh.12486
33. Wang Y, Liu Y, Struthers J, Lian M. Spatiotemporal characteristics of the COVID-19 epidemic in the United States. Clin Infect Dis. 2021;72:643–51. https://doi.org/10.1093/cid/ciaa934
34. Centers for Disease Control and Prevention. CDC Data, Analytics and Visualization Task Force. COVID-19 case surveillance restricted access detailed data [cited 2023 Nov 1]. https://data.cdc.gov/Case-Surveillance/COVID-19-Case-Surveillance-Restricted-Access-Detai/mbd7-r32t
35. National Notifiable Diseases Surveillance System. Coronavirus disease 2019 (COVID-19) 2021 case definition [cited 2023 Nov 1]. https://ndc.services.cdc.gov/case-definitions/coronavirus-disease-2019-2021
36. Weinberger DM, Chen J, Cohen T, Crawford FW, Mostashari F, Olson D, et al. Estimation of excess deaths associated with the COVID-19 pandemic in the United States, March to May 2020. JAMA Intern Med. 2020;180:1336–44. https://doi.org/10.1001/jamainternmed.2020.3391
37. Ingram DD, Franco SJ. 2013 NCHS urban–rural classification scheme for counties. Vital Health Stat 2. 2014;166:1–73.
38. Rossen LM, Branum AM, Ahmad FB, Sutton P, Anderson RN. Excess deaths associated with COVID-19, by age and race and ethnicity—United States, January 26–October 3, 2020. MMWR Morb Mortal Wkly Rep. 2020;69:1522–7. https://doi.org/10.15585/mmwr.mm6942e2
39. Huang Q, Cutter SL. Spatial-temporal differences of COVID-19 vaccinations in the U.S. Urban Inform. 2022;1:19. https://doi.org/10.1007/s44212-022-00019-9
40. Cuadros DF, Miller FD, Awad S, Coule P, MacKinnon NJ. Analysis of vaccination rates and new COVID-19 infections by US county, July–August 2021. JAMA Netw Open. 2022;5:e2147915. https://doi.org/10.1001/jamanetworkopen.2021.47915
41. Muhsen K, Maimon N, Mizrahi AY, Boltyansky B, Bodenheimer O, Diamant ZH, et al. Association of receipt of the fourth BNT162b2 dose with omicron infection and COVID-19 hospitalizations among residents of long-term care facilities. JAMA Intern Med. 2022;182:859–67. https://doi.org/10.1001/jamainternmed.2022.2658

42. Barda N, Dagan N, Cohen C, Hernán MA, Lipsitch M, Kohane IS, et al. Effectiveness of a third dose of the BNT162b2 mRNA COVID-19 vaccine for preventing severe outcomes in Israel: an observational study. Lancet. 2021; 398:2093–100. https://doi.org/10.1016/S0140-6736(21)02249-2
43. Baden LR, El Sahly HM, Essink B, Kotloff K, Frey S, Novak R, et al.; COVE Study Group. Efficacy and safety of the mRNA-1273 SARS-CoV-2 vaccine. N Engl J Med. 2021;384:403–16. https://doi.org/10.1056/NEJMoa2035389
44. Polack FP, Thomas SJ, Kitchin N, Absalon J, Gurtman A, Lockhart S, et al.; C4591001 Clinical Trial Group. Efficacy and safety of the BNT162b2 mRNA Covid-19 vaccine. N Engl J Med. 2020;383:2603–15. https://doi.org/10.1056/NEJMoa2034577
45. McConeghy KW, White EM, Blackman C, Santostefano CM, Lee Y, Rudolph JL, et al. Effectiveness of a second COVID-19 vaccine booster dose against infection, hospitalization, or death among nursing home residents—19 states, March 29–July 25, 2022. MMWR Morb Mortal Wkly Rep. 2022;71:1235–8. https://doi.org/10.15585/mmwr.mm7139a2
46. Johnson AG, Amin AB, Ali AR, Hoots B, Cadwell BL, Arora S, et al. COVID-19 incidence and death rates among unvaccinated and fully vaccinated adults with and without booster doses during periods of Delta and Omicron variant emergence—25 U.S. jurisdictions, April 4–December 25, 2021. MMWR Morb Mortal Wkly Rep. 2022;71:132–8. https://doi.org/10.15585/mmwr.mm7104e2
47. Tenforde MW, Self WH, Gaglani M, Ginde AA, Douin DJ, Talbot HK, et al.; IVY Network. Effectiveness of mRNA vaccination in preventing COVID-19–associated invasive mechanical ventilation and death—United States, March 2021–January 2022. MMWR Morb Mortal Wkly Rep. 2022;71:459–65. https://doi.org/10.15585/mmwr.mm7112e1
48. Natarajan K, Prasad N, Dascomb K, Irving SA, Yang DH, Gaglani M, et al. Effectiveness of homologous and heterologous COVID-19 booster doses following 1 Ad.26.COV2.S (Janssen [Johnson & Johnson]) vaccine dose against COVID-19–associated emergency department and urgent care encounters and hospitalizations among adults—VISION Network, 10 states, December 2021–March 2022. MMWR Morb Mortal Wkly Rep. 2022;71:495–502. https://doi.org/10.15585/mmwr.mm7113e2
49. Khazanchi R, Beiter ER, Gondi S, Beckman AL, Bilinski A, Ganguli I. County-level association of social vulnerability with COVID-19 cases and deaths in the USA. J Gen Intern Med. 2020;35:2784–7. https://doi.org/10.1007/s11606-020-05882-3
50. Li Z, Lewis B, Berney K, Hallisey E, Williams AM, Whiteman A, et al. Social vulnerability and rurality associated with higher severe acute respiratory syndrome coronavirus 2 (SARS-CoV-2) infection-induced seroprevalence: a nationwide blood donor study—United States, July 2020–June 2021. Clin Infect Dis. 2022;75:e133–43. https://doi.org/10.1093/cid/ciac105

Address for correspondence: Kai Ding, Hudson College of Public Health, 801 NE 13th St, Rm 329, PO Box 26901, Oklahoma City, OK 73104, USA; email: kai-ding@ouhsc.edu

etymologia revisited

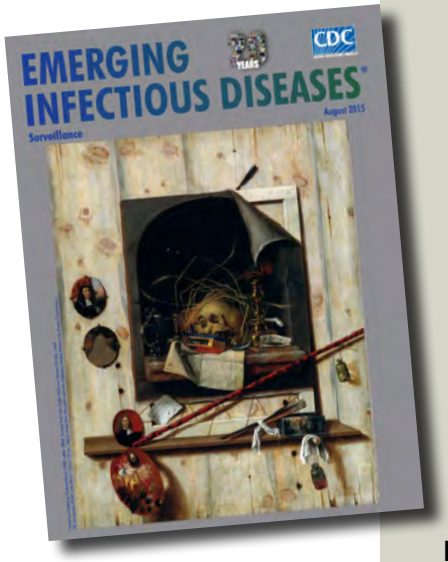

Originally published in August 2015

Escherichia coli

[esh″ə-rik′e-ə co′lī]

A gram-negative, facultatively anaerobic rod, *Escherichia coli* was named for Theodor Escherich, a German-Austrian pediatrician. Escherich isolated a variety of bacteria from infant fecal samples by using his own anaerobic culture methods and Hans Christian Gram's new staining technique. Escherich originally named the common colon bacillus *Bacterium coli commune*. Castellani and Chalmers proposed the name *E. coli* in 1919, but it was not officially recognized until 1958.

References:

1. Oberbauer BA. Theodor Escherich—Leben und Werk. Munich: Futuramed-Verlag; 1992.
2. Shulman ST, Friedmann HC, Sims RH. Theodor Escherich: the first pediatric infectious diseases physician? Clin Infect Dis. 2007;45:1025–9 .

https://wwwnc.cdc.gov/eid/article/21/8/et-2108_article

SARS-CoV-2 Infection in School Settings, Okinawa Prefecture, Japan, 2021–2022

Yoshihiro Takayama, Yusuke Shimakawa, Ryota Matsuyama, Gerardo Chowell, Ryosuke Omori, Tetsuharu Nagamoto, Taro Yamamoto, Kenji Mizumoto

During the COVID-19 pandemic, widespread school closures were implemented globally based on the assumption that transmission among children in the school environment is common. However, evidence regarding secondary infection rates by school type and level of contact is lacking. Our study estimated the frequency of SARS-CoV-2 infection in school settings by examining the positivity rate according to school type and level of contact by using data from a large-scale school-based PCR project conducted in Okinawa, Japan, during 2021–2022. Our results indicate that, despite detection of numerous positive cases, the average number of secondary infections remained relatively low at ≈0.5 cases across all types of schools. Considering the profound effects of prolonged closures on educational access, balancing public health benefits against potential long-term effects on children is crucial.

During the COVID-19 pandemic, many countries implemented extensive school closures from nurseries to high schools to reduce infection transmission within schools and curb community spread. School closures have proven effective against highly transmissible diseases (*1*–*3*). Closures may target specific classrooms, grades, or entire schools when positive cases are confirmed, and, in some instances, regional closures are enacted to contain outbreaks or curb epidemic spread.

During school closures, the shift to online learning places new demands on both students and teachers, particularly those unfamiliar with digital teaching methods. In addition, the cost of acquiring necessary online learning devices falls on families, posing a financial barrier for some. The prolonged closures during the COVID-19 pandemic have resulted in substantial learning setbacks; students lost ≈1.5 school years by the end of 2021. This lapse has led to a concerning rise in learning poverty; 70% of 10-year-olds cannot read and comprehend simple stories, especially in East Asia, South Asia, the Middle East, and Latin America (*4*). Face-to-face learning not only maximizes educational opportunities but also plays a crucial role in preventing the exacerbation of poverty issues. Moreover, the closure of nurseries and elementary schools has substantial socioeconomic effects, frequently necessitating parental leave to care for children (*5*).

The rationale for school closures rests on the assumption of high child-to-child transmission within schools. Both schools and households, where persons gather in close proximity for extended periods, are identified as high-risk settings for transmission (*6*). Some studies have suggested that reducing classroom sizes or increasing the distance between student seats can effectively reduce transmission rates (*7*). However, large-scale research on the extent of COVID-19 transmission among students, who now exhibit increased hygiene awareness and mask usage compared with prepandemic times, remains limited. Moreover, detailed data on the actual number of secondary infections that occur when positive cases occur in schools are scarce.

Author affiliations: Okinawa Chubu Hospital, Uruma, Japan (Y. Takayama); Okinawa Prefecture Epidemiological Statistics and Analysis Committee, Naha-shi, Japan (Y. Takayama, Y. Shimakawa, R. Matusuyama, R. Omori, T. Nagamoto, K. Mizumoto); Institute of Tropical Medicine Department of International Health and Medical Anthropology, Nagasaki University, Nagasaki, Japan (Y. Takayama, T. Yamamoto); Institut Pasteur, Université Paris Cité, Paris, France (Y. Shimakawa); Pasteur International Unit at Kumamoto University/National Center for Global Health and Medicine, Tokyo, Japan (Y. Shimakawa) Rakuno Gakuen Univerisity, Ebetsu, Japan (R. Matsuyama); Georgia State University School of Public Health, Atlanta, Georgia, USA (G. Chowell); International Institute for Zoonosis Control, Hokkaido University, Sapporo, Japan (R. Omori); Kyoto University Graduate School of Advanced Integrated Studies in Human Survivability, Kyoto, Japan (K. Mizumoto)

DOI: https://doi.org/10.3201/eid3011.240638

Okinawa Prefecture in Japan implemented the prefecture-wide School PCR Project to mitigate infection spread. Under this initiative, if a child or student tested positive for SARS-CoV-2, all persons within the affected class were subject to reverse transcription PCR (RT-PCR) testing. Those tested were then required to remain home until they received negative results. Although previous studies have reported positivity rates among contacts (*8*,*9*), data on the number of secondary infections per school and the extent of testing, stratified by school types and contact levels, are lacking.

In this study, we sought to estimate the frequency of SARS-CoV-2 infection in school settings by examining positivity rates according to school type and contact level. The goal was to guide the optimal implementation of school closures, balancing public health concerns with the children's educational needs.

Methods

Study Setting

Okinawa Prefecture, situated at the southwestern tip of the Japan archipelago and isolated by sea, comprises 1.17% of Japan's population of 14.47 million. In Okinawa, the School PCR Project ran from May 2021 to September 2022. We initially targeted all the elementary schools (n = 268), junior high schools (n = 149), high schools (n = 67), special support schools (n = 22), and after-school children's clubs (n = 501). In September 2021, the scope was expanded to include all nurseries (n = 456) and kindergartens (n = 303) in Okinawa (*10*–*12*). We excluded vocational training schools (n = 3) because of their small number and classification challenges. Since March 24, 2022, no close contacts have been identified, and after June 2022, the project's focus was narrowed down to support schools, after-school children's clubs, and nurseries and kindergartens (*13*,*14*).

The after-school children's clubs serve elementary school students whose parents work late and whose grandparents live far away. Those clubs typically use vacant classrooms or children's halls in elementary schools. During school closures of elementary schools affected by COVID-19, the clubs accommodated students during daytime hours (*15*,*16*).

The School's PCR Project protocol (Figure 1) begins when the Prefectural COVID-19 Task Force is notified of a SARS-CoV-2 infection in a student. The

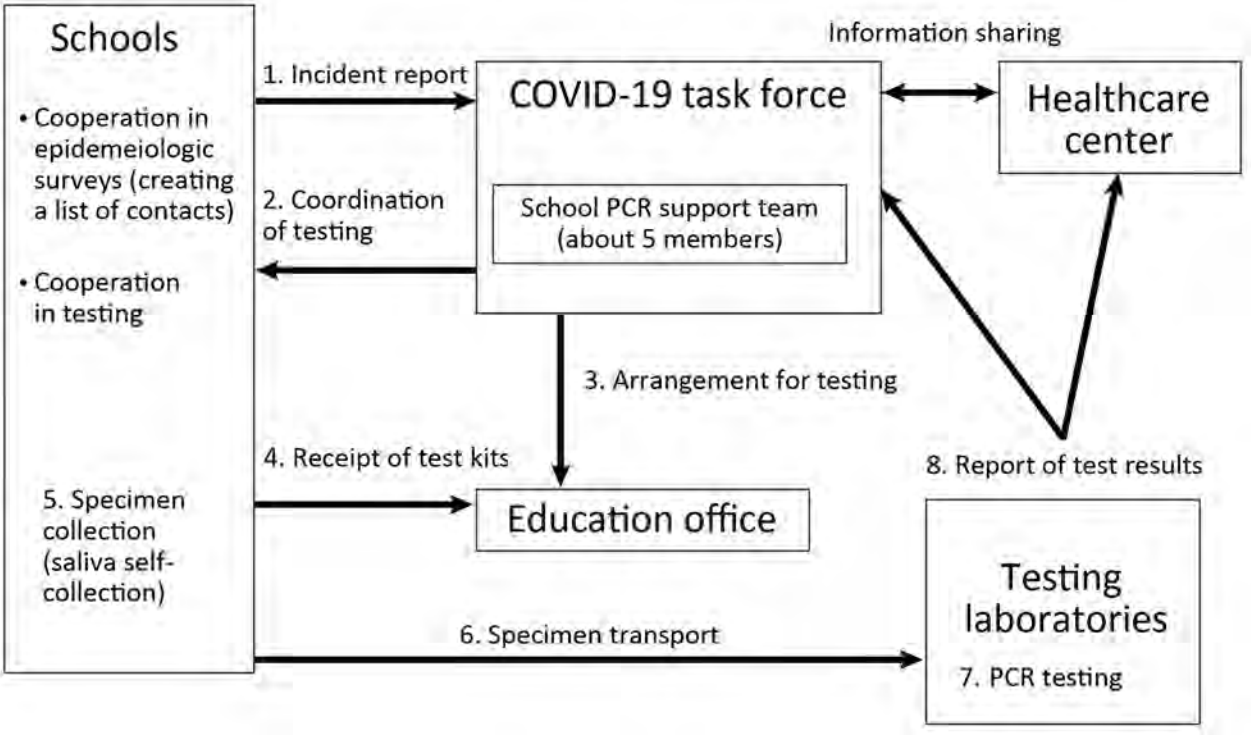

Figure 1. Overview of the SARS-CoV-2 PCR project conducted in school settings, Okinawa Prefecture, Japan, 2021–2022. The school's PCR Project protocol begins when the Prefectural COVID-19 Task Force is notified of a SARS-CoV-2 infection in a student. The prefectural school PCR support team will arrange for testing, with students providing saliva samples through self-collection of saliva. School officials receive test containers from the education office and transport the specimens to the testing laboratories. Contacts are generally all children or students in the class with a positive case, and close contacts are those within 1 meter from the index case-patient for ≥15 minutes without appropriate infection control measures.

prefectural school PCR support team will arrange for testing, and students provide saliva samples through self-collection of saliva. School officials receive test containers from the education office and transport the specimens to the testing laboratories. Contacts are generally all children or students in the class with a positive case, and close contacts are those who were within 1 meter of the index case-patient for ≥15 minutes without the appropriate infection control measures (*17*). Initially, contacts and close contacts were placed on home leave until test results were known (in the case of contacts) and for 7 days from the last exposure (in the case of close contacts). After March 24, 2022, no attendance suspension was required in elementary, junior high, and high schools for contacts. Close contacts remained in school if they were asymptomatic (*18*). Parental consent was obtained for the PCR tests (*17*); saliva testing was not invasive, and refusals from testing because of concerns about infection were rare. Samples were centrally tested at the following local laboratories using PCR: Anti Viral Screening System, Okinawa Institute of Science and Technology, SRL, Okinawa PCR Testing Center, Okinawa Prefecture Environmental Science Center, Okinawa Institute of Environmental Conservation, and Okinawa Clinical Laboratory Center.

During the study period, the predominant variants in Okinawa Prefecture shifted over time. The Alpha variant was dominant during May–June 2021, followed by the Delta variant during July 2021–November 2021, and then the Omicron variant from December 2021 onward (*19*).

Data Sources

The School PCR Project collected data on each event, including facility name, name of the index case-patient, date of birth, date of last contact between index case-patient and contacts, date of illness onset of index case-patient, lists of students who had contact with the index case-patient during the infectious period, and contact location (*16*). In this analysis, provided data included the date of illness onset of the index case-patient, type of school, health center with jurisdiction over that school, number of identified contacts with an index case-patient, and number of tested positives among contacts with information on the level of contacts from the Okinawa Prefecture government. We divided contacts into 2 groups by contact level: those in close contact (close contacts) and those in contact except for close contacts (non–close contacts) with the index case-patient.

Ethics Considerations

The School PCR project complied with Japan law and Okinawa Prefecture government policy. As part of the public health response to COVID-19, this study involved the secondary analysis of anonymized data provided by Okinawa Prefecture. The study was exempt from institutional review board review because no information in the dataset could directly or indirectly identify persons.

Statistical Analysis

This analysis defined the positivity rate as the proportion of contacts testing positive among those exposed to index case-patients. A negative binomial regression model with a log link identified factors associated with higher positivity rates among all contacts (close and non-close contacts) and close contacts. By setting the number of positive cases as a response variable and the number of tested students as an offset, we used the following school PCR project-related variables as explanatory variables: the type of school, health center with jurisdiction over that school, RT-PCR testing institute, and whether the PCR tests performed in the target school were the first implementation or subsequent implementations. We conducted multivariate analyses by using the explanatory variables, which showed a p value <0.20, as determined by the Wald test in the univariate analysis. We examined multicollinearity by using the variance inflation factor. We excluded variables exceeding the variance inflation factor value of 4.0 one by one from the multivariate analyses. We stratified data by whether they involved the school's first or subsequent RT-PCR test, reflecting increased infection control awareness after the initial outbreak. We performed all statistical analyses in R version 4.2.3 (The R Project for Statistical Computing, https://www.r-project.org).

Results

We calculated the number of events by school type and month (Figure 2, panel A; Appendix Table 1, https://wwwnc.cdc.gov/EID/article/30/11/24-0638-App1.pdf). The total number of events for the entire period was 6,736; of those, 1,311 (19.5%) occurred at elementary schools, 721 (10.7%) at junior high schools, 392 (5.8%) at high schools, 67 (1.0%) at special support schools, 830 (12.3%) at after-school children's clubs, and 3,415 (50.7%) at nurseries and kindergarten. Overall, the number of events increased dramatically after January 2022. Relative to the 2021 average, the increases in January 2022 were 108% for elementary schools, 161% for junior high schools, 54% for high schools, 271% for special support schools, 172% for

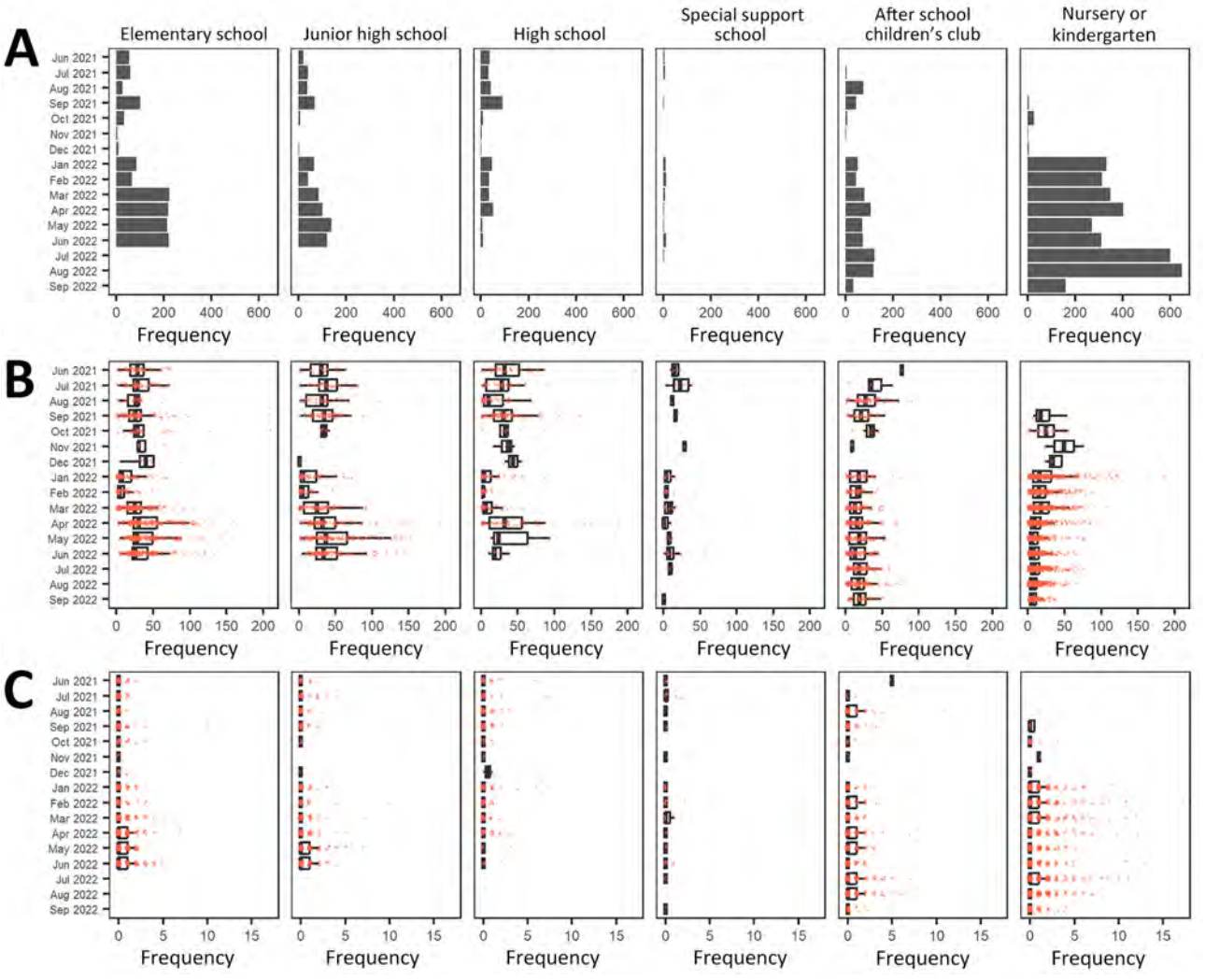

Figure 2. Results of SARS-CoV-2 PCR projects conducted in school settings, by month and school type, Okinawa Prefecture, Japan, 2021–2022. A) Number of events that results in school contact tracing, by month and school type. B) Number of PCR tests per event, by month stratified by school type. C) Number of secondary SARS-CoV-2 infection cases per event, by month and school type. Box-and-whisker plots indicate the median (solid black lines), the first and third quartiles (box left and right edges), and minimum and maximum values excluding outliers (error bars). Orange particles represent each observed datapoint.

after-school children's clubs, and 4,483% for nurseries and kindergarten.

We calculated the number of PCR tests per event by school type and month during June 2021–September 2022 (Figure 2, panel B; Appendix Table 1). In total, we identified 143,184 contacts, of whom 20,546 were classified as close contacts and all of whom underwent PCR tests. The median number of PCR tests per event was 15.0 (interquartile range [IQR] 6.0–29.0) for all tested schools for the entire period. By school type, the median number of PCR tests per event was 27.0 (IQR 19.0–40.0) for elementary schools, 31.0 (IQR 16.0–47.0) for junior high schools, 20.0 (IQR 4.0–37.0) for high schools, 8.0 (IQR 3.0–14.5) for special support schools, 18.0 (IQR 8.0–28.0) for after-school children's clubs, and 9.0 (IQR 4.0–18.0) for nurseries and kindergartens. With a few exceptions, the median number of PCR tests per event declined dramatically after January 2022. The relative reduction in medians from 2021 to 2022 was 76% in elementary schools, 83% in junior high schools, 86% in senior high schools, 78% in special support schools, 36% in after-school children's clubs, and 52% in nurseries and kindergartens.

We calculated the number of secondary infections per event by school type and month for June 2021–September 2022 (Figure 2, panel C; Appendix Table 1). Overall, the mean number of secondary infections per event was 0.43 (median 0, IQR 0–0) for all tested schools during the entire period. By school type, the mean number of secondary infections per

event was 0.34 (median 0, IQR 0–0) for elementary schools, 0.35 (median 0, IQR 0–0) for junior high schools, 0.28 (median 0, IQR 0–0) for high schools, 0.13 (median 0, IQR 0–0) for special support schools, 0.50 (median 0, IQR 0–1) for after-school children's clubs, and 0.49 (median 0, IQR 0–0) for nurseries and kindergartens. During January–February 2022, the mean number of secondary infections was much higher than the overall average for the period in 2021, having a relative increase of 47% in January 2022 and 104% in February 2022.

After we excluded the months when the number of events was small (<10 events/month/school type), the top 2 months with the highest average number of secondary infections per event were June 2022 (0.50) and April 2022 (0.45) for elementary schools, February 2022 (0.50) and May 2022 (0.58) for junior high schools, January 2022 (0.53) and April 2022 (0.40) for high schools, February 2022 (0.17) and June 2022 (0.17) for special support schools, February 2022 (0.68) and March 2022 (0.71) for nurseries and kindergartens, and July 2022 (0.67) and August 2022 (0.75) for after-school children's clubs. By school type, the widest monthly range of secondary infections for elementary school was 0–10 in September 2021; for junior high schools, 0–10 in February 2022; for high schools, 0–7 in July 2021; for special support schools, 0–2 in July 2021 and February 2022; for after-school children's clubs, 0–11 in August 2021; and for nurseries and kindergartens, 0–17 in February 2022.

We stratified positive rates among contacts by school type by the level of contacts (Figure 3; Appendix Table 2). Positivity rates among all contacts were 2.04% (95% CI 1.96%–2.11%) (2,914/143,184), among close contacts were 3.06% (95% CI 2.83%–3.31%) (629/20,546), and among non–close contacts were 1.86% (95% CI 1.79%–1.94%) (2,285/122,638). Among all contacts, the top 2 highest positivity rates were 3.44% (95% CI 3.28%–3.60%) (1,676/48,472) in nurseries and kindergartens and 2.51% (95% CI 2.27%–2.76%) (416/16,592) in after-school children's clubs, whereas this rate was ≈1.0% in other school types. Mean positivity rates among close contacts in all school types ranged from 2.0 to 3.5, with no significant differences. Among non–close contacts, the top 2 highest positivity rates were 3.50% (95% CI 3.31%–3.70%) (1,205/34,421) in nurseries and kindergartens and 2.48% (95% CI 2.24%–2.74%) (381/15,362) in after-school children's clubs, and the lowest positivity rate was 0.31% (95% CI 0.04–1.13) (2/637) in special support schools.

Regarding the proportion of the positives in close contacts among the positives in all contacts (Appendix Table 3), nurseries and kindergartens and high schools had the highest values: 74.6% (95% CI 71.0%–78.03%) for nurseries and kindergartens and 41.7% (95% CI 31.0%–52.9%) for high schools, excluding special support schools because of data scarcity. This proportion maintained relatively high values after January 2022.

We calculated the result from the regression analysis of positivity rates among all contacts on the basis of various factors (Appendix Tables 4, 5). Compared with elementary school, positivity rates were significantly lower in high school (relative risk [RR] 0.61, 95% CI 0.46–0.81; p<0.001) and special support school (RR 0.59, 95% CI 0.43–0.80; p<0.01) and significantly higher in after-school children's club (RR 1.34, 95% CI 1.05–1.72; p = 0.02), after adjusting for the first event, school type, area, and period. Compared with PCR tests in October 2021, PCR tests conducted starting in January 2022 were associated with significant increases in positivity rates: a 155% (95% CI 39%–382%) increase in January 2022, a 339% (95% CI 140%–728% [significant]) increase in February 2022, a 242% (95% CI 89%–537%) increase in March 2022, a 231% (95% CI 83%–516%) increase in April 2022, a 215% (95% CI 73%–491%) increase in May 2022, and a 237% (95% CI 86%–532%) increase in June 2022.

We calculated the results from the regression analysis of positivity rates among close contacts as a function of the variables (Appendix Tables 6, 7). Compared with October 2021, the positivity rates of PCR tests were significantly higher for January 2022 (RR 2.66, 95% CI 1.06–7.08; p = 0.04), February 2022 (RR 5.42, 95% CI 2.17–14.38), March 2022 (RR 4.41, 95% CI 1.77–11.66), and April 2022 (RR 3.40, 95% CI 0.89–13.49) after adjusting for the first event, school type, area, and period.

Discussion

This study assessed the effectiveness of screening tests in school PCR projects conducted in Okinawa Prefecture, Japan, during May 2021–September 2022. After January 2022, coinciding with the prevalence of the more infectious Omicron variant (*15*), the average number of secondary infections was almost the same or increased in all school types yet remained well below 1. Our findings suggest that, in schools where appropriate infection-control measures were in place, the risk for secondary infection was not necessarily high, and the actual status of infection in school settings should be considered when implementing school closures. In addition to households, schools have been cited as a major route of infection for children, and measures such as class closures and school closures have been deployed when even a limited number

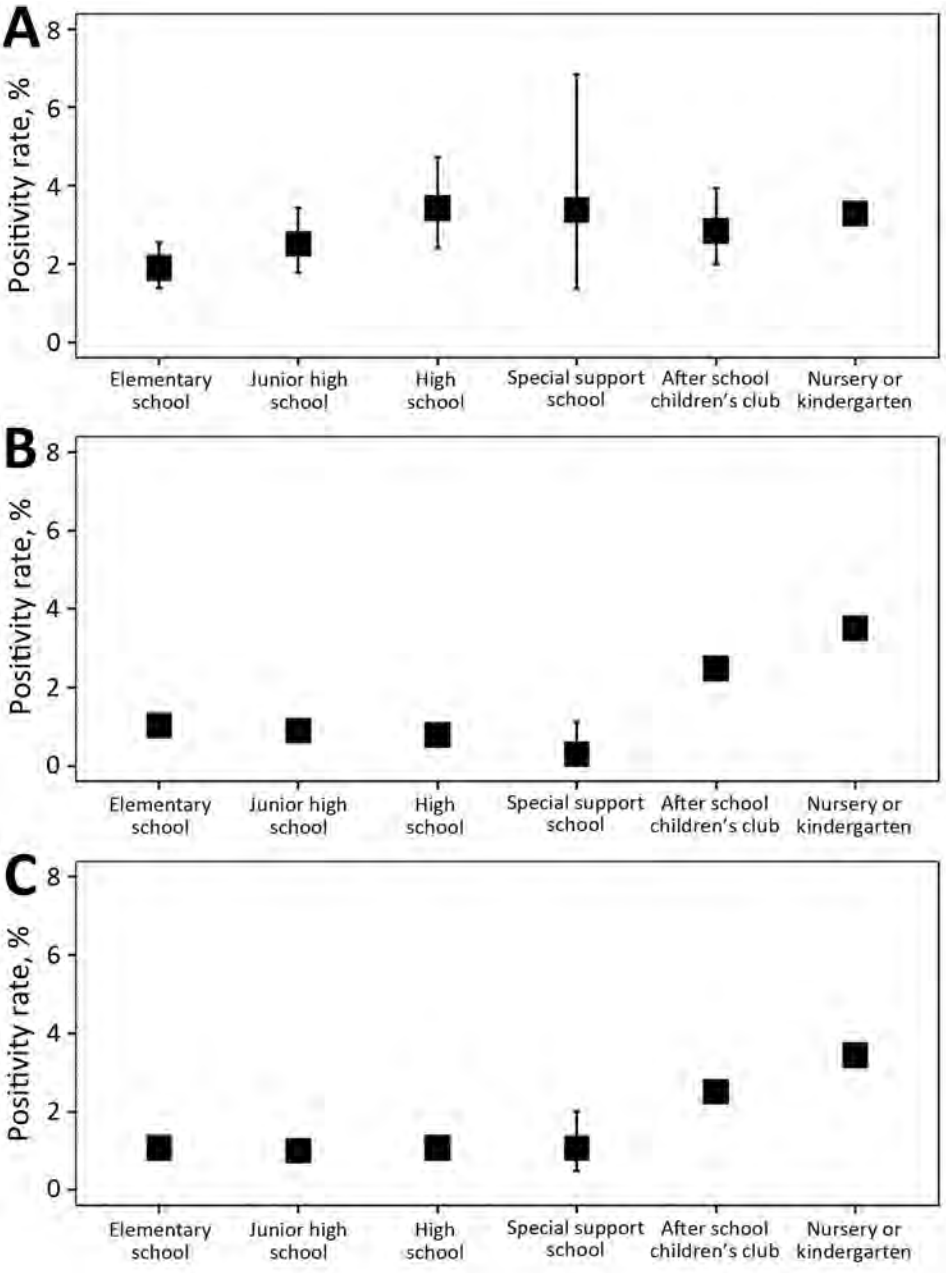

Figure 3. SARS-CoV-2 positivity rates in school settings among close contacts (A), non–close contacts (B), and all contacts (C) of infected children, by school type, Okinawa Prefecture, Japan, 2021–2022. In all panels, boxes indicate mean positivity rate and error bars indicate 95% CIs.

of positive cases were confirmed. In Japan, after the spread of the novel coronavirus, handwashing and hand sanitizing have been routinely encouraged, and wearing masks for elementary school students and older essentially became mandatory. Furthermore, during the study period, mokushoku ("silent eating") was recommended by the government, and students were prohibited from talking during lunch meals (*20*,*21*). This analysis shows that schools with appropriate infection-control measures are not always at high risk. Field epidemiologic investigations corroborate this low infection risk at schools, indicating that the transmission route constitutes only 4% of elementary schools, 6% of junior high schools, and 4% of high schools (*22*). In addition, students identified as close contacts with the infected person are required to stay at home for 7 days from the date of the last contact with the infected person (*23*). Given those findings, alternatives to canceling classes might include allowing only close contacts to stay home or requiring testing for all contacts, requiring only those testing positive to quarantine. Such approaches could also be considered for managing other infectious diseases, such as influenza.

During the study period, secondary infection risks were significantly higher at nurseries and kindergartens and after-school children's clubs. In nurseries and kindergartens, factors such as inappropriate masking and physical proximity because of younger ages probably contributed to increased risk. Despite overlapping age groups with elementary schools, after-school clubs showed significantly higher infection risks, suggesting factors unique to these settings (e.g., smaller spaces per child and higher population density when nonregular attendees join) exacerbate transmission risks. Moreover, during school closures, many younger elementary students, particularly from households with essential workers or dual-income parents unable to take leave, are sent to these clubs (*15*,*16*). Many after-school clubs in Okinawa Prefecture are privately operated and involve low usage of public facilities such as school spaces (*24*). Activities common in clubs, such as communal meal preparation, may also increase contact intensity and infection risk. Although the clubs are crucial for supporting working parents and are integral to social infrastructure, the challenges of enforcing strict infection controls in such environments suggest that flexible, rather than restrictive, measures are preferable during outbreaks.

Given that secondary infection risks vary by school type and level of contact, differences should be carefully considered when narrowing down the target population, especially under budget constraints. Depending on the type of school, the importance of RT-PCR testing for non–close contacts may need to be enhanced. Although nurseries and kindergartens and after-school children's clubs consistently showed high risks for all contacts and non–close contacts, we observed no significant differences among close contacts across school types. Of note, in after-school children's clubs, the positivity rate for non–close contacts occasionally exceeded that for close contacts. Furthermore, the absolute number of test-positive cases among non–close contacts was higher than among close contacts.

The multivariate analysis results, which showed that both the close contact and all contacts positivity rates were significantly higher after January 2022 compared with October 2021, are consistent with the higher infectivity of the Delta variant. We reconfirmed that the positivity rate for all contacts was significantly higher in after-school children's clubs than in elementary schools. The significantly lower positive rates in high and special-needs schools may be because of the students and their guardians' higher awareness of infection-control measures.

The relatively high percentage of positive test results among close contacts over all positive results after January 2022 is because of the effect of numerous reported cases of infection attributable to the outbreak of the contagious Omicron strain (Figure 2, panel A). This development led to a restriction on the number of tests performed on non–close contacts.

One limitation of our study is that the average number of secondary infections is well below 1.0. However, false negatives might have occurred, considering that the test was performed only once and the RT-PCR test has relatively low sensitivity using saliva specimens (*25*). Nevertheless, although an alternative, nasal swab tests also present disadvantages; of note, false-negative results may be more common in children because of the difficulty in obtaining adequate specimens (*26*). Second, because of the prolonged COVID-19 epidemic, unofficial reports indicated that some junior and high school students did not stay home but instead chose to socialize with friends during school closure periods. In addition, cases of infection might have occurred not in the classroom but in extracurricular activities involving physical contact. However, our analysis does not reflect these cases because of the lack of data. In addition, secondary infections include cases contracted outside of school, which is influenced by changes in local community prevalence. The secondary infection rate we report represents the maximum value, encompassing infections acquired outside school. The estimated value would probably be even lower if external cases were excluded. Furthermore, Japan's commuting and class systems differ from those in other countries, potentially affecting the generalizability of these findings. In Japan, students typically walk or ride bicycles to school instead of using school buses, and teachers, rather than students, move between classrooms because of the home-class system (*27*). Moreover, students eat lunch in their home classroom with their teachers, rather than in a cafeteria, as is common in the United States (*28*).

In summary, our analysis indicates that, during the 2021–2022 period of the COVID-19 pandemic, many positive cases were reported in school settings among students, with varying risks of infection by school type and the level of contact. However, the average number of secondary infections was generally low, limited to ≈0.5 cases across all school types. Remarkably, no large-scale child-to-child transmission occurred, a prerequisite for school closure. Because prolonged school closure deprives students of educational opportunities and leads to education poverty issues, it is worth reconsidering the target population

and the measures to be taken. In addition, national and local governments could consider enhancing control measures in after-school children's clubs to improve safety.

Acknowledgments

The authors appreciate the following institutions for their contribution to support this study: Okinawa Prefecture; Sanitary and Environmental Research Institute in Okinawa Prefecture; and public health centers, public health institutes, and medical facilities in Okinawa Prefecture.

K.M. acknowledges support from the Japan Society for the Promotion of Science (grant nos. 20H03940 and 20KK0367) and the Strategic International Collaborative Research Program of the Japan Science and Technology Agency (grant no. JPMJSC21U4). R.O. acknowledges support from the Japan Science and Technology Agency (grant nos. JPMJCR20H1 and JPMJSC21U4).

About the Author

Dr. Takayama is deputy director of the Department of Infectious Diseases and Community Care at Okinawa Prefectural Chubu Hospital. His primary research interests include infectious disease epidemiology, infection control, and community medicine.

References

1. Cauchemez S, Ferguson NM, Wachtel C, Tegnell A, Saour G, Duncan B, et al. Closure of schools during an influenza pandemic. Lancet Infect Dis. 2009;9:473–81. https://doi.org/10.1016/S1473-3099(09)70176-8
2. Cauchemez S, Valleron AJ, Boëlle PY, Flahault A, Ferguson NM. Estimating the impact of school closure on influenza transmission from sentinel data. Nature. 2008;452:750–4. https://doi.org/10.1038/nature06732
3. Jackson C, Vynnycky E, Hawker J, Olowokure B, Mangtani P. School closures and influenza: systematic review of epidemiological studies. BMJ Open. 2013; 3:e002149. https://doi.org/10.1136/bmjopen-2012-002149
4. Indermit Gill JS. We are losing a generation: the devastating impacts of COVID-19. 2022 Feb 1 [cited 2023 Aug 5]. https://blogs.worldbank.org/voices/we-are-losing-generation-devastating-impacts-covid-19
5. Mizumoto K, Yamamoto T, Nishiura H. Contact behaviour of children and parental employment behaviour during school closures against the pandemic influenza A (H1N1-2009) in Japan. J Int Med Res. 2013;41:716–24. https://doi.org/10.1177/0300060513478061
6. Cowling BJ, Lau MS, Ho LM, Chuang SK, Tsang T, Liu SH, et al. The effective reproduction number of pandemic influenza: prospective estimation. Epidemiology. 2010; 21:842–6. https://doi.org/10.1097/EDE.0b013e3181f20977
7. van den Berg P, Schechter-Perkins EM, Jack RS, Epshtein I, Nelson R, Oster E, et al. Effectiveness of 3 versus 6 ft of physical distancing for controlling spread of coronavirus disease 2019 among primary and secondary students and staff: a retrospective, statewide cohort study. Clin Infect Dis. 2021;73:1871–8. https://doi.org/10.1093/cid/ciab230
8. Hershow RB, Wu K, Lewis NM, Milne AT, Currie D, Smith AR, et al. Low SARS-CoV-2 transmission in elementary schools—Salt Lake County, Utah, December 3, 2020–January 31, 2021. MMWR Morb Mortal Wkly Rep. 2021;70:442–8. https://doi.org/10.15585/mmwr.mm7012e3
9. Dawson, Worrell MC, Malone S, Tinker SC, Fritz S, Maricque B, et al. Pilot investigation of SARS-CoV-2 secondary transmission in kindergarten through grade 12 schools implementing mitigation strategies—St. Louis County and City of Springfield, Missouri, December 2020. MMWR Morb Mortal Wkly Rep. 2021;70:449–55.
10. Okinawa Prefectural Board of Education. School list, Okinawa, Japan [in Japanese] [cited 2022 Aug 6]. https://www.pref.okinawa.jp/edu/edu/sagasu/index.html
11. Okinawa Prefectural Government, Children's Welfare Department. Digest version of survey of after-school children's clubs in Okinawa Prefecture in fiscal year 2020, Japan [in Japanese] [cited 2023 Aug 1]. https://www.okinawa gakudou.com/_files/ugd/b16a48_894b809302194b80918cb2 7939f3798a.pdf
12. The 125th Meeting of the Okinawa Prefectural COVID-19 Task Force, Sep 28, 2022, Okinawa Prefecture, Japan [in Japanese] [cited 2024 May 4]. https://www.pref.okinawa.jp/_res/projects/default_project/_page_/001/023/403/125siryo.pdf
13. The 165th Meeting of the Okinawa Prefectural COVID-19 Task Force, June 9, 2022, Okinawa Prefecture, Japan [in Japanese] [cited 2024 May 4]. https://www.pref.okinawa.lg.jp/_res/projects/default_project/_page_/001/023/402/165gijigaiyou.pdf
14. The 155th Meeting of the Okinawa Prefectural COVID-19 Task Force, March 24, 2022, Okinawa Prefecture, Japan [in Japanese] [cited 2024 May 4]. https://www.pref.okinawa.lg.jp/_res/projects/default_project/_page_/001/023/402/155-2.pdf
15. Okinawa Times. After-school children's clubs, which took on the role of accepting children after the school was closed during COVID-19 pandemic. Staff members are exhausted and face a shortage of funds. 2020 May 29 [in Japanese] [cited 2024 May 4]. https://www.okinawatimes.co.jp/articles/-/577266
16. Okinawa Prefecture After-School Childcare Management Support Association. COVID-19 countermeasures. Opening during elementary school closures, Wakuwaku and Maeda after-school children's club, March 2, 2020 [in Japanese] [cited 2024 May 4]. https://www.gakusapo.okinawa/entry_top_news.php?eid=53548
17. Okinawa Prefectural Government. Frequently asked questions. Okinawa Prefecture school and nursery PCR testing application site [in Japanese] [cited 2024 May 4]. https://mitsuwa.rdy.jp/mgc/wp-content/uploads/2022/03/%E3%82%88%E3%81%8F%E3%81%82%E3%82%8B%E8%B3%AA%E5%95%8F%EF%BD%9C%E6%B2%96%E7%B8%84%E7%9C%8C%E5%AD%A6%E6%A0%A1%E3%83%BB%E4%BF%9D%E8%82%B2PCR%E6%A4%9C%E6%9F%BB%E7%94%B3%E8%AB%8B%E3%82%B5%E3%82%A4%E3%83%88.pdf
18. Naha City Board of Education. Notice: attendance of students, teachers and staff at the reopening of Okinawa Prefecture school and daycare PCR tests. 2022 Mar 3 [in Japanese] [cited 2024 May 4]. https://www.city.naha.okinawa.jp/child/education/kyouikugakukyou/pcr.files/pcr.pdf
19. Okinawa Prefectural Government. Trends in proportion of SARS-CoV-2 variants [in Japanese] [cited 2024 Sep 3].

https://www.pref.okinawa.lg.jp/_res/projects/default_project/_page_/001/018/248/030318.pdf
20. Takahashi R, Igei K, Tsugawa Y, Nakamuro M. The effect of silent eating during school lunchtime on COVID-19 outbreaks. Soc Sci Med. 2024;348:116852. https://doi.org/10.1016/j.socscimed.2024.116852
21. Novel Coronavirus Response Headquarters. Basic policy on countermeasures against new coronavirus infections [in Japanese] [cited 2024 Sep 3]. https://www.kantei.go.jp/jp/singi/novel_coronavirus/th_siryou/kihon_r2_040908.pdf
22. Okinawa Prefecture Epidemiology and Statistical Analysis Committee. Outbreak surveillance report of COVID-19 in Okinawa. Japan: Okinawa Prefecture, March 1, 2022 [in Japanese] [cited 2024 Apr 30]. https://www.pref.okinawa.lg.jp/_res/projects/default_project/_page_/001/018/406/hp220301.pdf
23. Ministry of Health, Labour and Welfare, Japan, Headquarters for the Promotion of Countermeasures to Combat COVID-19. Notice: response to a confirmed outbreak of COVID-19 [in Japanese]. 2022 Jan 5 [cited 2024 Apr 30]. https://www.mhlw.go.jp/content/10900000/000895943.pdf
24. Okinawa Prefectural Government. After-school child health and development project [in Japanese]. [cited 2024 Apr 30]. https://www.pref.okinawa.jp/site/kodomo/kosodate/15846.html
25. White D, Gu J, Steinberg CJ, Yamamura D, Salena BJ, Balion C, et al. Investigation of discordant SARS-CoV-2 RT-PCR results using minimally processed saliva. Sci Rep. 2022;12:2806. https://doi.org/10.1038/s41598-022-06642-5
26. Waggoner JJ, Vos MB, Tyburski EA, Nguyen PV, Ingersoll JM, Miller C, et al. Concordance of SARS-CoV-2 results in self-collected nasal swabs vs swabs collected by health care workers in children and adolescents. JAMA. 2022;328:935–40. https://doi.org/10.1001/jama.2022.14877
27. Johnson ML, Johnson JR. Daily life in Japanese high schools. Stanford Program on International and Cross-Cultural Education. 1996 Oct [cited 2024 Sep 5]. https://spice.fsi.stanford.edu/docs/daily_life_in_japanese_high_schools
28. Japan National Tourism Organization. Lunch in Japanese schools. 2022 Jan 24 [cited 2024 Sep 5]. https://education.jnto.go.jp/en/school-in-japan/school-life-in-japan/lunch-in-japanese-schools

Address for correspondence: Kenji Mizumoto, Graduate School of Advanced Integrated Studies in Human Survivability, Kyoto University, Yoshida-Naka Adachi-cho, Sakyo-ku, Kyoto 606-8306, Japan; mizumoto.kenji.5a@kyoto-u.ac.jp

etymologia revisited

Originally published in June 2019

Neospora caninum

[ne-os′ pə-rə ca-nin′ um]

From the *neo-* (Latin, "new") + *spora* (Greek, "seed") and *canis* (Latin, "dog"), *Neospora caninum* is a sporozoan parasite that was first described in 1984. It is a major pathogen of cattle and dogs but can also infect horses, goats, sheep, and deer. Antibodies to *N. caninum* have been found in humans, predominantly in those with HIV infection, although the role of this parasite in causing or exacerbating illness is unclear.

References:

1. Bjerkås I, Mohn SF, Presthus J. Unidentified cyst-forming sporozoon causing encephalomyelitis and myositis in dogs. Z Parasitenkd. 1984;70:271–4. http://dx.doi.org/10.1007/BF00942230
2. Dubey JP. Review of *Neospora caninum* and neosporosis in animals. Korean J Parasitol. 2003; 41:1–16. http://dx.doi.org/10.3347/kjp.2003.41.1.1
3. Lobato J, Silva DA, Mineo TW, Amaral JD, Segundo GR, Costa-Cruz JM, et al. Detection of immunoglobulin G antibodies to *Neospora caninum* in humans: high seropositivity rates in patients who are infected by human immunodeficiency virus or have neurological disorders. Clin Vaccine Immunol. 2006;13:84–9. http://dx.doi.org/10.1128/CVI.13.1.84-89.2006

https://wwwnc.cdc.gov/eid/article/25/6/et-2506_article

Quantitative SARS-CoV-2 Spike Receptor-Binding Domain and Neutralizing Antibody Titers in Previously Infected Persons, United States, January 2021–February 2022

Anna Bratcher, Szu-Yu Kao, Kelly Chun, Christos J. Petropoulos, Adi V. Gundlapalli, Jefferson Jones,[1] Kristie E.N. Clarke[1]

We studied SARS-CoV-2 binding and neutralizing antibody titers among previously infected persons in the United States over time. We assayed SARS-CoV-2 spike protein receptor-binding domain and neutralizing antibody titers for a convenience sample of residual clinical serum specimens that had evidence of prior SARS-CoV-2 infection gathered during January 2021–February 2022. We correlated titers and examined them by age group (<18, 18–49, 50–64, and ≥65 years) across 4 different SARS-CoV-2 variant epochs. Among selected specimens, 30,967 had binding antibody titers and 744 had neutralizing titers available. Titers in specimens from children and adults correlated. In addition, mean binding antibody titers increased over time for all age groups, and mean neutralization titers increased over time for persons 16–49 and ≥65 years of age. Incorporating binding and neutralization antibody titers into infectious disease surveillance could provide a clearer picture of overall immunity and help target vaccination campaigns.

Since its emergence in late 2019, SARS-CoV-2 has posed a substantial challenge to public health surveillance worldwide. Seroprevalence, the proportion of a population that has detectable SARS-CoV-2 antibodies, has commonly been used to estimate population-level infection and vaccination history across geographic regions (*1*–*4*). However, seroprevalence studies only describe the presence or absence of antibodies. In addition, those studies generally refer only to binding antibodies, or antibodies that can recognize and attach to an antigen. However, binding antibody analyses neglect to describe the ability of antibodies to neutralize a pathogen, which is measured by neutralizing antibody titers. Therefore, additional information is needed when studying populations in which nearly all persons have detectible antibodies.

Binding and neutralizing antibody titers can be heterogeneous after SARS-CoV-2 infection or vaccination (*5*–*7*). Thus, those titers can be particularly valuable measures of protective immunity among populations where nearly all persons have detectible antibodies (*8*). In addition, the ability of those titers to detect heterogeneity in serologic status within fully seropositive populations, including changes in antibody levels over time, enables epidemiologists to provide a more nuanced description of serostatus for those populations. Furthermore, those antibody titers can clarify a population's continued risk because evidence shows that higher binding and neutralizing antibody titers are associated with lower probability of infection, re-infection, and severe disease (*9*–*11*; J.A.

Author affiliations: Epidemic Intelligence Service, Centers for Disease Control and Prevention, Atlanta, Georgia, USA (A. Bratcher); Alan Shawn Feinstein College of Education, University of Rhode Island, Kingston, Rhode Island, USA (S.-Y. Kao); Labcorp Esoterix, Calabasas, California, USA (K. Chun); Labcorp-Monogram Biosciences, South San Francisco, California, USA (C.J. Petropoulos); Centers for Disease Control and Prevention, Atlanta (A.V. Gundlapalli, J. Jones, K.E.N. Clarke)

DOI: https://doi.org/10.3201/eid3011.240043

[1]These co-senior authors contributed equally to this article.

Cohen et al., unpub. data, https://doi.org/10.1101/2021.05.31.21258018). Moreover, understanding the correlation between the 2 measures can inform clinical practice. Strong evidence that neutralizing antibody titers are a correlate of protection is available, but acceptance of binding antibodies as a correlate of protection is less prevalent (*12*). Limited evidence is available on the correlation of binding and neutralizing antibody levels, particularly among a large, nationwide population spanning all age groups.

Measuring binding and neutralizing antibody titers after SARS-CoV-2 infection and vaccination also can enable the study of differences across key demographics. Using those measures, epidemiologists can statistically test antibody titers across characteristics such as age and sex that are likely to be associated with differences in immune response and severity of SARS-CoV-2 outcomes (*13*). In addition to enabling the study of risk factors, titers can help examine the immunogenicity of vaccination, booster vaccines, and reinfection (*14*,*15*), as well as the effects of waning antibodies over time (*16*). Measuring binding and neutralizing antibody titers can improve understanding of the course of the SARS-CoV-2 pandemic. As correlates of protection, those measures can be indicative of future transmission levels and risks for severe disease. To supplement understanding of seroprevalence over the COVID-19 pandemic, we studied binding and neutralizing antibody titers among previously infected persons in the United States during January 2021–February 2022.

Methods

Study Design and Sample

A convenience sample of residual clinical serum specimens were collected as part of the Nationwide Commercial Laboratory Seroprevalence Survey (NCLS; https://data.cdc.gov/Laboratory-Surveillance/Nationwide-Commercial-Laboratory-Seroprevalence-Su/d2tw-32xv/about_data). NCLS is a repeated, cross-sectional survey conducted by the Centers for Disease Control and Prevention (CDC) and designed to monitor national seroprevalence of infection-induced antibodies to SARS-CoV-2. Detailed methods are discussed elsewhere (*17*). In brief, we collected data from specimens submitted for clinical testing across 50 US states, the District of Columbia, and Puerto Rico. To minimize selection bias, we excluded specimens for which SARS-CoV-2 antibody testing was ordered by the clinician. Specimen information included data on patient age, patient sex, jurisdiction, and date of blood collection.

For this analysis, we included specimens gathered during January 2021–February 2022 that had antibodies against the nucleocapsid protein (anti-N). Anti-N are produced in response to infection but are not produced in response to the COVID-19 vaccines authorized for use in the United States at the time of data collection. Anti-N were detected by using the Elecsys Anti-SARS-CoV-2 assay (Roche Diagnostics, https://diagnostics.roche.com), which has a sensitivity of 100% and specificity of 99.8% for the N protein (*18*). When testing with this assay, anti-N positivity remains high over a substantial follow-up period; >94% of persons retain a positive value 10 months after infection (*19*,*20*). Thus, we assumed anti-N positivity to be evidence of any prior infection, not just recent infections.

Among specimens with anti-N, we selected a subset for further testing with a quantitative assay that determines the spike protein receptor-binding domain IgG (anti-RBD) level. That subset was selected because samples were received until either a target number for each patient age category and state of residence was reached or the data collection period concluded. Among specimens tested for quantitative anti-RBD titers, we tested a random subset of collected specimens for neutralizing antibodies within each age category. We determined subset size according to available resources.

Quantitative Anti-RBD Assay

We used the electrochemiluminescent Cov2Quant IgG assay (LabCorp, https://www.labcorp.com) to quantify anti-RBD IgG in serum samples (*21*). We calculated the anti-RBD concentration of each serum sample by using a dilution series of affinity-purified human IgG standard and calibrated results with the World Health Organization international standard (international reference standard conversion factor for wild-type spike protein D614G mutation 50% infectious dose is 20/136) to convert results into binding antibody units (BAU) per milliliter. The threshold for anti-RBD positivity is 17.8 BAU/mL (sensitivity, 99.4% [95% CI 96.6%–99.9%]; specificity, 98.4% [95% CI 98.4%–99.6%]). For samples that returned a value <1.0, the lower quantitation limit of the assay, we used 1.0 as the value for quantitative results to enable statistic calculations on the logarithmic scale. Full methods are discussed elsewhere (*11*,*21*).

Neutralizing Antibody Assay

We used the PhenoSense SARS-CoV-2 Neutralizing Antibody Assay (Mongram Biosciences, https://monogrambio.labcorp.com) (*22*,*23*) to measure

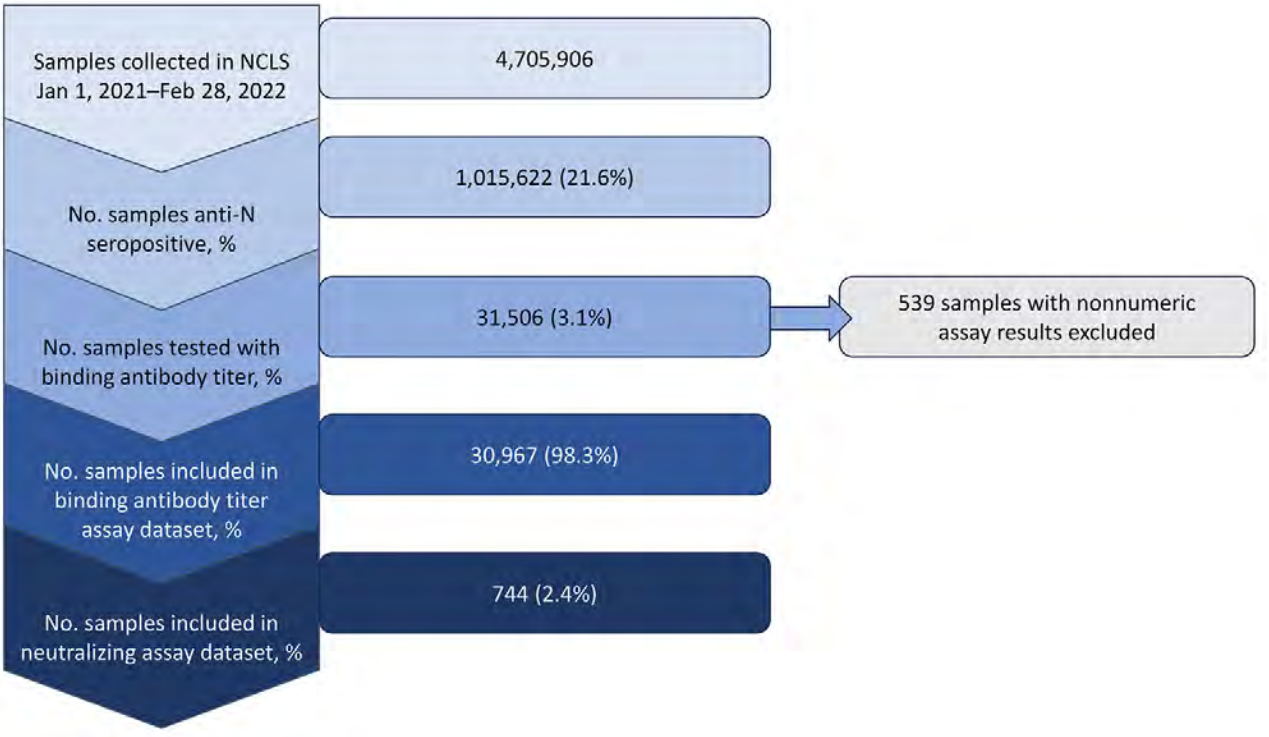

Figure 1. Flowchart of sample selection in study of quantitative SARS-CoV-2 spike receptor-binding domain and neutralizing antibody titers in previously infected persons, United States, January 2021–February 2022. Nonnumeric results are quantitative receptor-binding domain assays with invalid results due to insufficient serum volume, lost sample, or poor reproducibility. NCLS, Nationwide Commercial Laboratory Seroprevalence Survey.

neutralizing antibodies against the wild-type SARS-CoV-2 spike protein (GenBank accession no. MN908947.3). We recorded the 50% neutralization titer (NT_{50}) as the reciprocal of the serum dilution conferring 50% inhibition of pseudovirus infection, with an upper limit of detection of 787,320 IU/mL. Full methods are discussed elsewhere (*10*,*23*).

Statistical Analysis

We recorded counts and percents across covariates for anti-N seropositive samples, those with binding antibody titer results, and those with both binding and neutralizing antibody titer results. We compared distribution of age, sex, and metro status (i.e., living in a metropolitan statistical area or nonmetro area)

Table. Characteristics of subjects in a study of quantitative SARS-CoV-2 spike receptor-binding domain and neutralizing antibody titers in previously infected persons, United States, January 2021–February 2022*

Characteristics	% Total US population, 2021	Anti-N seropositive,† n = 1,015,622	Binding antibody titer available, n = 30,967	Neutralizing and binding antibody titers available, n = 744
Sex				
M	49.6	4.2 (41.3)	13,146 (42.5)	317 (42.6)
F	50.3	5.9 (58.1)	17,821 (57.5)	427 (57.4)
Age group, y				
<18	21.9	2.4 (23.6)	8,089 (26.1)	231 (31.0)
18–49	42.0	3.5 (34.5)	8,127 (26.2)	133 (17.8)
50–64	19.1	2.4 (23.6)	7,224 (23.3)	153 (20.5)
≥65	16.9	1.8 (17.7)	7,527 (24.3)	227 (30.5)
Residence				
Nonmetro	13.8	1.7 (16.7)	5,767 (18.6)	136 (18.3)
Metro	86.2	8.4 (82.7)	25,200 (81.4)	608 (81.7)
Variant epoch				
Wild-type		2.5 (24.6)	9,049 (29.2)	202 (27.2)
Alpha		3.1 (30.5)	6,868 (22.2)	75 (10.1)
Delta		3.7 (36.4)	10,808 (34.9)	361 (48.5)
Omicron		0.9 (8.9)	4,242 (13.7)	106 (14.2)

*Values are no. (%) except as indicated. Population data are from the US Census Bureau (https://www.census.gov). Anti-N, nucleocapsid antibody.
†Values are no. × 10^5 (%).

among patient specimens with US Census Bureau estimates of the total US population in 2021 (*24*). We calculated Pearson correlation coefficients between $\log_{10}$-transformed quantitative binding and neutralizing antibody assay results stratified by age: children 0–17 years of age and adults ≥18 years of age. Then, we stratified binding and neutralization titers by sex assigned at birth (male or female) and age group (<18, 18–49, 50–64, or ≥65 years). We used a *t*-test on $\log_{10}$-transformed data to statistically compare mean titer by sex and a simple linear regression to examine whether slope, indicated by β, was nonzero across age groups. We conducted further analyses to compare binding and neutralizing titers by age group and 4 epochs of the pandemic, delineated by which SARS-CoV-2 variant was responsible for >50% of US cases: wild-type during January 1–March 27, 2021; Alpha during March 28–June 25, 2021; Delta during June 26–December 17, 2021; and Omicron BA 1.1 during December 8, 2021–February 28, 2022 (*25*). We performed 4 simple linear regressions for each assay result, 1 for each age group, to statistically described that trend. We then compared trends in binding antibody titer, neutralizing antibody titer, and national vaccination rates as recorded by CDC (*26*), for each age group over time.

We performed all statistical analyses in R version 4.1.2 (The R Project for Statistical Computing, https://www.r-project.org). We considered $p<0.05$ statistically significant and did not correct for multiple comparisons.

Ethics Statement

This activity was reviewed by CDC and conducted consistent with applicable federal law and CDC policy (45 C.F.R. part 46, 21 C.F.R. part 56; 42 U.S.C. Sect. 241(d); 5 U.S.C. Sect. 552a; 44 U.S.C. Sect. 3501 et seq.). CDC determined that this project was public health surveillance and not research. Thus, approval by an institutional review board was waived. Informed consent was also waived because all data were deidentified.

Results

During January 1, 2021–February 28, 2022, the NCLS study collected 4,705,906 serum specimens, of which 1,015,622 (21.6%) were anti-N seropositive (Figure 1). Of those seropositive samples, we tested 31,506 (3.2%) for binding antibody titer, of which 30,967 (98.3%) had valid numeric anti-RBD assay results. We included data from samples with valid assay results in our binding antibody titer analysis. Of the specimens included in the anti-RBD dataset, 744 (2.4%) had neutralizing titer results from the same specimen.

When we compared anti-N–positive samples in NCLS, samples with binding antibody titer results, and samples with neutralizing antibody titer results, we found that all 3 groups originated from populations who had similar distributions by sex and residence in a metropolitan area (Table). Percentages in each age group varied by dataset. Among anti-N–positive specimens, the lowest percentage (18%) was among persons ≥65 years of age. Because of the sampling design, nearly equal percentages of specimens were available by age group among those with binding antibody titers (age range <1–99 years). Among specimens with neutralizing antibody titers, the neutralization assay dataset, most samples were from persons in the youngest (<18 years) or oldest (≥65) age groups (age range <1–93 years).

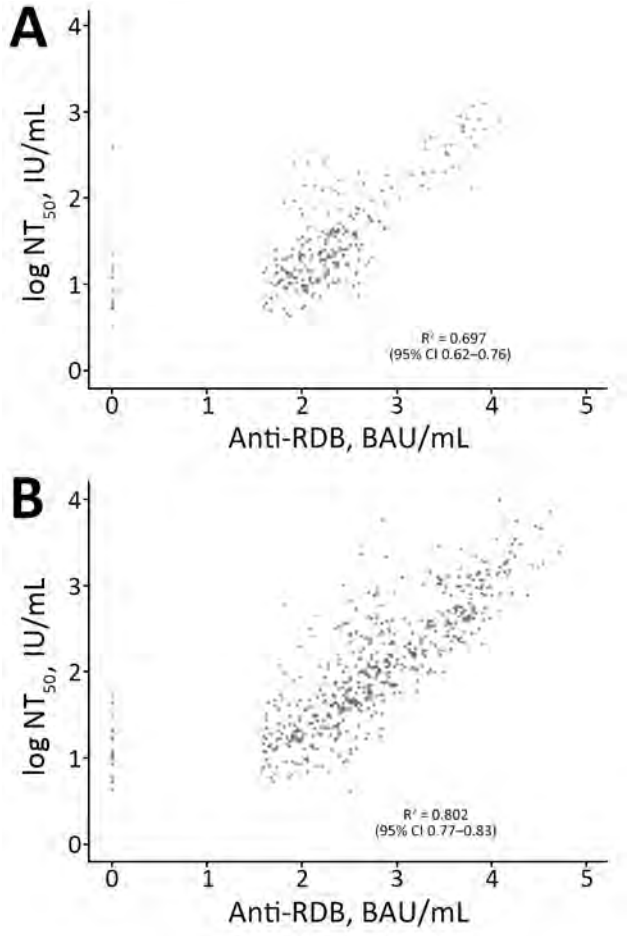

Figure 2. Pearson correlations in study of quantitative SARS-CoV-2 spike RBD and neutralizing antibody titers in previously infected persons, United States, January 2021–February 2022. A) Samples from children; B) samples from adults. Correlations are between the $\log_{10}$-transformed binding (anti-RBD IgG) and neutralizing antibody titers (NT_{50}) for 744 specimens with available results in the Nationwide Commercial Laboratory Seroprevalence Survey database. Neutralizing antibody titers are against the ancestral spike protein. BAU, binding antibody units; NT_{50}, 50% neutralization titer; RBD, receptor-binding domain.

The percentage of samples gathered during variant epochs also varied by dataset. The smallest percentage of specimens with anti-N (9%) and specimens with binding antibody titers (14%) were collected during the Omicron epoch but had representation of >20% from each earlier epoch. Specimens with neutralizing antibody titers were predominantly from the wild-type and Delta variant epochs and a lower percentage from the Alpha (10%) and Omicron (14%) epochs. Specimens collected from children and adults across all 4 variant epochs showed positive correlations between the $\log_{10}$-transformed binding and neutralizing antibody titers (children $R^2 = 0.70$ [95% CI 0.62–0.76]; adult $R^2 = 0.80$ [95% CI 0.77–0.83]) (Figure 2).

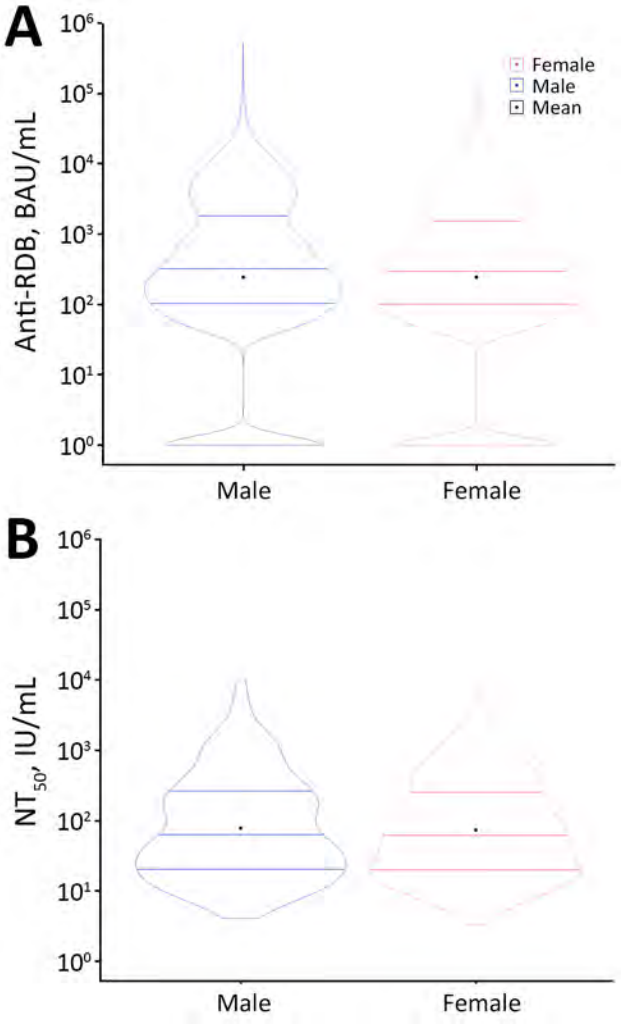

Figure 3. Violin plots of anti-RBD IgG and NT_{50} titer results by sex in study of quantitative SARS-CoV-2 spike RBD and neutralizing antibody titers in previously infected persons, United States, January 2021–February 2022. A) Anti-RBD, n = 30,967; B) NT_{50}, n = 744. Anti-RBD measured by Cov2Quant IgG (LabCorp, https://www.labcorp.com) and NT_{50} measured by PhenoSense SARS-CoV-2 Neutralizing Antibody Assay (Monogram Biosciences, https://monogrambio.labcorp.com). Horizontal lines in plots indicate first quantile, median, and third quantile; black dots indicates means. BAU, binding antibody units; NT_{50}, 50% neutralization titer; RBD, receptor-binding domain.

We noted no clear difference in distribution in either binding or neutralizing titers between sexes (binding titers mean difference = 0.002 [95% CI −0.02 to 0.03]; neutralizing titers mean difference = 0.03 [95% CI −0.08 to 0.13]) (Figure 3). In contrast, mean titers had a notable positive trend across age groups for both titers (binding titers $\beta = 0.24$ [95% CI 0.23–0.25]; neutralizing titers $\beta = 0.23$ [95% CI 0.20–0.27]) (Figure 4).

Violin plots of binding antibody titers showed an increasing trend in mean titer over the 4 variant epochs for all age groups: <18 years, $\beta = 0.15$ (95% CI 0.13–0.17); 18–49 years, $\beta = 0.29$ (95% CI 0.27–0.32); 50–64 years, $\beta = 0.30$ (95% CI 0.28–0.33); and ≥65 years, $\beta = 0.29$ (95% CI 0.27–0.32) (Figure 5, panel A). In addition, maximum values increased over time. Among all specimens, 11.9% had anti-RBD titers below the limit of detection: 1,275 (14.1%) in the wild-type epoch, 986 (14.4%) in the Alpha epoch, 1,101 (10.2%) in the Delta epoch, and 318 (7.5%) in the Omicron epoch. Of note, the distribution for persons <18 years of age appeared bimodal during the Alpha and Delta epochs before returning to a less bimodal shape during the Omicron epoch.

Neutralizing antibody titers showed an increasing trend in mean titer over the 4 variant epochs for all age groups. Mean titers showed statistical significance when tested for linear increases over time for persons 18–49 years of age ($\beta = 0.014$ [95% CI 0.03–0.24]) and those ≥65 years of age ($\beta = 0.09$ [95% CI 0.00–0.18]) (Figure 5, panel B). We noted no consistent changes in distribution shapes over time. Compared with temporal trends in US vaccination coverage by age, we found that distributions in assay results shifted upward as each corresponding age group experienced an increase in vaccination coverage (Figure 5, panel C; Appendix Table, https://wwwnc.cdc.gov/EID/article/30/11/24-0043-App.pdf).

Discussion

This analysis demonstrates the contribution of SARS-CoV-2 binding and neutralizing antibody titers in epidemiologic studies among populations in which nearly all persons have detectible antibodies. Using the range of titers detected in a population with 100% seroprevalence, we were able to study correlations between those 2 measures and compare the means, ranges, and shape of their distributions by demographic group and over time. The ability of those measures to detect serologic heterogeneity within populations

with high rates of seroprevalence is key to studying correlates of protection in previously infected or vaccinated persons (*12*).

We observed a highly positive correlation between SARS-CoV-2 binding and neutralizing antibody titers among a sample of persons with serologic evidence of previous infection. This correlation is consistent with previous studies showing that binding antibody titers could be an acceptable proxy for neutralizing antibody titers, which can be costly and difficult to obtain (*27*,*28*). Although neutralizing antibody titers have been determined to be a correlate of protection for COVID-19 vaccines (*12*), the assays are resource intensive and, thus, are unlikely to be used routinely in a clinical setting (*27*,*28*). Furthermore, that correlation establishes the relationship within our sample, enabling results for both binding and neutralizing titers to lend context to one another. However, interpreting antibody titers should be approached with caution because no threshold above which a person is completely protected from infection or severe disease has been established. Antibody titers have a dose-response effect, and higher titers lead to lower chance of infection or severe disease (*9*–*11*; J.A. Cohen et al., unpub. data). Of note, antibody levels cannot completely describe the risk for severe COVID-19. Despite higher vaccine rates and higher antibody levels, older adults remain at higher risk for severe COVID-19 than young adults (*29*). Moreover, the protection associated with an antibody titer differs by variant and by assay (*30*).

We observed increases in mean and range across age groups for both binding and neutralizing antibody titers, and persons ≥65 years of age had the largest means and ranges. Conversely, neither binding nor neutralizing antibody titers showed meaningful heterogeneity across sex. Those observations are consistent with previous research on antibody titers. One previous study observed an association between increased age and an increase in antibody titers, possibly due to increasing likelihood of vaccination (*6*). Although some studies have shown lower antibody titers among vaccinated older adults (*31*–*33*), those adults likely received a higher number of total vaccine doses. That increase in vaccination could overcome the negative correlation of older age and postvaccine antibody levels to produce the effect seen here. Other studies failed to find evidence of variations in antibody titer by sex (*6*,*7*).

Among this serial cross-sectional study of previously infected persons, we observed an increase in mean binding and neutralizing antibody titers in all age groups over the course of the COVID-19 pandemic in the United States. Increasing antibody levels in the population may be one of the reasons that, as COVID-19 community transmission continues to surge, the rate of hospitalizations and deaths has decreased over time. In addition, increases in titers corresponded with increases in nationwide vaccination rates within each age group. Thus, our observed increases over time and by age are consistent with a higher likelihood of being vaccinated over time and in older age groups (*34*,*35*). Similarly, reinfection could also be contributing to increases in mean titer,

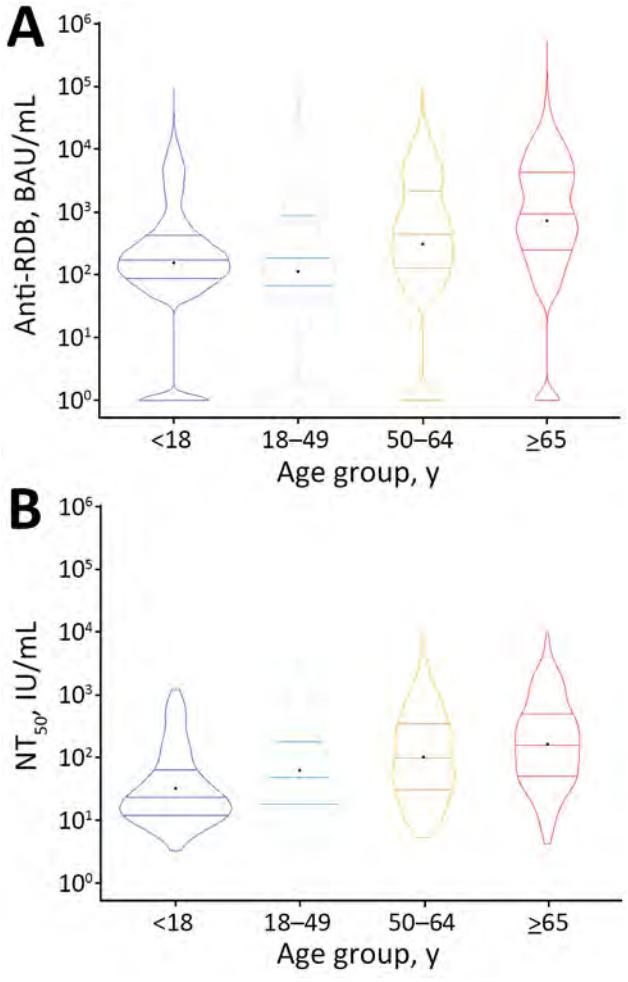

Figure 4. Violin plots of anti-RBD IgG and NT_{50} titer results by age group in a study of quantitative SARS-CoV-2 spike RBD and neutralizing antibody titers in previously infected persons, United States, January 2021–February 2022. A) Anti-RBD, n = 30,967; B) NT_{50}, n = 744. Anti-RBD measured by Cov2Quant IgG (LabCorp, https://www.labcorp.com) and NT_{50} measured by PhenoSense SARS-CoV-2 Neutralizing Antibody Assay (Monogram Biosciences, https://monogrambio.labcorp.com). Horizontal lines in plots indicate first quantile, median, and third quantile; black dots indicates means. BAU, binding antibody units; NT_{50}, 50% neutralization titer; RBD, receptor-binding domain.

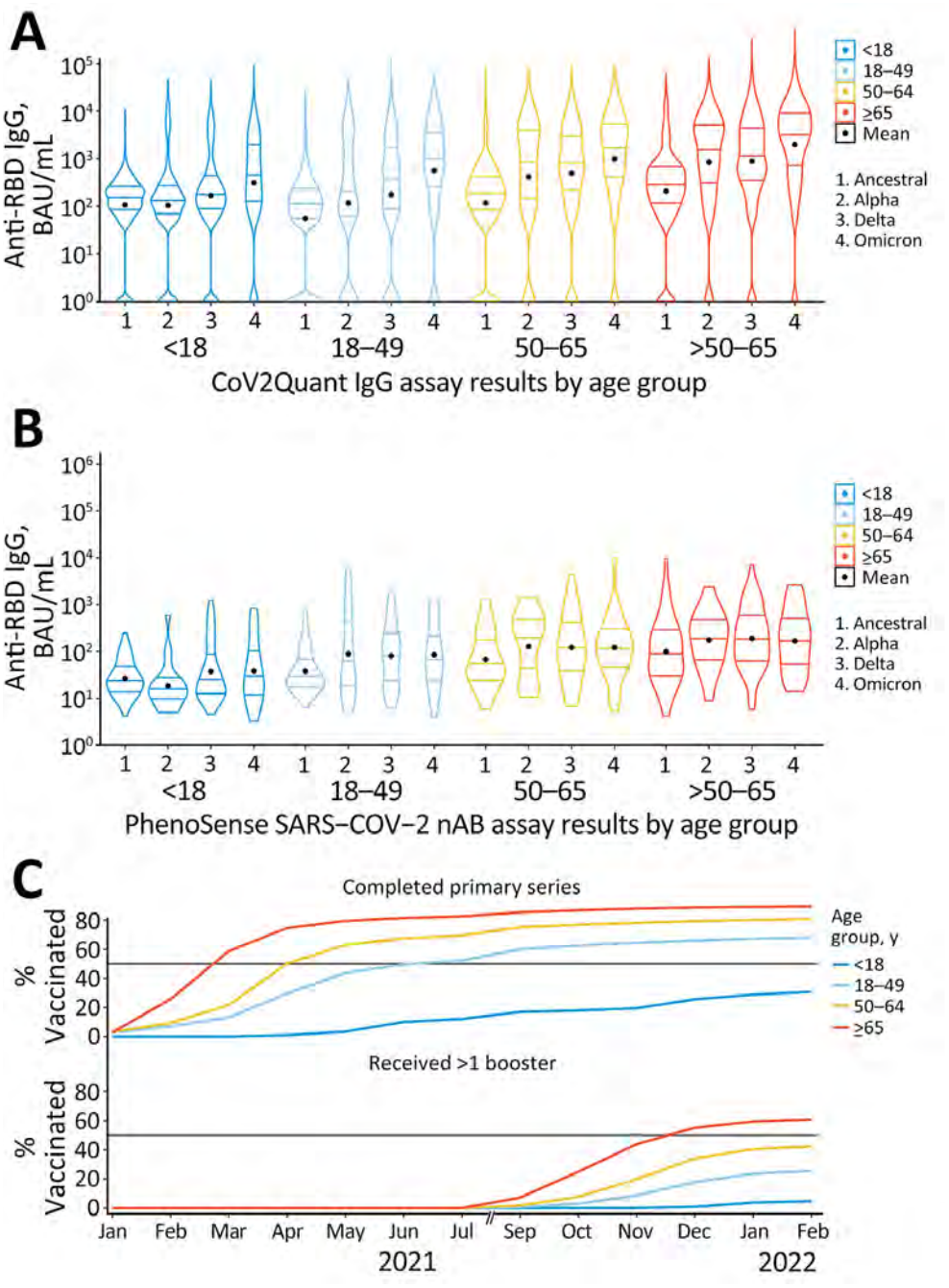

Figure 5. Violin plots of anti-RBD IgG and NT_{50} titer results by age group in study of quantitative SARS-CoV-2 spike RBD and neutralizing antibody titers in previously infected persons, United States, January 2021–February 2022. A) Anti-RBD, n = 30,967; B) NT_{50}, n = 744; C) vaccination coverage per SARS-CoV-2 epoch. Anti-RBD measured by Cov2Quant IgG (LabCorp, https://www.labcorp.com) and NT_{50} measured by PhenoSense SARS-CoV-2 Neutralizing Antibody Assay (Monogram Biosciences, https://monogrambio.labcorp.com). Horizontal lines in plots indicate first quantile, median, and third quantile; black dots indicates means. Persons ≥16 years of age were eligible for vaccination starting in December 2020. In May 2021, vaccination was approved for persons 12–15 years of age. In November 2021, vaccination was approved for persons 5–11 years of age. Note: August 2021 is omitted due to a gap in data collection. BAU, binding antibody units; NT_{50}, 50% neutralization titer; RBD, receptor-binding domain.

especially because likelihood of reinfection increases over time and with later variants (*36*).

In addition to showing differences in means, our analysis visualized distribution shapes over the 4 variant epochs. Upon detailed inspection, the distribution for persons <18 years of age appeared more bimodal during the Alpha and Delta epochs before returning to a more unimodal shape during the Omicron epoch. During the Alpha and Delta epochs, we observed a large mode of titers at lower levels along with a smaller but visible secondary mode at a higher antibody concentration (*37*). That observation is consistent with the staggered vaccine rollout, in which various age groups <18 years of age became eligible at various dates. In our data from the Alpha and Delta epochs, titers from older children who were eligible for vaccination contributed to the upper mode. Visualization of binding antibody titer distributions also highlighted another characteristic: the lower tails of each distribution remained over

epochs. Given that binding antibody titers below the limit of detection of the assay remained, some persons might have failed to mount a robust anti-RBD response to their infection, possibly related to mild or asymptomatic infections (*38*). Alternatively, some persons might have mounted an initial anti-RBD response but experienced titer waning over time (*38*), possibly correlated with an absence of vaccination or reinfection (*36*,*39*). Anti-RBD has been observed to wane faster than anti-N (*40*).

The first limitation of our analysis that race, ethnicity, and vaccination history of persons contributing specimens were not available from commercial laboratory data, precluding analysis with those variables. Second, we did not use information on prior infections, such as date of symptom onset or confirmation, because that information was only available for a small subset of persons. Similarly, we cannot generalize our findings to those who have never been infected, a valuable consideration for our comparison to nationwide vaccination rates. Third, sex, age, and metro status distribution among patients who provided specimens varied slightly from distributions among the general US population; however, we noted no extreme deviations signaling serious generalizability concerns. Finally, our neutralizing assay used a pseudovirion constructed by using the wild-type spike protein, which does not correlate with protection as closely as would neutralizing assays using variant-specific correlates. However, evidence suggests that neutralizing assays continue to correlate with protection against more recent variants (*41*,*42*)

In conclusion, binding and neutralizing antibody titers among persons with serologic evidence of prior SARS-CoV-2 infection have generally increased within age groups over variant epochs and in synchronization with increases in vaccination coverage. Those increases indicate a possible rise in protective immunity within age groups in previously infected populations over the study period, likely resulting from increases in vaccination coverage and reinfections. Our findings indicate that binding titers are acceptable in the absence of neutralizing titers in a clinical setting. In addition, our findings demonstrate the contribution of SARS-CoV-2 serologic surveys incorporating measures beyond seroprevalence for understanding immunity. Future serologic surveillance of infectious diseases would benefit from the incorporation of binding and neutralizing antibody titers. As the US population approaches 100% seroprevalence, those measures could help identify populations with less immunity to serve with vaccination campaigns.

Acknowledgments

We thank the following Labcorp team members for their contributions: Monique Bastidas, Manory Fernando, Terri Wrin, Suqin Cai, Dot Adcock, Deborah Sesok-Pizzini, and Stanley Letovsky. We would also like to thank Amy J. Schuh and L. Clifford McDonald for their contributions.

This work was supported by the Centers for Disease Control and Prevention, Atlanta, Georgia, USA.

About the Author

Dr. Bratcher is an Epidemic Intelligence Service officer at the Centers for Disease Control and Prevention, Atlanta, GA, USA. Her research interests include the study of large healthcare data sets with a focus on emerging infectious disease, vaccination, and health equity.

References

1. Rostami A, Sepidarkish M, Leeflang MMG, Riahi SM, Nourollahpour Shiadeh M, Esfandyari S, et al. SARS-CoV-2 seroprevalence worldwide: a systematic review and meta-analysis. Clin Microbiol Infect. 2021;27:331–40. https://doi.org/10.1016/j.cmi.2020.10.020
2. Bobrovitz N, Arora RK, Cao C, Boucher E, Liu M, Donnici C, et al. Global seroprevalence of SARS-CoV-2 antibodies: a systematic review and meta-analysis. PLoS One. 2021;16:e0252617. https://doi.org/10.1371/journal.pone.0252617
3. Lai C-C, Wang J-H, Hsueh P-R. Population-based seroprevalence surveys of anti–SARS-CoV-2 antibody: an up-to-date review. Int J Infect Dis. 2020;101:314–22. https://doi.org/10.1016/j.ijid.2020.10.011
4. Arora RK, Joseph A, Van Wyk J, Rocco S, Atmaja A, May E, et al. SeroTracker: a global SARS-CoV-2 seroprevalence dashboard. Lancet Infect Dis. 2021;21:e75–6. https://doi.org/10.1016/S1473-3099(20)30631-9
5. Wei J, Pouwels KB, Stoesser N, Matthews PC, Diamond I, Studley R, et al.; COVID-19 Infection Survey team. Antibody responses and correlates of protection in the general population after two doses of the ChAdOx1 or BNT162b2 vaccines. Nat Med. 2022;28:1072–82. https://doi.org/10.1038/s41591-022-01721-6
6. Arkhipova-Jenkins I, Helfand M, Armstrong C, Gean E, Anderson J, Paynter RA, et al. Antibody response after SARS-CoV-2 infection and implications for immunity: a rapid living review. Ann Intern Med. 2021;174:811–21. https://doi.org/10.7326/M20-7547
7. Qaseem A, Yost J, Etxeandia-Ikobaltzeta I, Forciea MA, Abraham GM, Miller MC, et al.; Scientific Medical Policy Committee of the American College of Physicians; Scientific Medical Policy Committee of the American College of Physicians. What is the antibody response and role in conferring natural immunity after SARS-CoV-2 infection? Rapid, living practice points from the American College of Physicians (version 2). Ann Intern Med. 2022;175:556–65. https://doi.org/10.7326/M21-3272
8. Buss L, Prete CA Jr, Whittaker C, Salomon T, Oikawa MK, Pereira RHM, et al. Predicting SARS-CoV-2 variant spread in a completely seropositive population using semi-quantitative antibody measurements in blood donors. Vaccines (Basel). 2022;10:1437. https://doi.org/10.3390/vaccines10091437

9. Khoury DS, Cromer D, Reynaldi A, Schlub TE, Wheatley AK, Juno JA, et al. Neutralizing antibody levels are highly predictive of immune protection from symptomatic SARS-CoV-2 infection. Nat Med. 2021;27:1205–11. https://doi.org/10.1038/s41591-021-01377-8
10. Schuh AJ, Satheshkumar PS, Dietz S, Bull-Otterson L, Charles M, Edens C, et al. SARS-CoV-2 convalescent sera binding and neutralizing antibody concentrations compared with COVID-19 vaccine efficacy estimates against symptomatic infection. Microbiol Spectr. 2022;10:e0124722. https://doi.org/10.1128/spectrum.01247-22
11. Earle KA, Ambrosino DM, Fiore-Gartland A, Goldblatt D, Gilbert PB, Siber GR, et al. Evidence for antibody as a protective correlate for COVID-19 vaccines. Vaccine. 2021;39:4423–8. https://doi.org/10.1016/j.vaccine.2021.05.063
12. Gilbert PB, Donis RO, Koup RA, Fong Y, Plotkin SA, Follmann D. A Covid-19 milestone attained—a correlate of protection for vaccines. N Engl J Med. 2022;387:2203–6. https://doi.org/10.1056/NEJMp2211314
13. Takahashi T, Ellingson MK, Wong P, Israelow B, Lucas C, Klein J, et al.; Yale IMPACT Research Team. Sex differences in immune responses that underlie COVID-19 disease outcomes. Nature. 2020;588:315–20. https://doi.org/10.1038/s41586-020-2700-3
14. Crotty S. Hybrid immunity. Science. 2021;372:1392–3. https://doi.org/10.1126/science.abj2258
15. Buss LF, Prete CA, Whittaker C, Salomon T, Oikawa MK, Pereira RHM, et al. Predicting SARS-CoV-2 variant spread in a completely seropositive population using semi-quantitative antibody measurements in blood donors. Vaccines (Basel). 2022;10:1437. https://doi.org/10.3390/vaccines10091437
16. Choudhary HR, Parai D, Dash GC, Peter A, Sahoo SK, Pattnaik M, et al. IgG antibody response against nucleocapsid and spike protein post-SARS-CoV-2 infection. Infection. 2021;49:1045–8. https://doi.org/10.1007/s15010-021-01651-4
17. Wiegand RE, Deng Y, Deng X, Lee A, Meyer WA III, Letovsky S, et al. Estimated SARS-CoV-2 antibody seroprevalence trends and relationship to reported case prevalence from a repeated, cross-sectional study in the 50 states and the District of Columbia, United States—October 25, 2020–February 26, 2022. Lancet Reg Health Am. 2023;18:100403. https://doi.org/10.1016/j.lana.2022.100403
18. Bajema KL, Wiegand RE, Cuffe K, Patel SV, Iachan R, Lim T, et al. Estimated SARS-CoV-2 seroprevalence in the US as of September 2020. JAMA Intern Med. 2021;181:450–60. https://doi.org/10.1001/jamainternmed.2020.7976
19. Muecksch F, Wise H, Batchelor B, Squires M, Semple E, Richardson C, et al. Longitudinal serological analysis and neutralizing antibody levels in coronavirus disease 2019 convalescent patients. J Infect Dis. 2021;223:389–98. https://doi.org/10.1093/infdis/jiaa659
20. Favresse J, Eucher C, Elsen M, Gillot C, Van Eeckhoudt S, Dogné J-M, et al. Persistence of anti–SARS-CoV-2 antibodies depends on the analytical kit: a report for up to 10 months after infection. Microorganisms. 2021;9:556. https://doi.org/10.3390/microorganisms9030556
21. Kappelman MD, Weaver KN, Boccieri M, Firestine A, Zhang X, Long MD, et al.; PREVENT-COVID Study Group. Humoral immune response to messenger RNA COVID-19 vaccines among patients with inflammatory bowel disease. Gastroenterology. 2021;161:1340–3.e2. https://doi.org/10.1053/j.gastro.2021.06.016
22. Huang Y, Borisov O, Kee JJ, Carpp LN, Wrin T, Cai S, et al. Calibration of two validated SARS-CoV-2 pseudovirus neutralization assays for COVID-19 vaccine evaluation. Sci Rep. 2021;11:23921. https://doi.org/10.1038/s41598-021-03154-6
23. Markmann AJ, Giallourou N, Bhowmik DR, Hou YJ, Lerner A, Martinez DR, et al. Sex disparities and neutralizing-antibody durability to SARS-CoV-2 infection in convalescent individuals. MSphere. 2021;6:e00275-21. https://doi.org/10.1128/mSphere.00275-21
24. US Census Bureau. Measuring America's people, places, and economy [cited 2024 Aug 20]. https://www.census.gov/data/datasets/time-series/demo/popest/2020s-national-detail.html
25. Centers for Disease Control and Prevention. COVID data tracker: monitoring variant proportions [cited 2023 Jan 13]. https://covid.cdc.gov/covid-data-tracker
26. Centers for Disease Control and Prevention. COVID-19 vaccination demographics in the United States, national [cited 2023 Jan 13]. https://data.cdc.gov/Vaccinations/COVID-19-Vaccination-Demographics-in-the-United-St/km4m-vcsb
27. Shi AC, Ren P. SARS-CoV-2 serology testing: progress and challenges. J Immunol Methods. 2021;494:113060. https://doi.org/10.1016/j.jim.2021.113060
28. Younes N, Al-Sadeq DW, Al-Jighefee H, Younes S, Al-Jamal O, Daas HI, et al. Challenges in laboratory diagnosis of the novel coronavirus SARS-CoV-2. Viruses. 2020;12:582. https://doi.org/10.3390/v12060582
29. Johnson AG, Linde L, Ali AR, DeSantis A, Shi M, Adam C, et al. COVID-19 incidence and mortality among unvaccinated and vaccinated persons aged ≥12 years by receipt of bivalent booster doses and time since vaccination—24 U.S. jurisdictions, October 3, 2021–December 24, 2022. MMWR Morb Mortal Wkly Rep. 2023;72:145–52. https://doi.org/10.15585/mmwr.mm7206a3
30. Khoury DS, Schlub TE, Cromer D, Steain M, Fong Y, Gilbert PB, et al. Correlates of protection, thresholds of protection, and immunobridging among persons with SARS-CoV-2 infection. Emerg Infect Dis. 2023;29:381–8. https://doi.org/10.3201/eid2902.221422
31. Bag Soytas R, Cengiz M, Islamoglu MS, Borku Uysal B, Yavuzer S, Yavuzer H. Antibody responses to COVID-19 vaccines in older adults. J Med Virol. 2022;94:1650–4. https://doi.org/10.1002/jmv.27531
32. Soeorg H, Jõgi P, Naaber P, Ottas A, Toompere K, Lutsar I. Seroprevalence and levels of IgG antibodies after COVID-19 infection or vaccination. Infect Dis (Lond). 2022;54:63–71. https://doi.org/10.1080/23744235.2021.1974540
33. Müller L, Andrée M, Moskorz W, Drexler I, Walotka L, Grothmann R, et al. Age-dependent immune response to the Biontech/Pfizer BNT162b2 coronavirus disease 2019 vaccination. Clin Infect Dis. 2021;73:2065–72. https://doi.org/10.1093/cid/ciab381
34. Klein NP. Added benefit of Covid-19 vaccination after previous infection. N Engl J Med. 2022;386:1278–9. https://doi.org/10.1056/NEJMe2201380
35. Lewis N, Chambers LC, Chu HT, Fortnam T, De Vito R, Gargano LM, et al. Effectiveness associated with vaccination after COVID-19 recovery in preventing reinfection. JAMA Netw Open. 2022;5:e2223917. https://doi.org/10.1001/jamanetworkopen.2022.23917
36. Siddiqui SM, Bowman KA, Zhu AL, Fischinger S, Beger S, Maron JS, et al. Serological markers of SARS-CoV-2 reinfection. MBio. 2022;13:e0214121. https://doi.org/10.1128/mbio.02141-21
37. Centers for Disease Control and Prevention. The changing threat of COVID-19 [cited 2024 Aug 23]. https://www.cdc.gov/ncird/whats-new/changing-threat-covid-19.html

38. Peluso MJ, Takahashi S, Hakim J, Kelly JD, Torres L, Iyer NS, et al. SARS-CoV-2 antibody magnitude and detectability are driven by disease severity, timing, and assay. Sci Adv. 2021;7:eabh3409. https://doi.org/10.1126/sciadv.abh3409
39. Coppeta L, Ferrari C, Somma G, Mazza A, D'Ancona U, Marcuccilli F, et al. Reduced titers of circulating anti–SARS-CoV-2 antibodies and risk of COVID-19 infection in healthcare workers during the nine months after immunization with the BNT162b2 mRNA vaccine. Vaccines (Basel). 2022;10:141. https://doi.org/10.3390/vaccines10020141
40. Yan LN, Liu PP, Li XG, Zhou SJ, Li H, Wang ZY, et al. Neutralizing antibodies and cellular immune responses against SARS-CoV-2 sustained one and a half years after natural infection. Front Microbiol. 2022;12:803031. https://doi.org/10.3389/fmicb.2021.803031
41. Röltgen K, Boyd SD. Antibody and B cell responses to SARS-CoV-2 infection and vaccination: the end of the beginning. Annu Rev Pathol. 2024;19:69–97. https://doi.org/10.1146/annurev-pathmechdis-031521-042754
42. Springer DN, Camp JV, Aberle SW, Deutsch J, Lammel O, Weseslindtner L, et al. Neutralization of SARS-CoV-2 Omicron XBB.1.5 and JN.1 variants after COVID-19 booster-vaccination and infection. J Med Virol. 2024;96:e29801. https://doi.org/10.1002/jmv.29801

Address for correspondence: Anna Bratcher, Centers for Disease Control and Prevention, 1600 Clifton Rd NE, Mailstop H21-8, Atlanta, GA 30329-4018, USA; email: tqx5@cdc.gov

Estimating Influenza Illnesses Averted by Year-Round and Seasonal Campaign Vaccination for Young Children, Kenya

Radhika Gharpure, Young M. Yoo, Ben Andagalu, Stefano Tempia, Sergio Loayza, Chiedza Machingaidze, Bryan O. Nyawanda, Jeanette Dawa, Eric Osoro, Rose Jalang'o, Kathryn E. Lafond, Melissa A. Rolfes, Gideon O. Emukule

In Kenya, influenza virus circulates year-round, raising questions about optimum strategies for vaccination. Given national interest in introducing influenza vaccination for young children 6–23 months of age, we modeled total influenza-associated illnesses (inclusive of hospitalizations, outpatient illnesses, and non–medically attended illnesses) averted by multiple potential vaccination strategies: year-round versus seasonal-campaign vaccination, and vaccination starting in April (Southern Hemisphere influenza vaccine availability) versus October (Northern Hemisphere availability). We modeled average vaccine effectiveness of 50% and annual vaccination coverage of 60%. In the introduction year, year-round vaccination averted 6,410 total illnesses when introduced in October and 7,202 illnesses when introduced in April, whereas seasonal-campaign vaccination averted 10,236 (October) to 11,612 (April) illnesses. In the year after introduction, both strategies averted comparable numbers of illnesses (10,831–10,868 for year-round, 10,175–11,282 for campaign). Campaign-style vaccination would likely have a greater effect during initial pediatric influenza vaccine introduction in Kenya; however, either strategy could achieve similar longer-term effects.

Influenza causes a substantial number of respiratory illnesses among young children in Kenya (*1*). The best time to vaccinate against seasonal influenza is before influenza viruses circulate, but because there are multiple periods of increased influenza activity each year in Kenya, the optimum timing and approach for influenza vaccination remains unclear (*2*–*4*). In 2016, the Kenya National Immunization Technical Advisory Group issued a provisionary recommendation to introduce seasonal influenza vaccination among children 6–23 months of age on the basis of national evidence demonstrating substantial disease in this age group and advised that a pilot vaccination project should be conducted to inform a potential national vaccination rollout (*5*). As a result, a subnational pediatric vaccination pilot was conducted in Kenya during 2019–2021 to compare 2 potential delivery strategies: year-round vaccination, in which influenza vaccine is offered all months of the year, and a once-yearly seasonal vaccination campaign, in which influenza vaccine is offered only for 4 consecutive months (*6*,*7*). Results of the pilot indicated that both strategies might achieve similar vaccine coverage and incur a similar cost per dose for delivery but that the seasonal campaign could require considerable operational needs (e.g., workforce and cold chain capacity) compared with the year-round strategy (*6*,*7*).

In addition to those pilot data on the real-world performance of the proposed strategies, estimating the number of illnesses averted through influenza vaccination can provide additional, relevant evidence to inform pediatric influenza vaccination policy

Author affiliations: Centers for Disease Control and Prevention, Atlanta, Georgia, USA (R. Gharpure, Y.M. Yoo, B. Andagalu, K.E. Lafond, M.A. Rolfes, G.O. Emukule); Centers for Disease Control and Prevention, Nairobi, Kenya (B. Andagalu, G.O. Emukule); World Health Organization, Geneva, Switzerland (S. Tempia, C. Machingaidze, M.A. Rolfes); Pan American Health Organization, Washington, DC, USA (S. Loayza); Kenya Medical Research Institute, Kisumu, Kenya (B.O. Nyawanda); Washington State University Global Health Kenya, Nairobi (J. Dawa, E. Osoro); Washington State University, Pullman, Washington, USA (E. Osoro); Ministry of Health, Nairobi (R. Jalang'o)

DOI: http://doi.org/10.3201/eid3011.240375

deliberations in Kenya. In other settings, averted illness estimates have provided actionable public health data for influenza vaccine implementation, such as optimizing campaign timing (*8*). In fact, a similar averted illness analysis was previously conducted for pregnant women and young children in Kenya and found that, given the year-round circulation of influenza, both year-round and twice-yearly vaccination strategies might avert a comparable number of illnesses compared with a single annual campaign (*9*). In this analysis, we adapted an existing model (*8*,*10*) to estimate the number of influenza illnesses and hospitalizations averted by influenza vaccine introduction for children 6–23 months of age in Kenya, comparing year-round to seasonal campaign vaccine delivery.

Methods

Base Model and Modifications

We adapted a static compartmental model jointly developed by the World Health Organization (WHO), US Centers for Disease Control and Prevention (CDC), and Pan American Health Organization (PAHO) to estimate the number of total influenza-associated illnesses (including hospitalized illnesses, outpatient illnesses, and non–medically attended illnesses) averted by vaccination. Model methods have been published previously (*8*); in brief, we first estimated the burden of disease among children 6–23 months of age in Kenya in the absence of an influenza vaccination program and then calculated the number of illnesses averted through a counterfactual vaccination program.

We made 3 major modifications to the model described in Chard et al. (*8*) (Appendix Table 1, Figure 1, https://wwwnc.cdc.gov/EID/article/30/11/24-0375-App1.pdf). First, we expanded the time horizon from 12 months to 24 months (as years 1 and 2) to better simulate the effect of residual vaccine protection from the prior year, which was of particular interest for longer-term implementation of year-round vaccine delivery. Second, whereas the original model assumed constant vaccine effectiveness (VE) over the model timeframe, we assumed VE waned in the months after vaccination, as described previously in evaluating influenza vaccination among children and older adults (*11*,*12*). Finally, because we expanded the time period for the new model, we assumed that natural immunity from infection lasted for 12 months, meaning infected persons could recover within the model's 24-month timeframe and return to the susceptible compartment for their remaining time. In addition, persons infected in the 12 months before the model's start (year 0) were also systematically returned to the susceptible population as their 12-month immunity expired.

Vaccination Strategies Modeled

We modeled 2 distinct vaccination strategies: seasonal campaigns, as traditionally used in countries with a Southern or Northern Hemisphere influenza season (*13*), and year-round vaccination, as has been proposed for countries with no clear influenza season (*14*). Although the 2019–2021 demonstration project included campaigns starting in June and July (*6*), we modeled 2 variations of the seasonal campaign with starting months of April (corresponding to the usual timing of Southern Hemisphere influenza vaccine availability) and October (corresponding to Northern Hemisphere vaccine availability) (*13*) (Figure). We assumed each vaccination campaign would last 4 months, as in the demonstration project (*6*). For year-round vaccination, we similarly modeled initial introduction of the vaccine in both April and October for comparability across the 24-month analysis timeframe. As a sensitivity analysis, we included 2

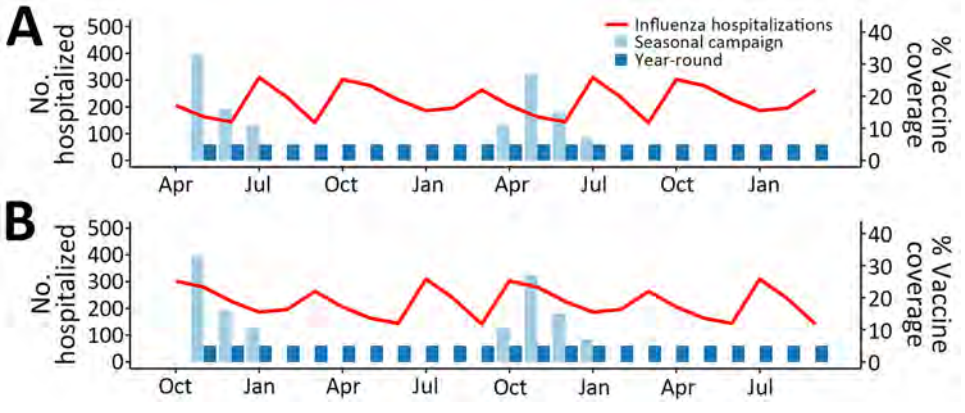

Figure. Modeled influenza hospitalizations and vaccine coverage among children 6–23 months of age in Kenya, by delivery strategy. Red line indicates no. monthly hospitalizations, corresponding to the left y-axis. Light blue bars represent percentage vaccine coverage for the seasonal-campaign strategy and dark blue bars the year-round strategy, corresponding to the right y-axis. Hospitalization curves are identical for both the introduction year (months 1–12) and postintroduction year (months 13–24). A) April introduction of vaccination. B) October introduction of vaccination.

additional start times for the seasonal campaign: June (halfway between Southern and Northern Hemisphere vaccine availability) and January (halfway between Northern and Southern Hemisphere vaccine availability).

Model Data Inputs

We estimated the 2022 population size for children 6–23 months of age in Kenya (n = 1,809,394) based on growth projections from 2019 census data (*15*,*16*) (Table 1). We used a previously published incidence of influenza-associated severe acute respiratory illness hospitalizations among children 0–23 months of age in Kenya during 2011–2014 (146.6/100,000 population; *17*) to calculate the annual expected number of hospitalizations (n = 2,653). In addition, we derived an average seasonal curve of influenza-associated disease burden from influenza surveillance data reported to the WHO Global Influenza Surveillance and Response System FluNet data platform (*21*) from Kenya for all ages during 2011–2019. Using an aggregate average method (*22*), we calculated a 3-week moving proportion of samples positive for influenza (Appendix Figure 2). We then distributed the 2,653 annual hospitalizations across weeks of the year using this seasonal curve and summed weekly counts to generate monthly hospitalizations; all years of the model (0–3) used the same hospitalization curve (Figure).

To estimate the number of influenza-associated events by different strata of severity of illness and care-seeking (i.e., hospitalized illnesses, outpatient illnesses, and total illnesses inclusive of non–medically attended), the model uses multipliers for the ratio of nonhospitalized to hospitalized illnesses and for the proportion of illnesses medically attended. We calculated a multiplier for the ratio of nonhospitalized to hospitalized cases based on a combination of sentinel surveillance data from Siaya County among children 6–23 months of age during 2011–2013 and a 2018 healthcare utilization survey of children <2 years of age in Kenya (*18*) (Appendix Figure 3). We obtained a multiplier for the proportion of illnesses that were medically attended using the same healthcare utilization survey (*18*).

On the basis of results of the demonstration project comparing year-round and campaign vaccine delivery in 2 counties during 2019–2021 (*6*), we assumed that both delivery strategies would achieve equal cumulative vaccine coverage; we set this value to 60% annually for both strategies. We allocated monthly coverage for the year-round strategy evenly across the year and coverage for the seasonal campaign according to the distribution of monthly coverage

Table 1. Model input variables and data sources in study to estimate influenza illnesses averted by year-round and seasonal campaign vaccination for young children, Kenya*

Model input	Value	Data source
Population characteristics		
Population size, children 6–23 mo of age	1,809,394	2022 census projection using 2019 census (*15*) and World Bank annual population growth rates (*16*)
Annual vaccination coverage, %	60	Assumption based on coverage calculated in first year of pediatric demonstration project; both strategies obtained similar coverage (*6*)
Influenza illnesses		
Influenza-associated hospitalization rate	146.6/100,000 population	Rate among children <2 y of age during 2011–2014 (*17*)
Ratio of nonhospitalized to hospitalized influenza illnesses	19.9 (IQR 17.6–21.6)	Calculated from Siaya County SARI surveillance data and healthcare utilization survey (Appendix Figure 3, https://wwwnc.cdc.gov/EID/article/30/11/24-0375-App1.pdf)
Influenza illnesses medically attended, %	47.9	Healthcare utilization survey: results for children <2 y of age in Kenya (*18*)
Vaccine effectiveness and natural immunity		
VE point estimate, %	50 (average)	2010–2012 clinical trial data for trivalent influenza vaccine in children <5 y of age in Kenya (*19*) and meta-analysis of influenza VE among children 6–23 mo of age (*20*)
Rate of waning (base scenario)	$VE_t = 70 - 1.37 \times biweeks + 0.18 \times biweeks^2 - 0.03 \times biweeks^3$ † (≈7% absolute decline per month)	Prior analyses evaluating influenza vaccination timing among older adults (*11*)
Duration of natural immunity from infection	12 mo	Assumption consistent with prior models that did not assume reinfections within a 12-mo time horizon (*8*,*10*)

*VE, vaccine effectiveness.
†VE_t refers to vaccine effectiveness at time t, calculated based on the number of biweeks (period of 2 weeks) elapsed.

Table 2. Estimated influenza illnesses averted through influenza vaccination for children 6–23 mo of age in the introduction year (base scenario), Kenya*

Vaccination strategy	Prevented fraction	Hospitalizations averted	Outpatient visits averted	Medically attended illnesses averted	Total illnesses averted
Year-round vaccination, April start	13.2 (10.9–15.7)	349 (286–416)	3,101 (2,456–3,846)	3,450 (2,751–4,251)	7,202 (5,898–8,616)
Year-round vaccination, October start	11.7 (9.6–13.9)	311 (254–371)	2,754 (2,173–3,414)	3,066 (2,431–3,769)	6,410 (5,218–7,692)
Seasonal campaign vaccination, Apr–Jul	21.2 (16.9–26.3)	562 (448–695)	4,988 (3,828–6,391)	5,546 (4,287–7,090)	11,612 (9,220–14,478)
Seasonal campaign vaccination, Oct–Jan	18.7 (14.9–23.3)	497 (394–621)	4,399 (3,377–5,684)	4,894 (3,787–6,286)	10,236 (8,082–12,837)

*Values are estimated no. (95% CI) except for prevented fraction, which was defined as the number of illnesses averted by vaccination divided by the number of illnesses in the absence of vaccine.

achieved during the demonstration project (Figure). We assumed that children would receive 2 doses of influenza vaccine ≥4 weeks apart, in accordance with recommendations for the age group (*23*), to be considered fully vaccinated; thus, no children were considered fully vaccinated at month 1 of vaccine introduction. However, for the first year after introduction (postintroduction year) of the seasonal campaign, we assumed that one third of children who were previously vaccinated would remain in the eligible age group (6–11 months of age in the first year and 18–23 months in the second year), receiving only 1 dose of vaccine and considered fully vaccinated in the first month of the postintroduction year campaign.

For influenza VE inputs, we used an average VE of 50% against any influenza-associated illness, consistent with 2010–2012 clinical trial data for trivalent influenza vaccine in children <5 years of age in Kenya (*19*), as well as a meta-analysis of influenza VE among children 6–23 months of age (*20*). The base scenario incorporated cubic waning of VE as previously described (*11*), with a starting VE of 70% in month 1 and an average VE of 50% over 8 months (Appendix Table 2). We explored 2 additional patterns: scenario A modeled a constant of 50% with vaccine protection lasting 8 months and then 0% VE (no protection) thereafter, and scenario B modeled a constant VE of 50% with protection lasting 12 months (Appendix Table 2).

Model Outputs

We estimated the number of hospitalizations, outpatient visits, medically attended illnesses (inclusive of both outpatient visits and hospitalizations), and total illnesses (inclusive of medically attended and non–medically attended illnesses) averted by each vaccination strategy and stratified results by year. We also calculated the prevented fraction, defined as the number of illnesses averted by vaccination divided by the number of illnesses in the absence of vaccine. We used Monte Carlo simulation with 5,000 iterati ons to sample parameter values at random from their distributions and obtained confidence intervals for all estimates. Monte Carlo simulation assumed a Poisson distribution for monthly hospitalizations, a uniform distribution for the ratio of nonhospitalized to hospitalized influenza illnesses, and normal distributions for the proportion of influenza illnesses non–medically attended, VE, and vaccine coverage. We performed all analyses in R version 4.0.2 (The R Project for Statistical Computing, https://www.r-project.org).

Results

From the modeled estimates, during the first year that seasonal influenza vaccination was introduced (introduction year), year-round vaccination starting in April averted an estimated 7,202 (95% CI 5,898–8,616) total influenza-associated illnesses in children 6–23 months of age, including 3,450 (95% CI 2,751–4,251) medically attended illnesses and 349 (95% CI 286–416) hospitalizations (Table 2). Year-round vaccination starting in October averted an estimated 6,410 (95% CI 5,218–7,692) total illnesses, including 3,066 (95% CI 2,431–3,769) medically attended illnesses and 311 (95% CI 254–371) hospitalizations (Table 2). The prevented fraction of total illnesses in the introduction year was 13% (95% CI 11%–16%) when year-round vaccination was introduced in April and 12% (95% CI 10%–14%) when introduced in October. In comparison, an April–July (Southern Hemisphere) seasonal campaign averted an estimated 11,612 (95% CI 9,220–14,478) total illnesses, including 5,546 (95% CI 4,287–7,090) medically attended illnesses and 562 (95% CI 448–695) hospitalizations; an October–January seasonal campaign (corresponding to Northern Hemisphere vaccine availability) averted an estimated 10,236 (95% CI 8,082–12,837) total influenza-associated illnesses, including 4,894 (95% CI 3,787–6,286) medically attended illnesses and 497 (95% CI 394–621) hospitalizations. The prevented fraction of total illnesses was 21% (95% CI 17%–26%) for the April–July campaign and 19% (95% CI 15%–23%) for October–January.

In the second year after influenza vaccination was introduced (postintroduction year), year-round vaccination averted an estimated 10,831 (95% CI 8,748–13,106) total illnesses, including 5,188 (95% CI 4,077–6,464) medically attended illnesses and 526 (95% CI 426–635) hospitalizations when introduced in April and 10,868 (95% CI 8,726–13,162) total illnesses, including 5,187 (95% CI 4,079–6,486) medically attended illnesses and 528 (95% CI 425–636) hospitalizations when introduced in October (Table 3). The prevented fraction of total illnesses was 20% (95% CI 16%–24%) for year-round vaccination regardless of the starting month. An April–July seasonal campaign averted an estimated 11,282 (95% CI 8,752–14,099) total illnesses, including 5,392 (95% CI 4,130–6,890) medically attended illnesses and 547 (95% CI 425–684) hospitalizations, and an October–January seasonal campaign averted an estimated 10,175 (95% CI 7,891–12,876) total illnesses, including 4,869 (95% CI 3,703–6,253) medically attended illnesses and 493 (95% CI 384–622) hospitalizations. The prevented fraction was 21% (95% CI 16–26) for the April–July campaign and 19% (95% CI 14–23) for October–January.

Sensitivity analyses indicated that assuming a constant 8-month VE without waning (scenario A) did not significantly change the estimate of averted illness for any strategy in the introduction or postintroduction years compared with the base scenario (Appendix Table 3, Figure 4). Assuming a constant 12-month VE (scenario B) increased the absolute number of averted illnesses for all strategies in the postintroduction year, but 95% CIs overlapped with the base scenario for the April seasonal campaign and year-round strategy with October introduction (Appendix Table 4, Figure 4). In addition, sensitivity analyses that changed the starting month of the seasonal campaign to January or June did not significantly affect the estimates of averted illnesses (Appendix Figure 5).

Discussion

Introducing influenza vaccination for children 6–23 months of age in Kenya would reduce the number of influenza-associated illnesses substantially. Our results indicate that campaign-style vaccination would likely have the greatest effect for initial introduction because it would most rapidly achieve high population protection in a vaccine-naive population. Our finding is consistent with recommendations for catch-up campaigns, or initial campaign-style rollout of vaccination to accelerate herd protection, for other vaccines; for example, modeling findings indicated that catch-up campaigns would increase the efficiency of pneumococcal conjugate vaccine introduction for children <5 years of age in Kenya (*24*). However, our results suggest that, after the initial introduction, either year-round vaccination or a seasonal campaign could have similar effects for long-term implementation. Therefore, national policy decisions regarding which strategy to implement for influenza vaccination should consider the full portfolio of evidence available from the demonstration project, including coverage, costs, effects on the wider health system, logistical feasibility, and perceptions from both the community and health workers (*6*,*7*,*25*). For example, implementation experiences from the vaccination pilot suggested greater operational demands within a short time for the campaign strategy (*6*), but year-round delivery could also be operationally complex (*9*,*14*); previously proposed options include using both Northern and Southern Hemisphere formulations during their respective influenza seasons or extending use of a single formulation for the entire year (*14*). More data are needed on clinical protection offered by those options and programmatic feasibility of changing formulations during a year to inform how year-round vaccination would be implemented. Prior analyses have also considered a twice-yearly vaccination campaign strategy which might offer an intermediate option to year-round and single annual

Table 3. Estimated influenza illnesses averted through influenza vaccination for children 6–23 mo of age in the postintroduction year (base scenario), Kenya*

Vaccination strategy	Prevented fraction	Hospitalizations averted	Outpatient visits averted	Medically attended illnesses averted	Total illnesses averted
Year-round vaccination, April start	19.8 (16.1–23.9)	526 (426–635)	4,656 (3,640–5,831)	5,188 (4,077–6,464)	10,831 (8,748–13,106)
Year-round vaccination, October start	19.9 (16.1–23.9)	528 (425–636)	4,658 (3,635–5,861)	5,187 (4,079–6,486)	10,868 (8,726–13,162)
Seasonal campaign vaccination, Apr–Jul	20.6 (16.1–25.7)	547 (425–684)	4,845 (3,697–6,221)	5,392 (4,130–6,890)	11,282 (8,752–14,099)
Seasonal campaign vaccination, Oct–Jan	18.6 (14.4–23.4)	493 (384–622)	4,371 (3,308–5,638)	4,869 (3,703–6,253)	10,175 (7,891–12,876)

*Values are estimated no. (95% CI) except for prevented fraction, which was defined as the number of illnesses averted by vaccination divided by the number of illnesses in the absence of vaccine.

vaccination (*5*,*9*); however, we did not include that strategy in this analysis for comparability with the 2019–2021 demonstration project (*6*).

The first limitation of our study is that the results from our analysis are greatly dependent on the 2011–2019 influenza seasonal curve that we calculated using FluNet data for Kenya. Because the seasonal curve we calculated from surveillance data showed no clear single seasonal peak, our results indicated that timing a vaccination program with either Southern or Northern Hemisphere vaccine availability might have similar results in Kenya. Previous analyses characterizing influenza seasonality in Kenya are not consistent; a recent analysis suggested that Kenya had 3 influenza seasons, occurring primarily during the Southern Hemisphere seasonal months (*19*), whereas others have suggested a primarily Northern Hemisphere epidemic (*26*), 2 major epidemics (*3*), or unascertainable seasonality (*4*). Even within the years included in the seasonal curve calculation, not all matched the average seasonality exactly; some years have larger peaks at different times, and, thus, use of a seasonal curve does not account for potential year-to-year variations in incidence or temporal distribution of influenza illnesses, which could influence the model results. In addition, to calculate the annual number of influenza hospitalizations, we used an estimate of incidence among children 0–23 months of age during 2011–2014, which might not be representative of all years; because incidence among children 0–5 months of age might be slightly lower than incidence for those 6–11 and 12–23 months (*17*), inclusion of this age group might have underestimated true incidence among the target population 6–23 months of age. Similarly, the results are dependent on the VE estimate used, which can also vary year-to-year based on the level of vaccine match with circulating viruses (*23*). We assumed the same VE for both the Northern and Southern Hemisphere vaccine formulations, as well as for both severe illness (i.e., hospitalization) and mild illness, which might in reality have differential VEs (*27*).

Second, we based our models on assumptions about duration of vaccine-induced immunity, which we modeled from earlier analysis of VE among older adults rather than young children. However, analyses have indicated similar patterns of waning of VE among children and older adults (*12*), and sensitivity analyses using a constant VE suggested that the base scenario might, in fact, be a conservative estimate of the vaccine's impact. Similarly, we assumed that previous infection would confer 12 months of natural immunity, consistent with earlier models that did not include reinfections within a 12-month timeframe (*8*,*10*). Cohort studies have indicated that reinfections with influenza virus are possible within a single season (*28*,*29*); thus, our model assumptions might not fully reflect the duration of natural immunity and likelihood of reinfection in Kenya, particularly given year-round influenza circulation. Third, given the relatively short timeframe examined (24 months), we assumed a stable population and did not account for potential changes in population size (e.g., births, deaths, and migrations) within the model period. Fourth, results in the postintroduction year include residual immunity from the previous year. If a catch-up campaign were used for initial vaccine introduction and the program transitioned to year-round vaccination, the effect of the vaccine would not be equivalent to the postintroduction year results until ≥2 years of year-round vaccination had occurred. Fifth, we assumed that both strategies would achieve the same annual vaccine coverage based on results of the vaccination pilot (*6*), but it is possible that a year-round strategy could reach more children during noncampaign months and result in higher coverage, as previously modeled for maternal influenza vaccination (*9*), or that differences in vaccination program costs could result in differential coverage achieved (*7*).

Finally, we assumed that vaccinated persons were either fully protected by their vaccine or unprotected. Alternative assumptions—for example, where all vaccinees experience a reduced rate of acquiring infection—might result in a higher estimated number of illnesses prevented by vaccination (*30*). In addition, the model did not include nonrespiratory manifestations of influenza illness (*31*), did not account for partial immunity received from a single dose of influenza vaccine among young children (*23*,*32*), and did not include indirect effects of the vaccine (*33*) or estimates of averted deaths (*34*). Furthermore, because less than one third (32%) of young children with severe pneumonia were hospitalized in a previous healthcare utilization survey in Kenya (*20*), a substantial burden of severe illness is missed by focusing on hospitalizations alone. Therefore, our results likely underestimate the full value and effect of influenza vaccination, which warrant further evaluation.

Our findings indicate that either year-round or seasonal campaign vaccination for influenza could substantially reduce influenza burden among children 6–23 months of age in Kenya, resulting in health and economic benefits to children and their families, as well as to the health system and broader society. The results of our analysis suggest that campaign-style vaccination would achieve the greatest impact for in the first year of introduction; however, longer-term implementation could employ either strategy to

achieve similar effect. Our data can be used to inform additional analyses, such as estimating averted cost burden, cost-benefit, or cost-effectiveness of vaccination. Policy decisions regarding the most appropriate vaccination strategy should holistically weigh the available evidence and local implementation context.

Acknowledgments

We thank Eduardo Azziz-Baumgartner, Anna Chard, and Vanessa Cozza for early input into the analysis design and conceptualization.

About the Author

Dr. Gharpure is an epidemiologist at the Coalition for Epidemic Preparedness Innovations; during the completion of this work, she was an epidemiologist in the Influenza Division at the US Centers for Disease Control and Prevention, National Center for Immunization and Respiratory Diseases. Her primary research interests are at the intersection of infectious disease epidemiology, vaccine implementation, and policy.

References

1. Emukule GO, Paget J, van der Velden K, Mott JA. Influenza-associated disease burden in Kenya: a systematic review of literature. PLoS One. 2015;10:e0138708. https://doi.org/10.1371/journal.pone.0138708
2. Emukule GO, Mott JA, Spreeuwenberg P, Viboud C, Commanday A, Muthoka P, et al. Influenza activity in Kenya, 2007–2013: timing, association with climatic factors, and implications for vaccination campaigns. Influenza Other Respir Viruses. 2016;10:375–85. https://doi.org/10.1111/irv.12393
3. Hirve S, Newman LP, Paget J, Azziz-Baumgartner E, Fitzner J, Bhat N, et al. Influenza seasonality in the tropics and subtropics—when to vaccinate? PLoS One. 2016; 11:e0153003. https://doi.org/10.1371/journal.pone.0153003
4. Dawa J, Emukule GO, Barasa E, Widdowson MA, Anzala O, van Leeuwen E, et al. Seasonal influenza vaccination in Kenya: an economic evaluation using dynamic transmission modelling. BMC Medicine. 2020;18:223.
5. Dawa J, Chaves SS, Ba Nguz A, Kalani R, Anyango E, Mutie D, et al.; Kenya National Immunization Technical Advisory Group (KENITAG). Developing a seasonal influenza vaccine recommendation in Kenya: process and challenges faced by the National Immunization Technical Advisory Group (NITAG). Vaccine. 2019;37:464–72. https://doi.org/10.1016/j.vaccine.2018.11.062
6. Dawa J, Jalang'o R, Mirieri H, Kalani R, Marwanga D, Lafond KE, et al. Comparing performance of year-round and campaign-mode influenza vaccination strategies among children aged 6–23 months in Kenya: 2019–2021. Vaccine. 2023;2023:125461. https://doi.org/10.1016/j.vaccine.2023.11.036
7. Gharpure R, Akumu AO, Dawa J, Gobin S, Adhikari BB, Lafond KE, et al. Costs of seasonal influenza vaccine delivery in a pediatric demonstration project for children aged 6–23 months—Nakuru and Mombasa Counties, Kenya, 2019–2021. Vaccine. 2023;125519. https://doi.org/10.1016/j.vaccine.2023.12.029
8. Chard AN, Machingaidze C, Loayza S, Gharpure R, Nogareda F, González R, et al. Estimating averted illnesses from influenza vaccination for children and pregnant women—El Salvador, Panama, and Peru, 2011–2018. Vaccine. 2024;125861. https://doi.org/10.1016/j.vaccine.2024.04.007
9. McMorrow ML, Emukule GO, Obor D, Nyawanda B, Otieno NA, Makokha C, et al. Maternal influenza vaccine strategies in Kenya: which approach would have the greatest impact on disease burden in pregnant women and young infants? PLoS One. 2017;12:e0189623. https://doi.org/10.1371/journal.pone.0189623
10. Tokars JI, Rolfes MA, Foppa IM, Reed C. An evaluation and update of methods for estimating the number of influenza cases averted by vaccination in the United States. Vaccine. 2018;36:7331–7. https://doi.org/10.1016/j.vaccine.2018.10.026
11. Ferdinands JM, Alyanak E, Reed C, Fry AM. Waning of influenza vaccine protection: exploring the trade-offs of changes in vaccination timing among older adults. Clin Infect Dis. 2020;70:1550–9. https://doi.org/10.1093/cid/ciz452
12. Belongia EA, Sundaram ME, McClure DL, Meece JK, Ferdinands J, VanWormer JJ. Waning vaccine protection against influenza A (H3N2) illness in children and older adults during a single season. Vaccine. 2015;33:246–51. https://doi.org/10.1016/j.vaccine.2014.06.052
13. Cox N. Influenza seasonality: timing and formulation of vaccines. Bull World Health Organ. 2014;92:311. https://doi.org/10.2471/BLT.14.139428
14. Lambach P, Alvarez AM, Hirve S, Ortiz JR, Hombach J, Verweij M, et al. Considerations of strategies to provide influenza vaccine year round. Vaccine. 2015;33:6493–8. https://doi.org/10.1016/j.vaccine.2015.08.037
15. Kenya National Bureau of Statistics. 2019 Kenya Population and Housing Census results. 2019 [cited 2023 Nov 8]. https://www.knbs.or.ke/2019-kenya-population-and-housing-census-results
16. The World Bank Group. World Bank open data. 2023 [cited 2022 Nov 1]. https://data.worldbank.org
17. Dawa JA, Chaves SS, Nyawanda B, Njuguna HN, Makokha C, Otieno NA, et al. National burden of hospitalized and non-hospitalized influenza-associated severe acute respiratory illness in Kenya, 2012–2014. Influenza Other Respir Viruses. 2018;12:30–7. https://doi.org/10.1111/irv.12488
18. Emukule GO, Osoro E, Nyawanda BO, Ngere I, Macharia D, Bigogo G, et al. Healthcare-seeking behavior for respiratory illnesses in Kenya: implications for burden of disease estimation. BMC Public Health. 2023;23:353. https://doi.org/10.1186/s12889-023-15252-3
19. Katz MA, Lebo E, Emukule GO, Otieno N, Caselton DL, Bigogo G, et al. Uptake and effectiveness of a trivalent inactivated influenza vaccine in children in urban and rural Kenya, 2010 to 2012. Pediatr Infect Dis J. 2016;35:322–9. https://doi.org/10.1097/INF.0000000000001035
20. Boddington NL, Pearson I, Whitaker H, Mangtani P, Pebody RG. Effectiveness of influenza vaccination in preventing hospitalization due to influenza in children: a systematic review and meta-analysis. Clin Infect Dis. 2021;73:1722–32. https://doi.org/10.1093/cid/ciab270
21. World Health Organization. FluNet [cited 2022 Nov 1]. https://www.who.int/tools/flunet
22. Igboh LS, Roguski K, Marcenac P, Emukule GO, Charles MD, Tempia S, et al. Timing of seasonal influenza epidemics for 25 countries in Africa during 2010–19: a retrospective analysis. Lancet Glob Health. 2023;11:e729–39. https://doi.org/10.1016/S2214-109X(23)00109-2

23. World Health Organization. Vaccines against influenza: WHO position paper—May 2022. Wkly Epidemiol Rec. 2022;97:185–208.
24. Flasche S, Ojal J, Le Polain de Waroux O, Otiende M, O'Brien KL, Kiti M, et al. Assessing the efficiency of catch-up campaigns for the introduction of pneumococcal conjugate vaccine: a modelling study based on data from PCV10 introduction in Kilifi, Kenya. BMC Med. 2017;15:113. https://doi.org/10.1186/s12916-017-0882-9
25. Liku N, Mburu C, Lafond KE, Ebama M, Athman M, Swaleh S, et al. A qualitative assessment of influenza vaccine uptake among children in Kenya. Vaccine X. 2024;19:100507. https://doi.org/10.1016/j.jvacx.2024.100507
26. Alonso WJ, Yu C, Viboud C, Richard SA, Schuck-Paim C, Simonsen L, et al. A global map of hemispheric influenza vaccine recommendations based on local patterns of viral circulation. Sci Rep. 2015;5:17214. https://doi.org/10.1038/srep17214
27. Regan AK, Arriola CS, Couto P, Duca L, Loayza S, Nogareda F, et al. Severity of influenza illness by seasonal influenza vaccination status among hospitalised patients in four South American countries, 2013–19: a surveillance-based cohort study. Lancet Infect Dis. 2023;23:222–32. https://doi.org/10.1016/S1473-3099(22)00493-5
28. Cohen C, Kleynhans J, Moyes J, McMorrow ML, Treurnicht FK, Hellferscee O, et al.; PHIRST group. Asymptomatic transmission and high community burden of seasonal influenza in an urban and a rural community in South Africa, 2017–18 (PHIRST): a population cohort study. Lancet Glob Health. 2021;9:e863–74. https://doi.org/10.1016/S2214-109X(21)00141-8
29. Horby P, Mai Q, Fox A, Thai PQ, Thi Thu Yen N, Thanh T, et al. The epidemiology of interpandemic and pandemic influenza in Vietnam, 2007–2010: the Ha Nam household cohort study I. Am J Epidemiol. 2012;175:1062–74. https://doi.org/10.1093/aje/kws121
30. Tokars JI, Patel MM, Foppa IM, Reed C, Fry AM, Ferdinands JM. Waning of measured influenza vaccine effectiveness over time: the potential contribution of leaky vaccine effect. Clin Infect Dis. 2020;71:e633–41. https://doi.org/10.1093/cid/ciaa340
31. Macias AE, McElhaney JE, Chaves SS, Nealon J, Nunes MC, Samson SI, et al. The disease burden of influenza beyond respiratory illness. Vaccine. 2021;39(Suppl 1):A6–14. https://doi.org/10.1016/j.vaccine.2020.09.048
32. Chung JR, Flannery B, Gaglani M, Smith ME, Reis EC, Hickey RW, et al. Patterns of influenza vaccination and vaccine effectiveness among young US children who receive outpatient care for acute respiratory tract illness. JAMA Pediatr. 2020;174:705–13. https://doi.org/10.1001/jamapediatrics.2020.0372
33. Eichner M, Schwehm M, Eichner L, Gerlier L. Direct and indirect effects of influenza vaccination. BMC Infect Dis. 2017;17:308. https://doi.org/10.1186/s12879-017-2399-4
34. Newall AT, Nazareno AL, Muscatello DJ, Boettiger D, Viboud C, Simonsen L, et al. The association between influenza vaccination uptake and influenza and pneumonia-associated deaths in the United States. Vaccine. 2024;42:2044–50. https://doi.org/10.1016/j.vaccine.2024.01.089

Address for correspondence: G.O. Emukule, US Centers for Disease Control and Prevention, Village Market, PO Box 606-00621, Nairobi, Kenya; email: uyr9@cdc.gov

Fatal Oropouche Virus Infections in Nonendemic Region, Brazil, 2024

Antonio Carlos Bandeira, Felicidade Mota Pereira, Arabela Leal, Sara P.O. Santos, Ana Claudia Barbosa, Marcia Sao Pedro Leal Souza, Daniele Ribeiro de Souza, Natalia Guimaraes, Vagner Fonseca, Marta Giovanetti, Luiz Carlos Junior Alcantara, André Alvarez A. Lessa, Ramon Costa Saavedra, Luiz Marcelo R. Tomé, Felipe Campos M. Iani, Rivia Mary Barros, Sandra Maria O. Purificação, Jaciara Prado de Jesus, Ricardo Rosário Fonseca, Marcio Luis Valença Araújo

We report acute Oropouche virus infections in 2 previously healthy women from a nonendemic region of Brazil outside the Amazon Basin. Infections rapidly progressed to hemorrhagic manifestations and fatal outcomes in 4–5 days. These cases highlight the critical need for enhanced surveillance to clarify epidemiology of this neglected disease.

Oropouche virus (OROV), the etiologic agent of Oropouche fever, is an arbovirus that belongs to the *Orthobunyavirus* genus of the Peribunyaviridae family (*1*). Discovered in 1955 in Trinidad and Tobago, the virus subsequently was isolated from a pale-throated sloth (*Bradypus tridactylus*) in Brazil in 1960 (*2*,*3*). Transmission to humans in urban settings is thought to occur mainly through the bites of infected *Culicoides paraensis* midges (*4*).

In 2020, a few OROV cases were retrospectively detected in the Salvador metropolitan region, Bahia state, Brazil (*5*), and OROV was considered nonendemic that region. However, in March 2024, the Central Public Health Laboratory detected OROV in Bahia again (*6*). Since then, a major outbreak has erupted in parallel with increasing case numbers in Brazil (*6*), but severe outcomes have not been reported. We report 2 cases of Oropouche fever in Bahia that progressed to death.

The Study

We retrospectively collected clinical information by analyzing digital records and conducting an epidemiologic investigation to collect clinical and laboratory data. In addition, we conducted interviews with the medical teams who cared for the patients and investigated residents living in the same households as the case-patients. The study was approved by the Brazil National Research Ethics Commission (approval no. CAAE 81053724.6.0000.0052).

Patient 1 was a 24-year-old woman whose symptoms began with fever lasting 1 day, headache, retroorbital pain, myalgia, severe abdominal pain, diarrhea, nausea, and vomiting. She had no underlying conditions, was not pregnant, had no history of miscarriage, and was admitted 3 days after symptom onset due to worsening symptoms and blurred vision. She continued to report severe abdominal pain and hypoactivity and had ocular edema 7 hours after admission.

At 10 hours after admission, psychomotor agitation developed, and in the subsequent 2 hours the patient began to experience hypotension and desaturation. Clinicians introduced a Venturi mask at 8 liters of oxygen per minute, followed by orotracheal intubation, when bronchial hemorrhage was detected. One hour later, the patient progressed to cardiorespiratory arrest and died the next day, 13

Author affiliations: Laboratório Central de Saúde Pública da Bahia, Salvador, Brazil (A.C. Bandeira, F. Mota Pereira, A. Leal, S.P.O. Santos); Diretoria de Vigilância Epidemiológica do Estado da Bahia, Salvador (A.C. Barbosa, M.S.P.L. Souza, D.R. de Souza, A.A.A. Lessa, R.C. Saavedra, S.M. de Oliveira da Purificação, J.P. de Jesus, M.L.V. Araújo); Fundação Ezequiel Dias, Belo Horizonte, Brazil (N. Guimaraes, F.C.M. Iani); University of the State of Bahia, Salvador (V. Fonseca); Universita Campus Bio-Medico di Roma, Rome, Italy (M. Giovanetti); Oswaldo Cruz Institute, Oswaldo Cruz Foundation, Rio de Janeiro, Brazil (M. Giovanetti); Instituto Rene Rachou, Fundação Oswaldo Cruz, Minas Gerais, Brazil (L.C.J. Alcantara, L.M.R. Tomé); Superintendência de Vigilância em Saúde, Salvador (R.M. Barros); Santa Casa de Misericórdia de Valença Hospital, Valença, Brazil (R.R. Fonseca); Instituto Federal de Educação, Salvador (M.L.V. Araújo)

DOI: https://doi.org/10.3201/eid3011.241132

Table 1. Laboratory results for patient 1 in a case of fatal Oropouche virus infections in nonendemic region, Brazil, 2024*

Variable	Time after admission	
	6 hours	13 hours
Hematocrit, %	50.3	20.9
Hemoglobin, %	16.7	7.0
Mean corpuscular volume, fL (reference <80 fL)	82	88
Mean corpuscular hemoglobin, pg (reference 27–31 pg)	27	29
Leukocytes, cells/mm^3	44,700	24,500
Neutrophils, %	71	80
Band forms, %	8	10
Metamyelocytes, %	1	1
Lymphocytes, %	16	6
Platelets, cells/mm^3	125,000	43,000
Bleeding time, min	ND	1
Clotting time, min	ND	>30
Clot retraction	ND	Complete
Aspartate aminotransferase, U/L	ND	970
Alanine aminotransferase, U/L	7	404
GGT, U/L	559	144
TB/DB, mg/dL	2.78/1.52	ND
Creatinine, mg/dL	4.1	2.3

*GGT, gamma-glutamyl transferase; ND, not done; TB/DB, total bilirubin/direct bilirubin.

hours after admission. Samples collected at 6 hours and 13 hours after admission (4 days after symptom onset) showed rapid decline in hematocrit, thrombocytopenia, and prolongation of clotting time, as well as elevated liver enzymes and renal dysfunction (Table 1).

Patient 2, a 21-year-old woman, had fever, myalgia, headache, retroorbital pain, pain in the lower limbs, asthenia, and joint pain. After 4 days, a rash and purple spots on her body developed, as did nose, gum, and vaginal bleeding. The patient reported weakness, drowsiness, and vomiting. She had no underlying conditions, denied pregnancy or previous miscarriage, and was admitted to a local hospital. After 9 hours she was transferred to a secondary facility and appeared drowsy, had cyanosis of the extremities and persistent vomiting, and had not eaten in several days. On examination, she had bleeding gums and epistaxis, vaginal bleeding, and cold and clammy skin, in addition to widespread petechia. She died 2 hours later. Samples collected 5 days after symptom onset showed thrombocytopenia, prolongation of clotting and bleeding time, and renal dysfunction (Table 2). A household member retrospectively had Oropouche fever confirmed.

We used Extracta Kit DNA and RNA of Pathogens (Loccus, https://www.loccus.com.br) to extract genetic material from 200 µL of clinical samples, following manufacturer's instructions. Subsequently, we conducted real-time reverse transcription PCR (RT-PCR) reactions for different pathogens. We used inputs produced by the Institute of Molecular Biology of Paraná (IBMP) for quantitative RT-PCR (qRT-PCR) for OROV, as previously described (*7*).

To differentiate Oropouche diagnoses, we conducted RT-PCR for other pathogens. For Mayaro virus, we used RT-PCR techniques from IBMP (*7*). For *Leptospira*, we used an in-house RT-PCR method for detecting the lipL32 target gene. We used the ZC D-Typing Molecular Kit (Bio-Manguinhos, https://www.bio.fiocruz.br) for Zika, chikungunya, and dengue viruses. For *Hemophilus influenzae*, *Neisseria meningitidis*, and *Streptococcus pneumoniae*, we used the Viasure PCR Detection Kit (Certest Biotec, https://www.certest.es) (Table 3).

For serologic tests (Table 3), we used Panbio Dengue IgM Capture ELISA (Abbott Point of Care, https://www.globalpointofcare.abbott) for dengue virus (DENV); Anti-Chikungunya virus ELISA (IgM) (EUROIMMUN, https://www.euroimmun.com) for chikungunya; and Panbio Leptospira IgM (Abbott Point of Care) for *Leptospira*. For hepatitis viruses, we used serologic tests from Roche Diagnostics (https://diagnostics.roche.com), including Elecsys HBsAg II and Elecsys Total Anti-HBc II for hepatitis B, Elecsys Anti-HCV II for hepatitis C, and Elecsys Anti-HAV for hepatitis A and IgM. We used all kits in accordance with the manufacturers' guidelines.

We sequenced samples using the viral metagenomics approach, according to the SMART-9N protocol (*8*). Initially, we subjected samples to nucleic acid extraction for DNA and RNA and concentrated to 10 µL by using Zymo RNA Clean and Concentrator-5

Table 2. Laboratory test results for patient 2 in a case of fatal Oropouche virus infections in nonendemic region, Brazil, 2024*

Variable	Time after admission	
	At admission	10 hours
Hematocrit, %	38.7	43.7
Hemoglobin, %	13.5	14.0
Mean corpuscular volume, fL (reference <80 fL)	86	82
Mean corpuscular hemoglobin, pg (reference 27–31 pg)	30	26
Leukocytes, cells/mm^3	9,500	19,400
Neutrophils, %	59	58
Band forms, %	0	0
Metamyelocytes, %	0	0
Lymphocytes, %	34	36
Platelets, cells/mm^3	147,000	91,000
Prothrombin time, sec	ND	>120
Partial thromboplastin time, sec	ND	>120
Bleeding time, min	ND	5
Clotting time, min	ND	>30
TB/DB, mg/dL	ND	2.71/1.54
Creatinine, mg/dL	ND	3.6
NS1	Nonreactive	ND

*Patient was transferred to a second hospital after initial admission. ND, not done; NS1, rapid immunochromatographic test for dengue virus; TB/DB, total/direct bilirubin.

Table 3. Molecular biology and serologic test results in 2 cases of fatal Oropouche virus infection in nonendemic region, Brazil, 2024*

Laboratory test	Patient 1	Patient 2
qRT-PCR		
Dengue virus	Undetectable	Undetectable
Chikungunya virus	Undetectable	Undetectable
Zika virus	Undetectable	Undetectable
Mayaro virus	Undetectable	Undetectable
Oropouche virus, Ct value	Detectable, 16	Detectable, 8
qPCR		
Leptospira	Not done	Undetectable
Neisseria meningitidis	Undetectable	Undetectable
Streptococcus pneumoniae	Undetectable	Undetectable
Hemophilus influenzae	Undetectable	Undetectable
Serology		
Dengue virus IgM	Nonreactive	Nonreactive
Leptospira IgM	Nonreactive	Nonreactive
Chikungunya virus IgM	Nonreactive	Nonreactive
Hepatitis C virus IgG, IgM	Not done	Nonreactive
Hepatitis B virus IgG, IgM	Not done	Nonreactive
Hepatitis A virus IgG, IgM	Not done	Nonreactive

*Performed in serum samples, except for *Leptospira* qPCR, which was performed on whole blood. Patient 1 samples collected 4 days after symptom onset; patient 2 samples collected 5 days after symptom onset. Ct, cycle threshold; qPCR, quantitative PCR; qRT-PCR, quantitative reverse transcription PCR.

(Zymo Research, https://www.zymoresearch.com). Next, we performed cDNA synthesis by using SuperScript IV Reverse Transcriptase (Thermo Fisher Scientific, https://www.thermofisher.com) and random primers RLB RT 9N and RLB TSO synthesized in-house (I.C. Morales, unpub. data, https://doi.org/10.17504/protocols.io.7w5hpg6). We prepared the sequencing library by using the Ligation Sequencing Kit (SQK-LSK109) and Native Barcoding Kit (Oxford Nanopore Technologies [ONT], https://nanoporetech.com). We loaded the final 60-ng library onto an R9.4.1 flow cell (ONT) and sequenced for 24 hours on the MinION nanopore sequencer (ONT). We used the Genome Detective pipeline (https://www.genomedetective.com) to assemble raw reads. We aligned all sequences by using MAFFT (*9*) and manually edited by using AliView (*10*). To explore the relationship between the sequenced genomes obtained in this study and those sampled globally, we constructed maximum-likelihood phylogenies for the small, medium, and large segments by using IQ-TREE 2 software under the Hasegawa-Kishino-Yano plus gamma 4 substitution model (*11*).

Sequencing the complete genome enabled generation of complete genomes of 3 segments. Analysis revealed that the genomes clustered with sequences recently isolated from the northern part of Brazil (F. Naveca et al., unpub. data, https://doi.org/10.1101/2024.07.23.24310415) (Figure). We did not identify any novel mutations. However, we plan further comparisons during this ongoing outbreak to check for point mutations.

Conclusions

By March 2024, an OROV outbreak was spreading in Bolivia, Colombia, Peru, and Cuba, and >7,800 cases were detected in Brazil (*12*). However, the clinical course of the 2 cases we describe highlights the possibility for rapid evolution from symptom onset to death in 4–5 days. In addition, severe coagulopathy was the probable mechanism that led to death, and

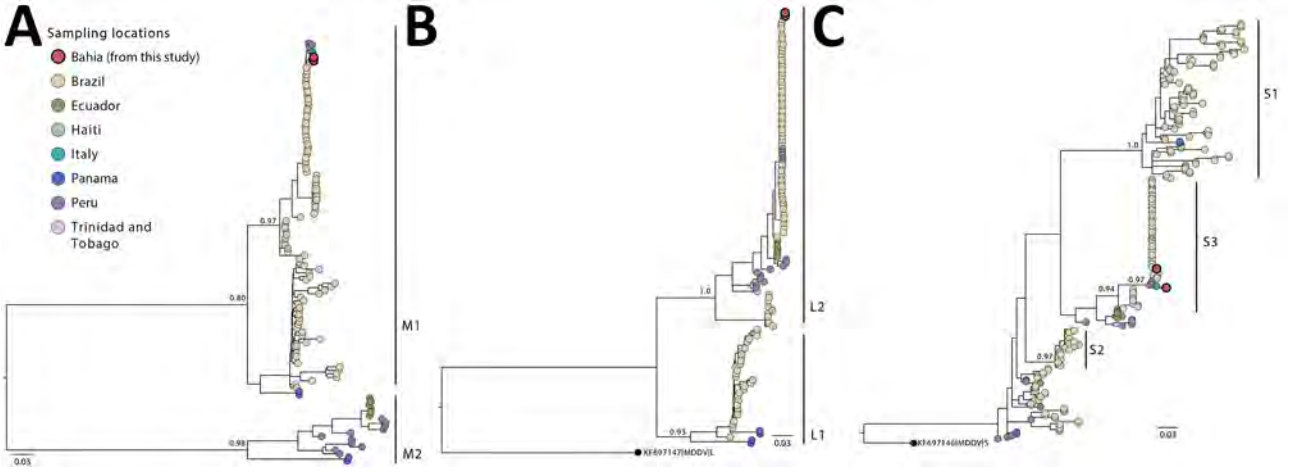

Figure. Maximum-likelihood phylogenetic trees of the 3 independent OROV segments from fatal Oropouche virus infections in nonendemic region, Brazil, 2024. A) Medium segment (n = 122); B) large segment (n = 138); C) small segment (n = 264). Tips of prototypical viruses and major clusters are color-coded according to locations of isolation. The trees included annotations indicating the bootstrap probability support for both major lineages and specific clades. Trees were constructed by using IQ-TREE 2 software under the Hasegawa-Kishino-Yano plus gamma 4 substitution model (*11*). MDDV was included as an outgroup in the large and small segment trees. Scale bars indicate nucleotide substitutions per site. MDDV, Madre de Dios virus; OROV, Oropouche virus.

we observed evidence of liver and kidney involvement that may have contributed to the coagulopathy and, consequently, to death.

One previous study observed hemorrhagic phenomena in 20 patients (15.5% of the sample) but did not present laboratory data (*13*). Another study demonstrated that OROV could be detected in the liver 6 hours after OROV was intracerebrally inoculated into 3-week-old hamsters (*14*), suggesting hematogenous virus transmission from the brain to liver lesions and substantial hepatocyte necrosis.

In both cases we describe, the clinical course was remarkably like that of severe dengue, but the mechanisms that triggered the events leading to death remain unknown. Our 2 case-patients did not share any family or household links, lived in different cities, and did not have any underlying conditions that would increase their risks for severe disease. Furthermore, coinfection with DENV is unlikely because the RT-PCR we used has a 97.3%–100% specificity for DENV, and having 2 undetected dengue cases by that assay is unlikely. Finally, we sequenced the samples using viral metagenomics and only identified OROV.

In conclusion, we describe clinical and laboratory findings and phylogeny from 2 fatal cases of OROV infection in the nonendemic region of Bahia, Brazil. An OROV outbreak continues to expand in the Americas, and our findings underscore the urgent need to clarify the pathophysiology of this neglected disease.

This article was preprinted at https://doi.org/10.1590/SciELOPreprints.9342.

Acknowledgments

We thank the Bahia state health professionals for their support during the investigation.

This work received financial support from the National Council for Scientific and Technological Development-CNPq (grant no. 306306/2021-2) and financial support from notice no. 20/2023/PRPGI/IFBA. This study was also supported by the National Institutes of Health, Bethesda, Maryland, USA (grant no. U01 AI151698 for the United World Arbovirus Research Network [UWARN]), and by the International Centre for Genetic Engineering and Biotechnology Research Grant 2020 Project CRP/BRA20-03 (contract no. CRP/20/03).

About the Author

Dr. Bandeira is an infectious diseases medical advisor at the Central Laboratory of the State of Bahia, Bahia, Brazil. His research interest is in integrating clinical expertise for the diagnosis of emerging diseases.

References

1. Sakkas H, Bozidis P, Franks A, Papadopoulou C. Oropouche fever: a review. Viruses. 2018;10:175. https://doi.org/10.3390/v10040175
2. Moreira HM, Sgorlon G, Queiroz JAS, Roca TP, Ribeiro J, Teixeira KS, et al. Outbreak of Oropouche virus in frontier regions in western Amazon. Microbiol Spectr. 2024;12:e0162923. https://doi.org/10.1128/spectrum.01629-23
3. Pinheiro F, Pinheiro M, Bensabath G, Causey OR, Shope RE. Oropouche virus epidemic in Bethlehem [in Tetum]. Revista do Serviço Especial de Saude Publica. 1962;12:13–23.
4. Pereira CS, Picanço MRS, Vale GP, Oliveira CS, Amorim FAS, Costa FS, et al. Epidemiology, diagnosis and treatment of Oropouche fever in Brazil: a literature review [in Portuguese]. Brazilian J Health Rev. 2021;4:23912–20. https://doi.org/10.34119/bjhrv4n6-023
5. Fonseca LMDS, Carvalho RH, Bandeira AC, Sardi SI, Campos GS. Oropouche virus detection in febrile patients' saliva and urine samples in Salvador, Bahia, Brazil. Jpn J Infect Dis. 2020;73:164–5. https://doi.org/10.7883/yoken.JJID.2019.296
6. Lorenz C, Chiaravalloti-Neto F. Brazil reports an increased incidence of Oropouche and Mayaro fever in the Amazon region. Travel Med Infect Dis. 2024;58:102692. https://doi.org/10.1016/j.tmaid.2024.102692
7. Naveca FG, Nascimento VAD, Souza VC, Nunes BTD, Rodrigues DSG, Vasconcelos PFDC. Multiplexed reverse transcription real-time polymerase chain reaction for simultaneous detection of Mayaro, Oropouche, and Oropouche-like viruses. Mem Inst Oswaldo Cruz. 2017;112:510–3. https://doi.org/10.1590/0074-02760160062
8. Claro IM, Ramundo MS, Coletti TM, da Silva CAM, Valenca IN, Candido DS, et al. Rapid viral metagenomics using SMART-9N amplification and nanopore sequencing. Wellcome Open Res. 2021;6:241. https://doi.org/10.12688/wellcomeopenres.17170.2
9. Katoh K, Rozewicki J, Yamada KD. MAFFT online service: multiple sequence alignment, interactive sequence choice and visualization. Brief Bioinform. 2019;20:1160–6. https://doi.org/10.1093/bib/bbx108
10. Larsson A. AliView: a fast and lightweight alignment viewer and editor for large datasets. Bioinformatics. 2014;30:3276–8. https://doi.org/10.1093/bioinformatics/btu531
11. Nguyen L-T, Schmidt HA, von Haeseler A, Minh BQ. IQ-TREE: a fast and effective stochastic algorithm for estimating maximum-likelihood phylogenies. Mol Biol Evol. 2015;32:268–74. https://doi.org/10.1093/molbev/msu300
12. Brazilian Ministry of Health. Oropouche [cited 2024 Aug 27]. https://app.powerbi.com/view?r=eyJrIjoiMzc0Mzg3NjMtMzBiNy00ODhhLWJhNmItZmYzYWM4ZjUxN2Q0IiwidCI6IjlhNTU0YWQzLWI1MmItNDg2Mi1hMzZmLTg0ZDg5MWU1YzcwNSJ9

13. Mourão MPG, Bastos MS, Gimaqu JBL, Mota BR, Souza GS, Grimmer GHN, et al. Oropouche fever outbreak, Manaus, Brazil, 2007–2008. Emerg Infect Dis. 2009;15:2063–4. https://doi.org/10.3201/eid1512.090917
14. Araújo R, Dias LB, Araújo MT, Pinheiro F, Oliva OF. Ultrastructural changes in the hamster liver after experimental inoculation with Oropouche arbovirus (type BeAn 19991) [in Portuguese]. Rev Inst Med Trop Sao Paulo. 1978;20:45–54.

Address for correspondence: Marcio Araújo, Federal Institute of Education Science and Technology of Bahia, IT, R. São Cristóvão, Novo Horizonte, Lauro de Freitas, Salvador, Bahia 42700-000, Brazil; email: marcioaraujo@ifba.edu.br

Co-Circulation of 2 Oropouche Virus Lineages, Amazon Basin, Colombia, 2024

Jaime Usuga,[1] Daniel Limonta,[1] Laura S. Perez-Restrepo, Karl A. Ciuoderis, Isabel Moreno, Angela Arevalo, Vanessa Vargas, Michael G. Berg, Gavin A. Cloherty, Juan P. Hernandez-Ortiz, Jorge E. Osorio

In early 2024, explosive outbreaks of Oropouche virus (OROV) linked to a novel lineage were documented in the Amazon Region of Brazil. We report the introduction of this lineage into Colombia and its co-circulation with another OROV lineage. Continued surveillance is needed to prevent further spread of OROV in the Americas.

Oropouche virus (OROV; *Orthobunyavirus oropoucheense*) is a reemerging arbovirus belonging to the family Peribunyaviridae. The large (L), medium (M), and small (S) single-stranded, negative-sense RNA segments of the OROV genome are susceptible to reassortments (*1*). Besides acute fever, OROV can cause meningitis and encephalitis. Although *Culicoides paraensis* biting midges are the main vector for OROV in urban cycles, different insect species are vectors in sylvatic cycles. Vertebrates, such as primates, small mammals, and possibly birds, are reservoir hosts (*1*,*2*).

OROV has spread rapidly in South America, causing >500,000 human infections (*2*,*3*). Most OROV cases have occurred in the Amazon in Brazil, where explosive outbreaks, sometimes affecting thousands of inhabitants, have been reported since OROV was identified in Trinidad and Tobago in 1955 (*2*,*4*,*5*). During 2019–2021, OROV was responsible for >10% and dengue virus (DENV) for 20% of acute febrile illness cases at 4 sites in Colombia: Cúcuta, Cali, Villavicencio, and Leticia (*6*). Phylogenetic analysis revealed 2 separate OROV introductions into those sites in Colombia from bordering Ecuador or Peru (*6*).

In early February 2024, the Pan American Health Organization and World Health Organization issued an epidemiologic alert because of the dramatic increase in OROV cases in 4 states within the Amazon Region of Brazil (*7*). The state of Amazonas, Brazil, alone had >1,000 quantitative reverse transcription PCR (qRT-PCR)–confirmed cases reported during 2023–January 2024 (*8*). After analyzing hundreds of full-length genomes isolated during the large-scale OROV outbreak in Brazil, multiple reassortment events were identified, indicating a new OROV lineage, BR-2015-2024 (*9*; F.C.M. Iani et al., unpub. data, https://doi.org/10.1101/2024.08.02.24311415). We report human OROV cases in Colombia caused by the novel BR-2015-2024 lineage, which is co-circulating with another previously characterized OROV lineage (*6*). The protocol for this study was approved by the ethics committee of the Corporación para Investigaciones Biológicas (protocol no. SC-6230-1).

The Study

In early January 2024, health authorities noticed a slight increase in acute febrile cases in Leticia municipality, which has >53,000 inhabitants, in the Amazonas department of Colombia. A total of 117 persons reporting chills (94.6%), headache (87.2%), arthralgia (65%), myalgia (41%), diarrhea (34.2%), fatigue (33.3%), and rash (6%) were treated at the emergency room of a Leticia hospital during a 5-week period. Although fever (≥38.5°C) was confirmed at the doctor's office in >46% of patients, <3% had respiratory symptoms. No hemorrhagic manifestations were

Author affiliations: National University of Colombia, Medellin, Colombia (J. Usuga, L.S. Perez-Restrepo, K.A. Ciuoderis, I. Moreno, A. Arevalo, V. Vargas, J.P. Hernandez-Ortiz, J.E. Osorio); University of Wisconsin, Madison, Wisconsin, USA (D. Limonta, K.A. Ciuoderis, J.E. Osorio); Abbott Diagnostics/Abbott Pandemic Defense Coalition, Abbott Park, Illinois, USA (M.G. Berg, G.A. Cloherty)

DOI: https://doi.org/10.3201/eid3011.240405

[1]These first authors contributed equally to this article.

observed in the febrile patients, and severe illnesses or hospitalizations were not reported. Patients were 7–92 years of age; 60 were male and 57 female. After obtaining written consent from adults and the children's parents or legal guardians, hospital staff collected serum samples.

Frozen serum samples were shipped by air >1,300 km to One Health Colombia in Medellin, Colombia, a center established by the Global Health Institute at the University of Wisconsin, Madison (Madison, WI, USA), and the National University of Colombia-Medellin. According to center guidelines at One Health Colombia (*6*), we tested the serum samples for Zika virus (ZIKV), Mayaro virus (MAYV), chikungunya virus, DENV, OROV, hepatitis B and C viruses, *Leptospira* spp., and *Plasmodium* spp. (Appendix Table 1, https://wwwnc.cdc.gov/EID/article/30/11/24-0405-App1.pdf).

We detected the DENV genome in 8 samples by using the Zika, chikungunya, and dengue virus Trioplex real-time qRT-PCR (Appendix Table 1); 4 samples were positive for the DENV nonstructural protein 1, and 3 samples were positive for DENV IgM. The study population (n = 117) had a high DENV IgG prevalence of 77.7%. All samples were negative for ZIKV, CHIKV, and MAYV RNA. We detected *Plasmodium* spp. DNA in 7 samples by quantitative PCR, and 5 samples were positive for the *P. vivax* antigen. No samples were positive for hepatitis B virus surface antigen, hepatitis C virus antibody, or *Leptospira* spp. DNA.

Using an OROV qRT-PCR designed at One Health Colombia (*6*), we detected OROV L and M segment RNA

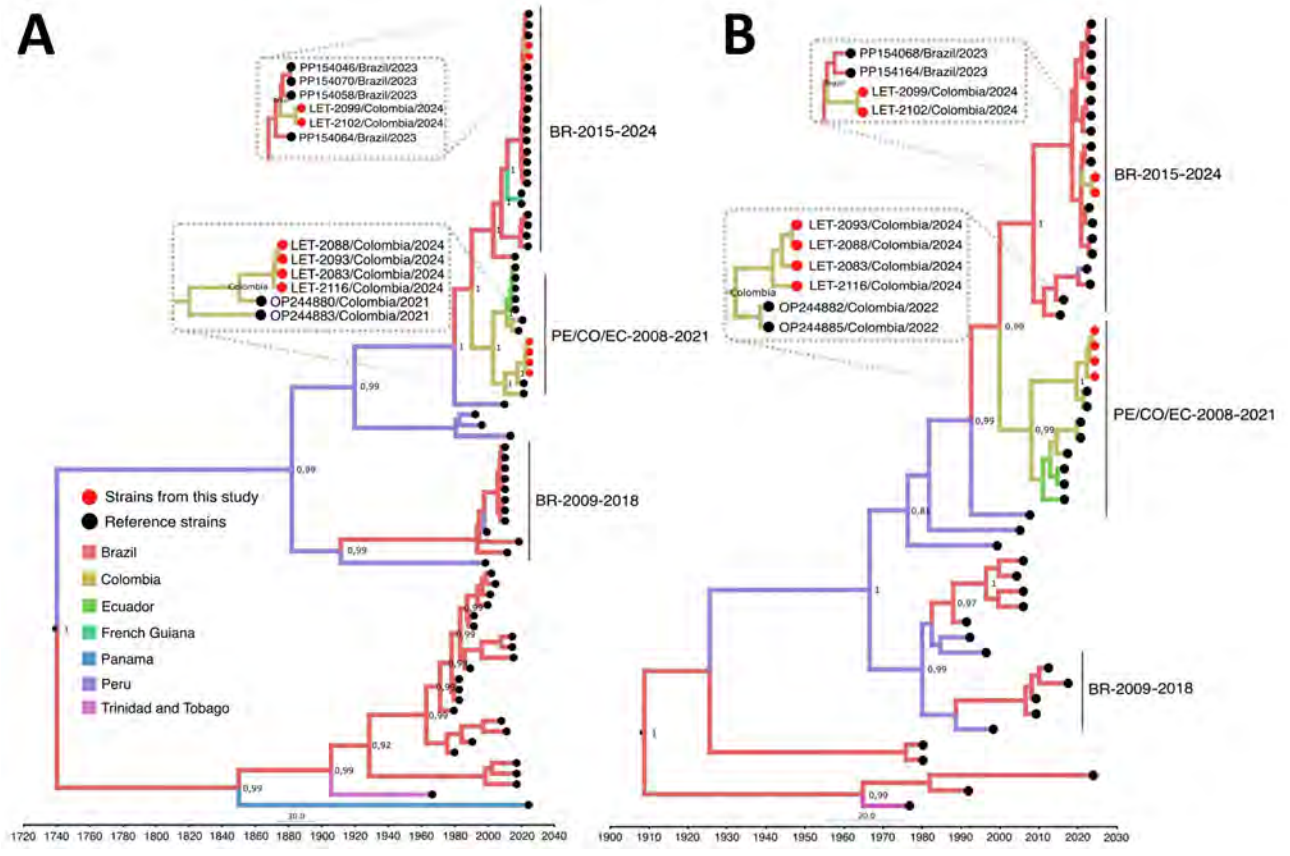

Figure 1. Time-scaled Bayesian phylogeographic analysis of large and small segments of co-circulating Oropouche virus lineages, Amazon Basin, Colombia, 2024. Bayesian phylogenetic trees of large (A) and small (B) gene segments were estimated by using the Bayesian Markov chain Monte Carlo method (>100 million generations) in Beast (https://beast.community) and ModelFinder in IQ-TREE (http://www.iqtree.org) (ultrafast bootstrapping and 1,000 replicates). Red solid circles indicate viruses from this study that begin with LET for Leticia, Colombia. Phylogeny branches are colored according to their descendant place of origin. Best-fit model was selected according to Bayesian information criteria, and a strict molecular clock model was used. Bayesian posterior values (≥0.8) are annotated at specific nodes of the trees. Sequences from this study were compared with reference sequences from other studies. Main clusters are indicated by using the following reference labels: BR-2015-2024 cluster represents the recent outbreak of the new OROV lineage in Brazil during 2015–2024; PE/CO/EC-2008-2021 cluster represents sequences from Colombia, Peru, and Ecuador during 2008–2021; and BR-2009-2018 cluster represents sequences from Brazil during 2009–2018. Scale bar indicates nucleotide substitutions per site.

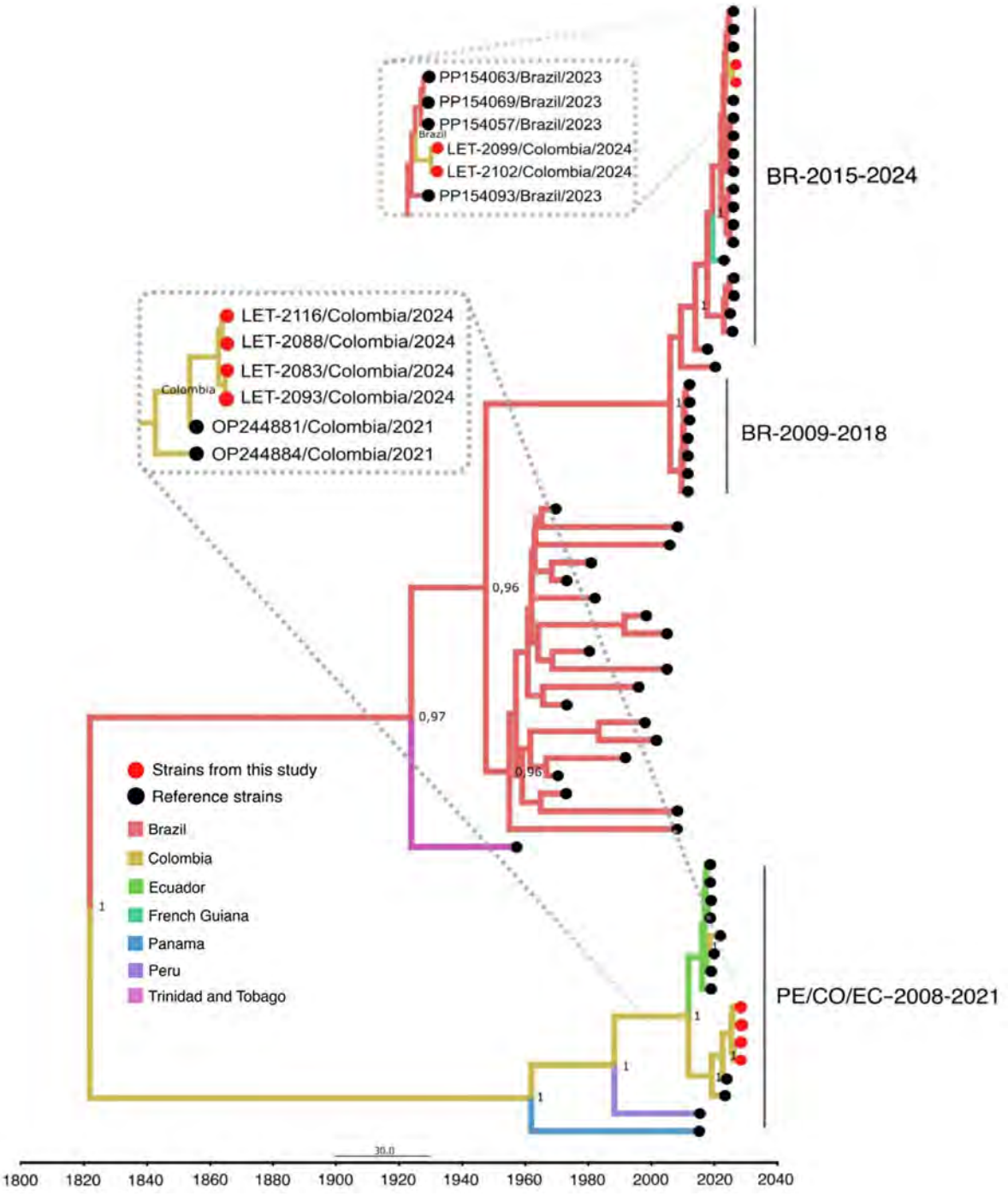

Figure 2. Time-scaled Bayesian phylogeographic analysis of medium segments of co-circulating Oropouche virus lineages, Amazon Basin, Colombia, 2024. Bayesian phylogenetic tree of medium gene segments were estimated by using the Bayesian Markov chain Monte Carlo method (>100 million generations) in Beast (https://beast.community) and ModelFinder in IQ-TREE (http://www.iqtree.org) (ultrafast bootstrapping and 1,000 replicates). Red solid circles indicate viruses from this study that begin with LET for Leticia, Colombia. Phylogeny branches are colored according to their descendant place of origin. Best-fit model was selected according to Bayesian information criteria, and uncorrelated relaxed molecular clock model was used. Bayesian posterior values (≥0.8) are annotated at specific nodes of the trees. Sequences from this study were compared with reference sequences from other studies. Main clusters are indicated by using the following reference labels: BR-2015-2024 cluster represents the recent outbreak of the new OROV lineage in Brazil during 2015–2024; PE/CO/EC-2008-2021 cluster represents sequences from Colombia, Peru, and Ecuador during 2008–2021; and BR-2009-2018 cluster represents sequences from Brazil during 2009–2018. Scale bar indicates nucleotide substitutions per site.

Figure 3. Leticia municipality and Three Borders (Colombia, Peru, and Brazil) region in study of co-circulation of 2 Oropouche virus lineages, Amazon Basin, Colombia, 2024. Symbols indicate residential locations of 8 patients infected with OROV in Leticia municipality. Colored circles and diamonds indicate patients infected with each OROV lineage. Macedonia, Vereda Santa Sofia, Santa Rosa de Yavari, and Tabatinga correspond to indigenous communities or cities. Map was created by using QGIS 3.36.0 RC (https://www.qgis.org). OROV, Oropouche virus.

in 8 samples. We conducted next generation sequencing by using metagenomic and target enrichment approaches for those 8 serum specimens, as described previously (*6*). We conducted phylogenetic analysis of the OROV L, M, and S segments isolated from patient samples by using available OROV genomes and sequences of the new clade from Brazil. OROV BR-2015-2024 from Brazil (*9*; F.C.M. Iani et al., unpub. data) was present in 2 samples from Leticia municipality, designated as LET-2099 and LET-2102 (Figures 1, 2). Although the L and S segments of those 2 OROV samples each branched as paraphyletic clades basal to OROV PE/CO/EC-2008-2021, the M segment sequences were more closely related to OROV BR-2009-2018 sequences.

Table. Characteristics of 8 human febrile cases of OROV infection in study of co-circulation of 2 Oropouche virus lineages, Amazon Basin, Colombia, 2024*

ID no.	Age, y/sex	Symptom onset date	Sampling date	Ct value	OROV clade
LET-2040	27/M	2024 Jan 16	2024 Jan 19	32.9	PE/CO/EC-2008-2021
LET-2083	23/M	2024 Feb 1	2024 Feb 5	28.6	PE/CO/EC-2008-2021
LET-2088	22/M	2024 Feb 4	2024 Feb 6	31.5	PE/CO/EC-2008-2021
LET-2093	15/F	2024 Feb 5	2024 Feb 8	33.2	PE/CO/EC-2008-2021
LET-2099	24/M	2024 Feb 8	2024 Feb 12	28.7	BR-2015-2024
LET-2102	27/M	2024 Feb 11	2024 Feb 13	30.1	BR-2015-2024
LET-2116	49/F	2024 Feb 13	2024 Feb 15	34.2	PE/CO/EC-2008-2021
LET-2117	66/F	2024 Feb 10	2024 Feb 15	34.4	PE/CO/EC-2008-2021

*OROV was detected in serum samples by using quantitative reverse transcription PCR, and Ct values were determined. Ct, cycle threshold; ID, identification; LET, Leticia; OROV, Oropouche virus.

Amino acid changes within lineage BR-2015-2024 indicated multiple mutations in L and M segments when compared with those in ancestral virus strains (Appendix Figure). In addition, in 6 of the 8 samples, we detected the OROV PE/CO/EC-2008-2021 lineage, which circulated in Colombia during 2019–2021 (Table) (*6*). The 8 OROV-positive patients did not exhibit co-infections with the other tested organisms, aside from clinical manifestations of acute undifferentiated fever (Appendix Table 2), and they had not traveled outside of Leticia municipality or its surrounding areas in the 2 weeks before symptom onset (Figure 3). We deposited 6 full-length OROV genomes analyzed in this study, including the 2 novel OROV lineages, into GenBank (accession nos. PP477303–20).

We report the circulation of the novel orthobunyavirus, OROV BR-2015-2024, in Colombia that has been documented in Brazil. The numerous mutations in OROV BR-2015-2024 RNA-dependent RNA polymerase and glycoproteins likely enhanced replication and immune evasion capabilities, increasing virus fitness and transmission. In addition, we detected co-circulation of OROV PE/CO/EC-2008-2021 lineage (*6*) in 6 patients. The identification of co-circulating strains of OROV exemplifies the evolving nature of orthobunyaviruses and raises concerns about future reassortment events and emergence of new lineages having more severe clinical phenotypes and enhanced vector competence. In an arbovirus hotspot, such as Leticia, it is unknown if cross-protective immunity will exist between the 2 OROV lineages. Previously, a reassortant OROV isolated from outbreaks in Iquitos, the largest city in the Amazon of Peru, provided limited cross-protection against a different OROV strain (*10*).

Leticia municipality, in the southernmost region in Colombia (Figure 3), remains isolated from the rest of Colombia's road network, and travelers typically reach Leticia by aircraft. Leticia city, the capital of Amazonas department of Colombia, is in Leticia municipality, where the borders of Colombia, Brazil, and Peru converge, forming an area known as the Three Borders. Tabatinga city, in the state of Amazonas in Brazil, is located across from Leticia city, forming a unique suburban area near Santa Rosa de Yavarí, Peru, which is on an island in the Amazon River (*11*). The new OROV lineage is likely spreading rapidly in those borderlands because of the considerable human mobility related to local businesses. Furthermore, we believe that the novel OROV lineage in Leticia came from either a nearby settlement or air travelers from the Amazon in Brazil, where persistent outbreaks are occurring.

Conclusions

One Health Colombia has previously reported outbreaks of ZIKV (*12*), DENV (*13*), OROV (*6*), and, in 2024, MAYV (*14*) in Colombia, which underscores the dynamic landscape of reemerging arboviruses in the region. The sustained transmission of established strains and the unpredictable reassortment events of OROVs causing outbreaks is yet another demonstration of the public health challenges associated with prevention and control of arbovirus reemergence in South America. Continued surveillance and molecular characterization of OROV and other arboviruses are needed to prevent the spread of arboviral diseases in the Americas.

Acknowledgments

We thank the clinical and laboratory staff at the Hospital San Rafael de Leticia and Fundación Clínica Leticia for their participation in our study; the staff of One Health Colombia, particularly the laboratory personnel, for their support of this work; Fundación Fraternidad Medellin and Fundación Sofia Perez de Soto for their unwavering support for One Health PhD awards; and Celeny Ortiz Restrepo for generating the map of Leticia municipality in the Amazon Basin, Colombia.

This research was supported by the Global Health Institute of the University of Wisconsin-Madison, the National University of Colombia-Medellin, and the virus discovery research program of the Abbott Pandemic Defense Coalition.

About the Author

Mr. Usuga is a research scientist and bioinformatician at the One Health Colombia center at the National University of Colombia in Medellin. His research interests focus on data modeling, genomics, and molecular epidemiology of emerging and reemerging viral diseases.

References

1. Wesselmann KM, Postigo-Hidalgo I, Pezzi L, de Oliveira-Filho EF, Fischer C, de Lamballerie X, et al. Emergence of Oropouche fever in Latin America: a narrative review. Lancet Infect Dis. 2024;24:e439–52. https://doi.org/10.1016/S1473-3099(23)00740-5
2. Pinheiro FP, Travassos da Rosa AP, Travassos da Rosa JF, Ishak R, Freitas RB, Gomes ML, et al. Oropouche virus. I. A review of clinical, epidemiological, and ecological findings. Am J Trop Med Hyg. 1981;30:149–60. https://doi.org/10.4269/ajtmh.1981.30.149
3. Forshey BM, Guevara C, Laguna-Torres VA, Cespedes M, Vargas J, Gianella A, et al.; NMRCD Febrile Surveillance Working Group. Arboviral etiologies of acute febrile illnesses in western South America, 2000–2007. PLoS Negl Trop Dis. 2010;4:e787. https://doi.org/10.1371/journal.pntd.0000787

4. Anderson CR, Spence L, Downs WG, Aitken TH. Oropouche virus: a new human disease agent from Trinidad, West Indies. Am J Trop Med Hyg. 1961;10:574–8. https://doi.org/10.4269/ajtmh.1961.10.574
5. Azevedo RSS, Nunes MR, Chiang JO, Bensabath G, Vasconcelos HB, Pinto AY, et al. Reemergence of Oropouche fever, northern Brazil. Emerg Infect Dis. 2007;13:912–5. https://doi.org/10.3201/eid1306.061114
6. Ciuoderis KA, Berg MG, Perez LJ, Hadji A, Perez-Restrepo LS, Aristizabal LC, et al. Oropouche virus as an emerging cause of acute febrile illness in Colombia. Emerg Microbes Infect. 2022;11:2645–57. https://doi.org/10.1080/22221751.2022.2136536
7. Pan American Health Organization, World Health Organization. Epidemiological alert—Oropouche in the Region of the Americas—2 February 2024 [cited 2024 Mar 10]. https://www.paho.org/en/documents/epidemiological-alert-oropouche-region-americas-2-february-2024
8. Pan American Health Organization, World Health Organization. Public health risk assessment related to Oropouche virus (OROV) in the Region of the Americas—9 February 2024 [cited 2024 Mar 10]. https://www.paho.org/en/documents/public-health-risk-assessment-related-oropouche-virus-orov-region-americas-9-february
9. Naveca FG, de Almeida TAP, Souza V, Nascimento V, Silva D, Nascimento F, et al. Human outbreaks of a novel reassortant Oropouche virus in the Brazilian Amazon region Nat Med. 2024 Sep 18 [Epub ahead of print]. https://doi.org/10.1038/s41591-024-03300-3
10. Aguilar PV, Barrett AD, Saeed MF, Watts DM, Russell K, Guevara C, et al. Iquitos virus: a novel reassortant *Orthobunyavirus* associated with human illness in Peru. PLoS Negl Trop Dis. 2011;5:e1315. https://doi.org/10.1371/journal.pntd.0001315
11. Farnsworth-Alvear A, Palacios M, López AMG, editors. The Colombia reader: history, culture, politics. Durham (NC): Duke University Press; 2016.
12. Camacho E, Paternina-Gomez M, Blanco PJ, Osorio JE, Aliota MT. Detection of autochthonous Zika virus transmission in Sincelejo, Colombia. Emerg Infect Dis. 2016;22:927–9. https://doi.org/10.3201/eid2205.160023
13. Ciuoderis KA, Usuga J, Moreno I, Perez-Restrepo LS, Flórez DY, Cardona A, et al. Characterization of dengue virus serotype 2 cosmopolitan genotype circulating in Colombia. Am J Trop Med Hyg. 2023;109:1298–302. https://doi.org/10.4269/ajtmh.23-0375
14. Perez-Restrepo LS, Ciuoderis K, Usuga J, Moreno I, Vargas V, Arévalo-Arbelaez AJ, et al. Mayaro virus as the cause of acute febrile illness in the Colombian Amazon Basin. Front Microbiol. 2024;15:1419637. https://doi.org/10.3389/fmicb.2024.1419637

Address for correspondence: Jorge E. Osorio, Global Health Institute, University of Wisconsin, 1050 MSC, 1300 University Ave, Madison, WI 53706, USA; email: jorge.osorio@wisc.edu

etymologia revisited

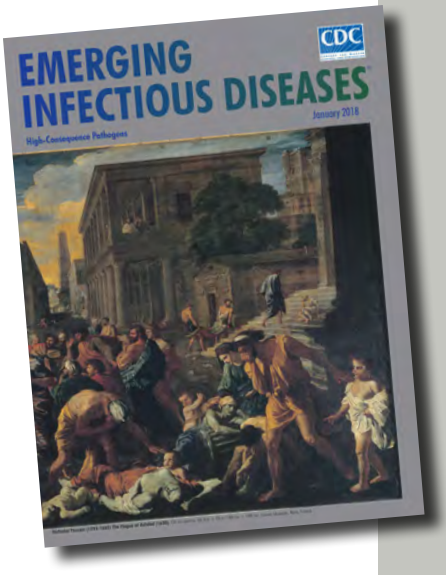

Originally published in January 2018

Plague
[plāg]

Plague (from the Latin *plaga*, "stroke" or "wound") infections are believed to have been common since at least 3000 BCE. Plague is caused by the ancestor of current *Yersinia* (named for Swiss bacteriologist Alexandre Yersin, who first isolated the bacterium) *pestis* strains. However, this ancestral *Y. pestis* lacked the critical *Yersinia* murine toxin (*ymt*) gene that enables vectorborne transmission. After acquiring this gene (sometime during 1600–950 BCE), which encodes a phospholipase D that protects the bacterium inside the flea gut, *Y. pestis* evolved the ability to cause pandemics of bubonic plague. The first recoded of these, the Justinian Plague, began in 541 ACE and eventually killed more than 25 million persons.

References:

1. Alexandre Yersin BW. Etymologia: yersinia. Emerg Infect Dis. 2010;16:496.
2. Centers for Disease Control and Prevention. History of plague [cited 2017 Oct 19]. https://www.cdc.gov/plague/history/index.html.
3. Rasmussen S, Allentoft ME, Nielsen K, Orlando L, Sikora M, Sjögren K-G, et al. Early divergent strains of Yersinia pestis in Eurasia 5,000 years ago. Cell. 2015;163:571–82.

https://wwwnc.cdc.gov/eid/article/24/1/et-2401_article

Analysis of Monkeypox Virus Exposures and Lesions by Anatomic Site

Sarah Anne J. Guagliardo, Teresa Smith, Davidson H. Hamer, Ralph Huits, Phyllis Kozarsky, Michael Libman, Andrea M. McCollum, Kristina M. Angelo, GeoSentinel Network Collaborators[1]

We used cross-sectional data from 226 patients with monkeypox virus to investigate the association between anatomic exposure site and lesion development. Penile, anorectal, and oral exposures predicted lesion presence at correlating anatomic sites. Exposure site also predicted the first lesion site of the penis and anus.

Monkeypox virus (MPXV) can be transmitted from person-to-person through contact with mucous membranes, percutaneous exposures, or, less commonly, inhalation of infectious particles (*1*). In the 2022 global clade II mpox outbreak, most transmission was associated with sexual contact, particularly among men who have sex with men (*2*).

MPXV lesions begin as macules and papules and progress to vesicles and pustules (*3*). Lesions crust over and heal within 2–4 weeks (*4*). In recent outbreaks, a high prevalence and early appearance of anogenital lesions has been observed (*2*,*5*). A hypothesis that a rash will occur at the inoculation site has been proposed (*3*), yet the relationship between exposures and lesion site has not been studied in published literature to date.

GeoSentinel, a global epidemiologic surveillance network, collected data on 226 patients with MPXV in 2022. We used those data to evaluate the correlation between exposures and lesion presence, site of first appearance, and the number of lesions by anatomic site.

Author affiliations: Centers for Disease Control and Prevention, Atlanta, Georgia, USA (S.A.J. Guagliardo, T. Smith, A.M. McCollum, K.M. Angelo); Boston University Chobanian & Avedisian School of Medicine, Boston, Massachusetts, USA (D.H. Hamer); Boston University Center on Emerging Infectious Diseases, Boston (D.H. Hamer); IRCCS Sacro Cuore Don Calabria Hospital, Verona, Italy (R. Huits); Emory University, Atlanta (P. Kozarsky); McGill University Health Centre, Montreal, Quebec, Canada (M. Libman)

DOI: https://doi.org/10.3201/eid3011.241120

The Study

We included in the study patients with a positive MPXV PCR test from skin or blood samples, who were ≥18 years of age and sought testing at a GeoSentinel site between May 1–July 1, 2022 (*5*). Although GeoSentinel surveillance typically includes only travel-associated cases, this study is from an enhanced surveillance project that included patients with and without international travel history. A questionnaire captured information about anatomic site of sexual exposures, physical examination, and underlying medical conditions. Healthcare practitioners completed the questionnaire by using medical record extraction and patient interviews. Lesion quantity was estimated ordinally on physical exam (1, 2–10, 10–50, 50–100, >100 lesions). Patients self-reported anatomic location of first lesions.

We focused our analysis on 3 anatomic sites (penis, anus, mouth) because there were sufficient patients exposed at these sites (>50%) to render statistical comparisons (*5*). We defined exposures at the rectum or anus as anorectal exposures and exposures at the oropharynx, including the mouth, oral mucosa, and pharynx, as oral exposures. MPXV lesion locations were described including at the penis, anus, oral mucosa, or lips. Rectal and oropharyngeal exams were not performed.

We calculated descriptive statistics for exposures and lesion outcomes. We evaluated the number of lesions by exposure site by using Mantel-Haenszel linear trend tests. For each anatomic site, we used univariable and multivariable logistic regression models to test the relationships between exposures, lesion presence, and site of lesion onset. We also adjusted multivariable models for other exposures and model assumptions. Participants recorded exposures by anatomic

[1]GeoSentinel Network Collaborators are listed at the end of this article.

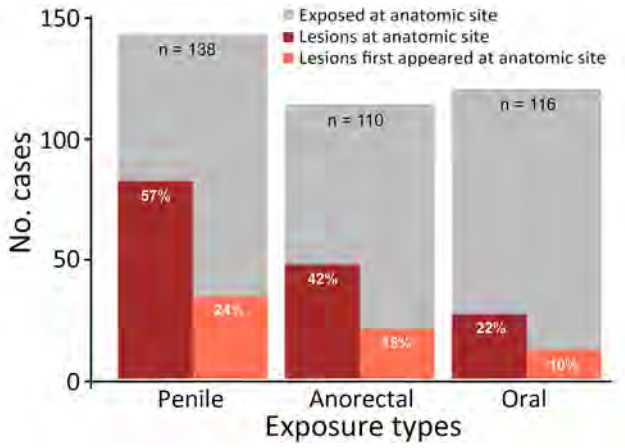

Figure. Locations of monkeypox virus exposures and locations and numbers of lesions reported by patients with monkeypox virus at GeoSentinel sites, May–July 2022. Percentages indicate numbers of patients who had lesions at the exposure site and those who reported the first lesion at the exposure site.

location as "yes" or "no/no response"; we assumed no response to indicate no exposure. To assess the influence of this assumption, we conducted a sensitivity analysis on 216 patients that reported sexual exposures and excluded patients who did not report sexual exposures.

Patients were from 15 countries, most of whom were from Spain (n = 79) and Canada (n = 66). All participants were assigned male sex at birth; median age was 37 (range 18–68) years, and 18% reported international travel in the 21 days before symptom onset (*5*). Most enrolled patients (99%) reported recent sexual contact with men, and 44% had HIV infection (median CD4 count 713 cells/mm^3) (*5*). Those demographic characteristics are similar to those reported in large-scale surveillance analyses from Europe (*6*).

From 22% to 57% of patients had lesions at the exposure site; 10%–24% of patients reported that lesions first appeared at the exposure site (Figure). The number of penile lesions was significantly greater for patients exposed at the penis compared with patients not exposed at the penis (χ^2 = 20.2; p<0.0001). The same pattern held for the anorectal exposures and anal lesions (χ^2 = 22.7; p<0.0001), but we found no significant association for oral exposures and lesions.

After accounting for other exposure types, the odds of having penile lesions were 14.6 (95% CI 5.6–45.0) times greater for patients with penile exposures compared with patients without penile exposures (Table 1). Anal lesions were 12.8 (95% CI 4.8–39.8) times more likely to occur among patients with anorectal exposures, and oral lesions were 5.4 (95% CI 1.7–19.7) times more likely to occur among patients with oral exposures.

The odds of developing penile lesions first were 7.3 (95% CI 2.7–21.2) times greater for persons with penile exposures after adjusting for other exposure types (Table 2). Among patients with anorectal exposures, lesions were 3.7 (95% CI 1.2–11.2) times more likely to first develop at the anus. There were no significant associations between oral exposures and first appearance of lesions. Sensitivity analyses revealed similar patterns (Appendix Table, https://wwwnc.cdc.gov/EID/article/30/11/24-1120-App1.pdf).

Conclusions

Exposures to MPXV influence the clinical manifestations of disease (*7*), but little is known about the quantitative relationship between exposures and lesion development. Results from this analysis showed that penile, anorectal, and oral exposures were associated with lesion development and quantity at the same anatomic site. We found increased odds of lesions first appearing at the exposure site for the penis and anus but not for the mouth. This discrepancy between sites might be because practices that cause abrasions, such

Table 1. Characteristics of lesions and exposures among patients with monkeypox virus infection reported to GeoSentinel, May–July 2022*

Characteristics	Total no. responses	No. (%) responses		
		Yes†	No/not reported	Missing‡
Exposure site				
Penis	226	138 (61.1)	88 (38.9)	0
Mouth	226	116 (51.3)	110 (48.7)	0
Rectum/anus	226	110 (48.7)	116 (51.3)	0
Lesion site				
Penis	221	101 (45.7)	120 (54.3)	5 (2.2)
Mouth	218	60 (27.5)	158 (72.4)	8 (3.5)
Rectum/anus	221	43 (19.5)	178 (80.5)	5 (2.2)
Initial lesion onset site				
Penis	226	41 (18.1)	185 (81.9)	0
Mouth	226	30 (13.2)	196 (86.7)	0
Rectum/anus	226	25 (11.1)	201 (88.9)	0

*Exposures at each anatomic location were recorded as yes or no/no response.
†Among complete responses.
‡Among all patients in dataset, N = 226.

Table 2. Logistic regression models assessing the relationship between exposures, lesion presence or absence, and lesion onset site by anatomic site among patients with monkeypox virus who reported to GeoSentinel, May–July 2022*

No. pts.†	Outcome (no. pts.)‡	Predictor	No. pts.§	Univariable models				Multivariable models¶			
				OR	(95% CI)	p value	AIC	aOR	(95% CI)	p value	AIC
221	Penis lesions (101)	Penis exposure	138	3.7	(2.1–6.8)	<0.001	288.4	14.6	(5.6–45.0)	<0.0001	272.4
		Rectum/anus exposure	110	0.7	(0.4–1.2)	0.25	307.4	0.3	(0.1–0.7)	<0.01	
		Mouth exposure	116	1.2	(0.7–2.0)	0.59	308.5	0.4	(0.1–0.9)	0.056	
218	Anal lesions (60)	Rectum/anus exposure	110	4.8	(2.5–9.8)	<0.0001	236.84	12.8	(4.8–39.8)	<0.0001	229.4
		Penis exposure	138	0.9	(0.5–1.7)	0.76	260.4	0.3	(0.1–0.4)	<0.05	
		Mouth exposure	116	1.5	(0.8–2.7)	0.21	259	0.6	(0.2–1.9)	0.41	
221	Mouth lesions (43)	Mouth exposure	116	1.5	(0.8–3.0)	0.24	220.4	5.4	(1.7–19.7)	<0.01	216.2
		Penis exposure	138	0.7	(0.4–1.4)	0.31	220.8	0.3	(0.2–0.5)	<0.05	
		Rectum/anus exposure	110	0.9	(0.4–1.7)	0.63	221.6	0.5	(0.2–1.3)	0.17	
226	Penis lesions first (41)	Penis exposure	138	3.4	(1.4–7.6)	<0.01	209.4	7.3	(2.7–21.2)	<0.001	204.3
		Rectum/anus exposure	110	0.7	(0.3–1.4)	0.3	216.9	0.5	(0.2–1.1)	0.078	
		Mouth exposure	116	1.0	(0.5–2.0)	0.9	218.0	0.5	(0.2–1.3)	0.17	
226	Anus lesions first (30)	Rectum/anus exposure	110	2.4	(1.1–5.5)	0.038	176.4	3.7	(1.3–11.2)	<0.05	176.9
		Penis exposure	138	0.8	(0.4–1.8)	0.60	180.7	0.4	(0.1–1.2)	0.11	
		Mouth exposure	116	1.3	(0.6–2.8)	0.53	180.6	1.1	(0.3–3.9)	0.91	
226	Mouth lesions first (25)	Mouth exposure	116	0.9	(0.4–2.0)	0.72	161.1	3.1	(0.8–13.1)	0.11	158.9
		Penis exposure	138	0.5	(0.2–1.3)	0.16	159.4	0.4	(0.1–1.3)	0.15	
		Rectum/anus exposure	110	0.5	(0.2–1.1)	0.083	158.0	0.3	(0.1–1.0)	0.06	

*For each model, the main predictor variable of interest is listed first, followed by additional predictor variables. AIC, akaike information criterion; aOR, adjusted odds ratio; OR, odds ratio; pts., patients.
†The number of observations included in the regression model. Missing observations: n = 5 for penis lesions, n = 8 for anus lesions, n = 5 for mouth lesions.
‡The number of patients who reported lesions at this anatomic site.
§The number of patients who reported exposure at this anatomic site.
¶Covariates included in each multivariable model are all exposure types (e.g., for the outcome of penis lesions, penile, anorectal and oral exposures were included).

as condomless anal sex, might contribute to direct inoculation, increased viral exposure, and early development of mucosal lesions at the penis and anus or rectum.

Previous studies have reported that receptive anal sex was associated with anogenital lesions in men who have sex with men (*2*); vaginal and anal sex were associated with anogenital lesions in cisgender women and nonbinary persons (*8*). Similar phenomena have been observed previously with MPXV and other orthopoxviruses. MPXV-contaminated and vaccinia virus–contaminated needlestick exposures and animal bites and scratches from MPXV and cowpox-infected animals have caused initial lesions to develop at the site of inoculation (*7*,*9*–*11*).

Some patients did not have lesions reported at the exposure site. MPXV infection has a wide spectrum of clinical manifestations, ranging from mild to severe; some recent data suggest a small number of asymptomatic cases have occurred (*12*–*14*). It is possible lesions that were small, painless, and few might have been missed. In addition, our data only captured binary exposures by anatomic location but did not assess duration or nature of exposures, which might influence lesion development.

The first limitation of this analysis is that patients might not have reported exposures because of social desirability or recall bias. Rectal and oropharyngeal exams were not conducted, so it is possible that lesions in those anatomic sites went undetected. Most patients with HIV infection were virally suppressed, so our findings may not be applicable to immunocompromised patients, who are at greater risk for disseminated rash (*14*). This study was cross-sectional, and therefore lesions that may have developed later were not captured. Finally, small sample sizes resulted in wide CIs for odds ratios.

Lesion presence, quantity, and onset site may be proxies for identifying the anatomic site of MPXV exposure. However, lesions may appear at anatomic sites where exposures did not occur and may be absent where exposures did occur. Our findings highlight the importance of clinicians conducting a complete physical examination, including a thorough skin and mucosal examination, for patients with suspected mpox. Patients with suspected mpox should be aware that lesions may occur first at mucosal sites, particularly at the sites of exposure. Findings from this study reinforce public health guidance about mpox prevention by avoiding close, skin-to-skin contact with persons who have a rash (*15*).

GeoSentinel Network Collaborators: Hilmir Asgeirsson, Leire Balerdi-Sarasola, Sapha Barkati, Michael Beadsworth, Emmanuel Bottieau, Lucille Blumberg, Daniel Camprubí-Ferrer, Marta Díaz Menéndez, Alexandre Duvignaud, Eric Florence, Simin Aysel Florescu, Albie de Frey, Christina Greenaway, Martin P. Grobusch, Kristina L.B. Huber, Marina Klein, Susana Lloveras, Carmello Licitra, Denis Malvy, Charlotte Martin, Diogo Mendes Pedro, José Muñoz, Duc Nguyen, Corneliu Petru Popescu, Laura A.S. Quilter, Mary G. Reynolds, Camilla Rothe, Eli Schwartz, Guillermo Servera-Negre, Patrick Soentjens, and Camille Tumiotto.

Acknowledgments

We thank Kathleen A. Jablonski, Ryan Wiegand, and Jef Vanhamel.

Funding for GeoSentinel is provided by a cooperative agreement (agreement no. 1 U01 CK000632-01) from the Centers for Disease Control and Prevention, the GeoSentinel Foundation, and the Public Health Agency of Canada.

About the Author

Dr. Guagliardo is an epidemiologist in the Division of Vector-Borne Diseases, National Center for Emerging and Zoonotic Infectious Diseases, the Centers for Disease Control and Prevention, Fort Collins, Colorado. Her research interests include applied epidemiology and ecology of vectorborne and zoonotic diseases.

References

1. Beeson A, Styczynski A, Hutson CL, Whitehill F, Angelo KM, Minhaj FS, et al. Mpox respiratory transmission: the state of the evidence. Lancet Microbe. 2023;4:e277–83. https://doi.org/10.1016/S2666-5247(23)00034-4
2. Tarín-Vicente EJ, Alemany A, Agud-Dios M, Ubals M, Suñer C, Antón A, et al. Clinical presentation and virological assessment of confirmed human monkeypox virus cases in Spain: a prospective observational cohort study. Lancet. 2022; 400:661–9. https://doi.org/10.1016/S0140-6736 (22)01436-2
3. Guarner J, Del Rio C, Malani PN. Monkeypox in 2022—what clinicians need to know. JAMA. 2022;328:139–40. https://doi.org/10.1001/jama.2022.10802
4. Mitjà O, Ogoina D, Titanji BK, Galvan C, Muyembe JJ, Marks M, et al. Monkeypox. Lancet. 2023;401:60–74. https://doi.org/10.1016/S0140-6736(22)02075-X
5. Angelo KM, Smith T, Camprubí-Ferrer D, Balerdi-Sarasola L, Díaz Menéndez M, Servera-Negre G, et al.; GeoSentinel Network Collaborators. Epidemiological and clinical characteristics of patients with monkeypox in the GeoSentinel Network: a cross-sectional study. Lancet Infect Dis. 2023;23:196–206. https://doi.org/10.1016/S1473-3099(22)00651-X
6. Vaughan AM, Afzal M, Nannapaneni P, Leroy M, Andrianou X, Pires J, et al. Continued circulation of mpox: an epidemiological and phylogenetic assessment, European Region, 2023 to 2024. Euro Surveill. 2024;29:2400330. https://doi.org/10.2807/1560-7917.ES.2024.29.27.2400330
7. Reynolds MG, Yorita KL, Kuehnert MJ, Davidson WB, Huhn GD, Holman RC, et al. Clinical manifestations of human monkeypox influenced by route of infection. J Infect Dis. 2006;194:773–80. https://doi.org/10.1086/505880
8. Thornhill JP, Palich R, Ghosn J, Walmsley S, Moschese D, Cortes CP, et al.; Share-Net writing group. Human monkeypox virus infection in women and non-binary individuals during the 2022 outbreaks: a global case series. Lancet. 2022;400:1953–65. https://doi.org/10.1016/S0140-6736(22)02187-0
9. Baxby D, Bennett M, Getty B. Human cowpox 1969–93: a review based on 54 cases. Br J Dermatol. 1994;131:598–607. https://doi.org/10.1111/j.1365-2133.1994.tb04969.x
10. MacNeil A, Reynolds MG, Damon IK. Risks associated with vaccinia virus in the laboratory. Virology. 2009;385:1–4. https://doi.org/10.1016/j.virol.2008.11.045
11. Carvalho LB, Casadio LVB, Polly M, Nastri AC, Turdo AC, de Araujo Eliodoro RH, et al. Monkeypox virus transmission to healthcare worker through needlestick injury, Brazil. Emerg Infect Dis. 2022;28:2334–6. https://doi.org/10.3201/eid2811.221323
12. Guagliardo SAJ, Monroe B, Moundjoa C, Athanase A, Okpu G, Burgado J, et al. Asymptomatic orthopoxvirus circulation in humans in the wake of a monkeypox outbreak among chimpanzees in Cameroon. Am J Trop Med Hyg. 2020;102:206–12. 10.4269/ajtmh.19-0467 https://doi.org/10.4269/ajtmh.19-0467
13. De Baetselier I, Van Dijck C, Kenyon C, Coppens J, Michiels J, de Block T, et al.; ITM Monkeypox study group. Retrospective detection of asymptomatic monkeypox virus infections among male sexual health clinic attendees in Belgium. Nat Med. 2022;28:2288–92. https://doi.org/10.1038/s41591-022-02004-w
14. Miller MJ, Cash-Goldwasser S, Marx GE, Schrodt CA, Kimball A, Padgett K, et al.; CDC Severe Monkeypox Investigations Team. Severe monkeypox in hospitalized patients—United States, August 10–October 10, 2022. MMWR Morb Mortal Wkly Rep. 2022;71:1412–7. https://doi.org/10.15585/mmwr.mm7144e1
15. Centers for Disease Control and Prevention. How to protect yourself: mpox prevention steps. 2024. [cited 2024 July 9]. https://www.cdc.gov/poxvirus/monkeypox/prevention/protect-yourself.html

Address for correspondence: Sarah Anne J. Guagliardo, Centers for Disease Control and Prevention, 3156 Rampart Rd, Fort Collins, CO 80521, USA; email: sguagliardo@cdc.gov.

Emerging Monkeypox Virus Sublineage C.1 Causing Community Transmission, Vietnam, 2023

Huynh Thi Thuy Hoa, Nguyen Thanh Dung, Le Manh Hung, Nguyen Thi Thu Hong, Vo Truong Quy, Nguyen Thi Thao, Nguyen Trong Duy, Hoang Truong, Tran Minh Hoang, Nguyen Thi Thanh, Mai Pham Hong Phuoc, Truong Ngoc Trung, Nguyen Nhut Thong, Nguyen Duc Huy, Vu Thi Kim Thoa, Vo Trong Vuong, Ngo Tan Tai, Huynh Kim Nhung, Dao Phuong Linh, Pham Thi Ngoc Thoa, Lam Minh Yen, Tran Ba Thien, Truong Hoang Chau Truc, Le Kim Thanh, Nguyen Thi Han Ny, Vo Tan Hoang, Nghiem My Ngoc, Dinh Nguyen Huy Man, Louise Thwaites, Tran Tan Thanh, Nguyen Van Vinh Chau, Guy Thwaites, Nguyen To Anh, Le Van Tan

We studied a community cluster of 25 mpox cases in Vietnam caused by emerging monkeypox virus sublineage C.1 and imported into Vietnam through 2 independent events; 1 major cluster carried a novel APOBEC3-like mutation. Three patients died; all had advanced HIV coinfection. Viral evolution and its potential consequences should be closely monitored.

To date, most globally reported mpox sequences have come from Europe and North America, where sustained human-to-human transmission has resulted in explosive mpox outbreaks, especially in 2022 (*1*). A hallmark of the monkeypox virus (MPXV) strain responsible for the ongoing global outbreaks is its high evolution rate, which is driven by the host APOBEC3 (apolipoprotein B mRNA editing enzyme, catalytic polypeptide 3) deaminases, causing a dinucleotide change from TC to TT (*2*). In addition, persons with advanced HIV might experience more severe outcomes (*3*) and delayed viral clearance, resulting in the emergence of new variants, as has been observed with SARS-CoV-2 (*4*). However, this possibility has not been well studied for MPXV infection (*5*).

Vietnam reported its first mpox cases in late 2022 in 2 female travelers returning from United Arab Emirates (*6*). No additional cases were reported until September 2023, when mpox was diagnosed in a 33-year-old man in Dong Nai Province in southern Vietnam (*7*). This case marked the start of ongoing community transmission in Vietnam, where the mpox vaccine has not been deployed.

Despite the ongoing challenges of mpox, existing literature has been dominated by reports from Europe and North America, where most cases have been reported (*1*). We therefore studied the longitudinal clinical, laboratory, and virological features in mpox patients admitted to a tertiary referral hospital in Ho Chi Minh City, Vietnam, in 2023. We also sought to study virus evolution in persons with advanced HIV over the course of hospitalization.

The Study

In Vietnam, all persons with mpox are subject to isolation at a designated healthcare center for ≥14 days or until clinical manifestations resolve. This study was conducted at the Hospital for Tropical Diseases (HTD) in Ho Chi Minh City. HTD is a tertiary referral infectious diseases hospital and a designated hospital for isolating and treating mpox patients in Ho Chi Minh City, which has a population of ≈10 million persons. The study was approved by the HTD Institutional Review Board and Oxford Tropical Research Ethics

Author affiliations: Hospital for Tropical Diseases, Ho Chi Minh City, Vietnam (H.T.T. Hoa, N.T. Dung, L.M. Hung, V.T. Quy, N.T. Duy, H. Truong, T.M. Hoang, N.T. Thanh, M.P.H. Phuoc, T.N. Trung, N.N. Thong, N.D. Huy, V.T.K. Thoa, V.T. Vuong, N.T. Tai, H.K. Nhung, D.P. Linh, P.T.N. Thoa, N.M. Ngoc); Oxford University Clinical Research Unit, Ho Chi Minh City (N.T.T. Hong, N.T. Thao, L.M. Yen, T.B. Thien, T.H.C. Truc, L.K. Thanh, N.T.H. Ny, V.T. Hoang, L. Thwaites, T.T. Thanh, G. Thwaites, N.T. Anh, L.V. Tan); Centre for Tropical Medicine and Global Health University of Oxford, Oxford, UK (L. Thwaites, G. Thwaites, L.V. Tan); Department of Health, Ho Chi Minh City (N.V.V. Chau)

DOI: https://doi.org/10.3201/eid3011.240729

Committee. Written informed consent was obtained from study participants.

We collected laboratory and clinical data from recruited patients at admission, as well as lesion swab samples for analysis. Where relevant, cerebrospinal fluid (CSF) samples, endotracheal aspirate (ETA) samples, and follow-up lesion swab samples were also collected from patients with clinical

Table. Baseline characteristics of 25 participants in study of emerging monkeypox virus sublineage C.1 causing community transmission, Vietnam, 2023*

Characteristic	Value
Median age, y (range)	31 (22–49)
From Ho Chi Minh City	20/25 (80)
Median time from symptom onset to admission, d (range)	6 (4–30)
Median hospitalization, d (range)	14 (11–43)
Sexual activity within 21 d before illness	18/25 (72)
Travel abroad within 21 d before illness	0/25 (0)
HIV-positive	21/25 (84)
Receiving antiretroviral therapy	16/21 (76)
Gonorrhea	5/25 (20)
Syphilis	9/25 (36)
Symptoms	
Fever	14/25 (56)
Sore throat	5/25 (20)
Myalgia	2/25 (8)
Headache	1/25 (4)
Fatigue	2/25 (8)
Oral pain	2/25 (8)
Diarrhea	2/25 (8)
Rectal pain	6/25 (24)
Pain with swallowing	2/25 (8)
Difficulty swallowing	1/25 (4)
Lymphadenopathy	16/25 (64)
Cervical	9/16 (56)
Inguinal	9/16 (56)
Median temperature, °C (range)	37 (37–38.5)
Median heart rate, bpm (range)	85 (75−130)
Median respiratory rate, bpm (range)	20 (18–22)
Median arterial pressure, mm Hg (range)	83 (73–107)
Laboratory findings, median (range)/(reference range)	
CD4+ count, cells/μL	451 (1–956)/(500–1600)
leukocyte count, 10^9 cells/L	9.98 (5.53–17.08)/(4.5–11)
Hemoglobin, g/L	147 (11–174)/(130–160)
Platelet count, 10^9/L	256 (131–473)/(140–440)
Glucose, mg/dL	83 (6–138)/(70–100)
Aspartate aminotransferase, U/L	24 (15–48)/(0–40)
Alanine aminotransferase, U/L	35 (11–85)/(0–40)
Creatinine, μmol/L	89 (70–147)/(53–120)
No. lesions	
1–5	1/25 (4)
6–25	11/25 (44)
26–100	12/25 (48)
>250	1/25 (4)
Lesion position	
Arm	20/25 (80)
Leg	19/25 (76)
Genitals	19/25 (76)
Oral mucosa	5/25 (20)
Perianal area	15/25 (60)
Lesion characteristics	
Macule	5/25 (20)
Papule	6/25 (24)
Early vesicle	11/25 (44)
Small pustule	21/25 (84)
Umbilicated pustule	12/25 (48)
Ulcerated lesion	6/25 (24)
Crusting of a mature lesion	10/25 (40)
Partially removed scab	3/25 (12)

*Values are no. (%) unless otherwise indicated. All patients were assigned male sex at birth; 24/25 reported having sex with men (2 men identified as bisexual). No participants had been vaccinated for mpox or had a tecovitimat prescription.

complications. Daily clinical follow-up of patients took place during hospitalization, including assessment for new and evolving lesions.

We diagnosed MPXV using LightMix Modular Mpox PCR (TIB Molbiol, https://www.tib-molbiol.de). We generated MPXV genomes directly from representatives of admission lesion swabs and other sample types (if available) with a PCR cycle threshold (Ct) value <30 using a metagenomics-based approach (*6*) (Appendix, https://wwwnc.cdc.gov/EID/article/30/11/24-0729-App1.pdf).

During September–December 2023, a total of 54 mpox patients were admitted to HTD, and 25 (46%) participated in the clinical studies. The participants were 22–49 (median 31) years of age; 88% (22/25) were men who have sex with men (Table). No patients reported recent travel history outside of Vietnam. HIV infection was documented in 21 (84%) persons; median CD4 cell count was 14 (range 1–579) cells/μL. Of those 21 patients, 16 (76%) were receiving antiretroviral therapy. Concurrent sexually transmitted diseases were documented in 12/24 (50%) persons; the most common were syphilis (n = 9) and gonorrhea (n = 5) (Table).

A total of 3 patients had severe disease that required intensive care unit admission for septic shock; the patients subsequently died (Appendix Table 1).

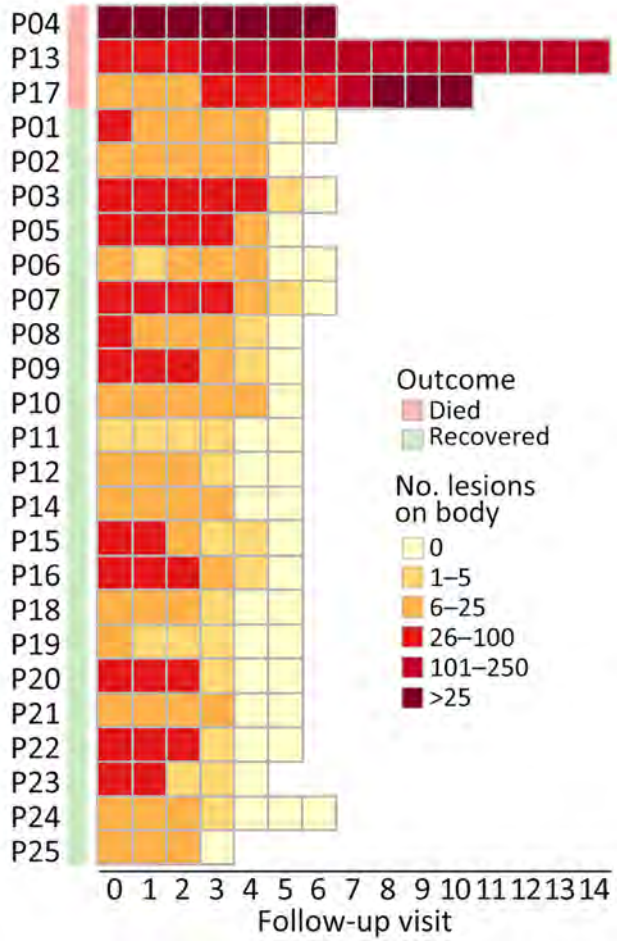

Figure 1. Heat map showing changes in the number of skin lesions over the course of hospitalization of 3 fatal (P04, P13, and P17) and 22 nonfatal cases in study of emerging monkeypox virus sublineage C.1 causing community transmission, Vietnam, 2023. Median follow-up was 3 (range 3–5) days. P, patient number.

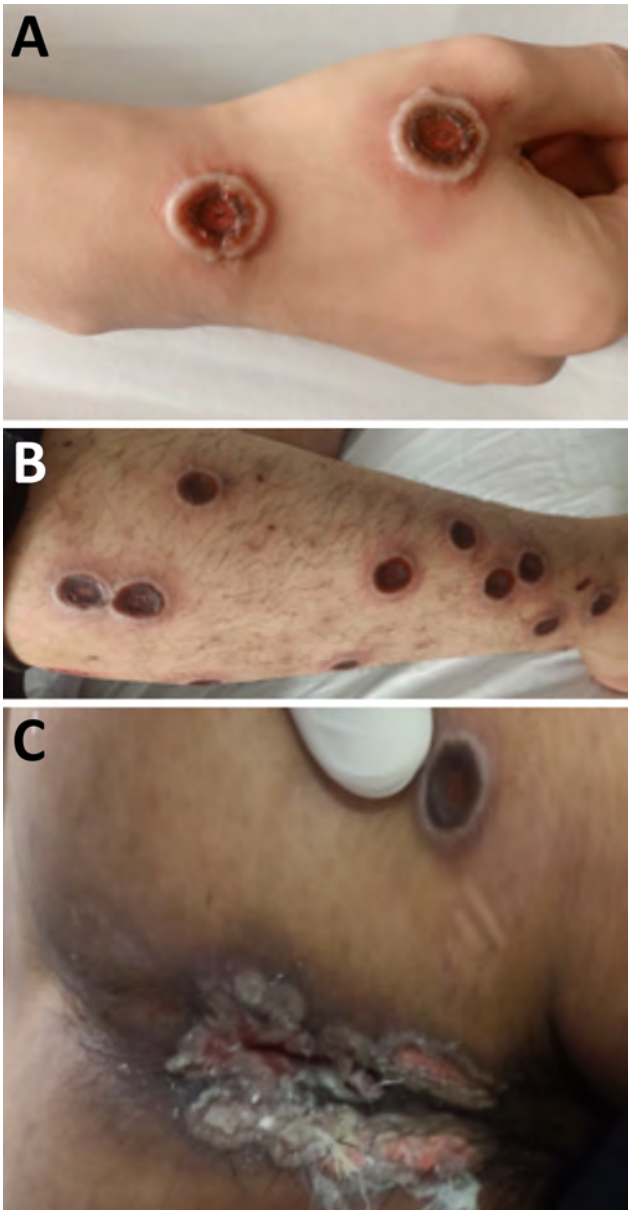

Figure 2. Natural progression of skin lesions of mpox patient who died in study of emerging monkeypox virus sublineage C.1 causing community transmission, Vietnam, 2023. Skin lesions shown are on the right hand (A), right leg (B), and perianal and buttock areas (C) of a patient with a CD4 cell count of 16 cells/μL.

Those patients were all young adults with advanced HIV infection (low CD4 cell counts) (Appendix Table 1); only 1 was receiving antiretroviral therapy. One patient had other opportunistic infections (tuberculosis and pneumocystis pneumonia) (Appendix Table 1), and MPXV DNA was detected in both ETA (PCR Ct 17.67) and CSF (PCR Ct 33.82). Lumbar puncture was indicated in this patient because he began hallucinating. We did not perform testing for other pathogens in the CSF, but the CSF parameters were with reference ranges (data not shown). All patients who died had prominent skin lesions (confluence and necrosis) (Figures 1, 2) that remained unhealed. The remaining 22 (88%) patients made a full recovery; all lesions resolved before hospital discharge.

We successfully obtained 14 complete-genome sequences from 14 patients (Appendix Table 1). Phylogenetically, they all exhibited a close relatedness with sublineage C.1 viruses of MPXV clade IIb but formed 2 separate clusters, including 1 cluster of 13 sequences sharing 2 nonsynonymous substitutions (Figure 3). Pairwise analysis identified 12 nonsynonymous mutations (2 APOBEC3-like and 10 non–APOBEC3-like) in the 14 Vietnam sequences but not in the global MPXV dataset as of July 29, 2024 (Appendix Figure 1). The 2 APOBEC3-like mutations were detected in 2/14 (14.3%) sequences and 13/14 (92.9%) sequences, as compared with 1/14 (7.1%) sequence for the 10 non–APOBEC3-like mutations (Appendix Figure 1). Subsequently, Sanger sequencing confirmed the presence of the APOBEC3-like mutation (OPG068: S428L) coexisting in 13/14 sequences in the original samples (Appendix Figure 2). We did not perform Sanger sequencing for the remaining 11 sporadic mutations because materials were unavailable. The 12 substitutions were mostly located in functional proteins concerning virus assembly, virulence, or replication (Appendix Table 3).

Of the patients who died, 1 person had 4 longitudinal lesion swab samples and an ETA available for

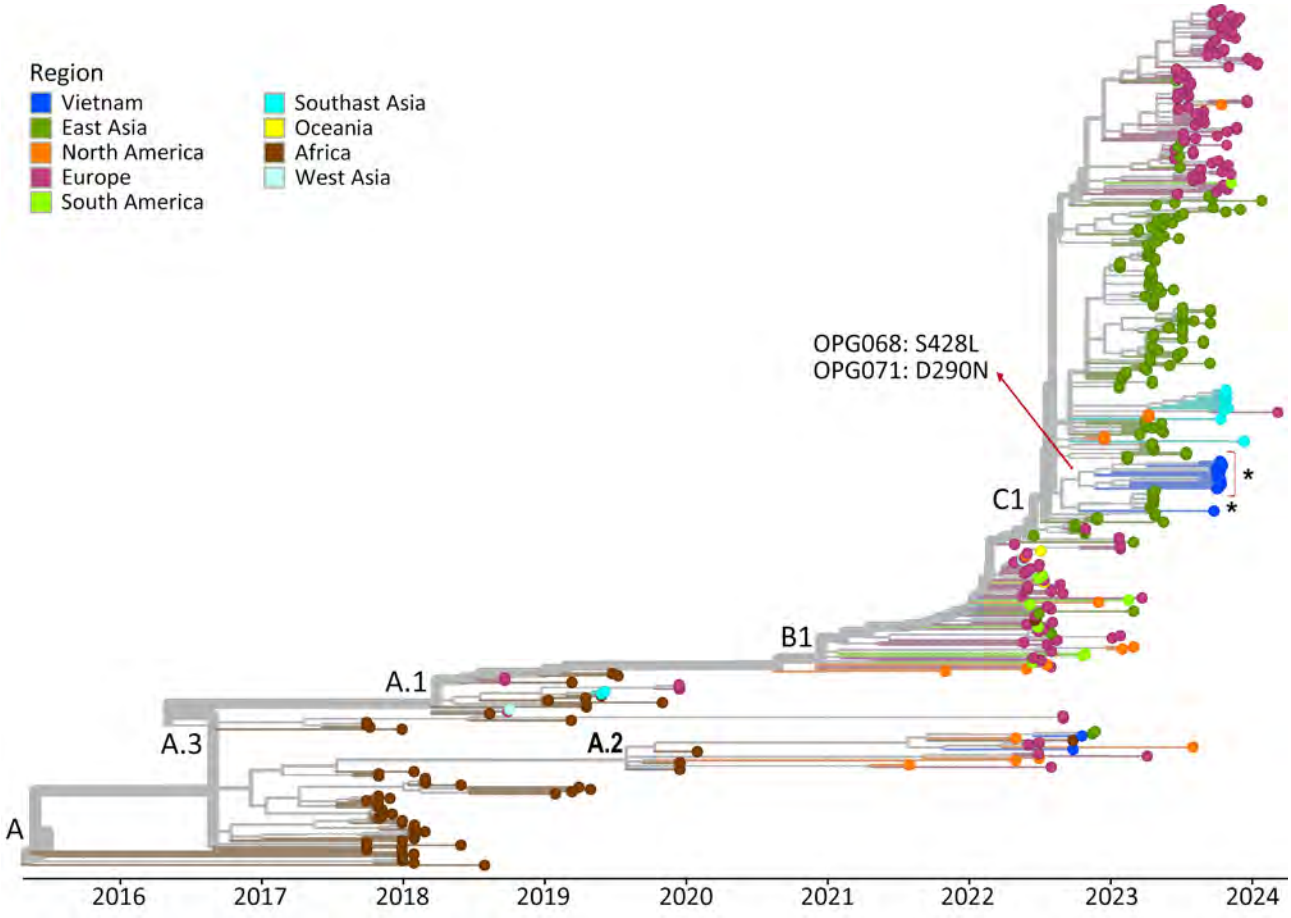

Figure 3. Assessment of genetic diversity of the monkeypox virus genomes obtained in study of emerging monkeypox virus sublineage C.1 causing community transmission, Vietnam, 2023. Time-scaled phylogenetic tree of 14 Vietnam monkeypox virus genomes from this study (asterisk) highlights 2 nonsynonymous substitutions shared by 13 sequences (red arrow), with substitution OPG068: S428L uniquely found in those 13 sequences. D, aspartate; L, leucine; N, asparagine; OPG, orthopoxvirus gene; S, serine.

intrahost evolution analysis. We found evidence of nonsynonymous substitutions (n = 2) and single-nucleotide polymorphisms (n = 6) in the metagenomics datasets (Appendix Table 4). However, subsequent Sanger sequencing failed to confirm their presence in the original samples (Appendix Figure 3).

Our findings emphasize that, although MPXV infections are usually self-limiting, severe clinical complications and death can occur, especially in persons with advanced HIV (*3*,*8*). Detecting MPXV in ETA and CSF samples is unusual, although it has been reported previously (*3*), and this finding supports further study of mpox pathogenesis.

The responsible viruses belonged to sublineage C.1, lineage B.1 of clade IIb, and were imported into Vietnam through 2 independent events, as demonstrated by their phylogenetically forming into 2 different clusters. Sublineage C.1 has only recently emerged and caused local transmission in China (*9*). In addition, C.1 sequences from various countries in Asia, Europe, and the Americas have been deposited to GISAID (https://www.gisaid.org), demonstrating its global dispersal. Those collective findings point to a rapid evolution of MPXV, of which the host APOBEC3 has been shown to be a main driver (*2*). Alternatively, immune suppression or antivirals might also enable intrahost evolution, as observed in a recent study (*5*). Similar findings were documented in our metagenomics datasets of longitudinal samples. However, subsequent Sanger sequencing failed to confirm those original findings, likely attributed to sequencing artifacts, emphasizing the importance subsequent Sanger sequencing–based confirmatory experiments.

The tight cluster on the global phylogenetic tree of the 13 sequences sharing 2 nonsynonymous substitutions suggested that those patients shared a transmission network, supporting findings from a recent report (*10*). Because direct skin-to-skin contact plays a key role in MPXV transmission, public education campaigns should raise awareness about behaviors that increase the risk for MPXV exposure (*11*). Vaccination remains the most effective tool to control mpox outbreaks (*12*).

Conclusions

We report the clinical, laboratory, and virological findings in 25 mpox patients infected with an emerging sublineage C.1 that was imported into Vietnam through 2 independent events; 1 major cluster carried a novel APOBEC3-like mutation concerning virus assembly. MPXV evolution and its potential consequences should be closely monitored. Clinicians should be aware of unusual skin lesions in patients with advanced HIV.

Acknowledgments

We are indebted to the participants for their participation in this study and our colleagues at the Hospital for Tropical Diseases for providing clinical care for the patients. We thank all data contributors and their laboratories for obtaining the specimens for this study, and we thank the laboratories that submitted and shared their generated genetic sequence and metadata via GISAID, on which this research is based.

This work was supported by the Wellcome Trust, United Kingdom (226120/Z/22/Z and 225437/Z/22/Z). The funder did not have any influence on the study design, study conduct, preparation of the manuscript, or decision to publish.

About the Author

Dr. Hoa is a senior infectious disease specialist at the Ho Chi Minh City Hospital for Tropical Diseases. Her research interests focus on infectious diseases, including mpox.

References

1. World Health Organization. 2022–24 mpox (monkeypox) outbreak: global trends [cited 2024 Apr 26]. https://worldhealthorg.shinyapps.io/mpx_global
2. O'Toole Á, Neher RA, Ndodo N, Borges V, Gannon B, Gomes JP, et al. APOBEC3 deaminase editing in mpox virus as evidence for sustained human transmission since at least 2016. Science. 2023;382:595–600. https://doi.org/10.1126/science.adg8116
3. Mitjà O, Alemany A, Marks M, Lezama Mora JI, Rodríguez-Aldama JC, Torres Silva MS, et al.; SHARE-NET writing group. Mpox in people with advanced HIV infection: a global case series. Lancet. 2023;401:939–49. https://doi.org/10.1016/S0140-6736(23)00273-8
4. Cele S, Karim F, Lustig G, San JE, Hermanus T, Tegally H, et al.; COMMIT-KZN Team. SARS-CoV-2 prolonged infection during advanced HIV disease evolves extensive immune escape. Cell Host Microbe. 2022;30:154–162.e5. https://doi.org/10.1016/j.chom.2022.01.005
5. Rueca M, Tucci FG, Mazzotta V, Gramigna G, Gruber CEM, Fabeni L, et al. Temporal intra-host variability of mpox virus genomes in multiple body tissues. J Med Virol. 2023;95:e28791. https://doi.org/10.1002/jmv.28791
6. Dung NT, Hung LM, Hoa HTT, Nga LH, Hong NTT, Thuong TC, et al. Monkeypox virus infection in 2 female travelers returning to Vietnam from Dubai, United Arab Emirates, 2022. Emerg Infect Dis. 2023;29:778–81. https://doi.org/10.3201/eid2904.221835
7. Adamson PC, Bui HTM, Kesteman T, Nguyen DTN, Nguyen TTH, Van Le T, et al. Screening for monkeypox virus infections in men who have sex with men in a sexual health clinic in Hanoi, Viet Nam. Lancet Microbe. 2023;4:e201–2. https://doi.org/10.1016/S2666-5247(22)00385-8
8. Philpott DC, Bonacci RA, Weidle PJ, Curran KG, Brooks JT, Khalil G, et al. Low CD4 count or being out of care increases the risk for mpox hospitalization among people with human immunodeficiency virus and mpox. Clin Infect Dis. 2024;78:651–4. https://doi.org/10.1093/cid/ciad482
9. Yu J, Zhang X, Liu J, Xiang L, Huang S, Xie X, et al. Phylogeny and molecular evolution of the first local monkeypox virus cluster in Guangdong Province, China.

Nat Commun. 2023;14:8241. https://doi.org/10.1038/s41467-023-44092-3
10. Borges V, Duque MP, Martins JV, Vasconcelos P, Ferreira R, Sobral D, et al. Viral genetic clustering and transmission dynamics of the 2022 mpox outbreak in Portugal. Nat Med. 2023;29:2509–17. https://doi.org/10.1038/s41591-023-02542-x
11. Allan-Blitz LT, Gandhi M, Adamson P, Park I, Bolan G, Klausner JD. A position statement on mpox as a sexually transmitted disease. Clin Infect Dis. 2023;76:1508–12. https://doi.org/10.1093/cid/ciac960
12. Deputy NP, Deckert J, Chard AN, Sandberg N, Moulia DL, Barkley E, et al. Vaccine effectiveness of JYNNEOS against mpox disease in the United States. N Engl J Med. 2023;388:2434–43. https://doi.org/10.1056/NEJMoa2215201

Address for correspondence: Nguyen Thanh Dung or LeVan Tran, Hospital for Tropical Diseases, 764 Vo Van Kiet, District 5, Ho Chi Minh City, Vietnam; email: bsdungbvbnd@gmail.com or tanlv@oucru.org

Dengue Outbreak Caused by Multiple Virus Serotypes and Lineages, Colombia, 2023–2024

Nathan D. Grubaugh, Daniela Torres-Hernández, Mónica A. Murillo-Ortiz, Diana M. Dávalos, Pio Lopez, Isabel C. Hurtado, Mallery I. Breban, Ellie Bourgikos, Verity Hill, Eduardo López-Medina

Dengue cases rose to record levels during 2023–2024. We investigated dengue in Valle del Cauca, Colombia, to determine if specific virus serotypes or lineages caused its large outbreak. We detected all 4 serotypes and multiple lineages, suggesting that factors such as climatic conditions were likely responsible for increased dengue in Colombia.

Reported cases of dengue caused by dengue virus (DENV) are increasing. DENV (genus *Orthoflavivirus*, family Flaviviridae) is composed of 4 genetically distinct serotypes, DENV-1–4. In 2023, a total of 4.6 million dengue cases were reported in the Americas, a record at the time and a 64% increase over 2022 (*1*). Those numbers were quickly surpassed in 2024, when almost 10 million dengue cases were reported through June (*1*). Of those cases, ≈8.4 million were from Brazil (*1*); however, many countries, including Colombia, reported large outbreaks. The Valle del Cauca State Health Department in Colombia reported ≈56,000 dengue cases through May 2024, compared with ≈23,000 for all of 2023 and <5,000 in 2022.

The cause of the substantial increase in dengue cases is likely multifaceted. Warming temperatures caused by climate change increase the transmission potential and expand the geographic range of the primary mosquito vector, *Aedes aegypti* (*2*). Moreover, Indian Ocean surface temperature anomalies, especially El Niño events, are associated with dengue epidemics in the Northern and Southern Hemispheres (*3*). A strong El Niño–Southern Oscillation event occurred during 2023–2024, the first since 2015–2016 (Golden Gate Weather Services, https://ggweather.com/enso/oni.htm). Moreover, new DENV introductions, perhaps related to resumption of travel after the COVID-19 pandemic (*4*), could be reaching large susceptible populations. For example, DENV-3 was rarely detected in the Americas during the 10 years before an introduction into the Caribbean from Asia around 2021 (*5*,*6*). We investigated whether a specific DENV serotype or lineage contributed to the recent surge in cases in Valle del Cauca, Colombia.

The Study

The Valle del Cauca State Health Department in Colombia reported 966 dengue cases in 2019, 655 in 2020, 8,940 in 2021, 4,630 in 2022, 22,988 in 2023, and 56,355 cases in 2024 (through May) (Figure 1, panel A). To determine which DENV serotypes and lineages were involved, we collected 150–500 μL of serum from all 266 confirmed dengue case-patients at Hospital Universitario del Valle (HUV) in Cali, Colombia, during April 2023–May 2024. Cases were diagnosed by VIDAS anti-DENV IgM and anti-DENV IgG (bioMérieux, https://www.biomerieux.com) assays at HUV. Patient ages were 0–77 (mean 16) years, and all participants signed an informed consent; parents or guardians signed for persons <18 years of age. HUV shipped samples to Yale University (New Haven, CT, USA) for molecular processing.

We used the QIAamp Viral RNA Mini Kit (QIAGEN, https://www.qiagen.com) to extract RNA from 140 μL of each serum sample. We initially determined DENV serotypes by using a multiplexed quantitative reverse transcription PCR (*7*) before attempting panserotype whole-genome amplicon sequencing with DengueSeq (*8*). We conducted bioinformatic

Author affiliations: Yale University, New Haven, Connecticut, USA (N.D. Grubaugh); Rega Institute KU Leuven, Leuven, Belgium (N.D. Grubaugh); Yale School of Public Health, New Haven (N.D. Grubaugh, M.I. Breban, E. Bourgikos, V. Hill); Universidad del Valle, Cali, Colombia (D. Torres-Hernández, M.A. Murillo-Ortiz, I.C. Hurtado, E. López-Medina); Centro de Estudios en Infectología Pediátrica CEIP, Cali (D.M. Dávalos, P. Lopez, E. López-Medina); Valle del Cauca State Health Department, Cali (I.C. Hurtado); Clínica Imbanaco, Cali (E. López-Medina)

DOI: https://doi.org/10.3201/eid3011.241031

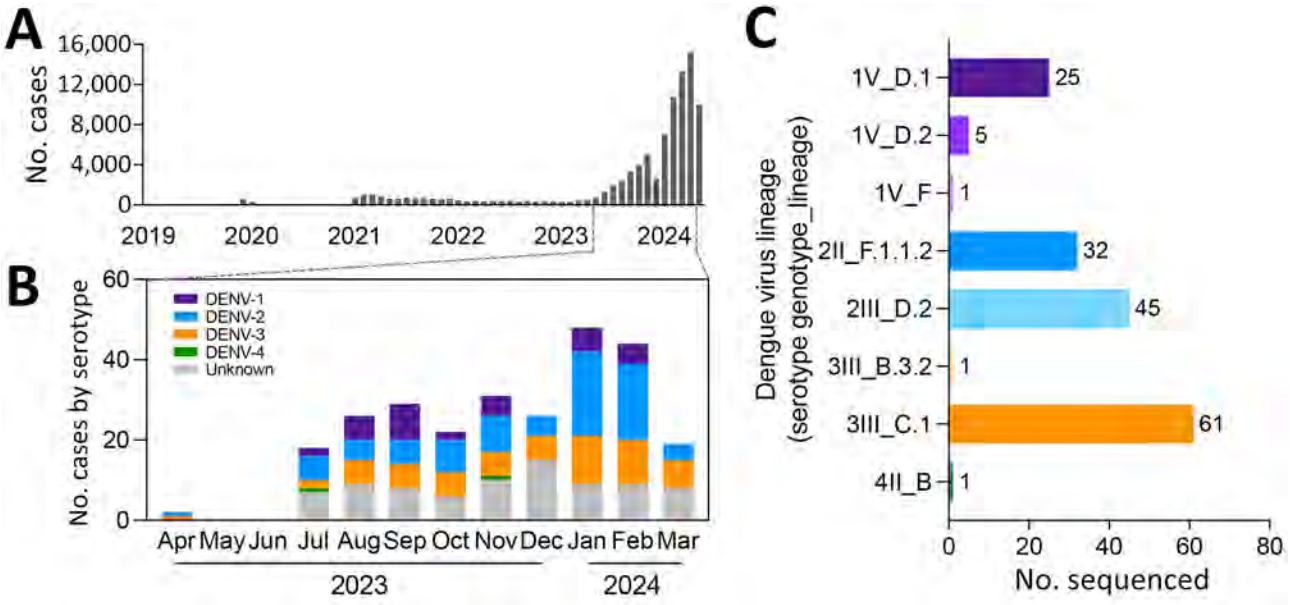

Figure 1. Cases in a study of multiple virus serotypes and lineages during dengue outbreak, Valle del Cauca, Colombia, 2023–2024. A) Monthly dengue cases reported by Valle del Cauca State Health Department in Colombia. Samples from confirmed dengue cases (n = 266) diagnosed at Hospital Universitario del Valle, Cali, Colombia. B) Number of cases per month by serotype during 2023–2024 period of increased dengue outbreaks. Serotypes detected by quantitative reverse transcription PCR. Samples with viral levels below detection limit are labeled unknown. C) DENV lineage by amplicon-based sequencing listed by serotype, genotype, and lineage. DENV, dengue virus.

analysis, including primer trimming and consensus sequence generation, by using a previously described iVar pipeline (*8*). We assigned DENV lineages to samples with ≥5% genome completeness, which was validated to be >93% accurate (*9*), by using the Dengue Virus Typing Tool nomenclature system (Genome

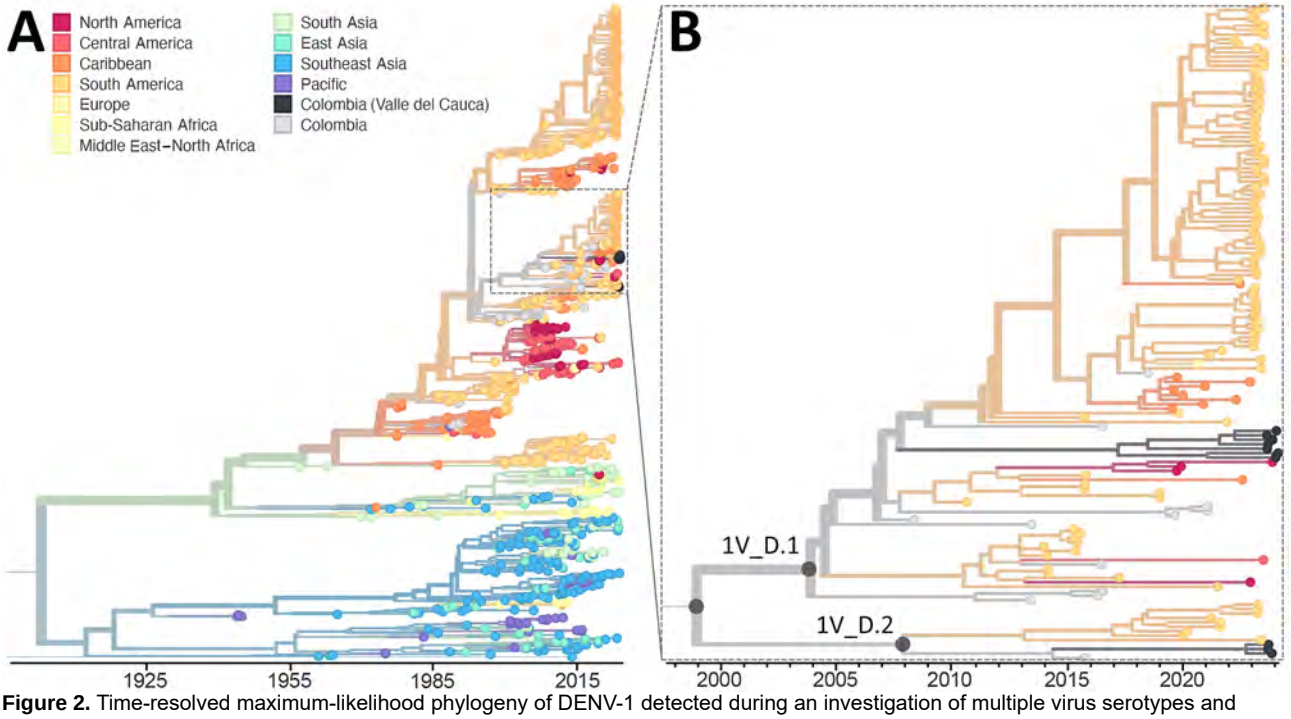

Figure 2. Time-resolved maximum-likelihood phylogeny of DENV-1 detected during an investigation of multiple virus serotypes and lineages during dengue outbreak, Valle del Cauca, Colombia, 2023–2024. The tree includes global DENV-1 sequences downloaded from GenBank and was constructed by using IQ-TREE (http://www.iqtree.org). A) Full reconstruction of 1,007 DENV-1 sequences from 1944–2024 colored by sampling location. B) Detail of the DENV-1V_D clade highlighting sequences from Valle del Cauca, Colombia (black) from 2023 through mid-2024. DENV, dengue virus.

Detective, https://www.genomedetective.com). We assigned serotypes to 185 (70%) samples (Figure 1, panel B); the assay was not able to detect serotypes in the remaining 81 samples because of low virus concentrations. Of the 185 samples with a serotype assignment, we assigned lineages to 171 (92%) samples via sequencing (Figure 1, panel C; Appendix Table, https://wwwnc.cdc.gov/EID/article/30/11/24-1031-App1.xlsx).

Among 2023–2024 samples, we detected all 4 DENV serotypes (DENV-1, 35; DENV-2, 85; DENV-3, 63; and DENV-4, 2) and 81 unknown serotypes (Figure 1, panel B). For part of 2023, we detected relatively equal proportions of DENV-1, DENV-2, and DENV-3, but then DENV-1 decreased as DENV-2 increased during late 2023 to early 2024. We also detected multiple lineages per serotype, except for DENV-4. DENV-3 genotype III lineage C.1 (3III_C.1 [*9*]), DENV-2III_D.2, DENV-2II_F.1.1.2, and DENV-1V_D.1 were most common (Figure 1, panel C).

To further investigate DENV lineages, we performed phylogenetic analysis using 79 sequenced samples for which we achieved >70% genome coverage: 10 DENV-1 sequences, 38 DENV-2 sequences, and 31 DENV-3 sequences. We combined our data with a background dataset downloaded from GenBank (Appendix Table) and then downsampled the data per serotype so that we kept all sequences from Colombia, 5 per year from the other countries in the Americas, and 1 per year from each country outside the Americas (1,007 DENV-1, 965 DENV-2, and 542 DENV-3 sequences). We analyzed the sequences using the Nextstrain bioinformatic and phylogenetic framework (*10*), and constructed maximum-likelihood trees using IQ-TREE (*11*) and a general time-reversible substitution model.

Our DENV-1 phylogenetic analysis revealed co-circulation of 2 distinct lineages, DENV-1V_D.1 and D.2 (Figure 2). Both lineages were previously detected in Colombia and elsewhere in South America (*5*,*12*), representing ongoing local and regional lineage persistence and diversification for the past ≈15–20 years.

Our DENV-2 phylogenetic analysis presents a more complicated picture of 3 genetic clusters and 3 individual sequences dispersed among 2 defined lineages, DENV-2III_D.2 and DENV-2II_F.1.1.2 (Figure 3). Lineage 2III_D.2 is a descendent of the original DENV-2 genotype III (i.e., Asian-American lineage) that was introduced in the Americas during the late 1970s and subsequently became established throughout

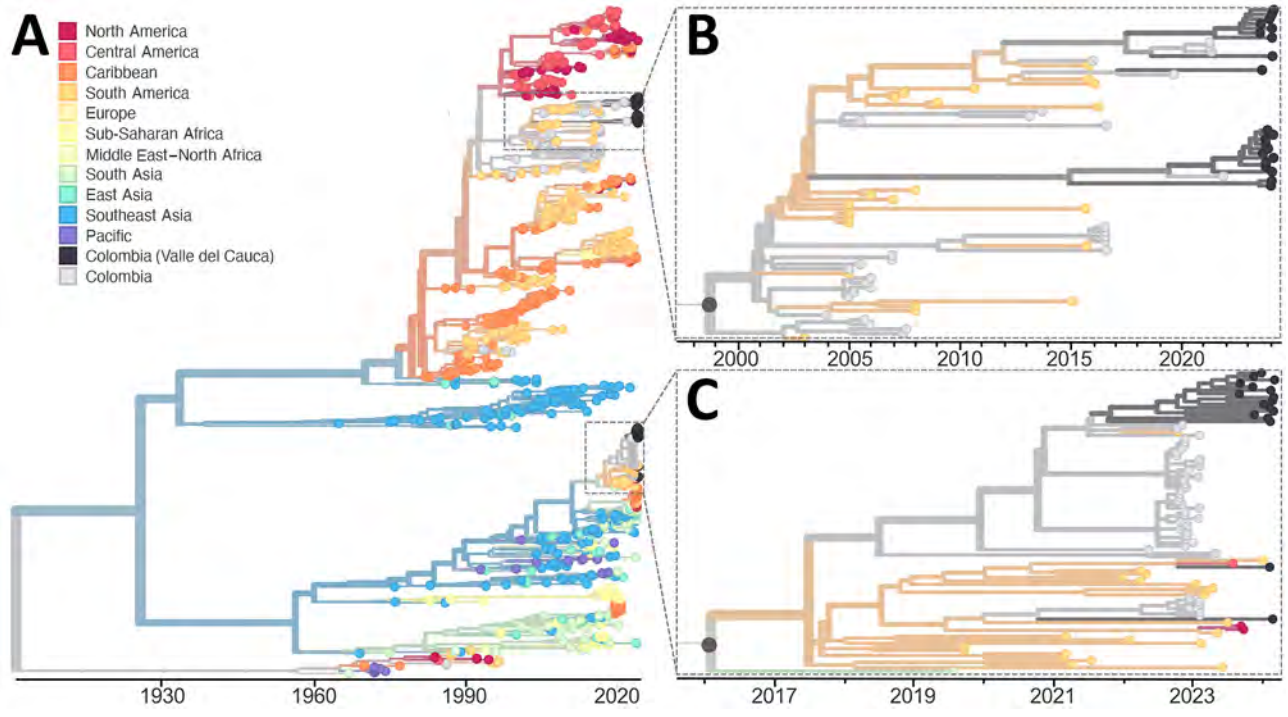

Figure 3. Time-resolved maximum-likelihood phylogeny of DENV-2 detected during an investigation of multiple virus serotypes and lineages during dengue outbreak, Valle del Cauca, Colombia, 2023–2024. The tree includes global DENV-2 sequences downloaded from GenBank and was constructed by using IQ-TREE (http://www.iqtree.org). A) Full reconstruction of 965 DENV-2 sequences from 1964–2024 colored by sampling location. B) Detail of the DENV-2III_D.2 clade highlighting sequences from Valle del Cauca, Colombia (black) from 2023 through mid-2024. C) Detail of DENV-2II_F.1.1.2 clades highlighting sequences from Valle del Cauca, Colombia (black) from 2023 through mid-2024. DENV, dengue virus.

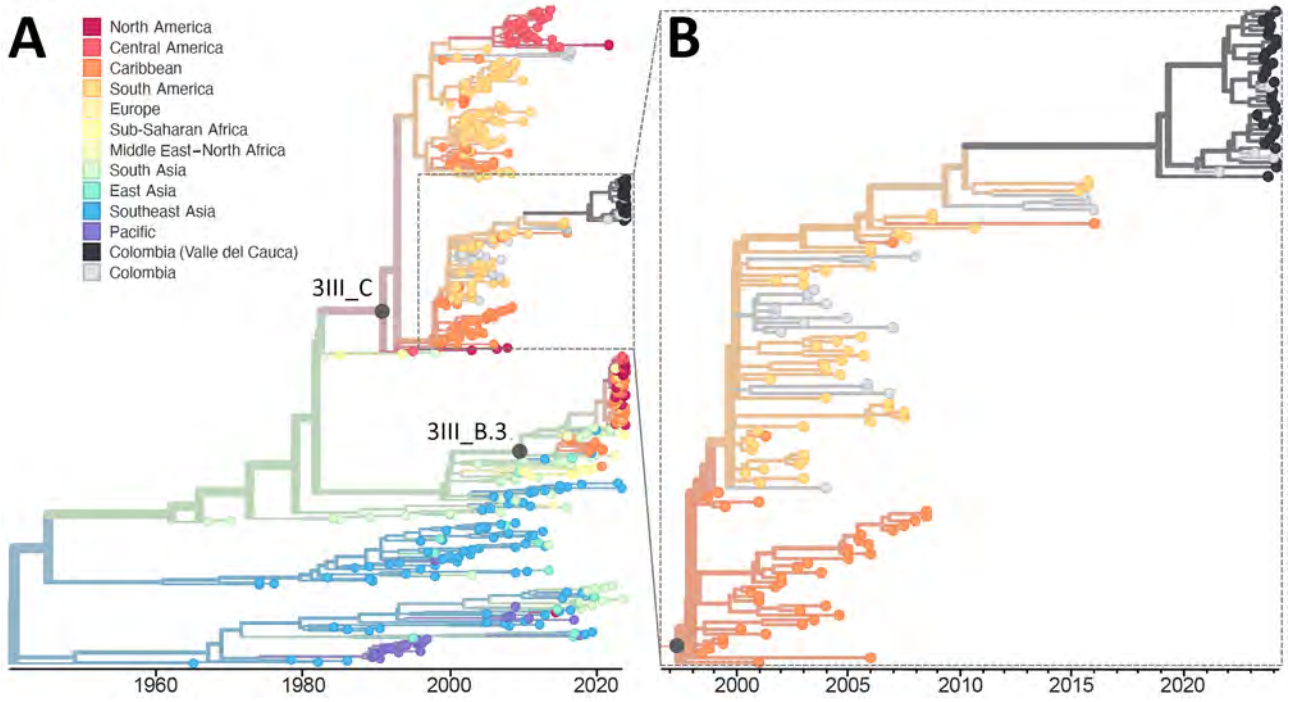

Figure 4. Time-resolved maximum-likelihood phylogeny of DENV-3 detected in an investigation of multiple virus serotypes and lineages during dengue outbreak, Valle del Cauca, Colombia, 2023–2024. The tree includes global DENV-3 sequences downloaded from GenBank and was constructed by using IQ-TREE (http://www.iqtree.org). A) Full reconstruction of 542 DENV-3 sequences from 1964 through 2024 colored by sampling location. B) Detail of the DENV-3III_C.1 clade highlighting sequences from Valle del Cauca, Colombia (black) from 2023 through mid-2024.

the region, including in Colombia (*13*). DENV-2 genotype II (a.k.a. Cosmopolitan lineage) was recently introduced into the Americas from Asia and was first detected during a dengue outbreak in Peru in 2019 (*14*). Detection of DENV-2II_F.1.1.2 in Valle del Cauca demonstrates that the emerging Cosmopolitan genotype can become established alongside the existing Asian-American genotype.

One hypothesis for the sudden increase in dengue cases is the introduction and rapid spread of a new DENV-3 lineage from Asia (*5*). DENV-3 can go undetected for long time periods in the Americas, sometimes for more than a decade, leaving large portions of the population potentially susceptible to this serotype (*4*,*6*,*15*). Therefore, detection of an emerging DENV-3III_B.3.2 lineage in the Caribbean (*5*), Brazil (*6*), Nicaragua (*4*), and elsewhere in the Americas was alarming. We detected 1 dengue case from January 2024 in Valle del Cauca with a likely 3III_B.3.2 infection (18% genome coverage), but 97% (61/63) of DENV-3 infections were lineage 3III_C.1 (Figure 1, panel C), and the lineage from 1 DENV-3 infection could not be assigned. DENV-3III_C was likely first introduced into the Americas in the early 1990s (*13*). Our findings show that DENV-3III_C has persisted through long periods of low detection (Figure 4), including sporadic detections of 3III_C.1 in Colombia since the early 2000s. Therefore, our results suggest that populations in the Americas might be susceptible to DENV-3 in general and not just the emerging 3III_B.3.2 lineage.

Conclusions

We investigated DENV infections from Valle del Cauca, Colombia, to determine if a specific virus serotype or lineage might be driving the record number of dengue cases in that state (*1*). We detected all 4 serotypes and found DENV-1, DENV-2, and DENV-3 shared dominance and at least 8 separate defined lineages were involved. Those lineages included multiple DENV-1 genotype V and DENV-2 genotype III lineages that have circulated in the Americas for ≈40 years (*13*), as well as an emerging DENV-2 genotype lineage. Moreover, despite the rapid spread of a new DENV-3III_B.3.2 lineage in the Americas (*4*–*6*), we found that the dominant DENV-3 lineage was 3III_C.1, which has been sporadically detected in Colombia for ≈20 years. Although multiple DENV serotypes are often detected during endemic transmission, our results were unexpected because outbreaks are typically dominated by a single serotype.

In summary, DENV lineages can have variable phenotypes that affect virulence, transmissibility, and

immune evasion. Detecting several co-dominating serotypes and lineages in Valle del Cauca suggests that the specific viruses were not the primary driver of the large outbreak. Our study demonstrates how genomic surveillance can help investigate causes of outbreaks and aid public health responses.

Sequencing data are available at National Center for Biotechnology Information BioProject (https://www.ncbi.nlm.nih.gov/bioproject; accession no. PRJNA1132139). Alignments, trees, and Nextstrain outputs are available at https://github.com/grubaughlab/DENV-genomics/tree/master/paper_2024-CO.

This study was approved by the research ethics committee at Hospital Universitario del Valle and Yale University Human Research Protection Program (protocol no. 2000033281). This publication was made possible by the National Institute of Allergy and Infectious Diseases of the National Institutes of Health (NIH) under award no. DP2AI176740 to N.D.G. and an NIH Shared Equipment grant (no. 1S10OD028669-01) award to the Yale Center for Genome Analysis. The findings and conclusions in this report are those of the author(s) and do not necessarily represent the official position of the NIH.

About the Author

Dr. Grubaugh is an associate professor at the Yale School of Public Health in Connecticut, USA. His research interests focus on integrating genomic epidemiology in public health systems to enhance virus surveillance and outbreak response, with a special emphasis on arthropodborne viruses.

References

1. Pan American Health Organization, World Health Organization. Data—dengue [cited 2024 Jul 1]. https://www3.paho.org/data/index.php/en/mnu-topics/indicadores-dengue-en.html
2. Messina JP, Brady OJ, Golding N, Kraemer MUG, Wint GRW, Ray SE, et al. The current and future global distribution and population at risk of dengue. Nat Microbiol. 2019;4:1508–15. https://doi.org/10.1038/s41564-019-0476-8
3. Chen Y, Xu Y, Wang L, Liang Y, Li N, Lourenço J, et al. Indian Ocean temperature anomalies predict long-term global dengue trends. Science. 2024;384:639–46. https://doi.org/10.1126/science.adj4427
4. Cerpas C, Vásquez G, Moreira H, Juarez JG, Coloma J, Harris E, et al. Introduction of new dengue virus lineages of multiple serotypes after COVID-19 pandemic, Nicaragua, 2022. Emerg Infect Dis. 2024;30:1203–13. https://doi.org/10.3201/eid3006.231553
5. Taylor-Salmon E, Hill V, Paul LM, Koch RT, Breban MI, Chaguza C, et al. Travel surveillance uncovers dengue virus dynamics and introductions in the Caribbean. Nat Commun. 2024;15:3508. https://doi.org/10.1038/s41467-024-47774-8
6. Naveca FG, Santiago GA, Maito RM, Ribeiro Meneses CA, do Nascimento VA, de Souza VC, et al. Reemergence of dengue virus serotype 3, Brazil, 2023. Emerg Infect Dis. 2023;29:1482–4. https://doi.org/10.3201/eid2907.230595
7. Santiago GA, Vergne E, Quiles Y, Cosme J, Vazquez J, Medina JF, et al. Analytical and clinical performance of the CDC real time RT-PCR assay for detection and typing of dengue virus. PLoS Negl Trop Dis. 2013;7:e2311. https://doi.org/10.1371/journal.pntd.0002311
8. Vogels CBF, Hill V, Breban MI, Chaguza C, Paul LM, Sodeinde A, et al. DengueSeq: a pan-serotype whole genome amplicon sequencing protocol for dengue virus. BMC Genomics. 2024;25:433. https://doi.org/10.1186/s12864-024-10350-x
9. Hill V, Cleemput S, Pereira JS, Gifford RJ, Fonseca V, Tegally H, et al. A new lineage nomenclature to aid genomic surveillance of dengue virus. PLoS Biol. 2024;22:e3002834. https://doi.org/10.1371/journal.pbio.3002834
10. Hadfield J, Megill C, Bell SM, Huddleston J, Potter B, Callender C, et al. Nextstrain: real-time tracking of pathogen evolution. Bioinformatics. 2018;34:4121–3. https://doi.org/10.1093/bioinformatics/bty407
11. Minh BQ, Schmidt HA, Chernomor O, Schrempf D, Woodhams MD, von Haeseler A, et al. IQ-TREE 2: new models and efficient methods for phylogenetic inference in the genomic era. Mol Biol Evol. 2020;37:1530–4. https://doi.org/10.1093/molbev/msaa015
12. Carrillo-Hernandez MY, Ruiz-Saenz J, Jaimes-Villamizar L, Robledo-Restrepo SM, Martinez-Gutierrez M. Phylogenetic and evolutionary analysis of dengue virus serotypes circulating at the Colombian–Venezuelan border during 2015–2016 and 2018–2019. PLoS One. 2021;16:e0252379. https://doi.org/10.1371/journal.pone.0252379
13. Allicock OM, Lemey P, Tatem AJ, Pybus OG, Bennett SN, Mueller BA, et al. Phylogeography and population dynamics of dengue viruses in the Americas. Mol Biol Evol. 2012;29:1533–43. https://doi.org/10.1093/molbev/msr320
14. García MP, Padilla C, Figueroa D, Manrique C, Cabezas C. Emergence of the Cosmopolitan genotype of dengue virus serotype 2 (DENV2) in Madre de Dios, Peru, 2019. Rev Peru Med Exp Salud Publica. 2022;39:126–8. https://doi.org/10.17843/rpmesp.2022.391.10861
15. Santiago GA, McElroy-Horne K, Lennon NJ, Santiago LM, Birren BW, Henn MR, et al. Reemergence and decline of dengue virus serotype 3 in Puerto Rico. J Infect Dis. 2012;206:893–901. https://doi.org/10.1093/infdis/jis426

Address for correspondence: Nathan D. Grubaugh, Yale School of Public Health, 60 College St, Ste 608, New Haven, CT 06510, USA; email: nathan.grubaugh@yale.edu

Evidence of Human Bourbon Virus Infections, North Carolina, USA

Diana L. Zychowski,[1] Gayan Bamunuarachchi,[1] Scott P. Commins, Ross M. Boyce, Adrianus C.M. Boon

Bourbon virus is a tickborne virus that can cause human disease. Cases have been reported in Kansas, Oklahoma, and Missouri, USA. We identified Bourbon virus–specific neutralizing antibodies in patients from North Carolina. Bourbon virus infections are likely more common than previously thought, highlighting the need for improved diagnostics and surveillance.

Vectorborne diseases are a growing public health concern in the United States. Whereas bacterial pathogens are responsible for most infections, tickborne viruses represent an emerging and poorly understood threat (*1*).

Bourbon virus (BRBV), a tickborne virus belonging to the family Orthomyxoviridae, was first isolated from a patient living in Bourbon County, Kansas, USA, in 2014 (*2*). To date, human cases have been reported only in the United States, with 5 cases reported in 3 states: Kansas, Oklahoma, and Missouri (*2*–*5*). However, serosurveillance of St. Louis, Missouri, residents identified BRBV-specific serum-neutralizing antibodies in 0.7% (3/440) of persons, suggesting that BRBV infections are likely underrecognized (*6*).

Because of the scarcity of confirmed cases, descriptions of the clinical disease spectrum are limited. Fever, arthralgia, diarrhea, headache, and rash are complaints recorded early in the course of infection, followed by progression to critical illness in some cases. Laboratory abnormalities include leukopenia, thrombocytopenia, and elevated levels of aspartate and alanine aminotransferase (*2*,*3*,*7*).

The primary vector of BRBV is the lone star tick (*Amblyomma americanum*), which is widely distributed throughout the central, eastern, southeastern, and south-central United States (*4*,*8*). Although no cases of human BRBV disease have been confirmed in North Carolina, BRBV was isolated from ticks (North Carolina Division of Public Health, pers. comm., email, 2022 Jul 13), and neutralizing antibodies were detected in white-tailed deer across the state (Figure 1) (*9*). BRBV may be circulating in North Carolina and being transmitted to humans, possibly causing disease, but is undiagnosed or interpreted as other tickborne diseases. We used previously collected human serum samples to screen for the presence of BRBV-neutralizing antibodies.

The Study

Serum from 518 residents of North Carolina, with variable known tick exposure, were screened for the presence of BRBV-neutralizing antibodies. Another 162 samples came from a cohort of patients with confirmed alpha-gal syndrome (AGS), a delayed-onset reaction following ingestion of mammal meat products that is associated with the bite of a lone star tick (*10*). An additional 156 samples were from a repository of recent heart valve recipients undergoing surveillance for the development of immunoglobulin E to galactose-α-1,3-galactose. The remaining 200 samples were from antenatal women. Those sample sources were selected because of availability, with the AGS group having the highest risk for tick exposure. Samples were collected during 2021–2023 and tested for BRBV antibodies in 2023.

We conducted testing by using previously validated methods (*6*). We diluted the serum samples 1:60 and screened in a rapid neutralization assay with a chimeric vesicular stomatitis virus (VSV) expressing the BRBV envelope protein to assess for the presence of BRBV-specific neutralizing antibodies. We conducted confirmatory testing on samples with ≥90% inhibition of VSV-BRBV by using a focus reduction neutralization test (FRNT) that used a BRBV St. Louis

Author affiliations: University of North Carolina at Chapel Hill, Chapel Hill, North Carolina, USA (D.L. Zychowski, S.P. Commins, R.M. Boyce); Washington University School of Medicine in St. Louis, St. Louis, Missouri, USA (G. Bamunuarachchi, A.C.M. Boon).

DOI: https://doi.org/10.3201/eid3011.240499

[1]These first authors contributed equally to this article.

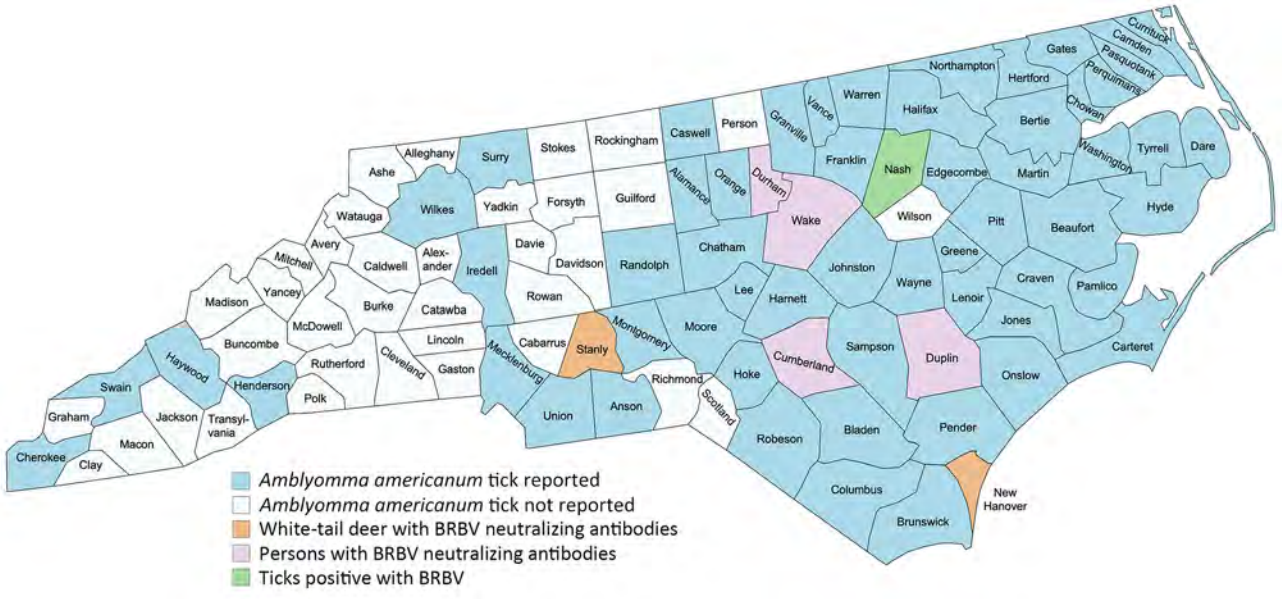

Figure 1. Distribution of the lone star tick (*Amblyomma americanum*) and evidence of Bourbon virus detection throughout North Carolina, USA. The map is adapted from a previous publication (*8*) and updated with locations of known bourbon virus carrying ticks (North Carolina Division of Public Health, pers. comm., email, 2022 Jul 13), white-tailed deer with positive bourbon virus–specific neutralizing antibodies (*9*), and persons with bourbon virus–specific neutralizing antibodies. Created by using http://www.mapchart.net.

strain. We serially diluted serum samples 3-fold and incubated them with BRBV to reach a final serum dilution of 1:40–1:29,160 in media. We tested samples in duplicate. Each assay included convalescent serum from BRBV-infected mice as positive controls and samples without serum as negative controls. We calculated inhibitory values at a concentration of 90% (IC_{90}) by using log (agonist) versus response. We defined samples with BRBV-neutralizing antibodies of $IC_{90} \geq$1:40 as positive and undertook a 10-year chart review of outpatient and inpatient records. The collection of the data used in the study was approved by the institutional review boards of Duke University (Durham, NC, USA) and the University of North Carolina, Chapel Hill (Chapel Hill, NC, USA).

Of the 518 samples, 6 (1.15%) demonstrated ≥90% inhibition of infection (Figure 2) in the VSV-BRBV rapid assay and underwent further testing by using BRBV FRNT. From the AGS cohort samples, 1 sample was positive for BRBV neutralizing antibodies, and from the heart valve group, 3 samples were positive for BRBV neutralizing antibodies. The IC_{90} for those 4 serum samples ranged from 1:100 to 1:200.

Among the 4 positive samples, all were residents of North Carolina (Table). Of those residents, 3 sought care for nonspecific viral respiratory symptoms within the previous 10 years, but there was no suspicion for a febrile tickborne illness. Only 1 person, with known AGS, had a documented history of tick bites.

Conclusions

The presence of BRBV-specific neutralizing antibodies in 4/518 (0.77%) persons provides evidence of human BRBV infection in North Carolina. Whereas some of the patients did seek care for respiratory infections, there was no documented history of illness compatible with previous descriptions of BRBV infection. This finding suggests that there are likely to be asymptomatic or more subtle manifestations of BRBV infection, particularly in immunocompetent hosts, which would be consistent with other arboviral infections. Overall, our findings suggest that BRBV may be an underappreciated cause of vectorborne disease in NC.

Our study likely underestimates the number of persons infected with BRBV in North Carolina. It is possible we missed exposed persons who have waning immunity from more remote infections, or the infection did not induce sufficiently high levels of neutralizing antibodies to be detected in our assays.

The first limitation of our study is that the presence of neutralizing antibodies does not equate to clinical disease. This study aimed to demonstrate the presence of human infection in North Carolina but was not designed to capture a history of typical symptoms or risk factors for disease severity. Second, we cannot exclude travel of persons positive for BRBV neutralizing antibody to states with known cases. However, given the evidence of BRBV in North Carolina wildlife and ticks (*9*), it is not surprising that

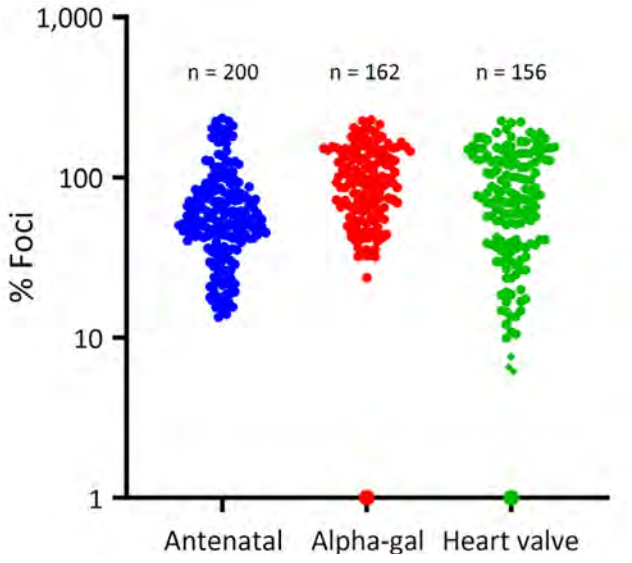

Figure 2. Results from a vesicular stomatitis virus and Bourbon virus rapid neutralization assay using serum samples from residents of North Carolina, USA. Normalized vesicular stomatitis virus-Bourbon virus neutralization (percentage foci compared with the control without serum) results are shown from 3 groups: antenatal women, persons with alpha-gal syndrome, and recent heart valve recipients. Colored dots represent singular serum sample.

local BRBV transmission to humans has occurred. Finally, whereas we found a higher proportion of persons with BRBV-specific neutralizing antibodies within the heart valve group compared with those with known AGS, this study was not designed to look for statistical differences between groups and is subject to small frequencies.

The laboratory diagnosis of BRBV infection is challenging because there are no commercially available tests within the United States. Samples can be sent for serologic and nucleic acid amplification testing at public health laboratories or FRNT at the Centers for Disease Control and Prevention. Unfortunately, those tests have limitations. The viremic window for nucleic acid detection may be short or limited to the asymptomatic phase, and antibodies may not be detectable until 1 week after symptom onset. New diagnostic approaches are needed to improve accessibility and time to diagnosis, which cannot only prevent further invasive testing and unnecessary antimicrobial exposure but can also provide anticipatory guidance.

In addition to improved diagnostics, clinicians must remain vigilant to identify patients in need of viral testing. A single, acute serologic titer result cannot be used for the diagnosis of tickborne *Rickettsia* or *Ehrlichia* infections. For example, a North Carolina seroprevalence study revealed high population point prevalence rates for *Ehrlichia* infection of 8.6% (95% CI 5.9%–11.3%) and *Rickettsia* infection of 17.1% (95% CI 12.6–21.5) (*11*). Therefore, a single positive bacterial antibody titer should not preclude further tickborne diagnostic workup, particularly in cases of severe disease or where the patient fails to respond to antimicrobials.

Because of the clinical manifestation of nonspecific viral symptoms, challenging laboratory diagnostics, and the lack of commercially available tests, the true incidence and clinical symptomatology of BRBV remain unknown and active surveillance for acute cases is needed. Our findings substantially expand the known geographic area at risk for this emerging virus and demonstrate the need for further investigation and more widespread testing in patients with suspected BRBV infection.

Table. Documented characteristics of patients with bourbon virus–specific neutralizing antibodies, North Carolina, USA*

Case	Group	Age, y	County	Recent travel?	Tickborne illness?	Tick bite history?	Outdoor exposures	Comorbidities	Medical history
1	Heart valve	77	Cumberland	No	No	No	Outdoor walks	AS, essential thrombocytopenia, prior nephrectomy, OSA, HTN	Received care for allergies, possible viral upper respiratory infection, spring 2022.
2	Heart valve	78	Durham	No	No	No	None	AS, DMII, CKD, HTN, HLD, MGUS, ILD	Received antibiotics for possible lower respiratory infection superimposed on ILD, spring 2023.
3	Heart valve	79	Wake	No	No	No	None	AS, CAD, childhood rheumatic fever, HTN, HLD, hypothyroidism	Received care for respiratory viral infection or possible conjunctivitis, 2014.
4	AGS	63	Duplin	Arkansas, Montana	No	Yes, many	None	HTN, nephrolithiasis	Received multiple empiric doxycycline courses.

*AGS, alpha-gal syndrome; AS, aortic stenosis; CAD, coronary artery disease; CKD, chronic kidney disease; DMII, type two diabetes mellitus; HLD, hyperlipidemia; HTN, hypertension; ILD, interstitial lung disease; MGUS, monoclonal gammopathy of undetermined significance; OSA, obstructive sleep apnea.

Acknowledgments

We thank Joseph Turek, Joseph Nellis, Berk Aykut, and Sean Whelan.

A.C.M.B. was supported by the National Institute of Allergy and Infectious Disease (grant nos. R01-AI173327 and U01-AI151810), R.M.B. was supported by a Creativity Hub Award from the University of North Carolina Office of the Vice Chancellor for Research, D.L.Z. was supported by the National Institute of Allergy and Infectious Disease (grant no. AI070114). S.P.C. was supported by the National Institute of Allergy and Infectious Disease (grant no. R01-AI135049).

Author contributions: study conception and design, A.C.M.B., R.M.B., and S.P.C.; funding procurement, A.C.M.B., R.M.B., and S.P.C.; laboratory testing, G.B.; first draft of manuscript, D.L.Z. and G.B.

About the Author

Dr. Zychowski is an Infectious Disease Fellow at the University of North Carolina at Chapel Hill. Her primary research focus is on the intersection of tickborne infections, public health surveillance, and population health sciences.

References

1. Rosenberg R, Lindsey NP, Fischer M, Gregory CJ, Hinckley AF, Mead PS, et al. Vital signs: trends in reported vectorborne disease cases—United States and territories, 2004–2016. MMWR Morb Mortal Wkly Rep. 2018;67:496–501. https://doi.org/10.15585/mmwr.mm6717e1
2. Kosoy OI, Lambert AJ, Hawkinson DJ, Pastula DM, Goldsmith CS, Hunt DC, et al. Novel thogotovirus associated with febrile illness and death, United States, 2014. Emerg Infect Dis. 2015;21:760–4. https://doi.org/10.3201/eid2105.150150
3. Roe MK, Huffman ER, Batista YS, Papadeas GG, Kastelitz SR, Restivo AM, et al. Comprehensive review of emergence and virology of tickborne bourbon virus in the United States. Emerg Infect Dis. 2023;29:1–7. https://doi.org/10.3201/eid2901.212295
4. Savage HM, Burkhalter KL, Godsey MS Jr, Panella NA, Ashley DC, Nicholson WL, et al. Bourbon virus in field-collected ticks, Missouri, USA. Emerg Infect Dis. 2017;23:2017–22. https://doi.org/10.3201/eid2312.170532
5. Bricker TL, Shafiuddin M, Gounder AP, Janowski AB, Zhao G, Williams GD, et al. Therapeutic efficacy of favipiravir against bourbon virus in mice. PLoS Pathog. 2019;15:e1007790. https://doi.org/10.1371/journal.ppat.1007790
6. Bamunuarachchi G, Harastani H, Rothlauf PW, Dai YN, Ellebedy A, Fremont D, et al. Detection of bourbon virus-specific serum neutralizing antibodies in human serum in Missouri, USA. MSphere. 2022;7:e0016422. https://doi.org/10.1128/msphere.00164-22
7. Centers for Disease Control and Prevention. Bourbon virus. [cited 2024 Jan 3]. https://www.cdc.gov/bourbon-virus/hcp/clinical-diagnosis-treatment
8. Dupuis AP II, Lange RE, Ciota AT. Emerging tickborne viruses vectored by *Amblyomma americanum* (Ixodida: Ixodidae): heartland and bourbon viruses. J Med Entomol. 2023;60:1183–96. https://doi.org/10.1093/jme/tjad060
9. Komar N, Hamby N, Palamar MB, Staples JE, Williams C. Indirect evidence of bourbon virus (Thogotovirus, Orthomyxoviridae) infection in North Carolina. N C Med J. 2020;81:214–5. https://doi.org/10.18043/ncm.81.3.214
10. Kersh GJ, Salzer J, Jones ES, Binder AM, Armstrong PA, Choudhary SK, et al. Tick bite as a risk factor for alpha-gal-specific immunoglobulin E antibodies and development of alpha-gal syndrome. Ann Allergy Asthma Immunol. 2023;130:472–8. https://doi.org/10.1016/j.anai.2022.11.021
11. Zychowski DL, Alvarez C, Abernathy H, Giandomenico D, Choudhary SK, Vorobiov JM, et al. Tick-borne disease infections and chronic musculoskeletal pain. JAMA Netw Open. 2024;7:e2351418–2351418. https://doi.org/10.1001/jamanetworkopen.2023.51418

Address for correspondence: Diana Zychowski, University of North Carolina at Chapel Hill, 111 Mason Farm Rd, Chapel Hill, NC 27514, USA; email: diana.zychowski@unchealth.unc.edu

Clinical and Molecular Characterization of Human *Burkholderia mallei* Infection, Brazil

Kleber G. Luz, Fernanda R.O. Bezerra, Miguel A. Sicolo, Anuska A.R.S. Silva, Andréa A. Egito, Paula A.P. Suniga, Jessica C.K. Moriya, Maria G. Santos, Cynthia Mantovani, Júlia S. Silva, Nalvo F. Almeida, Ana Marcia S. Guimarães, Alberto M.R. Dávila, Rodrigo Jardim, Lenita R. Santos, Flábio R. Araújo

We report a case of *Burkholderia mallei* causing glanders in a 73-year-old patient from the Northeast Region of Brazil. The patient was hospitalized with severe pneumonia. PCR and genomic sequencing confirmed *B. mallei* in pleural drainage. Genotyping revealed a novel genotype, emphasizing the need for genetic surveillance in zoonotic infections.

Burkholderia mallei is a gram-negative bacterium that causes glanders disease, which primarily affects equids. *B. mallei* can infect humans and cause clinical manifestations ranging from subclinical infections to severe conditions such as septicemia or pneumonia. Treatment and prevention are difficult because of antimicrobial resistance, intracellular survival, and lack of a vaccine (*1*). In Brazil, *B. mallei* infections in equids have occurred across various regions (*2*–*6*). However, genotyping studies of *B. mallei* strains are limited. In the Northeast Region of Brazil, strains with lineages and branches L3B2, L3B3, and L3B2 have been identified. In the Southeast Region of Brazil, genotype L3B2 has been reported (*2*,*4*,*5*).

Author affiliations: Universidade Federal do Rio Grande do Norte, Natal, Brazil (K.G. Luz); Universidade Potiguar, Natal (F.R.O. Bezerra); Casa de Saúde São Lucas, Natal (M.A. Sicolo); Laboratório DNA Center, Natal (A.A.R.S. Silva); Embrapa Beef Cattle, Campo Grande, Brazil (A.A. Egito, P.A.P. Suniga, J.C.K. Moriya, M.G. Santos, C. Mantovani, J.S. Silva, L.R. Santos, F.R. Araújo); Universidade Federal de Mato Grosso do Sul, Campo Grande (N.F. Almeida); University of São Paulo, São Paulo, Brazil (A.M.S. Guimarães), Oswaldo Cruz Institute, FIOCRUZ, Rio de Janeiro, Brazil (A.M.R. Dávila, R. Jardim)

DOI: https://doi.org/10.3201/eid3011.240549

Surveillance and scientific understanding of human *B. mallei* infection in Brazil remain limited. *B. mallei* was identified in a case involving a child from the Northeast Region of Brazil (*7*). However, that publication did not specify the diagnostic methodology used to confirm the pathogen's identity. Accurate diagnostics are crucial because melioidosis caused by *B. pseudomallei*, which can lead to similar clinical and pathological outcomes, is also found in Brazil (*8*).

We report a case of *B. mallei* infection in a patient from Brazil. This case provides insights into the probable transmission context, clinical symptoms, treatment approaches, and methods for detecting *B. mallei*.

The Study

A 73-year-old man residing in Natal, Rio Grande do Norte, northeast Brazil, was hospitalized with complaints of fever and respiratory symptoms (Appendix, https://wwwnc.cdc.gov/EID/article/30/11/24-0549-App1.pdf). The patient's medical history revealed his horse was in contact with a glanders-positive horse at a vaquejada training center. In the Northeast Region, equestrian events bring together horses from various sources, which increases the risk for *B. mallei* transmission and infection. Close interactions between horse owners and horses raise the likelihood of human exposure to infected animals. After 6 days of hospitalization, the patient underwent a computed tomography of his chest (Figure 1). On day 7 of hospitalization, a 25-mL sample of pleural drainage was collected and transported to the Embrapa Beef Cattle Biosafety Level 3 laboratory in Campo Grande, Brazil.

We extracted DNA from the pleural drainage by using a DNeasy Blood & Tissue Kit (QIAGEN,

https://www.qiagen.com). We conducted microbiome DNA enrichment by using the NEBNext microbiome DNA enrichment kit (New England Biolabs, https://www.neb.com). We inoculated 100 µL of pleural drainage onto 5% sheep blood agar with 2% glycerol and incubated aerobically at 37°C for 24–72 hours. We cultured 100 µL of pleural drainage in 3 mL of brain heart infusion medium with 2% glycerol, with and without penicillin G and polymyxin B, and incubated at 37°C with shaking for 24 hours. From each brain–heart infusion culture, we plated 50 µL on glycerinated blood agar and incubated at 37°C with shaking for 24 hours.

We subcultured colonies matching the macroscopic identification of *B. mallei* on semi-selective agar with penicillin G (100 U/mL), polymyxin B (50 U/mL), disodium ticarcillin (32 µg/mL), ampicillin (32 µg/mL), and trimethoprim/sulfamethoxazole (TMP/SMX) (50 µg/mL + 10 µg/mL), and incubated for ≤72 hours. The pleural drainage culture initially grew slowly on glycerinated blood agar. Subsequent plating on semiselective agar and agar without antimicrobial drugs led to the isolation of colonies with consistent morphology. We chose a single colony and cultivated on glycerinated blood agar, yielding multiple colonies with identical morphology. We then collected the colonies for DNA extraction and PCR analysis.

We extracted DNA from bacterial isolates by using a modified protocol (*9*). Conventional PCR targeted specific genetic loci from pleural drainage and bacterial isolates (Appendix Table 1). Each PCR reaction included a negative control and a positive control (*B. mallei* DNA, strain BAC 86/19) (*5*). We included PCR extraction controls (parallel DNA extraction of *E. coli*) in assays targeting fliP-IS407A (Appendix Table 1) with DNA from pleural drainage and fliP-IS407A (Appendix Table 1) with DNA from bacterial colonies. PCR conducted by using DNA extracted directly from bacterial colonies included control DNA from a field strain of *B. pseudomallei* supplied by the Ceará Central Laboratory, Brazil. We included the control DNA in reactions targeting the multiple-locus variable number tandem repeat analysis marker Bm17. We analyzed PCR products by using gel electrophoresis and whole-genome sequencing (Appendix).

PCR amplifications targeting *B. mallei* loci (Appendix Table 1) from pleural drainage and bacterial isolate DNA yielded positive results. In addition, Burk475 PCR, which is designed to detect both *B. mallei* and *B. pseudomallei*, demonstrated positive amplification. The PCR targeting the open reading frame 11 marker for *B. pseudomallei* was negative (Figures 1, 2; Appendix). The amplicon sequencing results (Appendix Table 2) confirmed exact matches with *B. mallei* from PCR targeting the species.

The bacterial genome sequencing revealed 5,506,149 reads (National Center for Biotechnology Information Sequence Read Archive accession no. PRJNA1130892). De novo assembly produced 881 contigs, with an N50 of 2,605,114 bp. Synteny analysis indicated 112 regions shared similarity with *B. mallei* (Figure 2). BLASTX analysis (https://blast.ncbi.nlm.nih.gov) showed 110 contigs (12.48%) matched both *B. mallei* and *B. pseudomallei* with 100% identity, whereas 59 contigs (6.69%) specifically matched *B. mallei*, differing from *B. pseudomallei* because of single-nucleotide polymorphisms (SNPs), insertions, or deletions (Appendix Table 3).

Analysis identified an SNP at position 1,163,826 in the reference genome of *B. mallei*. In the human-origin isolate studied (*B. mallei* Natal strain), this SNP manifested as a T allele, a characteristic

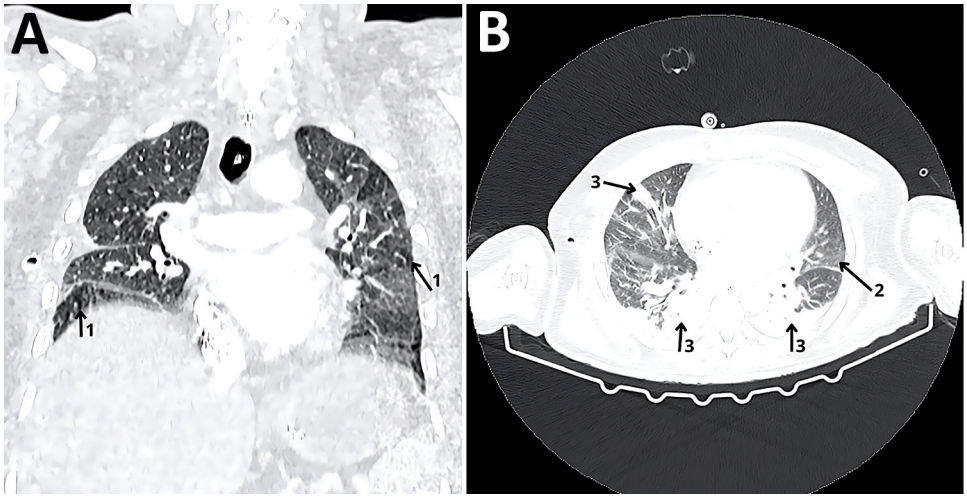

Figure 1. Computed tomography with contrast of the chest of a patient from Brazil infected with *Burkholderia mallei*. A) Coronal section, showing a heterogeneous pattern of lung attenuation. Arrows marked 1 indicate a suggestive disturbance in the ventilation-perfusion relationship. B) Axial section. Arrow marked 2 indicates consolidative opacities. Arrows marked 3 indicate subsegmental atelectasis in both lungs.

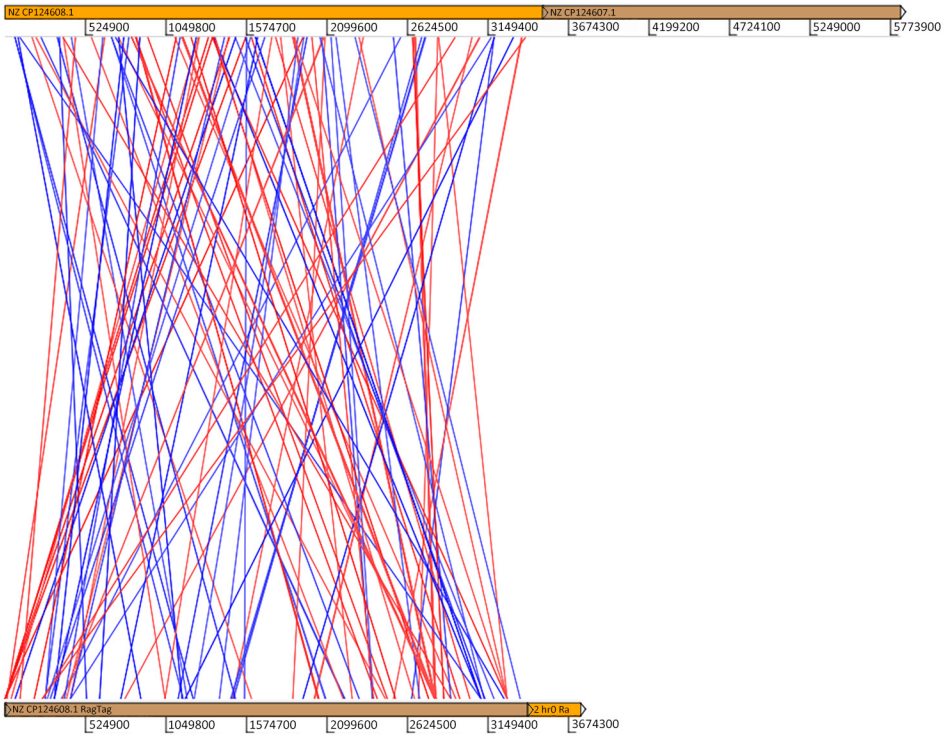

Figure 2. Synteny graph between the assembled genome (bottom) and the reference genome (top) of *Burkholderia mallei* recovered from a patient in Brazil. The lines represent regions of similarity; blue lines indicate sense and red lines antisense.

feature observed in isolates belonging to the L2B2sB1Gp1 lineage.

Conclusions

We successfully detected *B. mallei* in this patient by using various PCR targets, directly from both pleural drainage and bacterial cultures. The methodology included culturing a limited number of bacterial colonies from the sample, followed by subculturing to various media and antimicrobial drug conditions. Necessary to the process was the careful selection of colonies on the basis of consistent morphological characteristics, which was essential for the subsequent PCR detection.

The presence of a limited number of contigs showing identity with *Burkholderia* species in the genome sequencing of the PCR-positive colony suggests the potential coculturing of competing microbiota. However, 59 contigs showed exact matches with *B. mallei*, distinguishing them from *B. pseudomallei* because of variations such as SNPs, insertions, or deletions. Those matches aligned consistently with the reference *B. mallei* genome and were validated across multiple other *B. mallei* genomes, confirming the presence of this species in the sample through genome sequencing.

A SNP characteristic of isolates from the L2B2sB1Gp1 lineage was identified in the *B. mallei* Natal strain. This lineage includes strains from the United States and Burma (ATCC 23344) from humans and strains from Myanmar and China from equids (*10*). Of note, in Brazil only isolates from lineage 3 have been reported, all from equids (*2*,*4*,*5*).

Treating glanders disease is challenging because of *B. mallei*'s resistance to many common antimicrobial drugs. A recent case from China highlighted initial therapy failure with levofloxacin and cefotaxime/sulbactam, but success was achieved by adding meropenem, doxycycline, and TMP/SMX (*11*). In Iran, effective treatment involved imipenem and doxycycline (*12*), aligning with established guidelines for managing zoonotic glanders (*13*). In this case, initial treatment with ceftriaxone followed by meropenem and azithromycin did not improve symptoms. However, combining meropenem, linezolid, TMP/SMX, and levofloxacin resulted in improvement in the patient's condition.

Human glanders disease is likely underreported and underrecognized, underscoring the importance of increased awareness among medical professionals. The use of effective antimicrobial drugs is necessary for patient treatment. Management of human *B. mallei* infections requires enhanced coordination between veterinary and human health specialists.

This study was supported by Conselho Nacional de Desenvolvimento Científico e Tecnológico (grant no. 315857/2021-8).

About the Author

Dr. Luz is a professor at the Federal University of Rio Grande do Norte. His interests include tropical diseases, infectious and parasitic diseases, sepsis, hospital-acquired infections, arboviruses, viral hepatitis, and human T-lymphotropic virus 1 and 2 infections.

References

1. Waag DM, Chance TB, Trevino SR, Rossi FD, Fetterer DP, Amemiya K, et al. Comparison of three non-human primate aerosol models for glanders, caused by *Burkholderia mallei*. Microb Pathog. 2021;155:104919. https://doi.org/10.1016/j.micpath.2021.104919
2. Laroucau K, Lucia de Assis Santana V, Girault G, Martin B, Miranda da Silveira PP, Brasil Machado M, et al. First molecular characterisation of a Brazilian *Burkholderia mallei* strain isolated from a mule in 2016. Infect Genet Evol. 2018;57:117–20. https://doi.org/10.1016/j.meegid.2017.11.014
3. Abreu DC, Gomes AS, Tessler DK, Chiebao DP, Fava CD, Romaldini AHCN, et al. Systematic monitoring of glanders-infected horses by complement fixation test, bacterial isolation, and PCR. Vet Anim Sci. 2020;10:100147. https://doi.org/10.1016/j.vas.2020.100147
4. Falcão MVD, Laroucau K, Vorimore F, Deshayes T, Santana VLA, Silva KPC, et al. Molecular characterization of *Burkholderia mallei* strains isolated from horses in Brazil (2014–2017). Infect Genet Evol. 2022;99:105250. https://doi.org/10.1016/j.meegid.2022.105250
5. Suniga PAP, Mantovani C, Dos Santos MG, do Egito AA, Verbisck NV, Dos Santos LR, et al. Glanders diagnosis in an asymptomatic mare from Brazil: insights from serology, microbiological culture, mass spectrometry, and genome sequencing. Pathogens. 2023a;12:1250. https://doi.org/10.3390/pathogens12101250
6. Suniga PAP, Mantovani C, Santos MG, Rieger JSG, Gaspar EB, Dos Santos FL, et al. Molecular detection of *Burkholderia mallei* in different geographic regions of Brazil. Braz J Microbiol. 2023b;54:1275–85. https://doi.org/10.1007/s42770-023-00965-9
7. Santos Júnior ELD, Moura JCR, Protásio BKPF, Parente VAS, Veiga MHND. Clinical repercussions of glanders (*Burkholderia mallei* infection) in a Brazilian child: a case report. Rev Soc Bras Med Trop. 2020;53:e20200054. https://doi.org/10.1590/0037-8682-0054-2020
8. Velôso DS, da Silva SP, de Coelho CMS, Parente JML, Veloso TAE, Lima MM, et al. Emergence of melioidosis in Brazil: a case series. J Med Case Rep. 2023;17:362. https://doi.org/10.1186/s13256-023-04093-8
9. van Embden JD, Cave MD, Crawford JT, Dale JW, Eisenach KD, Gicquel B, et al. Strain identification of *Mycobacterium tuberculosis* by DNA fingerprinting: recommendations for a standardized methodology. J Clin Microbiol. 1993;31:406–9. https://doi.org/10.1128/jcm.31.2.406-409.1993
10. Girault G, Wattiau P, Saqib M, Martin B, Vorimore F, Singha H, et al. High-resolution melting PCR analysis for rapid genotyping of *Burkholderia mallei*. Infect Genet Evol. 2018;63:1–4. https://doi.org/10.1016/j.meegid.2018.05.004
11. He G, Zeng Y, He Q, Liu T, Li N, Lin H, et al. A case report of *Burkholderia mallei* infection leading to pneumonia. Comb Chem High Throughput Screen. 2023;26:241–5. https://doi.org/10.2174/1386207325666220509152221
12. Nasiri M, Zarrin A, RoshankarRudsari S, Khodadadi J. Glanders (*Burkholderia mallei* infection) in an Iranian man: a case report. IDCases. 2023;32:e01779. https://doi.org/10.1016/j.idcr.2023.e01779
13. Van Zandt KE, Greer MT, Gelhaus HC. Glanders: an overview of infection in humans. Orphanet J Rare Dis. 2013;8:131. https://doi.org/10.1186/1750-1172-8-131

Address for correspondence: Flábio Ribeiro de Araújo, Embrapa Beef Cattle, Avenida Rádio Maia, 830, Campo Grande, Mato Grosso do Sul 79106-550, Brazil; email: flabio.araujo@embrapa.br

Computerized Decision Support Systems Informing Community-Acquired Pneumonia Surveillance, France, 2017–2023

Tristan Delory,[1] Josselin Le Bel,[1] Raphaëlle Métras, Caroline Guerrisi, Ilona E. Suhanda, Elisabeth Bouvet, Sylvie Lariven, Pauline Jeanmougin

We show the value of real-time data generated by a computerized decision support system in primary care in strengthening pneumonia surveillance. The system showed a 66% (95% CI 64%–67%) increase in community-acquired pneumonia from 2018 to 2023 for the population of France, 1 month before a national alert was issued.

The COVID-19 pandemic has highlighted the importance of detecting novel or reemerging pathogens as they arise to enable the earliest possible response (*1*,*2*). The pandemic experience suggests that surveillance systems of routine health data collected at the primary healthcare level could rapidly identify emerging data patterns (signals) and inform future research to determine pandemic risk (*3*).

Since autumn 2023, health authorities in France have reported an increased rate of adults and children with pneumonia caused by *Mycoplasma pneumoniae*, including macrolide-resistant strains (*4*). *M. pneumoniae* circulates cyclically, with a higher rate in Europe and Asia every 3–7 years (*5*). In Europe, serologic surveys have observed a decline in the detection of specific antibodies from 2020 to mid-2023 (*6*,*7*). Prospective serologic surveillance in 2023 showed increased incidence compared with previous years, consistent with a resurgence of *M. pneumoniae* (*8*). Diagnosis of atypical pneumonia in primary care is challenging; hospital-based serologic surveillance may misestimate the potential threat of the epidemic and is not scalable to primary care (*5*). Indeed, hospital-based surveillance often reports patients who have failed initial empiric therapy or have risk factors or complications.

The computerized decision support system (CDSS) Antibioclic (*9*) is designed for antimicrobial drug prescriptions for a panel of infectious diseases in primary care (*9*,*10*). Antibioclic could provide real-time information on the ecology and surveillance of community-acquired pathogens (*11*,*12*). The data collected by the CDSS are not linked to patients' health records and do not allow patient identification (Appendix, https://wwwnc.cdc.gov/EID/article/30/11/24-0072-App1.pdf). Analyses of nonidentifiable data requests in Antibioclic do not require the approval of a research review board in France. Data collection and analysis follow European Union General Data Protection Regulation.

The Study

We examined the pattern of requests for community-acquired pneumonia (CAP) within the Antibioclic system during November 11, 2017–January 7, 2024. We first calculated the weekly number of requests made for each type of pathology to the system; they were CAP, sore throat with positive group A *Streptococcus* (strep-A) test, and Lyme disease. We chose sore throat and Lyme disease for a baseline comparison to ensure that signal for CAP was not related to a change in the

Author affiliations: Centre Hospitalier Annecy Genevois, Epagny Metz-Tessy, France (T. Delory); Antibioclic Steering Committee, Paris, France (T. Delory, J. Le Bel, E. Bouvet, S. Lariven, P. Jeanmougin); Sorbonne Université, INSERM, Institut Pierre Louis d'Épidémiologie et de Santé Publique, Paris (T. Delory, R. Metras, C. Guerrisi, I.E. Suhanda); Université Paris Cité, Paris (J. Le Bel); Université Paris Cité et Université Sorbonne Paris Nord, INSERM, Paris (J. Le Bel); Université de Nantes, Nantes, France (P. Jeanmougin)

DOI: http://doi.org/10.3201/eid3011.240072

[1]These co-primary authors contributed equally to this work.

pattern of use in the CDSS. For sore throat with positive strep-A tests (1,595,867 requests) we observed a resurgence in children in late 2022 (*13*). Lyme disease (691,889 requests) is a vectorborne bacterial disease not known to be transmissible from person to person (*14*).

We estimated the weekly incidence of requests made for each type of pathology per 1,000 overall requests (Appendix). The study period encompassed ≈27.7 million requests (21.4 million in adults and 6.3 million in children), of which 2,333,638 were for CAP (1,678,670 in adults and 567,849 in children), made mostly by primary care general practitioners (GPs) (92%, n = 46,762) (Appendix Table 1). Among requests performed in adults, 666,649 (39.7%) were for those >65 years of age, 417,094 (24.8%) involved other risk factors for severe CAP, and 189,304 (11.3%) were related to influenza-like illness (Appendix Table 2). We found that 1.49% (95% CI 1.46–1.52) of requests for CAP might be duplicated, defined as requests performed by a single user in ≤10 minutes.

We observed a seasonal pattern before the COVID-19 pandemic for both CAP and Lyme disease, winter peaks for CAP and summer peaks for Lyme disease; sore throat with positive strep-A test did not exhibit seasonal patterns (Figure 1). The COVID-19 pandemic affected the seasonal pattern of CAP. CDSS use was strongly reduced during the first lockdown; although its use recovered immediately after the release of the first restrictions, results showing seasonality of CAP did not resume until December 2022–March 2023. The seasonality of Lyme disease remains unchanged over the whole study period; peaks were as expected, in June 2022 and September 2023. We also observed a resurgence in streptococcal infections.

To compare seasonal patterns, we calculated rates by quarters and years for the whole study period (2018–2023) in the whole population and in adults and children. Then, we estimated relative risks (RRs) by comparing the quarterly rate for year 2023 to the same quarter for year 2018. The peak rate in winter 2022–2023 and 2017–2018 was ≈175 CAP/1,000 requests. However, from November 2023 onward, we observe an increase in incidence of CAP requests compared with previous years. The quarterly evolution between the reference year, 2018, and 2023 showed that both children and adults faced a resurgence of CAP during the 4th quarter but that the increase was higher for children: RR was 1.66 (95% CI 1.64–1.67) overall, 1.48 (95% CI 1.46–1.49) in adults, and 1.87 (95% CI 1.84–1.89) in children (Table). The resurgence also started earlier in children than in adults, which we observed in epidemiologic week 29 of 2023 (from 80 CAP/1,000 requests to 100 CAP/1,000 requests) and for weeks 39–52 of 2023 (Figure 2). In adults, the resurgence started during the 4th quarter, in week 40 of 2023.

The Ministry of Health in France issued a national alert 7 weeks (during week 47) after the start of the second surge involving both children and adults, 4 weeks after the rate of CAP rose by 25% in our system compared with prepandemic years. The peak during 2024 epidemiologic week 1, at 253 CAP/1,000 requests overall, corresponds to a 46% increase compared with the same week in winter 2017–2018, stratified as 232 CAP/1,000 adults (23% higher than 2017–2018) and 310 CAP/1,000 children (269% higher than 2017–2018).

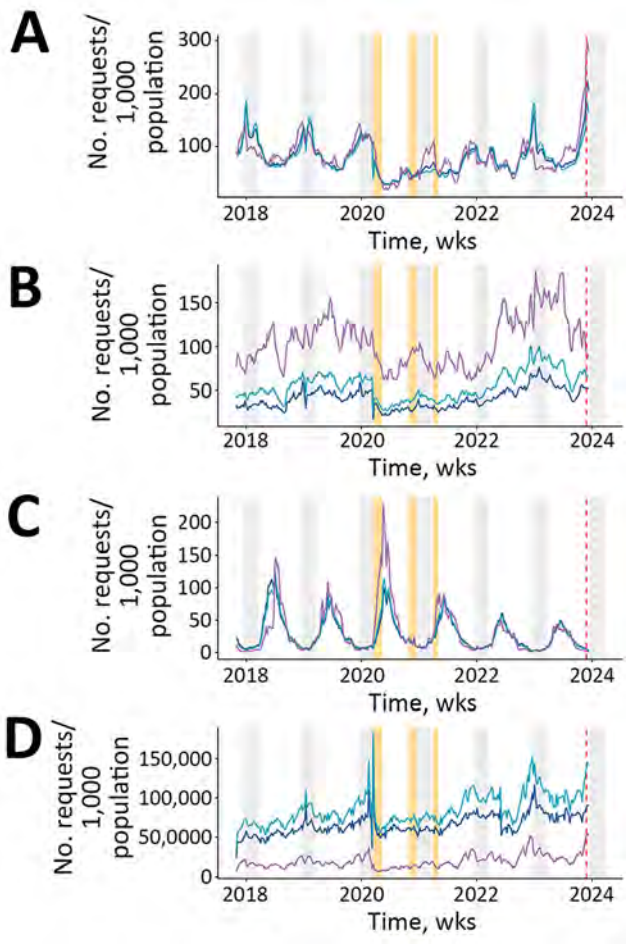

Figure 1. Temporal pattern of prescription data requests (per 1,000 population) within the Antibioclic computerized decision support system, France, December 2017–January 2024. A) Community-acquired pneumonia; (B) sore throat with positive group A *Streptococcus* test; C) Lyme disease; D) overall number of requests per week. Orange bars represent the 3 national lockdowns implemented in France during the COVID-19 pandemic. Light gray bars represent winter seasons. Purple lines represent evolution in children, light blue lines in adults, dark blue lines overall population. The dashed vertical red line represents the first national alert from the Ministry of Health associated with a possible outbreak of *Mycoplasma pneumoniae*, including macrolide-resistant strains.

Table. Prescription data requests within the Antibioclic computerized decision support system for community-acquired pneumonia, France, 2018–2023*

Quarter	No. requests/1,000 population						2023 vs. 2018 relative risk (95% CI)
	2018	2019	2020	2021	2022	2023	
Overall							
1	126.1	117.9	102.9	59.0	78.8	95.9	0.76 (0.75–0.77)
2	74.2	73.6	35.4	51.4	72.0	67.5	0.91 (0.90–0.92)
3	68.0	62.1	37.7	53.7	57.9	69.9	1.03 (1.02–1.04)
4	99.9	100.7	47.9	89.7	104.4	165.4	1.66 (1.64–1.67)
Adults							
1	135.5	120	99.4	51.9	80.2	107.9	0.80 (0.79–0.80)
2	73.9	73.4	35.9	47.4	74.1	68.9	0.93 (0.92–0.94)
3	65.7	60.2	37.8	53.4	57.7	63.8	0.97 (0.96–0.98)
4	93.4	95.5	48.0	86.3	107.0	138.0	1.48 (1.46–1.49)
Children							
1	94.6	110.8	116.5	84.8	74.0	60.2	0.64 (0.62–0.65)
2	75.1	74.5	31.6	67.8	65.3	62.8	0.84 (0.82–0.85)
3	77.7	70.3	37.1	55.1	58.7	94.0	1.21 (1.18–1.24)
4	119.9	117.0	47.2	99.1	98.6	223.6	1.87 (1.84–1.89)

*The rate of community-acquired pneumonia sharply decreased in all groups after introduction of nonpharmaceutical interventions for the COVID-19 pandemic (from the second quarter of 2020).

Finally, we estimated the expected numbers of CAP in 2023 in the absence of a resurgence. We trained a Poisson model with the 2018–2019 data (Appendix), projected for 2023 and compared those estimates to the observed 2023 data to compute excess CAP requests. We estimate an excess 17,876 requests (14.4% increase) for CAP (9,205 [9.9% increase] in adults, 8,671 [27.9% increase] in children) in 2023 compared with 2018–2019.

Conclusions

By analyzing the requests of CAP and 2 other control pathologies, we showed that Antibioclic data are successful in detecting early emergence of atypical CAP, observed elsewhere in Europe (*8*). This dataset, which covers many pathologies in primary care (n = 36), could be leveraged to monitor localized or national-level outbreaks and contribute to the assessment of emerging threats. Primary healthcare CDSSs that provide real-world and real-time data may effectively support pandemic pathogen intelligence by detecting or confirming signals of disease outbreaks. Those results can strengthen local surveillance or inform global surveillance centers. Our system does not identify specific pathogens involved in CAP and is not integrated into primary-care electronic health records (*9*). We plan to refine our estimates using field data.

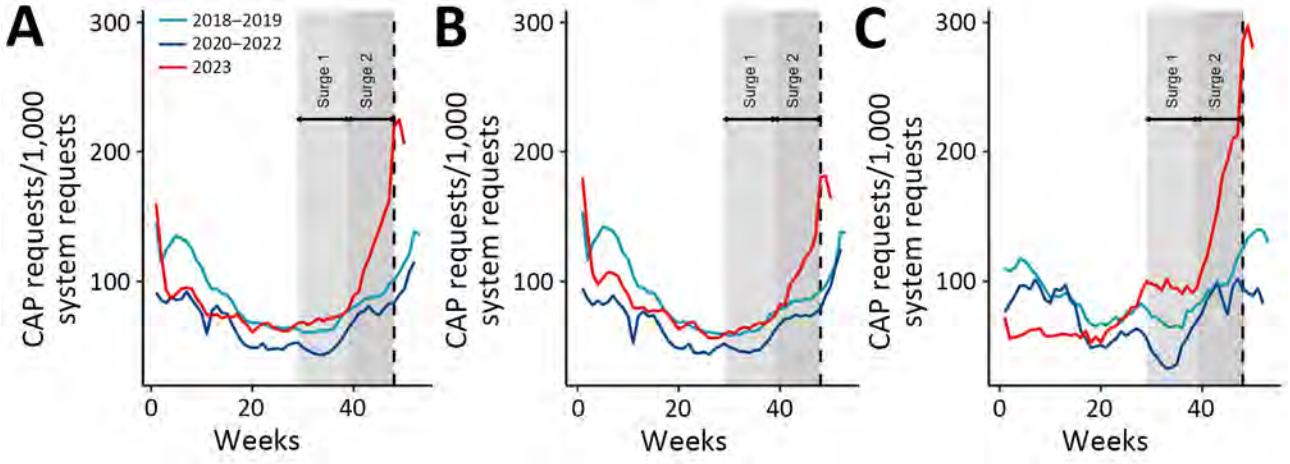

Figure 2. Rate of community-acquired pneumonia as indicated within the Antibioclic computerized decision support system, France, December 2017–January 2024. A) Overall population; (B) adults; (C) children. Light blue line indicates average number of system requests in 2018–2019 (pre–COVID-19 pandemic); dark blue line indicates average number of system requests in 2020–2022 (during pandemic); red line indicates average number of system requests in 2023. Light gray area indicates a surge in 2023 starting in epidemiologic week 29 and dark gray indicates surge in 2023 starting in week 39; we noted that surges began earlier in children than adults. The dashed vertical line represents the first national alert from the Ministry of Health associated with a possible outbreak of *Mycoplasma pneumoniae.*

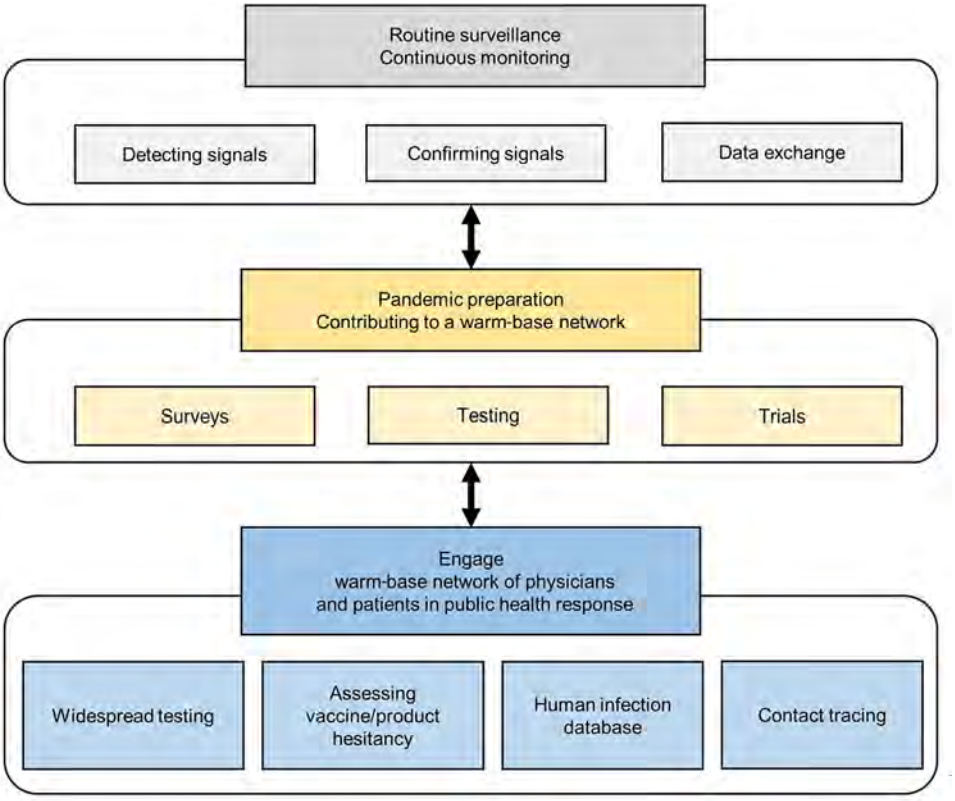

Figure 3. Potential contribution from primary healthcare computerized decision support system to global networks for pandemic preparedness by routine surveillance and continuous monitoring and a ready (warm-base) network of primary health care physicians already using the system that can be engaged for public health response in case of pandemic.

In France, ≈57% of 80,000 GPs use the CDSS; users are more likely to be younger than average (39 vs. 51 years of age), and more likely to be female (63.0% vs. 46.9%) than the whole population of GPs (*15*). Yet, CDSS was successful in confirming reemergence of CAP. Wide use of CDSS in primary care enabled creation and maintenance of a warm-base network of primary care physicians ready to engage against a pandemic (Figure 3). Those physicians could carry out widespread testing of the general population, improve contact tracing, and contribute to human infection databases. They could also be involved in surveys to better understand behaviors that lead to hesitancy toward new vaccines or products and use the knowledge gained to develop strategies to increase uptake before products are introduced.

Effective end-to-end communication between stakeholders, CDSS administrators, and users enables health authorities to maximize public information and health response. Between emerging or reemerging signals, the network can prepare by involving its users and their patients in surveys, tests, and trials.

Acknowledgments

We thank all Antibioclic users for their contribution to the system.

Antibioclic is a nonprofit organization and is not linked to pharmaceutical companies. The steering committee members are volunteers and funding is obtained through competitive calls for tenders from universities, the French health authorities, or learned societies. This study was self-subsidized by Antibioclic.

About the Author

Dr. Delory is the head of the clinical trial unit in Annecy Hospital, France. His primary research interests are computerized decision support systems and appropriateness of antimicrobial drugs. Dr. Bel is general practitioner and associate professor of general practice at Université Paris Cité. His primary research interests are the appropriate use of antibiotics and diagnostic strategies for infectious diseases in primary care.

References

1. Adjala AA, Watson M, Toner ES, Cicero A, Inglesby TV. The characteristics of pandemic pathogens. Baltimore: Johns Hopkins University, Bloomberg School of Public Health, Center for Health Security; 2018 [cited 2023 Dec 18]. https://centerforhealthsecurity.org/sites/default/files/2022-12/180510-pandemic-pathogens-report.pdf
2. May M. Tomorrow's biggest microbial threats. Nat Med. 2021;27:358–9. https://doi.org/10.1038/s41591-021-01264-2
3. Lal A, Schwalbe N. Primary health care: a cornerstone of pandemic prevention, preparedness, response, and

recovery. Lancet. 2023;401:1847. https://doi.org/10.1016/S0140-6736(23)00963-7
4. Société Française de Médicine d'Urgence. The DGS warns of an "unusual resurgence" of cases of respiratory infections from *Mycoplasma pneumoniae* [in French]. 2023 Nov 29 [cited 2023 Dec 18]. https://www.sfmu.org/fr/actualites/actualites-de-l-urgences/la-dgs-alerte-sur-une-recrudescence-inhabituelle-de-cas-d-infections-respiratoires-a-mycoplasma-pneumoniae/new_id/69481
5. Beeton ML, Zhang XS, Uldum SA, Bébéar C, Dumke R, Gullsby K, et al.; ESCMID Study Group for Mycoplasma and Chlamydia Infections (ESGMAC) Mycoplasma pneumoniae subgroup. *Mycoplasma pneumoniae* infections, 11 countries in Europe and Israel, 2011 to 2016. Euro Surveill. 2020;25:1900112. https://doi.org/10.2807/1560-7917.ES.2020.25.2.1900112
6. Meyer Sauteur PM, Beeton ML, Uldum SA, Bossuyt N, Vermeulen M, Loens K, et al.; ESGMAC–MyCOVID Study Team. *Mycoplasma pneumoniae* detections before and during the COVID-19 pandemic: results of a global survey, 2017 to 2021. Euro Surveill. 2022;27:2100746. https://doi.org/10.2807/1560-7917.ES.2022.27.19.2100746
7. Meyer Sauteur PM, Chalker VJ, Berger C, Nir-Paz R, Beeton ML; ESGMAC and the ESGMAC–MyCOVID study group. *Mycoplasma pneumoniae* beyond the COVID-19 pandemic: where is it? Lancet Microbe. 2022;3:e897. https://doi.org/10.1016/S2666-5247(22)00190-2
8. Meyer Sauteur PM, Beeton ML, European Society of Clinical Microbiology and Infectious Diseases (ESCMID) Study Group for Mycoplasma and Chlamydia Infections (ESGMAC), ESGMAC *Mycoplasma pneumoniae* Surveillance (MAPS) study group. *Mycoplasma pneumoniae:* delayed re-emergence after COVID-19 pandemic restrictions. Lancet Microbe. 2024;5:e100–e101.
9. Delory T, Jeanmougin P, Lariven S, Aubert JP, Peiffer-Smadja N, Boëlle PY, et al. A computerized decision support system (CDSS) for antibiotic prescription in primary care—Antibioclic: implementation, adoption and sustainable use in the era of extended antimicrobial resistance. J Antimicrob Chemother. 2020;75:2353–62. https://doi.org/10.1093/jac/dkaa167
10. Verger P, Fressard L, Jacquemot AF, Bergeat M, Vergier N, Pulicini C, et al. One in two general practitioners is confronted with antibiotic resistance problems. Report no. 1217 [in French]. 2022 Jan 11 [cited 2023 Dec 22]. https://drees.solidarites-sante.gouv.fr/publications-communique-de-presse/etudes-et-resultats/un-medecin-generaliste-sur-deux-est-confronte
11. Delory T, Le Bel J, Lariven S, Peiffer-Smadja N, Lescure FX, Bouvet E, et al. Computerized decision support system (CDSS) use for surveillance of antimicrobial resistance in urinary tract infections in primary care. J Antimicrob Chemother. 2022;77:524–30. https://doi.org/10.1093/jac/dkab392
12. Maillard A, Jeanmougin P, Bouvet E, Lariven S, Le Bel J, Delory T. Fluoroquinolones in primary care, a first step for patient empowerment towards antimicrobial stewardship? Clin Microbiol Infect. 2024;30:7–9. https://doi.org/10.1016/j.cmi.2023.06.011
13. Bamford A, Whittaker E. Resurgence of group A streptococcal disease in children. BMJ. 2023;380:43. https://doi.org/10.1136/bmj.p43
14. National Guideline Centre (UK). Evidence review for person-to-person transmission: Lyme disease: diagnosis and management: Evidence review M 2018 [cited 2023 Dec 18]. http://www.ncbi.nlm.nih.gov/books/NBK578131/
15. Delory T, Maillard A, Tubach F, Böelle PY, Bouvet E, Lariven S, et al. Appropriateness of intended antibiotic prescribing using clinical case vignettes in primary care, and related factors. Eur J Gen Pract. 2024;30:2351811. https://doi.org/10.1080/13814788.2024.2351811

Address for correspondence: Tristan Delory, Centre Hospitalier Annecy Genevois, 1 avenue de l'hôpital, Epagny Metz-Tessy 74370, France; email: tdelory@ch-annecygenevois.fr

Invasive Group A *Streptococcus* Hypervirulent $M1_{UK}$ Clone, Canada, 2018–2023

Alyssa R. Golden, Averil Griffith, Gregory J. Tyrrell, Julianne V. Kus, Allison McGeer, Marc-Christian Domingo, Jennifer Grant, Jessica Minion, Paul Van Caeseele, Guillaume Desnoyers, David Haldane, Yang Yu, Xiaofeng Ding, Laura Steven, Jan McFadzen, Courtney Primeau, Irene Martin

To determine invasive group A *Streptococcus* trends in Canada, we characterized *emm*1 isolates collected during 2018–2023. The percentage of hypervirulent $M1_{UK}$ lineage isolates increased significantly, from 22.1% in 2018 to 60.2% in 2023. Genomic analysis identified geographically and temporally associated clusters and genes associated with virulent bacteriophage acquisition.

The hypervirulent $M1_{UK}$ lineage of group A *Streptococcus* (GAS), originally identified in the United Kingdom in 2019, has been associated with increased notifications of scarlet fever and invasive GAS (iGAS) infections (*1*). The $M1_{UK}$ lineage is characterized by increased production of *speA* (streptococcal pyrogenic exotoxin A) and is differentiated from the $M1_{global}$ lineage by 27 key single-nucleotide variants (SNVs) (*1*). Initial characterization of a subset of *emm*1 isolates collected in Canada during 2016–2019 identified 10% of isolates as the $M1_{UK}$ lineage (*2*).

Beginning in 2022, several health organizations, including the World Health Organization and the Pan American Health Organization, reported increased cases of pediatric iGAS in numerous member countries, above seasonal expectations (*3*,*4*). Many countries in Europe, including Belgium, Netherlands, and the United Kingdom (*5*–*7*), have associated increased iGAS disease in the 2022–23 season with *emm*1, particularly the $M1_{UK}$ variant. In light of the worldwide increased iGAS disease activity and the association of those increases with *emm*1, we sought to describe the trends in *emm*1 and $M1_{UK}$ in Canada during 2018–2023.

The Study

We identified 2,582 isolates of iGAS *emm*1 collected during 2018–2023 as part of the passive, laboratory-based surveillance system for iGAS in Canada (*8*). Of those, we sequenced 2,315 isolates by using Illumina NextSeq technology (https://www.illumina.com); the remainder were received as line-listed typing data only. We identified $M1_{UK}$ isolates by mapping whole-genome sequencing reads to reference strain MGAS5005 and identifying 27 characteristic SNVs, as previously described (*1*). We performed core SNV phylogenetic analysis by using the SNVPhyl pipeline (*9*) and identified genomic clusters by using ClusterPicker with default settings (*10*). We assessed presence of

Author affiliations: Public Health Agency of Canada, Winnipeg, Manitoba, Canada (A. Golden, A. Griffith, I. Martin); Provincial Laboratory for Public Health (Microbiology), Edmonton, Alberta, Canada (G.J. Tyrrell); Public Health Ontario, Toronto, Ontario, Canada (J.V. Kus); University of Toronto, Toronto (J.V. Kus); Mount Sinai Hospital, Toronto (A. McGeer); Institut National de Santé Publique du Québec, Sainte-Anne-de-Bellevue, Québec, Canada (M-.C. Domingo); British Columbia Centre for Disease Control, Vancouver, British Columbia, Canada (J. Grant); Roy Romanow Provincial Laboratory, Regina, Saskatchewan, Canada (J. Minion); Cadham Provincial Laboratory, Winnipeg (P. Van Caeseele); Laboratoire de Santé Publique du New Brunswick, Moncton, New Brunswick, Canada (G. Desnoyers); Queen Elizabeth II Health Science Centre, Halifax, Nova Scotia, Canada (D. Haldane); Newfoundland and Labrador Public Health Laboratory, St. John's, Newfoundland, Canada (Y. Yu); Queen Elizabeth Hospital, Charlottetown, Prince Edward Island, Canada (X. Ding); Stanton Territorial Hospital Laboratory, Yellowknife, Northwest Territories, Canada (L. Steven); Yukon Communicable Disease Control, Whitehorse, Yukon, Canada (J. McFadzen); Public Health Agency of Canada, Ottawa, Ontario, Canada (C. Primeau)

DOI: https://doi.org/10.3201/eid3011.241068

antimicrobial resistance, toxin, and virulence genes by using the WADE pipeline (https://github.com/phac-nml/wade), the public virulence factor database (http://www.mgc.ac.cn/VFs), and custom database queries. The $M1_{UK}$ genomic data reported in our study have been deposited in the National Center for Biotechnology Information Sequence Read Archive (BioProject PRJNA1137869).

We assessed trends in lineage distribution for statistical significance by using the Cochran-Armitage test for trend and differences between lineages by using the 2-tailed Fisher exact test ($\alpha = 0.05$). We aggregated data regionally into the Western (British Columbia, Alberta), Prairie (Saskatchewan, Manitoba), Central (Ontario, Québec), Eastern (New Brunswick, Nova Scotia, Prince Edward Island, Newfoundland and Labrador), and Northern (Yukon, Northwest Territories, Nunavut) regions of Canada.

In 2018, *emm*1 accounted for 17.1% of iGAS isolates collected in Canada, after which the proportion of *emm*1 decreased significantly, to a low of 0.5% in 2021 ($p<0.0001$), followed by a sharp increase to 24.5% in 2023 ($p<0.0001$) (Figure 1, panel A). Overall, during 2018–2023, a total of 46.2% of the 2,315 sequenced *emm*1 isolates were the $M1_{UK}$ lineage. The proportion of $M1_{UK}$ isolates increased from 22.1% (110/497) in 2018 to 60.2% (711/1,182) in 2023 ($p<0.0001$) (Figure 1, panel B). In 2023, the proportion of $M1_{UK}$ was highest in the Prairie region (66.7%), followed by the Central (62.5%), Western (58.9%) and Eastern regions (35.3%); no $M1_{UK}$ was collected in the Northern region. The only common (n>20) *emm*1 subtype associated exclusively with the $M1_{UK}$ lineage was *emm*1.147; subtypes *emm*1.146 and *emm*1.25 were exclusively associated with the $M1_{global}$ genotype. Subtypes *emm*1.0 and *emm*1.3 were associated with both $M1_{global}$ and $M1_{UK}$ genotypes (40.8% of *emm*1.0 and 95.0% of *emm*1.3 were $M1_{UK}$).

Few antimicrobial resistance determinants were identified within the $M1_{global}$ or $M1_{UK}$ cohorts (Table).

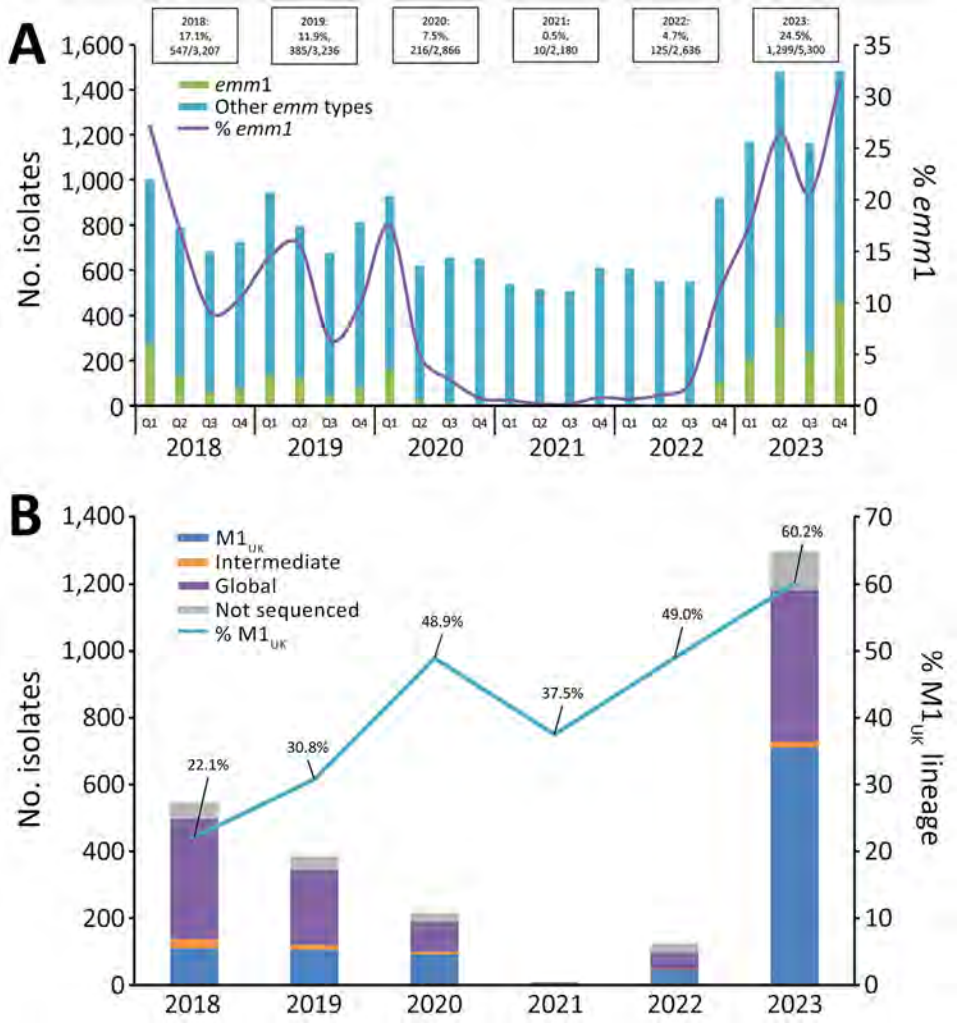

Figure 1. Expansion of invasive group A *Streptococcus emm*1 and the $M1_{UK}$ lineage in Canada, 2018–2023. A) Number of *emm*1 isolates collected, by quarter. B) Percentage of $M1_{UK}$ isolates among *emm*1 isolates collected. Q1, January–March; Q2, April–June; Q3, July–September; Q4, October–December. Annual proportions of *emm*1 are listed above the bars. Intermediate indicates an isolate with a partial $M1_{UK}$ genotype; not sequenced indicates an isolate that was submitted to the National Microbiology Laboratory as line-listed typing data only.

Table. Characteristics of $M1_{UK}$ lineage and other invasive group A *Streptococcus emm*1 isolates collected in Canada, 2018–2023

Isolate feature*	Lineage, no. (%) isolates		p value‡
	$M1_{UK}$, n = 1,069	Other *emm*1, n = 1,246†	
Antimicrobial susceptibility			
Penicillin	100	100	1.000
Erythromycin	99.5 (1,064)	99.2 (1,236)	0.4375
Clindamycin	99.8 (1,067)	99.5 (1,240)	0.2997
Chloramphenicol	100	100	1.000
Levofloxacin	99.9 (1,068)	99.8 (1,243)	0.6291
Tetracycline	99.6 (1,065)	99.1 (1,235)	0.1928
Toxin gene presence			
speA	98.4 (1,052)	97.4 (1,214)	0.1124
speC	43.8 (468)	8.3 (103)	<0.0001
speG	100 (1,069)	99.9 (1,245)	1.000
speH	0	0	1.000
speI	0	0	1.000
speJ	99.5 (1,064)	99.4 (1,238)	0.7817
speK	0.1 (1)	0	0.4618
speL	0	0	1.000
speM	0	0	1.000
smeZ	98.4 (1,052)	98.9 (1,232)	0.3674
ssa	35.5 (379)	4.4 (55)	<0.0001
Virulence gene presence			
Phage-associated DNase, *spd1*	43.9 (469)	8.3 (103)	<0.0001
Phage-associated hyaluronidase, *hylP*	37.8 (404)	3.9 (49)	<0.0001
Gene combinations			
speC + *ssa* + *spd1*	35.4 (378)	8.3 (55)	<0.0001
speC + *spd1*	8.3 (89)	3.9 (48)	<0.0001

*All isolate features (antimicrobial susceptibilities, toxin, and virulence gene presence) were inferred from whole-genome sequences.
†Other *emm*1 with whole-genome sequencing data available.
‡Two-tailed; p<0.05 considered significant.

Compared with other *emm*1 isolates, the $M1_{UK}$ variant demonstrated significantly higher presence of genes *speC* (streptococcal pyrogenic exotoxin C) and *ssa* (streptococcal superantigen), as well as virulence factors *spd1* (phage-associated DNase) and *hylP* (phage-associated hyaluronidase).

Phylogenetic analysis of all *emm*1 isolates identified clear separation of the $M1_{global}$ and $M1_{UK}$ lineages (Appendix Figure 1, https://wwwnc.cdc.gov/EID/article/30/11/24-1068-App1.pdf); the isolates within the $M1_{UK}$ cluster differed from those in the $M1_{global}$ cluster by an average of 46 (range 22–80) SNVs. Within the $M1_{UK}$ cluster, isolates differed by an average of 17.6 (range 0–41) SNVs, and there was more variability within isolates of the $M1_{global}$ lineage (average 32.6 [range 0–82] SNVs difference).

ClusterPicker identified 11 large clusters within the $M1_{UK}$ cohort, each cluster containing 10–280 isolates (Figure 2; Appendix Table). In general, the highest proportion of each cluster was collected in 2023, which is consistent with the surge of iGAS disease cases that year. Exceptions include clusters 4 and 11, which included isolates predominantly collected before the *emm*1 decrease that coincided with the COVID-19 pandemic. Clusters 1, 5–7, and 10 were identified exclusively after the COVID-19 pandemic period, and clusters 2 and 8 persisted across the study period. Clusters were generally associated with geographic region: clusters 1, 2, 5, 7, and 10 were strongly associated with the Central region, and clusters 3, 6, 8, and 9 were strongly associated with associated with the Western region. Cluster 4 was mostly found in the Eastern region; Cluster 11 was predominantly from the Prairie region. Within the Central region, approximately two thirds of the total isolates collected during the study period were part of either cluster 1 or cluster 2. Cluster 3 was most common for isolates collected from the Western (40.7%) and Prairie (25.0%) regions, and cluster 4 was most common in the Eastern region (53.8%).

More than 99% of isolates within $M1_{UK}$ cluster 1 possessed *speC*, *ssa*, *spd,1*, and *hylP* (Appendix Table). Within cluster 3, a total of 78.5% of isolates possessed *speC* and *spd1*; presence of *ssa* and *hylP* was sporadic. Those 4 genes were sporadically present within clusters 2 and 7.

Conclusions

Our study highlights expansion of the $M1_{UK}$ GAS lineage in Canada. Initial genomic characterization of *emm*1 isolates in Canada identified only 10% $M1_{UK}$ in a subset of *emm*1 isolates collected during 2016–2019 (*2*); by 2023, $M1_{UK}$ comprised 60.2% of *emm*1 isolates. The proportion of $M1_{UK}$ in Canada in 2023 is much higher than that most recently published from the United States (11%), although considerably lower

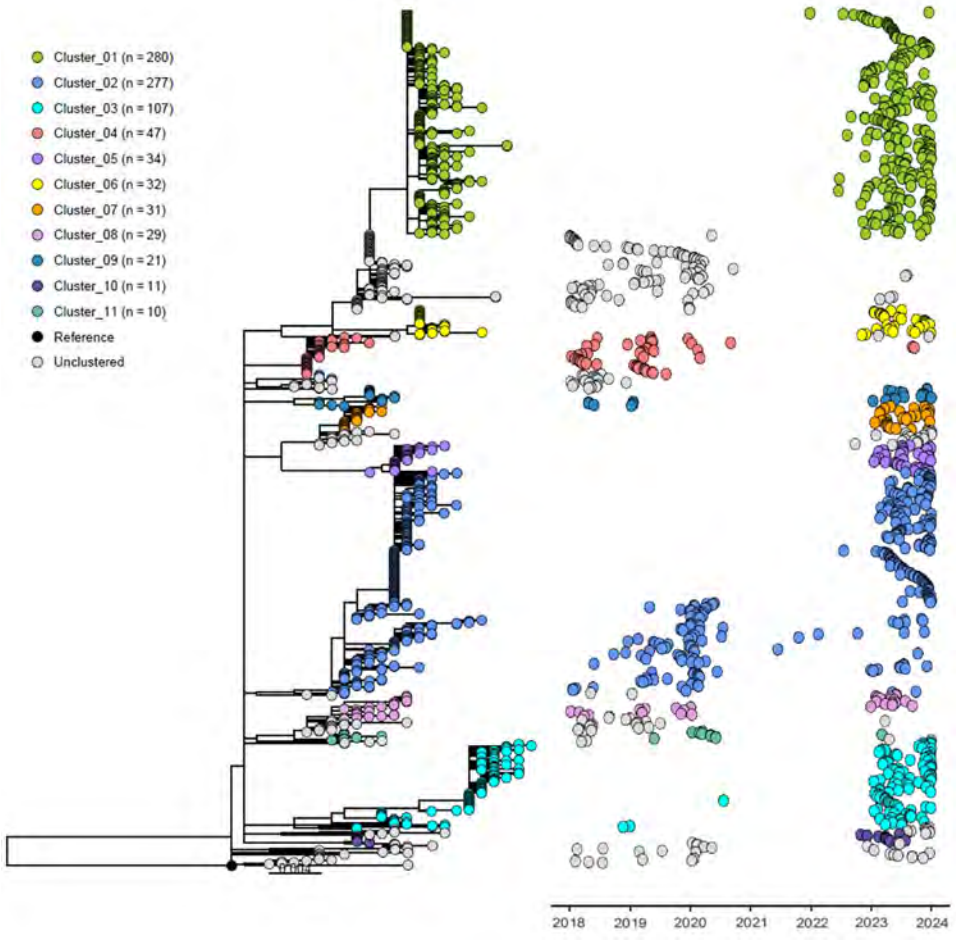

Figure 2. Maximum-likelihood core single-nucleotide variant phylogeny for 1,069 invasive group A *Streptococcus* $M1_{UK}$ lineage isolates collected in Canada, 2018–2023. Eleven large clusters are shown, each containing 10–280 isolates.

than that reported by recent studies from Belgium (78%) and the United Kingdom (95.7%) (*5*,*7*,*11*). Our study findings are consistent with findings of Vieira et al., who noted that the $M1_{UK}$ lineage showed less genomic diversity than the $M1_{global}$ lineage (*7*). Of note, we did not identify any isolates of the novel $M1_{DK}$ lineage, which was originally identified in Denmark and was responsible for 30% of iGAS cases in Denmark in winter 2022–23 (*12*).

Our study identified a large proportion of $M1_{UK}$ isolates with the bacteriophage-encoded DNase *spd1* and *speC*/*ssa* superantigens. The presence of those 3 genes suggests acquisition of a virulent prophage related to ΦHKU488.vir, which has been associated with outbreaks of *emm*12 scarlet fever in Asia (*13*,*14*). However, the lack of antimicrobial resistance determinants in Canadian *emm*1 isolates so far indicates limited transfer of the integrative conjugative elements that have been responsible for macrolide, lincosamide, and tetracycline resistance in GAS outbreaks in Asia (*14*). Although $M1_{UK}$ with this phage were present in Canada before the COVID-19 pandemic, their presence substantially expanded in 2023, particularly in central Canada (Figure 2, cluster 1). $M1_{UK}$ isolates within cluster 3 were associated with *speC* and *spd1* only; that combination is associated with a different prophage, ΦSP370.1 (*15*). Those isolates were more common in western Canada beginning in 2023, suggesting a different path of virulence gene acquisition compared with that of ΦHKU488.vir. Monitoring the spread of the variants of $M1_{UK}$, particularly for development of antimicrobial resistance, will remain critical. Our study underscores the value of linking laboratory data to epidemiologic variables to enhance our knowledge of how GAS variants affect clinical manifestations, outcomes, and risk groups.

Acknowledgments

We thank Angela Yuen, Rachel Hink, and Anastasia Anistratov from the Streptococcus and Sexually Transmitted Infections Section at the National Microbiology Laboratory for their laboratory technical assistance and the staff of provincial and territorial public health laboratories in Canada for participating in the national laboratory surveillance program.

This project was supported by internal funding from the Public Health Agency of Canada.

The authors have no conflicts of interest to declare. A.R.G. and I.M. contributed to study design; all authors contributed to data collection; and A.R.G. performed data analysis, produced visualizations, and wrote the manuscript. All authors reviewed and edited the manuscript.

About the Author

Dr. Golden is a biologist in the Streptococcus and Sexually Transmitted Infections Section at the National Microbiology Laboratory, Public Health Agency of Canada. She focuses on surveillance, antimicrobial resistance, and genomic epidemiology of invasive streptococcal diseases.

References

1. Lynskey NN, Jauneikaite E, Li HK, Zhi X, Turner CE, Mosavie M, et al. Emergence of dominant toxigenic M1T1 *Streptococcus pyogenes* clone during increased scarlet fever activity in England: a population-based molecular epidemiological study. Lancet Infect Dis. 2019;19:1209–18. https://doi.org/10.1016/S1473-3099(19)30446-3
2. Demczuk W, Martin I, Domingo FR, MacDonald D, Mulvey MR. Identification of *Streptococcus pyogenes* $M1_{UK}$ clone in Canada. Lancet Infect Dis. 2019;19:1284–5. https://doi.org/10.1016/S1473-3099(19)30622-X
3. World Health Organization. Disease outbreak news: increased incidence of scarlet fever and invasive group A *Streptococcus* infection—multi-country [cited 2023 Nov 26]. https://www.who.int/emergencies/disease-outbreak-news/item/2022-DON429
4. Pan American Health Organization/World Health Organization. Informative note: cases of diseases caused by group A *Streptococcus* in Uruguay [in Spanish] [cited 2023 Nov 28]. https://www.paho.org/es/documentos/nota-informativa-casos-enfermedades-causadas-por-estreptococo-grupo-uruguay
5. Rodriguez-Ruiz JP, Lin Q, Lammens C, Smeesters PR, van Kleef-van Koeveringe S, Matheeussen V, et al. Increase in bloodstream infections caused by *emm*1 group A *Streptococcus* correlates with emergence of toxigenic $M1_{UK}$, Belgium, May 2022 to August 2023. Euro Surveill. 2023;28:2300422. https://doi.org/10.2807/1560-7917.ES.2023.28.36.2300422
6. van der Putten BCL, Vlaminckx BJM, de Gier B, Freudenburg-de Graaf W, van Sorge NM. Group A streptococcal meningitis with the $M1_{UK}$ variant in the Netherlands. JAMA. 2023;329:1791–2. https://doi.org/10.1001/jama.2023.5927
7. Vieira A, Wan Y, Ryan Y, Li HK, Guy RL, Papangeli M, et al. Rapid expansion and international spread of $M1_{UK}$ in the post-pandemic UK upsurge of *Streptococcus pyogenes*. Nat Commun. 2024;15:3916. https://doi.org/10.1038/s41467-024-47929-7
8. Golden AR, Griffith A, Tyrrell GJ, Kus JV, McGeer A, Domingo MC, et al. Invasive group A streptococcal disease surveillance in Canada, 2021-2022. Can Commun Dis Rep. 2024;50:135–43. https://doi.org/10.14745/ccdr.v50i05a03
9. Petkau A, Mabon P, Sieffert C, Knox NC, Cabral J, Iskander M, et al. SNVPhyl: a single nucleotide variant phylogenomics pipeline for microbial genomic epidemiology. Microb Genom. 2017;3:e000116. https://doi.org/10.1099/mgen.0.000116
10. Ragonnet-Cronin M, Hodcroft E, Hué S, Fearnhill E, Delpech V, Brown AJ, et al.; UK HIV Drug Resistance Database. Automated analysis of phylogenetic clusters. BMC Bioinformatics. 2013;14:317. https://doi.org/10.1186/1471-2105-14-317
11. Li Y, Rivers J, Mathis S, Li Z, Chochua S, Metcalf BJ, et al. Expansion of invasive group A *Streptococcus* $M1_{UK}$ lineage in Active Bacterial Core Surveillance, United States, 2019–2021. Emerg Infect Dis. 2023;29:2116–20. https://doi.org/10.3201/eid2910.230675
12. Johannesen TB, Munkstrup C, Edslev SM, Baig S, Nielsen S, Funk T, et al. Increase in invasive group A streptococcal infections and emergence of novel, rapidly expanding sub-lineage of the virulent *Streptococcus pyogenes* M1 clone, Denmark, 2023. Euro Surveill. 2023;28:2300291. https://doi.org/10.2807/1560-7917.ES.2023.28.26.2300291
13. Davies MR, Keller N, Brouwer S, Jespersen MG, Cork AJ, Hayes AJ, et al. Detection of *Streptococcus pyogenes* $M1_{UK}$ in Australia and characterization of the mutation driving enhanced expression of superantigen SpeA. Nat Commun. 2023;14:1051. https://doi.org/10.1038/s41467-023-36717-4
14. Ben Zakour NL, Davies MR, You Y, Chen JHK, Forde BM, Stanton-Cook M, et al. Transfer of scarlet fever-associated elements into the group A *Streptococcus* M1T1 clone. Sci Rep. 2015;5:15877. https://doi.org/10.1038/srep15877
15. McShan WM, McCullor KA, Nguyen SV. The bacteriophages of *Streptococcus pyogenes*. Microbiol Spectr. 2019;7:7.3.8. https://doi.org/10.1128/microbiolspec.GPP3-0059-2018

Address for correspondence: Alyssa Golden, National Microbiology Laboratory, Public Health Agency of Canada, 1015 Arlington St, Winnipeg, MB R3E 3R2, Canada; email: alyssa.golden@phac-aspc.gc.ca

Genomic Epidemiology of Human Respiratory Syncytial Virus, Minnesota, USA, July 2023–February 2024

Daniel Evans, Henry Kunerth, Erica Mumm, Sarah Namugenyi, Matthew Plumb, Sarah Bistodeau, Scott A. Cunningham, Bryan Schmitt, Karen Martin, Katherine Como-Sabetti, Ruth Lynfield, Xiong Wang

We recently expanded the viral genomic surveillance program in Minnesota, USA, to include human respiratory syncytial virus. We performed whole-genome sequencing of 575 specimens collected at Minnesota healthcare facilities during July 2023–February 2024. Subgroups A and B differed in their genomic landscapes, and we identified 23 clusters of genetically identical genomes.

Human respiratory syncytial virus (RSV) is a major respiratory pathogen with increased risk of severe infections among infants and young children, elderly persons, and persons with underlying health conditions, including immunocompromise (*1*). Investigators have applied whole-genome sequencing (WGS) for retrospective RSV surveillance and outbreak investigation in the United States (*2*), but WGS has not yet been documented as a tool for prospective surveillance. Although researchers have developed and improved several genetic typing schemes to facilitate more granular characterization of RSV (*3*), application of those schemes in genomic epidemiology has not been thoroughly evaluated. We report preliminary findings from our recently established genomic surveillance program for RSV in Minnesota, USA. Because this study was conducted as a component of public health surveillance subject to Minnesota Reporting Rules, our investigation required no institutional review board approval.

Author affiliations: Health Protection Bureau, Minnesota Department of Health, St. Paul, Minnesota, USA (D. Evans, H. Kunerth, E. Mumm, S. Namugenyi, M. Plumb, S. Bistodeau, S.A. Cunningham, K. Martin, K. Como-Sabetti, R. Lynfield, X. Wang); Children's Minnesota Hospital, Minneapolis, Minnesota, USA (B. Schmitt)

DOI: http://doi.org/10.3201/eid3011.241000

The Study

During July 2023–February 2024, we collected RSV-positive nasal or nasopharyngeal specimens submitted voluntarily from outpatients and inpatients tested by quantitative reverse transcription PCR (qRT-PCR) or rapid antigen detection assays in 11 healthcare facilities in Minnesota. Specimens arrived with limited patient data (name, sex assigned at birth, date of birth, date of specimen collection, and outpatient or inpatient status).

We amplified genomes from specimens using 50 pairs of PCR primers that generated overlapping amplicons, as described by Maloney et al. (unpub. data, https://virological.org/t/preliminary-results-from-two-novel-artic-style-amplicon-based-sequencing-approaches-for-rsv-a-and-rsv-b/918), and sequenced genomes using the GridION platform with R9 flow cell chemistry (Oxford Nanopore Technologies, https://nanoporetech.com). We performed genome assembly, quality control, and viral subtyping using the nf-core Viralrecon pipeline (*4*), using a quality threshold of 20-fold coverage over 90% of the viral genome. We used Nextclade software to subgroup genomes based on the whole-genome lineage typing scheme described by Goya et al. (*3*) as available through Nextclade in June 2024 (*5*).

We successfully sequenced 575 RSV genomes from this cohort of case-patients. Median patient age was 2 years; 91.8% were <18 years of age, and 5% were ≥65 years of age. Patient sex was 53.4% male and 46.6% female. We classified 287 (49.9%) genomes as subgroup A and 288 (50.1%) as subgroup B (Table 1). Most RSV-A genomes (98.9%; n = 284) were distributed among 4 whole-genome lineages: A.D.1 (10.8%; n = 31), A.D.3 (18.5%; n = 53), A.D.5 (38.0%; n = 109), and A.D.5.2 (31.7%; n = 91). By contrast, most RSV-B genomes (95.1%; n = 274) belonged to a single lineage, B.D.E.1.

Table 1. Whole-genome sequencing results for RSV-A and RSV-B specimens collected from patients in Minnesota, USA, July 2023–February 2024*

Whole-genome lineage	No. (% of subgroup)	Cases in RSV-NET (% of WGS lineage)	Twin Cities metro (% of WGS lineage)	Mean pairwise phylogenetic distance	Earliest specimen collection, mo	Estimated time to most recent common ancestor (95% CI)
A.D.1	31 (10.8)	2 (6.5)	26 (83.9)	0.00555	2023 Sep	Jun 2017 (Jan 1996–Jan 2021)
A.D.3	53 (18.5)	5 (9.4)	40 (75.5)	0.00718	2023 Aug	Aug 2017 (Jun 1996–Jan 2021)
A.D.3.1	1 (0.3)	0	1 (100)	NA	2024 Jan	NA
A.D.5	109 (38.0)	25 (22.9)	103 (94.5)	0.00076	2023 Aug	Aug 2018 (Mar 2002–Nov 2021)
A.D.5.1	1 (0.3)	0	1 (100)	NA	2023 Dec	NA
A.D.5.2	91 (31.7)	32 (35.1)	74 (81.3)	0.00252	2023 Oct	Apr 2021 (May 2015–Oct 2022)
A.D.5.3	1 (0.3)	0	NA (unknown)	NA	2023 Sep	NA
B.D.4.1.1	12 (4.2)	4 (33.3)	12 (100)	0.00513	2023 Oct	Mar 2015 (Jun 1976–May 2019)
B.D.E.1	274 (95.1)	49 (17.9)	189 (69)	0.00384	2023 Jul	Oct 2019 (Nov 2000–Jul 2021)
B.D.E.2	2 (0.7)	0	2 (100)	NA	2023 Jul	NA

*Counts and percentages exclude cases with out-of-state or of unknown residence. Pairwise phylogenetic distances and estimated times of most recent common ancestors were calculated using Minnesota HRSV genomes only for lineages with ≥3 genomes. NA, not applicable; RSV, respiratory syncytial virus; RSV-NET, Respiratory Syncytial Virus Hospitalization Surveillance Network; Twin Cities Metro, Minneapolis-St Paul metropolitan area; WGS, whole-genome sequencing.

We constructed phylogenetic trees using Nextstrain's Augur pipeline version 24.3.0 (Figures 1, 2) (*6*,*7*). We aligned viral genome assemblies to Nextstrain's default reference sequences (hRSV/A/England/397/2017 and hRSV/B/Australia/VIC-RCH056/2019) by using MAFFT version 7.526 (*8*) and then constructed and refined distance-scaled and time-scaled trees from those alignments by using IQTree version 2.3.3 and TimeTree version 0.11.3 (*9*,*10*). Comparisons of tree architecture showed greater diversity among all RSV-A genomes (mean pairwise p-distance 0.00933) than among all RSV-B genomes (mean pairwise p-distance 0.00455) (*11*). We observed pairwise p-distances among lineages with ≥3 genomes to be more comparable across subgroups (Table 1). Time-scaled phylogenetic analyses specific to the genomes we sequenced estimated the divergence of lineages to have occurred between 2 and 8 years before their earliest specimen collection dates (Table 1; Appendix Figure, https://wwwnc.cdc.gov/EID/article/30/11/24-1000-App1.pdf). The 95% CIs excluded divergence dates that were more recent than 1–5 years before earliest specimen collection.

We identified single-nucleotide polymorphisms (SNPs) from reference-based whole-genome alignments using SNP-dists version 0.8.2 (*12*). Pairwise comparisons showed that 32.3% of genomes were identical to ≥1 other genome at 0 SNPs (RSV-A, 33.7%, n = 97; HRSV-B, 30.9%, n = 89) and 53% within 1 SNP (RSV-A, 54%, n = 155; RSV-B, 52.1%, n = 150). We found 23 clusters of at least 3 genomes with shared nucleotide identity at 0 SNPs (RSV-A, n = 14; RSV-B, n = 9). Those clusters included 19.5% of all genomes (RSV-A, 20.6%, n = 59; RSV-B, 18.4%, n = 53). Additionally, we identified 1 clade of 8 RSV-B genomes with the F protein amino acid mutation K68N, which is associated with nirsevimab resistance (*13*). This clade had an estimated time of most recent common ancestor of September–November 2023 (Figure 2).

To assess our ability to link RSV genomes to known severe infections, we cross-referenced the names and birthdates of case patients whose specimens we sequenced against the Respiratory Syncytial Virus Hospitalization Surveillance Network (RSV-NET). RSV-NET is a component of the Centers for Disease Control and Prevention Emerging Infections Program focused on sentinel population-based surveillance of RSV-associated hospitalizations and deaths (Table 2; Figure 1) (*14*). Among 531 genomes collected during October 2023–January 2024, the peak months of specimen collection, 117 (22%) were noted among RSV-NET cases (RSV-A, 55.2%, n = 64; RSV-B, 45.3%, n = 53). Those 117 genomes represented 6.3% of all hospitalized cases of RSV during that period. Nine (39.1%) of the 23 clusters we identified included ≥1 RSV-NET case (RSV-A, 50%, n = 7; RSV-B, 22.2%, n = 2), and 13.4% of clustered cases were in RSV-NET (RSV-A, 20.3%, n = 2; RSV-B, 5.7%, n = 3). Two RSV-NET case-patients with sequenced RSV—both with A.D.5.2 infections—were documented to have received nirsevimab (Figure 1). Of the 8 RSV-B cases whose genomes carried the K68N F protein mutation, 1 was documented in RSV-NET (Figure 2).

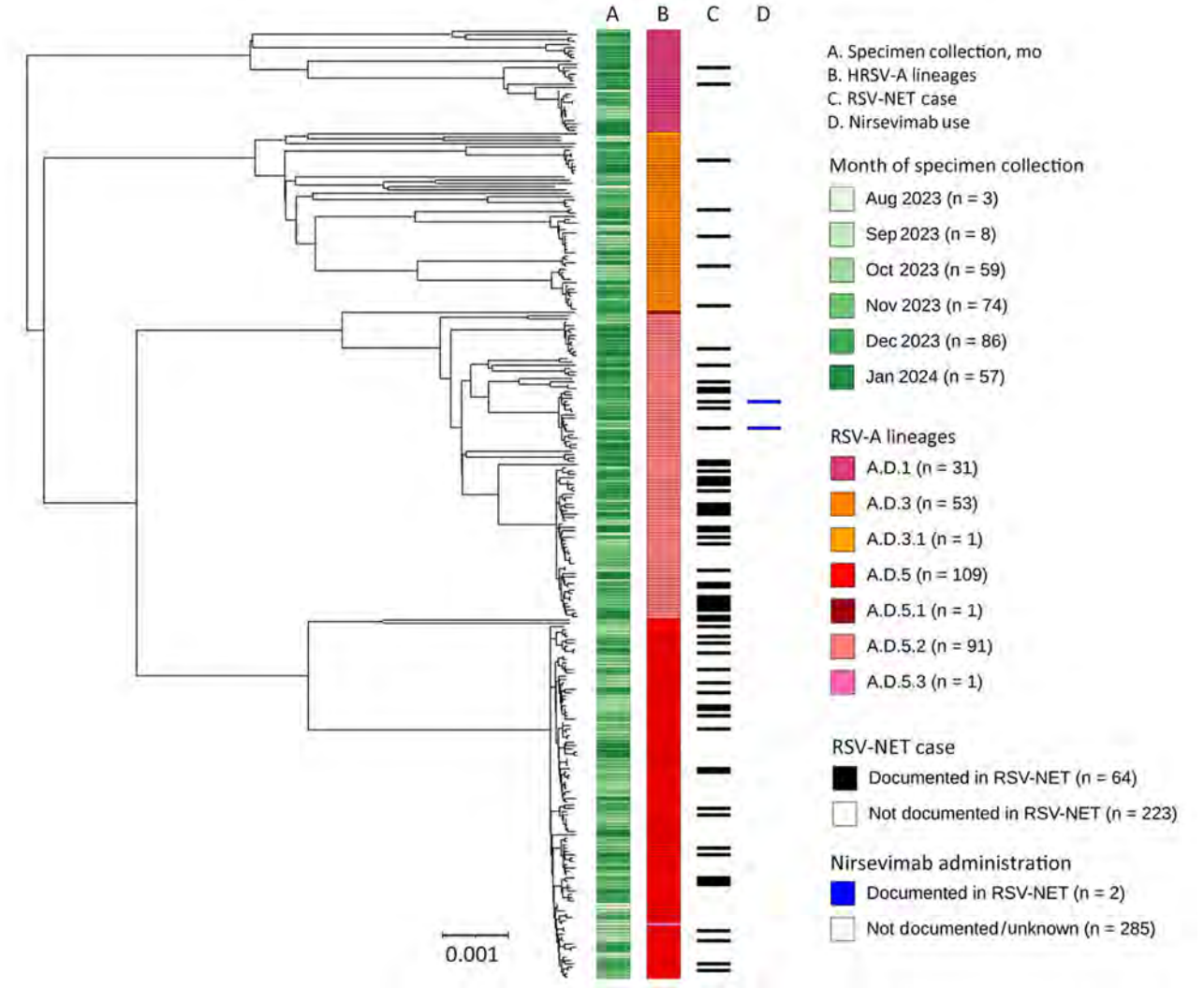

Figure 1. Midpoint-rooted, time-scaled phylogenetic tree of RSV-A whole-genome sequences, Minnesota, USA, October 2023–January 2024. Tree was generated using Interactive Tree of Life (https://itol.embl.de) software. Column annotations denote (from left to right) month of specimen collection, whole-genome lineage classification, documentation of the infected case in the RSV-NET surveillance database for RSV-associated hospitalizations, and administration of nirsevimab before infection as documented in RSV-NET. Scale bar indicates estimated substitution rate calculated from inputs of time and phylogenetic distance. RSV, respiratory syncytial virus; RSV-NET, Respiratory Syncytial Virus Hospitalization Surveillance Network.

To assess potential biases in our sampling for WGS, we performed a preliminary representativeness analysis of hospitalized RSV case-patients with or without collected WGS data. The cohort of sequenced cases documented in RSV-NET was not fully representative of all RSV-NET cases (Table 2). Compared with all RSV-NET case-patients, RSV-NET case-patients with sequenced RSV tended to be younger (median age 2 years for all RSV-NET vs. 1 year for sequenced RSV-NET; p = 0.0193), included a smaller proportion of cases of White versus non-White race (63.6% of all RSV-NET vs. 53.5% for sequenced RSV-NET; p = 0.0014), and were more likely to live within the Minneapolis-St. Paul metropolitan area (65% of all RSV-NET vs. 87.1% of sequenced RSV-NET; p<0.001).

Conclusions

Our findings from a new statewide genomic surveillance program of RSV infections in Minnesota, USA, show that applying WGS for RSV surveillance can yield insights into viral circulation and population dynamics. Prospective sequencing revealed differing genomic landscapes of subgroups A and B and contextualized their genetic diversity within the state. The detection of clusters within the viral population shows the potential use of WGS for detection and investigation of RSV out-

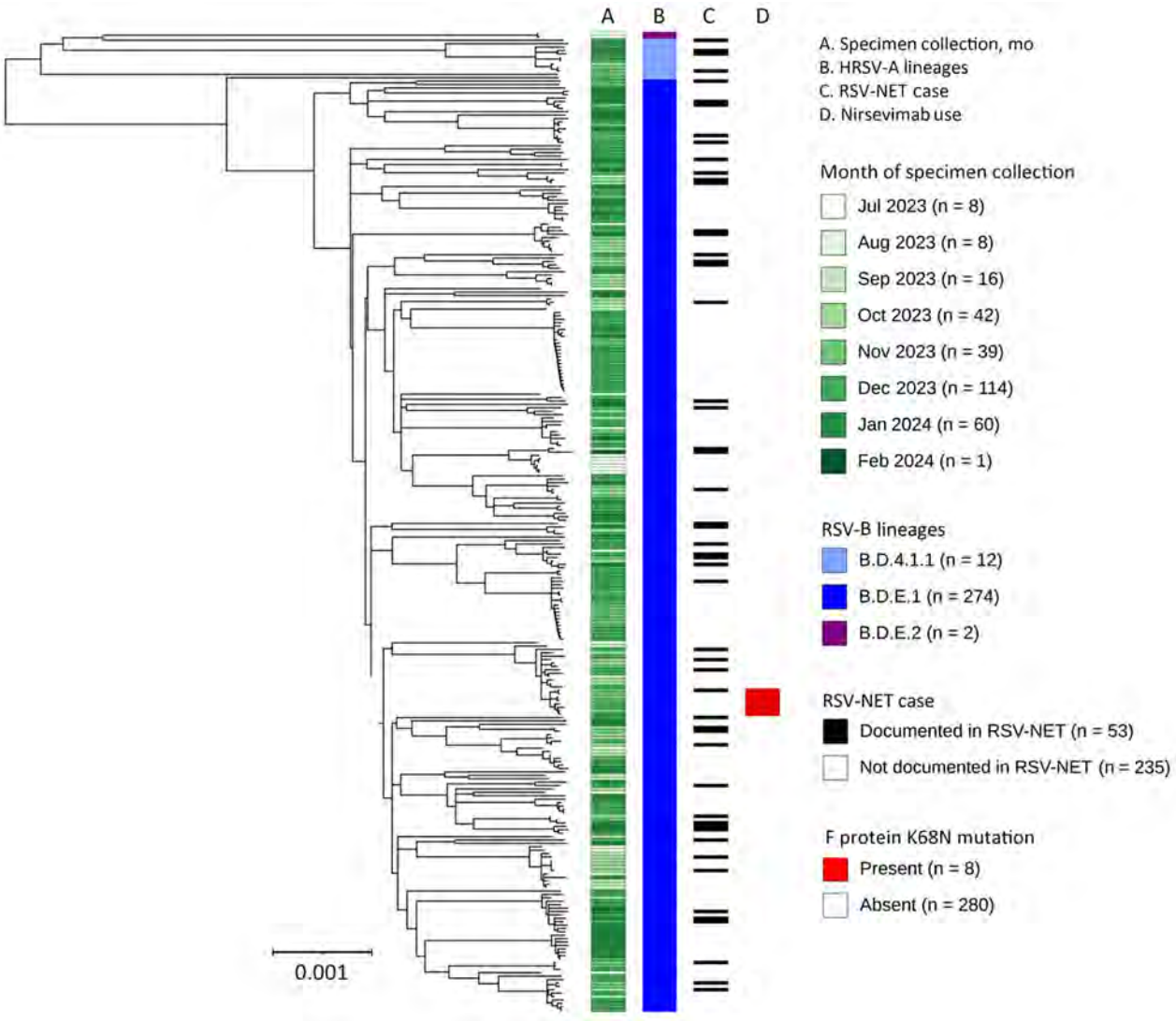

Figure 2. Midpoint-rooted, time-scaled phylogenetic tree of RSV-B whole-genome sequences, Minnesota, USA, October 2023–January 2024. Tree was generated using Interactive Tree of Life (https://itol.embl.de) software. Column annotations denote (from left to right) month of specimen collection, whole-genome lineage classification, documentation of the infected case in the RSV-NET surveillance database for RSV-associated hospitalizations, and the predicted nirsevimab resistance amino acid mutation K68N in the F protein gene sequence. Scale bar indicates estimated substitution rate calculated from inputs of time and phylogenetic distance. RSV, human respiratory syncytial virus; RSV-NET, Respiratory Syncytial Virus Hospitalization Surveillance Network.

Table 2. Comparison of RSV cases with WGS data to hospitalized or deceased case-patients documented in RSV-NET, Minnesota, USA, October 2023–January 2024*

Parameter	RSV-NET cases, Oct 2023–Jan 2024	RSV cases with WGS data, Oct 2023–Jan 2024	RSV-NET cases with WGS data, Oct 2023–Jan 2024
No.	1,847	524	116
Median age, y	2	1.7	1
Sex, %			
F	51.1	49.2	51.7
M	48.9	50.8	48.3
White race, %	63.6	45.2	53.5
Minneapolis-St. Paul metropolitan area, %	65.0	75.2	87.1
Total RSV-NET cases, %	NA	NA	6.3
Sequenced cases, %	NA	NA	20.2

*NA, not applicable; RSV-NET, RSV, respiratory syncytial virus; Respiratory Syncytial Virus Hospitalization Surveillance Network; WGS, whole-genome sequencing.

breaks at state or local levels. Our study also provided novel cross-referencing of viral genomic data against sentinel clinical surveillance of severe RSV infections.

Our study's skewed and localized convenience sampling limited the analytical potential of our findings. The limited geographic and temporal scope of our study also potentially introduced variability in our time-scaled analyses and location-specific discrepancies between RSV evolution in Minnesota and in other regions. In future work, we will expand the collection of genomic and epidemiologic data with more targeted collection of specimens, to improve the scope and representativeness of our sampling approach such that these questions can be investigated more thoroughly. We also intend to perform sufficiently powered epidemiologic analyses on the emergence of mutations linked to vaccine escape, virulence, and transmissibility. However, our results demonstrate that prospective genomic surveillance of RSV can identify the emergence of mutations and clades of epidemiologic significance, such as those linked to evolution of vaccines or monoclonal antibody resistance (*2*,*3*).

This article was preprinted at https://www.medrxiv.org/content/10.1101/2024.07.10.24310215v1.

Acknowledgments

We thank the following healthcare facilities for submitting specimens: Carris Rice, CCM Health-Montevideo, Children's Minnesota, Fairview Ridges, Fairview Southdale, Grand Itasca, Hennepin County Medical Center, Maple Grove Hospital, the Hennepin County medical examiner's office, Minnesota State University-Mankato clinic, Ridgeview-Waconia, and Riverview-Crookston. We thank the Centers for Disease Control and Prevention RSV-NET program and the Emerging Infections Program for their support of sentinel HRSV surveillance in Minnesota, as well as D. Maloney and colleagues for their support with laboratory methods.

All sequencing reads from this study are publicly available on the National Center for Biotechnology Information under BioProject no. PRJNA1048457.

This project was funded by Centers for Disease Control and Prevention Epidemiology and Laboratory Capacity grant no. NU50CK000508 and Pathogen Genomics Centers of Excellence grant no. NU50CK000628.

About the Author

Mr. Evans is a genomic epidemiologist with the Minnesota Department of Health. His work focuses on developing, implementing, and optimizing the use of genomics for pathogen surveillance and epidemiological intervention.

References

1. Shang Z, Tan S, Ma D. Respiratory syncytial virus: from pathogenesis to potential therapeutic strategies. Int J Biol Sci. 2021;17:4073–91. https://doi.org/10.7150/ijbs.64762
2. Goya S, Sereewit J, Pfalmer D, Nguyen TV, Bakhash SAKM, Sobolik EB, et al. Genomic characterization of respiratory syncytial virus during 2022–23 outbreak, Washington, USA. Emerg Infect Dis. 2023;29:865–8. https://doi.org/10.3201/eid2904.221834
3. Goya S, Ruis C, Neher RA, Meijer A, Aziz A, Hinrichs AS, et al. Standardized phylogenetic classification of human respiratory syncytial virus below the subgroup level. Emerg Infect Dis. 2024;30:1631–41. https://doi.org/10.3201/eid3008.240209
4. Patel H, Monzon S, Varona S, Espinosa-Carrasco J, Garcia MU, Heuer ML, et al. nf-core/viralrecon: v2.6.0-Rhodium Raccoon; 2023. [cited 2024 Aug 1]. https://zenodo.org/records/7764938
5. Aksamentov I, Roemer C, Hodcroft EB, Neher RA. Nextclade: clade assignment, mutation calling and quality control for viral genomes. J Open Source Softw. 2021;6:3773. https://doi.org/10.21105/joss.03773
6. Hadfield J, Megill C, Bell SM, Huddleston J, Potter B, Callender C, et al. Nextstrain: real-time tracking of pathogen evolution. Bioinformatics. 2018;34:4121–3. https://doi.org/10.1093/bioinformatics/bty407
7. Huddleston J, Hadfield J, Sibley TR, Lee J, Fay K, Ilcisin M, et al. Augur: a bioinformatics toolkit for phylogenetic analyses of human pathogens. J Open Source Softw. 2021;6:2906. https://doi.org/10.21105/joss.02906
8. Katoh K, Standley DM. MAFFT multiple sequence alignment software version 7: improvements in performance and usability. Mol Biol Evol. 2013;30:772–80. https://doi.org/10.1093/molbev/mst010
9. Minh BQ, Schmidt HA, Chernomor O, Schrempf D, Woodhams MD, von Haeseler A, et al. IQ-TREE 2: new models and efficient methods for phylogenetic inference in the genomic era. Mol Biol Evol. 2020;37:1530–4. https://doi.org/10.1093/molbev/msaa015
10. Kumar S, Suleski M, Craig JM, Kasprowicz AE, Sanderford M, Li M, et al. TimeTree 5: an expanded resource for species divergence times. Mol Biol Evol. 2022;39:174. https://doi.org/10.1093/molbev/msac174
11. Seemann T. SNP-distances. 2018 [cited 2024 Aug 1]. https://github.com/tseemann/snp-dists
12. Paradis E, Schliep K. ape 5.0: an environment for modern phylogenetics and evolutionary analyses in R. Bioinformatics. 2019;35:526–8. https://doi.org/10.1093/bioinformatics/bty633
13. Langedijk AC, Harding ER, Konya B, Vrancken B, Lebbink RJ, Evers A, et al. A systematic review on global RSV genetic data: identification of knowledge gaps. Rev Med Virol. 2022;32:e2284. https://doi.org/10.1002/rmv.2284
14. Havers FP, Whitaker M, Melgar M, Chatwani B, Chai SJ, Alden NB, et al. Characteristics and outcomes among adults aged ≥60 years hospitalized with laboratory-confirmed respiratory syncytial virus—RSV-NET, 12 states, July 2022–June 2023. MMWR. 2022;72:1075-1082.

Address for correspondence: Daniel Evans, Minnesota Department of Health, 625 Robert St N, St. Paul, MN 55101, USA; email: dan.r.evans@state.mn.us

Transmission of Severe Fever with Thrombocytopenia Syndrome Virus to Human from Nonindigenous Tick Host, Japan

Qiang Xu, Takeshi Nabeshima, Koichiro Hamada, Takashi Sugimoto, Mya Myat Ngwe Tun, Kouichi Morita, Hirotomo Yamanashi, Takahiro Maeda, Koya Ariyoshi, Yuki Takamatsu

We report a human case of severe fever with thrombocytopenia syndrome virus infection transmitted by a tick, confirmed by viral identification. *Haemaphysalis aborensis*, a tick species not native to Japan that has been observed to transmit the virus to humans, is now recognized as a potential vector of this virus in Japan.

Blood-feeding ticks can transmit viruses to vertebrates, including humans. A previously unknown flavivirus, Saruyama virus, was detected in Japan in 2018 (*1*); similar viral sequences have also been identified in wild deer and boars in Japan. Severe fever with thrombocytopenia syndrome (SFTS) is an emerging tickborne disease caused by SFTS virus (SFTSV), which belongs to the family Phenuiviridae, genus *Bandavirus*. The first SFTS case was reported in China in 2010 (*2*), followed by cases in Japan and South Korea in 2013 (*3*,*4*); those 3 countries are the primary endemic areas for SFTSV.

Tick bites are the primary route of SFTSV transmission (*2*,*5*). *Haemaphysalis longicornis* ticks, native to east Asia, have been identified as a major SFTSV vector (*2*,*6*). SFTSV cases have been reported in several countries in Southeast Asia, including Vietnam and Thailand, and in South Asia, including Pakistan (*7*), suggesting that SFTSV might expand from endemic regions in tandem with its host animals or through tick migration. In Japan, several tick species, including *H. flava*, *H. megaspinosa*, *H. kitaokai*, *H. formosensis*, and *H. hystricis*, carry the SFTSV genome (*8*,*9*). The mortality rate for SFTS infection ranges from 5% to 28%; the elderly are at higher risk for fatal clinical outcomes (*10*), indicating its potential public health consequences. No antiviral drugs or vaccines are available for SFTSV infection.

We report a human case of SFTS transmitted by a novel tick host, *H. aborensis*, a tick not endemic to Japan that has been identified as a potential vector of SFTSV, indicating possible expansion of habitats of infectious ticks. That finding highlights the importance of comprehensive viral genome analysis as part of routine tick-borne viral surveillance. We obtained informed consent for publication from the patient and ethics approval from the Clinical Research Ethics Committee of Nagasaki University Hospital (record no. 23112012).

The Study

An 80-year-old female patient with a medical history of hypertension, bronchial asthma, and cerebral aneurysm (postoperative), but no history of smoking, alcohol consumption, or recent travel, experienced fever and dizziness. The case-patient resided in Nagasaki, Japan, close to the forest, and reported that she frequently encountered wild animals, such as wild boars and civets. She engaged in daily activities, regularly tended her garden, and had no companion animals. She sought medical consultation with a primary care physician on day 3 after onset of symptoms.

Blood tests revealed a drop in her leukocyte count to 3,180 cells/μL (reference range 3,300–8,600 cells/μL) and platelet count to 104,000/μL (reference range 158,000–348,000/μL). Subsequent blood tests showed further decreases in leukocytes to 1,690 cells/μL and platelets to 72,000/μL. On day 5, the case-patient was

Author affiliations: Nagasaki University, Nagasaki, Japan (Q. Xu, T. Nabeshima, K. Hamada, T. Sugimoto, M.M. Ngwe Tun, K. Morita, H. Yamanashi, T. Maeda, K. Ariyoshi, Y. Takamatsu); Shimane University, Izumo, Japan (M.M. Ngwe Tun)

DOI: https://doi.org/10.3201/eid3011.240912

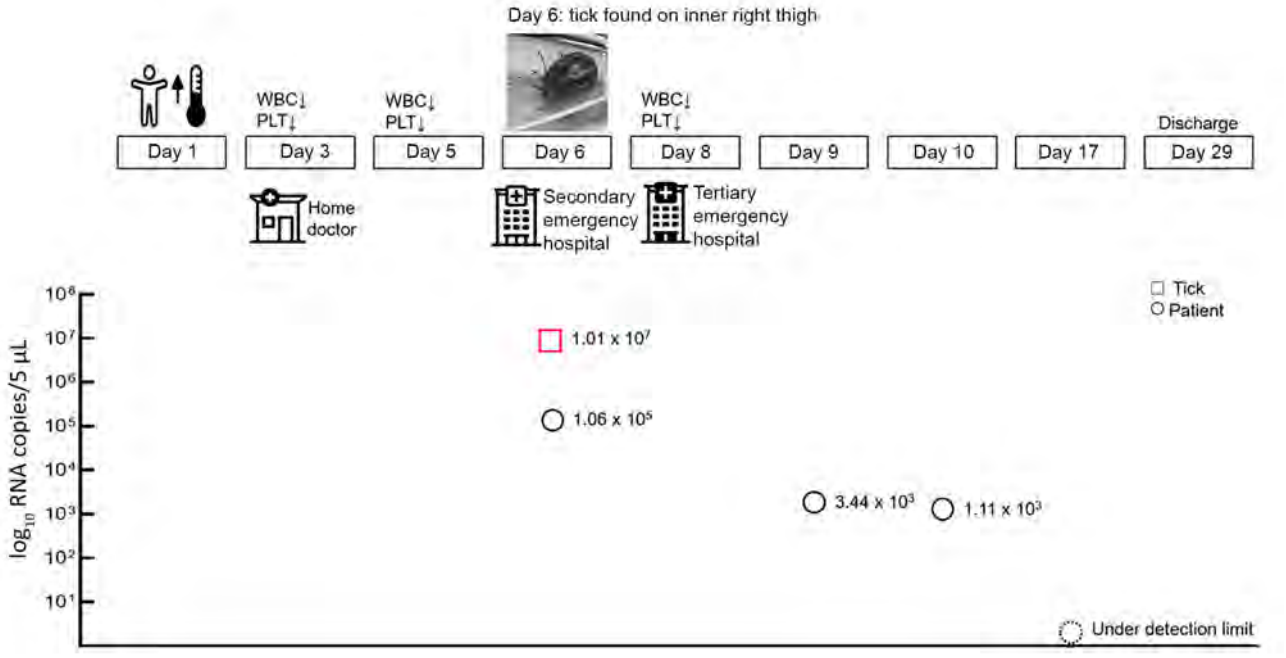

Figure 1. Timeline of SFTSV progression in a human patient in Japan and photograph of *Haemaphysalis aborensis* tick collected from the patient. WBC, white blood cells (leukocytes); PLT, platelets; SFTSV, severe fever with thrombocytopenia syndrome virus.

referred to a secondary emergency hospital for further evaluation. A blood-engorged tick was found on her inner right thigh (Figure 1). Presence of leukopenia, thrombocytopenia, and tick bites indicated SFTSV infection. A serum specimen from the patient was sent to the laboratory at Nagasaki City Health Center, which is responsible for administrative inspections for SFTS diagnosis. The results revealed SFTSV positivity on day 12 after symptom onset.

The patient was transferred from the secondary hospital to the Department of Internal Medicine of Infectious Diseases at Nagasaki University Hospital, a tertiary emergency hospital, on day 8 after onset. Physical examination at time of admission indicated a body temperature of 36.0°C, heartbeat of 66 beats/min, blood pressure of 121/72 mm Hg, SpO_2 of 94% (room air), and respiratory rate of 28 breaths/min. The patient's level of consciousness was unclear, but

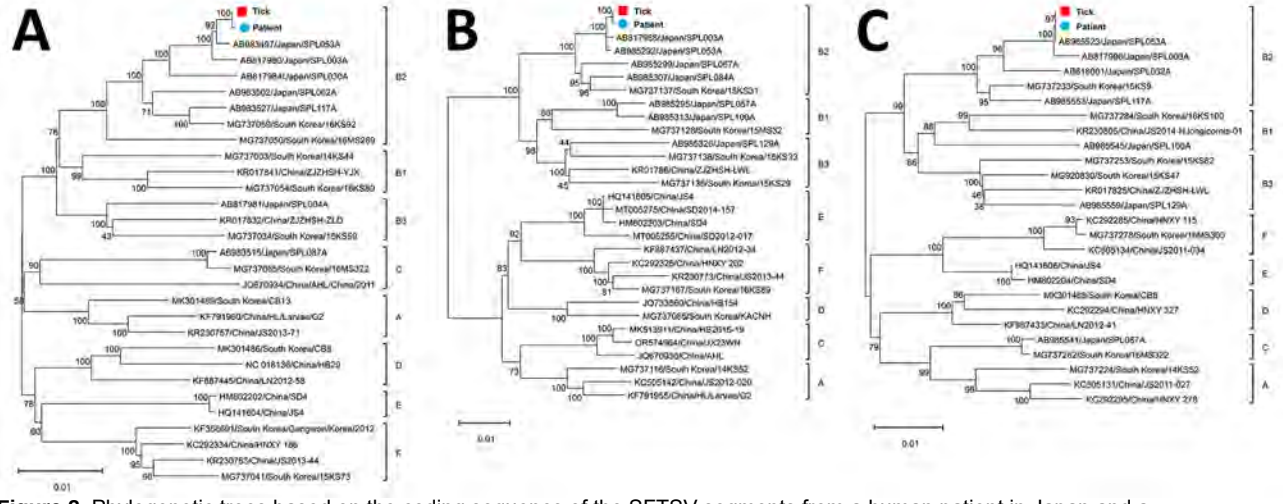

Figure 2. Phylogenetic trees based on the coding sequence of the SFTSV segments from a human patient in Japan and a *Haemaphysalis aborensis* tick collected from the patient. A) Large segment; B) medium segment; C) small segment. Blue circles indicate patient-derived SFTSV strains and red squares tick-derived strains from this study. Labels at right of each tree represent SFTSV genotypes A–F. We derived the phylogenetic trees using the maximum-likelihood method and general time-reversible model and ran 1,000 bootstrap replicates using MEGA 11.0.13 (https://www.megasoftware.net). Scale bars indicate the number of base differences per site. SFTSV, severe fever with thrombocytopenia syndrome virus.

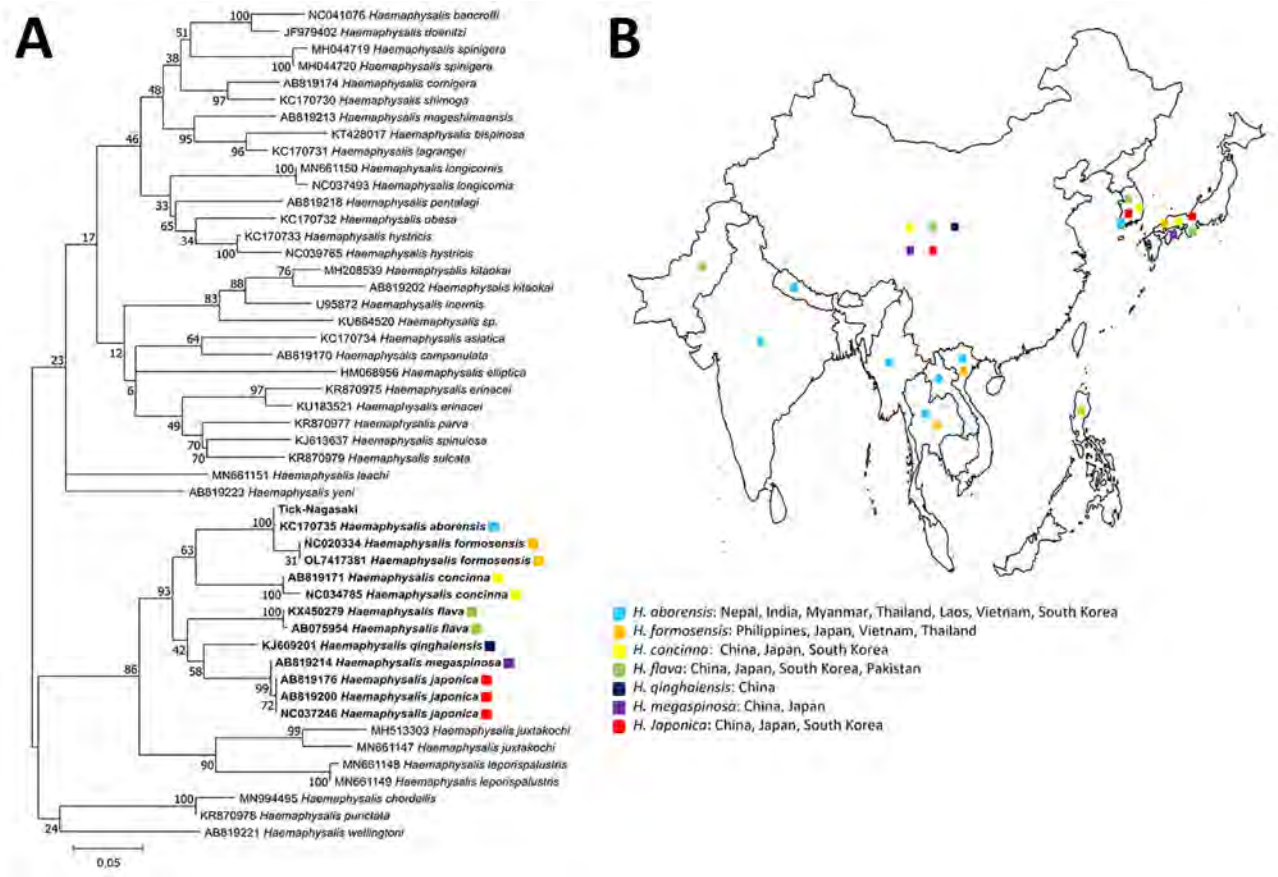

Figure 3. Phylogenetic tree (A) and geographic distribution (B) of 36 tick species from the genus *Haemaphysalis*. Bold indicates tick sequences analyzed in this study; Tick-Nagasaki indicates tick collected from a human patient in Japan who had severe fever with thrombocytopenia syndrome virus. Colors indicate locations where ticks have been found. We used 49 16S rRNA sequences to construct the maximum-likelihood tree based on 1,000 replicates in MEGA 11.0.13 (https://www.megasoftware.net). Bootstrap values are indicated next to the branches. Scale bar indicates nucleotide substitutions per site.

she responded when called, which is indicative of a II-10 rating on the Japan Coma Scale. Blood chemical examination demonstrated results with reference ranges for hemoglobin (12.3 g/dL), sodium (137 mEq/L), potassium (3.8 mEq/L), chloride (108 mEq/L), blood urea nitrogen (6 mg/dL), creatinine (0.7 mg/dL), and C-reactive protein (0.04 mg/dL). Compared with earlier test results, we noted further decreases in leukocyte count, to 2,300 cells/μL (neutrophils 920 cells/μL, lymphocytes 1,080 cells/μL), and platelet count, to 53,000/μL; we also saw increases in aspartate transferase (133 U/L, reference range 13–30 U/L), alanine transaminase (64 U/L, reference range 7–23 U/L), lactate dehydrogenase (770U/L, reference range 124–222 U/L), and creatine kinase (471 U/L, reference range 41–153 U/L). Urine examination revealed high protein 2+ and occult blood 2+ results. Results of blood cultures on days 6 and 10 and urine cultures on day 10 after onset were negative for bacterial infections. The patient gradually recovered and was discharged on day 29 after symptom onset without any specified lasting effects.

We sent the tick from the patient and serum specimens collected on days 6, 9, 10, and 17 after onset to the Department of Virology, Institute of Tropical Medicine, at Nagasaki University for examination. We extracted total RNA from the homogenized tick sample (Appendix, https://wwwnc.cdc.gov/EID/article/30/11/24-0912-App1.pdf) and subjected serum specimens to quantitative reverse-transcription PCR (qRT-PCR) (Appendix). The specimen from day 6 demonstrated the highest number of SFTSV RNA copies (1.06×10^5/5 μL). The SFTSV RNA copies in the serum specimens decreased and were undetectable on day 17 after onset (Figure 1). Homogenates from the tick demonstrated a substantially higher number of SFTSV RNA copies (1.01×10^7/5 μL) than the patient samples. We isolated viruses only from the tick, not from patient specimens.

To explore the genomic similarity of SFTSV strains derived from tick and human samples, we determined the full-length protein-coding sequences of the large (L), medium (M), and small (S) segments of viruses from the tick (GenBank accession nos. PP813867–9) and patient (accession nos. PP839300–2) by using next-generation sequencing (Appendix). We conducted phylogenetic analysis using MEGA11 (https://www.megasoftware.net) to determine the genetic relationships between the sequences from our study and previously identified SFTSV sequences from countries in Asia, including Japan (*11*). The sequences of patient- and tick-derived SFTS L/M/S segments were identical. SFTSV identified in our study's belonged to B-2 clade (Figure 2, panels A–C), the genotype most prevalent in Japan and South Korea (*10*).

Morphologic characteristics (Figure 1) identified the tick collected from the patient as belonging to the genus *Haemaphysalis*. To confirm species identification, we sequenced the 16S ribosomal RNA (accession no. PP813416) (Appendix). Phylogenetic analysis identified it as most closely related to *H. aborensis*, a species not endemic to Japan (Figure 3, panel A). We found no previous reports of SFTSV isolation or gene detection in *H. aborensis* ticks.

H. aborensis ticks are primarily distributed in Nepal and India in South Asia and Laos, Vietnam, and Thailand in Southeast Asia (Figure 3, panel B) (*12*); porcupines, wild boars, and deer are the primary hosts (*12*). A previous study identified *H. aborensis* ticks collected from *Turdus pallidus* (pale thrush) on Hong Island, South Korea (*13*). The *T. pallidus* thrush is a migratory bird that breeds in areas from northeast China to far eastern Russia and overwinters in southern and central Japan, South Korea, and southern China (*14*). Because the B-2 clade has been isolated only in Japan and South Korea (*10*), SFTSV-infected ticks were likely carried by infected birds from South Korea. Although it is possible that ticks were carried by birds from South Korea, then acquired and transmitted SFTSV through infected animals in Japan, this scenario is unlikely because *H. aborensis* ticks had not been previously identified in Japan.

Conclusions

We report a case of tick-transmitted SFTSV infection in a human patient. Virus isolation and identification of the tick species confirmed that *H. aborensis* ticks can transmit SFTSV to humans. The phylogenetic analysis revealed no differences between sequences of SFTSV from the tick and the patient. Identifying an additional host tick highlights the importance of routine tick surveillance for monitoring SFTSV expansion.

Acknowledgments

The authors acknowledge Katsuaki Motomiya for contributing to obtaining patient specimens and Mitsuru Hattori and Akira Yoshikawa for fruitful discussions. The authors acknowledge Tomomi Kurashige and Megumi Tsubota for their technical support and all members of the Department of Virology, Institute of Tropical Medicine, Nagasaki University for their cooperation.

This study was supported by the Japan Agency of Medical Research and Development (grant nos. JP24fk0108656, JP24fk0108695, JP24wm0125006, JP24wm0125011, JP23fm0208101, JP23fk0108656, JP23wm0125006, JP22wm0325023, JP22fm0208101, JP21fm0208101, JP21wm0325023, and JP20wm0323023); the Japan Society for Promotion of Sciences (grant nos. 21K07059, 22KK0115, and 24K02288); Takeda Science Foundation, MSD Life Science Foundation, the Naito Foundation, Kurozumi Medical Foundation, the Asahi Glass Foundation, and Joint/Research Center on Tropical Disease, Institute of Tropical Medicine, Nagasaki University (2022-Ippan-12, 2023-Ippan-16).

About the Author

Mr. Xu is a doctoral student in the Program for Nurturing Global Leaders in Tropical and Emerging Communicable Diseases at the Graduate School of Biomedical Sciences, Nagasaki University, Nagasaki, Japan. His research interests include the epidemiology of SFTSV and the elucidation of the molecular mechanism of the SFTSV replication cycle.

References

1. Kobayashi D, Inoue Y, Suzuki R, Matsuda M, Shimoda H, Faizah AN, et al. Identification and epidemiological study of an uncultured flavivirus from ticks using viral metagenomics and pseudoinfectious viral particles. Proc Natl Acad Sci U S A. 2024;121:e2319400121. https://doi.org/10.1073/pnas.2319400121
2. Yu XJ, Liang MF, Zhang SY, Liu Y, Li JD, Sun YL, et al. Fever with thrombocytopenia associated with a novel bunyavirus in China. N Engl J Med. 2011;364:1523–32. https://doi.org/10.1056/NEJMoa1010095
3 Takahashi T, Maeda K, Suzuki T, Ishido A, Shigeoka T, Tominaga T, et al. The first identification and retrospective study of severe fever with thrombocytopenia syndrome in Japan. J Infect Dis. 2014;209:816–27. https://doi.org/10.1093/infdis/jit603
4. Kim YR, Yun Y, Bae SG, Park D, Kim S, Lee JM, et al. Severe fever with thrombocytopenia syndrome virus infection, South Korea, 2010. Emerg Infect Dis. 2018;24:2103–5. https://doi.org/10.3201/eid2411.170756
5. Yun SM, Lee WG, Ryou J, Yang SC, Park SW, Roh JY, et al. Severe fever with thrombocytopenia syndrome virus in ticks collected from humans, South Korea, 2013. Emerg Infect Dis. 2014;20:1358–61. https://doi.org/10.3201/eid2008.131857

6. Park SW, Song BG, Shin EH, Yun SM, Han MG, Park MY, et al. Prevalence of severe fever with thrombocytopenia syndrome virus in *Haemaphysalis longicornis* ticks in South Korea. Ticks Tick Borne Dis. 2014;5:975–7. https://doi.org/10.1016/j.ttbdis.2014.07.020
7. Kim EH, Park SJ. Emerging tick-borne *Dabie bandavirus*: virology, epidemiology, and prevention. Microorganisms. 2023;11:2309. https://doi.org/10.3390/microorganisms11092309
8. Sato Y, Mekata H, Sudaryatma PE, Kirino Y, Yamamoto S, Ando S, et al. Isolation of severe fever with thrombocytopenia syndrome virus from various tick species in area with human severe fever with thrombocytopenia syndrome cases. Vector Borne Zoonotic Dis. 2021;21:378–84. https://doi.org/10.1089/vbz.2020.2720
9. National Institute of Infectious Diseases. Japan. Infectious agents surveillance report, volume 37. Severe fever with thrombocytopenia syndrome (SFTS) in Japan, as of February 2016 [cited 2024 Jun 5]. https://www.niid.go.jp/niid/en/iasr-vol37-e/865-iasr/6339-tpc433.html
10. Casel MA, Park SJ, Choi YK. Severe fever with thrombocytopenia syndrome virus: emerging novel phlebovirus and their control strategy. Exp Mol Med. 2021;53:713–22. https://doi.org/10.1038/s12276-021-00610-1
11. Yun SM, Park SJ, Kim YI, Park SW, Yu MA, Kwon HI, et al. Genetic and pathogenic diversity of severe fever with thrombocytopenia syndrome virus (SFTSV) in South Korea. JCI Insight. 2020;5:e129531. https://doi.org/10.1172/jci.insight.129531
12. Hoogstraal H, Dhanda V, Kammah KME. *Aborphysalis*, a new subgenus of Asian *Haemaphysalis* ticks; and identity, distribution, and hosts of *H. aborensis* Warburton (resurrected) (Ixodoidea: Ixodidae). J Parasitol. 1971;57:748–60. https://doi.org/10.2307/3277792
13. Kim HC, Chong ST, Choi CY, Nam HY, Chae HY, Klein TA, et al. Tick surveillance, including new records for three *Haemaphysalis* species (Acari: Ixodidae) collected from migratory birds during 2009 on Hong Island (Hong-do), Republic of Korea. Syst Appl Acarol. 2016;596–606.
14. Collar N, de Juana E. Birds of the world 2020. Pale thrush (*Turdus pallidus*) [cited 2024 Jun 6]. https://birdsoftheworld.org/bow/species/palthr1/cur/introduction

Address for correspondence: Yuki Takamatsu, Department of Virology, Institute of Tropical Medicine, Nagasaki University, 1-12-4 Sakamoto, Nagasaki 852-8523, Japan; email: yukiti@nagasaki-u.ac.jp

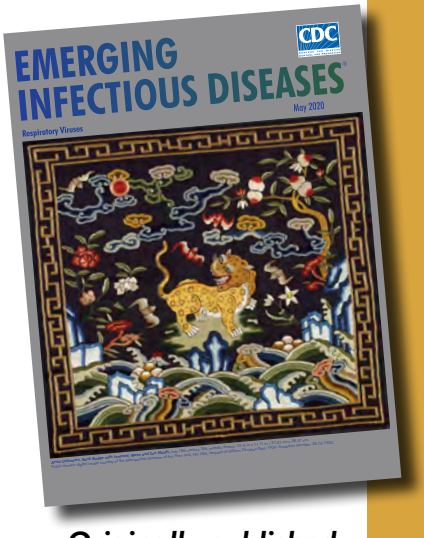

Originally published in May 2020

etymologia revisited

Coronavirus

The first coronavirus, avian infectious bronchitis virus, was discovered in 1937 by Fred Beaudette and Charles Hudson. In 1967, June Almeida and David Tyrrell performed electron microscopy on specimens from cultures of viruses known to cause colds in humans and identified particles that resembled avian infectious bronchitis virus. Almeida coined the term "coronavirus," from the Latin *corona* ("crown"), because the glycoprotein spikes of these viruses created an image similar to a solar corona. Strains that infect humans generally cause mild symptoms. However, more recently, animal coronaviruses have caused outbreaks of severe respiratory disease in humans, including severe acute respiratory syndrome (SARS), Middle East respiratory syndrome (MERS), and 2019 novel coronavirus disease (COVID-19).

References

1. Almeida JD, Tyrrell DA. The morphology of three previously uncharacterized human respiratory viruses that grow in organ culture. J Gen Virol. 1967;1:175–8. https://doi.org/10.1099/0022-1317-1-2-175
2. Beaudette FR, Hudson CB. Cultivation of the virus of infectious bronchitis. J Am Vet Med Assoc. 1937;90:51–8.
3. Estola T. Coronaviruses, a new group of animal RNA viruses. Avian Dis. 1970;14:330–6. https://doi.org/10.2307/1588476
4. Groupe V. Demonstration of an interference phenomenon associated with infectious bronchitis virus of chickens. J Bacteriol. 1949;58:23–32. https://doi.org/10.1128/JB.58.1.23-32.1949

https://wwwnc.cdc.gov/eid/article/26/5/et-2605_article

Outbreak of Listeriosis Likely Associated with Baker's Yeast Products, Switzerland, 2022–2024

Roger Stephan, Jule Anna Horlbog, Magdalena Nüesch-Inderbinen, Nicola Dhima

Author affiliations: Institute for Food Safety and Hygiene, Zurich, Switzerland (R. Stephan, J.A. Horlbog, M. Nüesch-Inderbinen); National Centre for Enteropathogenic Bacteria and *Listeria*, Zurich (J.A. Horlbog, M. Nüesch-Inderbinen); Swiss Federal Office of Public Health, Bern, Switzerland (N. Dhima)

DOI: https://doi.org/10.3201/eid3011.240764

We traced back a nationwide outbreak of human listeriosis in Switzerland to a persisting production line contamination of a factory producing baker's yeast with *Listeria monocytogenes* serotype 1/2a sequence type 3141. We used whole-genome sequencing to match clinical isolates to isolates from product samples.

We report a prolonged and diffuse outbreak of listeriosis in Switzerland that involved 34 patients. The first case was reported in April 2022, and the outbreak peak occurred in 2023 (Figure 1). The last known case was in June 2024. A questionnaire-based outbreak investigation was initiated by the Swiss Federal Office of Public Health but did not identify a specific food exposure. The median age of the patients was 79 years (range 0–93 years); 18 (53%) were female and 16 (47%) male. The distribution of patients within Switzerland was wide (across different cantons) (Appendix Figure, https://wwwnc.cdc.gov/EID/article/30/11/24-0764-App1.pdf).

Of the 34 persons with documented cases, 7 died, and listeriosis was reported as the primary cause of death in all 7 cases according to the notification data. Of the 34 human *Listeria monocytogenes* isolates recovered, 28 were from blood, 2 from cerebrospinal fluid, and 1 from a swab specimen of a facial skin lesion; for 3 isolates, no information about the clinical sample was available.

We performed whole-genome sequencing (WGS) by using Illumina MiSeq next-generation sequencing technology (Illumina, https://www.illumina.com). We mapped sequencing reads against a multilocus sequence typing scheme based on 7 housekeeping genes and a 1,701-locus core genome multilocus sequence typing (cgMLST) scheme by using Ridom SeqSphere+ software version 9.0.2 (https://www.ridom.de/seqsphere) (*1*). We determined sequence types and cluster types upon submission to the *L. monocytogenes* cgMLST Ridom SeqSphere+ server (*1*).

We defined a cluster as a group of isolates with ≤10 different alleles between neighboring isolates (*1*). We assigned all 34 isolates to *L. monocytogenes* serotype 1/2a, sequence type 3141, cgMLST cluster type 18049; all isolates harbored *fosX* genes (coding for fosfomycin resistance) and *vga*(G) genes (coding for lincosamides and streptogramin A resistance). Furthermore, all isolates were genetically closely related (≤2 allelic difference) to *L. monocytogenes* isolated from baker's yeast (*Saccharomyces cerevisiae*) products from a commercial yeast factory and its production lines.

The baker's yeast products were sold in retail stores and supplied the food industry throughout Switzerland. During 2022, the baker's yeast manufacturer had determined the occurrence of *L. monocytogenes* in yeast product samples. Analysis had been conducted as part of the manufacturer's self-control

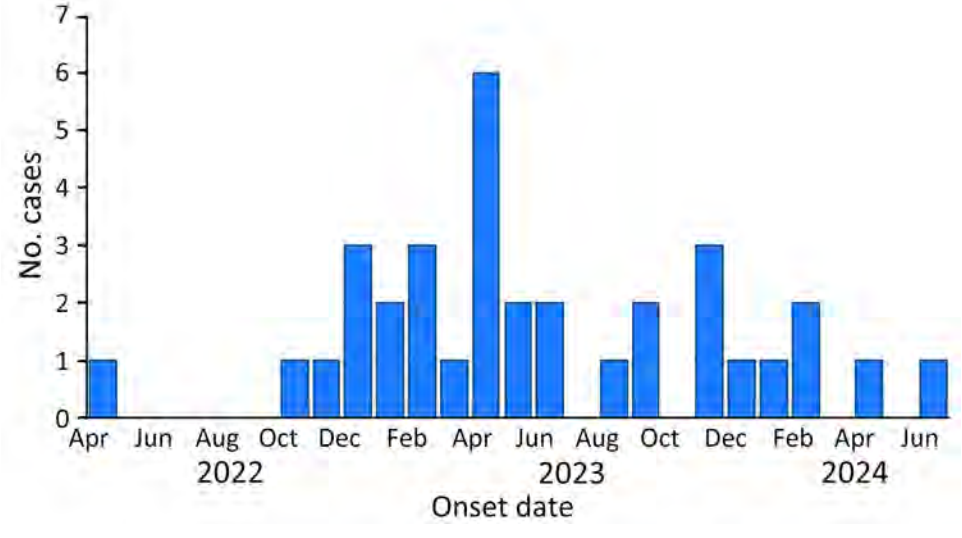

Figure 1. Listeriosis cases (N = 34), by illness onset date, in an outbreak likely linked to baker's yeast products, Switzerland, April 2022–June 2024. The outbreak involved single distinct core-genome multilocus sequence typing cluster type 18049 of *Listeria monocytogenes* serotype 1/2a, sequence type 3141.

practices; however, in the absence of legal requirements for non–ready-to-eat (non-RTE) products, the findings were not reported. In July 2023, official random and risk-based food checks performed by a cantonal laboratory in Switzerland revealed the presence of *L. monocytogenes* (isolate N23-1507) in a yeast product. WGS analysis confirmed the presence of the outbreak strain (Figure 2). The finding prompted extensive environmental sampling on the production site of the manufacturer and retrospective WGS analysis of all available isolates.

During July 2023–August 2024, the manufacturer commissioned microbiological testing on different production steps, and we obtained product samples or swabs from the yeast cream, vats, pipe systems, drying filters, extruders, conveyor belts, and cutting machines. All sequenced *L. monocytogenes* isolated from the production line and the strains obtained from yeast products matched the outbreak strain (Figure 2). Within the production line, the laboratory identified a flow pipe connecting a starch vat to the yeast drying bed as the first point of contamination. Subsequently, the manufacturer started deep cleaning of all processing equipment at the part of the production line where the positivity was detected. An official product recall was not warranted because baker's yeast is not classified as RTE food. However, only batches of the product that had been subjected to extensive controls and yielded <10 colony forming units of *L. monocytogenes* per gram were released for sale. This approach was supported by further investigations that showed no growth of *L. monocytogenes* during the shelf-life of the baker's yeast (data not shown).

Products made with baker's yeast normally undergo a heating step that would control the contamination. However, as evident from raw dough–associated illness outbreaks caused by *Escherichia coli* and *Salmonella* in Canada and the United States (*2*,*3*), contaminated dough represents a health hazard if consumed raw, and cross-contamination can occur through the handling of contaminated baker's yeast or contaminated raw dough. That aspect is reflected by the fact that the outbreak strain also was detected in food items in several restaurants and institutional catering establishments in different cantons (data not shown).

Listeriosis is a potentially lethal infection, and the young, the elderly, pregnant women, and immunocompromised persons are at particular risk (*4*). Foods, mainly RTE foodstuffs that include meat, fish, dairy products, fruit, and vegetables, represent major vehicles for sporadic cases and outbreaks of listeriosis (*5*).

This outbreak, likely linked to baker's yeast, highlights the lack of data on contamination of non-RTE products by foodborne pathogens, including *L. monocytogenes*, and the need for manufacturers of baker's yeast to consider this risk in their production processes. Moreover, this outbreak should raise awareness that compliance with basic hygiene measures to prevent cross-contamination is particularly important when handling food that is not RTE.

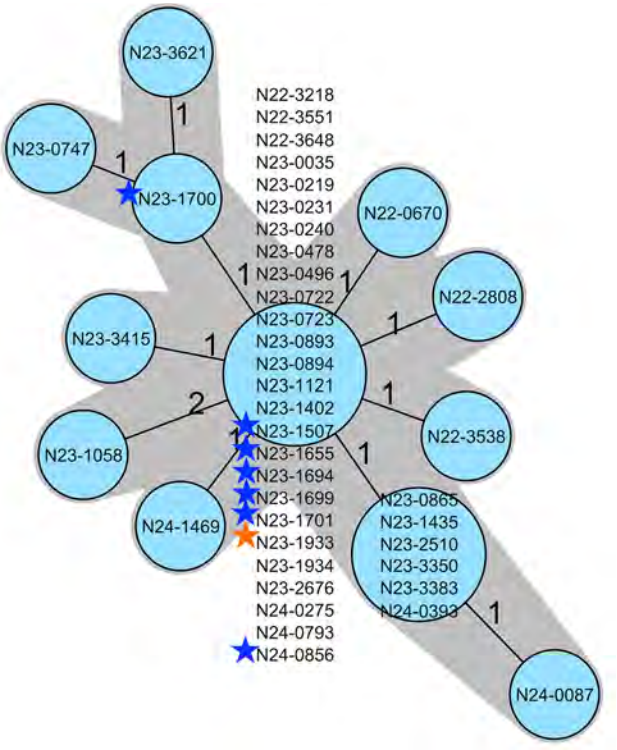

Figure 2. Minimum-spanning tree based on core-genome multilocus sequence typing allelic profiles of 34 human infections by *Listeria monocytogenes* sequence type 3141, a representative selection consisting of 7 baker's yeast product isolates, and 1 isolate from a flow pipe in the baker's yeast production line, Switzerland, 2022–2024. Each circle represents an allelic profile based on sequence analysis of 1,701 core-genome multilocus sequence typing target genes. Values on connecting lines indicate number of allelic differences between 2 strains. Each circle contains the identification of the strain or strains. Blue stars indicate the yeast product isolates; orange star indicates the environmental strain. Strain N23-1507 was isolated from baker's yeast product during an official food check.

Acknowledgments

We thank Nicole Cernela and Marc Stevens for the technical support with Illumina sequencing and bioinformatic analysis.

This work was partly supported by the Swiss Federal Office of Public Health's Division Communicable Diseases and the Swiss Federal Office of Public Health's Federal Food Safety and Veterinary Office.

The sequence data for clinical outbreak strain *L. monocytogenes* N23-0035 have been deposited in the National Center for Biotechnology Information Nucleotide database under BioProject no. PRJNA935533 and accession no. JBDQYW000000000.

About the Author

Mr. Stephan is the director of the Institute for Food Safety and Hygiene at the University of Zurich. His research activities are focused on the epidemiology and characteristics of foodborne pathogens in the food chain.

References

1. Ruppitsch W, Pietzka A, Prior K, Bletz S, Fernandez HL, Allerberger F, et al. Defining and evaluating a core genome multilocus sequence typing scheme for whole-genome sequence-based typing of *Listeria monocytogenes*. J Clin Microbiol. 2015;53:2869–76. https://doi.org/10.1128/JCM.01193-15
2. Gill A, Carrillo C, Hadley M, Kenwell R, Chui L. Bacteriological analysis of wheat flour associated with an outbreak of Shiga toxin–producing *Escherichia coli* O121. Food Microbiol. 2019;82:474–81. https://doi.org/10.1016/j.fm.2019.03.023
3. Rahman R, Scharff RL, Wu F. Foodborne disease outbreaks in flour and flour-based food products from microbial pathogens in the United States, and their health economic burden. Risk Anal. 2023;43:2519–26. https://doi.org/10.1111/risa.14132
4. Allerberger F, Wagner M. Listeriosis: a resurgent foodborne infection. Clin Microbiol Infect. 2010; 16:16–23. https://doi.org/10.1111/j.1469-0691.2009.03109.x
5. Buchanan RL, Gorris LGM, Hayman MM, Jackson TC, Whiting RC. A review of *Listeria monocytogenes*: an update on outbreaks, virulence, dose-response, ecology, and risk assessments. Food Control. 2017;75:1–13. https://doi.org/10.1016/j.foodcont.2016.12.016

Address for correspondence: Magdalena Nüesch-Inderbinen, Institute for Food Safety and Hygiene, Vetsuisse Faculty, University of Zurich, Winterthurerstrasse 272, 8057 Zurich, Switzerland; email: magdalena.nueesch-inderbinen@uzh.ch

Influenza A(H5N1) Virus Resilience in Milk after Thermal Inactivation

C. Joaquin Caceres, L. Claire Gay, Flavio Cargnin Faccin, Dikshya Regmi, Roberto Palomares, Daniel R. Perez

Author affiliation: University of Georgia College of Veterinary Medicine, Athens, Georgia, USA

DOI: https://doi.org/10.3201/eid3011.260772

Highly pathogenic avian influenza A(H5N1) detected in dairy cows raises concerns about milk safety. The effects of pasteurization-like temperatures on influenza viruses in retail and unpasteurized milk revealed virus resilience under certain conditions. Although pasteurization contributes to viral inactivation, influenza A virus, regardless of strain, displayed remarkable stability in pasteurized milk.

Recent detection of highly pathogenic avian influenza A(H5N1) virus in US dairy cows raises serious public health concerns (*1*–*3*). Pasteurization, a common process for ensuring milk safety, involves heating milk to specific temperatures for specific lengths of time to eliminate disease-causing bacteria. The most common methods in the United States (*4*) are low-temperature long-time (LTLT, 63°C for 30 minutes) and high-temperature short-time (HTST, 72°C for 15–20 seconds) pasteurization. Recent studies have shown that unpasteurized milk from H5N1-infected cows contains enough virus to infect susceptible animals (*5*).

We examined pasteurizing milk at various temperatures to evaluate how temperature affects virus viability (Figure 1). It is crucial to emphasize that we do not assert that those conditions in a test tube setting simulate the actual pasteurization process. We used 4 influenza virus strains in this study: 1 laboratory-adapted strain (PR8) and 3 H5N1 strains (Figures 1, 2; Appendix; https://wwwnc.cdc.gov/EID/article/30/11/24-0772-App1.pdf). We spiked commercially available pasteurized whole milk (3.25% fat) with virus strains at a concentration of 10^8 50% tissue culture infectious dose/mL of milk or Opti-MEM control media (Fisher Scientific, https://www.fishersci.com). We subjected varying sample volumes (200 μL, 20 μL, and 2 μL) to 3 distinct heat treatments: 63°C for 30 minutes, 72°C for 20 seconds, and 91°C for 20 seconds. In addition, we tested the PR8 strain in both pasteurized and unpasteurized

milk to investigate the effect of preheating milk at 37°C for 1 minute before subjecting it to HTST-like conditions. After treatment, we adjusted samples to a final volume of 200 μL and titrated (*6*).

We observed no significant (i.e., $p<0.05$) difference in viral titer between influenza viruses diluted in control media and in milk. All 3 viruses tested in this assay (PR8, VN/04 ΔH5N1, and ty/IN/22) behaved similarly (Figure 1, panels A–C). Heat treatment at 63°C for 30 minutes effectively reduced viral viability below the limit of detection. For samples treated at 72°C for 20 seconds, titer reduction was inversely proportional to sample volume, with a nonsignificant decrease observed in 200-μL samples. Conversely, we observed significant ($p<0.05$) titer reduction in 20 μL and 2-μL samples at 72°C. Treatment at 91°C for 20 seconds also resulted in significant titer reduction inversely proportional to sample volume. Preheating samples to 37°C for 1 minute before beginning HTST (Figure 1, panels D, E) accelerated virus inactivation and was more pronounced in smaller volumes of milk (Figure 1, panel A).

To investigate how different types of milk and storage temperatures affected the stability of influenza virus strains (Figure 2, panel B), we tested pasteurized milk, unpasteurized colostrum milk (Figure 2, panel C), and unpasteurized mature milk (Figure 2, panel D). We stored the milk samples spiked with viruses at different temperatures for up to 4 days. We included a control sample in virus media for comparison. Those viruses showed remarkable resilience in unpasteurized milk, remaining infectious for ≥4 days at temperatures other than 63°C, at which temperature virus was inactivated within 24 hours. Unpasteurized colostrum milk showed increased virus inactivation, perhaps because of the presence of immunoglobulins.

Although our study offers valuable insights, it is critical to note that spiking viruses into milk might not perfectly mimic a natural infection. However,

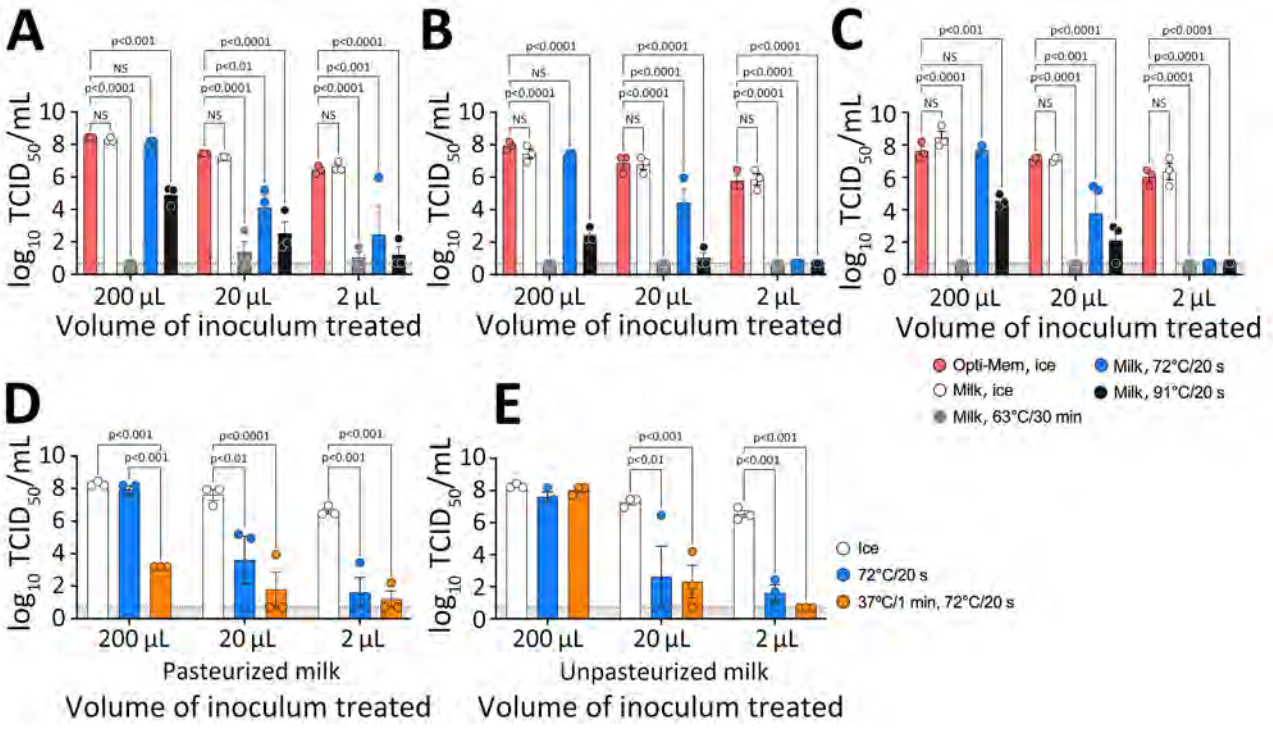

Figure 1. Heat treatment of influenza virus in milk. A–C) We diluted influenza A viruses in Opti-Mem control media (Fisher Scientific, https://www.fishersci.com) or commercial off-the-shelf pasteurized whole milk and heat-treated samples of different volumes at the times and temperatures shown; we calculated time from the moment the sample was placed in the heat block. A sandwich design in a heat block ensured uniform temperature exposure. After treatment, we chilled samples on ice for 5 minutes, adjusted them to a final volume of 200 μL, and titrated by $TCID_{50}$ in MDCK cells (*10*). Results are shown for reverse genetics wild-type strain A/Puerto Rico/8/1934 (H1N1) (A); Vietnam/1203/04, a reverse genetics virus carrying the H5 hemagglutinin and N1 neuraminidase segments from A/Vietnam/1203/2004 (H5N1) in the background of PR/8/34, with the H5 segment modified with a monobasic cleavage site (Δ) (B); and a field isolate of the wild-type highly pathogenic strain A/turkey/Indiana/3707-003/2022 (H5N1) (C). D, E) A/Puerto Rico/8/1934 (H1N1) strain was spiked on pasteurized (D) and unpasteurized (E) milk samples at the times and temperatures shown. Circles indicate individual measurements; error bars indicate 95% CIs. Light gray shaded area indicates $\log_{10}$ $TCID_{50}$ value of 1. NS, not significant; $TCID_{50}$, 50% tissue culture infectious dose.

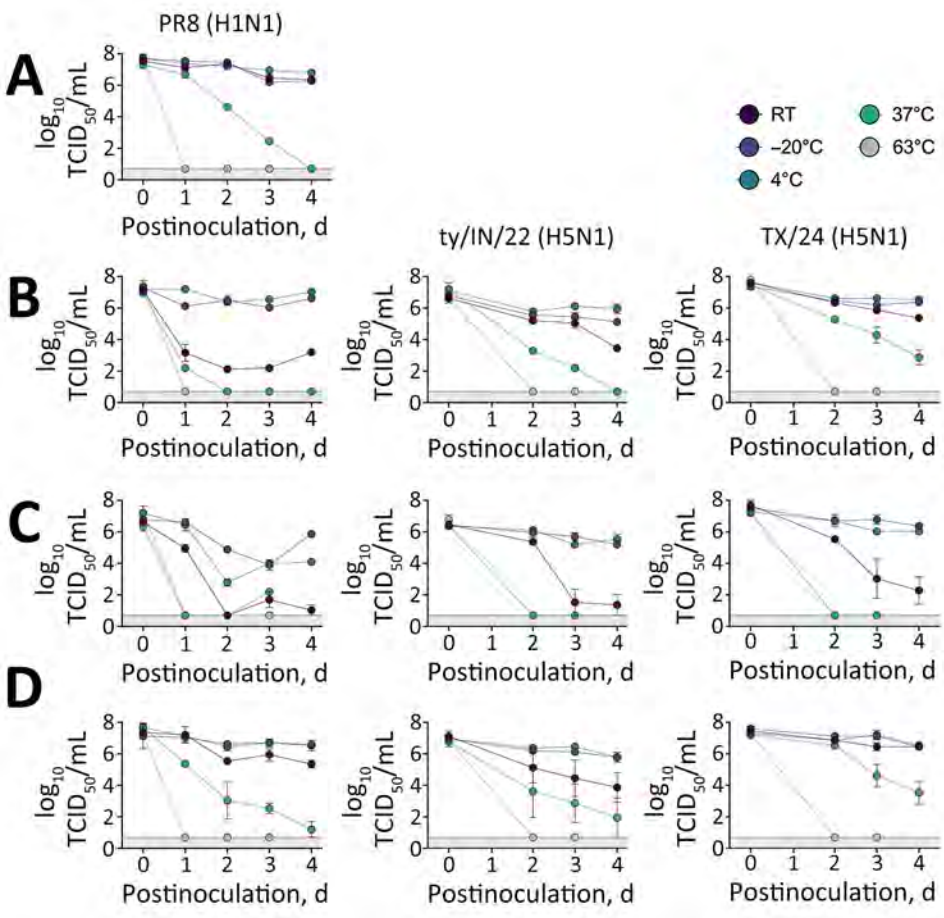

Figure 2. Stability of influenza A in retail and unpasteurized milk. We diluted influenza A viruses in either Opti-Mem control media (Fisher Scientific, https://www.fishersci.com) (A), retail off-the-shelf pasteurized whole milk (B), or 2 different sources of unpasteurized milk: colostrum milk (C) or mature milk (D). We then incubated 200-μL samples for several days at various temperatures, as shown. We subsequently titrated samples by $TCID_{50}$ in MDCK cells. We tested 3 strains: PR8 (H1N1), ty/IN/22 (H5N1), and the reverse genetics version of TX/24 (H5N1). Unpasteurized colostrum milk produced during the first few days after birth contains high levels of immunoglobulins and antimicrobial peptides that might have had an effect in decreasing virus survival. PR8 (H1N1), wild-type strain A/Puerto Rico/8/1934 (H1N1); RT, room temperature; $TCID_{50}$, 50% tissue culture infectious dose; TX/24, wild-type strain A/Texas/37/2024 (H5N1); ty/IN/22, wild-type highly pathogenic strain A/turkey/Indiana/3707-003/2022 (H5N1).

influenza viruses, being enveloped, are generally less stable than the nonenveloped viruses used in previous studies, showcasing this limitation (*7*).

Commercially available milk undergoes pasteurization and homogenization processes. Whereas H5N1 vRNA has been detected in some store-bought milk, the consistent absence of viable virus suggests the pasteurization and homogenization processes might contribute to viral inactivation. Several studies have investigated temperature conditions that mimic HTST pasteurization, with conflicting results. One study (*5*) observed complete virus inactivation only when samples were heated in a PCR machine with the lid on at 105°C but not at 72°C when the lid was replaced with a heat block. That observation aligns with our findings. Another study (*8*) demonstrated complete H5N1 inactivation in spiked milk samples treated under HTST conditions using a thermomixer; however, the timer was initiated only after the samples reached the target temperature (≈58 seconds later), potentially influencing the results. There is compelling evidence of virus inactivation under real-life HTST conditions, suggesting it can effectively lead to complete virus inactivation (*9*). That study estimated that standard US continuous flow HTST parameters would inactivate a significantly higher viral load than typically detected in unpasteurized milk, suggesting the milk supply is likely safe. However, caution is warranted because the industry lacks mandatory testing for H5N1 in milk. Definitively ruling out the presence of live virus might require multiple blind passages in eggs, as is standard procedure in surveillance studies. Our results with the laboratory-adapted PR8 strain are significant in this context, because PR8-spiked milk could serve as an ideal surrogate for testing under commercial pasteurization conditions. Our research, along with understanding factors influencing virus survival in milk, will inform targeted interventions to enhance milk safety and reassure consumers regarding emerging viral threats.

Funding for this work included grants, contracts, and subawards to D.R.P. including National Institute of Food and Agriculture and US Department of Agriculture grant award nos. 2020-67015-31539, 2021-67015-33406, and 2024-67015-42736, and National Institute of Allergy and

Infectious Diseases, National Institutes of Health, grant award nos. R21AI146448 and R01AI154894, contract no. 75N93021C00014, and options 15A, 15B, and 17A. Additional funds were provided to D.R.P. by the Georgia Research Alliance and the Caswell S. Eidson Chair in Poultry Medicine endowment funds.

About the Author

Dr. Caceres is a non–tenure track assistant research scientist at the University of Georgia. His expertise is in RNA viruses, reverse genetics, and animal models of virus disease.

References

1. Ly H. Highly pathogenic avian influenza H5N1 virus infections of dairy cattle and livestock handlers in the United States of America. Virulence. 2024;15:2343931. https://doi.org/10.1080/21505594.2024.2343931
2. Garg S, Reed C, Davis CT, Uyeki TM, Behravesh CB, Kniss K, Budd A, et al. Outbreak of highly pathogenic avian influenza A(H5N1) viruses in US dairy cattle and detection of two human cases—United States, 2024. MMWR Morb Mortal Wkly Rep. 2024;73:501–5.
3. Cohen J, Enserink M. Bird flu appears entrenched in US dairy herds. Science. 2024;384:493–4. https://doi.org/10.1126/science.adq1771
4. US Food and Drug Administration. 2019. Grade A pasteurized milk ordinance [cited 2024 Aug 28]. https://www.fda.gov/food/milk-guidance-documents-regulatory-information/national-conference-interstate-milk-shipments-ncims-model-documents
5. Guan L, Eisfeld AJ, Pattinson D, Gu C, Biswas A, Maemura T, et al. Cow's milk containing avian influenza A(H5N1) virus—heat inactivation and infectivity in mice. N Engl J Med. 2024;391:87–90. https://doi.org/10.1056/NEJMc2405495
6. Reed LJ, Muench H. A simple method of estimating fifty per cent endpoints. Am J Epidemiol. 1938;27:493–7. https://doi.org/10.1093/oxfordjournals.aje.a118408
7. Tomasula PM, Kozempel MF, Konstance RP, Gregg D, Boettcher S, Baxt B, et al. Thermal inactivation of foot-and-mouth disease virus in milk using high-temperature, short-time pasteurization. J Dairy Sci. 2007;90:3202–11. https://doi.org/10.3168/jds.2006-525
8. Kaiser F, Morris DH, Wickenhagen A, Mukesh R, Gallogly S, Yinda KC, et al. Inactivation of avian influenza A(H5N1) virus in raw milk at 63°C and 72°C. N Engl J Med. 2024;391:90–2. https://doi.org/10.1056/NEJMc2405488
9. Spackman E, Anderson N, Walker S, Suarez DL, Jones DR, McCoig A, et al. Inactivation of highly pathogenic avian influenza virus with high temperature short time continuous flow pasteurization and virus detection in bulk milk tanks. J Food Prot. 2024;87:100349. https://doi.org/10.1016/j.jfp.2024.100349
10. World Health Organization, Global Influenza Program, Global Influenza Surveillance and Response System. Manual for the laboratory diagnosis and virological surveillance of influenza: 2011 [cited 2024 May 20]. https://www.who.int/publications/i/item/manual-for-the-laboratory-diagnosis-and-virological-surveillance-of-influenza

Address for correspondence: Daniel R. Perez, University of Georgia Population Health, 953 College Station Rd, Athens, GA 30602, USA; email: dperez1@uga.edu

Prevalence of Pertactin-Deficient *Bordetella pertussis* Isolates, Slovenia

Alex-Mikael Barkoff,[1] Tamara Kastrin,[1] Katja Seme, Marta Grgič Vitek, Jussi Mertsola, Qiushui He

Author affiliations: National Reference Laboratory for Pertussis and Diphtheria, Institute of Biomedicine, University of Turku, Turku, Finland (A.-M. Barkoff, J. Mertsola, Q. He); InFLAMES Research Flagship Center, University of Turku, Turku (A.-M. Barkoff, J. Mertsola, Q. He); National Laboratory of Health, Environment and Food Department for Public Health Microbiology, Ljubljana, Slovenia (T. Kastrin); Institute of Microbiology and Immunology, Faculty of Medicine, University of Ljubljana, Ljubljana (K. Seme); Communicable Diseases Centre, National Institute of Public Health, Ljubljana (M. Grgič Vitek)

DOI: https://doi.org/10.3201/eid3011.231393

In Slovenia, primary acellular pertussis vaccines (ACVs) containing pertactin (PRN) were mostly used during 1999–2016; ACVs without PRN were introduced in 2017. Among 123 *Bordetella pertussis* strains collected during 2002–2020, a total of 48 were PRN-deficient; 44 were collected after 2017. Changes to ACVs could increase PRN-deficient *B. pertussis* and infections.

In Slovenia, whole-cell pertussis vaccine was introduced in 1959 and replaced by acellular pertussis vaccine (ACV) in 1999. ACVs containing pertactin (PRN), a highly immunogenic virulence factor of

[1]These first authors contributed equally to this article.

Bordetella pertussis, were used during 1999–2016, but since 2017, ACVs with and without PRN have been used, excluding during 2011, when only ACV without PRN was used. During 2006–2016, ACVs with and without PRN were used for primary immunization (Table). Since 2009, a booster vaccine including PRN has been given to children 8 years of age, and coverage for primary and booster vaccinations has been high (>90%).

A recent study from Japan showed a decreased frequency of PRN-deficient *B. pertussis* isolates after a change to an ACV without PRN (*1*). Similar observations have been made in Finland (Q. He et al., unpub. data), and partly in Spain (*2*). In Finland, primary vaccination using ACV without PRN was implemented in 2019, and all isolates collected during 2022–2023 were PRN-positive (Q. He et al., unpub. data). Previously, we have shown a high frequency of PRN-deficient *B. pertussis* isolates in Slovenia (*3*); such isolates could evade vaccine-induced immunity. We investigated how the compositional change in the current ACV has affected circulating *B. pertussis* strains.

We studied all 123 *B. pertussis* isolates collected during 2002–2020 in Slovenia, including 27 previously published isolates (*3*). Isolates were collected from different locations; 74 were collected during 2002–2016 and 49 during 2017–2020. Vaccination history was available for 45/49 (91.8%) patients reported during 2017–2020, among whom 31/45 (68.9%) were fully vaccinated. We used a standardized ELISA method with monoclonal antibodies to measure antigen expression of PRN, pertussis toxin (PT), filamentous hemagglutinin (FHA), and fimbriae (Fim) 2 and 3, as described previously (*4*). We used whole-genome sequencing of the *prn* gene to identify mechanisms causing PRN deficiency (*5*). For genotyping, we used PCR-based methods to identify allele specificity of *prn*, *ptxP*, and *ptxA* genes (*6*).

Altogether, 48 (39.0%) isolates did not express PRN. All but 4 isolates collected during 2002–2016 (70/74 [94.6%]) expressed PRN, but 44/49 (91.8%) isolates collected during 2017–2020 did not (Figure). One isolate collected in 2020 did not produce PRN or FHA. All isolates produced PT, and all but

Table. Pertussis vaccines assessed in study of prevalence of pertactin-deficient *Bordetella pertussis* isolates, Slovenia*

	Primary vaccines with PRN				Primary vaccines without PRN		Booster vaccines with PRN	
Year	Infanrix†	Zagreb dTP‡	Infanrix/Hib§	Infanrix/IPV+Hib¶	Pentaxim#	Hexacima**	Boostrix††	Adacel‡‡
1999	X	X						
2000			X	X				
2001	X		X					
2002			X					
2003			X	X				
2004				X				
2005				X				
2006				X	X			
2007				X	X			
2008				X	X			
2009				X	X		X	
2010				X	X		X	
2011					X		X	
2012				X	X		X	
2013				X			X	
2014				X			X	
2015				X			X	
2016				X	X		X	
2017					X		X	
2018					X		X	
2019					X		X	
2020					X	X	X	X
2021						X		X
2022						X		X
2023						X		X

*X indicates year vaccine was in use. Vaccination coverage for the primary series has been 90% higher since 2002; booster dose given at 8 years of age was introduced in 2009, and its coverage has ranged from 90.0% to 96.9% since its introduction. DT, diphtheria toxoid; FHA, filamentous hemagglutinin; FIM, fimbriae; HBsAg, hepatitis B virus surface antigen; Hib, *Hemophilus influenzae* type B; IPV, inactivated polio virus; PRN, pertactin; PT, pertussis toxin; TT, tetanus toxoid.
†GlaxoSmithKline (https://www.gsk.com); formulation PT-FHA-PRN-DT-TT.
‡Institute of Immunology and Tumor Genetics (https://www.info.hazu.hr); pertussis whole-cell vaccine.
§GlaxoSmithKline; formulation PT-FHA-PRN-DT-TT-Hib.
¶GlaxoSmithKline; formulation PT-FHA-PRN-DT-TT-IPV-Hib.
#Sanofi Pasteur (https://www.sanofi.us); formulation PT-FHA-DT-TT-IPV-Hib.
**Sanofi Pasteur; formulation PT-FHA-DT-TT-IPV-Hib-HBsAg.
††GlaxoSmithKline; formulation PT-FHA-PRN-DT-TT.
‡‡Sanofi Pasteur; formulation PT-FHA-PRN-FIM2-FIM3-DT-TT.

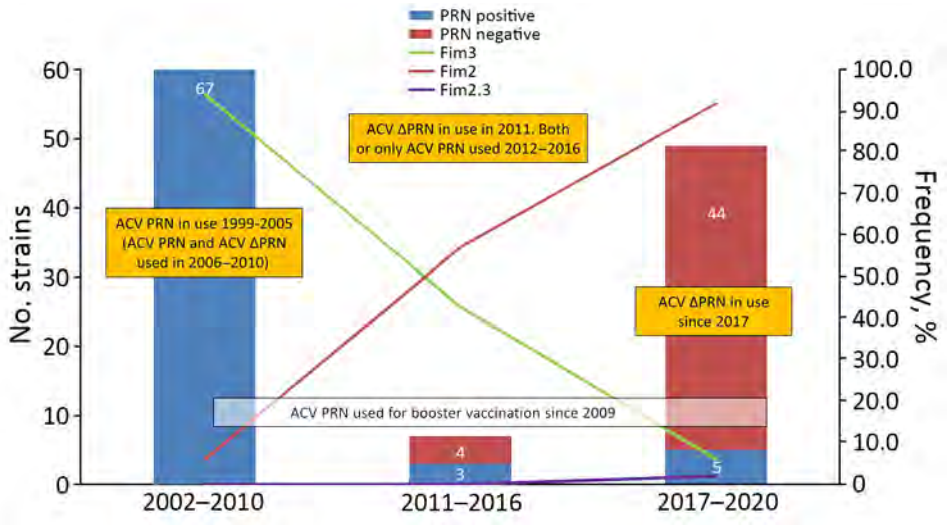

Figure. Number of PRN-deficient isolates and frequency of fimbrial serotypes in a study of pertactin-deficient *Bordetella pertussis* isolates, Slovenia, 2002–2020. Vaccines in yellow boxes are those used for primary vaccination; those in the white box are used for booster vaccination. ACV, acellular pertussis vaccine; ACV PRN, ACV containing pertactin; ACV ΔPRN, ACV without pertactin; Fim, fimbriae; PRN, pertactin.

2 isolates produced FHA. Most (43/48 [89.6%]) PRN-deficient isolates carried the IS*481* insertion within the *prn* gene at positions 1613 (n = 40) or 2735 (n = 3). Among the other 5 isolates, 2 had a 22-kb conversion in the promoter region of *prn* gene, 1 isolate had a large deletion of nucleotides within the *prn* promoter–gene area, and 2 others had single nucleotide deletions, 1 at ΔT 632 and 1 at ΔG 793. The mechanism behind FHA deficiencies remains unknown.

For serotypes, 53/123 (43.1%) isolates harbored Fim2, 69/123 (56.1%) Fim3, and 1/123 (0.8%) Fim2,3. From 2017 onward, 45/49 (91.8%) isolates harbored Fim2, and 66/74 (89.2%) isolates collected during 2002–2016 harbored Fim3 (Figure). Genotyping showed that 122/123 (99.2%) isolates carried *ptxA1*, and 120/123 (97.6%) carried *ptxP3* alleles. For *prn*, *prn2* was dominant 99/123 (80.5%), but *prn*6–8 alleles (23/123, 18.7%) were also notified among the PRN-deficient isolates with an IS*481* insertion. For 1 strain, *prn* was untypable.

Prevalence of PRN-deficient *B. pertussis* isolates remains high in Slovenia, although the current primary vaccines do not contain PRN. That finding differs from findings in Spain, Japan, and Finland (*1*,*2*; Q. He et al., unpub. data), where decline in frequency of PRN-deficient isolates was observed after the change to an ACV without PRN. Although the current vaccination schedule in Slovenia is effective and has high coverage, a 2021 seroprevalence study indicated high circulation of pertussis (*7*), which might affect selection pressure on PRN from natural infection. In addition, since 2009, Slovenia has implemented an additional booster containing PRN in 8-year-old children, which has high vaccination coverage (>90%). That booster could affect the number of PRN-negative strains. In addition, the effect of the frequent changes in vaccines on selection pressure for PRN-deficient isolates cannot be excluded.

We also observed a change in serotype frequency from Fim3 to Fim2 during the study period (Figure). In Slovenia, most ACVs do not contain Fim. Therefore, the change from Fim3 to Fim2 among isolates is likely because of natural selection, which may bias population immunity toward the dominant serotype (*8*). Furthermore, Fim2 strains could express both Fim2 and Fim3 during infection, as described in antibody findings among persons infected by Fim2 *B. pertussis* strains (*9*). Our finding of increasing frequency of both *B. pertussis* PRN-deficiency and Fim2 strains aligns with findings from a study in Spain that suggest a possible link between the 2 characteristics (*2*), which may provide an advantage of the isolates to escape population immunity. Most isolates in this study carried the genotype ptxA1/prn2/ptxP3, which is common in countries using ACVs (*6*).

In conclusion, the unique evading mechanisms of *B. pertussis* against vaccine-induced immunity in Slovenia remain unclear. To maintain optimal vaccination programs to prevent pertussis, Slovenia should continue monitoring circulating *B. pertussis* isolates to inform possible implications for disease incidence and vaccination strategies.

Acknowledgments

We thank Liisa Lund for the excellent laboratory work.

This study is partly supported by Tampere Tuberculosis Foundation (grant no. 26006205), Sigrid Juselius Foundation (grant no. 240045), and EUpertstrain project (project nos. 26004877 and 26004878).

About the Author

Mr. Barkoff is a project researcher at the Institute of Biomedicine, University of Turku, Turku, Finland. His research interests include pertussis vaccine studies in different age groups, *Bordetella pertussis* molecular typing, and surveillance of pertussis in Europe.

References

1. Hiramatsu Y, Miyaji Y, Otsuka N, Arakawa Y, Shibayama K, Kamachi K. Significant decrease in pertactin-deficient *Bordetella pertussis* isolates, Japan. Emerg Infect Dis. 2017;23:699–701. https://doi.org/10.3201/eid2304.161575
2. Mir-Cros A, Moreno-Mingorance A, Martín-Gómez MT, Abad R, Bloise I, Campins M, et al. Pertactin-deficient *Bordetella pertussis* with unusual mechanism of pertactin disruption, Spain, 1986–2018. Emerg Infect Dis. 2022;28:967–76. https://doi.org/10.3201/eid2805.211958
3. Kastrin T, Barkoff AM, Paragi M, Vitek MG, Mertsola J, He Q. High prevalence of currently circulating *Bordetella pertussis* isolates not producing vaccine antigen pertactin in Slovenia. Clin Microbiol Infect. 2019;25:258–60. https://doi.org/10.1016/j.cmi.2018.10.005
4. Barkoff AM, Guiso N, Guillot S, Xing D, Markey K, Berbers G, et al. A rapid ELISA-based method for screening *Bordetella pertussis* strain production of antigens included in current acellular pertussis vaccines. J Immunol Methods. 2014;408:142–8. https://doi.org/10.1016/j.jim.2014.06.001
5. Barkoff AM, Mertsola J, Pierard D, Dalby T, Hoegh SV, Guillot S, et al. Pertactin-deficient *Bordetella pertussis* isolates: evidence of increased circulation in Europe, 1998 to 2015. Euro Surveill. 2019;24:1700832. https://doi.org/10.2807/1560-7917.ES.2019.24.7.1700832
6. Barkoff AM, Mertsola J, Pierard D, Dalby T, Hoegh SV, Guillot S, et al. Surveillance of circulating *Bordetella pertussis* strains in Europe during 1998 to 2015. J Clin Microbiol. 2018;56:e01998-17. https://doi.org/10.1128/JCM.01998-17
7. Berbers G, van Gageldonk P, Kassteele JV, Wiedermann U, Desombere I, Dalby T, et al.; Serosurveillance Study Team. Circulation of pertussis and poor protection against diphtheria among middle-aged adults in 18 European countries. Nat Commun. 2021;12:2871. https://doi.org/10.1038/s41467-021-23114-y
8. Hot D, Antoine R, Renauld-Mongénie G, Caro V, Hennuy B, Levillain E, et al. Differential modulation of *Bordetella pertussis* virulence genes as evidenced by DNA microarray analysis. Mol Genet Genomics. 2003;269:475–86. https://doi.org/10.1007/s00438-003-0851-1
9. Heikkinen E, Xing DK, Olander RM, Hytönen J, Viljanen MK, Mertsola J, et al. *Bordetella pertussis* isolates in Finland: serotype and fimbrial expression. BMC Microbiol. 2008;8:162. https://doi.org/10.1186/1471-2180-8-162

Address for correspondence: Qiushui He, Institute of Biomedicine, University of Turku, Kiinamyllynkatu 10, Turku 20520, Finland; email: qiushui.he@utu.fi

Suspected Acute Pulmonary Coccidioidomycosis in Traveler Returning to Switzerland from Peru

Andreas Neumayr,[1] Volker Rickerts,[1] Sina Ackermann, Felipe Castelblanco, Esther Kuenzli, Ana Durovic,[1] Carlos Seas[1]

Author affiliations: James Cook University, Townsville, Queensland, Australia (A. Neumayr); Swiss Tropical and Public Health Institute, Basel, Switzerland (A. Neumayr, E. Kuenzli, A. Durocic); University of Basel, Basel (A. Neumayr, E. Kuenzli, A. Durocic); Robert Koch Institute, Berlin, Germany (V. Rickerts, S. Ackermann); Institute Art Gender Nature Basel Academy of Art and Design FHNW, Basel (F. Castelblanco); Universidad Peruana Cayetano Heredia, Lima, Peru (C. Seas); Hospital Cayetano Heredia, Lima (C. Seas).

DOI: https://doi.org/10.3201/eid3011.241034

We report a suspected case of acute pulmonary coccidioidomycosis contracted in Peru, where the disease is not known to occur, in a patient from Switzerland. Although not confirmed by direct diagnostic testing, the clinical manifestations and serologic testing results of this case are highly suggestive of coccidioidomycosis.

In November 2022, a 37-year-old man from Switzerland was referred by his general practitioner for further evaluation of an unknown febrile illness with respiratory symptoms. The patient had returned 3 weeks earlier from Peru, where he spent several days touring the southern coastal region, Ica, and Nazca and spent multiple weeks in the southeastern Amazon Basin region of Peru conducting field research in September 2022. The patient experienced an acute febrile illness with headache, myalgia, night sweats, dry cough, and dyspnea beginning 10 days after his return to Switzerland. The patient's general practitioner ruled out malaria and dengue fever and referred him to the Swiss Tropical and Public Health Institute (Basel, Switzerland) when symptoms did not improve over a 2-week period.

The patient's initial physical examination was unremarkable. Laboratory testing revealed an unremarkable complete blood count and creatinine level but found elevated C-reactive protein level of 46 mg/L (reference range ≤5 mg/L), aspartate aminotransferase level of 99 U/L (reference range ≤40 U/L), alanine aminotransferase level of 142 U/L (reference range ≤40 U/L), gamma-glutamyl transferase

[1]These authors contributed equally to this article.

level of 69 U/L (reference range ≤68 U/L), and lactate dehydrogenase level of 305 U/L (reference range ≤225 U/L). Results of blood cultures, HIV screening, interferon-γ release assay, *Histoplama capsulatum* immunodiffusion antibody test, *Cryptococcus* antigen test, *Coxiella burnetii* serologic test, and urine *H. capsulatum* and *Legionella pneumophila* antigen tests were negative. Computed tomography (CT) scan revealed a consolidation (sized 4.4 × 2 cm) in the right lower lung lobe (Figure 1), enlarged lymph nodes in the infracarinal region (3.8 × 2.3 cm), and less-pronounced enlarged lymph nodes (≤1 cm) in the right hilar, hepatic hilar, celiac trunk, and retroperitoneal regions. We repeated the serologic testing 2 weeks later because of the possibility of delayed seroconversion in histoplasmosis cases, but results remained negative.

We suspected an endemic mycosis infection and ordered serologic testing for *Paracoccidioides* and *Coccidioides*, which were positive with a titer of 1:2. We ordered a complement fixation assay for *Coccidioides* that was positive with a titer of 1:16. The pattern of the *Paracoccidioides* band on the immunodiffusion plate appeared to be a nonidentity reaction, suggesting cross reactivity. To confirm the serologic result, we performed a bronchoalveolar lavage (BAL) of the right lower lobe and endobronchial ultrasound-guided transbronchial needle biopsy of the right upper hilar and subcarinal lymph node. We found an elevated CD4/CD8 ratio in the BAL fluid and a lymphocytic cell count with epithelioid cell granulomas in the biopsy samples. Results of all additional testing for fungi were negative.

We initiated treatment with itraconazole under the suspected diagnosis of coccidiomycosis or paracoccidioidomycosis. The patient experienced resolution of symptoms, and laboratory parameters returned to reference limits over the following weeks. We conducted a CT scan and serologic examination 6 months after the initiation of treatment. The CT scan revealed almost complete regression of the lung lesion and the

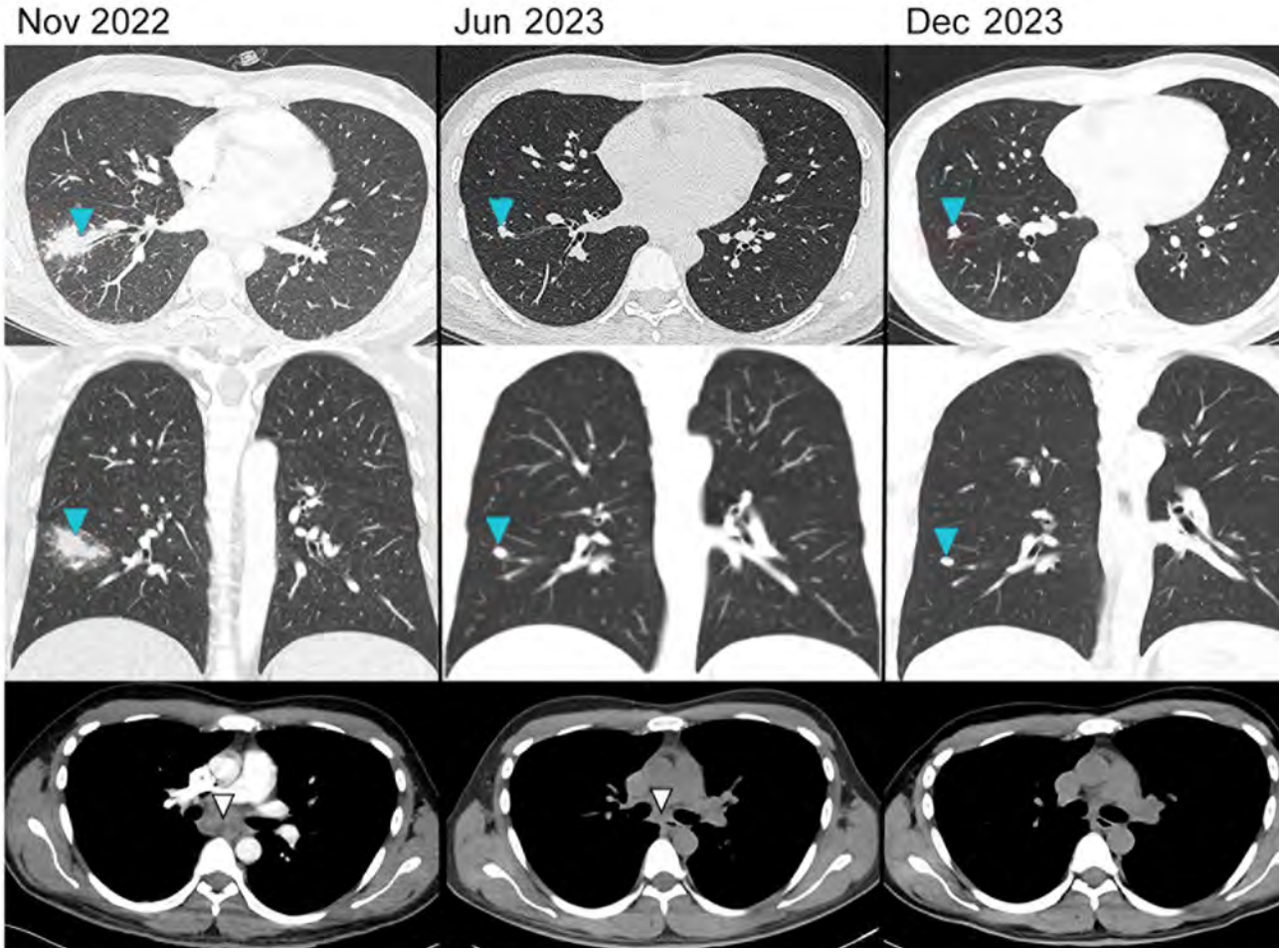

Figure 1. Computed tomography scan findings of a patient with a suspected case of coccidioidomycosis contracted in Peru and the changes in findings seen over 12 months while in treatment in Switzerland, 2022 and 2023. Blue arrows highlight the pulmonary consolidation and regression over time. White arrows highlight the enlarged infracarinal lymphnodes and their regression and normalization over time.

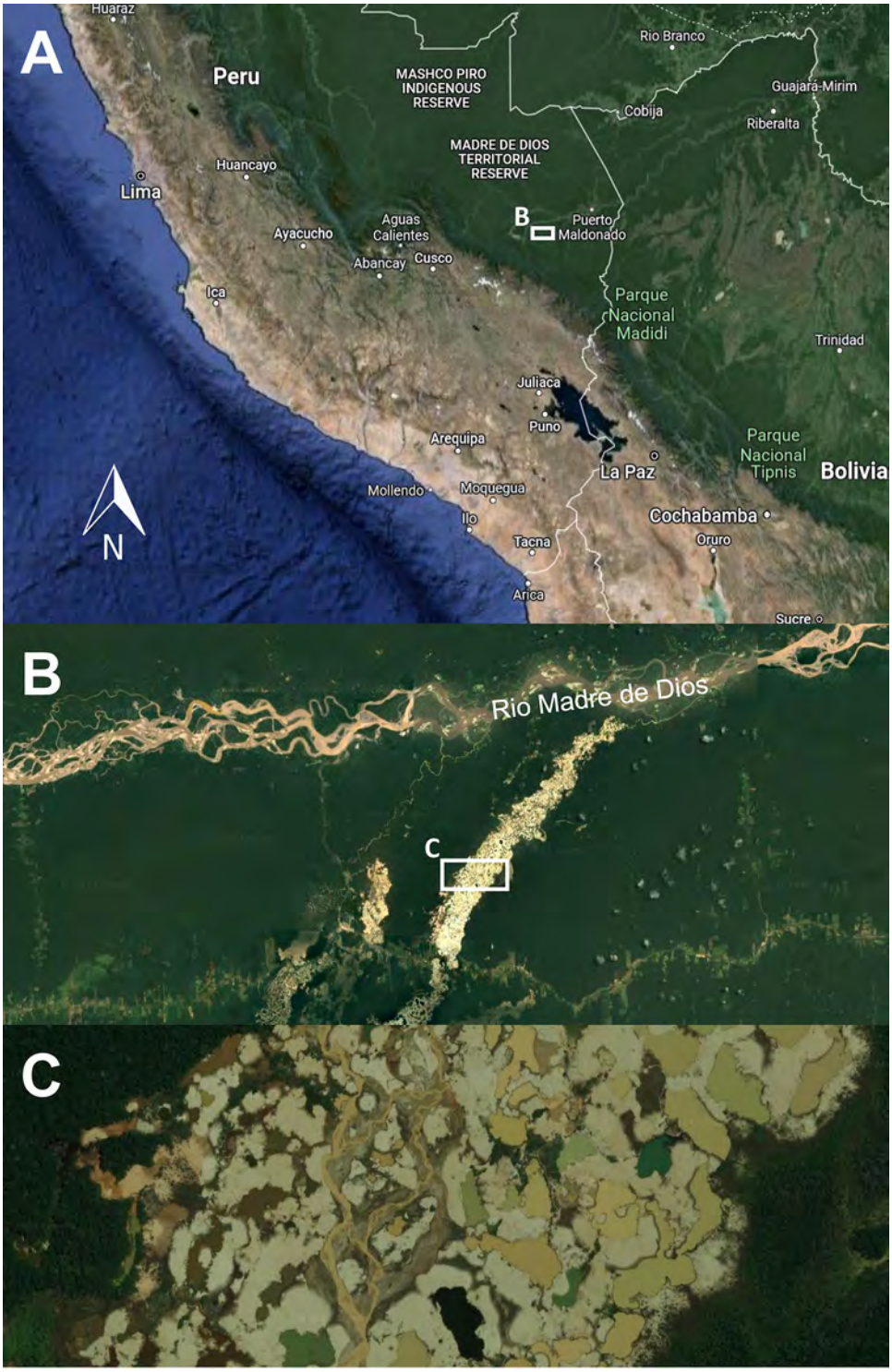

Figure 2. Satellite images of the region in Madre de Dios, Peru, where a patient from Switzerland contracted a suspected case of coccidioidomycosis while conducting field research, 2022. A) Map of southern Peru; B, C) enlargements of the area affected by mining-induced deforestation and desertification, visited by the patient. Images were obtained by using Google Maps (https://maps.google.com).

lymphadenopathies (Figure 1). The *Coccidioides* serologic testing remained positive, but the *Paracoccidioides* serologic testing was negative. The patient tolerated treatment well, and we made the decision to continue itraconazole for 12 months, after which a final CT scan and serologic testing was performed. The CT scan revealed only a nodular parenchymatous scar remained, and all previous lymphadenopathies had completely disappeared (Figure 1). The *Coccidioides* serologic testing revealed seroreversion and negative results after antifungal therapy concluded. We determined the patient likely contracted coccidioidomycosis on the basis of the

clinical manifestations and the serologic results. Coccidioidomycosis is a better fit than paracoccidioidomycosis, and the *Paracoccidioides* serology results are likely because of cross-reactivity between the assays.

Coccidioides is a saprotrophic soil fungus and feeds on decayed organic matter. Humans are infected by inhaling airborne arthroconidia when contaminated soil is disturbed (e.g., dust storms, manmade environmental interventions) (*1*). Most cases are reported from the arid and semiarid desert areas of the southwestern United States, but endemic foci also exist in Latin America (*2*). In Peru, coccidioidomycosis is not known to occur, and the single case reported in 1966 is unproven (*7*). Geospatial climate modeling suggests suitable conditions exist along the coast of Peru (*2*), but because there are no previously reported and confirmed coccidioidomycosis cases, we initially limited the serologic testing to histoplasmosis and paracoccidioidomycosis. The patient conducts his field research in the Madre de Dios region, which is an area experiencing heavy mining-related deforestation and desertification (Figure 2). Coccidioidomycosis might surface as an emerging disease in Peru because of manmade environmental changes, as seen in other regions of Latin America (*1*,*4*). In addition, the emergence of coccidioidomycosis in Washington, USA, in 2013 highlights the pathogen's occurrence in areas previously not considered endemic (*5*–*7*).

We believe this case provides evidence that *Coccidioides* might exist in Peru. Coccidioidomycosis could emerge in arid locations in Peru, and clinicians should actively test for it, especially in cases of suspected histoplasmosis or tuberculosis lacking diagnostic confirmation.

The patient consented to the publication of this case report.

About the Author

Dr. Neumayr heads the Center for Tropical and Travel Medicine at the Swiss Tropical and Public Health Institute in Basel, Switzerland. His interests include clinical tropical medicine, parasitology, and rare infectious diseases.

References

1. Boro R, Iyer PC, Walczak MA. Current landscape of coccidioidomycosis. J Fungi (Basel). 2022;8:413. https://doi.org/10.3390/jof8040413
2. Gorris ME, Ardon-Dryer K, Campuzano A, Castañón-Olivares LR, Gill TE, Greene A, et al. Advocating for coccidioidomycosis to be a reportable disease nationwide in the United States and encouraging disease surveillance across North and South America. J Fungi. 2023;5;9:83.
3. Campins H. Coccidioidomycosis in South America. A review of its epidemiology and geographic distribution. Mycopathol Mycol Appl. 1970;41:25–34. https://doi.org/10.1007/BF02051481
4. Eulálio KD, Kollath DR, Martins LMS, Filho AD, Cavalcanti MDAS, Moreira LM, et al. Epidemiological, clinical, and genomic landscape of coccidioidomycosis in northeastern Brazil. Nat Commun. 2024;15:3190. https://doi.org/10.1038/s41467-024-47388-0
5. Marsden-Haug N, Goldoft M, Ralston C, Limaye AP, Chua J, Hill H, et al. Coccidioidomycosis acquired in Washington state. Clin Infect Dis. 2013;56:847–50. https://doi.org/10.1093/cid/cis1028
6. Marsden-Haug N, Hill H, Litvintseva AP, Engelthaler DM, Driebe EM, Roe CC, et al; Centers for Disease Control and Prevention. *Coccidioides immitis* identified in soil outside of its known range - Washington, 2013. MMWR Morb Mortal Wkly Rep. 2014;23;63:450.
7. Engelthaler DM, Chatters JC, Casadevall A. Was *Coccidioides* a pre-Columbian hitchhiker to southcentral Washington? MBio. 2023;14:e0023223. https://doi.org/10.1128/mbio.00232-23

Address for correspondence: Andreas Neumayr, Swiss Tropical and Public Health Institute, Aeschenplatz 2, 4052 Basel, Switzerland; email: andreas.neumayr@swisstph.ch

Epidemiology of *Streptococcus pyogenes* Disease before, during, and after COVID-19 Pandemic, Germany, 2005–2023

Irene Burckhardt, Florian Burckhardt

Author affiliations: Heidelberg University, Heidelberg, Germany (I. Burckhardt); Baden-Württemberg Ministry of Social Affairs, Health and Integration Baden-Württemberg, Stuttgart, Germany (F. Burckhardt)

DOI: https://doi.org/10.3201/eid3011.231667

We analyzed 3,081 invasive and noninvasive *Streptococcus pyogenes* cases (January 2005–December 2023) at a tertiary care hospital in southwest Germany. Absolute numbers of case-patients increased each year from 2005 until the COVID-19 pandemic. Odds ratios for invasive streptococcal disease were significantly influenced by year, male sex, and older age.

Streptococcus pyogenes (group A *Streptococcus*) infection in humans can cause both benign and severe disease, including death. In addition, immune sequelae are described, and a vaccine does not exist (*1*). Recent reports on *S. pyogenes* infections have ranged from case series to national surveillance, covered periods of weeks to years, focused on invasive disease in children or on all types of infection in all age groups, and focused primarily on Europe (*2*–*10*).

In Germany, *S. pyogenes* infections are nonnotifiable. Strains can be referred for further analysis to the National Reference Centre for Streptococci (Aachen, Germany), but data on population trends are patchy at best. We studied cases of invasive and noninvasive *S. pyogenes* disease occurring during January 1, 2005–December 31, 2023, at University Hospital Heidelberg (Heidelberg, Germany).

We screened the hospital database for all *S. pyogenes* case-patients and designated sample year, sample type, samples collected during the pandemic (cases during 2020–2022), age, and sex. We inferred invasiveness from sample type (Appendix Table 1, https://wwwnc.cdc.gov/EID/article/30/11/23-1667-App1.pdf). Recent studies focused on varying age groups; we designated age categories of 0–5, 6–17, 18–34, 35–49, 50–65, and >65 years. We used linear regression to model numbers of prepandemic invasive and noninvasive cases by year (2005–2019) and tested residuals for lack of autocorrelation using the Breusch-Godfrey test and homoscedasticity using the Breusch-Pagan test. Using those models, we predicted numbers of case-patients during 2020–2023 and calculated differences between predictions and actual numbers. We used multivariable logistic regression (2005–2023) to model odds of invasiveness by year, sex, age group, and occurrence during pandemic. Descriptive and regression analyses were conducted using R version 4 (The R Project for Statistical Computing, https://www.r-project.org).

For the period January 2005–December 2023, we identified 3,081 case-patients. Total numbers per year ranged from 72 in 2021 to 341 in 2023 (Appendix Table 2). We identified 2,853 noninvasive and 228 invasive cases; the lowest number of invasive disease cases was registered in 2005 and the highest in 2023 (2 vs. 36 cases). Ratios between invasive and noninvasive disease were lowest in 2005 (2%) and highest in 2022 (15.8%) (Appendix Table 2).

More case-patients were male (1,745 [57%]) than female (1,333 [43%]); we excluded 3 patients with missing data. Each year, the number of male patients exceeded that of female patients (Appendix Table 3).

Linear regression showed an increase of 6.73 noninvasive and 1.25 invasive cases per year (Figure; Appendix Table 4). Multivariable logistic regression for odds of invasive disease showed an increase of odds ratios [ORs] of 1.08 per year and of 2.14 for male sex. Compared with the reference category of patients 6–17 years of age, patients <6 years of age showed increased ORs of 2.19; 18–34 years, OR 2.74; 35–49 years, OR 5.26; 50–65 years, OR 7.18; and >65 years, 16.73. Infection during the pandemic did not significantly increase odds for invasive disease (Table). Men >65 years of age had the highest OR for invasive disease. An additional logistic regression model with the interaction term age*sex did not improve overall model fit compared with the base model (p = 0.63).

Comparing published data is difficult because age groups studied, proportions calculated, and

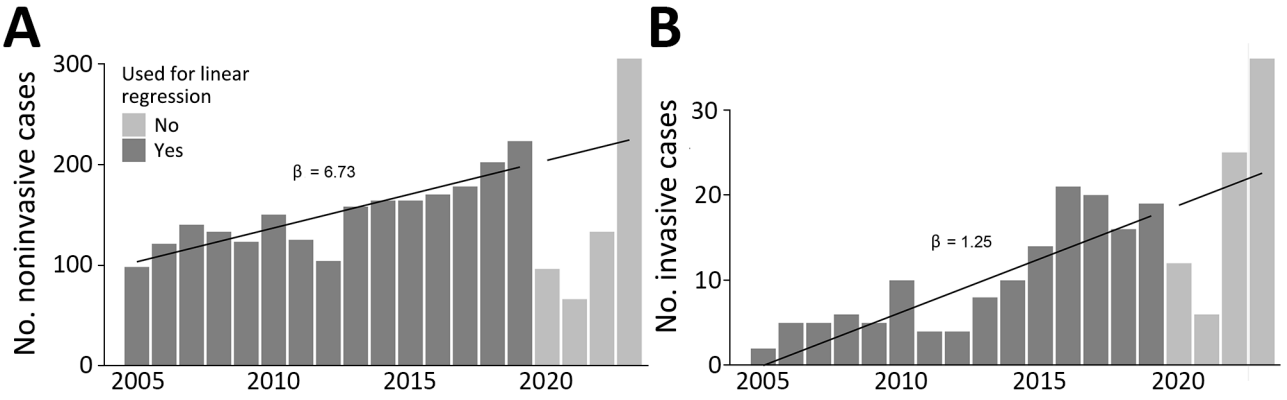

Figure. Number of cases in study of epidemiology of *Streptococcus pyogenes* disease before, during and after COVID-19 pandemic, Germany, 2005–2023. A) Noninvasive cases; B) invasive cases. Values indicate-patients per year; regression line and slope are shown. Dark gray indicates data used for calculation of linear regression (prepandemic); light gray indicates pandemic and postpandemic data, including regression line extrapolated from prepandemic data. β values indicate increases.

Table. Results of logistic regression models for *Streptococcus pyogenes* case-patients, Germany, 2005–2023

Characteristic	Odds ratio (95% CI)	p value
Sex		
F	Referent	
M	2.14 (1.58–2.94)	<0.001
Year	1.08 (1.04–1.11)	<0.001
Age group		
0–5	2.19 (1.11–4.54)	0.028
6–17	Referent	
18–34	2.74 (1.41–5.64)	0.004
35–49	5.26 (2.88–10.42)	<0.001
50–65	7.18 (3.89–14.35)	<0.001
≥66	16.73 (9.02–33.55)	<0.001
Pandemic	1.13 (0.75–1.75)	0.56

time period stratifications vary greatly. One study examining invasive *S. pyogenes* disease in the Netherlands in children <6 years of age found a mean of 6 invasive disease cases in 2016–2019 versus 42 in 2022 (*6*). Lassoued et al. (*3*) studied 135 case-patients <18 years of age with invasive disease in France, stratifying time by nonpharmaceutical interventions (NPIs), and reported stable incidences (cases/1,000 hospital admissions) during 2008–2019 (pre-NPI), a drop during the NPI period, and an increase after April 2021 (post-NPI).

Our study looked at 18 years of data across all ages and disease entities in 1 administrative district in Germany. We found numbers of *S. pyogenes* case-patients have increased since at least 15 years before the pandemic (100 case-patients in 2005 vs. 178 in 2019). Our linear models predicted 19 invasive cases and 204 noninvasive cases for 2020, but only 12 invasive and 96 noninvasive cases were observed. In 2021, predicted versus observed numbers were 20 versus 6 for invasive and 210 versus 66 for noninvasive. In 2022, those numbers were 21 versus 25 for invasive and 217 versus 133 for noninvasive. That finding equates to a mismatch during the pandemic of 60 invasive and 631 noninvasive cases predicted and 43 invasive and 295 noninvasive cases observed, ≈30%–50% less than expected. In 2023, however, our model predicted 22 invasive and 224 noninvasive cases, compared with 36 and 305 observed cases. Unlike previous studies, we calculated odds for invasive disease by year and demonstrated that the increase was unaffected by the pandemic, although total numbers dropped during that time.

We speculate that pandemic NPIs reduced the number of *S. pyogenes* cases. In February 2023, mandatory NPIs ended in this region. The observed increase in numbers of case-patients during 2023 will likely decrease in coming years, and case numbers will revert to prepandemic levels.

About the Authors

Dr. I. Burckhardt is an associate professor for medical microbiology at Heidelberg University, Heidelberg, Germany. Her main interests are the epidemiology of streptococcal disease and the refining of diagnostic procedures in microbiology.

Mr. Burckhardt is an epidemiologist with Baden-Württemberg Ministry of Social Affairs, Health and Integration Baden-Württemberg, Stuttgart, Germany. His main interest is the epidemiology of infectious diseases.

References

1. Brouwer S, Rivera-Hernandez T, Curren BF, Harbison-Price N, De Oliveira DMP, Jespersen MG, et al. Pathogenesis, epidemiology and control of Group A Streptococcus infection. Nat Rev MIcrobiol. 2023;21:431–47. https://doi.org/10.1038/s41579-023-00865-7
2. Johannesen TB, Munkstrup C, Edslev SM, Baig S, Nielsen S, Funk T, et al. Increase in invasive group A streptococcal infections and emergence of novel, rapidly expanding sub-lineage of the virulent *Streptococcus pyogenes* M1 clone, Denmark, 2023. Euro Surveill. 2023;28:2300291. https://doi.org/10.2807/1560-7917.ES.2023.28.26.2300291
3. Lassoued Y, Assad Z, Ouldali N, Caseris M, Mariani P, Birgy A, et al. Unexpected increase in invasive Group A Streptococcal infections in children after respiratory viruses outbreak in France: a 15-year time-series analysis. Open Forum Infect Dis. 2023;10:ofad188. https://doi.org/10.1093/ofid/ofad188
4. MacPhail A, Lee WJI, Kotsanas D, Korman TM, Graham M. A rise in invasive and non-invasive group A streptococcal disease case numbers in Melbourne in late 2022. Med J Aust. 2023;218:378–9. https://doi.org/10.5694/mja2.51909
5. Alcolea-Medina A, Snell LB, Alder C, Charalampous T, Williams TGS, Tan MKI, et al.; Synnovis Microbiology Laboratory Group. The ongoing *Streptococcus pyogenes* (Group A *Streptococcus*) outbreak in London, United Kingdom, in December 2022: a molecular epidemiology study. Clin Microbiol Infect. 2023;29:887–90. https://doi.org/10.1016/j.cmi.2023.03.001
6. de Gier B, Marchal N, de Beer-Schuurman I, Te Wierik M, Hooiveld M, de Melker HE, et al.; ISIS-AR Study Group; GAS Study group; Members of the GAS study group; Members of the ISIS-AR study group. Increase in invasive group A streptococcal (*Streptococcus pyogenes*) infections (iGAS) in young children in the Netherlands, 2022. Euro Surveill. 2023;28:2200941. https://doi.org/10.2807/1560-7917.ES.2023.28.1.2200941
7. de Ceano-Vivas M, Molina Gutierrez MA, Mellado-Sola I, Garcia Sanchez P, Grandioso D, Calvo C, et al. *Streptococcus pyogenes* infections in Spanish children before and after the COVID pandemic. Coming back to the previous incidence. Enferm Infecc Microbiol Clin (Engl Ed). 2024;42:88–92. https://doi.org/10.1016/j.eimce.2023.04.021
8. Holdstock V, Twynam-Perkins J, Bradnock T, Dickson EM, Harvey-Wood K, Kalima P, et al. National case series of group A streptococcus pleural empyema in children: clinical and microbiological features. Lancet Infect Dis. 2023;23:154–6. https://doi.org/10.1016/S1473-3099(23)00008-7
9. Davies PJB, Russell CD, Morgan AR, Taori SK, Lindsay D, Ure R, et al. Increase of severe pulmonary infections in adults

caused by M1$_{UK}$ *Streptococcus pyogenes*, central Scotland, UK. Emerg Infect Dis. 2023;29:1638–42. https://doi.org/10.3201/eid2908.230569
10. Erat T, Parlakay AO, Gulhan B, Konca HK, Yahsi A, Ozen S, et al. Emergency in Group A Streptococcal infections: single center data from Turkey. Pediatr Infect Dis J. 2023;42:e259-e61. https://doi.org/10.1097/INF.0000000000003926

Address for correspondence: Irene Burckhardt, Heidelberg University, Medical Faculty Heidelberg, Department of Infectious Diseases, Medical Microbiology and Hygiene, Im Neuenheimer, Feld 324, 69120 Heidelberg, Germany; email: irene.burckhardt@med.uni-heidelberg.de

Wastewater Surveillance for Norovirus, California, USA

Alexander T. Yu,[1] Elisabeth Burnor,[1] Angela Rabe, Sarah Rutschmann, Marlene K. Wolfe, Jessie Burmester, Chao-Yang Pan, Alice Chen, Hugo Guevara, Christina Morales, Debra A. Wadford, Alexandria B. Boehm, Duc J. Vugia

Author affiliations: California Department of Public Health, Richmond, California, USA (A.T. Yu, E. Burnor, A. Rabe, S. Rutschmann, C.-Y. Pan, A. Chen, H. Guevara, C. Morales, D.A. Wadford, D.J. Vugia); Emory University Rollins School of Public Health, Atlanta, Georgia, USA (M.K. Wolfe); County of San Luis Obispo Public Health Department, San Luis Obispo, California, USA (J. Burmester); Stanford University, Stanford, California, USA (A.B. Boehm)

DOI: https://doi.org/10.3201/eid3011.241001

Norovirus is a leading cause of acute gastroenteritis and imposes a substantial disease burden. In California, USA, norovirus surveillance is limited. We evaluated correlations between wastewater norovirus concentrations and available public health surveillance data. Wastewater surveillance for norovirus genotype GII in California provided timely, localized, and actionable data for public health authorities.

[1]These authors contributed equally to this article.

Norovirus infection causes substantial disease burden, but public health surveillance is limited, and cases are not routinely reported (*1*,*2*). Wastewater surveillance has the potential to provide localized data on norovirus transmission and outbreaks, which may improve public health awareness, communication, and prevention efforts. This study assessed whether wastewater-based norovirus surveillance data correlates with existing norovirus surveillance data and can improve the timeliness and representativeness of norovirus surveillance and inform public health action.

In 2022, the WastewaterSCAN program (https://www.wastewaterscan.org) began monitoring for norovirus genotype GII RNA in wastewater in California, USA, with the California Department of Public Health (CDPH) (*3*,*4*). We collected wastewater data during December 17, 2022–December 17, 2023, from 76 California wastewater utilities, including sites in all 5 California public health officer regions (*4*,*5*). We extracted viral RNA from wastewater settled solids and quantified norovirus concentrations by using digital droplet reverse transcription PCR (*5*). We normalized norovirus wastewater concentrations from individual sewersheds to pepper mild mottle virus (an internal recovery and fecal strength control), population-weighted them, and combined them into 5 California public health officer regional aggregates and a state aggregate (*4*,*5*).

We compared wastewater norovirus data to Centers for Disease Control and Prevention National Respiratory and Enteric Virus Surveillance System (NREVSS) norovirus test positivity at the national and western US regional level and to monthly California Norovirus Laboratory Network (NLN)–confirmed GII norovirus outbreaks. NREVSS receives norovirus test results from outbreaks or sporadic community cases from select participating laboratories (*2*,*6*). We did not analyze California-specific NREVSS test positivity data because of a paucity of data (average total reported monthly specimens <10). NLN tracks laboratory-confirmed norovirus outbreaks (≥2 confirmed, epidemiologically linked cases). We compared 10-day center-aligned moving averages of wastewater aggregates (a wastewater averaging window routinely used at CDPH) to NREVSS test positivity data, which are reported as 21-day center-aligned moving averages. We summed NLN outbreaks over 30 days (because of low numbers of reported outbreaks) and compared them to 30-day averages of wastewater aggregates. We used Kendall rank correlation, a nonparametric test measuring the strength of dependence between 2 variables, for

Table. Kendall correlations between 10-day center-aligned rolling averages of regional wastewater aggregated data and 21-day center-aligned averages of NREVSS test positivity (NREVSS analysis) and 30-day averages of regional wastewater aggregated data and 30-day counts of statewide norovirus outbreaks (NLN outbreak analysis), California, USA, December 17, 2022–December 17, 2023*

	NREVSS analysis			NLN outbreak analysis	
Wastewater region	NREVSS region	Kendall τ	p value	Kendall τ	p value
State	National	0.754	<0.001	0.701	0.002
State	Western region	0.682	<0.001		
Bay Area	National	0.770	<0.001	0.734	0.001
Bay Area	Western region	0.751	<0.001		
Greater Sacramento	National	0.644	<0.001	0.734	0.001
Greater Sacramento	Western region	0.666	<0.001		
Rural Northern California	National	0.464	<0.001	0.571	0.01
Rural Northern California	Western region	0.458	<0.001		
San Joaquin Valley	National	0.487	<0.001	0.603	0.01
San Joaquin Valley	Western region	0.641	<0.001		
Southern California	National	0.654	<0.001	0.603	0.002
Southern California	Western region	0.564	<0.001		

*NLN, California Norovirus Laboratory Network; NREVSS, Centers for Disease Control and Prevention National Respiratory and Enteric Virus Surveillance System.

comparison because it is robust to small samples sizes and skewed data (*7*,*8*). We defined strong correlations as τ values >0.49 (*9*). We performed statistical analyses in R version 4.0.4 (The R Project for Statistical Computing, https://www.r-project.org).

We observed positive, statistically significant (p<0.001), moderate-to-strong correlations between California regional and statewide wastewater aggregates and US national and western regional NREVSS test positivity (median τ value 0.65 [range 0.46–0.77]). We also observed positive, statistically significant (p<0.01), moderate-to-strong correlations between California wastewater aggregates and monthly California norovirus outbreaks (median τ value 0.65 [range 0.57–0.73]) (Table). We observed the lowest correlations for the Rural Northern California region, possibly because that region has the lowest wastewater surveillance population coverage, a largely rural population, and no NREVSS reporting laboratory. The lack of NREVSS reporting laboratories suggests that local norovirus activity may not be represented in western US regional- or national-level surveillance, highlighting the potential value of wastewater surveillance to provide localized information.

Wastewater norovirus data suggested distinct regional and temporal patterns of norovirus activity within California, peaking as early as February 22, 2023, in Southern California and as late as March 24, 2023, in the San Joaquin Valley (Figure). Those regional patterns were not discernable from NLN or NREVSS data. NLN outbreak data suggested that norovirus outbreaks peaked in March 2023 (Appendix Figure, https://wwwnc.cdc.gov/EID/article/30/11/24-1001-App1.pdf), whereas NREVSS test positivity peaked nationally on March 18, 2023, and in the western US region on April 22, 2023 (Figure).

Existing norovirus surveillance is limited and lacks widespread testing and reporting to public health authorities. California surveillance relies on successful outbreak investigations. Weekly California outbreak counts reported by NLN during 2022–2023 were small (median 0 [range 0–8]), which may represent a fraction of the actual number of outbreaks.

Wastewater results are available within 24–48 hours of sample collection and summarized into regular reports distributed to CDPH teams and local health departments (LHDs). In response to sustained wastewater norovirus increases, CDPH has issued California Health Alert Network notifications and Communicable Disease Briefs alerting LHDs of increasing norovirus activity and outbreak potential. Given that no other local California norovirus surveillance data are available, wastewater data have been used as a local and leading indicator to support investigations of gastrointestinal illness outbreaks. Those data have enabled LHDs to more (or less) aggressively pursue investigation and control efforts during gastroenteritis outbreaks, efforts that are time- and resource-intensive for LHDs, the public, and affected establishments. Further statistical analyses exploring lag times between wastewater concentrations and norovirus surveillance data and investigations into how different wastewater data smoothing and aggregation methods affect correlations will provide further insight into interpreting wastewater concentrations.

In conclusion, wastewater norovirus GII data from California during 2022–2023 correlated well with existing public health surveillance data. The wastewater data provided otherwise unavailable situational awareness, enabled timely identification of distinct California regional norovirus trends, and led to direct public health action, including guiding local outbreak investigations.

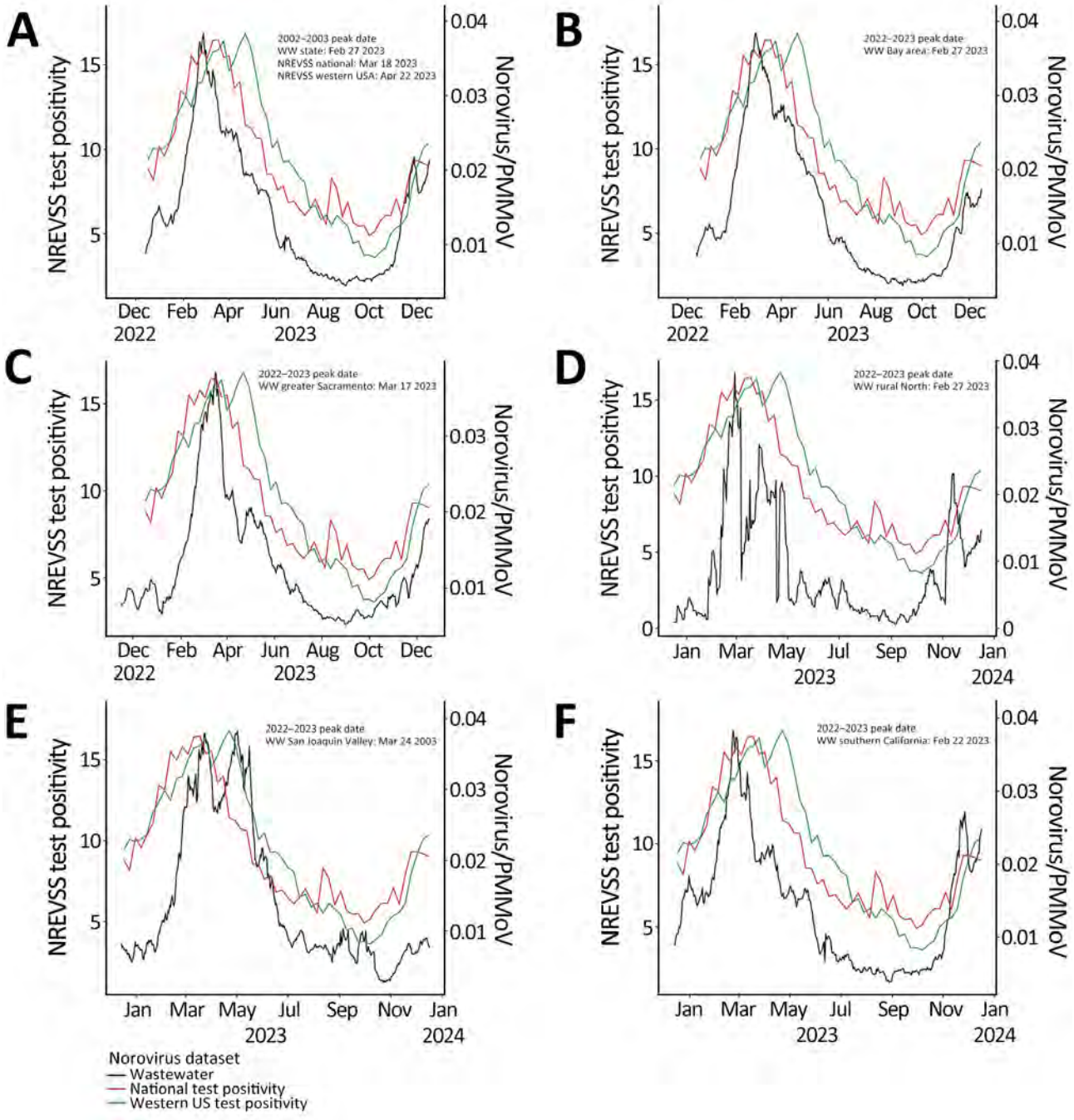

Figure. NREVSS norovirus test positivity (21-day center-aligned moving average) nationally (orange lines) and for the western United States (green lines) and wastewater aggregates (10-day center-aligned moving average) for norovirus, normalized by PMMoV (black lines), California, USA, December 17, 2022–December 17, 2023. A) Statewide; B) Bay Area; C) greater Sacramento; D) rural northern California; E) San Joaquin Valley; F) southern California. NREVSS, Centers for Disease Control and Prevention National Respiratory and Enteric Virus Surveillance System; PMMoV, pepper mild mottle virus; WW, wastewater.

Acknowledgments

We acknowledge and thank the staff of NLN and county public health laboratories in California who perform primary testing for norovirus and submit weekly data to CDPH. We also acknowledge the indispensable effort and extra work of participating wastewater utilities to collect and provide samples for analysis to Verily Life Sciences as part of the WastewaterSCAN project. Further, we thank the laboratory team at the CDPH Viral and Rickettsial Disease Laboratory, including April Hatada, Tasha Padilla, and Chelsea Wright.

This study was supported, in part, by the Epidemiology and Laboratory Capacity for Infectious Diseases Cooperative Agreement (no. 6NU50CK000539-04-02) from the Centers for Disease Control and Prevention and the Sergey Brin Family Foundation.

The findings and conclusions in this article are those of the authors and do not necessarily represent the views or opinions of the California Department of Public Health or the California Health and Human Services Agency.

Address for correspondence: Elisabeth Burnor, California Department of Public Health, 850 Marina Bay Pkwy, Richmond, CA 94804, USA; email: elisabeth.burnor@cdph.ca.gov

About the Author

Dr. Yu is an infectious diseases physician and serves as chief of the Surveillance Section at the California Department of Public Health. Ms. Burnor is an epidemiologist and research scientist on the California Surveillance of Wastewaters Program at the California Department of Public Health.

References

1. Inns T, Harris J, Vivancos R, Iturriza-Gomara M, O'Brien S. Community-based surveillance of norovirus disease: a systematic review. BMC Infect Dis. 2017;17:657. https://doi.org/10.1186/s12879-017-2758-1
2. Centers for Disease Control and Prevention. Norovirus reporting and surveillance. 2024 Apr 24 [cited 2024 May 16]. https://www.cdc.gov/norovirus/php/reporting/index.html
3. Boehm AB, Wolfe MK, Wigginton KR, Bidwell A, White BJ, Hughes B, et al. Human viral nucleic acids concentrations in wastewater solids from Central and Coastal California USA. Sci Data. 2023;10:396. https://doi.org/10.1038/s41597-023-02297-7
4. Boehm AB, Wolfe MK, White BJ, Hughes B, Duong D, Banaei N, et al. Human norovirus (HuNoV) GII RNA in wastewater solids at 145 United States wastewater treatment plants: comparison to positivity rates of clinical specimens and modeled estimates of HuNoV GII shedders. J Expo Sci Environ Epidemiol. 2024;34:440–7. https://doi.org/10.1038/s41370-023-00592-4
5. California Department of Public Health. Public health order questions and answers: hospital and health care system surge. 2021 Oct 1 [cited 2024 May 15]. https://www.cdph.ca.gov/Programs/CID/DCDC/Pages/COVID-19/Order-of-the-State-Public-Health-Officer-Hospital-Health-Care-System-Surge-FAQ.aspx
6. Centers for Disease Control and Prevention. National Respiratory and Enteric Virus Surveillance System interactive dashboard. [cited 2024 May 16]. https://www.cdc.gov/surveillance/nrevss/index.html
7. Field A. Kendall's coefficient of concordance. In: Encyclopedia of Statistics in Behavioral Science. Everitt B, Howell D, editors. Hoboken (New Jersey): Wiley; 2005. p. 1010–11. https://doi.org/10.1002/0470013192.bsa327
8. Arndt S, Turvey C, Andreasen NC. Correlating and predicting psychiatric symptom ratings: Spearman's r versus Kendall's tau correlation. J Psychiatr Res. 1999;33:97–104. https://doi.org/10.1016/S0022-3956(98)90046-2
9. Wicklin R. Weak or strong? How to interpret a Spearman or Kendall correlation. SAS Blogs. 2023 April [cited 2024 Jan 8]. https://blogs.sas.com/content/iml/2023/04/05/interpret-spearman-kendall-corr.html

Environmental *Vibrio cholerae* Strains Harboring Cholera Toxin and *Vibrio* Pathogenicity Island 1, Nigeria, 2008–2015

Sergio Morgado, Akinsinde Adewale, Iwalokun Abiodun, Salako Lawal, Fernanda Freitas, Érica Fonseca, Ana Carolina Vicente

Author affiliations: Instituto Oswaldo Cruz, Rio de Janeiro, Brazil (S. Morgado, F. Freitas, É. Fonseca, A.C. Vicente); Nigerian Institute of Medical Research, Yaba, Nigeria (A. Adewale, I. Abiodun, S. Lawai)

DOI: https://doi.org/10.3201/eid3011.240495

Analysis of clinical and environmental *Vibrio cholerae* O1 strains obtained during 2008–2015 in Nigeria showed that lineages Afr9 and Afr12 carrying cholera toxin and *Vibrio* pathogenicity island 1 can be isolated from water. Our findings raise concerns about the role of the environment in maintenance and emergence of cholera outbreaks in Nigeria.

Nigeria is one of the current cholera hotspots in Africa (*1*). The World Health Organization report on cholera cases in countries in Africa for January 2022–December 2023 showed that most cases in West Africa were in Nigeria (n = 26,452) (*2*).

In 1970, the seventh cholera pandemic in Africa was initiated by the *Vibrio cholerae* O1 El Tor lineage (7PET), which became endemic to many countries in Africa (*3*). The pathogenicity of that lineage is characterized by 2 factors: cholera toxin, encoded by the *ctx*AB operon in the lysogenic bacteriophage CTXΦ, and the toxin coregulated pilus (TCP), encoded on the *Vibrio* pathogenicity island 1 and an essential factor for intestinal colonization and CTXΦ uptake (*4*). Weill et al. reconstructed the spatiotemporal spread of

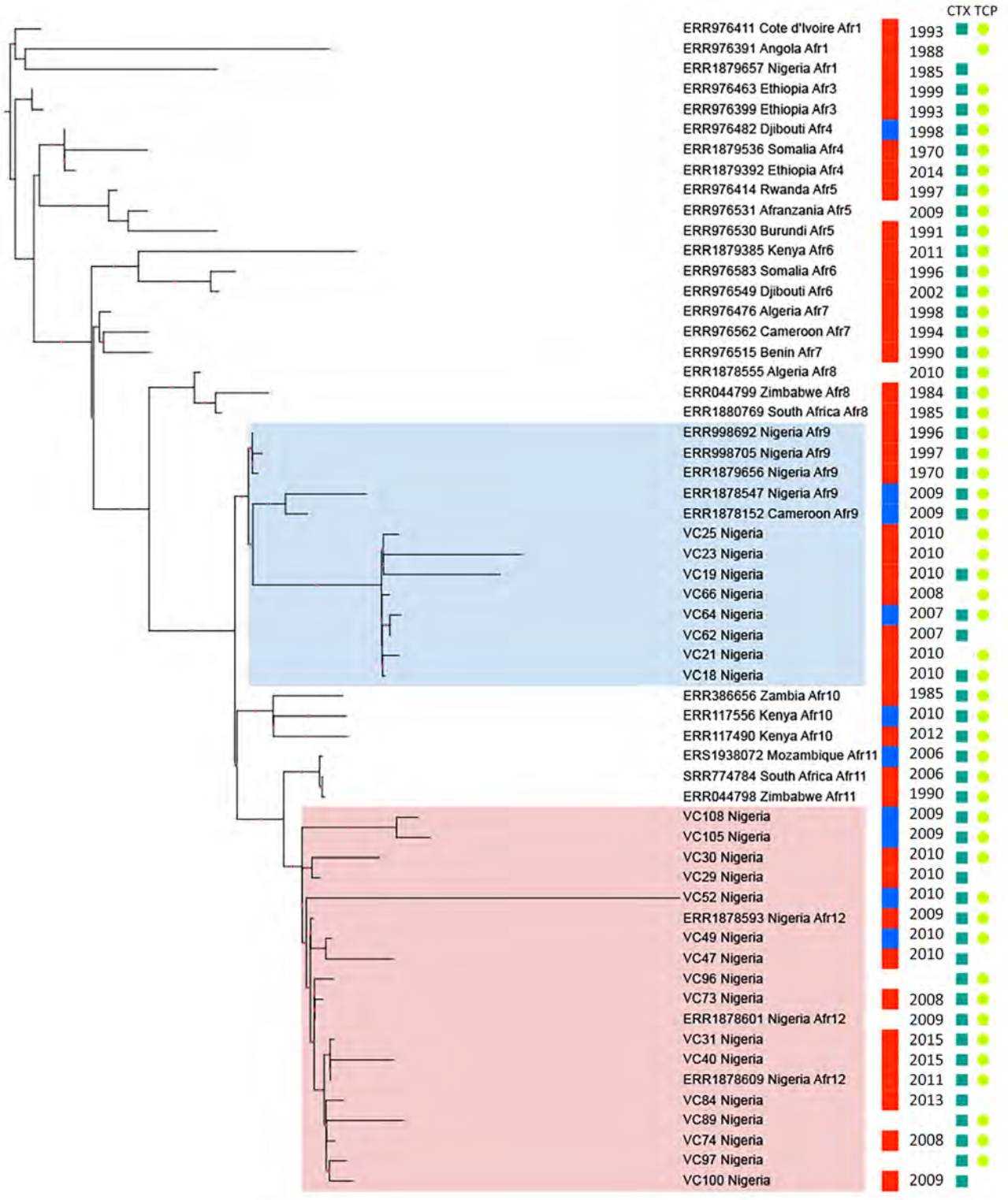

Figure. Maximum-likelihood tree of clinical and environmental *Vibrio cholerae* O1 strains, Nigeria, 2008–2015. The best evolutionary model was Kimura 3-parameter plus ascertainment bias correction plus FreeRate model 2 selected by Bayesian information criterion. The highlighted clusters represent genomes from Afr9 (blue) and Afr12 (pink) lineages. To the right of the genome name is information about source of isolation (red, human; blue, environment), year of isolation, presence of *ctx*AB genes (dark green block), and complete TCP cluster (light green circle). Red dots on branches represent >70% bootstrap values. Available GenBank accession numbers are provided. CTX, cholera toxin; TCP, toxin coregulated pilus.

cholera in Africa during the seventh and current pandemics, showing that the 7PET lineage evolved into ≥13 sublineages and that the Afr9 and Afr12 lineages are the main sublineages causing cholera outbreaks in Nigeria and Cameroon (West Africa) (*3*). As part of efforts to provide information for cholera control, we used conventional microbiology, whole-genome sequencing, comparative genomics, and phylogenetic analysis to characterize clinical and environmental *V. cholerae* O1 strains obtained during the 2008–2015 cholera outbreaks in Nigeria.

We analyzed 24 *V. cholerae* strains comprising isolates from clinical (n = 16), environmental (n = 5), and unknown (n = 3) sources (Appendix, https://wwwnc.cdc.gov/EID/article/30/11/24-0495-App1.xlsx). We used standard culture methods to identify and confirm that all strains were *V. cholerae* serogroup O1. We sequenced the genomes of those strains by using an Illumina Hiseq 2500 (https://www.illumina.com), assembled them with SPAdes v3.15.2 (https://github.com/ablab/spades), and analyzed them with Abricate by using the CARD and VFDB databases (https://github.com/tseemann/abricate). We analyzed the 24 environmental/clinical genomes from our study along with 36 other representative environmental/clinical *V. cholerae* genomes from Africa spanning all Afr sublineages (Afr1–12) of the seventh pandemic (*3*). We subjected genomes to a phylogenomic analysis that used Roary version 3.13.0 (https://github.com/sanger-pathogens/Roary), snp-dist version 2.5.1 (https://github.com/sanger-pathogens/snp-sites), and IQtree version 1.6.12 (https://github.com/Cibiv/IQ-TREE).

On the basis of the *V. cholerae* core genome, we determined that the 24 genomes from our study belonged to the Afr9 or Afr12 sublineages, including the clinical and environmental strains (Figure); those 2 sublineages have been associated with cholera outbreaks in countries in West Africa (*3*). The Afr9 genomes showed the wild-type sequence for GyrA and ParC, and the Afr12 genomes showed the S83I (GyrA) and S85L (ParC) mutations. *V. cholerae* strains from Nigeria had been previously characterized with those mutations, which were associated with resistance to nalidixic acid and decreased susceptibility to ciprofloxacin (*5*). The differences between the resistance profile of the Afr9 and Afr12 strains could be observed in the antimicrobial susceptibility profile (Table). Furthermore, we observed other resistance differences, mainly concerning resistance to streptomycin, sulfonamide, trimethoprim/sulfamethoxazole, and chloramphenicol (Table). By analyzing the resistome of the genomes (Appendix), we identified genes associated with resistance to those antimicrobials: *aph*(3″)-Ib (*str*A) and *aph*(6)-Id (*str*B) (streptomycin), *sul*2 (sulfonamide), *dfr*A1 (trimethoprim/sulfamethoxazole), and *flo*R (chloramphenicol). The genes were located in the integrative and conjugative element STX, which is predominant in genomes of current *V. cholerae* O1 strains, contrasting with 7PET strains from the 1970s (*5*). Of note, VC23, VC62, VC64 (Afr9), and VC105 (Afr12) presented a deletion in the integrative and conjugative element STX region that contained the *str*A/B, *flo*R, and *sul*2 genes, which resulted in differences in the antimicrobial resistance profile between those strains and the others (Table).

Environmental and clinical genomes were related, particularly observed in 2 pairs of genomes: VC64 (Afr9/environmental/2007) and VC62 (Afr9/clinical/2007), and VC49 (Afr12/environmental/2010) and VC47 (Afr9/clinical/2010) (Figure). All Afr9 and Afr12 environmental genomes from Nigeria harbored the 2 major virulence determinants of epidemic *V. cholerae* O1, the *ctx*AB operon, and the TCP cluster, as well as most clinical genomes (Appendix). Those data represent evidence that strains belonging to the Afr9 and Afr12 epidemic lineages could be recovered from the environment in a West Africa country (Nigeria) and would still harbor the main virulence determinants of *V. cholerae*. A study conducted in East Africa (Tanzania) showed that the Afr10e sublineage, associated with a cholera outbreak in that region, could also be isolated from the environment (fish and water) and, as shown here, also harbored the *ctx*AB operon and the TCP cluster (*8*).

Table. Antimicrobial susceptibility profile of environmental and clinical strains of *Vibrio cholerae*, Nigeria*

Strains	Lineage	Source	Isolation date	ICE STX	GEN	STR	NAL	CIP	SUL	SXT	TET	CHL
VC18 VC19 VC21 VC25 VC66	Afr9	Clinical	2008/2010	+	S	R	S	S	R	R	S	S
VC23 VC62	Afr9	Clinical	2007/2010	–	S	I	S	S	S	S	S	S
VC64	Afr9	Water	2007	–	S	I	S	S	S	S	S	S
VC29 VC30 VC31 VC40 VC47 VC73 VC74 VC84 VC100	Afr12	Clinical	2008/2009/20 10/2013/2015	+	S	R	R	S	R	R	S	I
VC105	Afr12	Water	2009	–	S	I	R	S	S	S	S	S
VC49 VC52 VC108	Afr12	Water	2009/2010	+	S	R	R	S	R	R	S	I
VC89 VC96 VC97	Afr12	Unknown	Unknown	+	S	R	R	S	R	R	S	I

*Phenotypic resistance was determined according to Clinical and Laboratory Standards Institute breakpoints (*6*,*7*). CHL, chloramphenicol; CIP, ciprofloxacin; GEN, gentamicin; ICE, integrative and conjugative element; NAL, nalidixic acid; STR, streptomycin; SUL, sulfonamide; SXT, trimethoprim/sulfamethoxazole; TET, tetracycline; +, indicates presence of the region with antimicrobial resistance genes in ICE STX; –, indicates absence of the region with antimicrobial resistance genes in ICE STX.

The global initiative for cholera control aims to reduce cholera deaths by 90% by 2030 (*9*). However, despite adoption of cholera elimination measures by many countries, cholera cases in 2023 demonstrated a huge and alarming resurgence across Africa, including Nigeria. The recent resurgence of cholera in some countries in Africa may be associated with climate change (*10*), but evidence of the presence of cholera-agenic *Vibrio* in the environment reveals the fundamental role of safe drinking water, sanitation, and hygiene in preventing and controlling cholera. Overall, our study highlights the need for continued genomic surveillance considering clinical and environmental *V. cholerae* strains.

The *V. cholerae* whole-genome sequences from this study were deposited in GenBank. Accession numbers are listed in the Appendix.

This study was financed by FAPERJ (Fundação Carlos Chagas Filho de Amparo à Pesquisa do Estado do Rio de Janeiro), Processo SEI-260003/019688/2022.

A.C.V. was responsible for conceptualization, methodology, writing the original draft, review, editing, and funding acquisition. S.M. was responsible for methodology, formal analysis, writing the original draft, writing, review, and editing. É.F. was responsible for writing, review, and editing. F.F. was responsible for investigation. A.A was responsible for conceptualization, methodology, investigation, writing the original draft, and resources. I.A. was responsible for conceptualization, methodology, investigation, and writing the original draft. S.L. was responsible for conceptualization and resources.

About the Author

Mr. Sergio is a postdoctoral fellow in bioinformatics at the Oswaldo Cruz Institute in Rio de Janeiro, Brazil. His primary research comprises genomic surveillance of environmental and clinical bacteria, also exploring their resistome, virulome, and mobilome.

References

1. Charnley GEC, Jean K, Kelman I, Gaythorpe KAM, Murray KA. Association between conflict and cholera in Nigeria and the Democratic Republic of the Congo. Emerg Infect Dis. 2022;28:2472–81. https://doi.org/10.3201/eid2812.212398
2. World Health Organization. Cholera in the WHO African Region: Weekly Regional Cholera Bulletin: 18 December 2023 [cited 2024 Mar 25]. https://iris.who.int/bitstream/handle/10665/375789/AFRO%20Cholera%20Bulletin.43.pdf
3. Weill FX, Domman D, Njamkepo E, Tarr C, Rauzier J, Fawal N, et al. Genomic history of the seventh pandemic of cholera in Africa. Science. 2017;358:785–9. https://doi.org/10.1126/science.aad5901
4. Ramamurthy T, Mutreja A, Weill FX, Das B, Ghosh A, Nair GB. Revisiting the global epidemiology of cholera in conjunction with the genomics of *Vibrio cholerae*. Front Public Health. 2019;7:203. PubMed https://doi.org/10.3389/fpubh.2019.00203
5. Marin MA, Thompson CC, Freitas FS, Fonseca EL, Aboderin AO, Zailani SB, et al. Cholera outbreaks in Nigeria are associated with multidrug resistant atypical El Tor and non-O1/non-O139 *Vibrio cholerae*. PLoS Negl Trop Dis. 2013;7:e2049. https://doi.org/10.1371/journal.pntd.0002049
6. Clinical and Laboratory Standards Institute. Methods for antimicrobial dilution and disk susceptibility testing of infrequently isolated or fastidious bacteria; approved guideline. 3rd ed. Austin (TX); The Institute; 2010.
7. Clinical and Laboratory Standards Institute. Performance standards for antimicrobial susceptibility testing, 26th ed. Supplement M100S. Wayne (PA): The Institute; 2016.
8. Hounmanou YMG, Njamkepo E, Rauzier J, Gallandat K, Jeandron A, Kamwiziku G, et al. Genomic microevolution of *Vibrio cholerae* O1, Lake Tanganyika Basin, Africa. Emerg Infect Dis. 2023;29:149–53. https://doi.org/10.3201/eid2901.220641
9. World Health Organization. Ending cholera: a global roadmap to 2030 [cited 2024 Mar 25]. https://www.gtfcc.org/wp-content/uploads/2019/10/gtfcc-ending-cholera-a-global-roadmap-to-2030.pdf
10. Kaseya J, Dereje N, Tajudeen R, Ngongo AN, Ndembi N, Fallah MP. Climate change and malaria, dengue and cholera outbreaks in Africa: a call for concerted actions. BMJ Glob Health. 2024;9:e015370. https://doi.org/10.1136/bmjgh-2024-015370

Address for correspondence: Sergio Morgado, Instituto Oswaldo Cruz, Av Brasil 4365, Rio de Janeiro 21040-360, Brazil; email: sergio.morgado@ioc.fiocruz.br

Mpox Hepatic and Pulmonary Lesions in HIV/Hepatitis B Virus Co-Infected Patient, France

Ruxandra Calin, Claire Périllaud-Dubois, Stéphane Marot, Khaldoun Kerrou, Gilles Peytavin, Marwa Bachir, Anne Laure Kirch, Ludovic Lassel, Vincent Fallet, Joel Gozlan, Jean Baptiste Pain, Patricia Senet, Olivier Ferraris, Sébastien Bine, Mathieu Hubert, Olivier Schwartz, Laurence Morand-Joubert, Gilles Pialoux

Author affiliations: Sorbonne University Tenon Hospital, Paris, France (R. Calin, K. Kerrou, M. Bachir, A.L. Kirch, L. Lassel, V. Fallet, J.B. Pain, P. Senet, G. Pialoux); Sorbonne University Saint-Antoine Hospital, Paris (C. Périllaud-Dubois, J. Gozlan, L. Morand-Joubert); Sorbonne University Pitié-Salpêtrière Hospital, Paris (S. Marot); Université Paris Cité Bichat Claude Bernard Hospital, Paris (G. Peytavin); Institut de Recherche Biomédicale des Armées National Reference Center for Orthopoxviruses, Brétigny-sur-Orge, France (O. Ferraris); Directorate-General for Health, Paris (S. Bine); Université Paris Cité Institut Pasteur, Paris (M. Hubert, O. Schwartz)

DOI: https://doi.org/10.3201/eid3011.241331

We report a case of persistent disseminated mpox evolving over >6 months in an HIV/hepatitis B virus co-infected patient in France who had <200 CD4+ cells/mm^3, pulmonary and hepatic necrotic lesions, persistent viremia, and nasopharyngeal excretion. Clinical outcome was favorable after 90 days of tecovirimat treatment and administration of human vaccinia immunoglobulins.

By November 2023, the global mpox outbreak that began in May 2022 had resulted in >92,000 cases and 171 deaths across 116 countries (*1*). Among HIV-infected persons, prevalence was high (27%–60%); the most severe and fatal outcomes were observed in those who had advanced infections (*2*,*3*). A new mpox strain in Africa prompted the World Health Organization to declare a global emergency (*4*). Despite ongoing clinical trials, no established guidelines exist for managing severe mpox cases (*3*). We report successful management of persistent disseminated mpox having nodular liver and bilateral lung involvement in an immunosuppressed patient co-infected with HIV and hepatitis B virus (HBV).

A 49-year-old HIV/HBV–co-infected patient who identified as a man who has sex with men was hospitalized in September 2022 for disseminated necrotizing mpox skin and anal lesions. Despite a low HIV-1 virus load (54 copies/mL) under multidrug therapy, his CD4+ cell count was low (82 cells/μL), and HBV virus load was high (8.02 log IU/mL) because of poor tenofovir adherence. A 14-day tecovirimat course (Appendix Figure, https://wwwnc.cdc.gov/EID/article/30/11/24-1331-App1.pdf) improved his skin and anal lesions. However, after discontinuing treatment, new cutaneous nodular lesions appeared, and existing lesions worsened. A computed tomography (CT) scan revealed a 4-cm necrotic mass in the right upper lung lobe, nodules in the opposite lung, and perirectal and nodular liver lesions. Rehospitalized and suspected of having metastatic cancer, he also had ulceronecrotic lesions on his foot, hands, and forearm.

A positron emission tomography/CT scan showed hypermetabolic foci in the skin, rectum, lungs, and liver (Figure, panel A). Liver magnetic resonance imaging (MRI) (Figure, panel B) showed multiple 1–2 cm abscesses across all lobes. Brain MRI and cardiac ultrasound results were unremarkable. The foot lesion sample was positive for monkeypox virus (MPXV) by PCR (cycle threshold 13.47) (Appendix Figure). Anal and skin biopsies revealed massive necrosis; a liver biopsy showed necrotic tissue without tumor cells but had a high MPXV PCR result. Blood and nasopharyngeal swab samples tested positive for MPXV (Appendix Figure). A lung biopsy indicated the presence of pulmonary adenocarcinoma that was positive for MPXV but negative for other pathogens.

We readministered tecovirimat on November 25, 2022, and treated a secondary skin infection. After 1 month, the skin lesions deteriorated; blood and respiratory samples remained MPXV positive. Tecovirimat plasma levels were adequate, and virus sequencing at different time points revealed no resistance-associated mutations (i.e., *F13L* gene). We administered 2 doses of 6,000 IU/kg vaccinia immune globulin intravenous (VIGIV), which led to gradual improvement, although blood remained MPXV positive for 5 weeks. We continued tecovirimat treatment for 90 days.

We measured humoral responses to MPXV by using serologic and seroneutralization assays (Table) (*5*). Neutralizing antibody (NAb) titers in serum samples without added complement decreased when lesions reappeared but increased substantially after the first VIGIV injection. Nab titers in serum samples with added complement remained consistently high. Follow-up positron emission tomography/CT scan and MRI showed reduced lung and liver lesions (Figure, panels C, D). On February 7, 2023, we performed a right lobectomy and removed a 0.7-cm adenocarcinoma in a 2.5-cm necrotic mass; lymph nodes had no metastatic cells. By March 20, the hepatic lesions

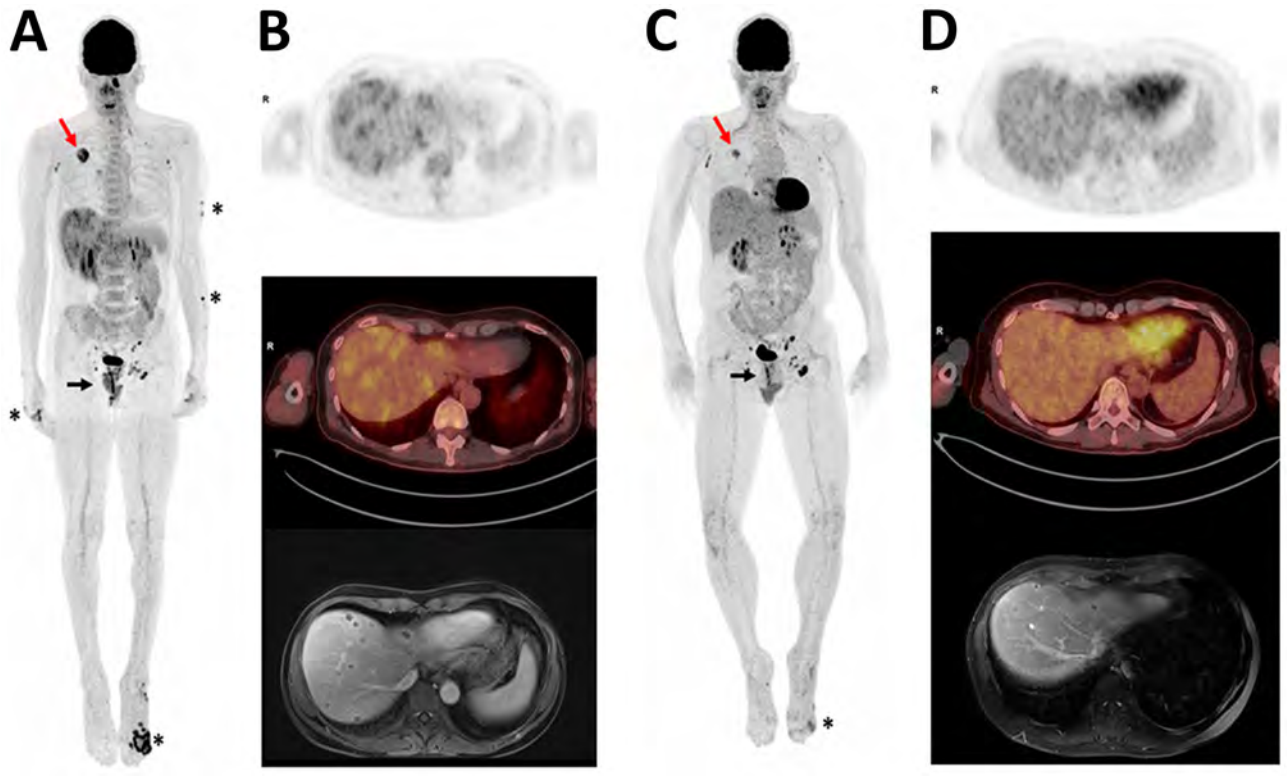

Figure. Positron emission tomography/computed tomography (PET/CT) scans and magnetic resonance imaging (MRI) of HIV/hepatitis B virus co-infected patient in case study of mpox hepatic and pulmonary lesions, France. A) Whole-body ^{18}F-fluorodeoxyglucose (^{18}F-FDG) PET/CT 3-dimensional maximum intensity projection performed in December 2022. Asterisks indicate anterior view of skin lesions. Black arrow indicates lesions in lower rectum; maximum standard uptake value (SUVmax) = 7. Red arrow indicates tumor in upper right lung; SUVmax = 6.4. Heterogeneous hepatic metabolism and multiple small foci of uptake were observed on liver transaxial views, which showed more intense metabolic ranges in the subcapsular region (SUVmax = 3.6). A hypermetabolic contralateral apical pulmonary nodule (SUVmax = 2.7) was also observed but is not visible in this image. B) Upper image shows liver transaxial ^{18}F-FDG PET, middle image is fused PET/CT, and lower image is liver MRI (axial liver acceleration volume acquisition). C) Follow-up whole-body ^{18}F-FDG PET/CT 3-dimensional maximum intensity projection performed in January 2023. Anterior view indicates substantial decreases in metabolic uptake intensities in foot lesion (asterisk), rectum (black arrow), and right lung tumor (red arrow). Tumor was 36 mm versus 46 mm in December, SUVmax 3.9 versus 6.4. Decrease in left apical pulmonary nodule, 9 mm versus 11 mm, SUVmax 1.3 versus 2.7; nodule was not visible in this image. D) Follow-up images indicate substantial decrease of liver abscesses. Upper image shows liver transaxial ^{18}F-FDG PET, middle image is fused PET/CT, and lower image is liver MRI (axial T1 fat suppression volumetric interpolated breath-hold examination portal).

regressed, and the patient fully recovered, with no relapse as of November 2023.

MPXV can persist in HIV patients, causing prolonged lesions that might be fatal (*6*). However, disease persistence for >6 months is rare. Relapse after initial tecovirimat treatment is also uncommon; immune reconstitution inflammatory syndrome was considered, but it was unlikely because of the

Table. MPXV antibody titers in case study of mpox hepatic and pulmonary lesions in HIV/hepatitis B virus co-infected patient, France*

Date	No. days after mpox diagnosis	MPXV E8L IgG titer,† AU/mL	MPXV NAb titer without complement‡	MPXV NAb titer with complement‡
2022 Sep 21	35	186	160	1,280
2022 Oct 17	61	>400	0	1,280
2022 Nov 16	91	>400	40	2,560
2023 Jan 6	142	>400	1,280	2,560
2023 Jan 10	146	>400	640	2,560
2023 Feb 14	181	>400	320	2,560

*AU, arbitrary unit; MPXV, monkeypox virus; NAb, neutralizing antibody.
†IgG against MPXV E8L protein was measured by using the Monkeypox Virus E8L Protein Human IgG ELISA Kit (RayBiotech, https://www.raybiotech.com). All serum samples were positive and reached the upper limit of detection (400 AU/mL) by 2 months after mpox diagnosis.
‡MPXV neutralizing antibody titers were determined in serum samples with or without added complement, as previously described (*5*). Nab titers decreased in serum samples without added complement when new skins lesions appeared and older lesions deteriorated; NAbs only increased after the first injection of vaccinia immune globulins. However, Nab titers were higher when complement was added to the assay and did not decrease; we did not see an increase after the first or second vaccinia immune globulins injections. Upper limit of MPXV neutralization titer was 1:2,560.

patient's low virus load. A longer initial tecovirimat treatment course might have been beneficial (*7*,*8*). Disseminated MPXV with lung, gastrointestinal, and neurologic involvement in HIV patients has been documented (*2*,*3*,*9*), but liver nodules were unexpected. Although initial radiologic description suggested tumor lesions, biopsies confirmed MPXV was present without cancer cells. The lung adenocarcinoma, an incidental finding, was surgically managed, and the tumor tested positive for MPXV.

Tecovirimat effectiveness was limited, despite adequate plasma levels. Tecovirimat is generally considered safe, but its efficacy in treating mpox remains uncertain (*3*,*10*). Drug resistance was a concern because of the patient's prolonged immunosuppression and MPXV replication, but virus sequencing revealed no resistance-associated mutations. Thus, we continued tecovirimat treatment for the maximum US Food and Drug Administration–approved duration of 90 days without adverse effects.

We administered VIGIV at day 31 of tecovirimat treatment, leading to gradual lesion improvement. Although lesions healed, blood was MPXV positive for 5 weeks. Nab titers (without complement) decreased before the second hospitalization, potentially reflecting clinical disease progression. The first VIGIV injection considerably increased NAb titers, but they quickly declined, suggesting that measuring Nab titers without adding complement to the serum sample might have more clinical relevance.

In conclusion, disseminated MPXV in HIV patients with low CD4 counts can cause prolonged, severe, and potentially fatal outcomes. This case highlights the need to monitor tecovirimat concentrations and resistance mutations and underscores the potential critical role of VIGIV treatment in severe mpox cases. As mpox continues to spread, atypical manifestations and severe forms need to be acknowledged and managed, especially in at-risk patients.

The patient provided written informed consent.

About the Author

Dr. Calin is an infectious diseases specialist based in Paris, France. Her research interests focus on management of infectious complications in immunosuppressed patients, especially in the field of HIV.

References

1. World Health Organization. Multi-country outbreak of mpox: external situation report 31. December 22, 2023 [cited 2024 May 23]. https://www.who.int/docs/default-source/coronaviruse/situation-reports/20231222_mpox_external-sitrep_31.pdf
2. Mitjà O, Alemany A, Marks M, Lezama Mora JI, Rodríguez-Aldama JC, Torres Silva MS, et al.; SHARE-NET writing group. Mpox in people with advanced HIV infection: a global case series. Lancet. 2023;401:939–49. https://doi.org/10.1016/S0140-6736(23)00273-8
3. Shishido AA, Street S. Optimal management of severe mpox in patients with uncontrolled human immunodeficiency virus. J Med Virol. 2023;95:e29277. https://doi.org/10.1002/jmv.29277
4. Harris E. As mpox cases surge in Africa, WHO declares a global emergency—here's what to know. JAMA. 2024;332:862–4. PubMed https://doi.org/10.1001/jama.2024.17797
5. Hubert M, Guivel-Benhassine F, Bruel T, Porrot F, Planas D, Vanhomwegen J, et al. Complement-dependent mpox-virus-neutralizing antibodies in infected and vaccinated individuals. Cell Host Microbe. 2023;31:937–48.e4. https://doi.org/10.1016/j.chom.2023.05.001
6. Triana-González S, Román-López C, Mauss S, Cano-Díaz AL, Mata-Marín JA, Pérez-Barragán E, et al. Risk factors for mortality and clinical presentation of monkeypox. AIDS. 2023;37:1979–85. https://doi.org/10.1097/QAD.0000000000003623
7. Martinez AE, Frattaroli P, Vu CA, Paniagua L, Mintz J, Bravo-Gonzalez A, et al. Successful outcome after treatment with cidofovir, vaccinia, and extended course of tecovirimat in a newly-diagnosed HIV patient with severe mpox: a case report. Vaccines (Basel). 2023;11:650. https://doi.org/10.3390/vaccines11030650
8. Miller MJ, Cash-Goldwasser S, Marx GE, Schrodt CA, Kimball A, Padgett K, et al.; CDC Severe Monkeypox Investigations Team. Severe monkeypox in hospitalized patients—United States, August 10–October 10, 2022. MMWR Morb Mortal Wkly Rep. 2022;71:1412–7. https://doi.org/10.15585/mmwr.mm7144e1
9. Simadibrata DM, Lesmana E, Pratama MIA, Annisa NG, Thenedi K, Simadibrata M. Gastrointestinal symptoms of monkeypox infection: a systematic review and meta-analysis. J Med Virol. 2023;95:e28709. https://doi.org/10.1002/jmv.28709
10. Grosenbach DW, Honeychurch K, Rose EA, Chinsangaram J, Frimm A, Maiti B, et al. Oral tecovirimat for the treatment of smallpox. N Engl J Med. 2018;379:44–53. https://doi.org/10.1056/NEJMoa1705688

Address for correspondence: Ruxandra Calin, Infectious Diseases Department, Tenon Hospital, AP-HP, Sorbonne University, INSERM 1135, 4 rue de la Chine 75020, Paris, France; email: ruxandra.calin@aphp.fr

Iquitos Virus in Traveler Returning to the United States from Ecuador

Katherine Baer,[1] Itika Arora,[1] Jayden Kimbro, Ali Haider, Michelle Mott, Kyleigh Marshall, Henry M. Wu, Jessica Fairley, Anne Piantadosi, David R. Myers, Jesse J. Waggoner

Author affiliations: Emory TravelWell Center, Atlanta, Georgia, USA (K. Baer); Emory University School of Medicine, Atlanta (K. Baer, I. Arora, J. Kimbro, A. Haider, M. Mott, H.M. Wu, J. Fairley, A. Piantadosi, J.J. Waggoner); Emory University Rollins School of Public Health, Atlanta (K. Marshall, J. Fairley, J.J. Waggoner); Emory University, Atlanta (D.R. Myers); Georgia Institute of Technology, Atlanta (D.R. Myers); American and Asian Centers for Arboviral Research and Enhanced Surveillance, Atlanta (J.J. Waggoner)

DOI: https://doi.org/10.3201/eid3011.240708

We describe the case of a returned traveler to the United States from Ecuador who had an acute febrile illness, initially diagnosed as Oropouche fever. This illness was later confirmed to be a rare infection with Iquitos virus, a related bunyavirus that shares 2 of 3 genome segments with Oropouche virus.

Oropouche virus (OROV) is a species in the Simbu serogroup of bunyaviruses (genus *Orthobunyavirus*) that includes the reassortant species Iquitos virus (IQTV) and Madre de Dios virus. The species share common small and large genome segments but differ in the medium segment (*1*,*2*). Symptomatic human infections with the viruses typically manifest with nonspecific signs and symptoms (e.g., fever, headache, myalgias, and arthralgias) that cannot be clinically differentiated from other common tropical febrile illnesses such as dengue, malaria, and leptospirosis (*2*–*4*).

In 2024, a large OROV outbreak has affected countries of the Amazon River Basin, with cases occurring in Brazil, Peru, Colombia, and Bolivia (*5*). However, despite previous detection of OROV transmission in Ecuador in 2016–2017 (*3*), cases have not been reported to the Pan American Health Organization from Ecuador in 2024 (*5*).

In early April 2024, a 38-year-old man with no notable medical history visited a healthcare system in Atlanta, Georgia, USA, with an acute febrile illness after returning from Ecuador. During a 10-day itinerary, he visited the capital city of Quito, Esmeraldas Province in the northwest, and Napo Province in the Amazon Basin (Figure 1), where he noted numerous bug bites. The patient did not take malaria prophylaxis but consistently used a DEET-containing insect repellant during the trip. He had 1 day of diarrhea on his last day in Ecuador; then, 2 days after returning to the United States, he had fevers reaching 102°F and chills, sweats, headache, and pain with eye movement. He was seen in an emergency department and was found to have a slight elevation in his creatinine (1.3 mg/dL [reference range 0.6-1.2 mg/dL]) but otherwise normal complete metabolic panel and complete blood count results. He was discharged home with an outpatient referral to the Emory TravelWell Center (also in Atlanta) the following day.

During that visit, he reported fatigue, sleeping 12–14 hours a day, and numerous itchy "bug bites" on his arms and ankles. Examination revealed he had unremarkable vital signs and a diffuse papular rash across his forearms and lower legs. The patient's illness was reported in the GeoSentinel database (*6*), and he consented to the collection and testing of EDTA whole blood and serum as part of a research study into the causes of infection in returned travelers. At a follow-up visit the next week, he reported that the fever had resolved after 2 days and that the headache and fatigue resolved over 10 days. The rash initially evolved to hyperpigmented plaques

Figure 1. Provinces of Ecuador (light blue), including areas visited by a traveler from the United States who was infected with Iquitos virus (medium and dark blue); the provinces of Esmeraldas and Napo (dark blue) highlighted as areas of highest concern for contracting the virus. Surrounding provinces with confirmed Oropouche virus infection cases in Brazil, Colombia, Peru, and Bolivia are shown; shading indicates the number of reported cases, based on data from the Pan American Health Organization (*5*).

[1]These first authors contributed equally to this article.

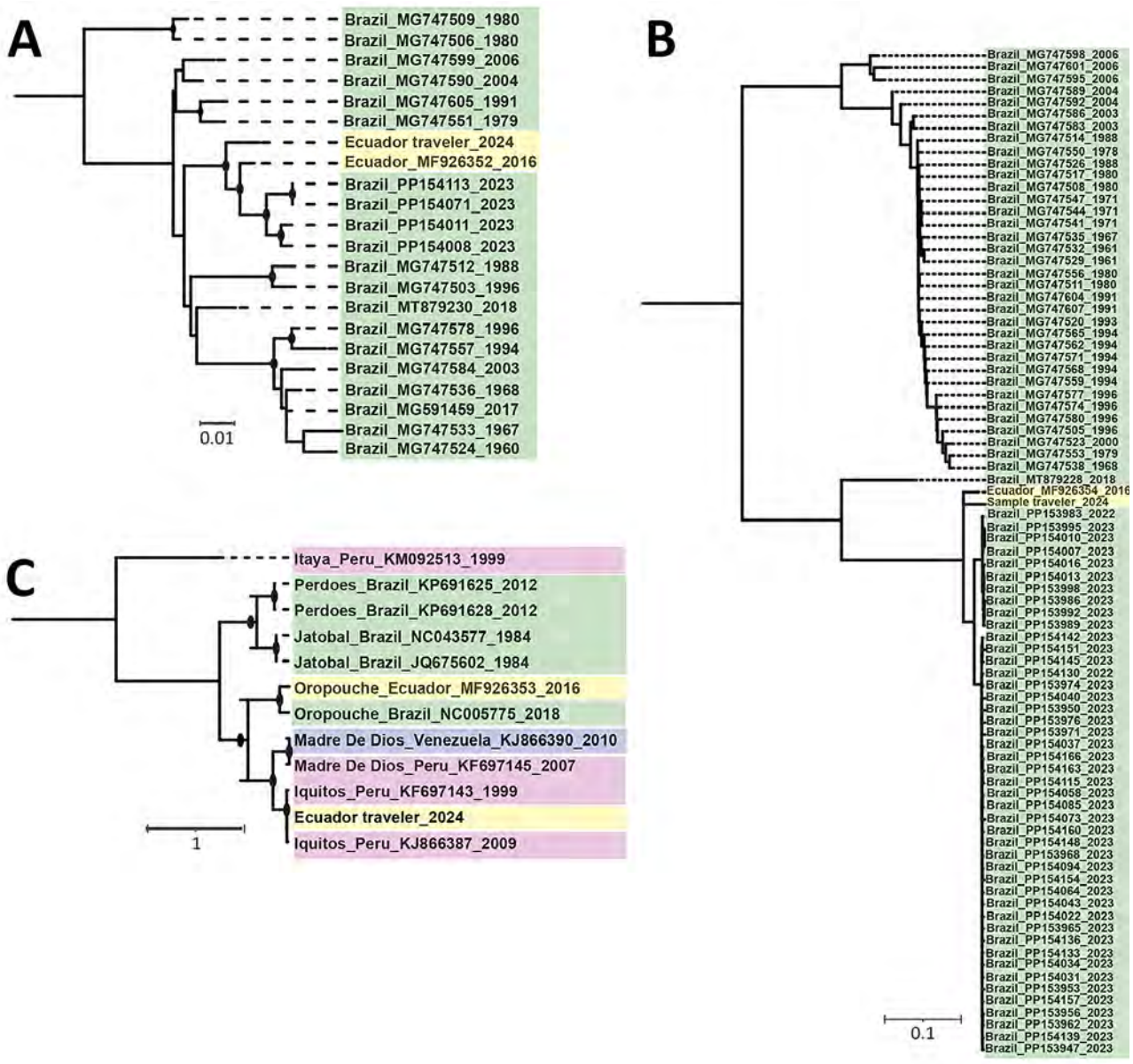

Figure 2. Maximum-likelihood phylogenetic analyses of the small segment (A), large segment (B), and medium segment (C) of Iquitos virus from a traveler returning to the United States from Ecuador. Sequences from the study have been deposited into GenBank (accession nos. PQ325301–4); reference sequences were obtained from National Center for Biotechnology Information Virus database. Panels A and B contain all available complete Oropouche small and large virus sequences, after removing identical sequences; panel C contains all available complete medium sequences for Iquitos, Oropouche, Itaya, Jatobal, Madre de Dios, and Perdoes viruses. Nodes with black circles have ultrafast bootstrap values ≥90. Sequence names are color-coded according to country of origin. Nucleotide substitution models were as follows: small segment, transversion model with empirical base frequencies and a gamma distribution of rates with 4 categories and α = 0.081; medium segment; transition model with empirical base frequencies and a gamma distribution of rates with 4 categories and α = 5.156; and large segment: general time-reversible model with empirical base frequencies, allowing for invariant sites and a gamma distribution of rates with 2 categories and α = 0.125. Scale bars indicate number of nucleotide substitutions per site.

and then resolved with topical hydrocortisone and diphenhydramine.

We processed whole blood and serum with a laboratory-developed nucleic acid extraction and storage protocol (i.e., the RNA extraction and storage [RNAES] protocol) (*7*). All eluates were negative for Zika, chikungunya, and dengue viruses on a laboratory-developed assay and negative for *Leptospira* and *Plasmodium* species (*8*). Eluates from serum and whole blood tested positive

in a laboratory-developed real-time reverse transcription PCR (RT-PCR) that targets the small genome segment of OROV and related bunyaviruses (Appendix Figure, panel A, https://wwwnc.cdc.gov/EID/article/30/11/24-0708-App1.pdf) (*4*). We confirmed this finding by reextraction and retesting of an aliquot of whole blood using a second real-time RT-PCR targeting a different portion of the small genome segment (Appendix Figure, panel B) (*9*).

We successfully generated partial sequences for the coding regions of the small (83%), medium (27%), and large (37%) segments (GenBank accession nos. PQ325301–4) (Appendix). Phylogenetic analysis indicated that the small and large segments from the returned traveler were most closely related to an Oropouche virus sample obtained in Ecuador in 2016, and they clustered just basal to sequences from samples obtained from Brazil in 2023 (Figure 2, panel A, B). However, phylogenetic analysis of the medium segment confirmed that it was most closely related to IQTV, the only other available sequences of which were from Peru (Figure 2, panel C).

Fever in a returned traveler can result from myriad etiologies that may be unfamiliar to providers in nonendemic areas and for which diagnostic testing is often limited (*6*). For the case we describe, systematic screening tools and economical laboratory solutions enabled the initial detection of OROV or a related bunyavirus, which has important implications for clinical management, given that meningitis and relapsing disease have been reported in OROV infection (*2*). However, further characterization by next-generation sequencing identified this virus as IQTV, a related bunyavirus that also circulates in the Amazon Basin and may have contributed to reassortment events that led to current OROV genetic diversity in South America (*10*). IQTV reportedly causes a clinical illness similar to Oropouche fever; of note, however, infection with OROV does not appear to protect against future IQTV infection (*1*). Finally, this case provides support for increased bunyavirus monitoring in Ecuador (*3*), where these viruses may have gone undetected or underreported because of limited diagnostics, poor healthcare access, sociopolitical instability, or a combination of those factors.

Acknowledgments

We appreciate the patient's willingness to participate in this study and the technical and clinical staff who made this possible.

New sequences generated for this study have been uploaded into GenBank and have the following accession numbers: small segment, PQ325301; medium segment, PQ325302 and PQ325303; large segment, PQ325304.

This work was supported by the Georgia Research Alliance (grant no. GRA.VL24.C4), a pilot project grant from the International Society of Travel Medicine, the National Institutes of Health's National Institute of Allergy and Infectious Diseases–funded Centers for Research in Emerging Infectious Diseases Network (awarded to the American and Asian Centers for Arboviral Research and Enhanced Surveillance Center under grant no. U01AI151788-03), the Center for the Advancement of Diagnostics for a Just Society based at Emory University, and the Centers for Disease Control and Prevention–funded Georgia Pathogen Genomics Center of Excellence.

The content is solely the responsibility of the authors and does not necessarily represent the official views of the Advancement of Diagnostics for a Just Society Center, Emory University, or the Centers for Disease Control and Prevention.

About the Author

Ms. Baer is a physician assistant at the Emory TravelWell Center. Her primary research centers on improving medical care for international travelers and migrants. Dr. Arora is an associate bioinformatics scientist in the Department of Infectious Diseases at Emory University School of Medicine. Her primary research interests are developing bioinformatics pipelines for next-generation sequencing to study emerging viruses.

References

1. Aguilar PV, Barrett AD, Saeed MF, Watts DM, Russell K, Guevara C, et al. Iquitos virus: a novel reassortant Orthobunyavirus associated with human illness in Peru. PLoS Negl Trop Dis. 2011;5:e1315. https://doi.org/10.1371/journal.pntd.0001315
2. Sakkas H, Bozidis P, Franks A, Papadopoulou C. Oropouche fever: a review. Viruses. 2018;10:175. https://doi.org/10.3390/v10040175
3. Wise EL, Pullan ST, Márquez S, Paz V, Mosquera JD, Zapata S, et al. Isolation of Oropouche virus from febrile patient, Ecuador. Emerg Infect Dis. 2018;24:935–7. https://doi.org/10.3201/eid2405.171569
4. Rojas A, Stittleburg V, Cardozo F, Bopp N, Cantero C, López S, et al. Real-time RT-PCR for the detection and quantitation of Oropouche virus. Diagn Microbiol Infect Dis. 2020;96:114894. https://doi.org/10.1016/j.diagmicrobio.2019.114894
5. Pan American Health Organization. Epidemiological update: Oropouche in the Americas Region. 2024 Sep 6

[cited 2024 Sep 16]. https://www.paho.org/en/documents/epidemiological-update-oropouche-americas-region-6-september-2024
6. Brown AB, Miller C, Hamer DH, Kozarsky P, Libman M, Huits R, et al. Travel-related diagnoses among U.S. nonmigrant travelers or migrants presenting to U.S. GeoSentinel sites—GeoSentinel Network, 2012–2021. MMWR Surveill Summ. 2023;72:1–22. https://doi.org/10.15585/mmwr.ss7207a1
7. Hernandez S, Cardozo F, Myers DR, Rojas A, Waggoner JJ. Simple and economical RNA extraction and storage packets for viral detection from serum or plasma. Microbiol Spectr. 2022;10:e0085922. https://doi.org/10.1128/spectrum.00859-22
8. Waggoner JJ, Abeynayake J, Balassiano I, Lefterova M, Sahoo MK, Liu Y, et al. Multiplex nucleic acid amplification test for diagnosis of dengue fever, malaria, and leptospirosis. J Clin Microbiol. 2014;52:2011–8. https://doi.org/10.1128/JCM.00341-14
9. Weidmann M, Rudaz V, Nunes MR, Vasconcelos PF, Hufert FT. Rapid detection of human pathogenic orthobunyaviruses. J Clin Microbiol. 2003;41:3299–305. https://doi.org/10.1128/JCM.41.7.3299-3305.2003
10. Naveca FG, de Almeida TAP, Souza V, Nascimento V, Silva D, Nascimento F, et al. Emergence of a novel reassortant Oropouche virus in the Brazilian Amazon region. Nat Med. 2024 [Epub ahead of print]. https://doi.org/10.1038/s41591-024-03300-3

Address for correspondence: Jesse J. Waggoner, Emory University School of Medicine, 1760 Haygood Dr NE, Rm E-132, Atlanta, GA 30322, USA; email: jjwaggo@emory.edu

COMMENT LETTERS

Estimating Underdetection of Foodborne Disease Outbreaks

Craig W. Hedberg, Melanie J. Firestone, Thuy N. Kim, Alexandra R. Edmundson, Jeff B. Bender

Authors affiliation: University of Minnesota School of Public Health, Minneapolis, Minnesota, USA

DOI: https://doi.org/10.3201/eid3011.240198

To the Editor: In the February issue, Ford et al. used the power law to estimate underdetection of foodborne disease outbreaks in the United States (*1*). Two of their main conclusions are entirely reasonable: small outbreaks are more likely to go undetected than large outbreaks, and the use of whole-genome sequencing (WGS) has improved the detection of small outbreaks caused by pathogens for which WGS is used. However, their conclusion on the usefulness of the power law itself needs further consideration.

Ford et al. analyzed the size of all foodborne outbreaks reported to the national Foodborne Disease Outbreak Surveillance System during 1998–2019. They defined outbreak size as the number of laboratory-confirmed cases. However, laboratory-confirmed cases are only good estimators for the size of outbreaks detected through pathogen-specific surveillance, such as for *Salmonella*, where outbreak detection follows the accumulation of confirmed cases. For outbreaks associated with events or establishments, identification might rely on reports from consumers, many of whom do not seek healthcare; thus, stool specimens might only be collected from a few cases to confirm the etiology. Consumer complaints are the primary means for identifying foodborne outbreaks caused by norovirus. The Council to Improve Foodborne Outbreak Response recommends collecting clinical specimens from ≥5 members from the ill group in such settings (*2*). Thus, the number of confirmed cases in an outbreak is dependent on how the outbreak is detected. Outbreaks detected by complaint generally have few confirmed cases, even though they can involve large numbers of illnesses.

To provide a fair evaluation for the usefulness of the power law, it may be better to restrict analyses to outbreaks with common detection pathways. For outbreaks detected by pathogen-specific surveillance, counting confirmed cases seems appropriate. For outbreaks detected through consumer complaints, analyses should include all outbreak-associated illnesses.

References

1. Ford L, Self JL, Wong KK, Hoekstra RM, Tauxe RV, Rose EB, et al. Power law for estimating underdetection of foodborne disease outbreaks, United States. Emerg Infect Dis. 2023;30:337–40. https://doi.org/10.3201/eid3002.230342
2. Council to Improve Foodborne Outbreak Response. CIFOR guidelines for foodborne disease outbreak ||response, 3rd ed. Atlanta: Council of State and Territorial Epidemiologists; 2019.

Address for correspondence: Craig Hedberg, University of Minnesota School of Public Health, MMC 807, 420 Delaware St. SE, Minneapolis, MN 55455, USA; email: hedbe005@umn.edu

Laura Ford,[1] Julie L. Self,[1] Karen K. Wong, Robert M. Hoekstra, Robert V. Tauxe, Erica Billig Rose, Beau B. Bruce

Authors affiliation: Centers for Disease Control and Prevention, Atlanta, Georgia, USA

DOI: https://doi.org/10.3201/eid3011.241351

In Response: Our analysis of foodborne outbreaks reported in the United States demonstrated that foodborne outbreaks are distributed approximately according to a family of probability distributions—that is, power laws—based on our analysis of culture-confirmed cases in a national surveillance system (*1*). Hedberg et al. suggest restricting analyses by common detection pathways, hypothesizing that distinct pathways may follow distinct power law distributions (*2*). That is a notable idea based on real surveillance concerns, but it is challenging to explore in the available data. Analyses of the distribution of events, which vary by many orders of magnitude, require large amounts of data because identifying the underlying distribution is primarily based on the distribution of the rarer events in the tails of the distribution. Furthermore, the detection pathway is not generally contained in the surveillance record.

However, the reported estimated case count is available from the surveillance record and likely captures aspects of the distinct pathways noted by Hedberg et al. Notable variation exists in their reporting over time and by jurisdiction and is, in part, why we did not choose estimated cases for our primary analysis. We did explore the power law fit of 2 very common pathogens, *Salmonella* and norovirus, which Hedberg et al. noted are likely to have different pathways for how cases are reported to surveillance. The fit of confirmed *Salmonella* cases and estimated norovirus cases appear consistent with approximate power law distributions (Figure): *Salmonella* Kolmogorov-Smirnov statistic (KS) = 0.028, p = 0.607; norovirus KS = 0.036, p = 0.437. The fit of estimated cases overall also appears consistent with an approximate power law distribution (KS = 0.026, p = 0.191; minimum threshold 80, 90% credible interval 49–117; slope 2.64, 90% credible interval 2.50–2.79), which further supports the validity of power laws as descriptors of outbreak size, regardless of the underlying mechanism of discovery and reporting.

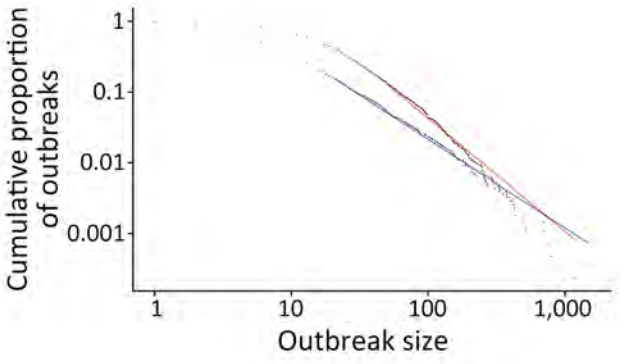

Figure. Log-log scale of foodborne *Salmonella* and norovirus outbreak size versus frequency from a power law for estimating underdetection of foodborne outbreaks, United States. Actual *Salmonella* (blue points) versus expected *Salmonella* (blue line) using laboratory-confirmed cases (minimum threshold 21, 90% credible interval [CrI] 11–43; slope 2.2, 90% CrI 2.1–2.5) and actual norovirus (red points) versus expected norovirus (red line) using estimated cases (minimum threshold 42, 90% CrI 22–123; slope 2.6, 90% CrI 2.3–3.3).

[1]These first authors contributed equally to this article.

References

1. Ford L, Self JL, Wong KK, Hoekstra RM, Tauxe RV, Rose EB, et al. Power law for estimating underdetection of foodborne disease outbreaks, United States. Emerg Infect Dis. 2023;30:337–40. https://doi.org/10.3201/eid3002.230342
2. Hedberg CW, Firestone MJ, Kim TN, Edmundson AR, Bender JB. Foodborne outbreak size is dependent on how the outbreak is detected. Emerg Infect Dis. 2024;30:2451. https://doi.org/10.3201/eid3011.240198

Address for correspondence: Laura Ford, Centers for Disease Control and Prevention, 1600 Clifton Rd NE, Mailstop H24-11, Atlanta, GA 30329-4017, USA; email: qdz4@cdc.gov

Revenge of the Microbes: How Bacterial Resistance Is Undermining the Antibiotic Miracle, 2nd Edition

Brenda A. Wilson and Brian T. Ho; ASM Press, Washington, DC, USA; ISBN: 978-1-683-67008-7; Pages: 160; Price: $29.95 (paperback)

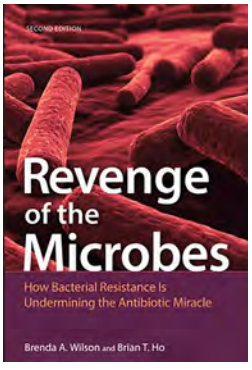

Revenge of the Microbes: How Bacterial Resistance Is Undermining the Antibiotic Miracle, 2nd edition, by Brenda A. Wilson and Brian T. Ho, is an intriguing and detailed narrative of the history of antibiotics, the mechanisms by which bacteria become resistant, and the spread of antibacterial resistance across the globe. The second edition comes at a critical time. While the attention of the general public, medical communities, and pharmaceutical companies is understandably focused on the development of vaccines and antivirals in response to the COVID-19 pandemic, this book shifts attention back to the ongoing crisis of antibiotic resistance.

The order of the chapters guides the reader seamlessly through the evolution of global antimicrobial resistance. The book begins with a brief overview of the history of antibiotics, diving into the groundbreaking antibiotic developments and discoveries. The chapters then explore the mechanisms by which bacteria gain resistance and how bacteria acquire resistance genes to existing antibiotics, providing the specific examples of avoparcin and fluroquinolones, which are of substantial public health interest.

The authors present readers with points to ponder, summarizing critical facts and discoveries while highlighting important unanswered questions at the conclusion of each chapter. That section provides an opportunity to pause, digest the material, and critically consider the potential impact of the "revenge of the microbes."

The photographs, figures, and tables also enhance comprehension, especially for those who are new to the topic. For example, chapter 6 describes the processes in which bacteria become resistant to antibiotics, which include restricting the antibiotic's access to the target, inactivating the antibiotic, and mutating the target itself. Figure 6.1 depicts a mechanism in which a membrane-embedded efflux pump actively removes tetracyclines, a class of antibiotics, in an easy-to-understand diagram. In addition, the included photograph of Anne Sheafe Miller, the first US patient to receive penicillin, emphasizes the authors' claim that antibiotics are miracle drugs.

Wilson and Ho tactfully describe the intricacies of the antimicrobial resistance crisis, including discussions regarding antibacterial use in livestock, the economic pressures faced by pharmaceutical companies related to antibiotic development and assessment, and the importance of antibiotic stewardship in hospital settings. The book concludes by offering a multidisciplinary framework for key stakeholders and interest groups to tackle the antibiotic resistance crisis. For example, treating patients with antibiotic-resistant bacterial infections is costly and requires additional supplies, space, and equipment. Consequently, hospital administrators are allocating more resources to establish effective infection-control practices. The final chapter serves as a call to action, underscoring the necessity of participation from many sectors.

Revenge of the Microbes offers an insightful examination of a critical global public health threat. This text succinctly meets the objectives outlined in the preface, focusing on "bridging the informational divide by presenting a more holistic view of antibiotics and antibiotic resistance." This book offers the opportunity for a general audience, including students, educators, scientists, medical professionals, and concerned citizens, to gain an appreciation for the successes of antibiotics and understand the intricacies of antibiotic use and stewardship.

Isabella Caruso

Author affiliation: University of Massachusetts Amherst, School of Public Health and Health Sciences, Amherst, Massachusetts, USA

DOI: https://doi.org/10.3201/eid3011.240228

Address for correspondence: Isabella Caruso, University of Massachusetts Amherst School of Public Health and Health Sciences, 715 N Pleasant St, Amherst, MA 01003, USA; email: igcaruso@umass.edu

Abraham Mignon (1640–1679, *Still Life with Fruits, Oysters and a Porcelain Bowl* (1660–1679) (detail). Oil on panel, 21.7 in × 17.7 in/55 cm × 45 cm. Digital image courtesy of Rijksmuseum, Amsterdam, the Netherlands.

Not Everything Is as It First Appears

Byron Breedlove

Although Abraham Mignon was born in Frankfurt, Germany, he is associated with the Dutch painters of his time. When Mignon was 9 years old, his parents, who were shopkeepers, arranged an apprenticeship with Jacob Marrel, a German still-life painter. Marrel had previously traveled to Utrecht, the Netherlands, to work and study, and he returned there in 1664 accompanied by Mignon, who was then 24.

Author affiliation: Centers for Disease Control and Prevention, Atlanta, Georgia, U:SA

DOI: https:l/doi.org/10.3201/eid3011.AC3011

In 1669, both artists became members of the Guild of Saint Luke, and for several years Mignon studied and worked with fellow guild member, Jan Davidsz de Heem, a Dutch still-life specialist. The Rijksmuseum states, "Mignon's paintings of flowers and fruit feature the same opulent style of composition and the same brilliant colours as De Heem's work." Mignon further assimilated into Dutch society when he married Maria Willaerts in 1675, but the union proved short, as he died at age 39 in March 1679.

Throughout the 17th Century, still-life painting in the Netherlands flourished. Art historian Walter

Liedtke wrote, "In general, the rise of still-life painting in the Northern and Spanish Netherlands (mainly in the cities of Antwerp, Middelburg, Haarlem, Leiden, and Utrecht) reflects the increasing urbanization of Dutch and Flemish society, which brought with it an emphasis on the home and personal possessions, commerce, trade, learning—all the aspects and diversions of everyday life."

Still Life with Fruits, Oysters and a Porcelain Bowl, featured on this month's cover, is among an estimated 400 paintings attributed to Mignon and exemplifies his eye for detail, precision, and texture. The Rijksmuseum, where the painting may be viewed, notes: "The composition of this still life is both sumptuous and inventive. Mignon set the roemer, the green glass at the left, upside down. Reflected in it is a window, and a view of a church tower in Utrecht, where Mignon lived. The porcelain bowl from Asia was a sign of prosperity as well as being a showpiece on the table."

In the painting, the vivid colors and lifelike textures are enhanced by a black background. The canvas is crowded with resplendent grapes and berries, the top of a green pumpkin or gourd, a halved pomegranate, an orange slice, cherries hanging from a snippet of a branch, charred chestnuts, a split walnut, glistening raw oysters, and various leaves and vines. Smoke tendrils drift from tobacco stuffed into a white clay pipe and the glowing tip of a twist of rope used to light the pipe. Mignon's expertise in creating textures is also shown by an ornate porcelain bowl, the hard-to-see inverted green drinking glass, or roemer, on the left, and drops and pools of a viscous liquid.

Symbolic and allegorical interpretations in still-life paintings from the Dutch Golden Age are abundant. Art historian Emily Snow wrote, "Grapes symbolize the themes of pleasure and lust associated with Bacchus, the Roman god of wine. Pomegranates are associated with Persephone, the Greek goddess of spring and queen of the underworld." Snow explains, "Oysters were especially popular in still life paintings of the Dutch Golden Age and were not considered a luxury food at the time. Like other shells, they symbolize birth and fertility."

Beneath its veneer of abundance, however, Mignon's painting reveals a more complicated commentary. Entomologists (meant in the broadest sense of the historical term) could describe which moth, spider, and caterpillar have taken residence, and a malacologist could identify the snail exploring the side of the table. Several grapes have split or shriveled, and the ripe cherries have already fed the hungry caterpillar. One oyster shell is overturned on the table, and others are piled over an ornate harlequin-handled knife lying on a smaller table. All may be interpreted as symbols of decay and death, the transience of life and beauty.

Modern viewers, accustomed to hearing about outbreaks of foodborne diseases and recalls of various foods, might ponder whether Mignon's colorful feast would be safe to eat. Could those grapes and berries have been grown near contaminated water or picked by people practicing poor hygiene? Might those oysters harbor some form of *Vibrio* bacteria that live in coastal waters and can contaminate shellfish with a bacteria or toxin?

Several articles in this issue of *Emerging Infectious Disease* address foodborne disease outbreaks. One reports food poisoning in Australia caused by *Vibrio parahemolyticus* in oysters. Another documents disease in Nigeria caused by *Vibrio cholerae*, a bacteria endemic to the environment there and a source of cholera through contact with contaminated food and water. A third recounts a prolonged outbreak of listeriosis in Switzerland, linked with a disease typically spread through contaminated dairy products, meat, fish, fruits, or vegetable—in this case, baker's yeast products.

More than 200 various types of foodborne diseases have been identified. The Centers for Disease Control and Prevention reports that in 1 year in the United States, 48 million people will get sick from a foodborne illness, nearly 130,000 will be hospitalized, and 3,000 will die. The World Health Organization estimates, "Each year worldwide, unsafe food causes 600 million cases of foodborne diseases and 420,000 deaths." The exact toll from foodborne illness is, however, not known.

Scallan, Hoekstra, and Angulo et al. noted in a 2011 research article in *Emerging Infectious Diseases* that "Estimates of the overall number of episodes of foodborne illness are helpful for allocating resources and prioritizing interventions," but they also explained that various factors make it difficult to develop accurate estimates: many different agents can contaminate food (bacteria, viruses, parasites, and toxins), contact with animals or drinking contaminated water may cause illness, and foodborne pathogens have different effects on their hosts depending on the person's age and overall health. They point out that "only a small proportion of illnesses are confirmed by laboratory testing and reported to public health agencies."

Public health investigators often assess information that relies on the people's memories. Responding to outbreaks of foodborne illnesses requires following clues, and as is the case with studying Dutch still-life paintings, requires an eye for detail, because not everything is as it first appears.

Bibliography

1. Centers for Disease Control and Prevention. About food safety [cited 2024 Sep 30]. https://www.cdc.gov/food-safety/about/#cdc_disease_basics_prevention-prevention
2. Fearnley E, Leong LEX, Centofanti A, Dowsett P, Hocking H, Combs B, et al. *Vibrio parahaemolyticus* foodborne illness associated with oysters, Australia, 2021–2022. Emerg Infect Dis. 2024;30:2271–8. https://doi.org/10.3201/eid3011.240172
3. Liedtke W. Still-life painting in northern Europe, 1600–1800 [cited 2024 Sep 23]. http://www.metmuseum.org/toah/hd/nstl/hd_nstl.htm
4. Morgado S, Adewale A, Abiodun I, Lawal S, Freitas F, Fonseca E, et al. Environmental *Vibrio cholerae* strains harboring cholera toxin and *Vibrio* pathogenicity island 1, Nigeria, 2008–2015. Emerg Infect Dis. 2024;30:2441–4. https://doi.org/10.3201/eid3011.240495
5. Rijksmuseum. Abraham Mignon [cited 2024 Sep 20]. https://www.rijksmuseum.nl/en/rijksstudio/artists/abraham-mignon
6. Rijksmuseum. Still Life with Fruit, Oysters, and a Porcelain Bowl, Abraham Mignon, 1660–1679 [cited 2024 Sept 20]. https://www.rijksmuseum.nl/en/rijksstudio/artists/abraham-mignon/objects#/SK-A-2329,1
7. Scallan E, Hoekstra RM, Angulo FJ, Tauxe RV, Widdowson MA, Roy SL, et al. Foodborne illness acquired in the United States—major pathogens. Emerg Infect Dis. 2011;17:7–15. https://doi.org/10.3201/eid1701.P11101
8. Snow E. 10 common symbols in still-life paintings & what they mean [cited 2024 Sep 25]. https://www.thecollector.com/still-life-paintings-what-they-mean
9. Stephan R, Horlbog JA, Nüesch-Inderbinen M, Dhima N. Outbreak of listeriosis likely associated with baker's yeast products, Switzerland, 2022–2024. Emerg Infect Dis. 2024;30:2424–6. https://doi.org/10.3201/eid3011.240764
10. Wheelock AK. Abraham Mignon: Biography. National Gallery of Art [cited 2024 Sept 20]. https://www.nga.gov/collection/artist-info.6626.html
11. World Health Organization. Estimating the burden of foodborne diseases [cited 2024 Sep 30]. https://www.who.int/activities/estimating-the-burden-of-foodborne-diseases

Address for correspondence: Byron Breedlove, EID Journal, Centers for Disease Control and Prevention, 1600 Clifton Rd NE, Mailstop H16-2, Atlanta, GA 30329-4018, USA; email: wbb1@cdc.gov

EMERGING INFECTIOUS DISEASES®

Upcoming Issue • December 2024
Zoonotic Infections

- Increase in Adult Patients with Varicella-Zoster Virus–Related Central Nervous System Infections, Japan
- Historical Assessment and Mapping of Human Plague, Kazakhstan, 1926–2003
- Cost-Effectiveness Analysis of Japanese Encephalitis Vaccination for Children <15 Years of Age, Bangladesh
- Clinical Manifestations, Antifungal Drug Susceptibility, and Treatment Outcomes for Emerging Zoonotic Cutaneous Sporotrichosis, Thailand
- Effect of Sexual Partnerships on Zika Virus Transmission in Virus-Endemic Region, Northeast Brazil
- Highly Pathogenic Avian Influenza Virus A(H5N1) Infection in Cats, South Korea, 2023
- Human Circovirus in Patients with Hepatitis, Hong Kong
- Novel Mastadenovirus Infection as Cause of Pneumonia in Imported Black-and-White Colobuses (*Colobus guereza*), Thailand
- Possible New Focus of Diphyllobothriosis, Central Europe
- *Mycobacterium leprae* in Nine-Banded Armadillos (*Dasypus novemcinctus*), Ecuador
- Transmission of Swine Influenza A(H1N1) Virus along Pig Value Chains in Cambodia, 2020–2022
- Chikungunya Outbreak Risks in the Dominican Republic since the 2014 Outbreak
- Mpox Vaccine Acceptance, Democratic Republic of the Congo
- Lobomycosis in Andes-Amazon Region, Bolivia, 2022
- Heartland Virus Infection in Elderly Patient Initially Suspected of Having Ehrlichiosis, North Carolina, USA
- Replication-Competent Oropouche Virus in Semen of Traveler Returning to Italy from Cuba, 2024
- Bacteriologic and Genomic Investigation of *Bacillus anthracis* Isolated from World War II Site, China
- Sporotrichosis Cluster in Domestic Cats and Veterinary Technician, Kansas, USA, 2022

Complete list of articles in the December issue at https://wwwnc.cdc.gov/eid/#issue-316

Earning CME Credit

To obtain credit, you should first read the journal article. After reading the article, you should be able to answer the following, related, multiple-choice questions. To complete the questions (with a minimum 75% passing score) and earn continuing medical education (CME) credit, please go to http://www.medscape.org/journal/eid. Credit cannot be obtained for tests completed on paper, although you may use the worksheet below to keep a record of your answers.

You must be a registered user on http://www.medscape.org. If you are not registered on http://www.medscape.org, please click on the "Register" link on the right hand side of the website.

Only one answer is correct for each question. Once you successfully answer all post-test questions, you will be able to view and/or print your certificate. For questions regarding this activity, contact the accredited provider, CME@medscape.net. For technical assistance, contact CME@medscape.net. American Medical Association's Physician's Recognition Award (AMA PRA) credits are accepted in the US as evidence of participation in CME activities. For further information on this award, please go to https://www.ama-assn.org. The AMA has determined that physicians not licensed in the US who participate in this CME activity are eligible for AMA PRA Category 1 Credits™. Through agreements that the AMA has made with agencies in some countries, AMA PRA credit may be acceptable as evidence of participation in CME activities. If you are not licensed in the US, please complete the questions online, print the AMA PRA CME credit certificate, and present it to your national medical association for review.

Article Title

Clinical and Genomic Epidemiology of Coxsackievirus A21 and Enterovirus D68 in Homeless Shelters, King County, Washington, USA, 2019–2021

CME Questions

1. Which of the following viruses was most commonly isolated from nasal swabs among persons experiencing homelessness in the current study?

A. Severe acute respiratory syndrome coronavirus 2 (SARS-CoV-2)
B. Enterovirus D68 (EV-D68)
C. Rhinovirus
D. Coxsackievirus A21 (CVA21)

2. Which of the following variables was the most significant risk factor for a positive test for enterovirus in the current study?

A. Being a child
B. Being female transgender
C. Recent homelessness <1 year
D. Higher rates of comorbid illness

3. Which of the following statements regarding the clinical presentation of participants with a positive test for CVA21 in the current study is most accurate?

A. The most common symptoms associated with a positive test were rhinorrhea and cough
B. The most common symptoms associated with a positive test were abdominal cramping and diarrhea
C. <10% of participants with a positive test reported some loss of function
D. About three-quarters of participants with a positive test had healthcare visits to address symptoms

4. Which of the following statements regarding environmental testing for viruses in the current study is most accurate?

A. Only the adult shelters had positive environmental tests for CVA21
B. Nearly all of the positive environmental tests for CVA21 were recorded at the shelter for older male persons
C. EV-D68 was more commonly found on surfaces compared with CVA21
D. 12% of bioaerosol samples were positive for enteroviruses

Earning CME Credit

To obtain credit, you should first read the journal article. After reading the article, you should be able to answer the following, related, multiple-choice questions. To complete the questions (with a minimum 75% passing score) and earn continuing medical education (CME) credit, please go to http://www.medscape.org/journal/eid. Credit cannot be obtained for tests completed on paper, although you may use the worksheet below to keep a record of your answers.

You must be a registered user on http://www.medscape.org. If you are not registered on http://www.medscape.org, please click on the "Register" link on the right hand side of the website.

Only one answer is correct for each question. Once you successfully answer all post-test questions, you will be able to view and/or print your certificate. For questions regarding this activity, contact the accredited provider, CME@medscape.net. For technical assistance, contact CME@medscape.net. American Medical Association's Physician's Recognition Award (AMA PRA) credits are accepted in the US as evidence of participation in CME activities. For further information on this award, please go to https://www.ama-assn.org. The AMA has determined that physicians not licensed in the US who participate in this CME activity are eligible for AMA PRA Category 1 Credits™. Through agreements that the AMA has made with agencies in some countries, AMA PRA credit may be acceptable as evidence of participation in CME activities. If you are not licensed in the US, please complete the questions online, print the AMA PRA CME credit certificate, and present it to your national medical association for review.

Article Title

Extrapulmonary *Mycobacterium abscessus* Infections, France, 2012–2020

CME Questions

1. What was the most common anatomic site of extrapulmonary infections due to *Mycobacterium abscessus* (EP-MAB) in the current study?

A. Skin and soft tissue
B. Lymph nodes
C. Biliary tract
D. Bone and joint

2. What was the most common clinical sign of EP-MAB in the current study?

A. Fever
B. Cutaneous lesions
C. Asthenia
D. Palpable lymph nodes

3. Which of the following statements regarding the etiology of EP-MAB in the current study is most accurate?

A. Approximately one-quarter of EP-MAB was related to penetrating injury
B. Patients with EP-MAB due to an environmental source were generally symptomatic within 2 weeks
C. Most EP-MAB were incurred in France
D. All EP-MAB in the breast were associated with healthcare injury

4. What is the cure rate without relapse in the current study of patients with EP-MAB?

A. 73%
B. 45%
C. 22%
D. 11%

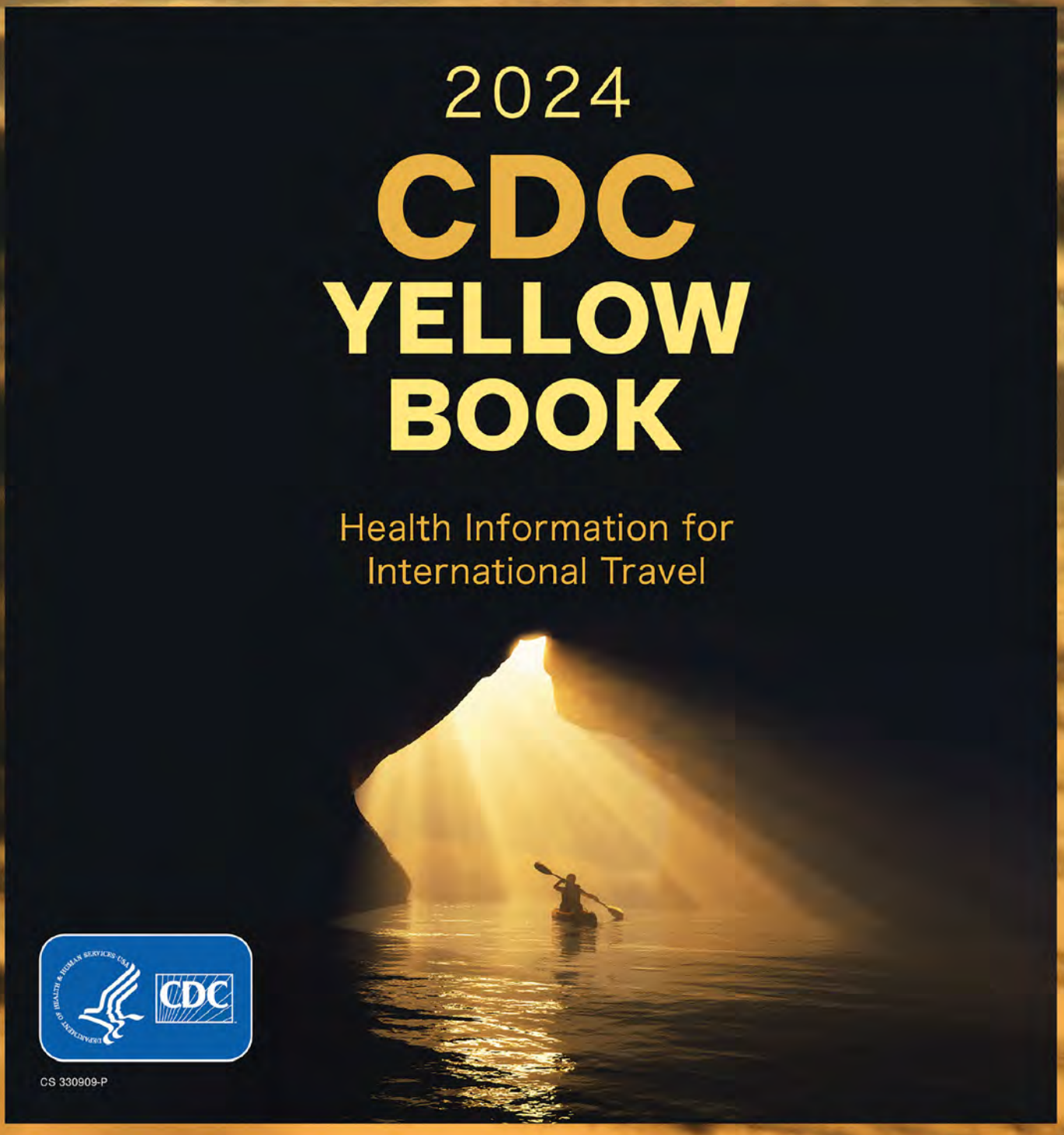

Launch of CDC Yellow Book 2024 – A Trusted Travel Medicine Resource

CDC is pleased to announce the launch of the CDC Yellow Book 2024. The CDC Yellow Book is a source of the U.S. Government's recommendations on travel medicine and has been a trusted resource among the travel medicine community for over 50 years. Healthcare professionals can use the print and digital versions to find the most up-to-date travel medicine information to better serve their patients' healthcare needs.

The CDC Yellow Book is available in print through Oxford University Press and online at www.cdc.gov/yellowbook.